

AD-A058 797

GEORGIA INST OF TECH ATLANTA

F/G 4/1

FEDERAL AVIATION ADMINISTRATION-GEORGIA INSTITUTE OF TECHNOLOGY--ETC(U)

MAY 78

UNCLASSIFIED

FAA-RD-78-83

NL

1 of 5  
AD  
A058 797





REPORT NO. FAA-RD-78-83

AD A058797

DDC FILE COPY

LEVEL

9

**FEDERAL AVIATION ADMINISTRATION-GEORGIA  
INSTITUTE OF TECHNOLOGY WORKSHOP ON  
GROUNDING AND LIGHTNING PROTECTION.**

*Held at Atlanta, Georgia on  
May 2-4/1978.*



MAY 1978

Final Report

Document is available to the U.S. public through  
the National Technical Information Service,  
Springfield, Virginia 22161.

78 08 29 023  
Prepared for

**U.S. DEPARTMENT OF TRANSPORTATION  
FEDERAL AVIATION ADMINISTRATION  
Systems Research & Development Service  
Washington, D.C. 20590**

153 800

mt

# NOTICE

This document is disseminated under the sponsorship of the Department of Transportation in the interest of information exchange. The United States Government assumes no liability for its contents or use thereof.

Technical Report Documentation Page

1. Report No. FAA-RD-78-83 ✓	2. Government Accession No.	3. Recipient's Catalog No.	
4. Title and Subtitle Federal Aviation Administration - Georgia Institute of Technology Workshop on Grounding and Lightning Protection		5. Report Date May 1978	
		6. Performing Organization Code	
7. Author(s)		8. Performing Organization Report No.	
9. Performing Organization Name and Address  Georgia Institute of Technology Atlanta, Georgia 30332		10. Work Unit No. (TRAIS)	
		11. Contract or Grant No.	
12. Sponsoring Agency Name and Address Federal Aviation Administration Department of Transportation System Research and Development Service Washington, DC 20590		13. Type of Report and Period Covered Final May 2-4, 1978	
		14. Sponsoring Agency Code ARD-350	
15. Supplementary Notes			
<p>16. Abstract</p> <p>A state-of-art review and background research reveals a number of opinions as to the preferred techniques of grounding of electronic equipment and systems. These techniques become important when protection must be provided for transients induced by lightning, electromagnetic pulses (EMP) and other sources. The Systems Research and Development Service of the Federal Aviation Administration in conjunction with the Georgia Institute of Technology conducted a workshop which brought together distinguished experts in the fields of grounding, lightning, transient protection, EMP protection for electrical and electronic facilities and lightning transient protection of aircraft electronics. This report contains the papers presented at the workshop. This is the fifth workshop conducted on the subject.</p>			
17. Key Words  Grounding, Bonding, Shielding, Electrical Noise, Lightning, EMP		18. Distribution Statement  Document is available through the National Technical Information Service, Springfield, VA 22151.	
19. Security Classif. (of this report)  UNCLASSIFIED	20. Security Classif. (of this page)  UNCLASSIFIED	21. No. of Pages  425	22. Price  023



# METRIC CONVERSION FACTORS

## Approximate Conversions to Metric Measures

Symbol When You Know Multiply by To Find Symbol

### LENGTH

in inches  
ft feet  
yd yards  
mi miles

\*2.5  
30  
0.9  
1.6

cm centimeters  
m meters  
km kilometers

### AREA

in<sup>2</sup> square inches  
ft<sup>2</sup> square feet  
yd<sup>2</sup> square yards  
mi<sup>2</sup> square miles  
acres

6.5  
0.09  
0.8  
2.6  
0.4

cm<sup>2</sup> square centimeters  
m<sup>2</sup> square meters  
km<sup>2</sup> square kilometers  
ha hectares

### MASS (weight)

oz ounces  
lb pounds  
short tons (2000 lb)

28  
0.45  
0.9

g grams  
kg kilograms  
t tonnes

### VOLUME

tsp teaspoons  
Tbsp tablespoons  
fl oz fluid ounces  
c cups  
pt pints  
qt quarts  
gal gallons  
cu ft cubic feet  
cu yd cubic yards

5  
15  
30  
0.24  
0.47  
0.95  
3.8  
0.03  
0.76

ml milliliters  
l liters  
m<sup>3</sup> cubic meters

### TEMPERATURE (exact)

°F Fahrenheit temperature

5/9 (after subtracting 32)

°C Celsius temperature

## Approximate Conversions from Metric Measures

When You Know Multiply by To Find Symbol

### LENGTH

mm millimeters  
cm centimeters  
m meters  
km kilometers

0.04  
0.4  
3.3  
1.1  
0.6

in inches  
ft feet  
yd yards  
mi miles

### AREA

cm<sup>2</sup> square centimeters  
m<sup>2</sup> square meters  
km<sup>2</sup> square kilometers  
ha hectares (10,000 m<sup>2</sup>)

0.16  
1.2  
0.4  
2.5

in<sup>2</sup> square inches  
ft<sup>2</sup> square feet  
mi<sup>2</sup> square miles  
acres

### MASS (weight)

g grams  
kg kilograms  
t tonnes (1000 kg)

0.035  
2.2  
1.1

oz ounces  
lb pounds  
short tons

### VOLUME

ml milliliters  
l liters  
m<sup>3</sup> cubic meters

0.03  
2.1  
1.06  
0.26  
35  
1.3

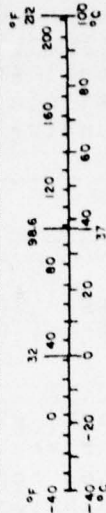
fl oz fluid ounces  
pt pints  
qt quarts  
gal gallons  
cu ft cubic feet  
cu yd cubic yards

### TEMPERATURE (exact)

°C Celsius temperature

9/5 (then add 32)

°F Fahrenheit temperature



\*1 in is 2.54 in exactly. For other exact conversions and more detailed tables, see NBS Mon. Pub. 298, Units of Weights and Measures, Pt. 2, Sec. 25, SI Tables, Vol. 1 (1975).

[illegible]111

FLORIDA LIGHTNING ELECTROMAGNETIC-FIELD MEASUREMENTS USING AN INSTRUMENTED NASA JET AIRCRAFT	
J. E. Nanevich, R. C. Adamo, E. F. Vance and R. T. Bly	305
IN-FLIGHT LIGHTNING DATA MEASUREMENT SYSTEM FOR FLEET APPLICATION	
G. J. Von Bokern, L. D. Piszker and R. O. Brick . . . . .	345
THE USE OF CW TEST AND ANALYSIS TECHNIQUES IN LIGHTNING VULNERABILITY ASSESSMENT OF AIRCRAFT SYSTEMS	
D. E. Young and L. D. Piszker . . . . .	365
A ONE MEGAJOULE LIGHTNING SIMULATOR	
E. H. Schulte and G. W. Kamerman . . . . .	385
PROTECTION AGAINST LIGHTNING-INDUCED LINE SURGES AND TRANSIENTS	
Rodney B. Bent . . . . .	405
LIST OF ATTENDEES . . . . .	A-1



FINAL PROGRAM

FEDERAL AVIATION ADMINISTRATION/GEORGIA INSTITUTE OF TECHNOLOGY  
WORKSHOP ON  
GROUNDING AND LIGHTNING PROTECTION  
ATLANTA, GEORGIA  
May 2-4, 1978

TUESDAY, MAY 2

Registration - Space Science Building

Introduction - Dr. D. G. Grace, Director, Engineering Experiment Station,  
Georgia Institute of Technology

Welcome - Dr. T. E. Stelson, Vice President for Research, Georgia  
Institute of Technology

Opening Remarks - Mr. P. H. Swatek, Director, Souther Region,  
Federal Aviation Administration

SESSION MODERATOR: Mr. H. W. Denny, Engineering Experiment Station,  
Georgia Institute of Technology

"Use of Stainless Steel in Ground Rod Systems" - Mr. H. W. Denny,  
Engineering Experiment Station, Georgia Institute of Technology,  
Atlanta, Georgia and Mr. Keith Switzer, ERICO Products, Inc.,  
Cleveland, Ohio.

"Improvements in the Measurements of Earth Resistance" - Mr. J. A.  
Woody, Engineering Experiment Station, Georgia Institute of  
Technology, Atlanta, Georgia.

"A Continuous Ground Bed Monitor" - Mr. W. L. Cooley and Mr. E. K.  
Stanek, University of West Virginia, Morgantown, West Virginia, and  
Mr. R. L. King, U. S. Bureau of Mines, Bruceton, Pennsylvania.

"Frequency Division Multiplex Baseband Cable Protection" - Mr. F.  
LaDieu, Air Force Communications Service, Scott Air Force Base,  
Illinois.

"The Role of Inductance in Lightning Protection" - Mr. J. A. Plumer,  
Lightning Technologies, Inc., Pittsfield, Massachusetts.



"Condition for Evaluating the Protection Zone of the Lightning Rod" - Dr. A. Vorgucic, School of Electrical Engineering, Georgia Institute of Technology, Atlanta, Georgia.

Discussion of MIL-STD-188-124: Grounding, Bonding, Shielding - Mr. W. L. Keller, Air Force Communication Service, Scott Air Force Base, Illinois.

WEDNESDAY, MAY 3

SESSION MODERATOR: Mr. C. W. Bergman, Defense Communications Engineering Center, Reston, Virginia.

"Protection Against Lightning-Induced Line Surges and Transients" - Dr. R. B. Bent, Atlantic Scientific Corporation, Indian Harbour Beach, Florida.

"EMP Protection of Minuteman Launch Facilities" - Mr. A. Brockschmidt, Boeing Aerospace Company, Renton, Washington.

"Reliability of the Silicon Avalanche Suppressor" - Mr. O. M. Clark, General Semiconductor Industries, Inc., Tempe, Arizona. (Paper presented by Joseph Pizzicaroli)

"Protecting Facilities and Equipment from Induced Lightning and Power Line Switching Transients" - Mr. R. Odenberg, Transtector Systems, Monterey Park, California.

"A Study of Lightning Transients in Telephone Cables" - Mr. K. E. Crouch, Lightning Technologies, Inc., Pittsfield, Massachusetts and Mr. B. I. Wolff, General Electric Company, Syracuse, New York. (Paper presented by J. A. Plumer)

"Transient Intrusion into Cable Television Systems: - Mr. W. L. Braun, ComSonics, Inc., Harrisonburg, Virginia.

SESSION MODERATOR: Mr. John Reed, System Research and Development Service, Federal Aviation Administration, Washington, DC.

"The Transient Responses of a Two-Wire Transmission Line Inside a Missile Due to EMP (Electromagnetic Pulse) and Lightning" - Mr. A. F. Rashid, General Dynamics/Convair, San Diego, California.

"Laboratory Simulation of Lightning Induced Electrical Transients" - Mr. J. E. Lee, McDonnell Douglas Corporation, St. Louis, Missouri. (Paper presented by William G. Butters)

THURSDAY, MAY 4

"Florida Lightning Electromagnetic Field Measurements Using a NASA Learjet Aircraft" - M. J. E. Nanevich, Mr. R. C. Adamo,, Mr. R. T. Oly, SRI International, Menlo Park, California. (Paper presented by Edward F. Vance)

"In-Flight Lightning Data Measurement System for Fleet Applications" - Mr. G. J. Von Bokern, Mr. L. D. Piszker, MR. R. O. Brick, Boeing Commercial Airplane Company, Seattle, Washington.

"The Use of CW Test and Analysis Techniques in Lightning Vulnerability Assessment of Aircraft Systems" - Mr. D. E. Young and Mr. L. D. Piszker, The Boeing Company, Seattle, Washington.

"A One Megajoule Lightning Simulator" - Mr. E. H. Schulte, and Mr. G. W. Kamerman, McDonnell Douglas Corporation, St. Louis, Missouri. (Paper presented by William G. Butters)

TECHNICAL PROGRAM COMMITTEE

Federal Aviation Administration/Georgia Institute of Technology

Workshop on

Grounding and Lightning Protection

MAY 2-4, 1978

R. Barkalow, Chairman	Federal Aviation Administration
B. Bergman	Defense Communication Agency
R. Cosel	Florida Institute of Technology
H. Denny	Engineering Experiment Station Georgia Institute of Technology
K. Huddleston	Georgia Institute of Technology
J. Reed	Federal Aviation Administration

USE OF STAINLESS STEEL IN GROUND ROD SYSTEMS

by

H. W. Denny  
Engineering Experiment Station  
Georgia Institute of Technology  
Atlanta, Georgia

and

W. Keith Switzer  
ERICO Products, Inc.  
Cleveland, Ohio

Presented at

Federal Aviation Administration - Georgia Institute of Technology  
Workshop on Grounding and Lightning Protection

May 1978



## ABSTRACT

The corrosion resistant properties of stainless steel are well known. Its corrosion resistance makes it as attractive for earth electrode construction as copper or copper-clad steel. An added feature of stainless steel is that it is electrochemically closer to iron, steel, and lead than is copper. Thus, the buried stainless steel presents less of a cathodic corrosion threat to pilings, pipings, and cable sheaths. Stainless rods and cables are available and are price competitive with copper or copper-clad materials. Installation is straightforward with the use of thermite bonding.

## Use of Stainless Steel in Ground Rod Systems

H. W. Denny  
Engineering Experiment Station  
Georgia Institute of Technology  
Atlanta, Georgia 30332

W. Keith Switzer  
ERICO Products, Inc.  
Cleveland, Ohio 44139

### Abstract

The corrosion resistance properties of stainless steel have been established. Its corrosion resistance makes it as attractive for earth electrode construction as copper or copper-clad steel. An added feature of stainless steel is that it is electrochemically more compatible with iron, steel, and lead than is copper. Thus, buried stainless steel presents less of a cathodic corrosion threat to pilings, piping, and cable sheaths. Stainless rods and cables are available and are price competitive with copper materials. Installation is straightforward with the use of thermite bonding.

### 1. Corrosion Properties of Stainless Steel in Soil

Corrosion is the deterioration of a metallic substance because of a reaction with its environment. Most environments are corrosive to some degree. Soils are corrosive because of the presence of moisture, dissolved mineral salts, and bacteria. In particular, low resistivity soils tend to be highly corrosive: the generally high level of moisture and dissolved salts that are responsible for the low resistivity also encourage corrosion.

The basic corrosion process for metals is illustrated in Figure 1. The requirements for corrosion to take place are that (1) an anode (positive) and a cathode (negative) must be present and form an electrochemical cell and (2) a complete path for the flow of direct current must exist. On the surface of many metals, anodic and cathodic regions are present because of impurities, grain boundaries and grain orientations, or localized stresses. These positively and negatively charged regions are in electrical contact

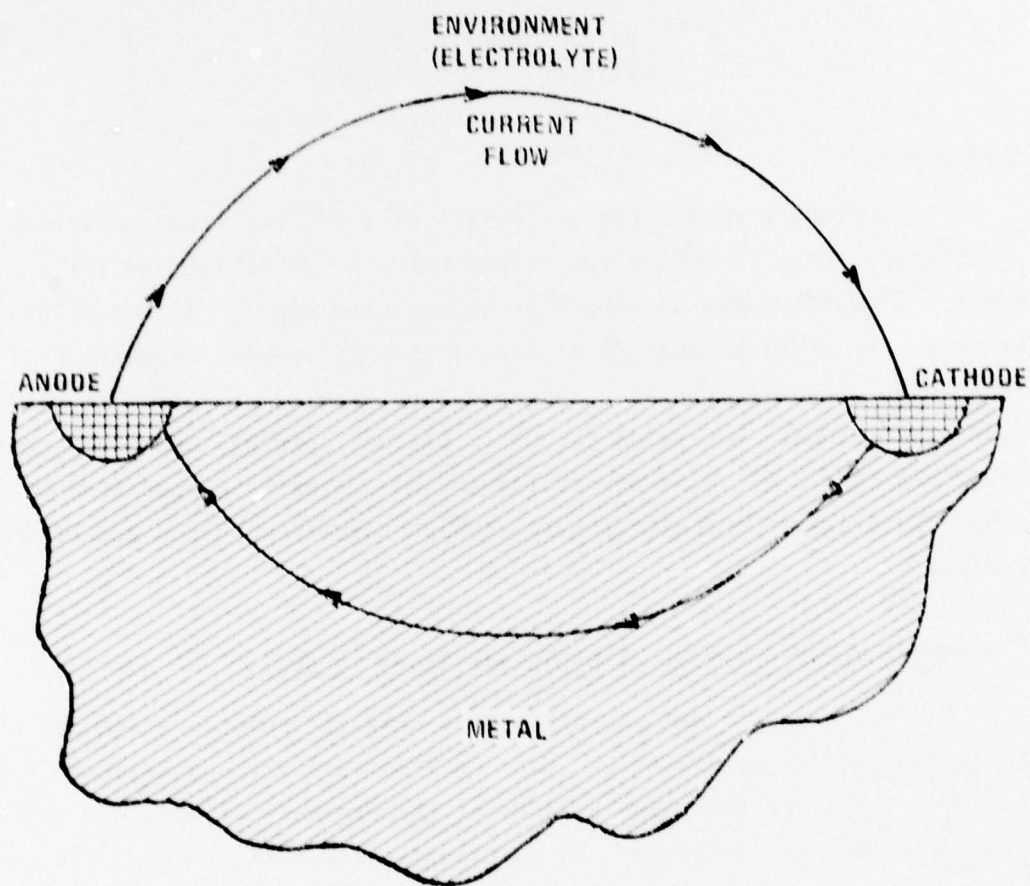


Figure 1. Basic Diagram of a Corrosion Cell.



through the body of metal. For corrosion to occur, however, an additional current path through an electrolyte (conducting fluid) must exist. In the presence of water or other appropriate liquid, the circuit is completed and current will flow from the anode to the cathode of the corrosion cell, with subsequent erosion of the anode.

The oxidation of metal involves the transfer of electrons from the metal to the oxidizing agent. In this process of oxidation, an electromotive force (EMF) is established between the metal and the solution containing the oxidizing agent. A metal in contact with an oxidizing solution containing its own metallic ions establishes a fixed potential difference with respect to every other metal in the same condition. The set of potentials determined under a standardized set of conditions, including temperature and ion concentration in the solution, is known as the EMF (or electrochemical) series [1]. The importance of the EMF series is that it qualitatively shows the relative tendencies of (pure) metals to corrode. Metals high in the series, such as aluminum and iron, react more readily in a conducting solution and thus are more prone to corrosion than metals, such as copper, which are low in the series.

The EMF series is based on metals in their free state--free of oxides and other films--in contact with a standardized solution. Of greater interest in practice, however, is the relative ranking of metals in a typical environment with the effects of surface films (which in some cases provide a high degree of protection) included. This ranking is referred to as the galvanic series. An abbreviated version of the most commonly referenced galvanic series is shown in Table I. Note that both copper and the stainless steels fall near the noble, or least corrosive, end of the series and are well below wrought iron and galvanized steel. This particular series is based on tests performed in sea water and should be used only as a relative indicator of possible corrosion rates in soils. Experience has shown that copper and copper clad materials are highly corrosion resistant in most soils. Thus the nearness of the stainless steels to copper in the galvanic series indicates that stainless steel materials should be similarly effective in resisting corrosion in soil.

Table I

Galvanic Series of Common Metals and Alloys in Seawater [2]

---

---

(ANODIC OR ACTIVE END)

Magnesium

Zinc

Galvanized Steel

2024 Aluminum

Mild Steel

Wrought Iron

Cast Iron

Ni-Resist (high-Ni cast iron)

Lead

Tin

Manganese Bronze

Brasses

Aluminum Bronze

Copper

Silicon Bronze

Nickel

Inconel

Monel

Chromium Steel

18-8 Stainless Steel Type 304

Silver

Gold

---

---

(CATHODIC OR MOST NOBLE END)

From 1962 to 1969, the Naval Civil Engineering Laboratory at Port Hueneme, California, in cooperation with the National Association of Corrosion Engineers, conducted a seven-year test program on the corrosion of ground rods [3]. Single rods of galvanized steel, copper-clad steel, Ni-Resist cast iron, Type 302 stainless steel, Type 304 stainless-clad steel, zinc, magnesium, and aluminum were tested along with couples of these rods to mild steel rods. Sets of both single and coupled rods were removed, cleaned, and weighed after 1, 3, and 7 years. Weight losses were used as the measure of relative corrosion effects.\*

Selected results from this series of tests are presented in Tables II, III, and IV. The data of Table II confirms the better corrosion resistance of copper and stainless steels over mild steel. The galvanized steel rods rapidly lost their galvanizing coat and thus reverted to a simple mild steel rod. The weight losses of the copper-clad and 304 stainless-clad rods appeared to be primarily the result of core erosion at the tip of the rod, which was not clad. Over the same time periods, the copper-clad rods showed greater core erosion. The Type 302 solid stainless rod did show evidence of pitting near the tip and close to the surface of the soil. Overall, the corrosion resistance of the copper and stainless materials seemed equally strong.

When electrically coupled (wired) to mild steel rods, each of these types (except for galvanized rods) showed a decrease in their corrosion rate as shown by Table III. This decrease generally occurred at the expense of the mild steel, however, as borne out by Table IV. (The galvanized rods showed an increase in weight loss when coupled to mild steel. This acceleration occurs because zinc, i.e., the galvanizing, is anodic to iron and thus is sacrificial to iron or mild steel. Note that the corrosion rate of the mild steel rods decreased when coupled to galvanized rods.) The copper-clad rods, in particular, produced a dramatic increase--approximately 4-fold--in the corrosion rate of a mild steel rod. The Type 302 stainless rods caused a slight increase (from 7.61% to 11.8% over 7

---

\* Complete details of this testing program are given in Reference 3 which may be obtained from the Department of Commerce's National Technical Information Service, Springfield, VA, 22151. Request Report No. AD 702040.

Table II  
Measured Weight Loss of Single Rods [3]

Material	Weight Loss		
	<u>1-year</u> (%)	<u>3-years</u> (%)	<u>7-years</u> (%)
Mild Steel	2.6	6.11	7.61
Galvanized Steel	1.5	2.4	2.2
Copper-Clad Steel	0.52	0.93	1.4
Ni-Resist Cast Iron	0.68	1.2 <sup>*</sup>	1.9
Type 302 Stainless	0.2	0.53	1.4
Type 304 Stainless-Clad	0.29	0.63	0.87 <sup>**</sup>

<sup>\*</sup> Different manufacturer than 1- and 7-year rods.

<sup>\*\*</sup> 5-year test only.



Table III

Measured Weight Loss of Test Rods Coupled to Mild Steel Rods [3]

Test Rod Material	Weight Loss		
	1-year (%)	3-years (%)	7-years (%)
Galvanized Steel	3.72	6.24	5.66
Copper-Clad Steel (to 1 mild steel rod)	0.38	0.35	0.73
Copper-Clad Steel (to 2 mild steel rods)	0.35	0.32	0.1
Ni-Resist Cast Iron	0.26	0.35	0.29
Type 302 Stainless	0.05	0.01	0.05
Type 304 Stainless-Clad	0.1	0.1	0.58*

\* 5-year test only.

Table IV  
Measured Weight Loss of Coupled Mild Steel Rods [3]

Material of Coupled Rods	Weight Loss		
	<u>1-year</u> (%)	<u>3-years</u> (%)	<u>7-years</u> (%)
Galvanized Steel	1.2	2.85	5.95
Copper-Clad Steel (to 1 mild steel rod)	4.83	14.8	25.9
Copper-Clad Steel <sup>*</sup> (to 2 mild steel rods)	3.84	11.85	17.05
Ni-Resist Cast Iron	2.4	7.46	10.9
Type 302 Stainless	2.5	6.79	11.8
Type 304 Stainless-Clad	2.3	5.56	6.84 <sup>**</sup>
<sup>*</sup> Average of two tests.			
<sup>**</sup> 5-year test only.			

years) in the corrosion rate of the mild steel rods. The Type 304 stainless-clad did not produce any noticeable increase (in fact, a slight decrease was measured) in the corrosion rate of the mild steel rods. Thus, Type 304 stainless is not only highly resistant to corrosion itself; it is electrochemically compatible with mild steels. It is also expected to be similarly more compatible with other buried metals, such as lead cable sheaths, than is copper.

In recognition of the corrosion resistance of stainless steel rods and their compatibility with lead and steel, Bell System Practices [4] require their use in the grounding of central exchange facilities. Also, based on the expected long lifetime and reduced corrosive threat to foundations and reinforcing materials, stainless materials were recommended for use for grounding systems in the Metropolitan Atlanta Rapid Transit Authority (MARTA) system [5].

## 2. Availability, Workability, and Cost

Type 304 stainless-clad rods are available in standard 5/8 in., 3/4 in., and 1 in. diameters from Teledyne/Mefco of Elkart, Indiana. (Other sources may be available but the authors are not aware of them.)

Stainless steel cable is available from a number of manufacturers. Stainless cable is more readily available than rods because of its widespread use as aircraft control cables. It is manufactured in various sizes, i.e., 1/4", 3/8", 1/2", etc. and in various strand combinations e.g., 6 x 19, 7 x 17, etc., to give it flexibility.

Comparative costs (in 1978 dollars) between Type 304 stainless-clad, copper and copper clad materials are listed in Table V. At this time, the costs of stainless clad and copper clad rods are competitive. Stainless cable however, is somewhat more expensive than either copper or copper clad cable.

For installation purposes, ease of handling (workability) is an important consideration. The relative ease with which copper cable can be handled (bent, routed, positioned, etc.,) is well known. Copper-clad steel is stiffer; however, it is frequently used for ground mat conductors.



Table V  
1978 Comparative Dollar Costs

<u>Item</u>	<u>Cost</u>		
	<u>304 Stainless*</u>	<u>Copper</u>	<u>Copper-Clad</u>
<u>Ground Rods†</u>			
5/8" x 10'	\$12.90		\$ 9.56
3/4" x 10'	16.30		15.36
<u>Cable††</u>			
1/4" (.250)	0.568/ft.		
No. 4 (.204)		\$0.229/ft.	
5/16" (.312)	0.792		
No. 2 (.257)		0.363	
0.385			.469/ft.
3/8" (0.375)	1.046		
1/0 (0.325)		0.510	
0.433			0.592
7/16" (0.438)	1.455		
2/0 (0.365)		0.633	
0.486			0.510
1/2" (0.500)	1.798		
4/0 (0.460)		0.981	
0.613			0.819

\*Stainless clad rods; solid stainless cables

†Price each for 10-100 pieces

††Price for 5000-ft. lots

Catalog prices provided courtesy of Arnold Hoge Assoc., Atlanta, GA

Stainless cable is manufactured with several small strands which gives it considerable flexibility. Experience indicates that a stainless cable poses no undue problems in installation.

### 3. Connections or Bonds

Another concern with the possible use of stainless steel materials for ground system construction is the ability to realize low resistance, long life electrical connections between the rods and the mat and with the various risers. Various types of connections are used with copper materials; the most common are bolted or clamped, brazed, gas welded, and exo-thermically welded. Stainless steel, being hard and requiring high high working temperatures, does not lend itself to brazing or gas welding as does copper or copper-clad materials. Bolted or clamped connections, particularly where their locations will be inaccessible as under a building or concrete pad, are not preferred for several reasons. Typically, the clamps are made of brass which forms an electrolytic cell with stainless or with other buried steels in the vicinity. Unless adequately sealed against moisture, the produced cell will result in corrosion of the brass or the stainless steel, depending upon the relative polarity of the stainless steel. The corrosion will produce a deteriorating connection with time.

Under fault conditions such as those likely to be encountered in a substation, the bolted connection requires derating the path by approximately 40% for a copper conductor [6]; it would be about the same for a stainless steel conductor.

Exothermic welding offers an attractive means for making connections between stainless conductors. This process provides: (1) a connection which seals the joint against moisture; (2) is rated the same as the cable in current-carrying capacity; (3) is made with easily portable equipment; and (4) does not require highly skilled personnel for implementation.

The exothermic weld is made by first positioning the two members to be joined in an appropriately configured mold. The different parts of the mold include: (1) the crucible which holds the welding material and

starting material; (2) the disk which holds the material in the crucible; (3) the tap hole leading down to the weld cavity; and (4) the conductors in the weld cavity.

The starting powder, which is ignited from a spark from a flint igniter, will start the reaction in the welding material. The powdered metals unite chemically to produce a super-heated copper compound at about 4,500°F. This compound melts through the disk, flows down the tap hole and over the conductor ends. The conductor ends are melted and then the weld material solidifies, resulting in a complete weld. The time involved for this complete reaction is 10-to-20 seconds, depending upon the size of the joint.

Since the finished joint contains copper, the entire joint must be sealed against moisture. An effective technique is to encapsulate the joint in a bitumastic compound. Sealing in this manner prevents the development of small corrosion cells between the copper and any buried steels or other metals in the area.

#### 4. References

1. American Institute of Physics Handbook, Second Edition (1963).
2. Reference Data For Radio Engineers, Fifth Edition, Howard W. Sams and Co., Inc., New York, NY (1968).
3. R. W. Drisko, et al, "Field Testing of Electrical Grounding Rods," TR-660, Naval Civil Engineering Laboratory, Port Hueneme, CA, February 1970, AD-702 040.
4. Bell System Practices, No. 876-210-100, "Electrical Protection of Radio Stations," November 1973.
5. S. L. Robinette, "Rationale for Grounding and Lightning Protection Recommendations for Metropolitan Atlanta Rapid Transit Authority," Final Report, Contract ENI-1, Georgia Tech Engineering Experiment Station, Atlanta, GA., July 1976.
6. "IEEE Guide for Safety in Substation Grounding," IEEE Std. 80-1976, June 30, 1976.

A CONTINUOUS GROUND-BED MONITOR

BY

Wils L. Cooley\*  
Roger L. King \*\*  
and  
E. K. Stanek\*

\*Department of Electrical Engineering  
West Virginia University  
Morgantown, WV 26506

\*\*U. S. Department of Interior  
Bureau of Mines  
4800 Forbes Ave.  
Pittsburgh, PA 15213

Presented at

Federal Aviation Administration/  
Georgia Institute of Technology

Workshop on Grounding and Lightning Protection



## ABSTRACT

West Virginia University, under U.S. Bureau of Mines sponsorship, has developed an instrument that will continuously monitor the integrity of a ground bed. Design requirements are briefly summarized for the currently developed ground bed monitor. In addition, field problems are reviewed from the performance of a prototype monitor that was used at several different mine sites.

## Introduction

Electrically powered equipment used in and about mines is required to be grounded by federal law. A good ground connection is necessary to prevent the development of dangerous potentials on the exposed surfaces of machines in the event of an electrical insulation failure. Since the equipment is constantly changing location, it is necessary that a fixed contact with earth be made remote from the machine. The machine frame is then connected to this point via grounding conductors within the cable supplying power to the machine. This paper describes an instrument that will continuously monitor the integrity of this fixed contact with earth -- the ground bed.

The work reported herein, was done at West Virginia University under sponsorship of Bureau of Mines Grant G0144138, as part of the Bureau's program of improving safety in mines.

## Low Resistance Requirement

Under normal operating conditions, and even under most fault conditions, the only currents flowing through the ground bed are small magnitude a.c. and d.c. stray currents. However, a ground bed must maintain a constant low-resistance to earth at all times to provide personnel safety. This is important because the ground bed will conduct current during conditions such as those illustrated in Figures 1 and 2. This current flow through the ground bed will elevate the frames of all equipment connected to the bed to a voltage determined by the IR voltage drop across the bed. Since the magnitude of the current cannot be controlled, the only way to maintain the frame voltage at an acceptable level is to maintain a low resistance ground bed.

## Measurement Technique

Periodic checks of ground bed resistance are absolutely necessary for electrical safety in the mine. Since bed resistance can change significantly in a short time due to weather conditions, corrosion, or unknown causes (Figures 3 and 4), continuous monitoring of bed resistance is desirable. Continuous monitoring also avoids the time involved and the possibility of error in making what is often a difficult measurement.

The fall-of-potential method (Figure 5) is used for the measurement of ground bed resistance. It is a method that is widely accepted and is accurate enough for most practical purposes. A known current,  $I$ , is passed between the auxiliary current electrode and the ground bed. The potential difference,  $V$ , is then measured between the auxiliary potential electrode and the ground bed. Then the ratio  $V/I$  will give a resistance which, with proper electrode spacings, results in the required resistance of the ground bed.

If a series of measurements is made with the auxiliary potential electrode at various distances from the ground bed, a curve as shown in Figure 6 can be plotted in which the ratio  $V/I$  is plotted against the position of the potential electrode. If the starting point was from the center of an equivalent hemisphere for the ground bed (Figure 7) the true earth resistance can be read at a potential electrode distance of 61.8 percent of the distance to the auxiliary current electrode.

This result is widely used in practice since it eliminates plotting an earth resistance curve. There are some difficulties associated with the application of the 61.8 percent rule, however, but they will not be covered at this time and the reader is referred to references 1, 2, and 3 for more information.

#### Ground Bed Monitor Device Requirements

In the design of a device to continuously monitor ground bed resistance, several criteria must be met:

1. The device must be able to continuously monitor the resistance of the ground bed, even during system operation. This means it must be unaffected by stray currents or induced voltages which may be present.
2. It should be unaffected by other connections to earth. Otherwise these connections could cause apparent variations in ground bed resistance.
3. The circuitry must be protected from transients on the mine power system and ground fault currents.
4. It must be able to operate for a reasonable range of supply voltage variations and other conditions which can be expected on a mine power system.
5. It should be easy to install; otherwise, all or a large portion of a mine would be down for a considerable time while the device is being installed.

#### Basic Monitor Design

The ground bed monitor drives an 11 Hz test current between the ground bed and the current electrode. A current transformer (Figure 8) measures the amount of test current flowing into the ground bed to avoid erroneous readings caused by equipment sitting on earth and other remote ground connections. The voltage electrode is driven into the ground at a distance from the bed which corresponds to 61.8 percent of the distance to the current electrode. The current and the voltage measured are then synchronously rectified and filtered to eliminate any spurious 60 Hz signals, fed to a divider network, and the final



output, (ground bed resistance) is recorded on a chart recorder.

Figure 9 shows the interior of the device. The boards shown contain a regulated d.c. power supply, 11 Hz oscillator, synchronous rectifiers and filters, and a divider network. The large output transformer is rated 250 watts. Although the ground bed monitor output is only 40 watts, the larger output capacity is required due to the 11 Hz output signal. The input voltage for the device is 110 volts a.c. However, the power supply has been carefully designed to operate properly over a wide range of line voltage fluctuations.

#### Field Tests

The ground bed monitor was first installed on December 22-23, 1975, at a mine in southwestern Pennsylvania. The ground bed that the device was to monitor had been constructed a few years earlier by driving ground rods along the banks of a small stream near the substation. It was about a 100 feet long by 15 feet wide, and was comprised of twenty-two rods and some buried copper trolley wire. Although the rods were 8 feet long, they were only driven to a depth of 5 feet because of a subsurface layer of solid rock. The last measurement taken on the bed indicated a resistance of 9 ohms.

The monitor was installed in the relaying cabinet of the substation and a series of preliminary measurements (soil resistivity and fall-of-potential) were taken. The auxiliary potential and current electrodes were driven and connected to the monitor. However, initially problems with the chart recorder and saturation of the output stages of the current source forced removal of the monitor.

Approximately 2½ months later the monitor was reinstalled for a two-month test. The monitor operated satisfactorily from March 12 to May 13, 1976, and portions of the recorded data are shown in Figures 10 and 11.

Since that test the monitor has been installed on two other ground beds to test circuit changes and to increase our confidence in its reliability. Three monitors have now been fabricated and this summer our plans call for testing all the units for an extended period.

The most significant fact of the field tests so far has been the locating of two broken conductors in a ground bed on different dates. The first was located during initial setup by the research team and the second was recorded by the monitor. This experience would suggest a real need for continuous monitoring.

#### Conclusions

A device to continuously monitor the integrity of a ground bed has been fabricated, tested, and proved viable. By using such devices

to continuously monitor the ground bed's resistance to earth the safety of mining personnel can be greatly improved.

#### Reference

1. Cooley, Wils L. Evaluation of In-Mine Grounding System and Codification of Ground Bed Construction and Measurement Techniques. USBM Grant G0144138 Annual Report. West Virginia University, August 1, 1975.
2. Cooley, Wils L. Mine Grounding Systems, Evaluation of Ground Beds, and Ground Bed Monitors and Evaluation of Modular Ground Wire Monitor. USBM Grant G0144138 Annual Report. West Virginia University, May 6, 1977.
3. King, R. L., H. W. Hill, Jr., R. R. Bafana, W. L. Cooley. Guide for the Construction of Driven-Rod Ground Beds. USBM Information Circular 8767, 1978.

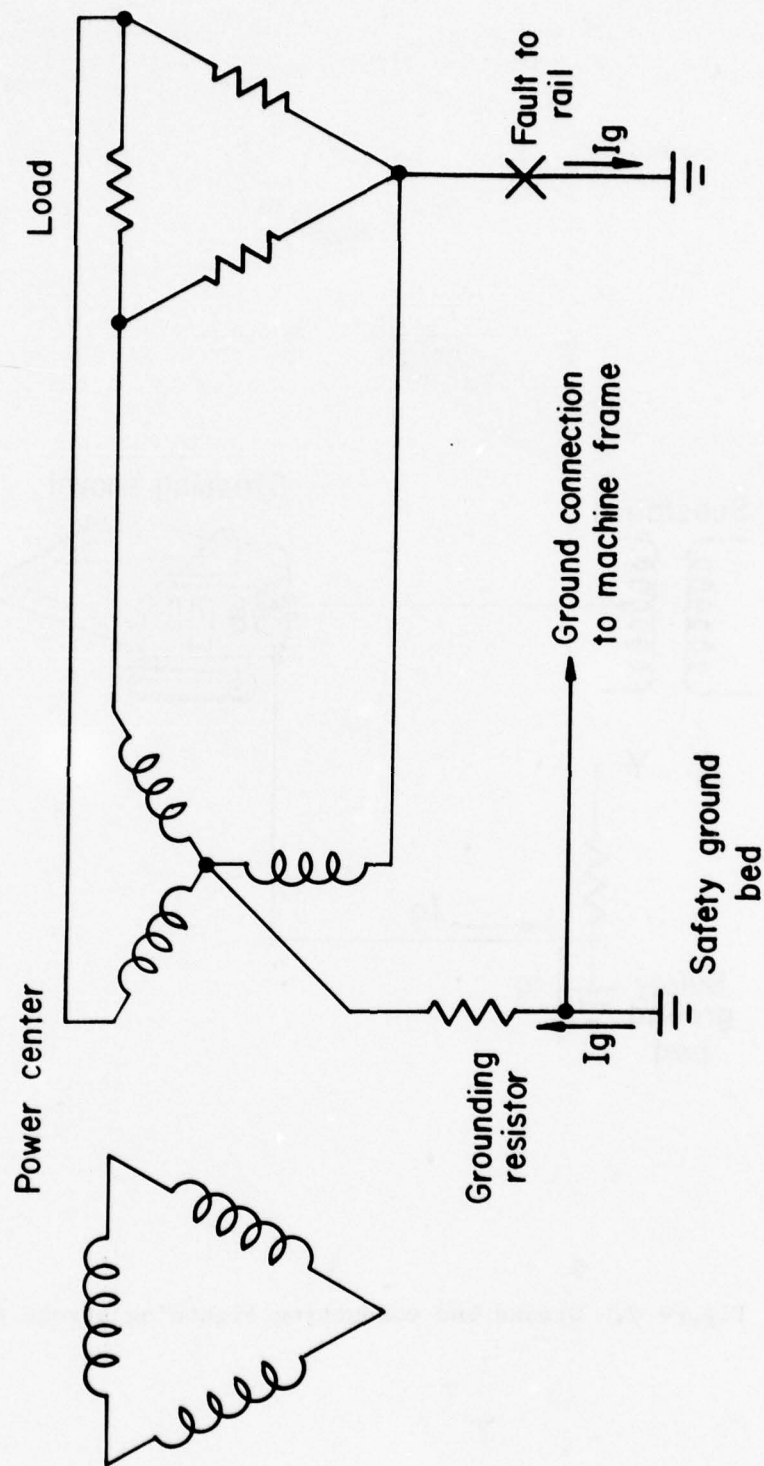


Figure 1. Ground bed conducting fault current during a phase-to-rail fault.

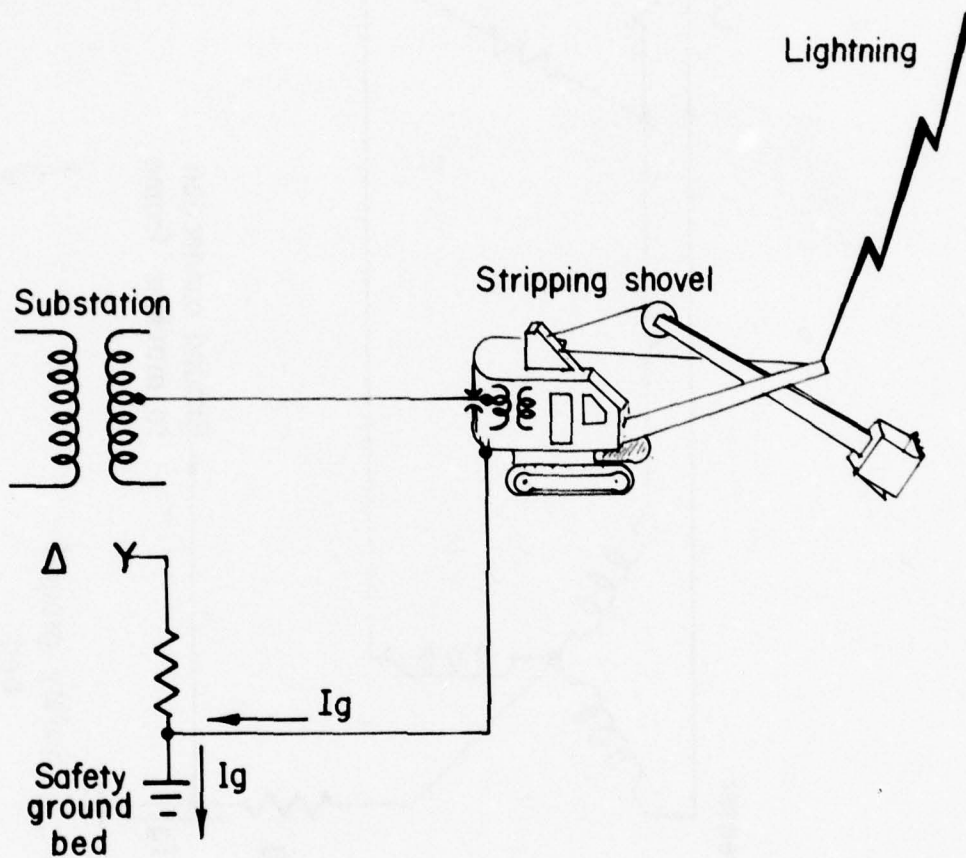


Figure 2. Ground bed conducting lightning stroke to earth.





Figure 3. Example of a safety ground rod destroyed by corrosion.



Figure 4. Example of a broken ground conductor in the safety ground bed.

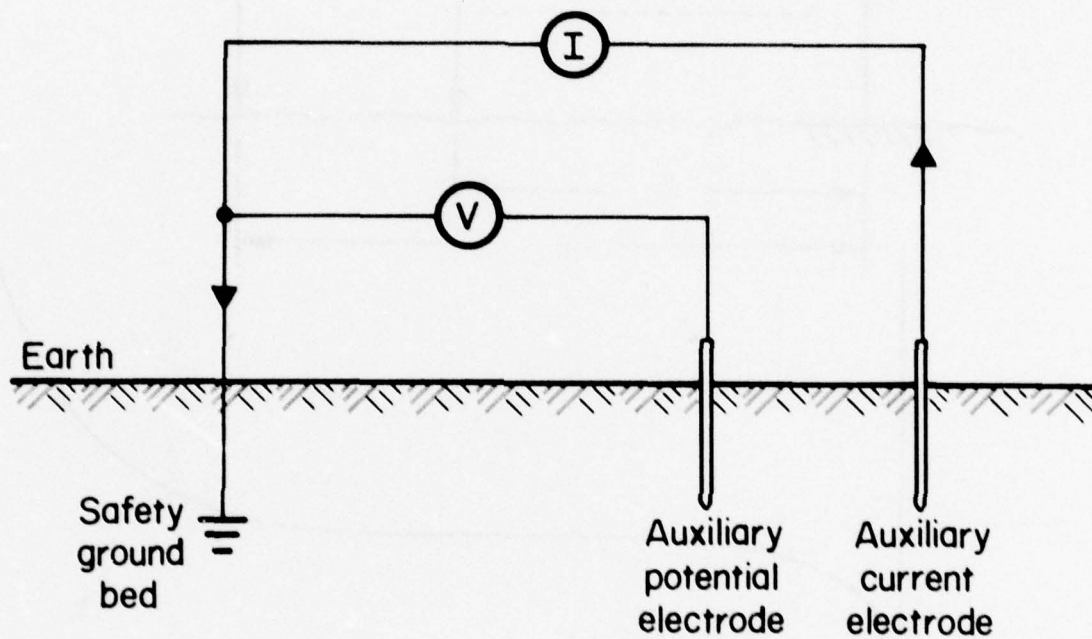


Figure 5. Electrode placement for fall-of-potential measurement.

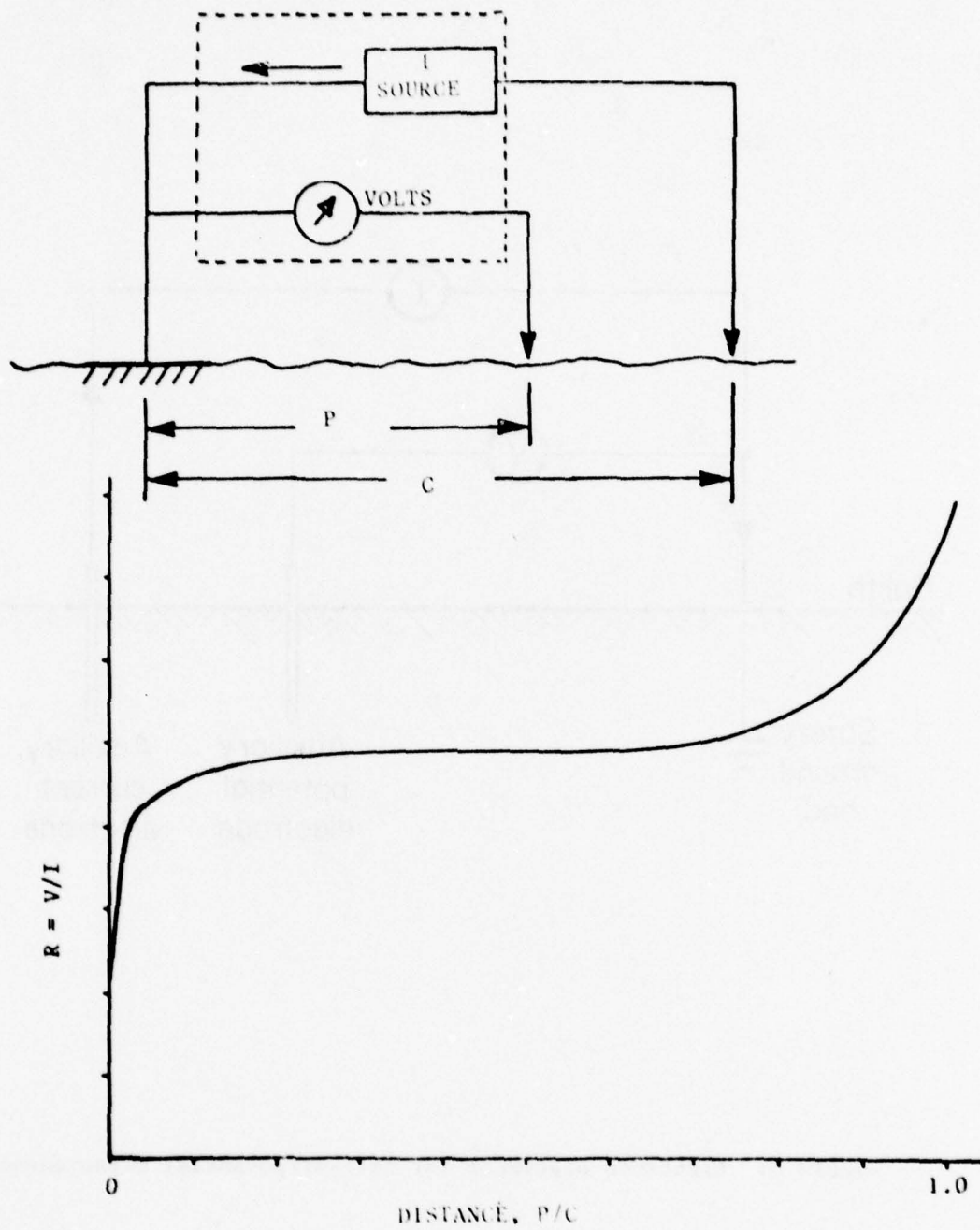


Figure 6. Fall-of-potential determination of ground bed resistance.



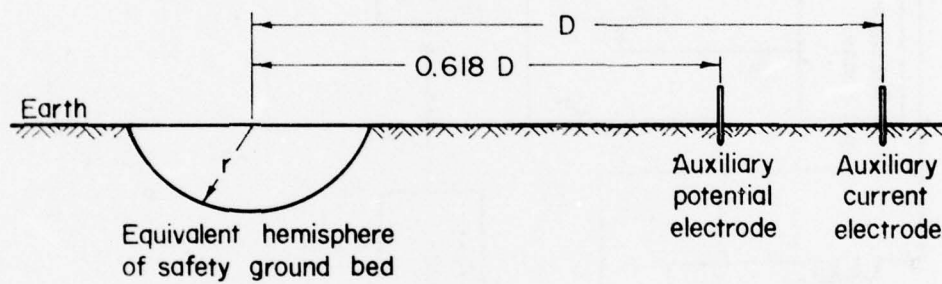


Figure 7. Measurement of ground bed resistance using fall-of-potential technique.

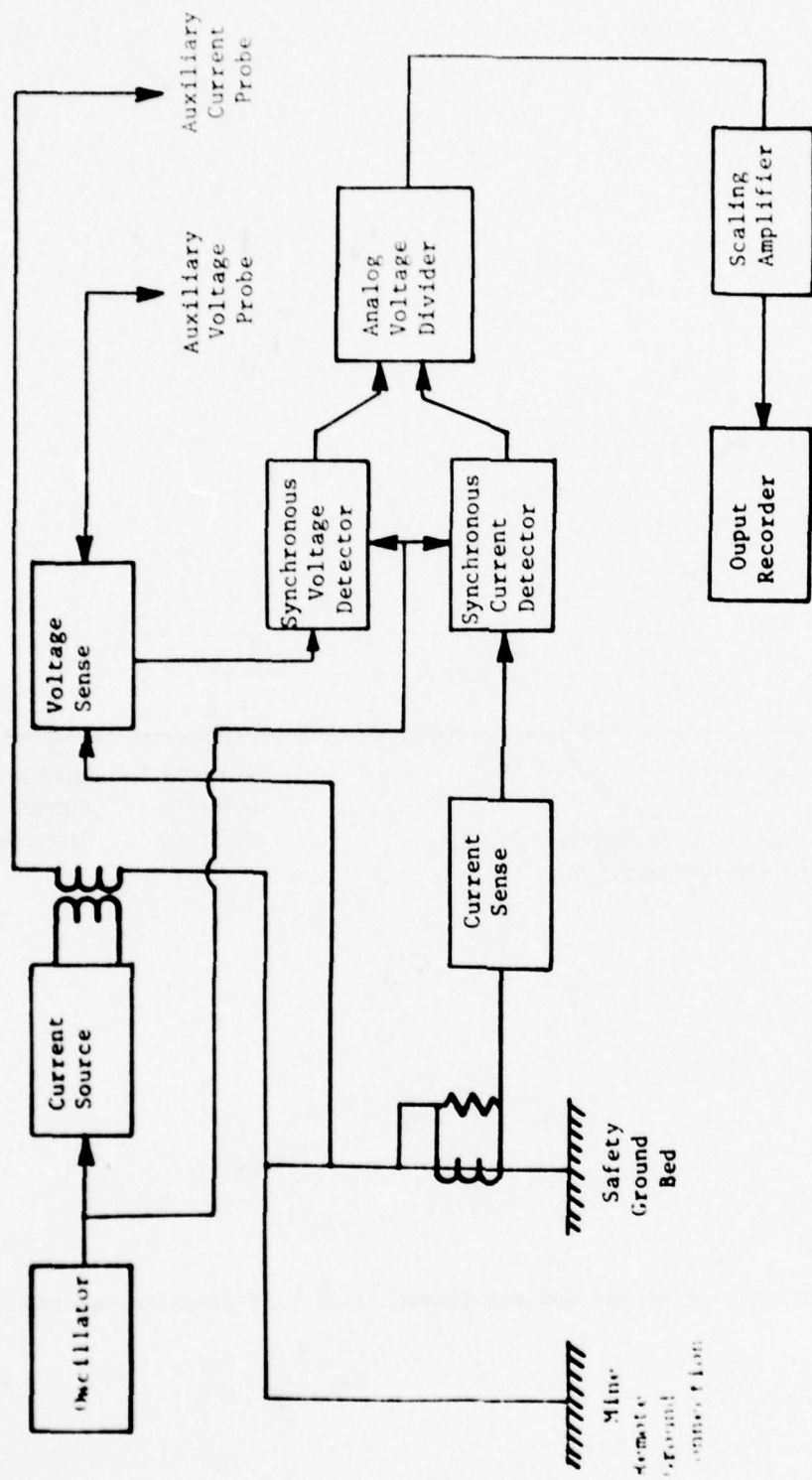


Figure 8. Block diagram of ground bed resistance monitor.

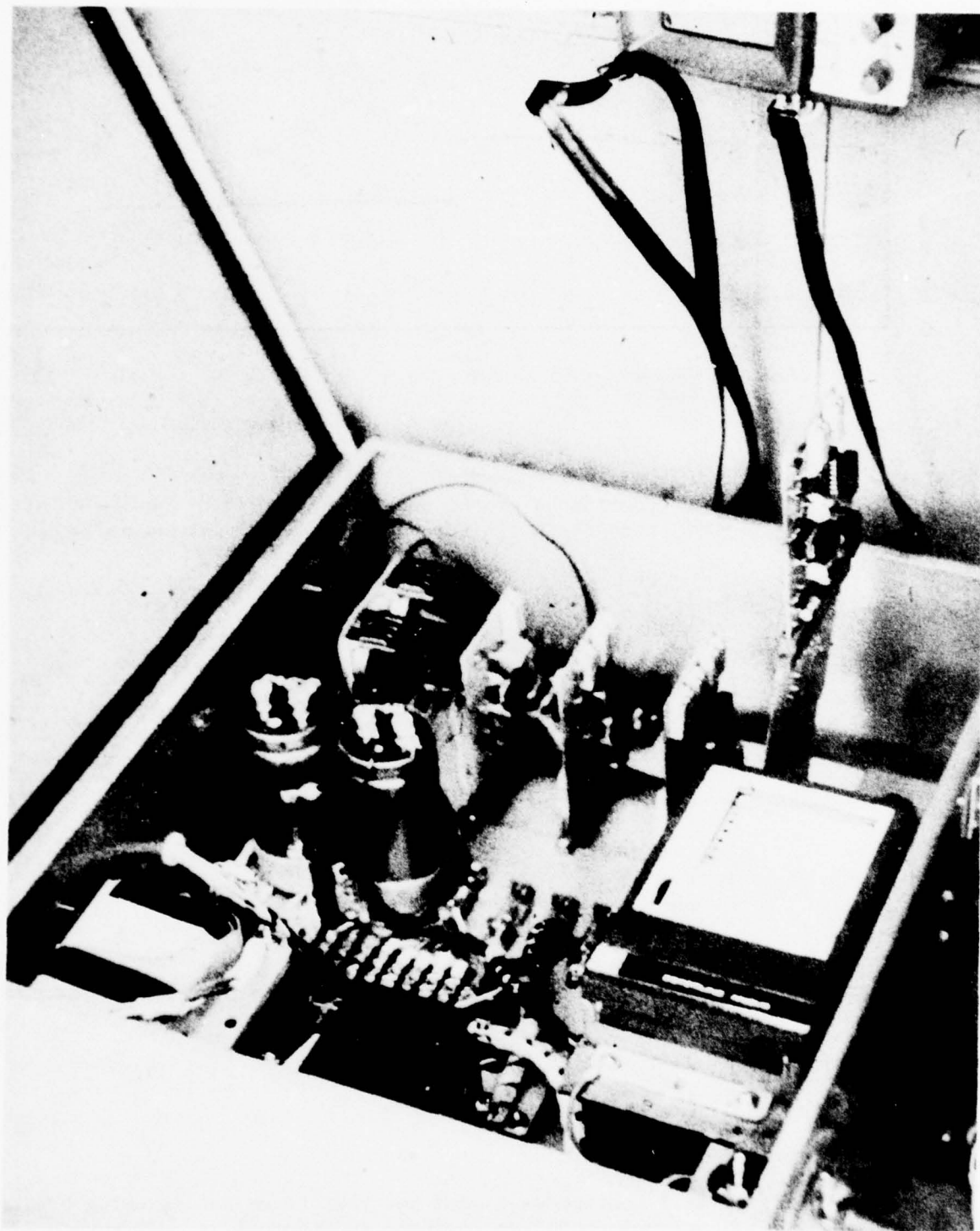


Figure 9. Interior view of ground bed monitor.

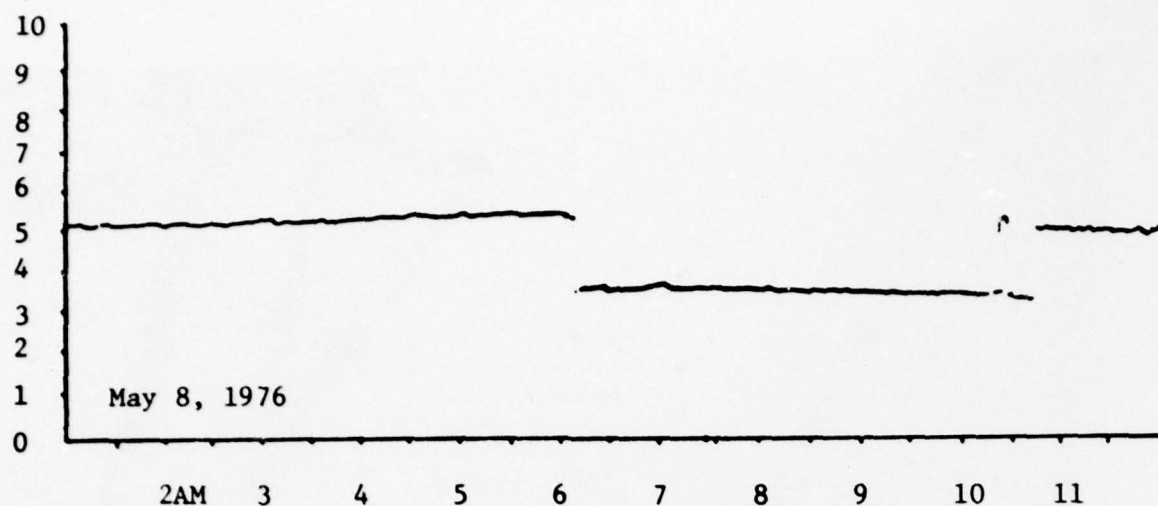


Figure 10. Continuous ground bed resistance data showing abrupt changes in resistance of a failing ground bed.

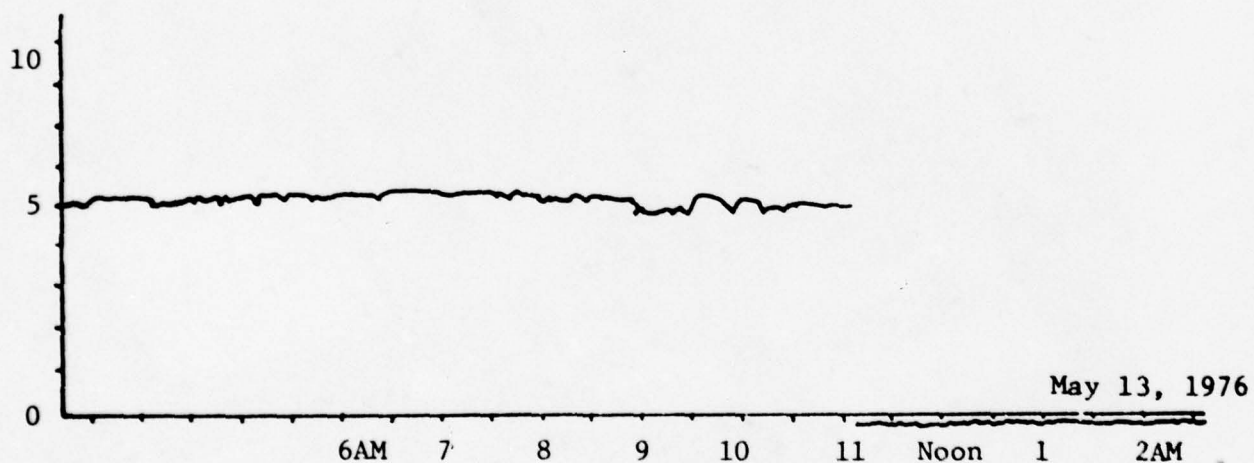


Figure 11. Continuous ground bed resistance data showing breakage of conductor pictured in Figure 4.



FREQUENCY DIVISION MULTIPLEX  
BASEBAND CABLE PLANT  
IMPROVEMENTS

BY  
Frank LaDieu

Transmission Systems Branch  
1842 Electronics Engineering Group (AFCS)

Presented At  
Federal Aviation Administration/  
Georgia Institute of Technology  
Workshop on Grounding and Lightning Protection

## ABSTRACT

Radio frequency interference, crosstalk and ground loop noise in baseband cable plants interfacing frequency division multiplex and wideband radios is depriving the Defense Communications System of hundreds of communications channels and degrading the performance of thousands of others. This paper discusses the fundamental characteristics of these baseband cable plants, details their deficiencies and describes a new technology for their testing, evaluation and correction.

## 1.0 INTRODUCTION

1.1 General. Radio frequency interference (RFI), crosstalk and ground loop noise in baseband cable plants interfacing frequency division multiplex (FDM) and wideband communications radios is depriving the Defense Communications System (DCS) of hundreds of communications channels while degrading the performance of thousands of others. This report discusses the fundamental characteristics of FDM baseband cable plants currently in use, details their deficiencies and describes the technology for their correction.

## 1.2 References.

1.2.1 AFCS/EPZ Report dated 5 September 1975, Subject: Scope Communications Baseband Cable Plants-Engineering, Installation and Testing.

1.2.2 AFCS-1839 E-I GP-EMC-75-59 Report dated 1 December 1975, Subject: Interference Investigation to AN/UCC-4 Multiplex Equipment at Selected Scope Comm Sites.

1.2.3 AFCS-1839 E-I GP-EMC-77-52 Report dated 15 August 1977, Subject: Radio Frequency Interference Measurements of the New Wideband Cable Plant at RAF Croughton and RAF Uxbridge. United Kingdom.

## 1.3 BACKGROUND

1.3.1 Baseband cable technology is believed by the author to be a new area of engineering investigation. In past times, installing connectors on a pair of cables and using the cables to interface multiplex equipment and radios seemed to be a straightforward enough task. What could go wrong with the cables if the connectors were on right? Nothing much was the standard answer. The radios and the multiplex and, yes, those poor station grounds were the bad fellows. Not to forget RSLs which were often low enough to justify any noise problems. Then something went wrong. Suddenly high performance radios along with high performance multiplex were being installed in Europe under the Task 21 Scope Comm Program by contractor personnel. The basic systems engineering was good; RSLs were excellent. Yet, the system performance was unacceptable in terms of RFI, crosstalk, and idle channel noise. The contractor correctly identified the problem as poor isolation in the baseband cable plants, but incorrectly laid the fault to GFE-balanced baseband composite video cables. AFCS/EPZ was tasked to investigate and correct these cable plants. The findings are cited in Ref 1.2.1 which is included in Appendix A of this report. From this start grew a new technology consisting of theory, evaluation techniques, and test methods. New test equipment and recent applications engineering has resulted in major improvements in the testing and evaluation of baseband cable plants with increased accuracy and greatly reduced test time. These tools have been applied to the investigations described in this report. Indeed, without these new equipments and test procedures, the data for this report would have required years to assemble because of the combinations of tests required and the time needed to plot isolation curves by hand.

## 2.0 EVALUATION TECHNIQUES

**2.1 Old Methods.** Methods used by AFCS personnel during early investigations of baseband cable plants are described in detail in Appendix A. In brief, a +10 dBm signal was inserted into the radio end of the receive cable and the power induced into the transmit cable was measured at the radio end. Both cables were terminated in the combining panel by 75 ohm loads. A frequency selective voltmeter such as the Sierra 128A read the power directly in dBm to which was added 10 dB to obtain the absolute isolation between receive and transmit cables for a 3kHz slot. This data was plotted versus frequency on a graph to obtain a display of cable plant isolation throughout the baseband. Although crude and time consuming, this method provided a tool with which to assess isolation and thereby predict the performance of the cable plant in an operational configuration. First, the alternate cable plant would be inspected for installation defects and tested to determine their presence or absence. When the alternate cable plant was found to have an isolation of 85 dB or higher across the baseband, the cable plant was judged adequate. Traffic was switched to the alternate cables after baseline data consisting of idle channel noise, crosstalk, and test tone level was taken on the primary cable plant. Immediately on cutover to the alternate cables, baseline data would be taken to insure that link performance was not degraded and evaluate noise and crosstalk improvements. Isolation tests would then be made on the primary cables and problems cleared. When the required isolation was obtained, traffic would be cut back to the primary cables and new baseline data taken. To appreciate the full scope of effort involved in this method, consider a 300 channel system from Hillingdon, U.K. to Martlesham Heath and consider three measurements per channel at both locations each time a cable was removed and returned to traffic. Using this method, it required from 3 days to a week at each location to correct a baseband cable plant. Often this effort was disrupted and data made invalid by necessary maintenance actions and equipment malfunctions occurring at sites between the facilities under test. However, despite the drawbacks to this method, it resulted in excellent system performance at a time when no other techniques were available.

**2.2 New Methods.** The next major breakthrough in baseband cable plant analysis came in the fall of 1975 when Mr. Wilhelm Stoeckle, electronic technician, and Mr. Fritz Liebrich, electrical engineer, both members of European Comm Area's 1945 Comm Group, were directed to investigate baseband cable plants at various USAF sites in Germany. Mr. Stoeckle's prior experience in cable plant troubleshooting gained with the AFCS Scope Comm Office coupled with Mr. Liebrich's expertise in applications of the HP 141T frequency spectrum analyzer resulted in a new evaluation capability. Using baseband amplifiers (available in various configurations depending on the radios used) for amplification and decoupling, the residual signals in the transmit(XMIT) baseband cable could be displayed and graphed automatically by an X-Y recorder. The information obtained clearly showed the presence of any RFI, crosstalk, and ground loop noise existing in the baseband cable plant exclusive of traffic which was



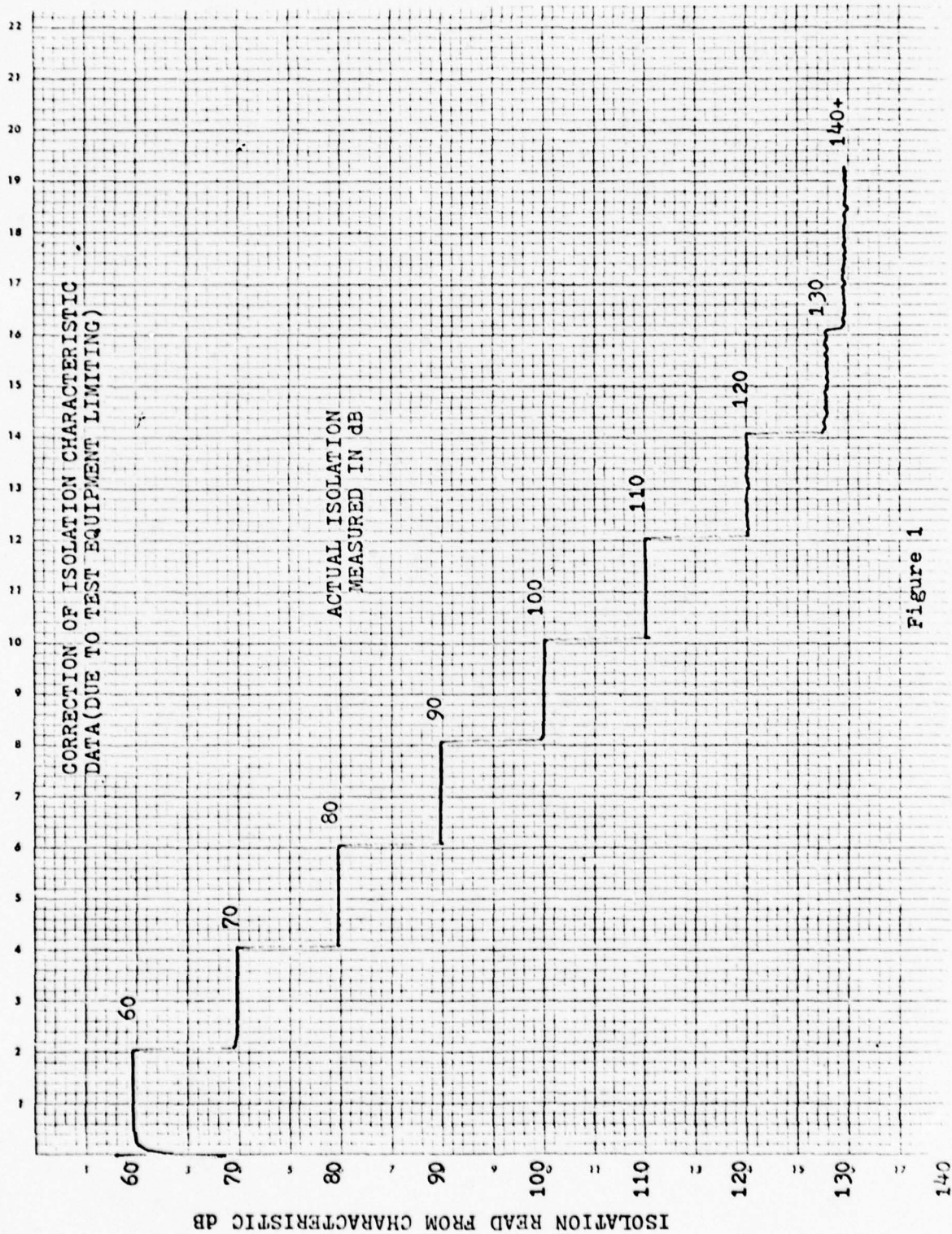


Figure 1

removed by pulling the supergroup looping plugs at the combining panel. A ten second sweep with a bandwidth of 3 kHz provided a distinct, unique, signature of the baseband cable plant's noise contribution. The approach here was to run an initial frequency signature of the transmit spectrum as installed and look for excessive RFI or noise across the baseband. If there appeared to be excessive noise present, inspection of the cable plant was made to insure that all grounds were intact and connectors properly installed. When the plant was deemed technically correct, a new signature was run to verify that the noise had been cleared or satisfactorily reduced. The use of this technique was demonstrated to the author in July 1977 at RAF Croughton, U.K. by Messrs. Liebrich and Stoeckle during investigation of Task 44 England baseband cable installation problems at that location. The power of this new technique was readily apparent as was its shortcoming. While it was possible to rapidly test, correct, and retest cable plants, there was no companion method to display cable plant isolation, a key performance indicator. Only through characterization of the baseband cable plant's isolation under varying conditions and lengths could a basic understanding of their performance be developed and a baseline for their evaluation established. In short, it remained for baseband cable evaluation to be converted from an art based on empirical experience to an applied engineering science.

2.2.2 Working from previous developments, what could well be the final technique in baseband cable evaluation was implemented at the Richards-Gebaur AFB Prototype Test Facility (PTF) in September 1977. This was the addition of a HP 8443A Tracking Generator to the HP 141T Spectrum Analyzer. Applying a signal to the receive (REC) baseband cable from the tracking generator, the power induced into the transmit cable is measured and displayed on the 141T and plotted by an X-Y recorder. This provides a continuous isolation plot throughout the baseband spectrum which can be compared with the baseband frequency signature. The effect of isolation changes on baseband cable performance in terms of RFI and noise is readily apparent. Using isolation and frequency plotting, it is possible to completely characterize the performance of a baseband cable plant and establish performance standards.

2.3 DATA PRODUCTS. Data products resulting from the new baseband cable test methods take three forms: the frequency signature, the isolation characteristic and the composite frequency signature and isolation characteristic.

2.3.1 The Frequency Signature (See Fig 200.1). The frequency signature is displayed on graph paper 8 x 10 inches. Frequency is read horizontally from 100 kHz to 2,000 kHz (Supergroups 1 thru 8); signal amplitude is read vertically in -dBm $\emptyset$ . To convert the value read in dBm $\emptyset$  to dBm, add -45 dBm (XMIT TLP). Levels displayed are measured with a 3 kHz slot filter and 10 second sweep rate.

2.3.2 The Isolation Characteristic (See Fig 200.2). The isolation characteristic utilizes the same format as the frequency signature except for vertical levels which are read as absolute values of isolation in dB. Subtraction of 10 dB from the value read provides the level of the signal induced in the XMIT cable when treated as NEGATIVE dBm. Values of isolation read correctly to 120 dB however, limiting in the test set up results in nonlinearity for larger values. For example: a value of 127 dB read from the graph is actually 130 dB; 130 dB as read from the graph is 140 dB. A test calibration graph is shown in Fig 1.

2.3.3 Composite Display. Where amplitude and shape of the frequency signature and isolation characteristic permit dual presentation without confusion, a composite display of the signature and characteristic is shown on one graph. This simplifies their comparison and analysis. The sole change in format is that the upper portion of the graph is given in dBm $\emptyset$  while the lower portion is in dB.

#### 2.4 TEST CONDITIONS.

2.4.1 TRIAX and COAX baseband cable plants in Fig 2 are shown in the NORMAL configuration. These configurations were found to provide maximum RFI, crosstalk, and ground loop noise reduction during previous field tests and were, therefore, adopted for use at many Air Force wideband facilities in West Germany and the United Kingdom.

2.4.1.1 NORMAL grounding for a TRIAX cable plant begins with a BNC connector at the radio end. The center conductor of the TRIAX is soldered inside of the BNC center pin and the inner and outer TRIAX shields are gathered together and clamped together within the BNC connector. At the multiplex combining panel the TRIAX center conductor terminates in a WECO jack and is connected to the multiplex HYBRID input or output transformer by a looping plug. The inner shield of both the alternate and primary cable share a mutual, isolated ground with the HYBRID. The outer shields of the primary and alternate TRIAX cables are connected to station (equipment) ground within the combining panel cabinet. The alternate cable center conductor terminates on a WECO jack and may be placed in service by removing the looping plug from the primary-HYBRID jacks and inserting it in the HYBRID-alternate jacks. Cabling is installed the same for both XMIT and REC cables. Special note should be taken that the HYBRID and TRIAX inner shields are NOT connected to cabinet ground in the NORMAL TRIAX configuration.

2.4.1.2 NORMAL grounding for a COAX cable plant differs from that of a TRIAX plant because only one braid (shield) is available. The single braid must serve as both a shield and a signal return path. Double braid COAX presents the same problem. At the radio end, the COAX cable terminates in a BNC connector. At the multiplex combining panel, the COAX center conductor terminates on a WECO jack. The looping plug provides connection of the cable center conductor to the HYBRID. The shields of the primary and alternate cables are connected to the common, isolated,



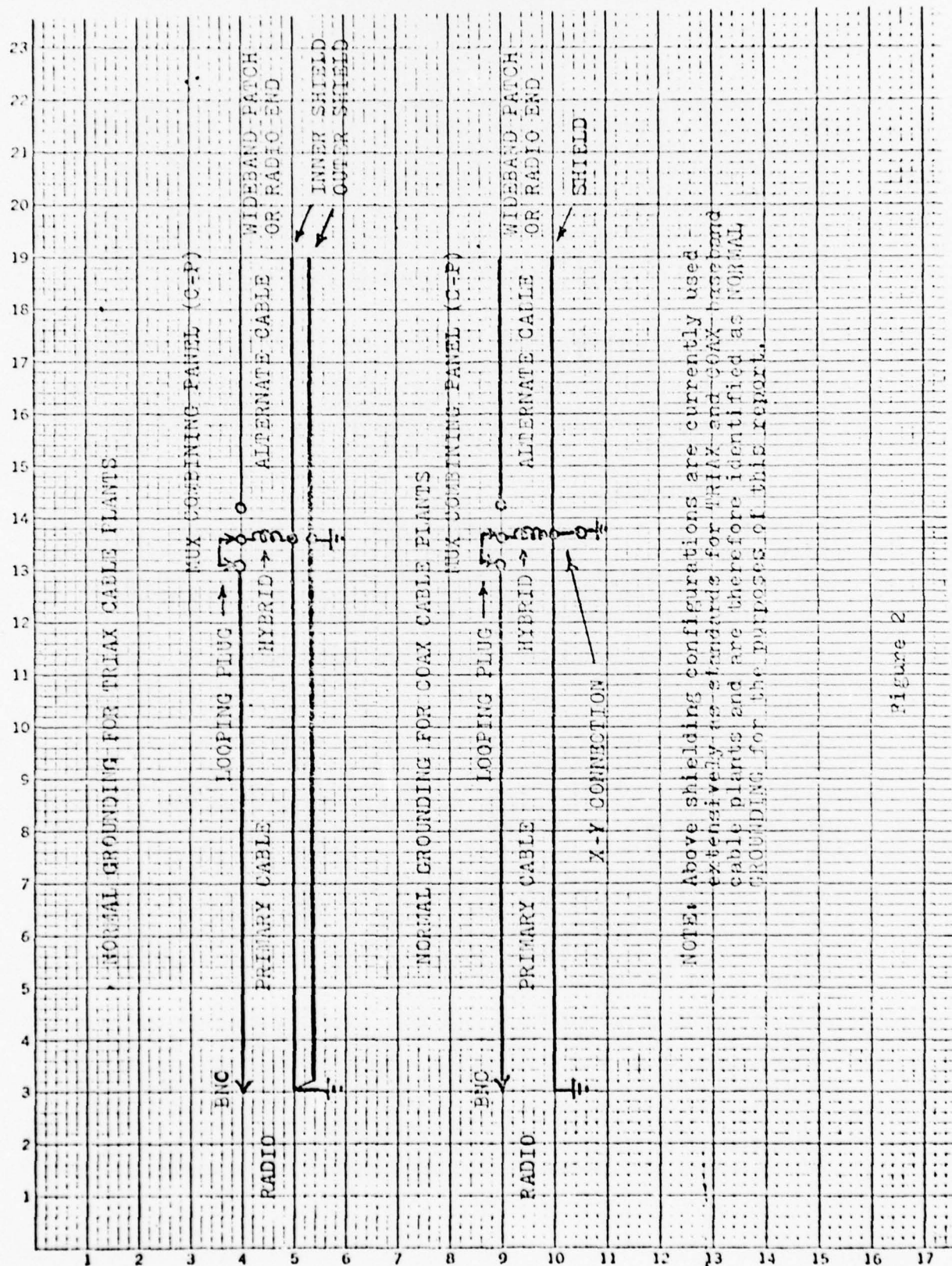


Figure 2



HYBRID ground which is strapped to cabinet ground. This strapping is called X-Y strapping. The use of X-Y strapping with COAX is required to reduce RFI.

2.4.1.3 During recent tests, many variations from NORMAL grounding have been made to explore their effect on TRIAX and COAX cable plants. The results of these tests are discussed later in this report.

## 2.5 TEST EQUIPMENT AND PROCEDURES.

2.5.1 A block diagram of the standard test set up used to obtain frequency signatures and isolation characteristics is provided in Fig 3. The test equipment used consists of:

- a. H.P. 7035B X-Y Recorder
- b. H.P. 8443A Tracking Generator
- c. H.P. 141T Mainframe equipped with: H.P. 8553B R.F. Section and H.P. 8552B I.F. Section.

In addition, use is made of the LC-8 radio adder and insertion amplifier to expand the range of the H.P. 141T. The new DCA standard radio series has a baseband amplifier which can be utilized for the same application. The value of using the as-installed radio components vice external amplifiers is that all basic components of the baseband cable plant are tested as a system. Excess noise in the amplifier modules can be checked for by terminating their inputs with 75 ohm terminations and sweeping the amplifier output.

2.5.2 XMIT and REC baseband cables were spaced close together for all tests reported herein unless otherwise indicated on the signature and characteristic. Primary cable lengths of 200 ft or greater were laid out in rectangular loop configuration on the test building roof. Care was required to insure that cables were dry unless damp test conditions were required. Primary and alternate cable lengths of 100 ft or less were dressed about the interior of the test facility.

2.5.3 To obtain an isolation characteristic, test equipment and baseband cables are connected as shown in Fig 3. The tracking generator is set to sweep from 100 kHz to 2,000 kHz with 1 kHz resolution. The output is set for +10 dBm into the REC cable at the radio end. The radio end of the XMIT cable is connected to the 141T input. The R.F. section of the 141T is set for a 3 kHz bandwidth and a 0.2 MHz SCAN WIDTH PER DIVISION. The I.F. section is set up for: SCAN TIME 10 sec., LOG REF LEVEL -50, SINGLE SCAN, VIDEO FILTER OFF. The X-Y recorder "Y" input is connected to the 141T vertical output; the "X" input is connected to the 141T SCAN OUT terminal. To obtain a frequency signature, use the same test set up with the exception that the XMIT cable terminates on the adder module input, the output of the adder module is applied

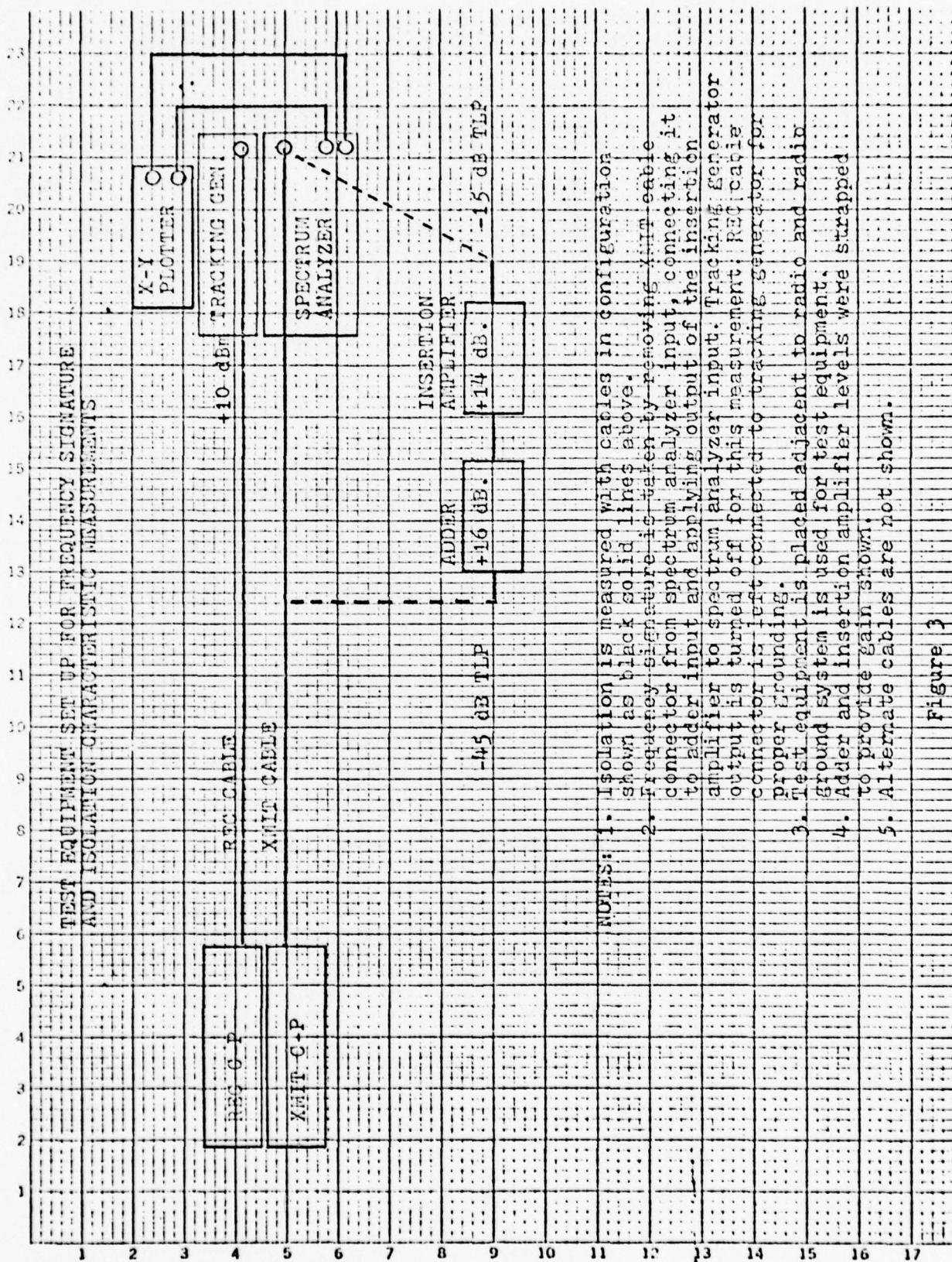


Figure 3

to the input of the insertion amplifier and the output of the insertion amplifier is connected to the 141T input. The output of the tracking generator is set to maximum attenuation (120 dB) and the REC cable left in place on the generator's input connection.

## 2.6 SIGNATURE AND CHARACTERISTIC ANALYSIS.

2.6.1 A frequency signature for a 75 ft primary cable (with 50 ft alt cable) is shown in Fig 75.1. The -35 dBm $\emptyset$  reference level corresponds to a -50 dBm level measured at a -15 dB TLP (Note: dBm = dBm $\emptyset$  + TLP). Looking at the signature, six distinct RFI blips are shown located at 610, 710, 810, 980, 1190, and 1380 kHz. Three of these are significant: 810 kHz at -68.5 dBm $\emptyset$ , 980 kHz at -59 dBm $\emptyset$ , and 1380 kHz at -69 dBm $\emptyset$ . The 980 kHz signal level does not meet the -60 dBm $\emptyset$  single tone interference specification cited in MIL-STD-188C. The noise floor of the cable plant is -77 dBm $\emptyset$  or better. No ground loop noise is seen in this signature.

2.6.2 An isolation characteristic of the same 75 ft primary cable is also shown in Fig 75.1. The 110 dB reference level shown corresponds to a -100 dBm signal induced into the XMIT cable by the +10 dBm signal level in the REC cable. The isolation shown at 1250 kHz is read on the characteristic as 130 dB. This corresponds to an absolute isolation of 140 dB (see para 2.3.2) which is the upper limit for this test method. Isolations greater than 180 dB are found to exist at certain frequencies in TRIAX cable plants and can be calculated at specific frequencies through signature and characteristic RFI comparison for known lower values of isolation. For baseband cable plant evaluation, an upper limit of 140 dB suffices. In Fig 75.1 the characteristic isolation antinode is clearly displayed centered around 980 kHz. This antinode is a breakdown in isolation between the XMIT and REC cable plants. In this case, the minimum isolation is seen to be 117 dB which is more than enough to prevent cable crosstalk.

## 3.0 APPLICATION.

3.1 Baseband Cable Plant Noise Evaluation. The tools for baseband cable plant noise evaluation are the frequency signature and the isolation characteristic. They are quickly obtained once the test equipment has been set up and calibrated. Less than three minutes of down time is required.



3.1.1 The reason for making a frequency signature is that this datum provides a documented, visual display of the noise existing in the baseband cable plant under test. The noise seen in the signature will be transmitted to the distant station and is the noise floor for this particular cable plant configuration. Under operational conditions, this noise floor will combine with multiplex, radio, and waveguide noise contributions and be added to the baseband traffic. RFI and ground loop noise is displayed in terms of level and frequency. That portion of the baseband spectrum used for link traffic can be closely examined for the baseband cable plant's contribution to noise at the distant end. Should excessive RFI levels or ground loop noise be found in the signature, corrective action must be taken on the baseband cable plant as only baseband cable plant noise contributions are shown in the signature.

3.1.2 The isolation characteristic provides the value of absolute isolation between the XMIT and REC portions of the baseband cable plant throughout the desired frequency spectrum. This information is vital to an accurate assessment of a plant's performance. Usually a multiplex is found to be operating under partially loaded conditions and, therefore, crosstalk may not be seen in the signature yet become a problem under full loading. Examination of the isolation characteristic will show what the absolute isolation is between cable plants over the frequency range utilized by the link traffic. For a single link, a minimum of 85 dB is required to prevent crosstalk from the REC to the XMIT portion of the cable plant. This level of isolation will not be sufficient if the facility is located in an area of high RFI sources. Here again, correction of the cable plant may be required to optimize its isolation over portions of the baseband where RFI disturbs mission traffic. The isolation characteristic will reveal the location of isolation antinodes and provide firm data on which corrective actions can be based.

\* Isolation requirements are discussed in para 2.4 of reference 1.2.1.

3.2 Baseband Cable Plant Comparison. Comparative evaluations of baseband cable plants in the past have required excessive amounts of time to accomplish. During such testing, variations in system loading and maintenance actions have frequently invalidated much of the data acquired. To obtain accurate data, constant involvement of highly experienced personnel was required to spot inconsistent test results. The frequency signature and isolation characteristic provide two powerful new tools for cable plant analysis and make possible evaluations in minimum time using less experienced personnel. TRIAX, COAX, TWINAX (balanced), and Fiber Optic plants for FDM-radio interfaces can be checked for relative and absolute performance in the laboratory or in operational facilities. Minimal test time is required; reliable data is recorded.



3.3 Facility Baseline Data for Baseband Cable Plants. Taking the signature and characteristic of a baseband cable plant is a logical step in the location and correction of wideband system noise problems. Testing for radio and multiplex equipment is standardized on a component basis. The radio must meet specifications when tested alone; the multiplex must meet specifications when tested alone. When these two equipments are connected together by the baseband cable plant (and thereby become a subsystem) their combined performance is often disappointing. Neither the performance of the radio or the multiplex has changed. The change has resulted from the noise contributions of the baseband cable plant. Because of this, the baseband cable plant must be treated as a distinct subsystem component. It must be made to meet specifications that will complement the radio and multiplex performance; it must be characterized in terms of its signature and characteristic; and it must be tested again at periodic intervals to insure that variations from this baseline data do not go unaccounted for. A stabilized baseband cable plant (a plant unaffected by physical or environmental changes) will have a signature and characteristic that remain constant with time. Defective connectors, changes to the cable plant's grounding configuration and new sources of RFI will be easily detected by comparison of new signatures and characteristics with the original baseline data. Characterization of the baseband cable plant for baseline data will make possible a systematic technique for troubleshooting subsystem noise problems.

4.0 BASEBAND CABLE PLANT DATA ANALYSIS. The tests performed during the preparation of this report use the NORMAL (Ref para 2.4.1) grounding configuration as a baseline for comparison. Changes to the NORMAL configuration (removal of shield grounds, etc.) are followed with new signatures and characteristics to show the effects on the cable plant tested. The same procedure is used for both TRIAX and COAX baseband interfaces.

4.1 TRIAX Cable Plant Tests. Appendix B contains sets of data for TRIAX baseband cable lengths of: 25, 50, 75, 100, 200, 300, 400, and 500 feet. Study of this data provides information vital to the design and installation of low noise baseband cable plants.

4.1.1 Isolation Antinodes. (See Figs 25.1, 50.1, 75.1, 100.1, 200.1 and 200.2, 300.1 and 300.2, 400.1 and 400.2, and 500.1) The isolation antinode is a breakdown in cable plant isolation caused by resonance of the inner and outer TRIAX cable shields. Antinodes exist within the baseband frequency spectrum of each cable plant tested. The frequency

at which they occur is a function of the combined length of the primary and alternate cables. For cable plants less than 100 feet, only the fundamental antinodes affect the cable isolation. Third and fifth harmonic of the fundamental antinode are above the baseband frequency spectrum. For cable lengths of 100 feet or longer, a second and then third antinode appear with increasing length. Cable plants of 200 feet or longer (with 50 foot alternate cables) suffer isolation degradation of 24 to 35 dB over portions of the baseband spectrum while cable plants of 100 feet or shorter are seen to lose 13 dB or less. The worst case degradation due to antinodes is shown in Fig 300.2 where the second antinode (third harmonic) reduces the cable pair isolation to 94.5 dB. While this value of isolation is adequate to prevent cable crosstalk, it falls far short of the isolation needed to effectively combat radio frequency interference.

4.1.1.1 Radio Frequency Interference and Antinodes. It is no accident that RFI and the antinodes are seen to affect the same portions of the frequency spectrum. Looking at the signature of Fig 25.1, a broadcast station is seen at 1380 KHz at a level of -49 dBm $\emptyset$  and the antinode isolation is 121 dB. The measured field intensity of the broadcast station is 73 dBuV/m. At 610 KHz, a station is seen at a level of -74 dBm $\emptyset$ . The measured field intensity of this second station is 84 dBuV/m. The RFI seen in the frequency signature is limited by the isolation of the transmit cable. The single cable isolation is roughly (within 6 dB) equal to one half of the pair isolation or, at 1380 KHz, 60.5 dB. By comparing levels and field intensities, the single cable isolation of the baseband cables at 610 KHz can be estimated at 96.5 dB based on actual performance. Or, the pair isolation at 610 KHz is approximately 193 dB. It can be seen by this example that a radical difference in cable plant isolation takes place in that portion of the baseband spectrum affected by the isolation antinodes. Removal of isolation antinodes from the baseband spectrum is needed to reduce or eliminate RFI in the baseband cable plant. When this is not possible because of excessive cable lengths, isolation antinode shifting techniques may be utilized to move the antinode to a portion of the baseband where it does not affect mission traffic.

4.1.1.2 Shifting Isolation Antinodes. There are a variety of techniques that can be employed to shift the antinodes.

4.1.1.2.1 Alternate Cable Removal. Fig 25.8 shows the effects of removal of the 50 foot alternate cables from the multiplex combining panels. Based on the data provided in para 4.1.1.1, the per cable isolation at 1380 KHz has increased to 87.5 dB. The actual paired isolation is in the vicinity of 175 dB. The fundamental antinode has been shifted to the 5 megacycle region leaving behind a smooth isolation characteristic. All RFI has been reduced to -73 dBm $\emptyset$  or lower. Antinode shifting has produced an ideal baseband interface with a noise contribution well

below the multiplex idle channel noise specified for any 3 kHz slot throughout the baseband. A similar improvement in the performance of a 50 foot baseband cable plant is shown in Fig 50.8 where again the alternate 50 foot baseband cables have been removed from the combining panel. The RFI spike located at 1380 kHz in Fig 50.1 is reduced by 5 dB resulting in a single tone interference level of -66 dBmØ from one broadcast station while all other RFI levels are reduced to -73 dBmØ or less. Figs 75.1, 75.8, 75.9, 100.1 and 100.14 show the improvement obtained by alternate cable removal from 75 and 100 feet cable plants.

4.1.1.2.2 Coaxial Shorting. A second shifting technique that is easily employed where needed is coaxial shorting of the alternate baseband cable. This is accomplished by shorting the inner and outer shield braids of each of the alternate cables together at the wideband patch (or radio end) of the cables. The symmetry of the braids should be maintained and clamped together or soldered. A BNC connector can be used for this purpose provided its shell is not grounded. Grounding of the alternate cable shields will result in a severe loss of cable plant isolation and cause increased levels of RFI to appear in the transmit cable. Application of coaxial shorts to the alternate cables will cause the frequency at which the isolation antinode appears in the baseband spectrum to double. Also, the 2nd and 3rd antinodes appear at the 2nd and 3rd harmonics of the first antinode. Looking at figure 100.1 and 100.16 the antinode is seen to shift from 840 kHz to 1710 kHz as read from the graphs. While this technique can be very effective, it must be used only in conjunction with testing that provides frequency signatures and isolation characteristics to insure that no ground loop noise has developed in the traffic carrying portion of the baseband spectrum. Shorting of the inner and outer shields together provides a low frequency - direct current X-Y connection at the combining panel. This will permit ground loop currents to flow on the inner shield of the TRIAX cable between radio and multiplex grounds. Should a significant difference in ground potential exist, the noise generated can be quickly identified in the signature and an alternative method of shifting used to obtain the desired improvement.

4.1.2 Variations from NORMAL Grounding. Variations from NORMAL grounding in TRIAX cable plants should be considered as plant defects unless they result from utilization of the techniques described above for antinode shifting. Tests performed on TRIAX cable plants have shown that variation from the NORMAL configuration results in loss of cable plant isolation and generally significantly higher levels of RFI and noise. The effects of variations on a 25 foot cable plant are shown in Figs 25.2 thru 25.17.



#### 4.1.2.1 Removal of Cable Shields from Ground at Combining Panel (C-P).

The most common cause of RFI and ground loop noise encountered in TRIAX cable plants is failure of the installer to ground the outer shields of the REC and XMIT cables (primary and alternate) to the equipment grounds within the combining panels. The results are clearly shown as follows:

4.1.2.1.1 Isolation Losses. Fig 25.2 shows the isolation losses between the XMIT and REC cable plants for: XMIT shield ungrounded in C-P; REC shield ungrounded in C-P; and XMIT and REC (simultaneously) ungrounded in C-P. In each case, major losses in isolation are seen when compared with the NORMAL (shields grounded in C-P) configuration.

4.1.2.1.2 RFI Increase. Figs 25.3, 25.4, and 25.5 show the frequency signatures for the three conditions described above. While loss of the shield ground from the REC cable has had slight effect on the signature (when compared with the NORMAL signature) in the existing RFI environment, the loss in isolation will permit entrance of RFI into the REC cable in the presence of exceptionally strong broadcast stations.

#### 4.1.2.2 Special Shielding and Grounding Techniques.

4.1.2.2.1 Fig 25.13 shows the application of a special shielding technique suggested for baseband cables. On the receive cable, the outer TRIAX shield is ungrounded at the radio and grounded at the C-P; the transmit cable outer shield is ungrounded at the C-P and grounded at the radio. Fig 25.14 shows the reverse of this technique. This shielding technique was tested for a number of cable lengths with similar results. The data shows that this technique cannot be used for FDM-radio interfaces currently used in the DCS. Its applicability to other situations was not investigated.

4.1.2.2.2 Fig 200.37 shows another method of shielding and grounding the TRIAX cable plant. The 200 foot transmit and receive cables have had their outer shield cut into five segments each of which is grounded at one end. The results were disastrous in terms of isolation loss and increased RFI. Again, no comments can be made as to the usefulness of this technique in other applications; however, it is evident that it cannot be used for FDM baseband interfaces.

4.1.2.2.3 An often suggested method for reduction of RFI on TRIAX cable plants is to ground the outer shield frequently or every one tenth wavelength. This was tried for both 200 foot and 500 foot baseband cable plants. Figs 200.16 thru 200.20 show the effect of adding 1, 3, and then 5 additional grounds to the outer shields of a 200 foot cable plant



which was otherwise NORMAL configured. Figs 500.20 thru 500.47 are a similar series showing the effects of grounding the outer shields of the XMIT and REC cables of a 500 foot plant at various points and in various combinations. What is seen from this data is that numerous grounds (much more frequent than every one tenth wavelength) are required to achieve a significant reduction in RFI and that random application of grounds may increase the incidence and level of RFI in the cable plant. It is clearly evident that attaching any grounds to the outer cable shield beyond those used for the NORMAL installation should be avoided at operational facilities unless trained test personnel and test equipment are present to determine their effect upon the cable plant. Generally, multiple grounding of the cable plants outer shields is impractical due to the physical placement of the cables within conduits, cable troughs, and within buildings. Where the length of the grounding wires is equal to the length of the cable shield from connecting point to a normal ground point, little is accomplished by adding an extra ground. A final consideration here is that performance equal to or better than that obtained through multiple grounding is more easily obtained through the antinode shifting techniques discussed previously (see Figs 200.27 and 500.61).

4.2.1 COAX Cable Plant Isolation. Fig 25.19 shows the isolation characteristic for a 25 foot NORMAL connected COAX baseband cable plant. The pair isolation is seen to be less than 130 dB and the single cable isolation approximately 65 dB. RFI spikes are seen to breakthrough the isolation throughout the full baseband spectrum (within broadcast band). Figs 50.16, 75.17, and 100.23 verify even worse isolation performance for longer length cable plants. Looking at Fig 75.18, the COAX cable plant isolation deteriorates rapidly because the X-Y connections have been removed at the combining panels. Although this would not be NORMAL configuration for a COAX cable plant, it can occur as an installation error and go undetected if only supergroup one is utilized. In Europe, RFI spikes would be seen in the frequency range of 60 kHz and upward as this portion of the spectrum is used for broadcast purposes. Tables I and II have been extracted from reference 1.2.3 to show the RFI environment at RAF Croughton and RAF Uxbridge, England. Study of these tables show strong sources of RFI distributed throughout the full baseband spectrum (60 to 2540 kHz) at those locations.

4.2.2 RFI in COAX Cable Plants. Again looking at Figs 25.19, 50.16, 75.17, and 100.23, high levels of RFI are seen throughout the broadcast band portion of the signatures. Comparison of these COAX cable plant signatures with equivalent NORMAL TRIAX installations illustrates the exceptionally high performance of the TRIAX cable plants. Fig 25.19 shows 7 hits (RFI spikes  $-60$  dBm $\emptyset$  or higher) on the 25 foot COAX plant; Fig 25.1 shows 1 hit on the NORMAL TRIAX plant; and Fig 25.8 shows no hits taking place on the antinode shifted NORMAL TRIAX plant and all

spikes reduced to -74 dBm $\emptyset$  or less. Fig 100.23 shows 4 hits on a 100 foot COAX plant; Fig 100.1 shows no hits on a NORMAL TRIAX plant and all spikes -61 or lower; Fig 100.14 shows no hits on one form of shifted antinode NORMAL TRIAX plant (maximum spike -65 dBm $\emptyset$ ); and no hits on a second form of shifted antinode NORMAL TRIAX plant (maximum spike -71 dBm $\emptyset$ ).

4.2.3 Double Shielded COAX. Fig 31.1 provides a signature and characteristic for a 31 foot NORMAL configured double shielded COAX cable plant. Its RFI performance is better than either the 25 or 50 foot COAX plants as only one hit is seen. While the pair isolation is less than that of the 25 foot plant, the isolation of the XMIT cable is several dB better than the REC cable isolation. The overall performance of the double shielded COAX plant does not measure up to that of the 25 foot NORMAL TRIAX plant except in the vicinity of the TRIAX plant antinode. With a shift of the antinode, as in Fig 25.8, the TRIAX plant is found to be significantly better in RFI rejection than the double shielded COAX plant.

5.0 BASEBAND CABLES AND SYSTEM NOISE. Modern FDM-radio systems such as those installed in Europe under the Scope Communications Program and the Augsburg Upgrade Program have provided the DCS with links capable of excellent and highly stable noise performance when NORMAL TRIAX baseband interfaces are utilized. Large variations in idle channel noise due to crosstalk from increased system loading are eliminated by the high isolation characteristics of the TRIAX cable plants. Fully quieted receivers result from high RSLs; the multiplex equipment is designed for low noise and long term stability. The outcome of this is that those facilities that have TRIAX cable plants installed in the NORMAL configuration are reporting exceptional idle channel noise performance through their Link Performance Assessment (LPA) data submissions. Thirty day averages for two of these links are shown in Table III. While these links demonstrate what is possible, they are in no way typical of a large percentage of DCS links. Noise in baseband cable plants is the primary limiting factor for many of these. Every FDM baseband cable plant appearance throughout the DCS provides a potential entry point for RFI. Every facility with a broadcast station in its vicinity has 10 kHz of its baseband spectrum subject to noise introduction. This noise is usually observed at the distant site rather than at the facility where it is introduced. Because of the broad coverage of most AM radio stations, efforts to identify the point of entrance of RFI into the system are frustrated.

With the new techniques for baseband cable plant evaluation described in this report, it is possible to systematically isolate and identify the entrance points

of RFI into the DCS. Then, the cable plant, if TRIAX, can be NORMAL configured and antinode corrected, if required. COAX cable plants can be replaced with TRIAX where the output/input hybrids of the multiplex can be isolated from ground. In short, effective means are now available to minimize the effects of or completely eliminate RFI from the DCS and greatly reduce the idle channel noise distributed throughout its systems.

TABLE IV

FIELD INTENSITY OF BROADCAST STATIONS  
MEASURED IN THE VICINITY OF THE PROTOTYPE  
TEST FACILITY AT RICHARDS-GEBAUR AFB MO.

Frequency (kHz)	Field Intensity (dBuV/m.)
610	84.5
710	85
810	83
970	82
1190	71
1380	73
1510	66.5
1590	60

\* dBuV/m. is read as decibels above one microvolt per meter.

NOTE: The above information has been extracted from AFCS 1839 E-I Group Report - FMEA-77-16 Radio Frequency Survey of the AM Radio Band at the Test Facility, Bldg 1700, Richards-Gebaur AFB MO.



TABLE III

THIRTY DAY LINK IDLE CHANNEL NOISE DATA FOR  
COMPARISON OF NOISE PERFORMANCE ON SELECTED  
LINKS BEFORE AND AFTER TRIAX CABLE PLANTS  
WERE INSTALLED IN THE NORMAL CONFIGURATION

## LANGERKOPF TO MUHL (GERMANY)

BEFORE		(dBm0) (3 kHz Flat)	AFTER (NORMAL)	
FEB 1974	JUL 1974		FEB 1977	JUL 1977
64	66		69	70
61	65		69	69
64	65		68	69
66	64		68	70
65	65		68	69
66	66		68	70
66	66		69	70
64	67		69	69
67	65		69	68
68	67		69	68
68	64		68	69
67	65		69	70
68	65		70	70
68	65		70	69
67	66		65	69
64	67		70	69
63	67		69	69
61	68		69	70
68	68		69	70
68	67		69	70
68	67		69	69
64	69		69	69
66	67		68	69
63	68		69	69
67	68		69	70
68	69		69	69
67	68		69	69
67	69		69	70
67	69		68	70
68	66		68	69
65.8	66.6	(30 day average)	68.7	69.3

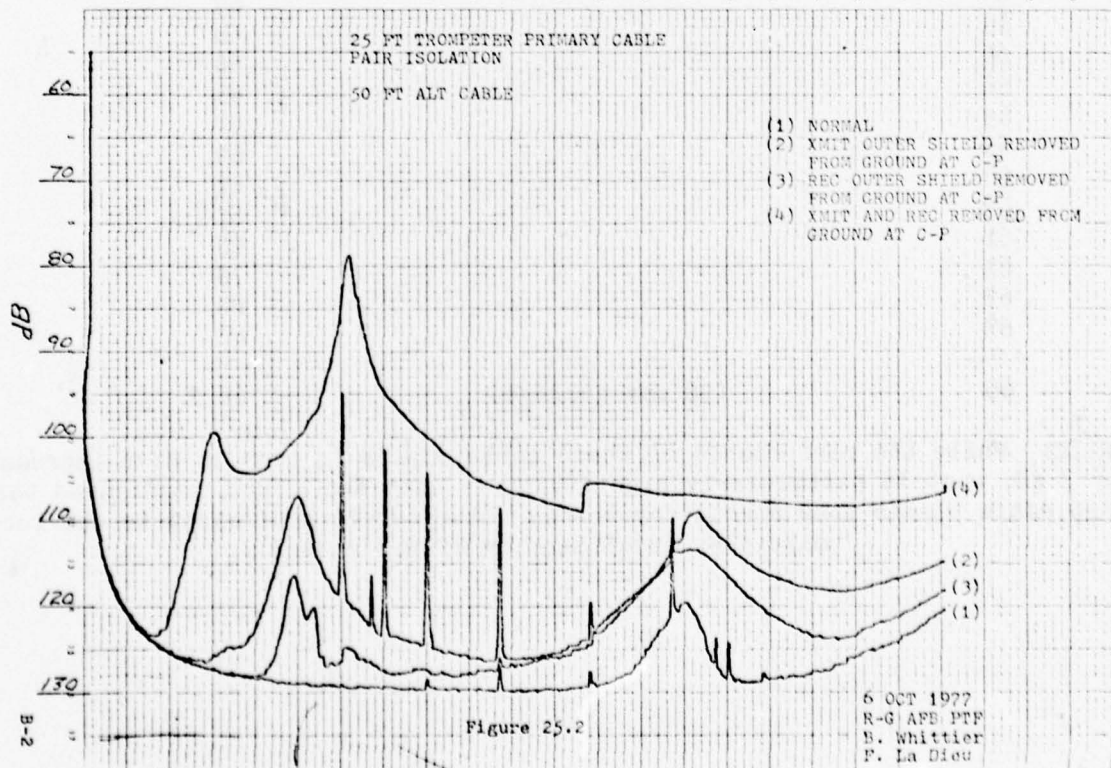
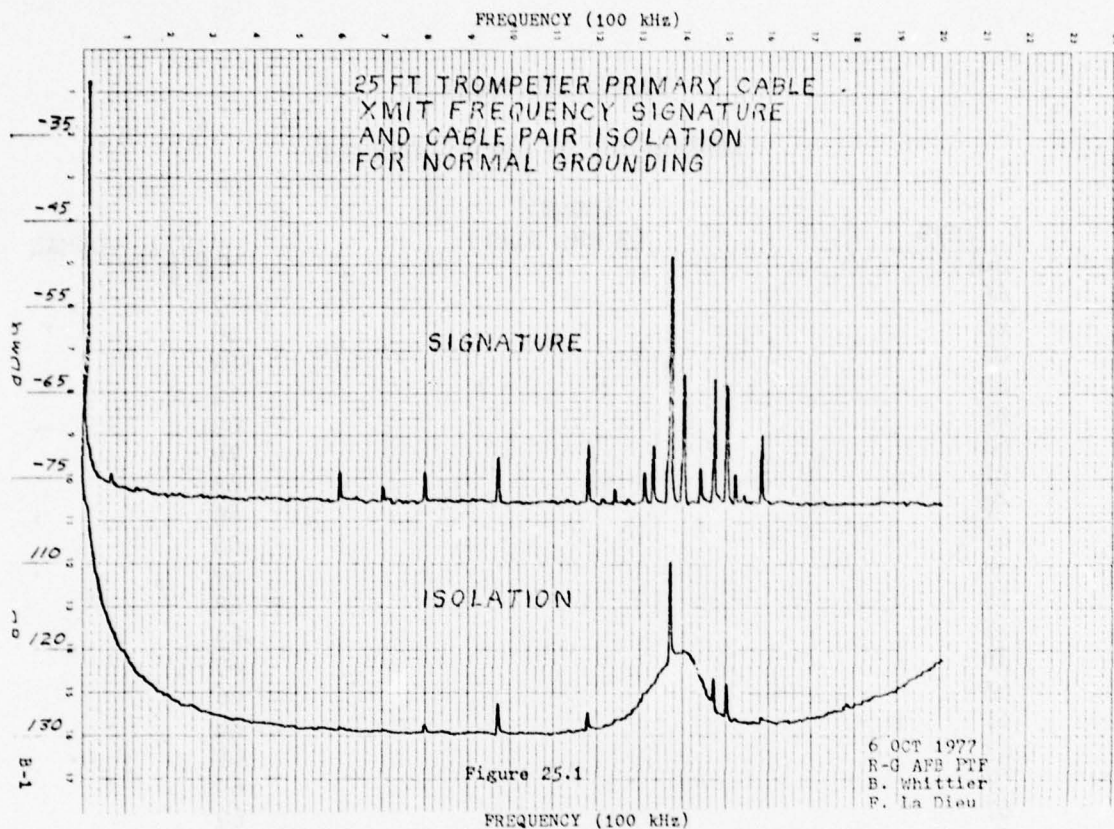


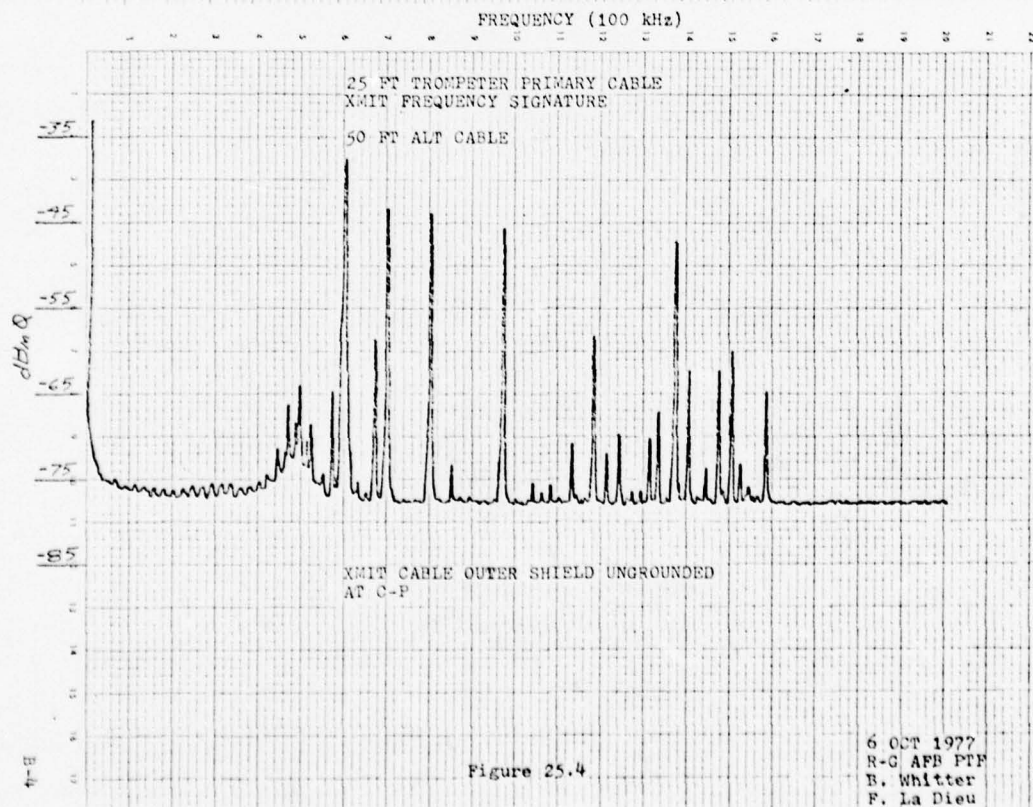
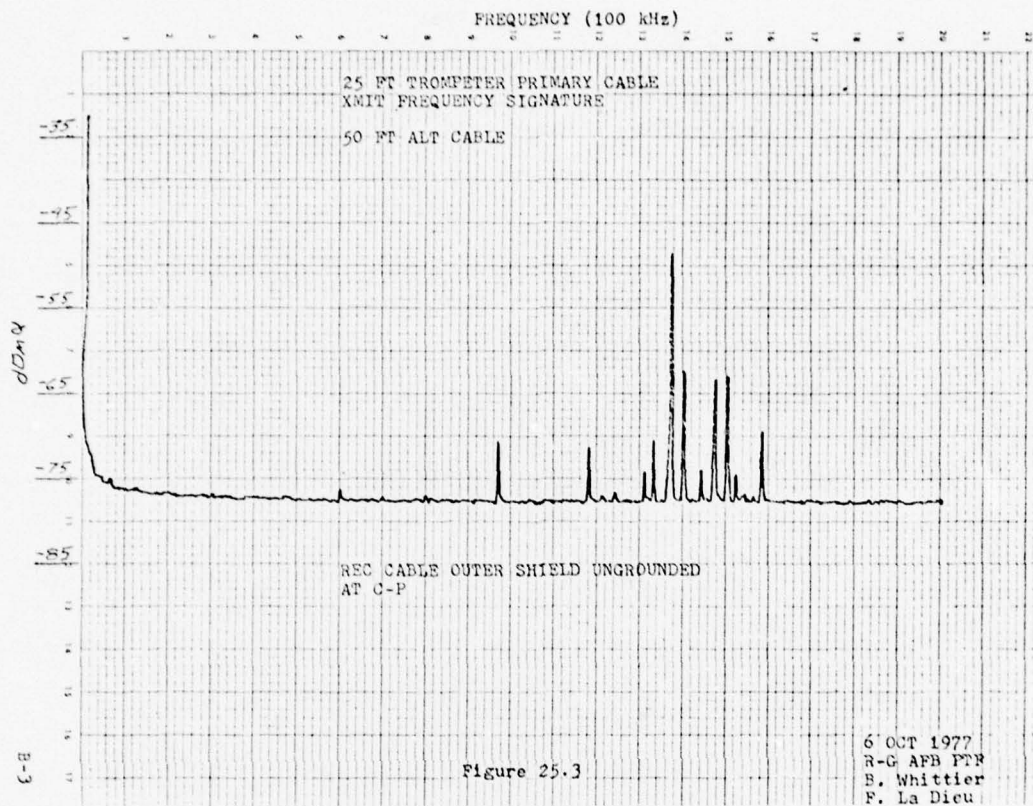
TABLE III (Page 2)

## LANGERKOPF TO RANN (GERMANY)

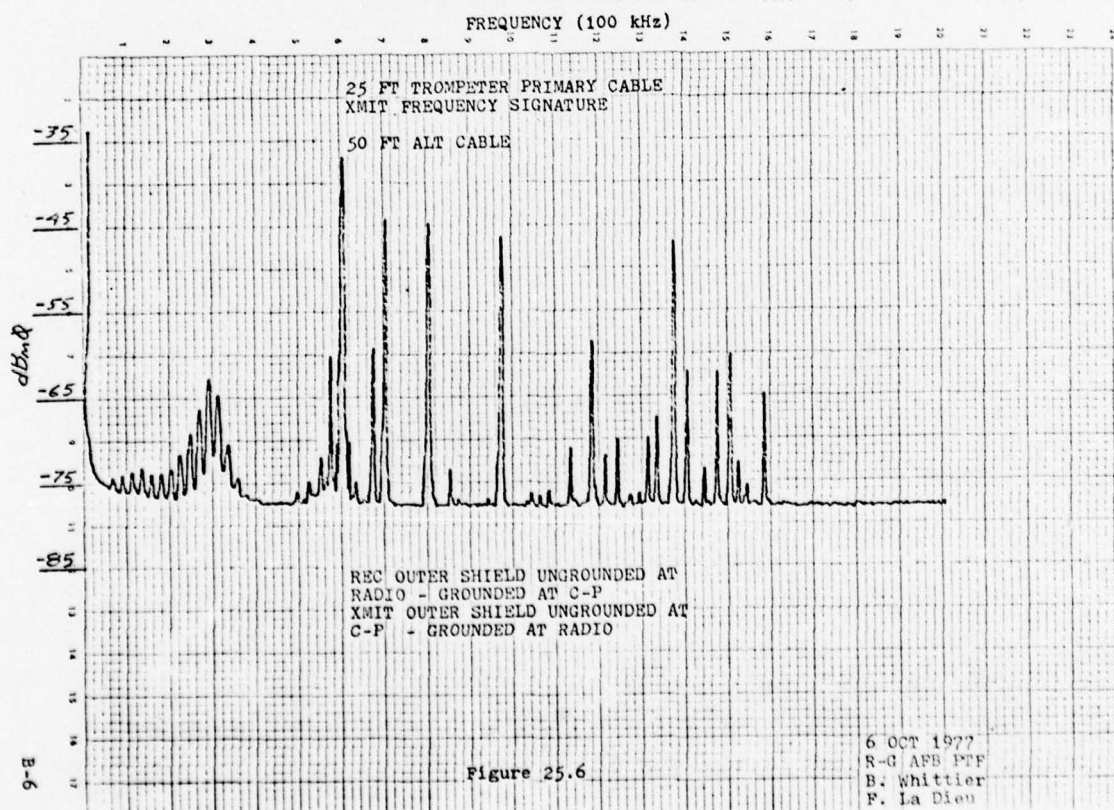
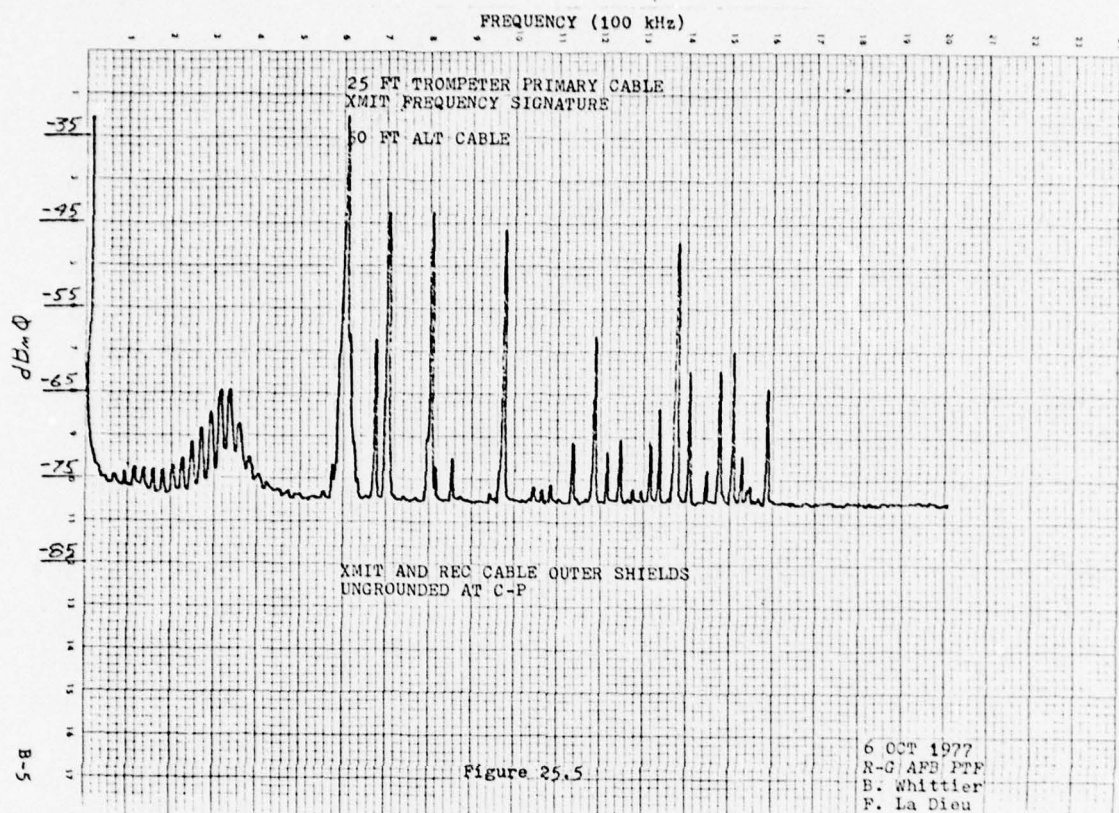
(dBmØ) (3 kHz Flat)		
1975		1977 NORMAL
Jul.1		Jul.1
66		67
63		66
60		69
63		69
66		69
68		70
68		68
67		69
67		68
68		69
64		68
65		69
65		67
63		66
61		68
63		69
67		69
67		69
65		69
65		68
66		68
68		68
63		67
65		69
66		67
63		67
61		68
63		70
67		68
67		68
65	(30 day average)	68.2

NOTE: While the performance of these cable plants is seen to have increased by 3 dB, what is particularly significant is that the NORMAL configured base-band cable plants show stable day-to-day noise levels equivalent to the looped multiplex specification of -68.7 dBmØ.

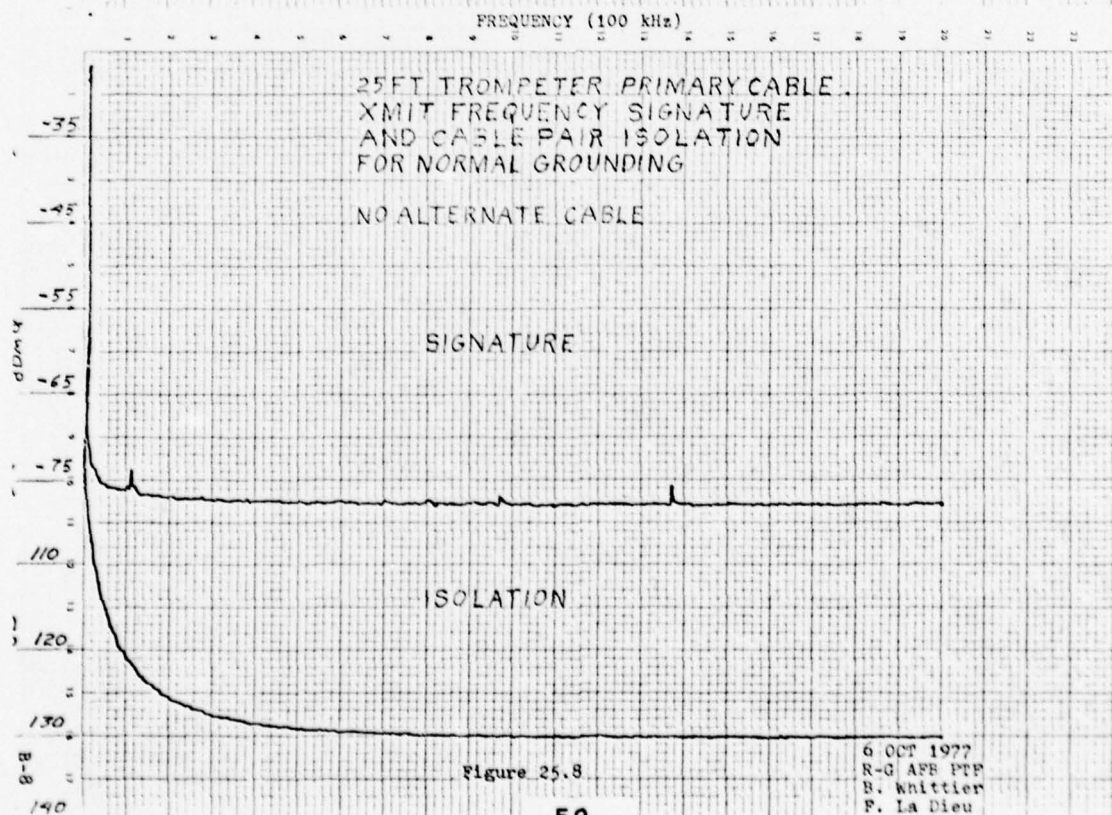
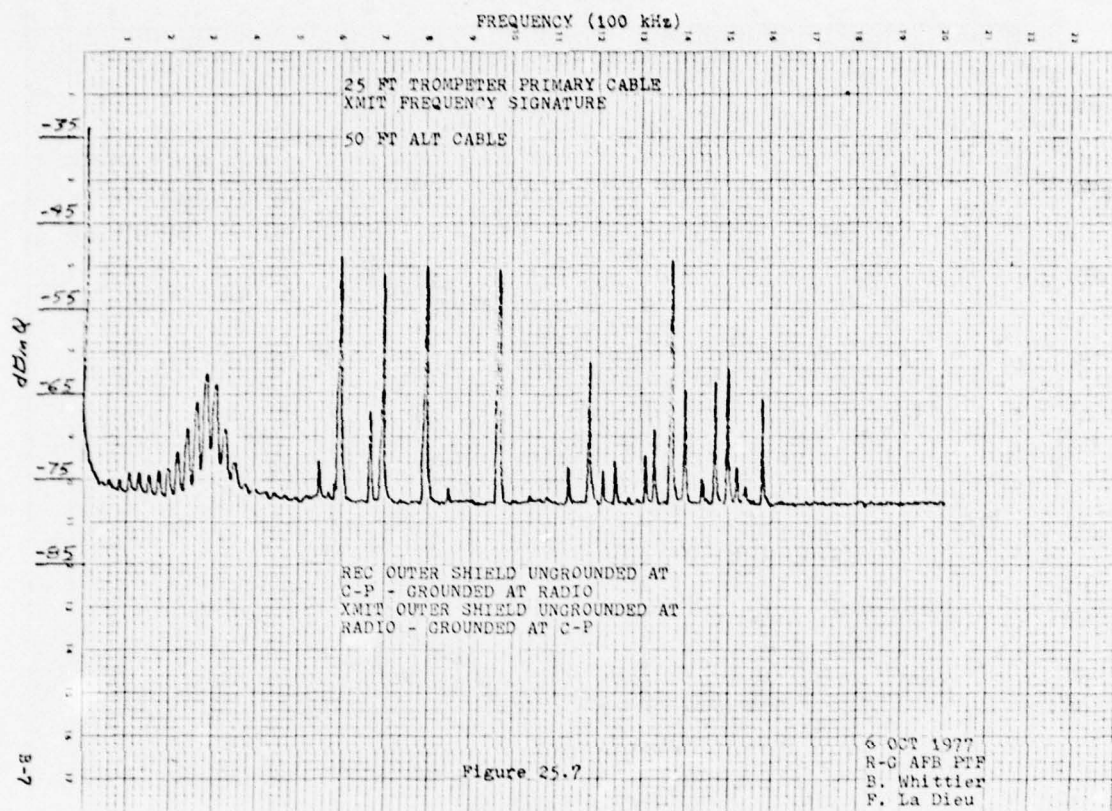


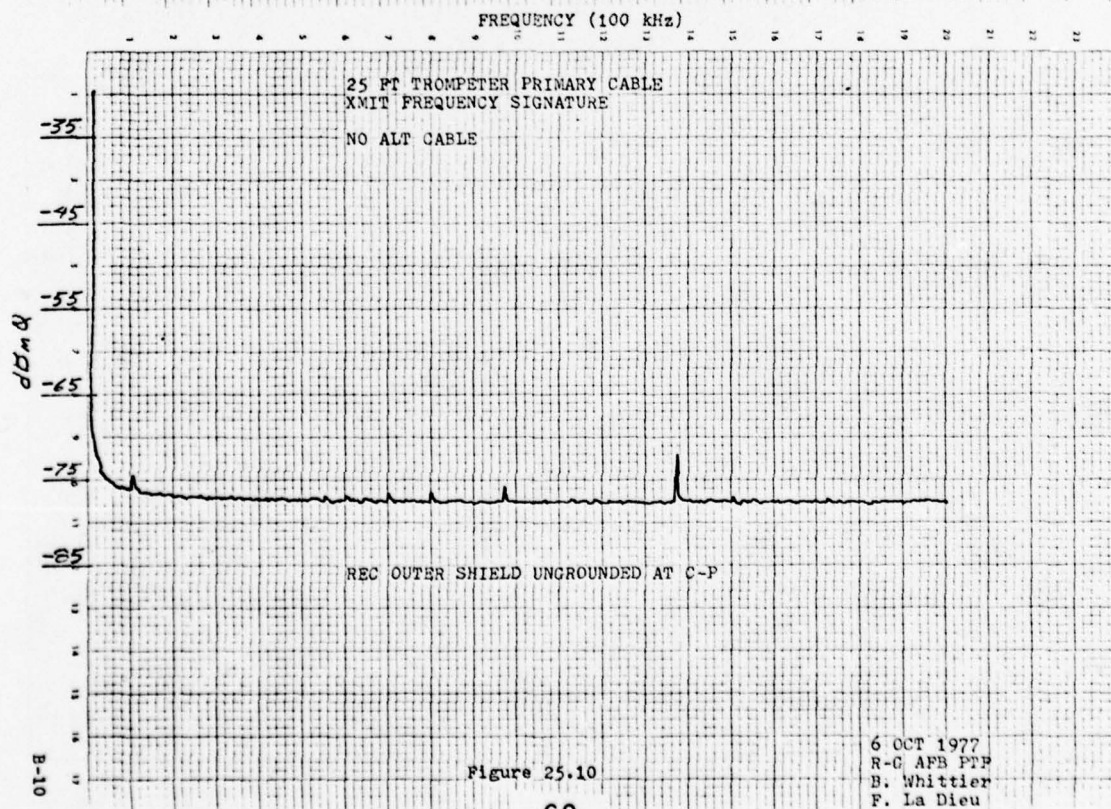
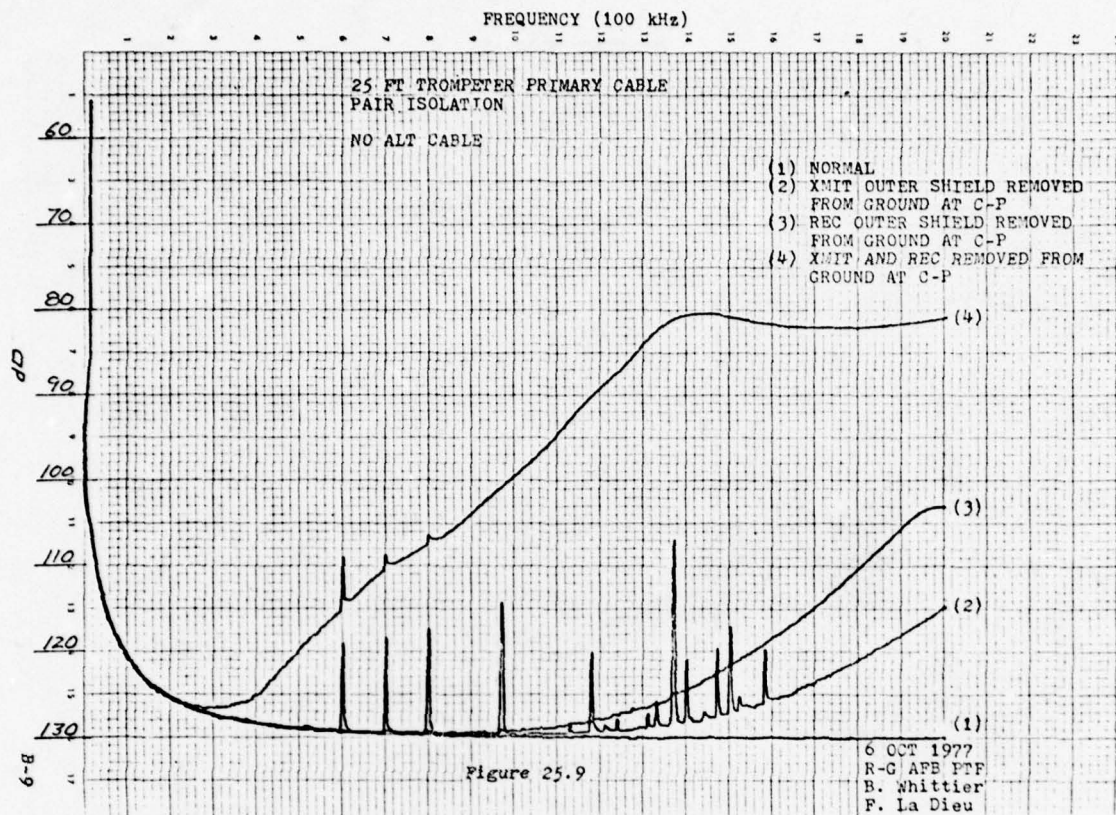




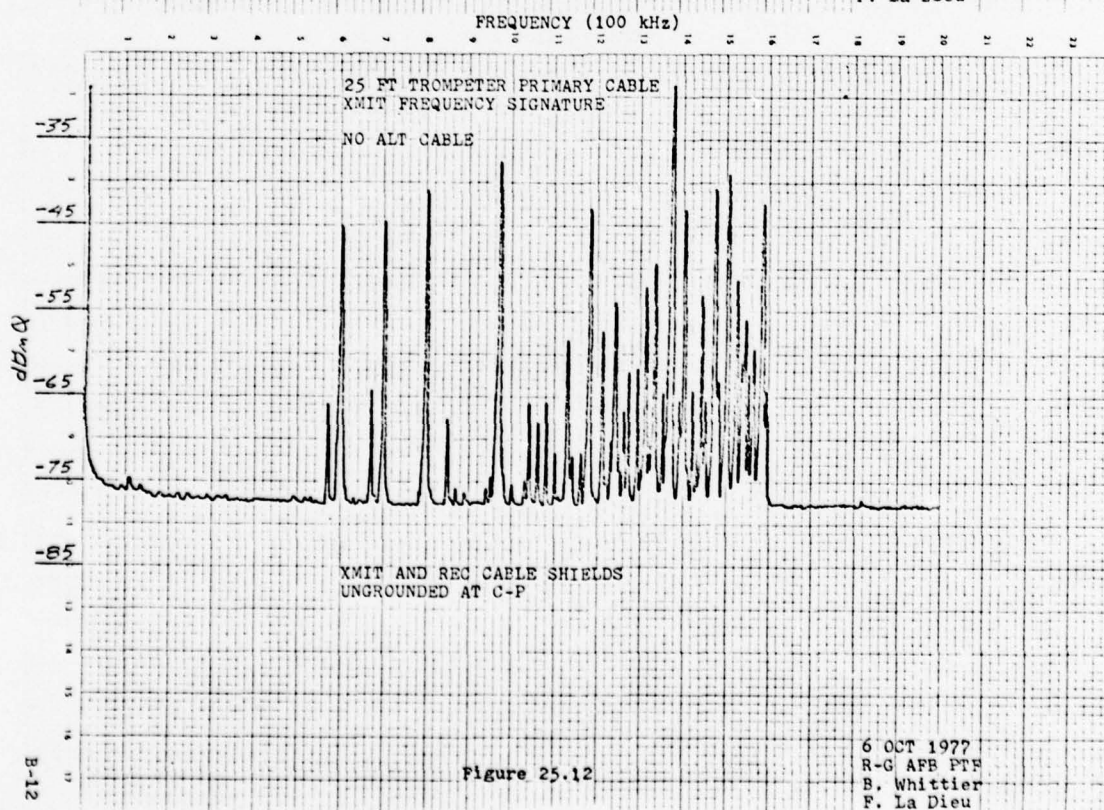
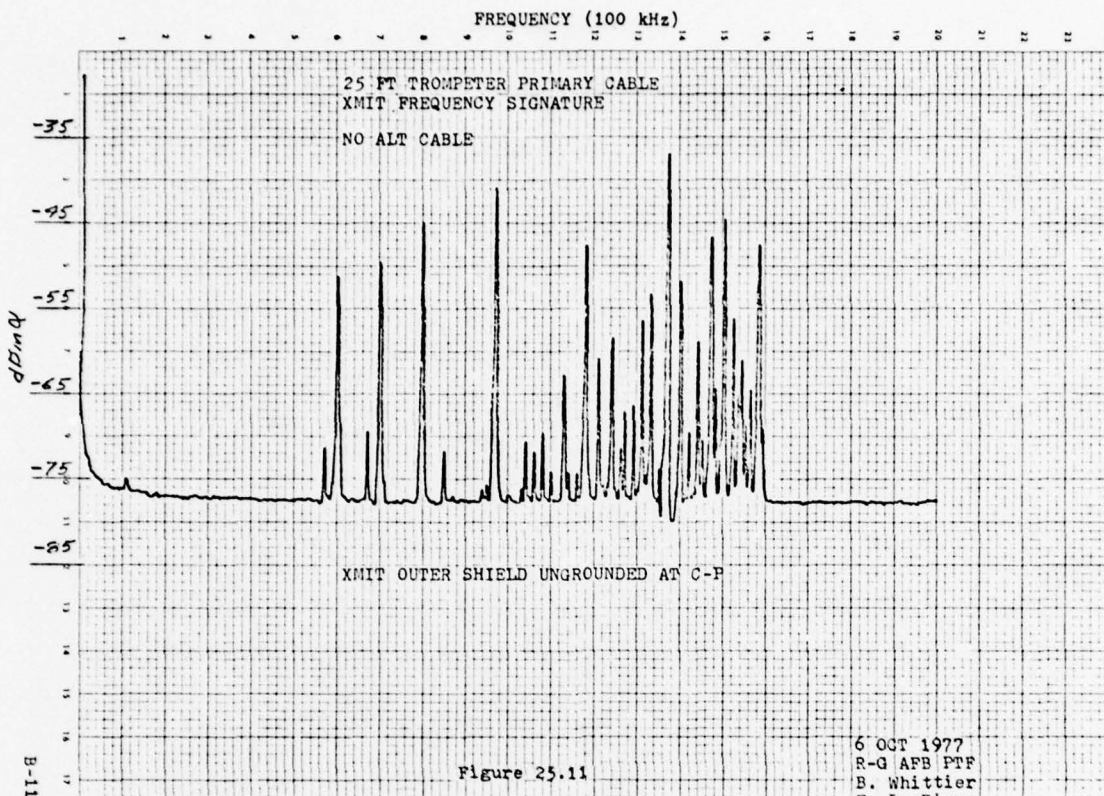


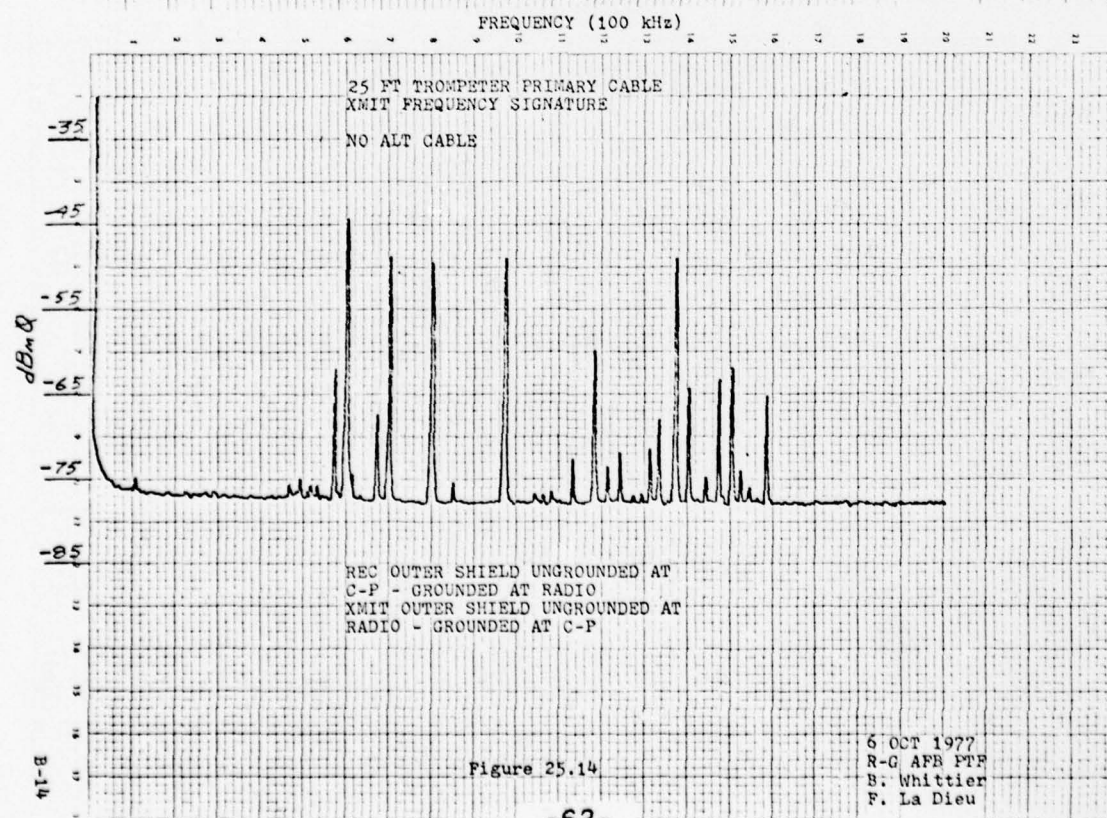
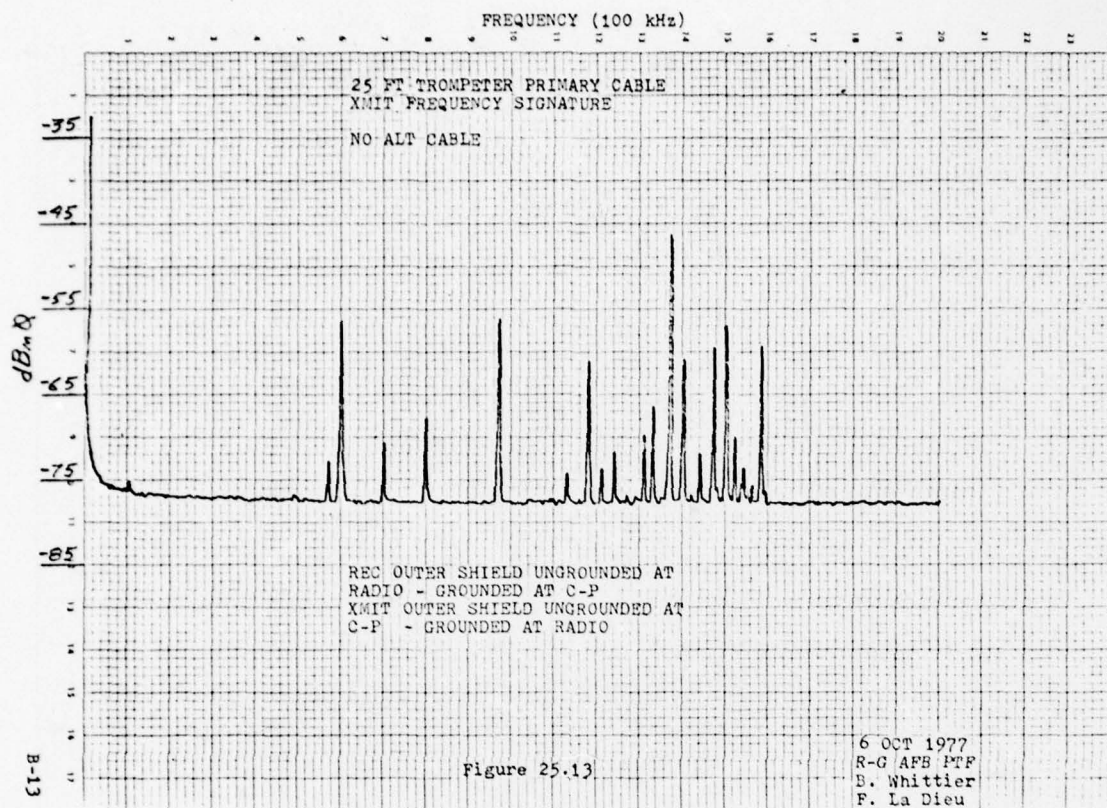




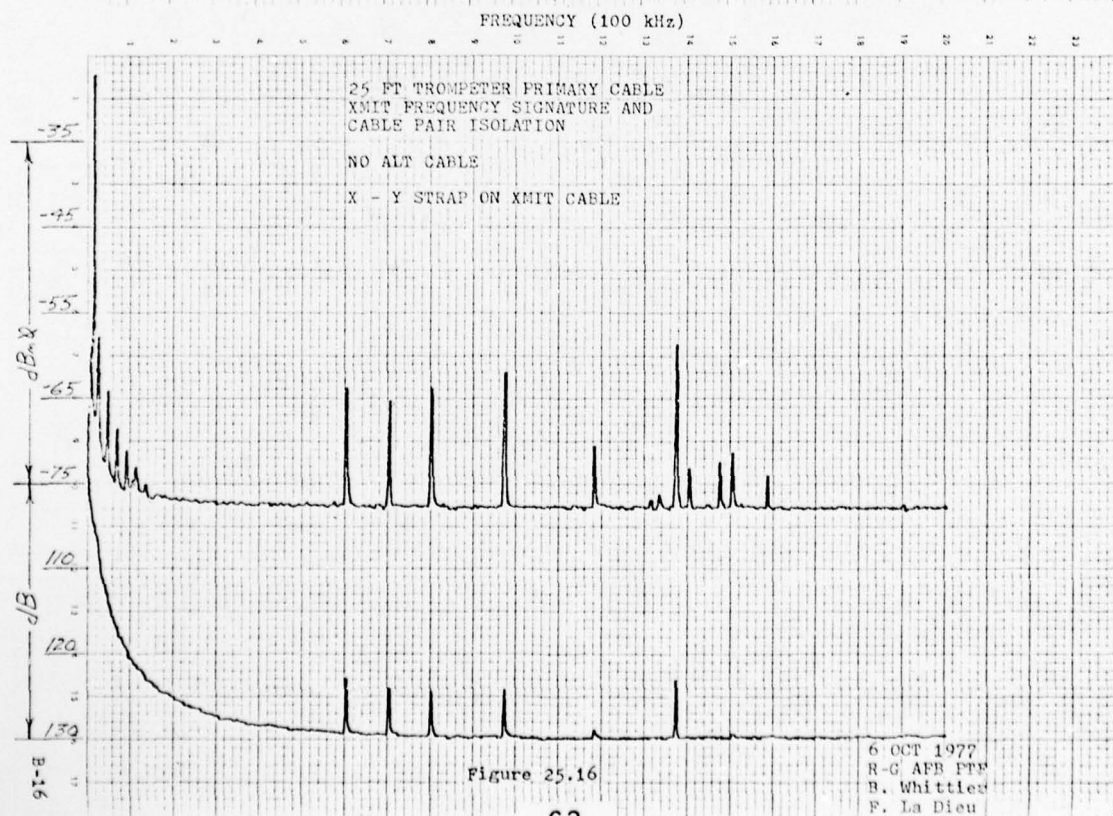
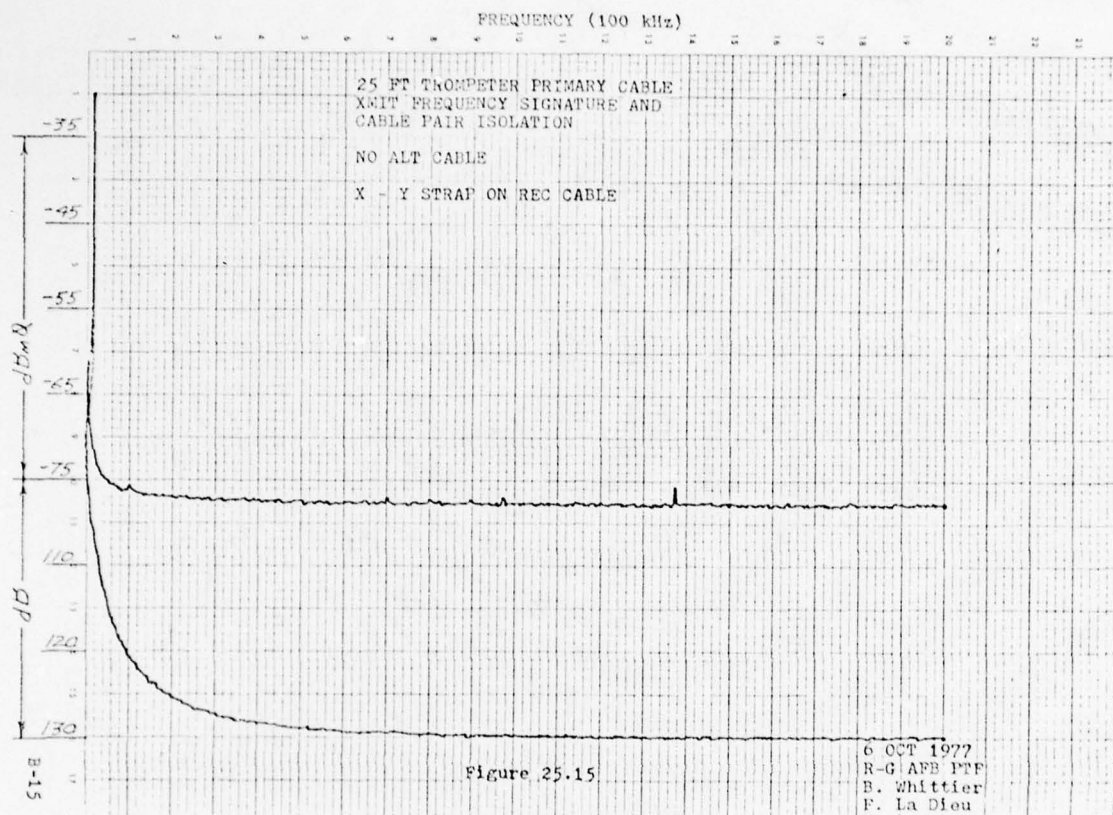


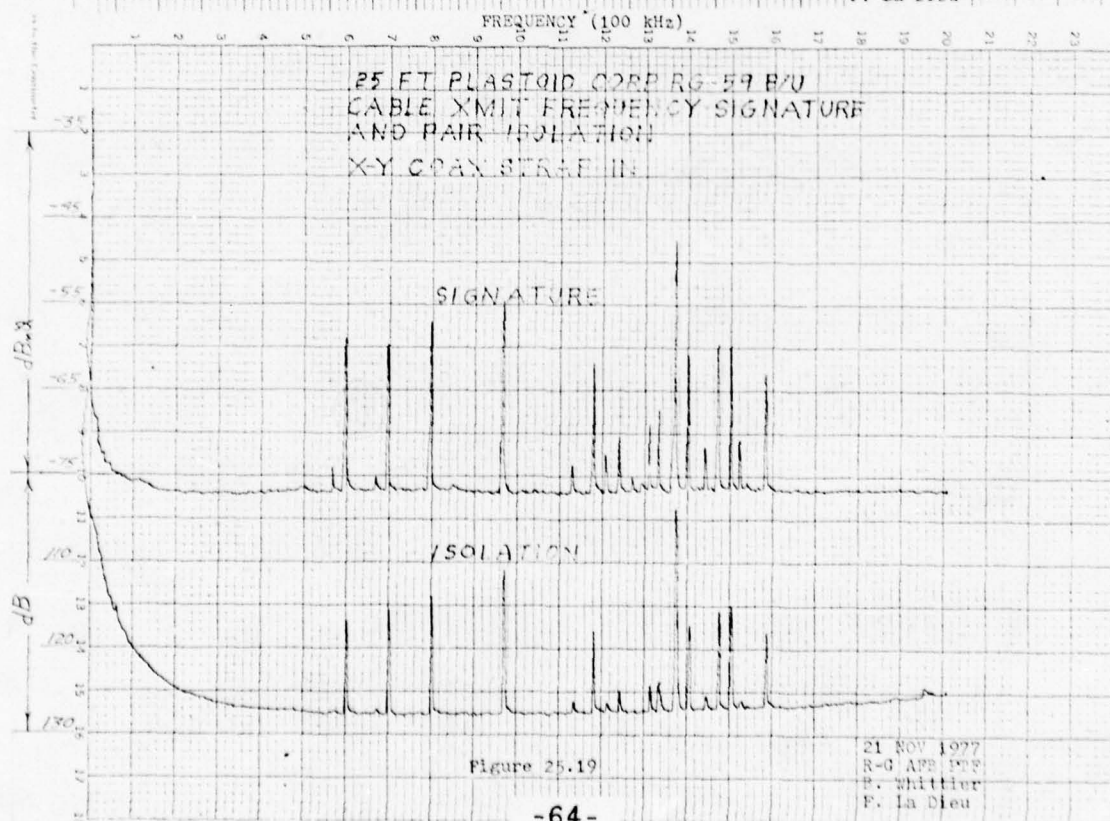
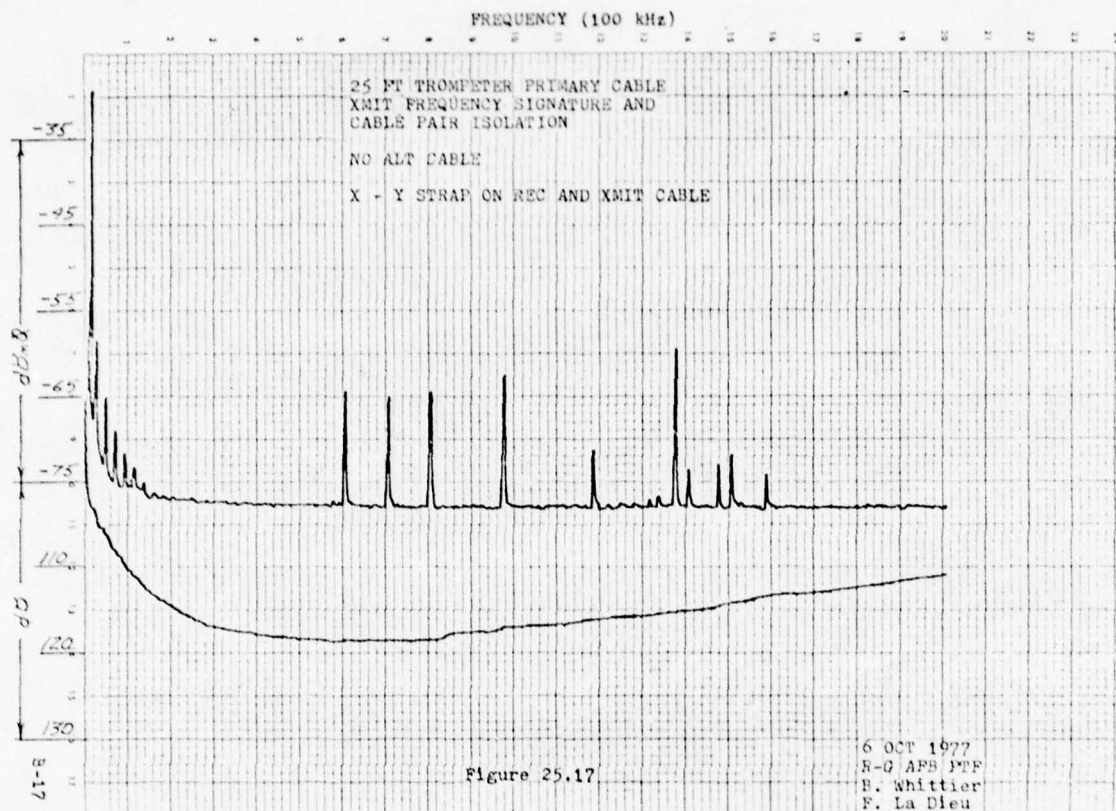


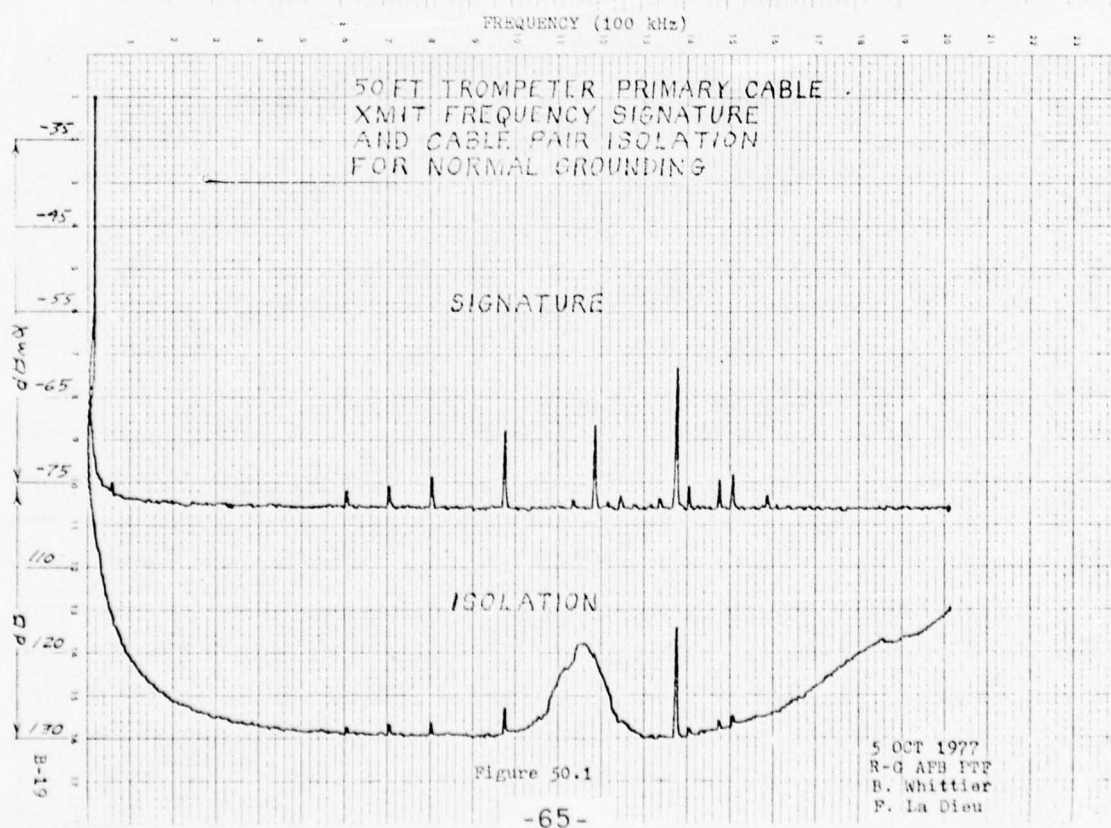
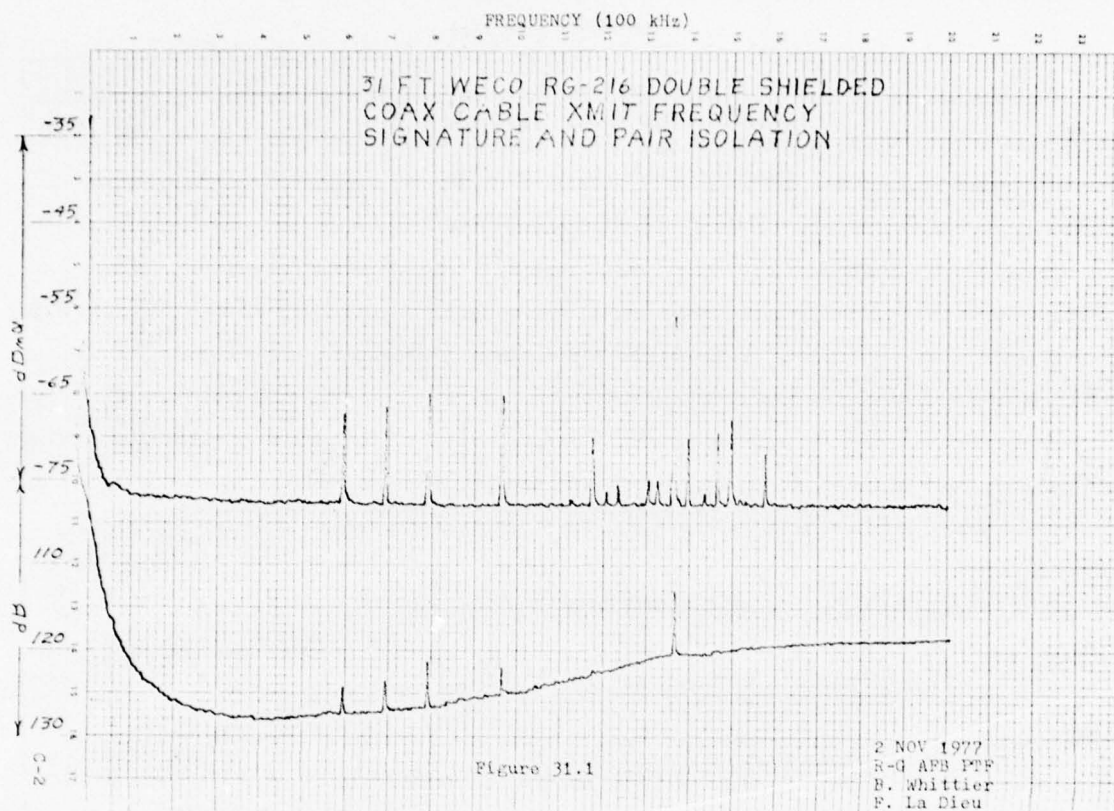




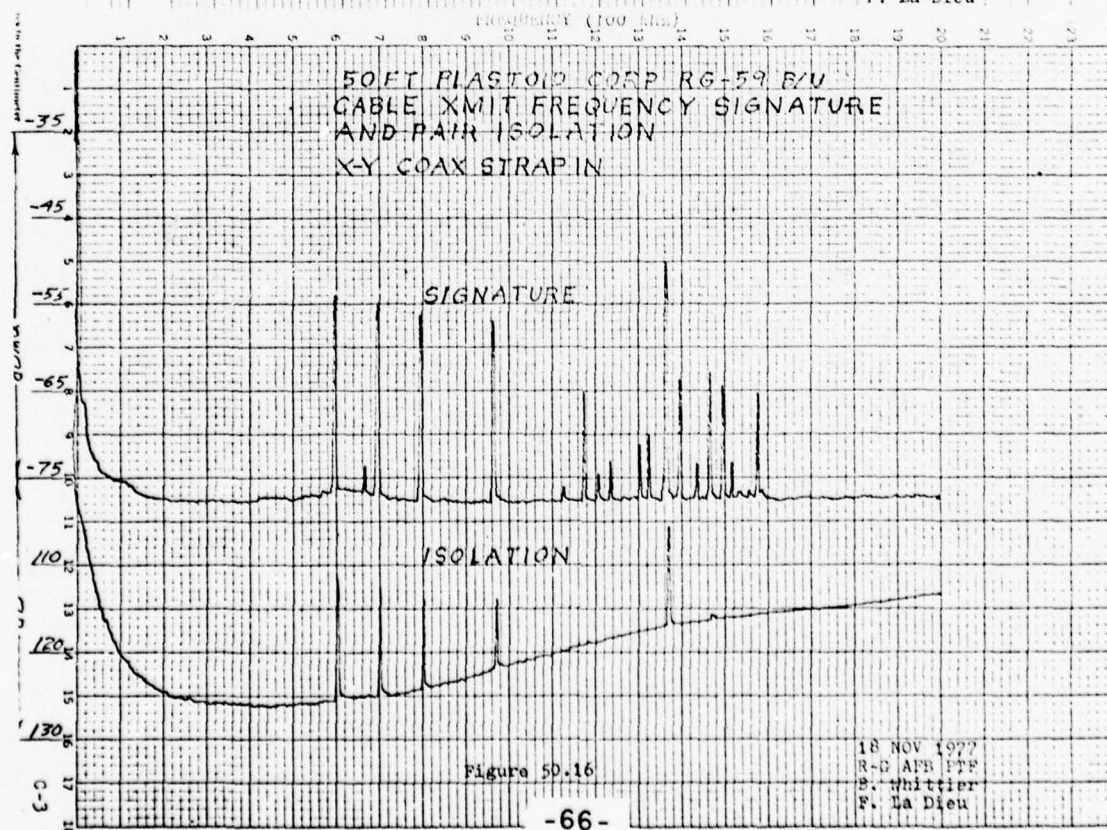
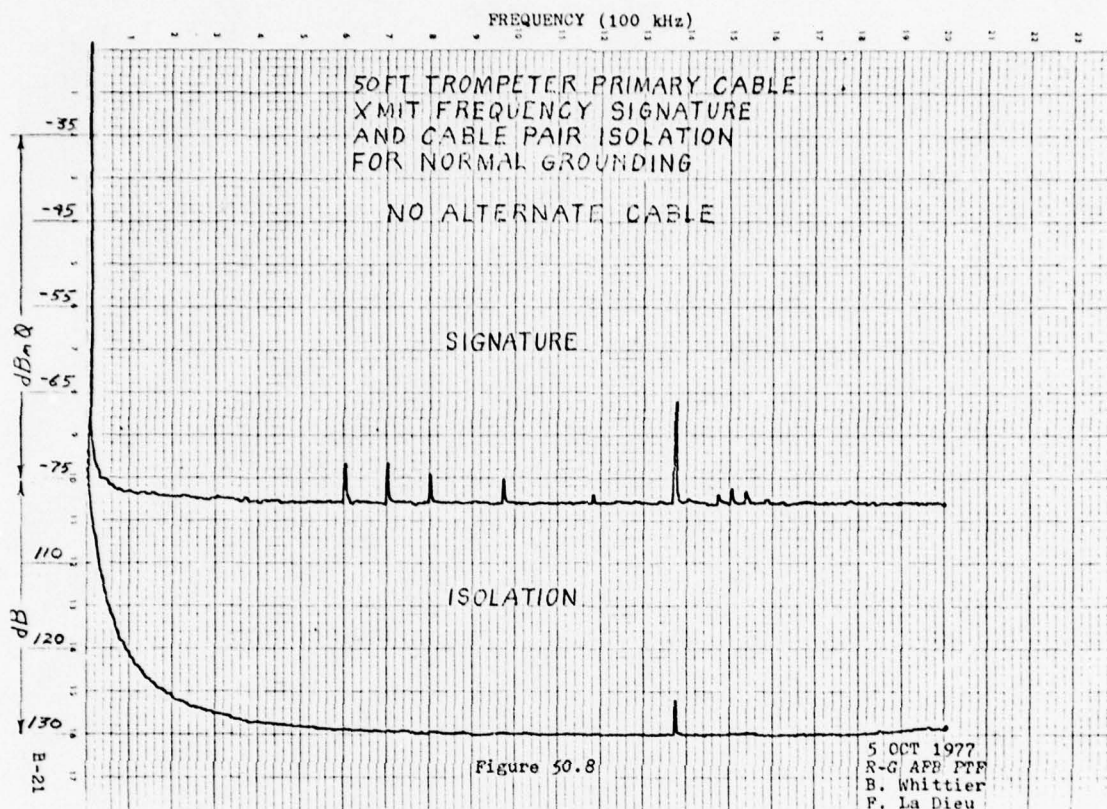




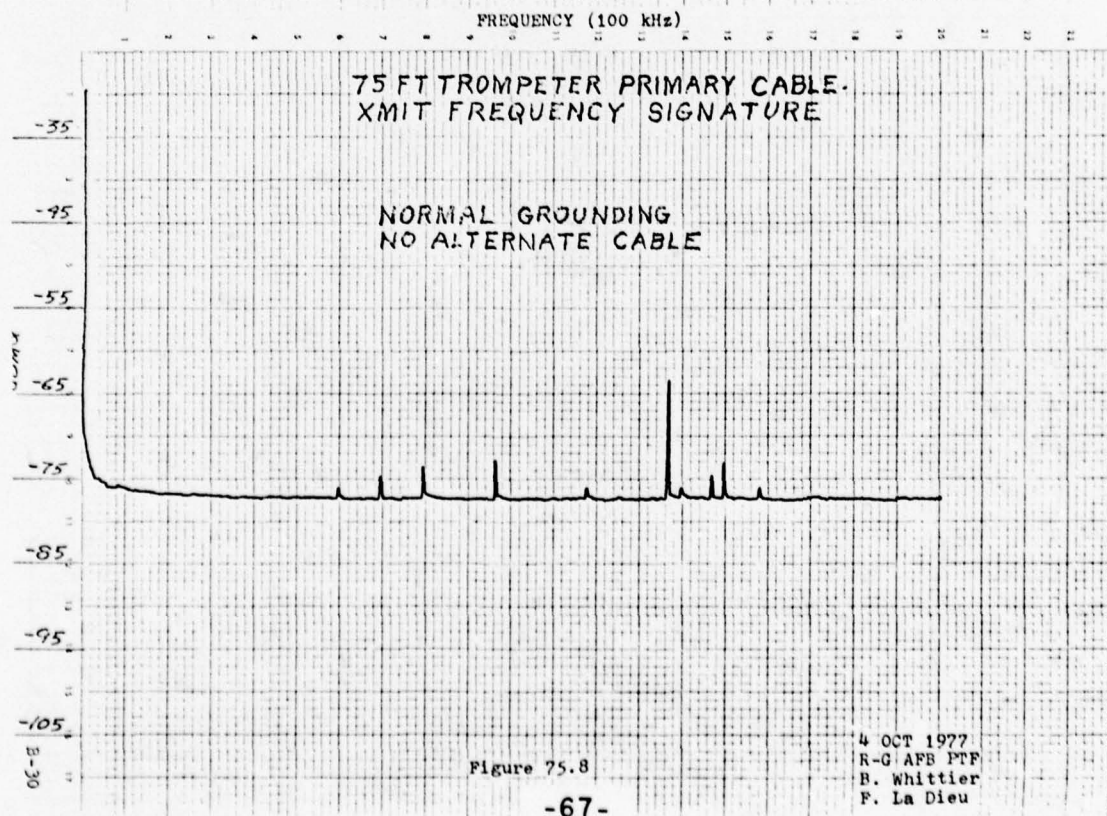
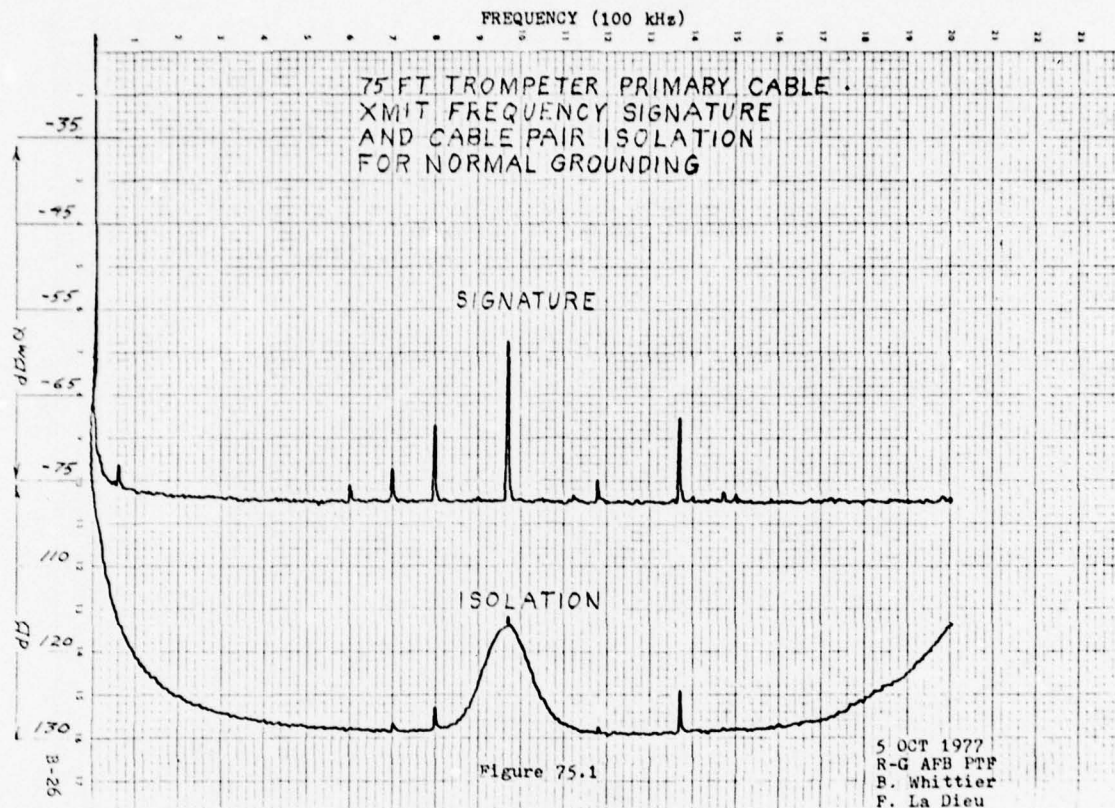


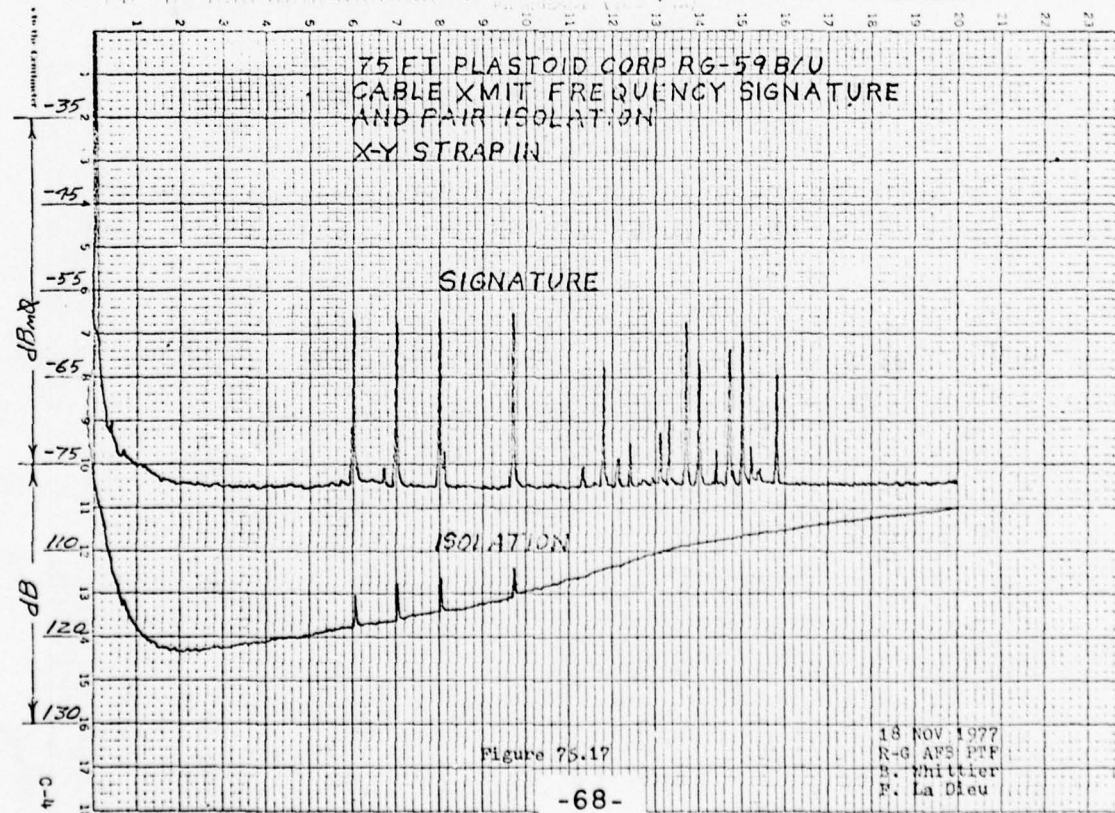
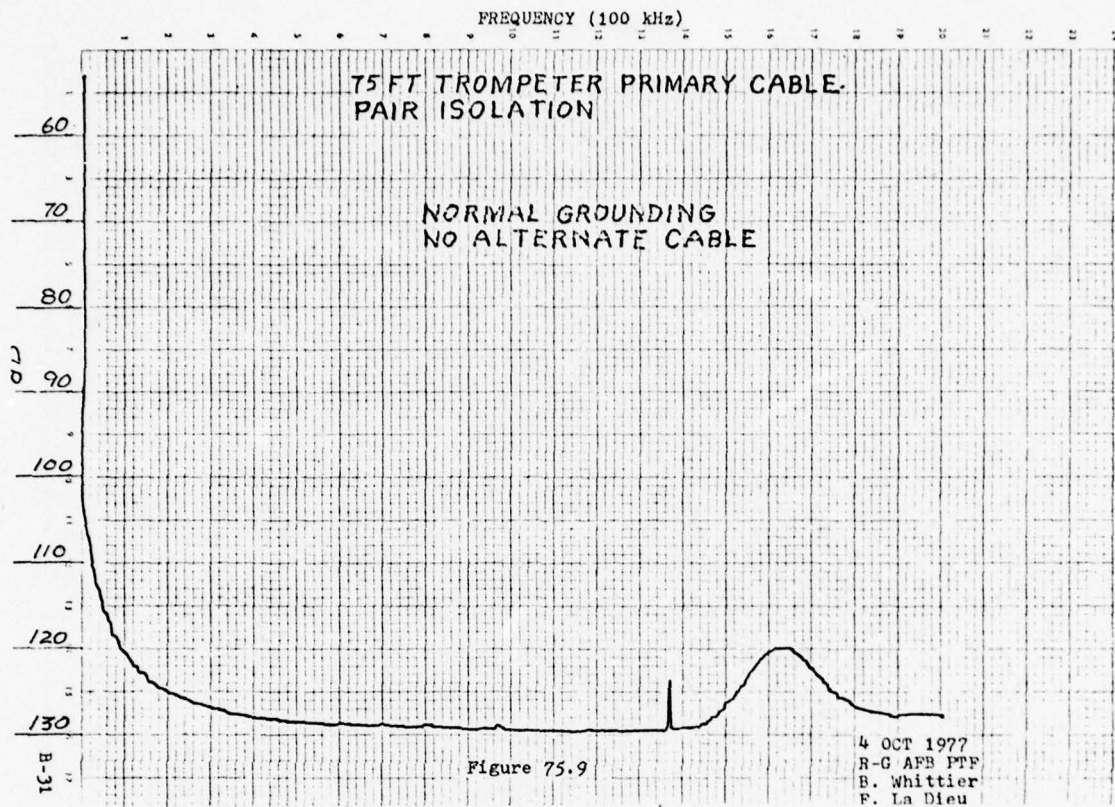




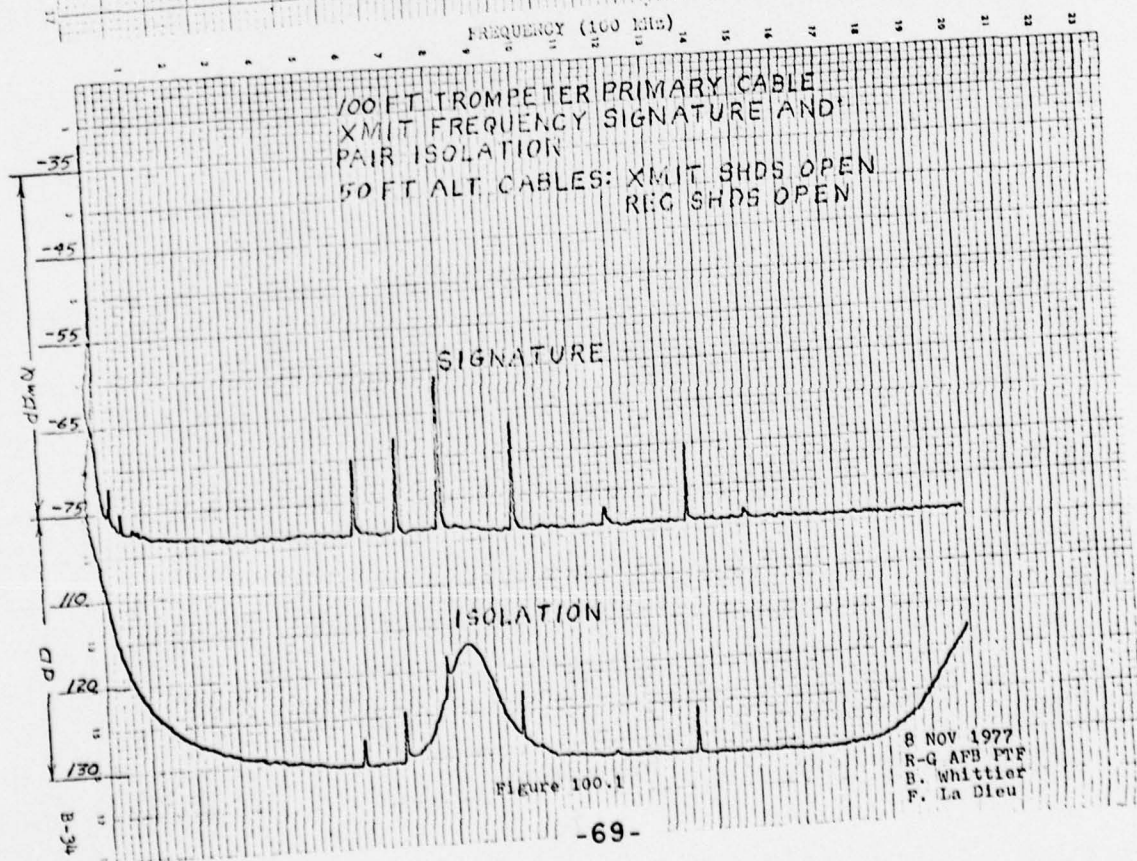
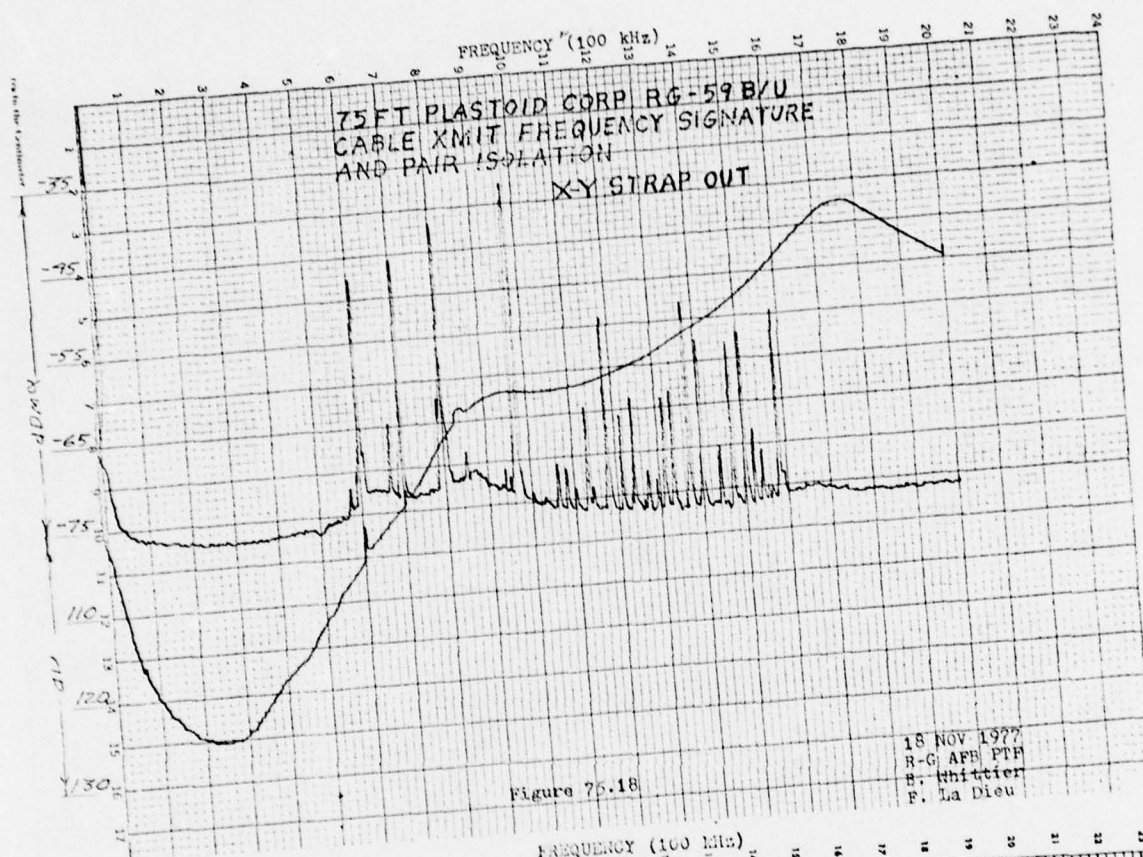




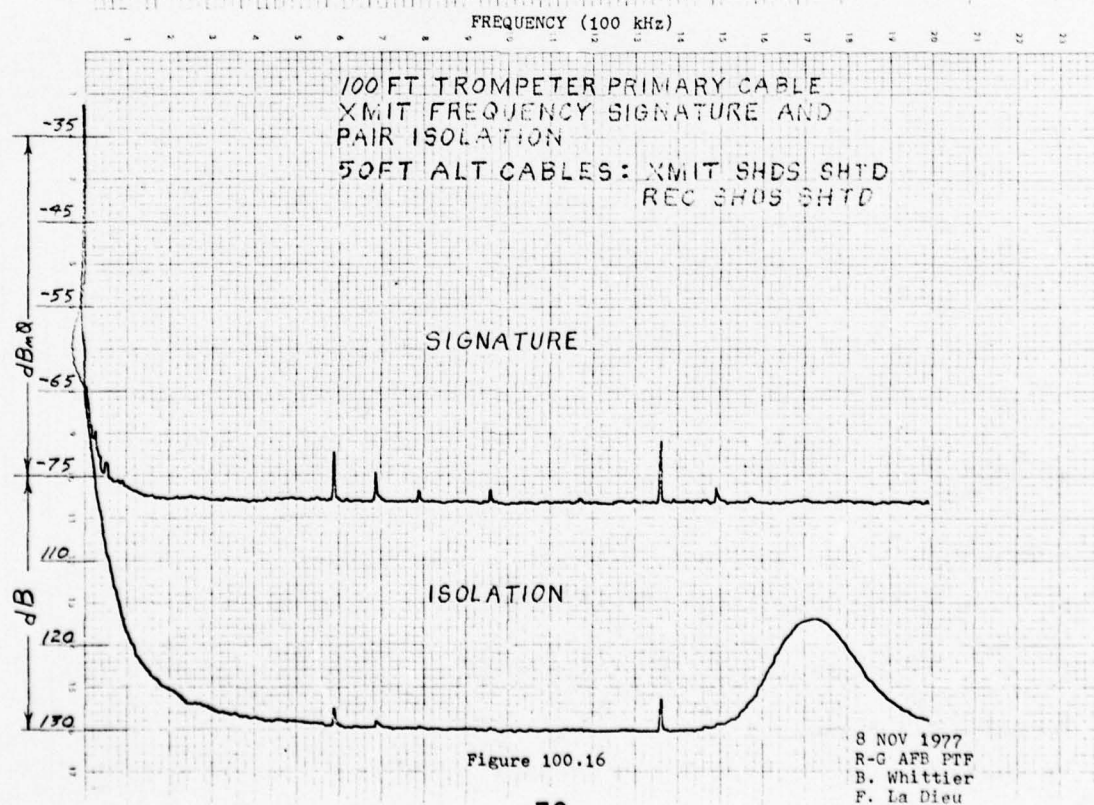
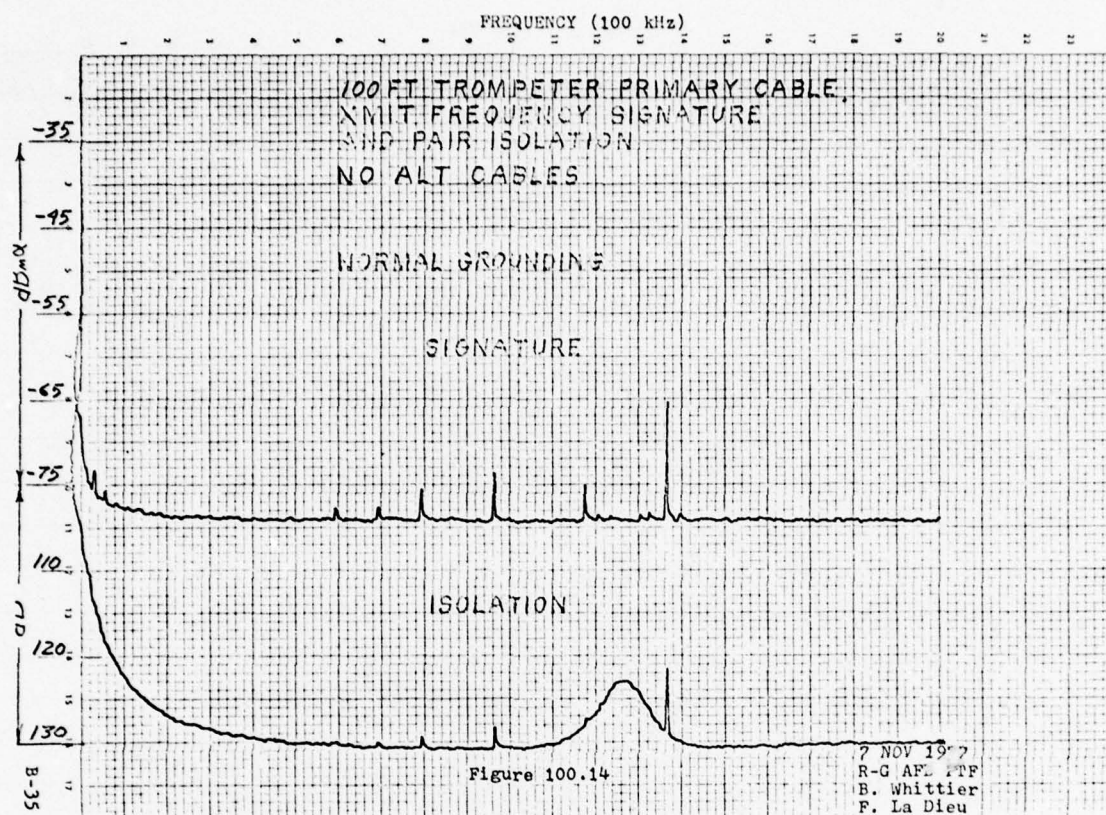


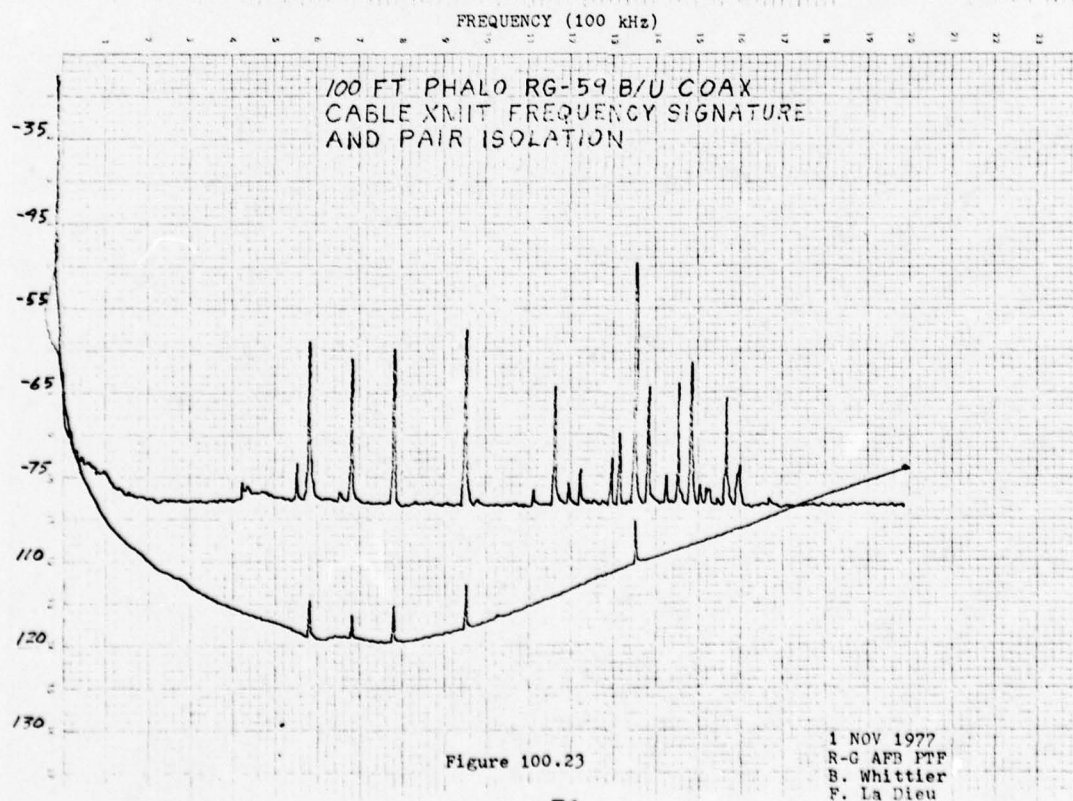
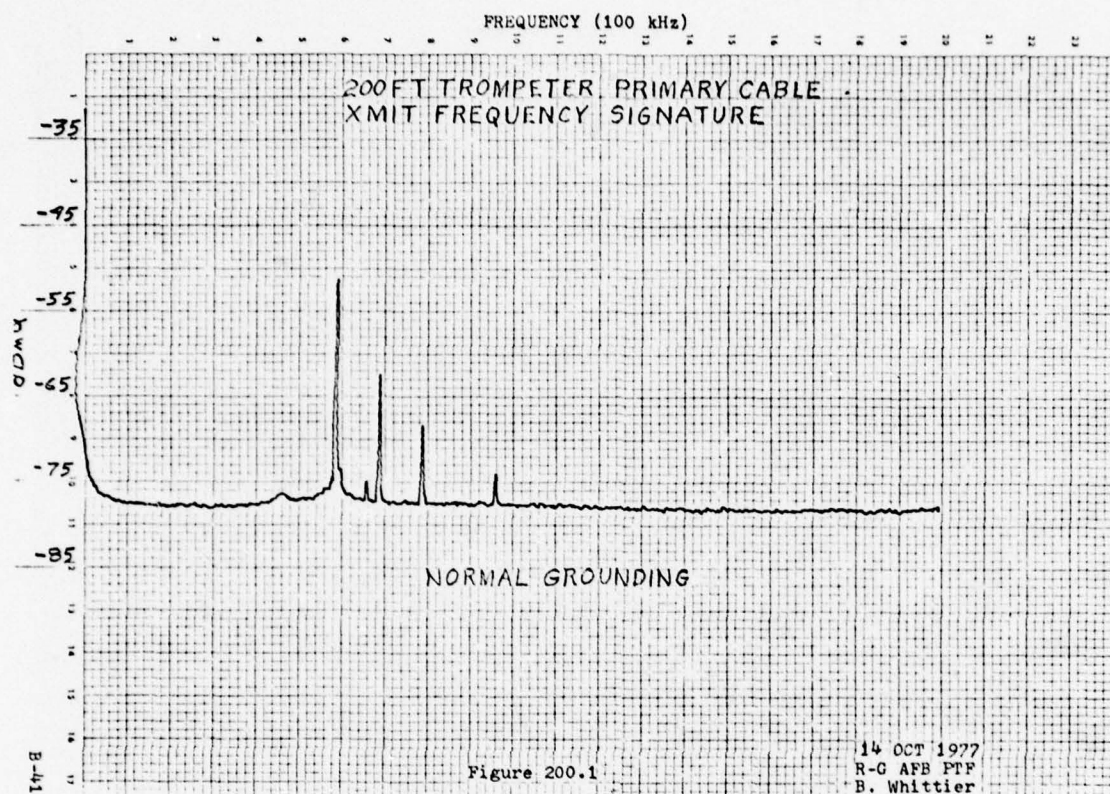


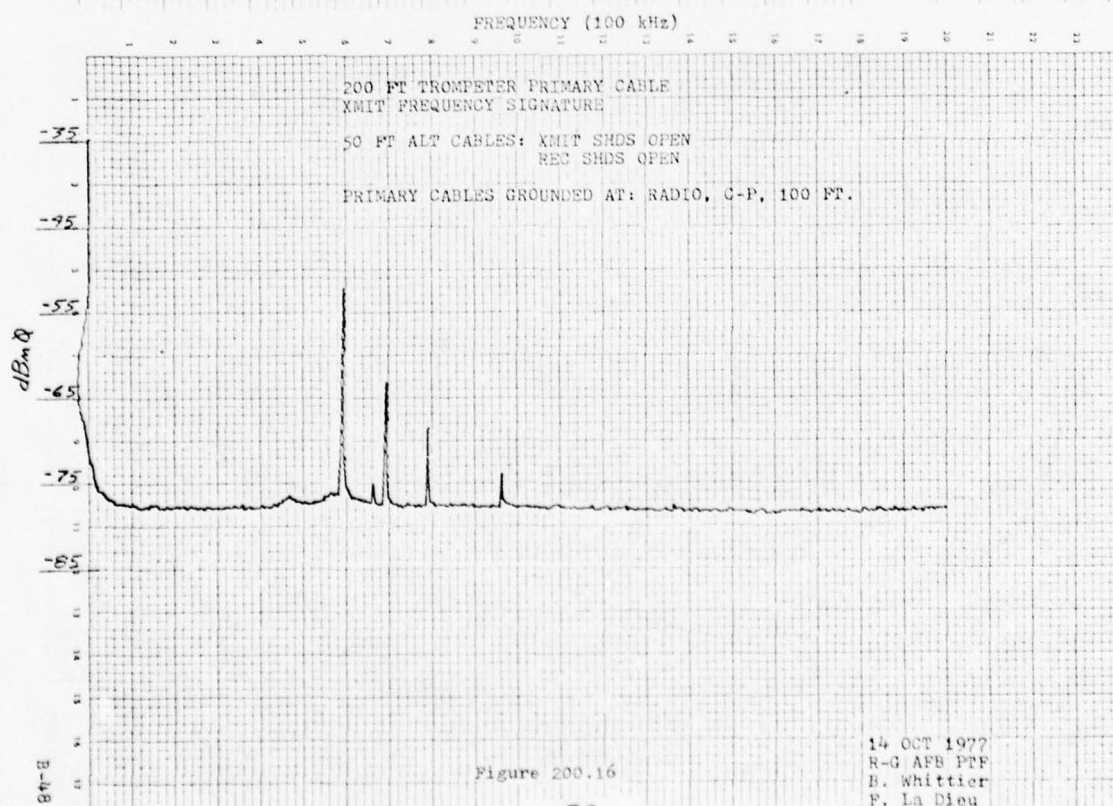
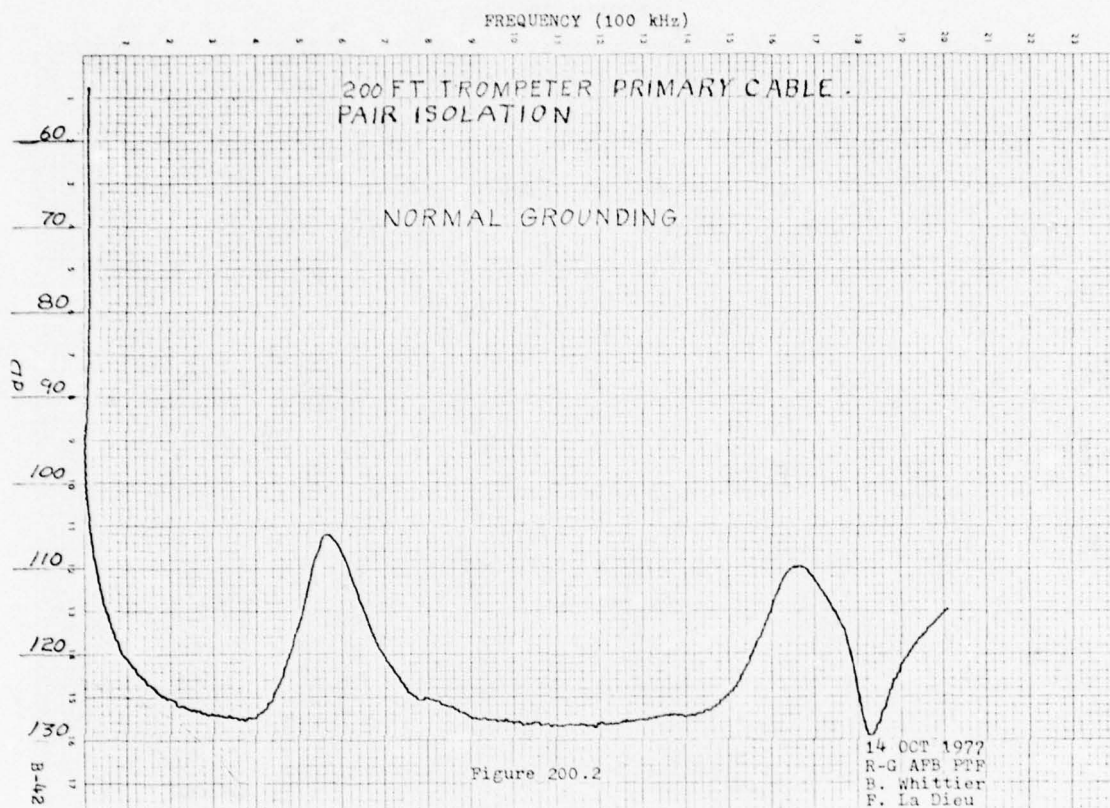




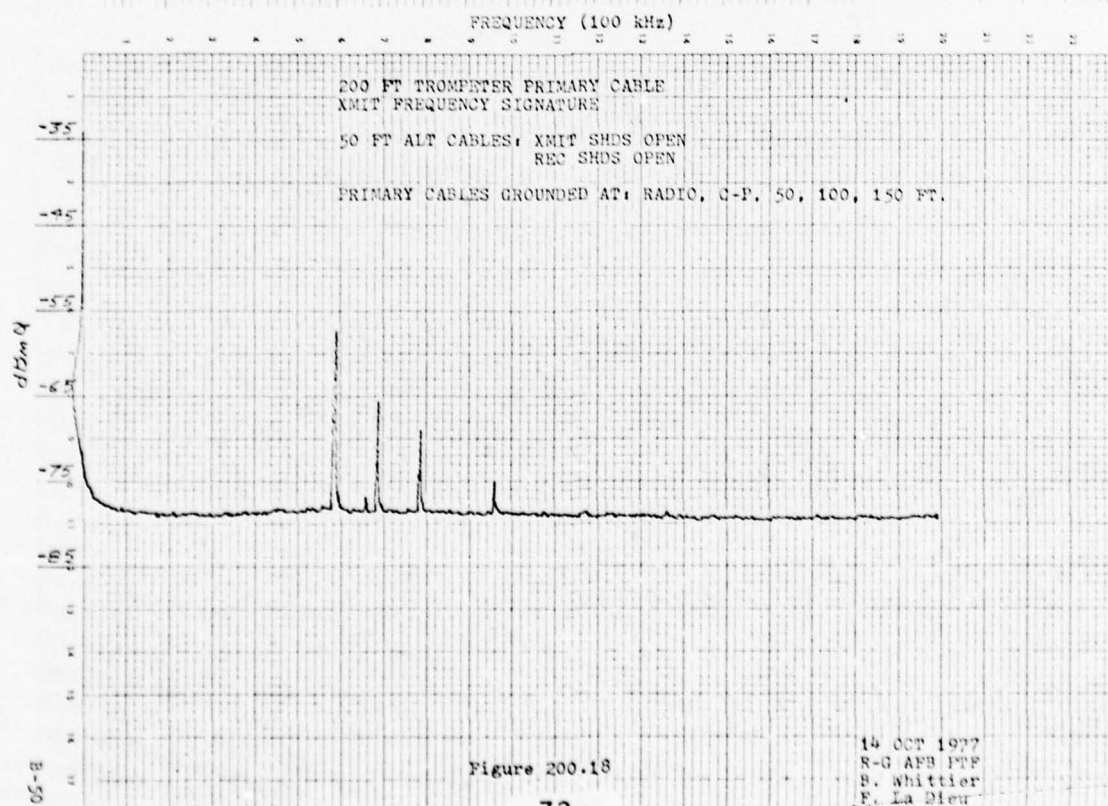
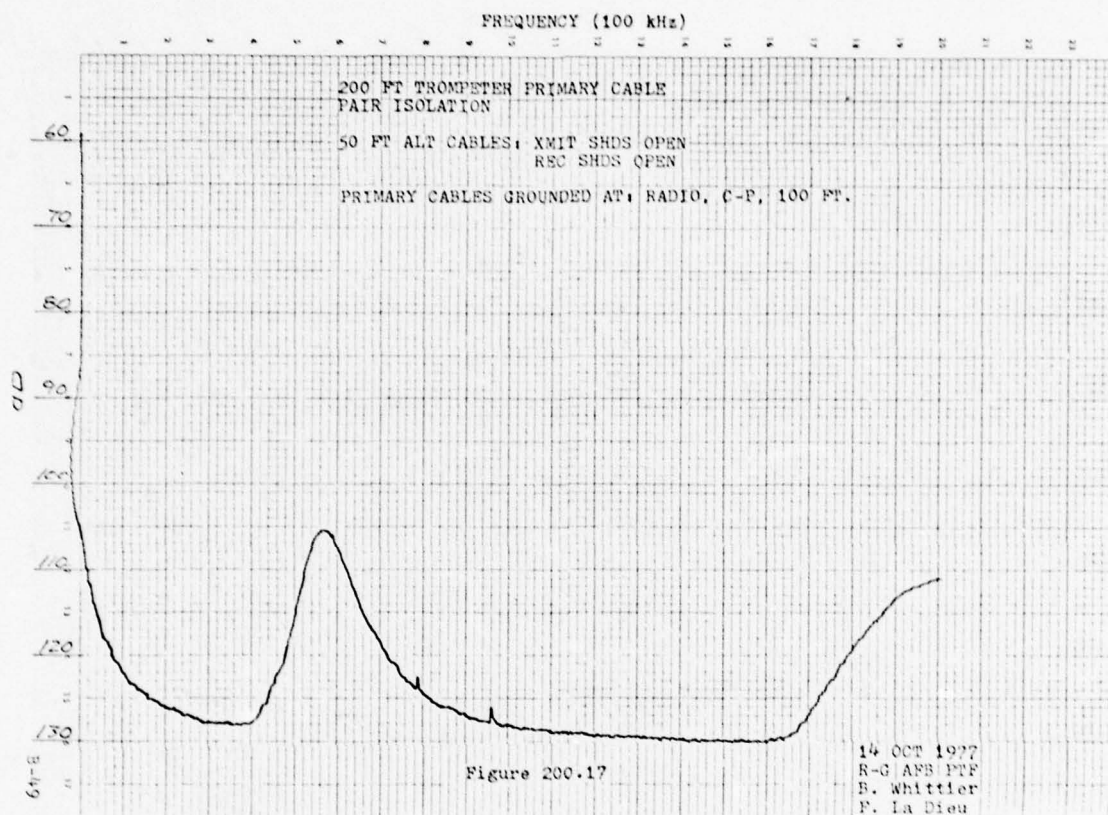


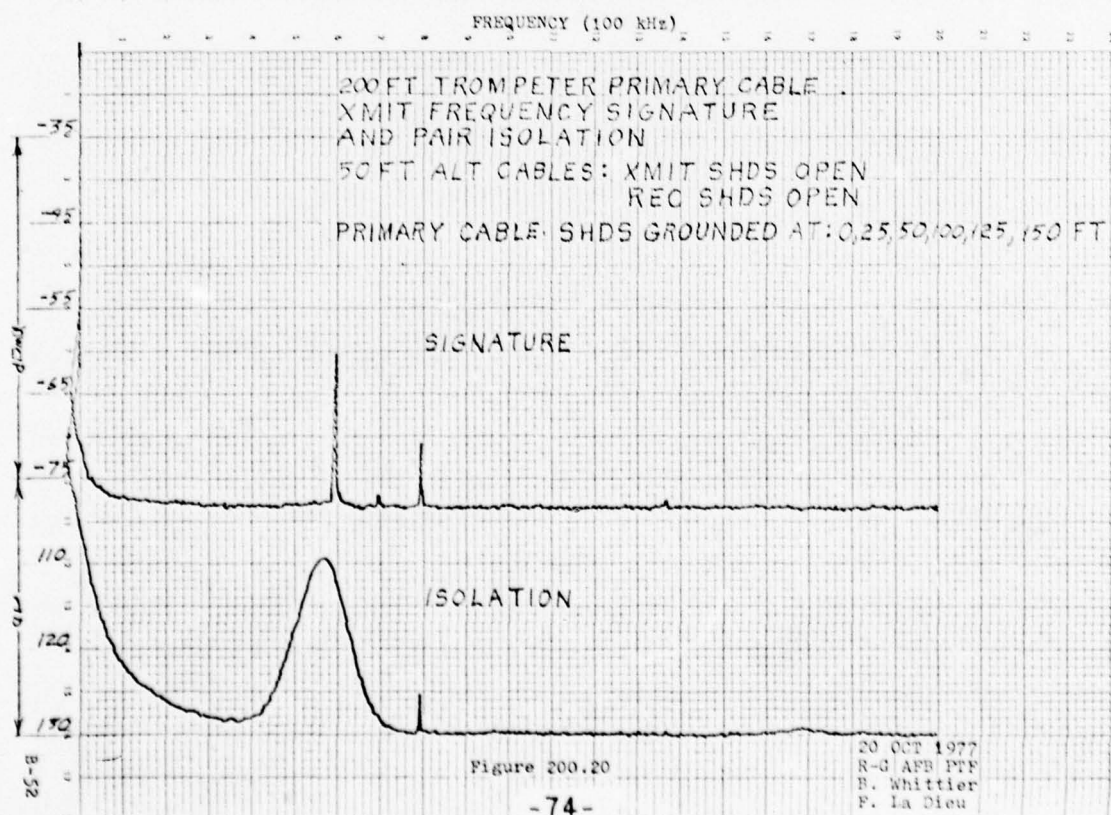
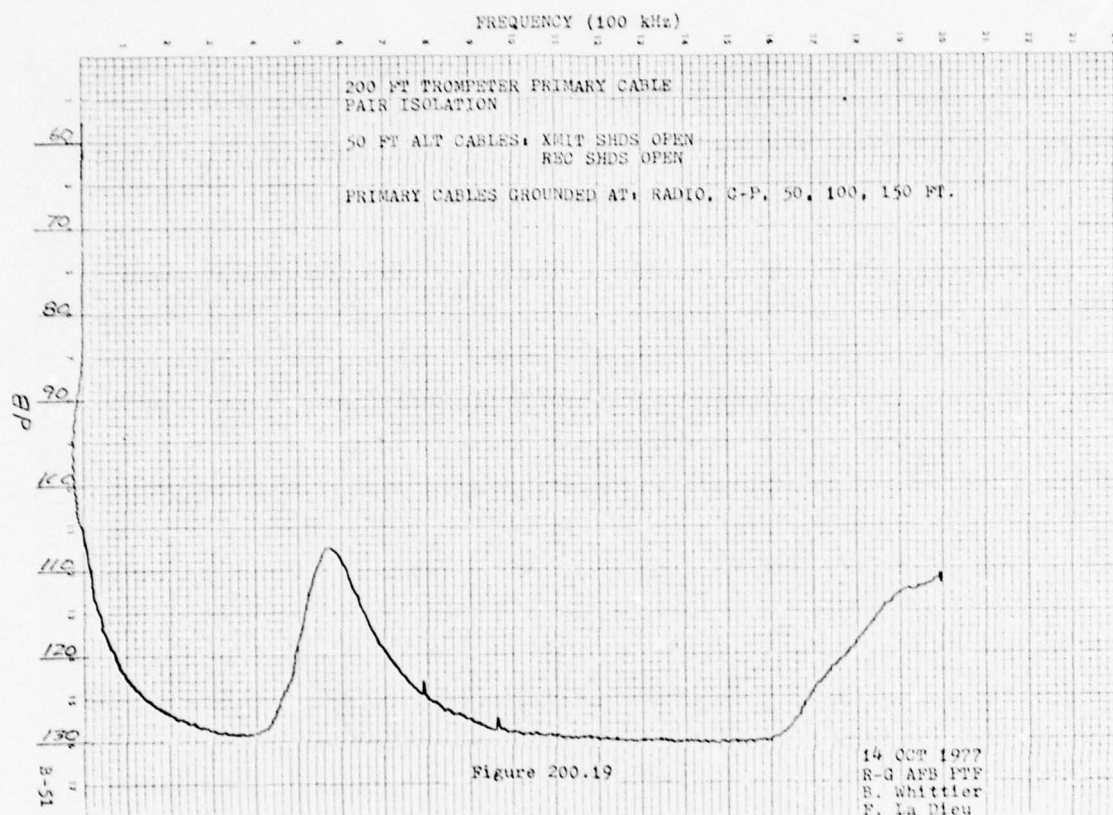


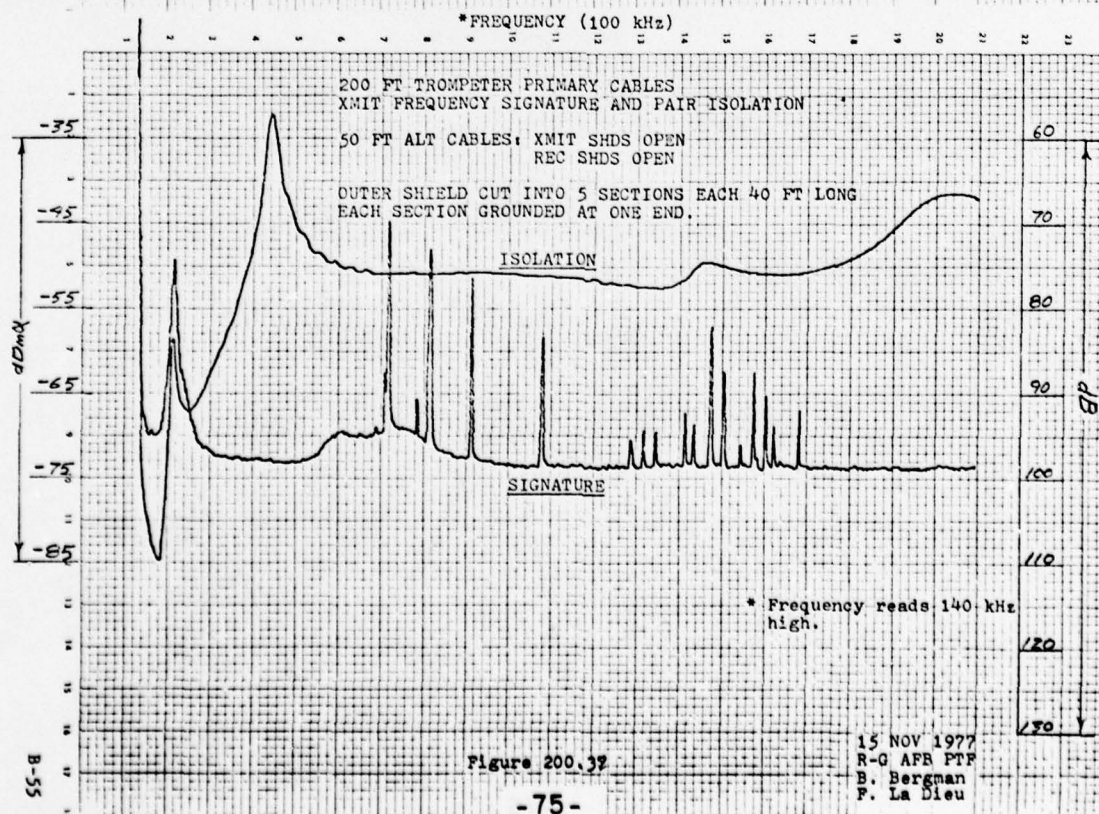
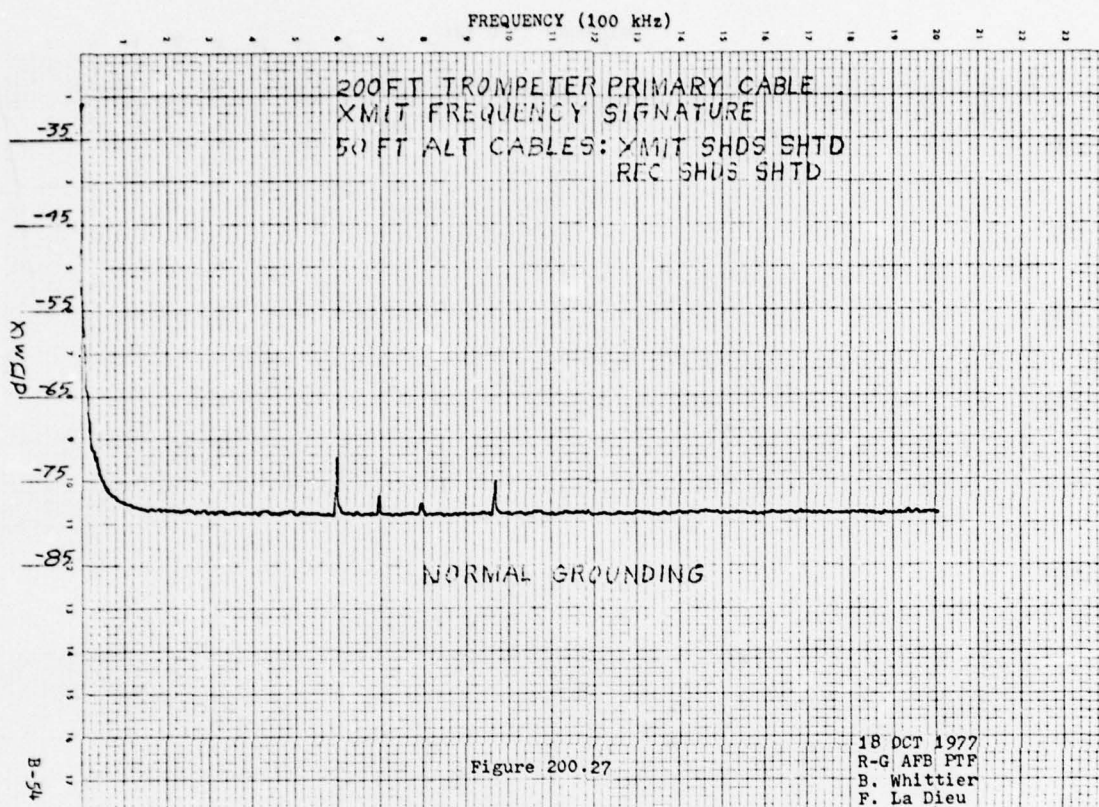




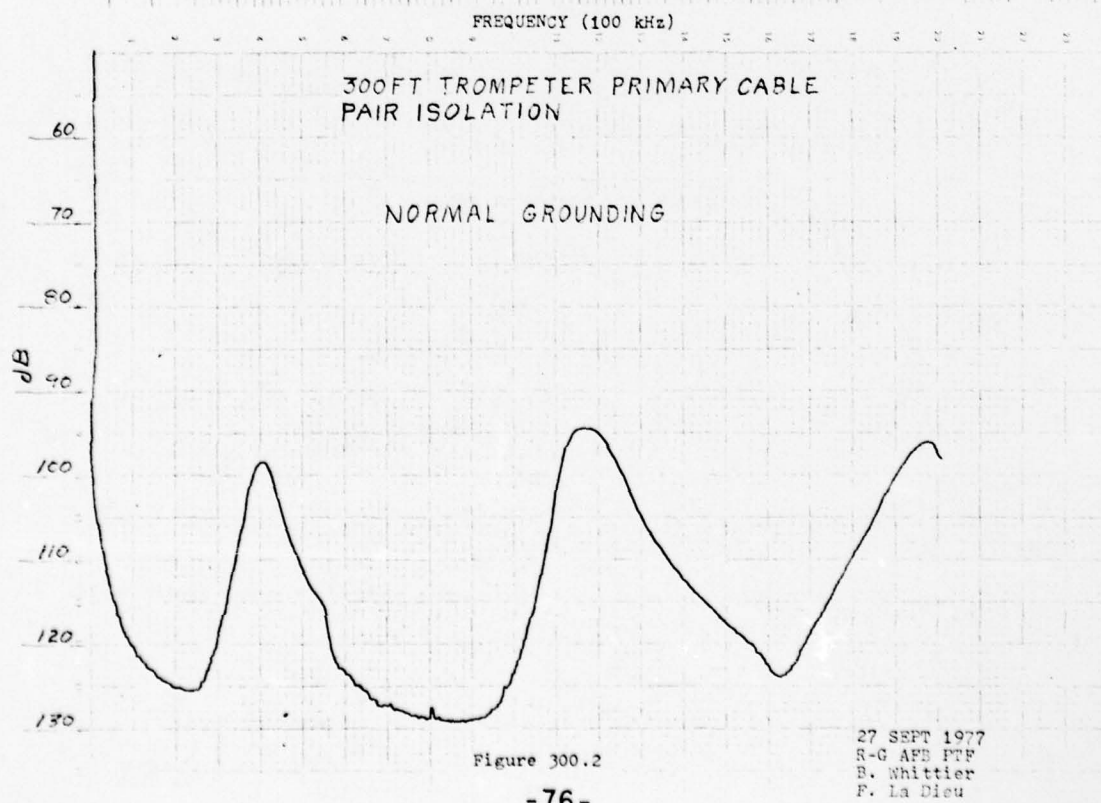
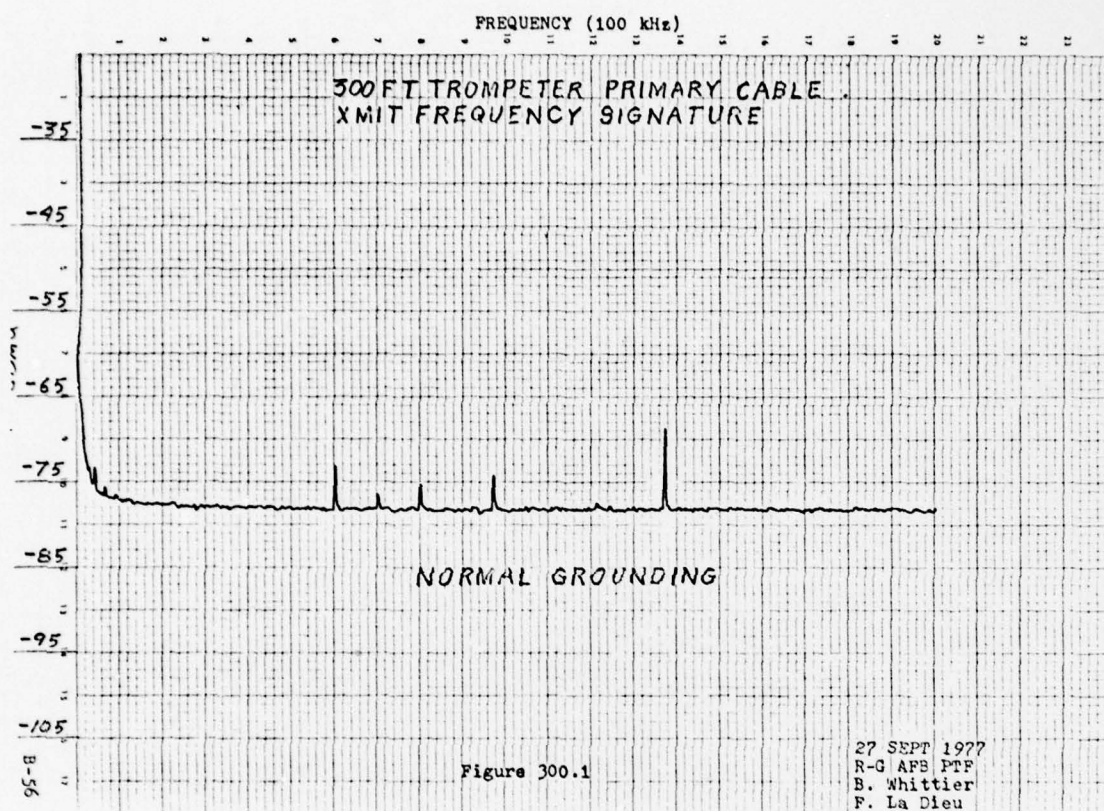


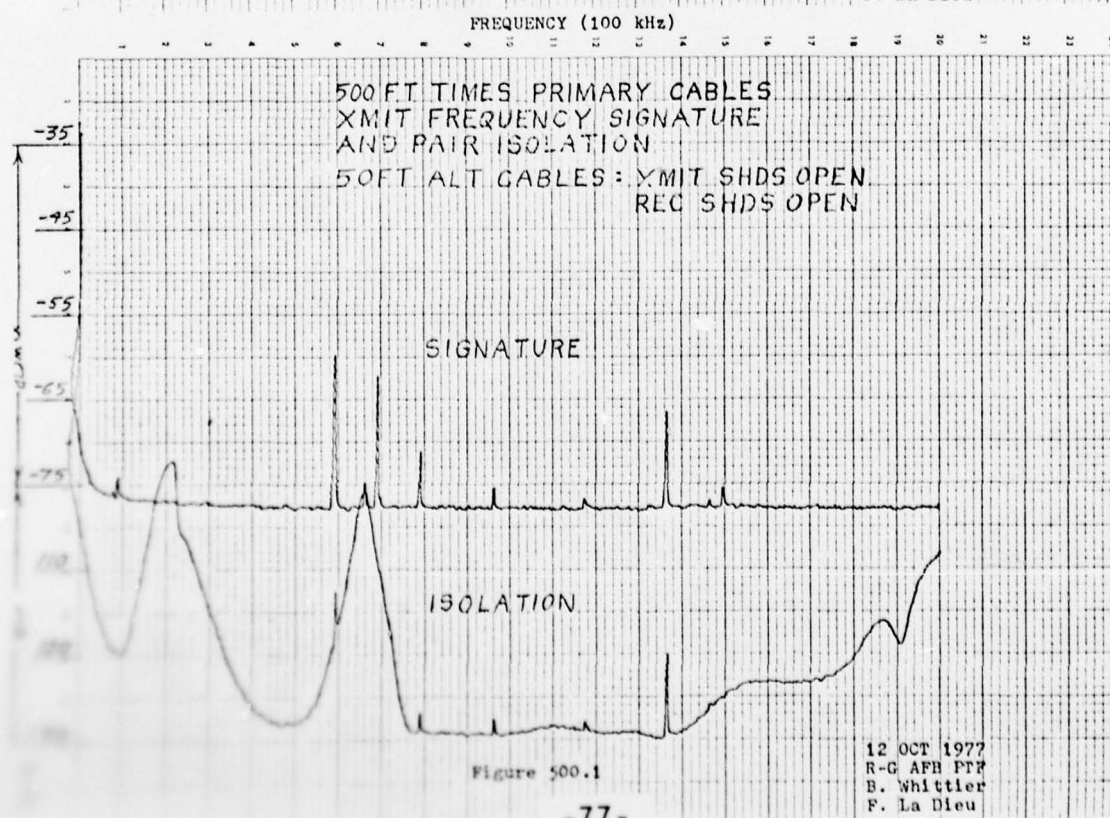
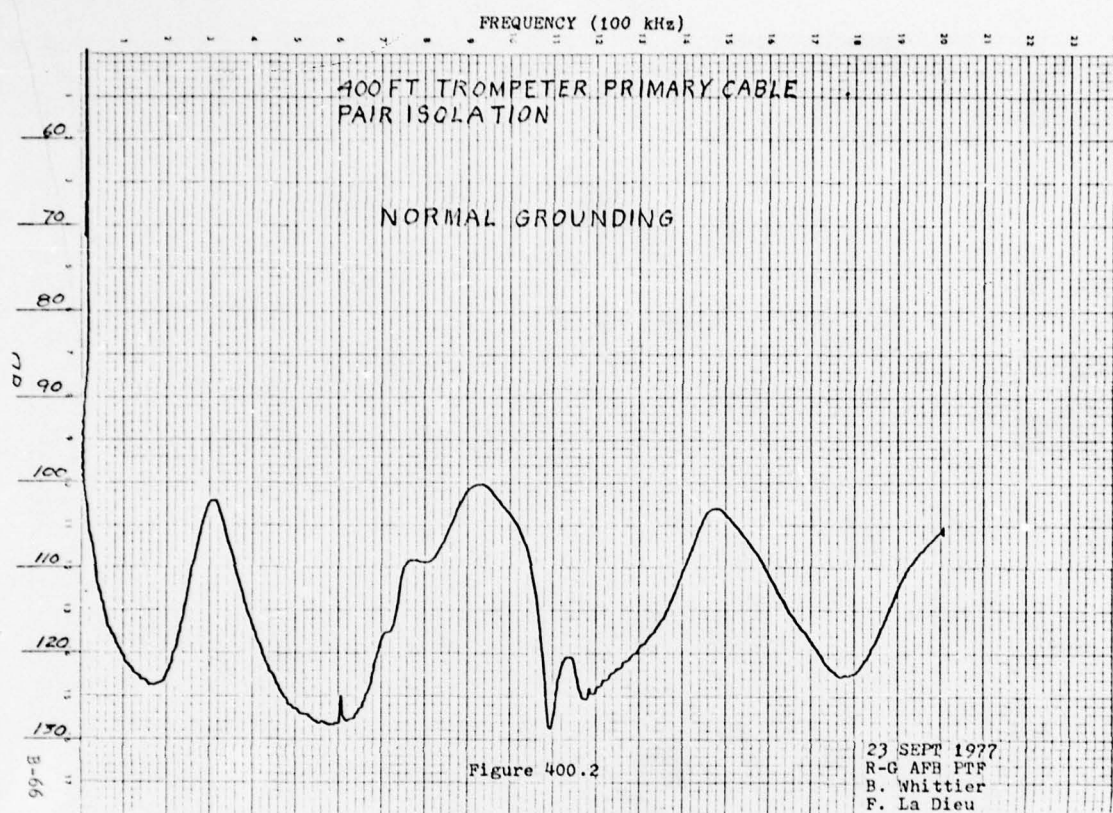


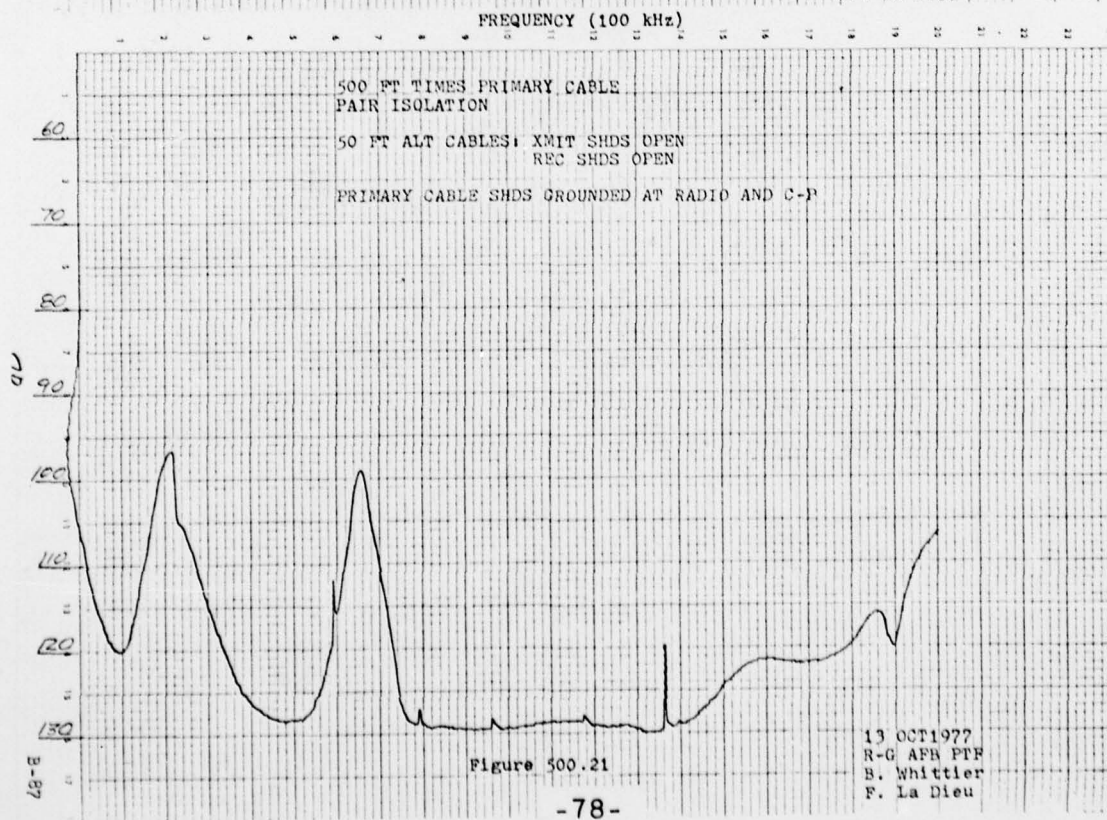
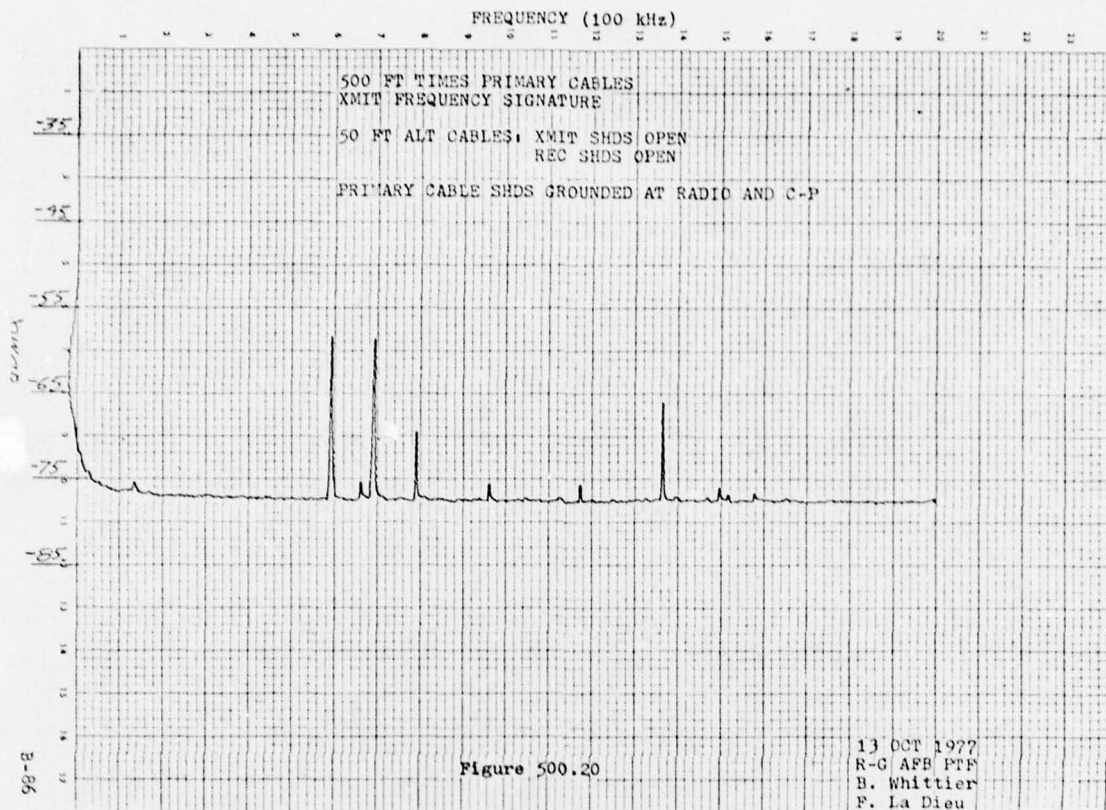




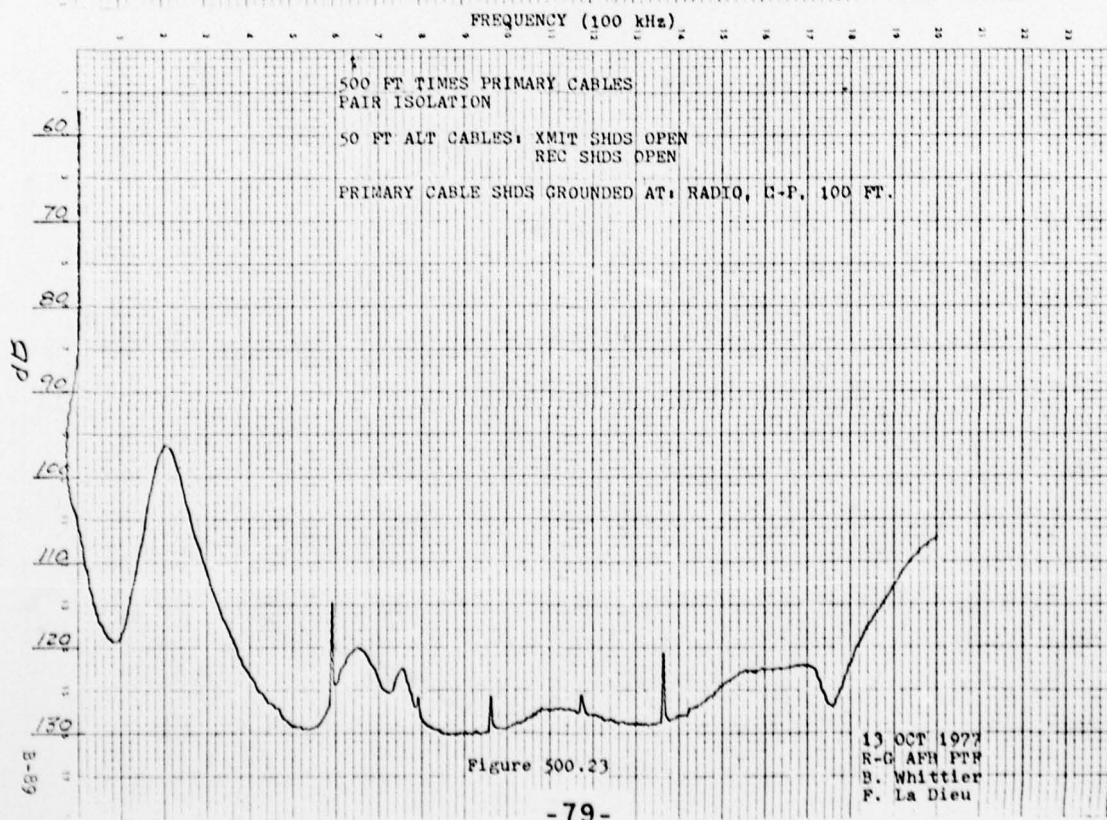
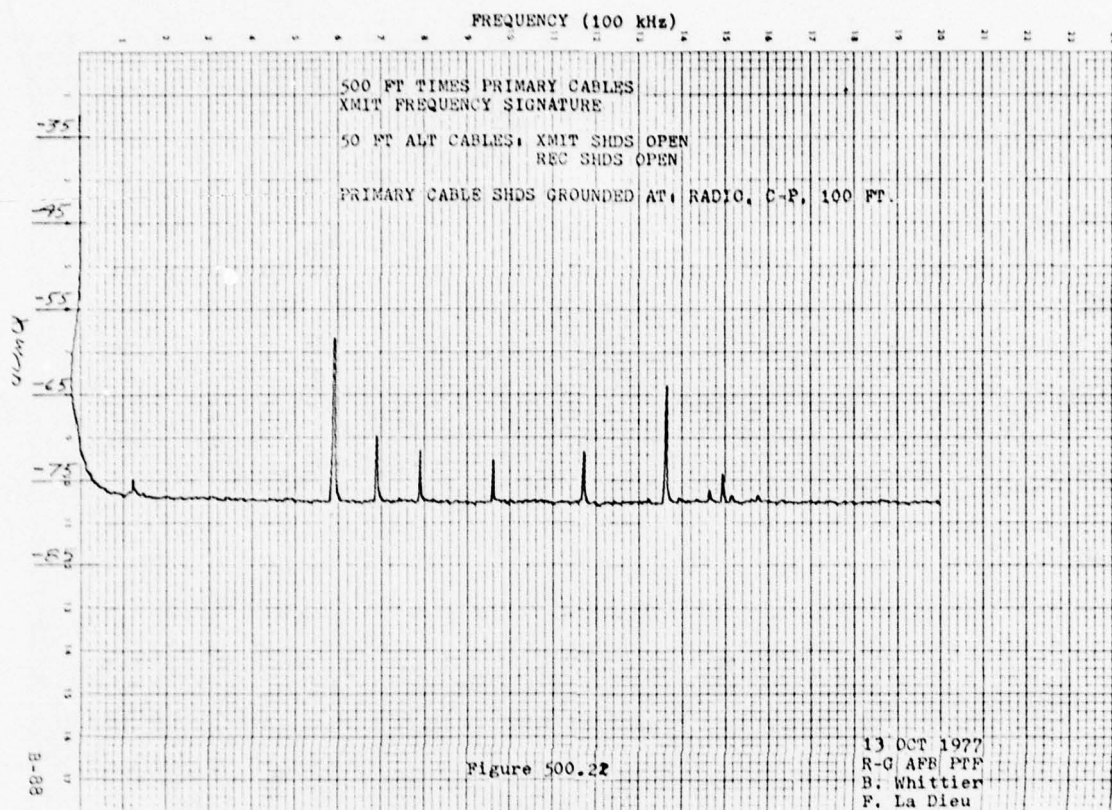


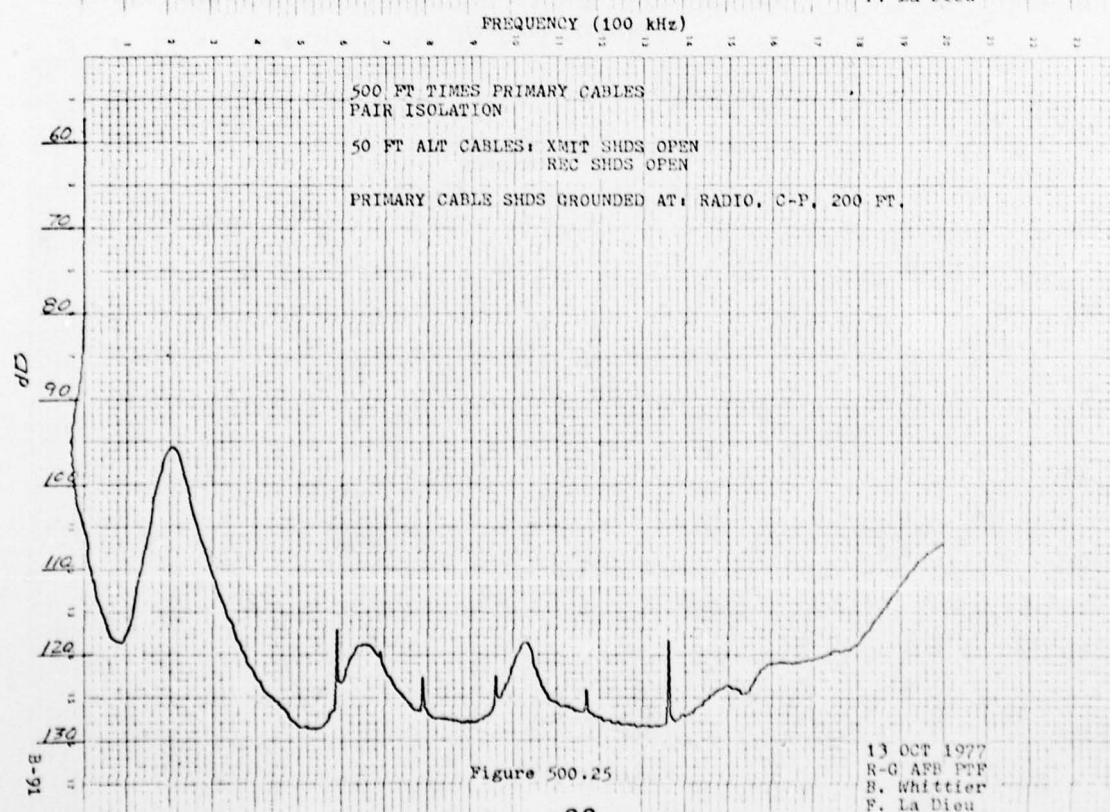
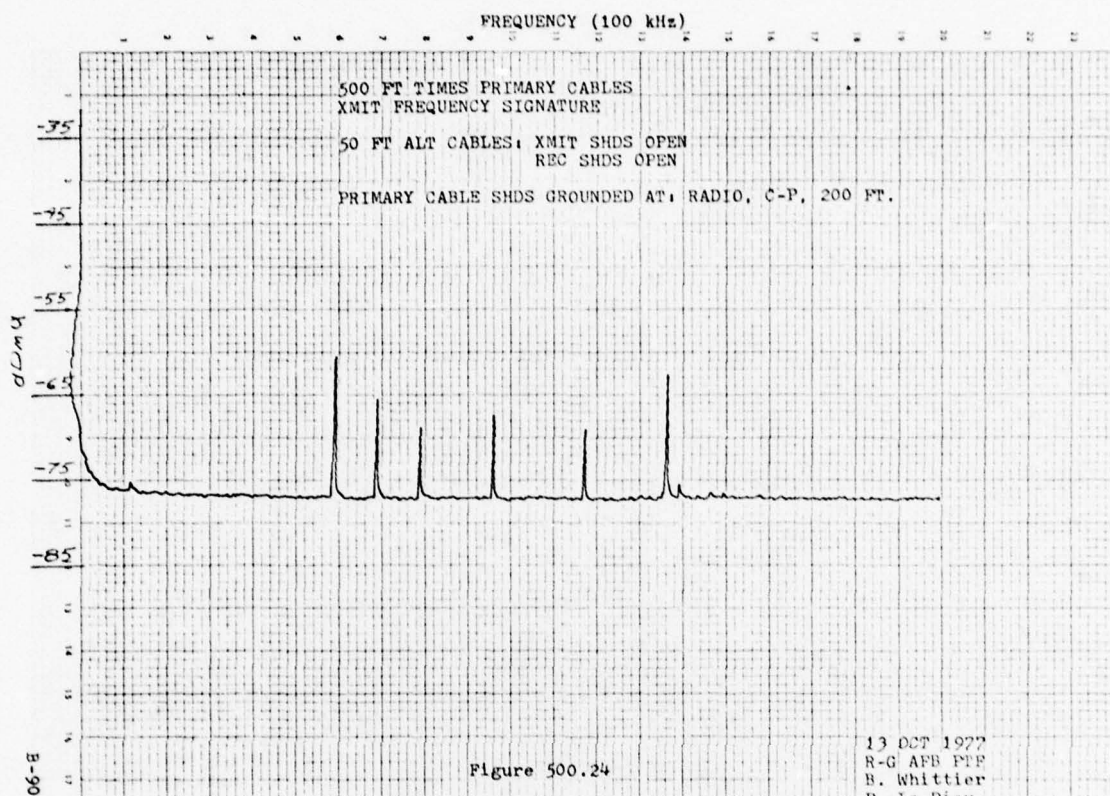


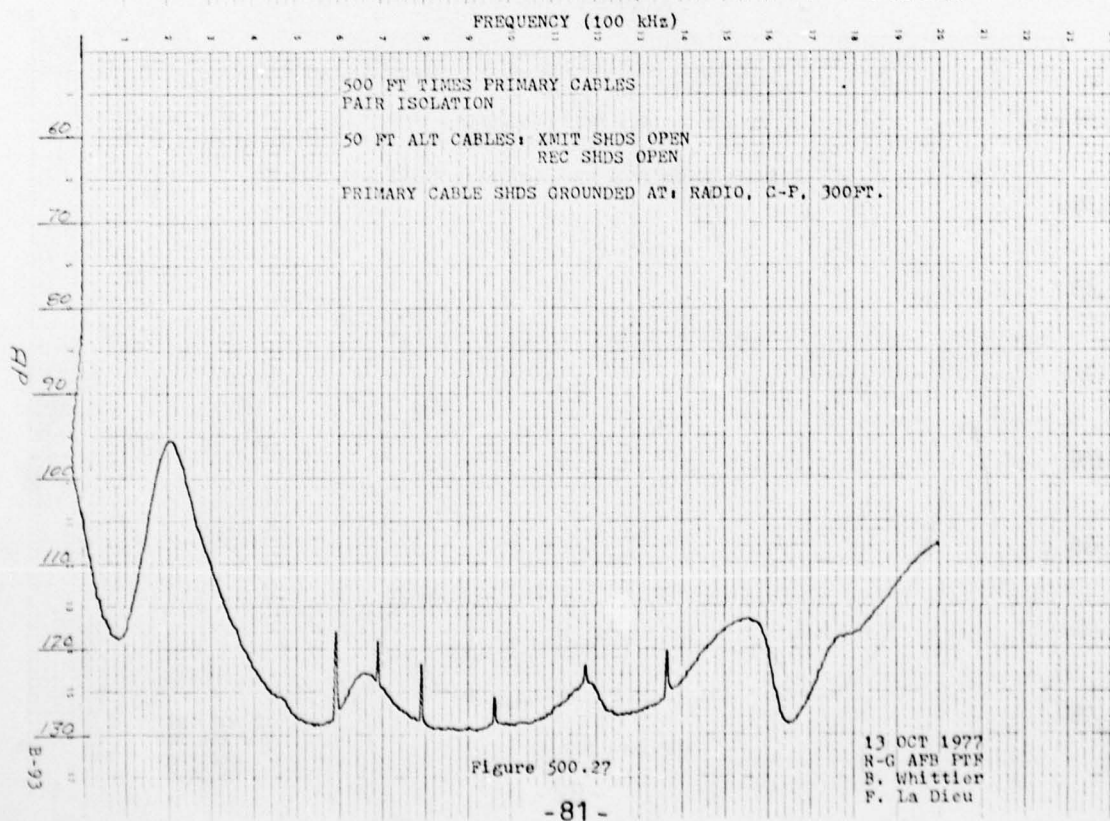
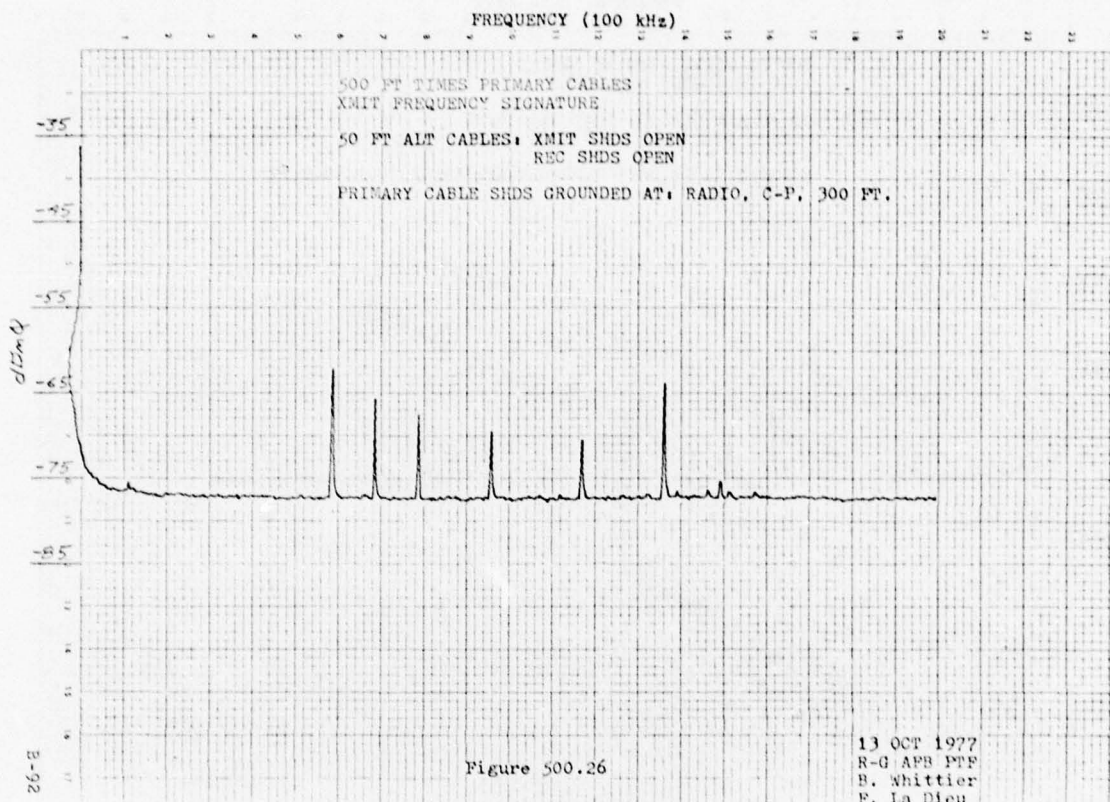




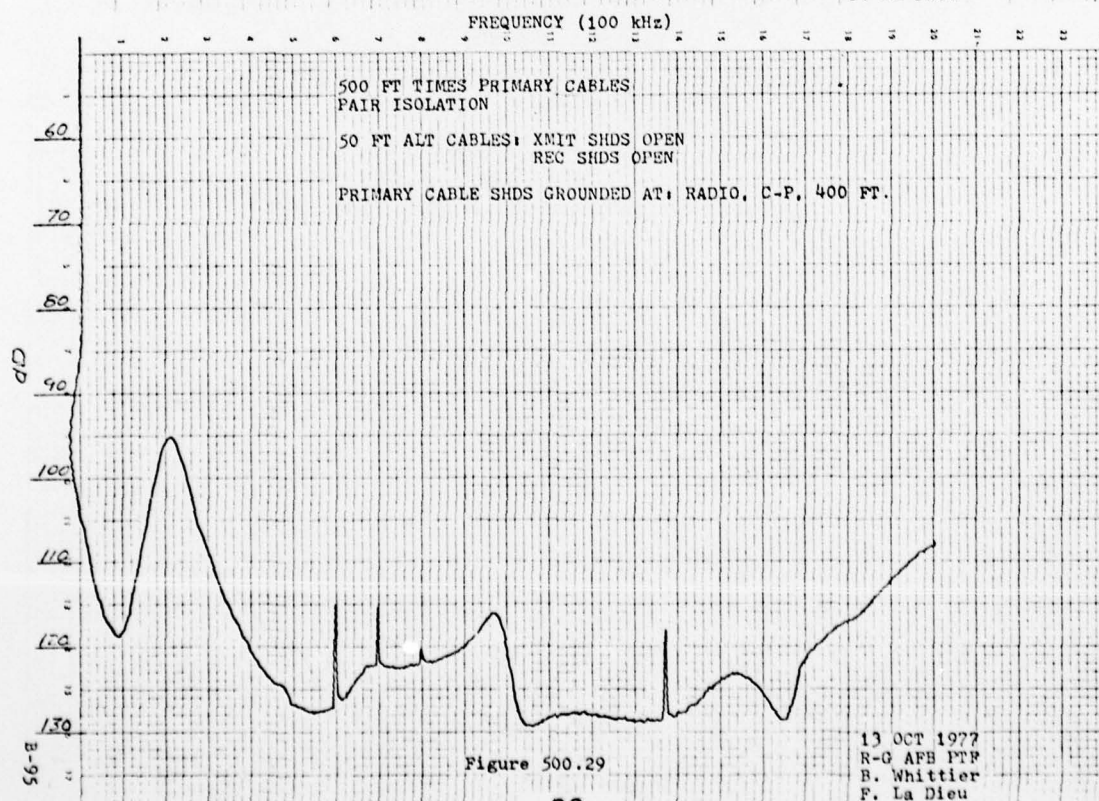
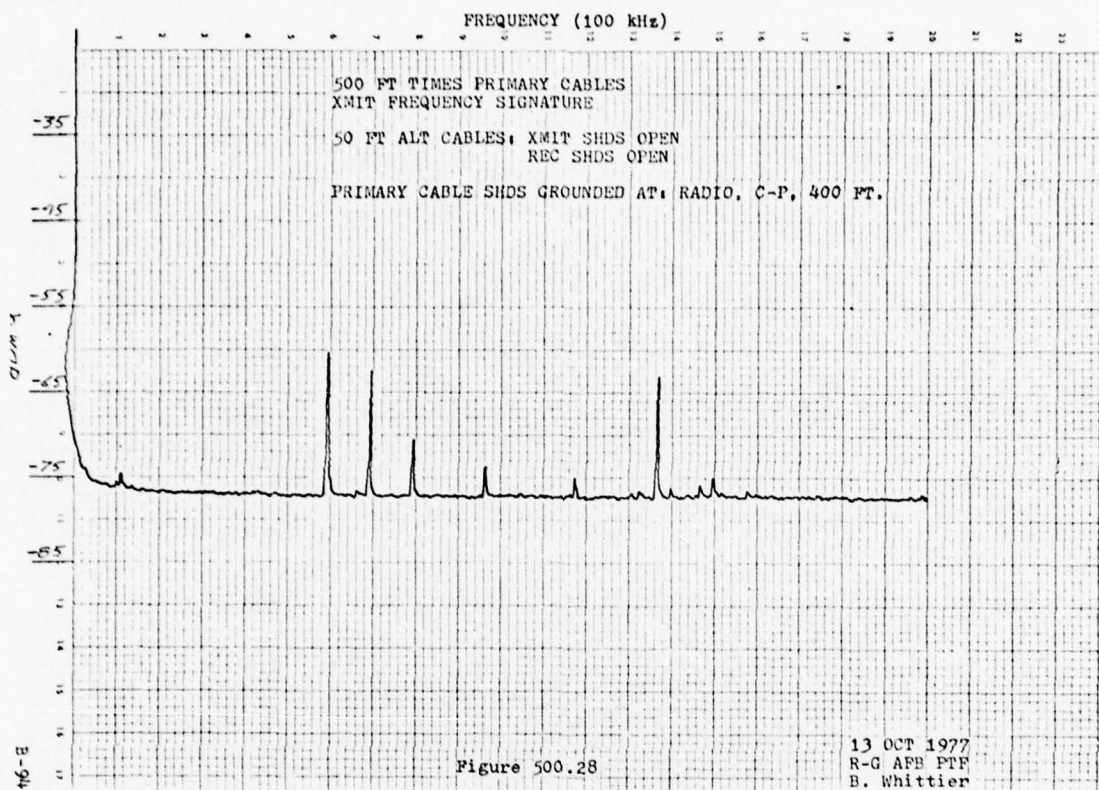


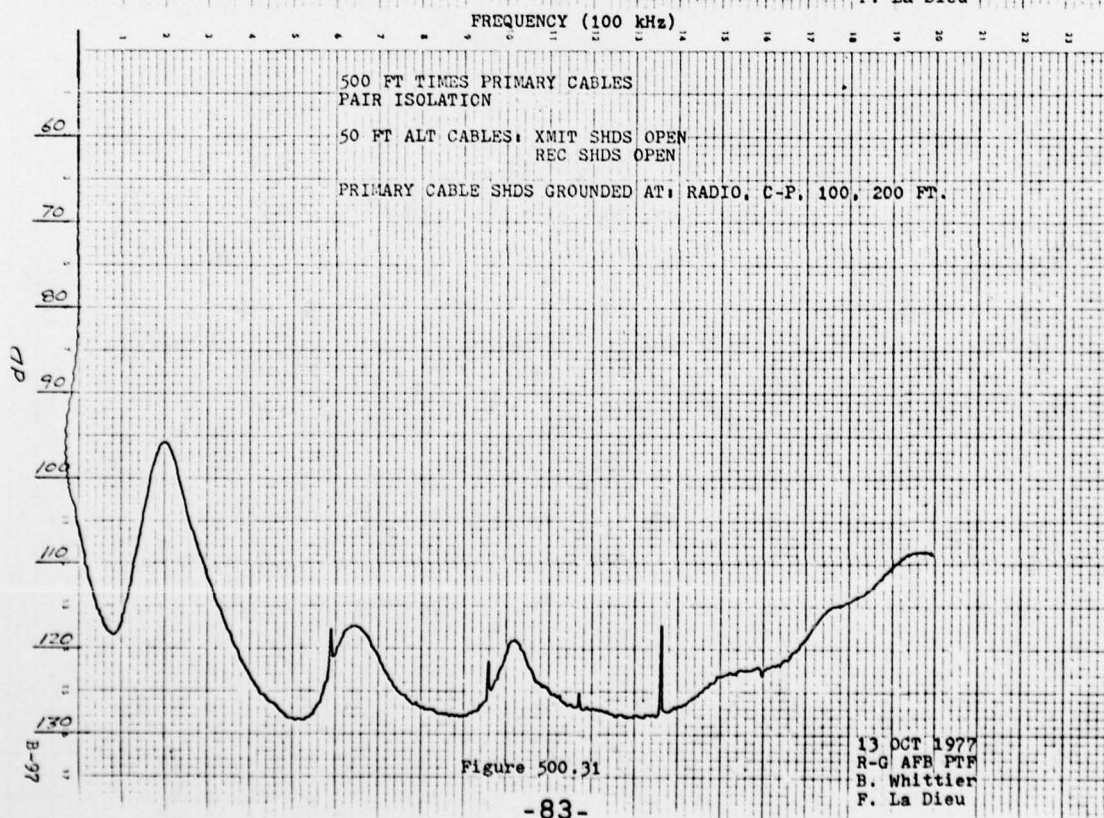
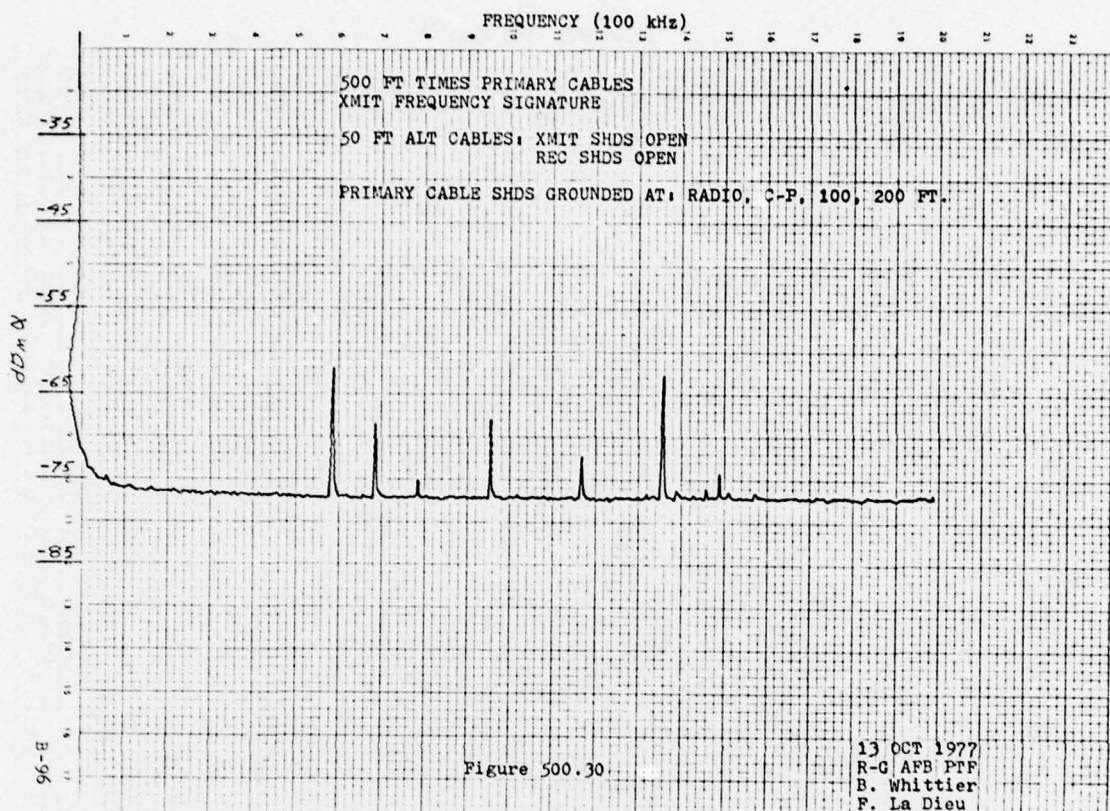




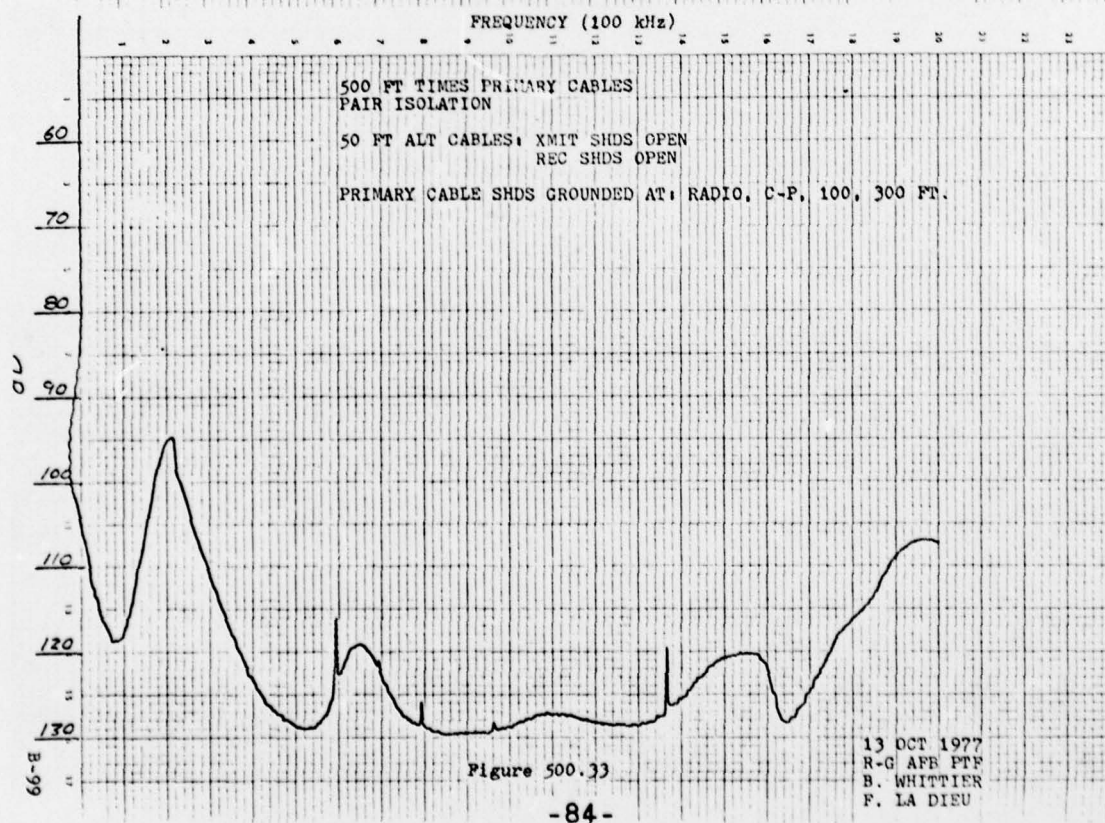
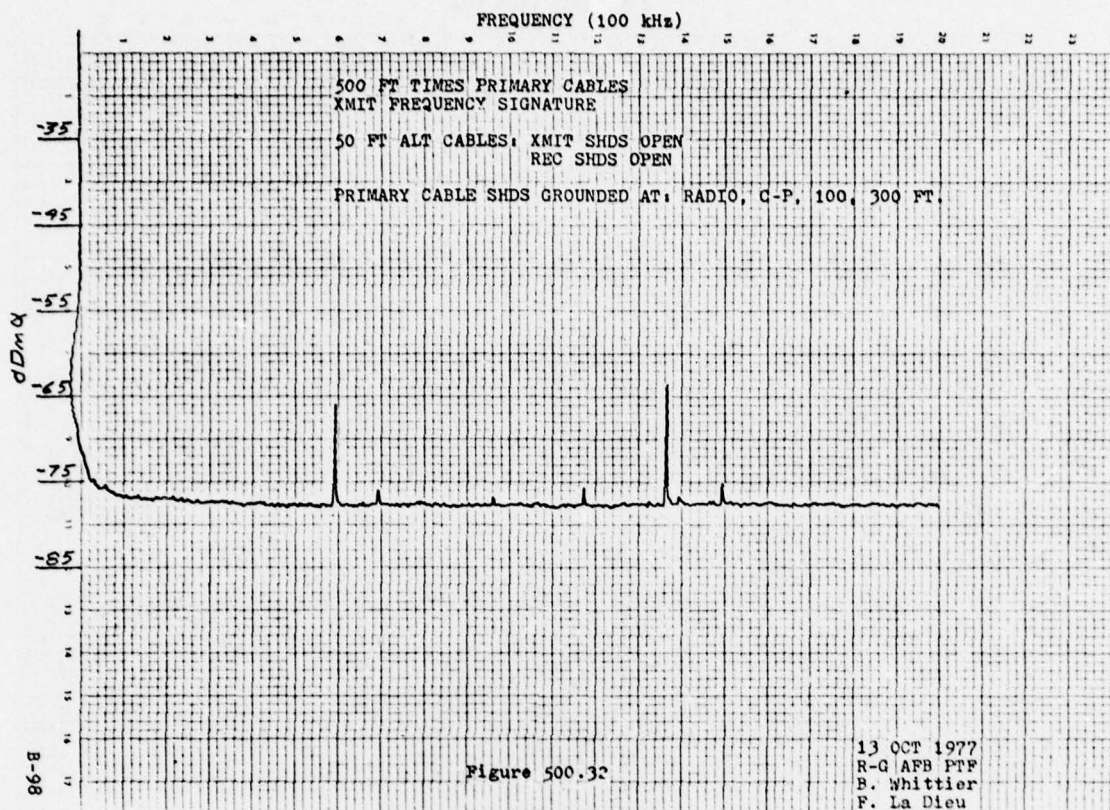




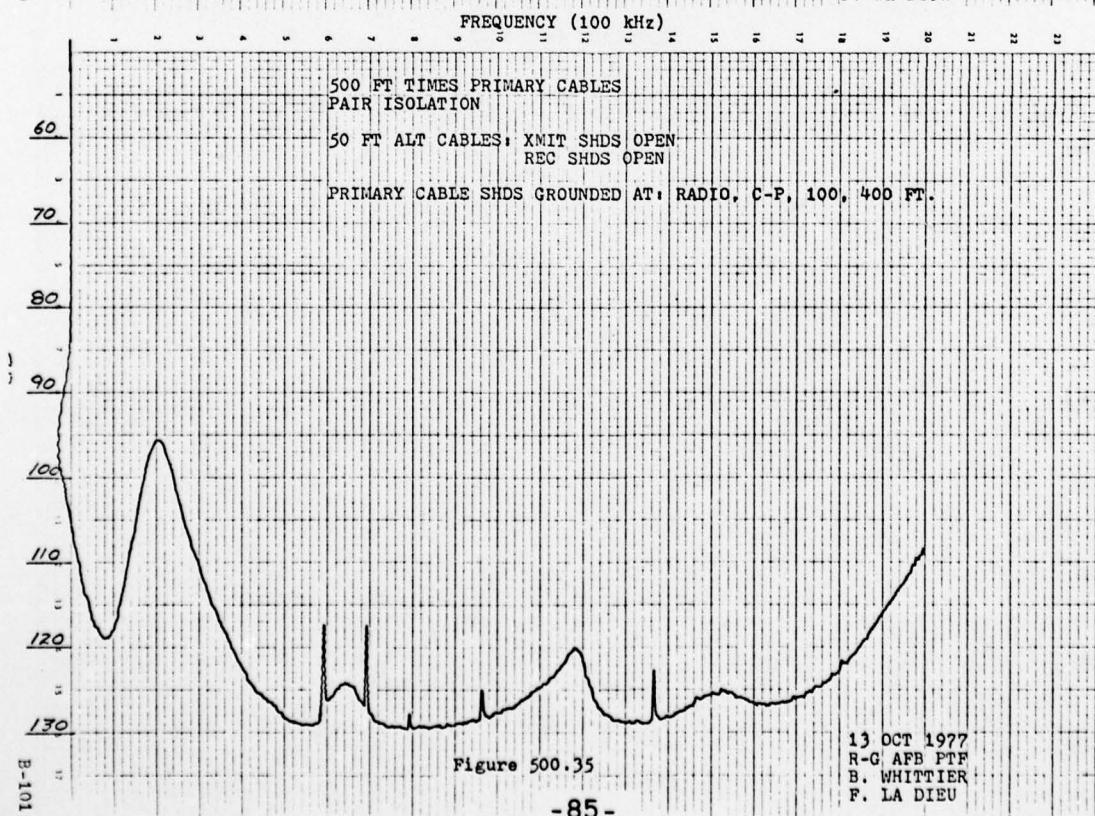
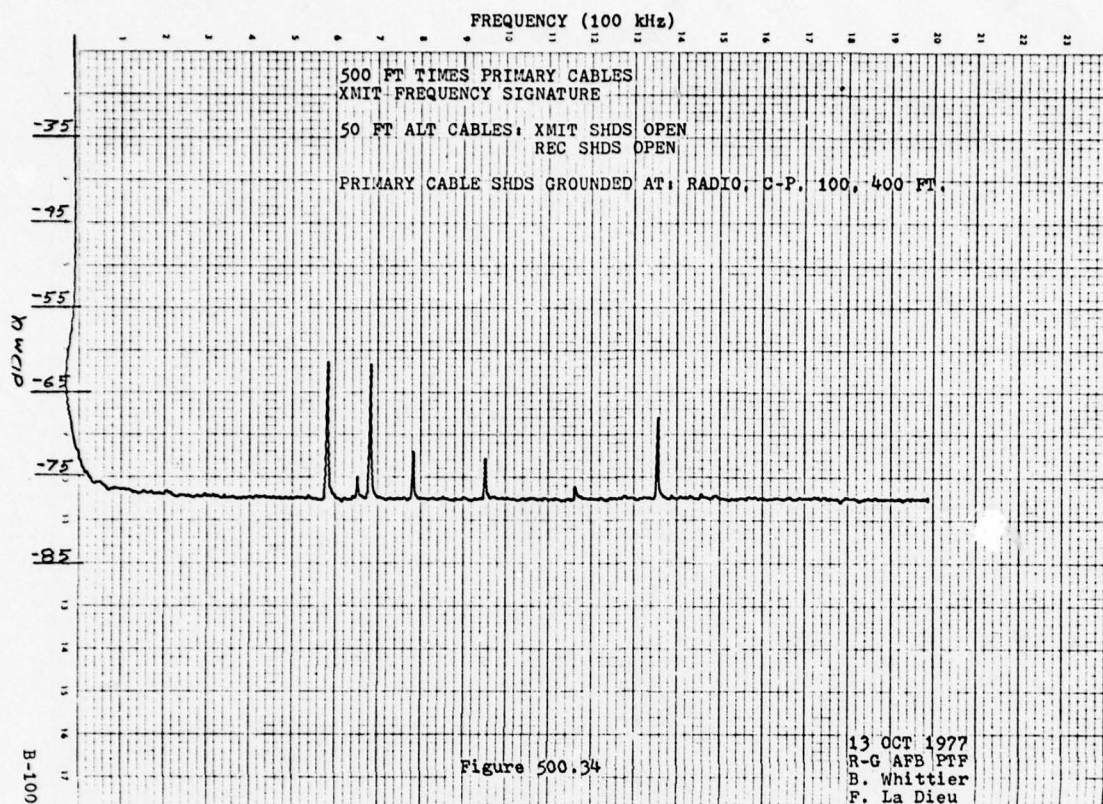


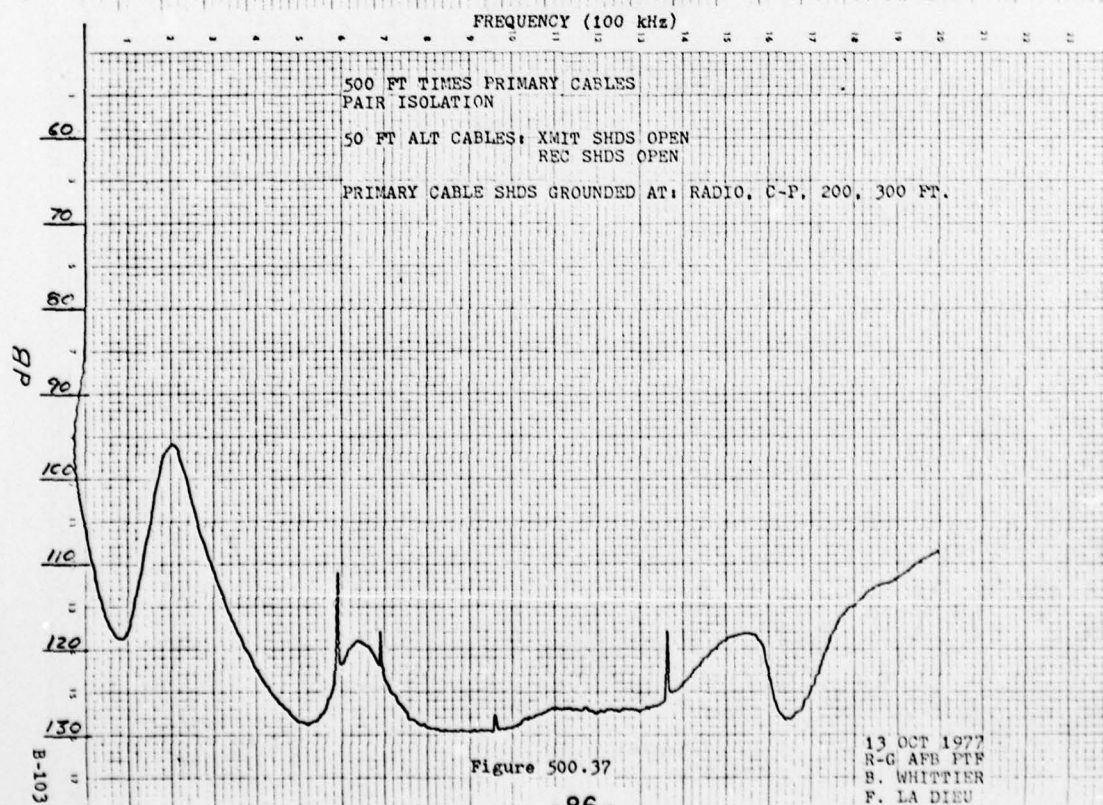
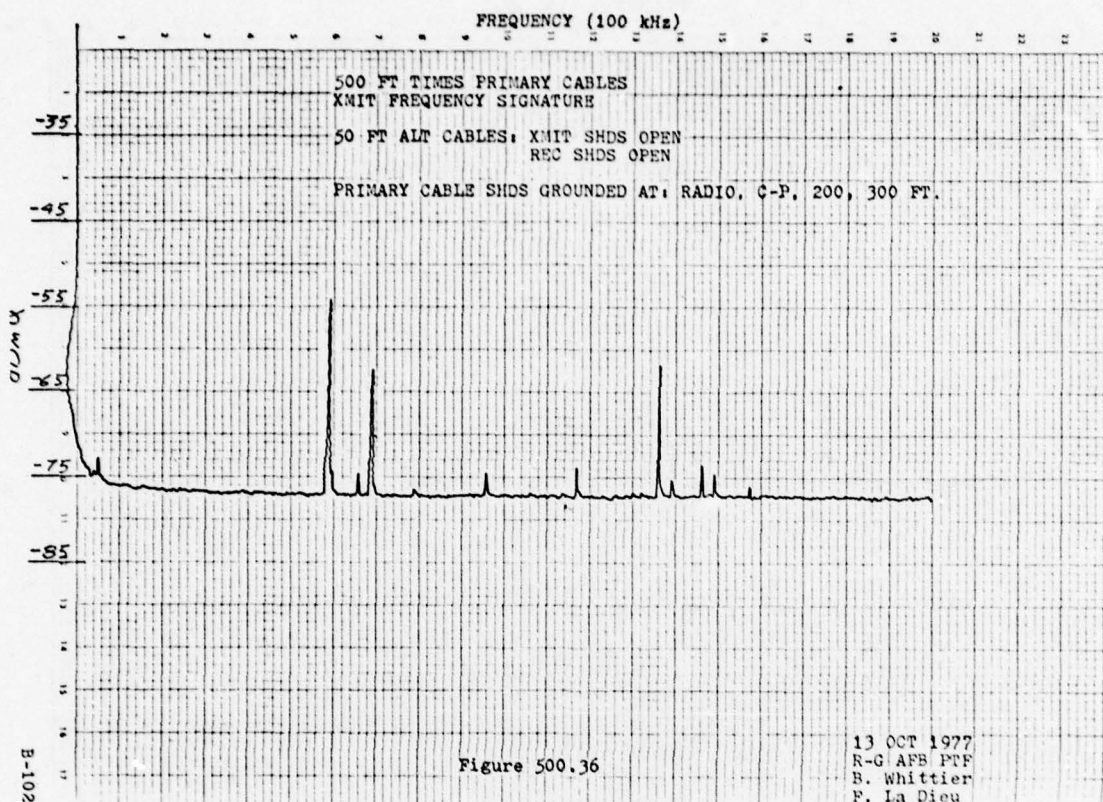




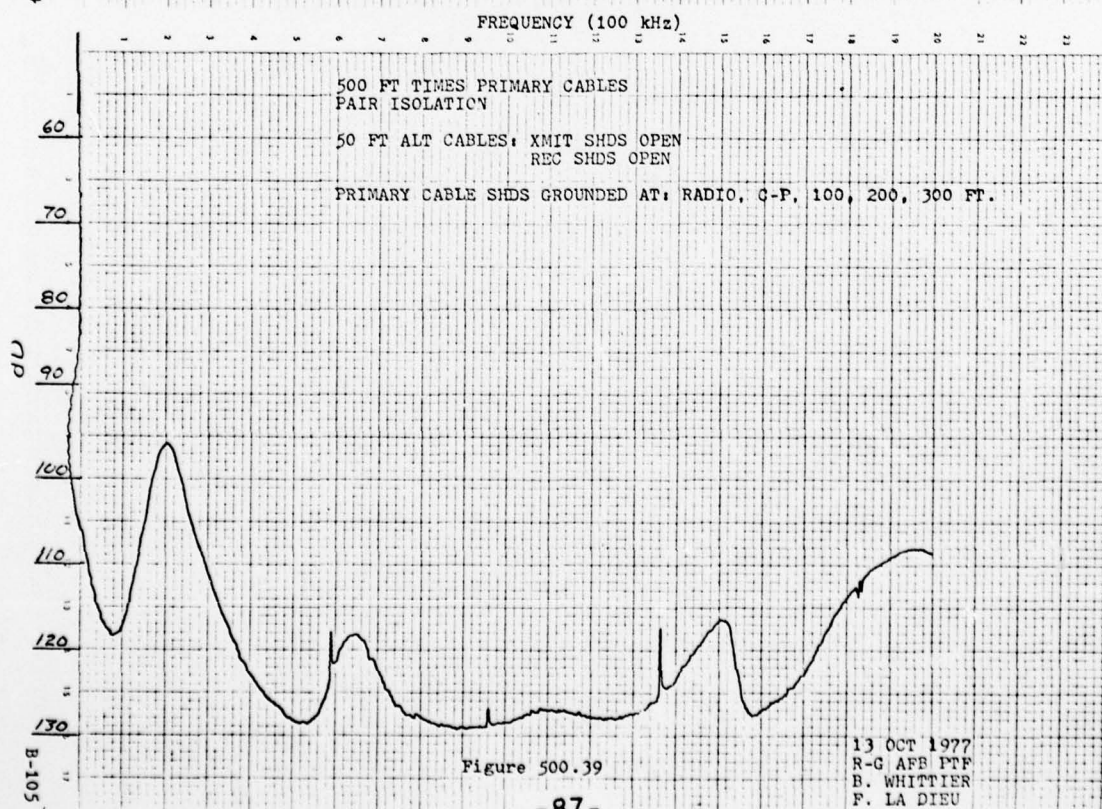
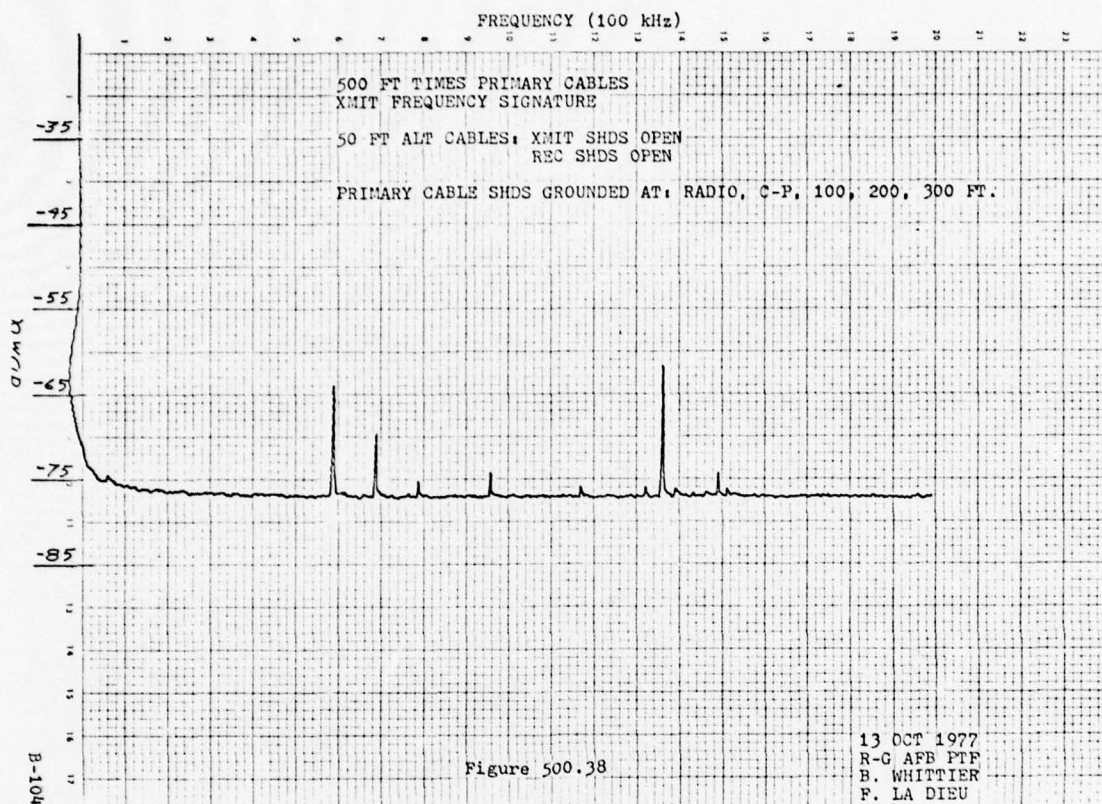




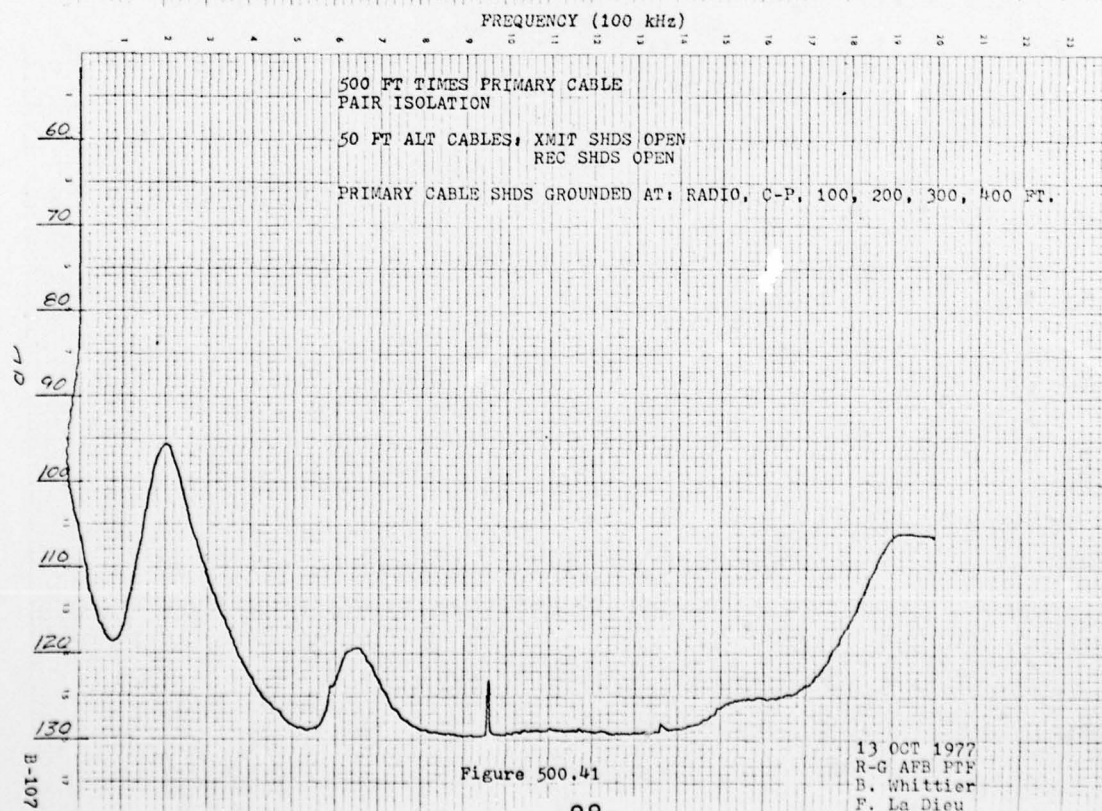
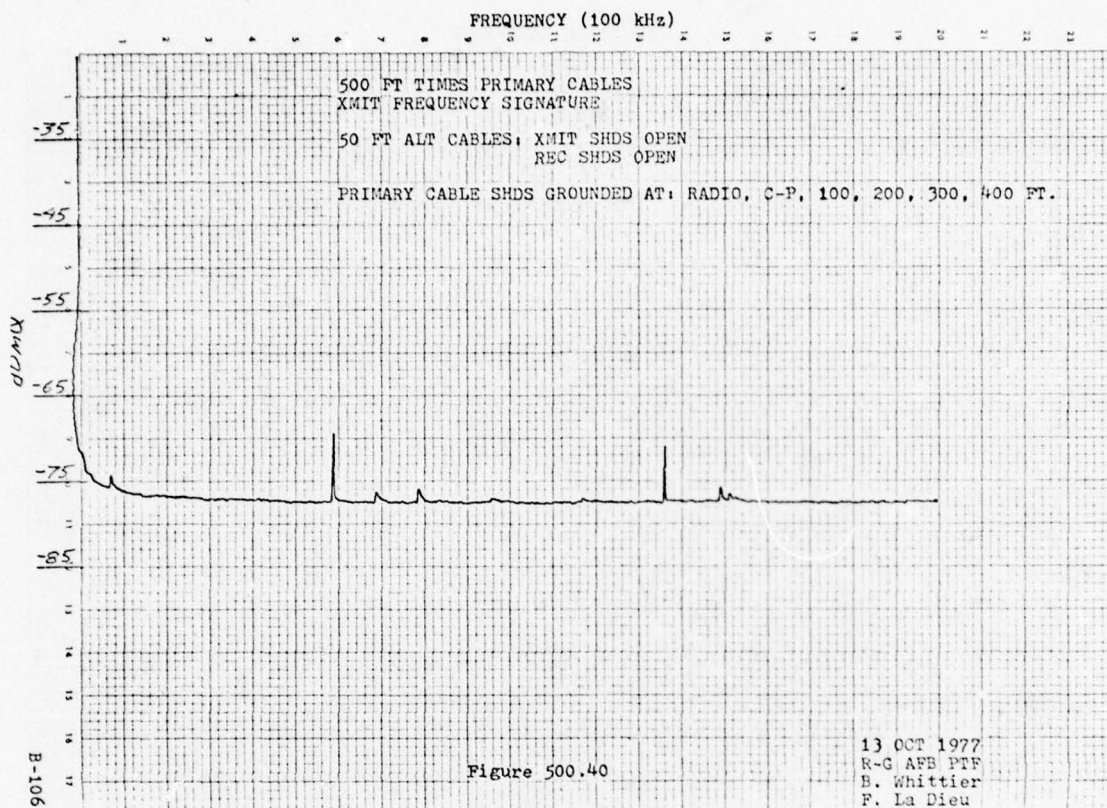












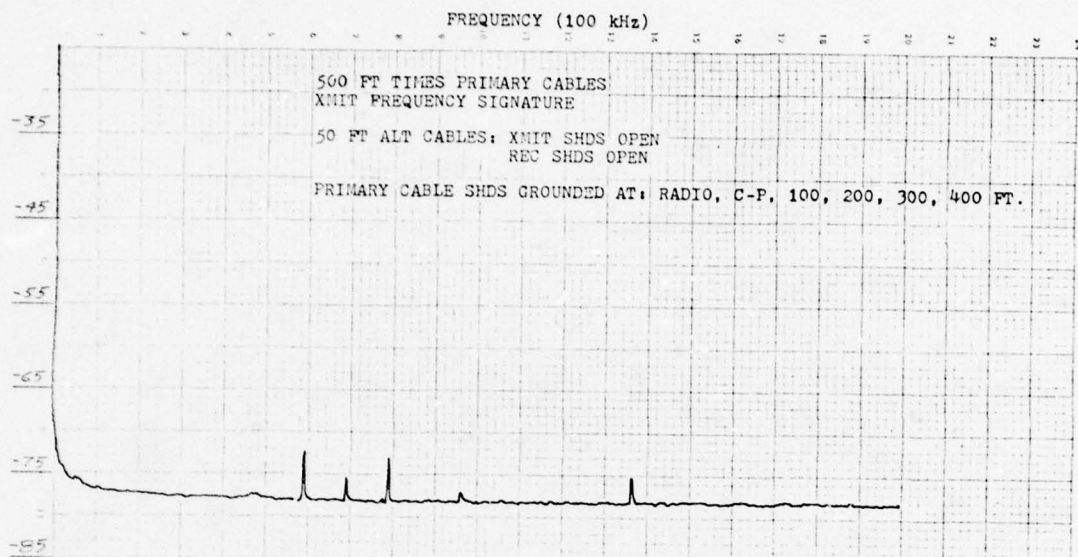


Figure 500.42

14 OCT 1977  
R-G AFB PTF  
B. Whittier  
F. La Dieu

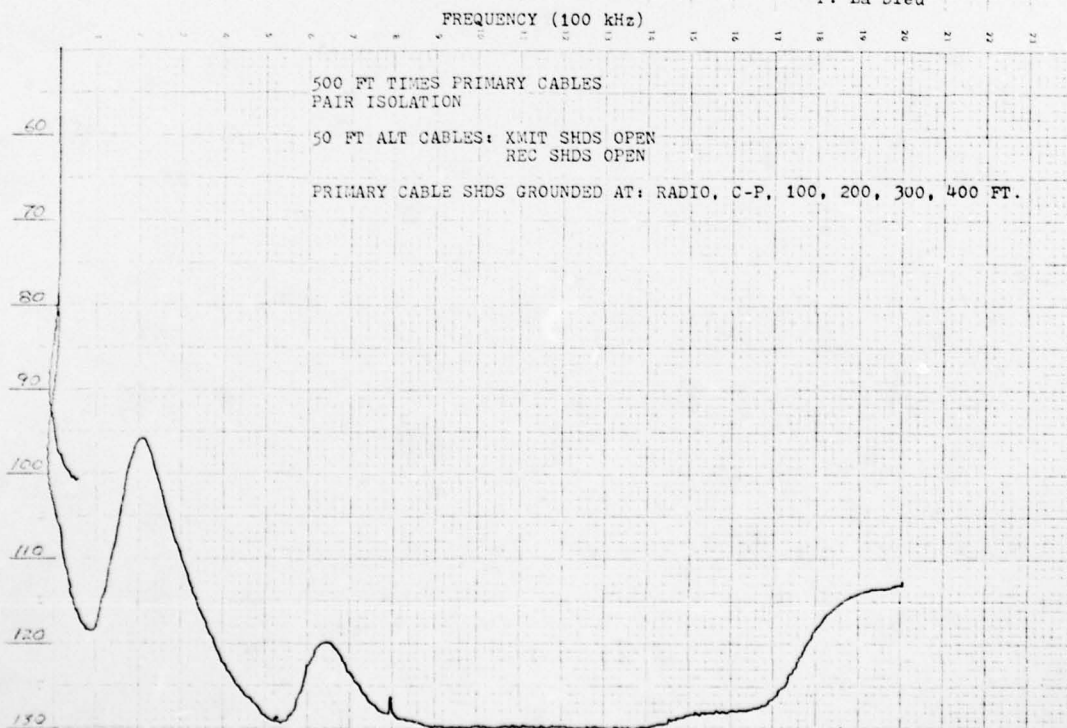
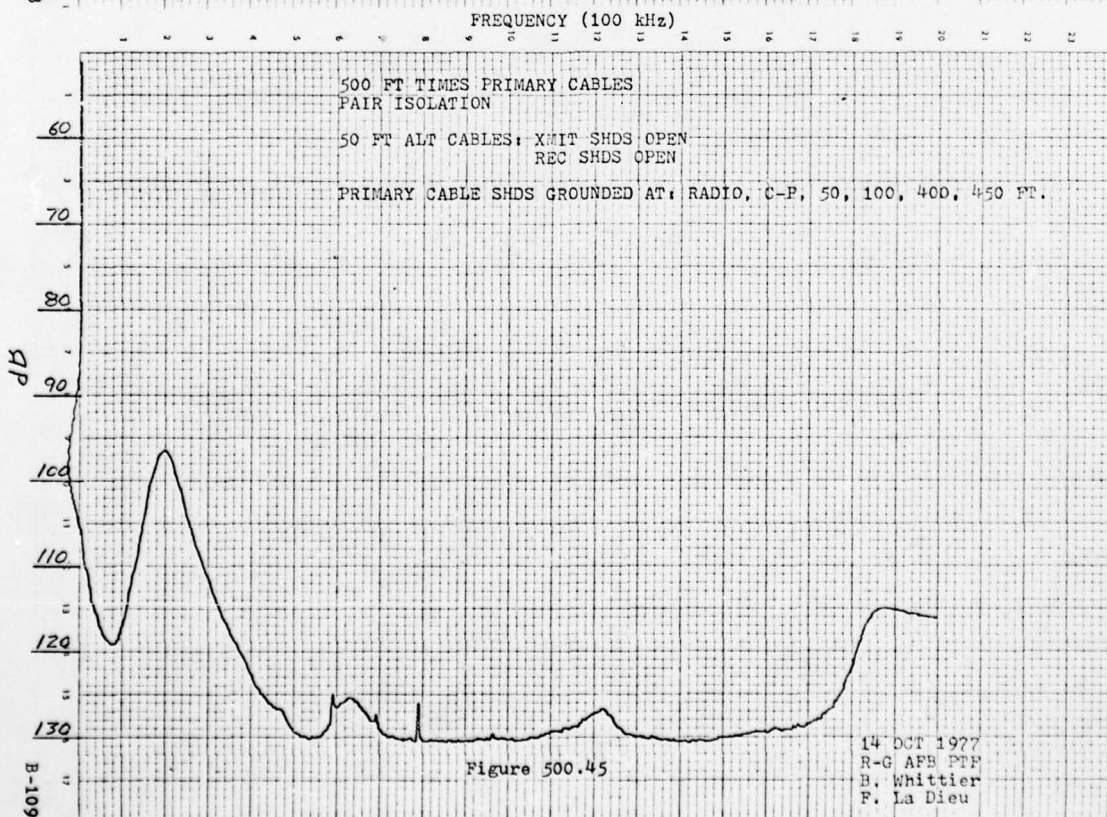
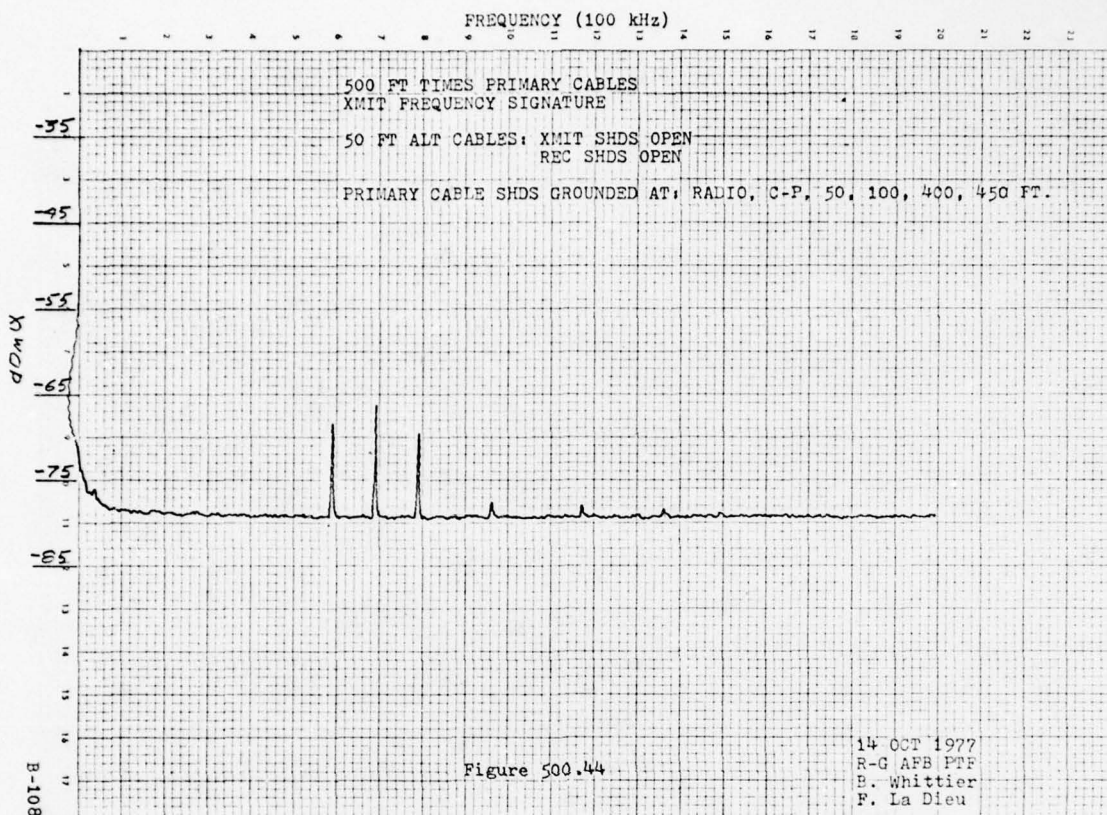


Figure 500.43

14 OCT 1977  
R-G AFB PTF  
B. Whittier  
F. La Dieu





AD-A058 797 GEORGIA INST OF TECH ATLANTA

GEORGIA INST OF TECH ATLANTA

F/G 4/1

FEDERAL AVIATION ADMINISTRATION-GEORGIA INSTITUTE OF TECHNOLOGY--ETC(U)

MAY 78

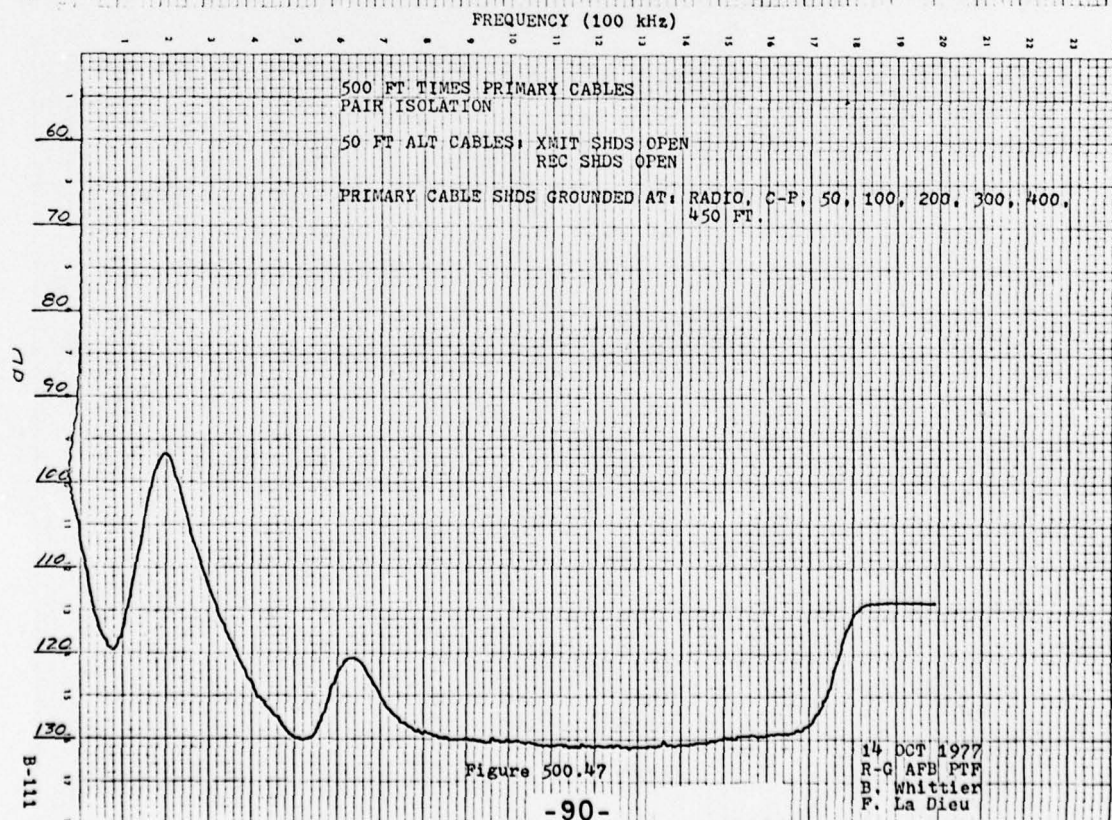
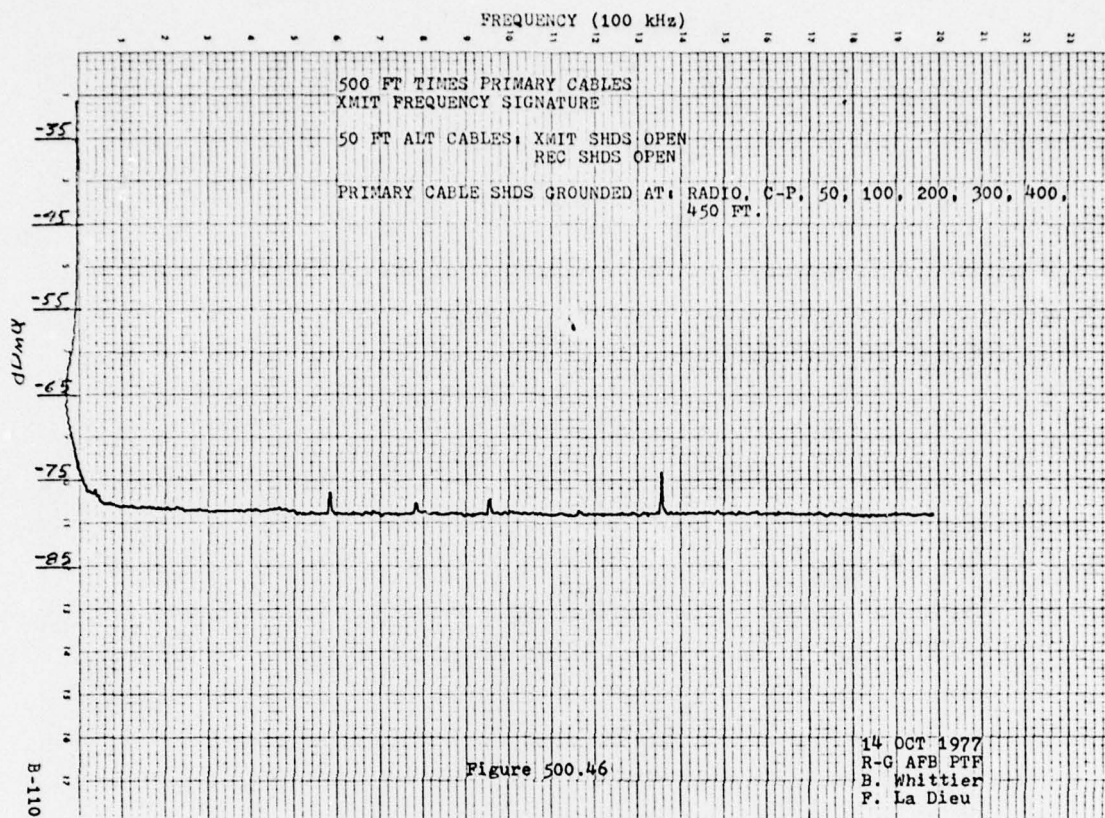
UNCLASSIFIED

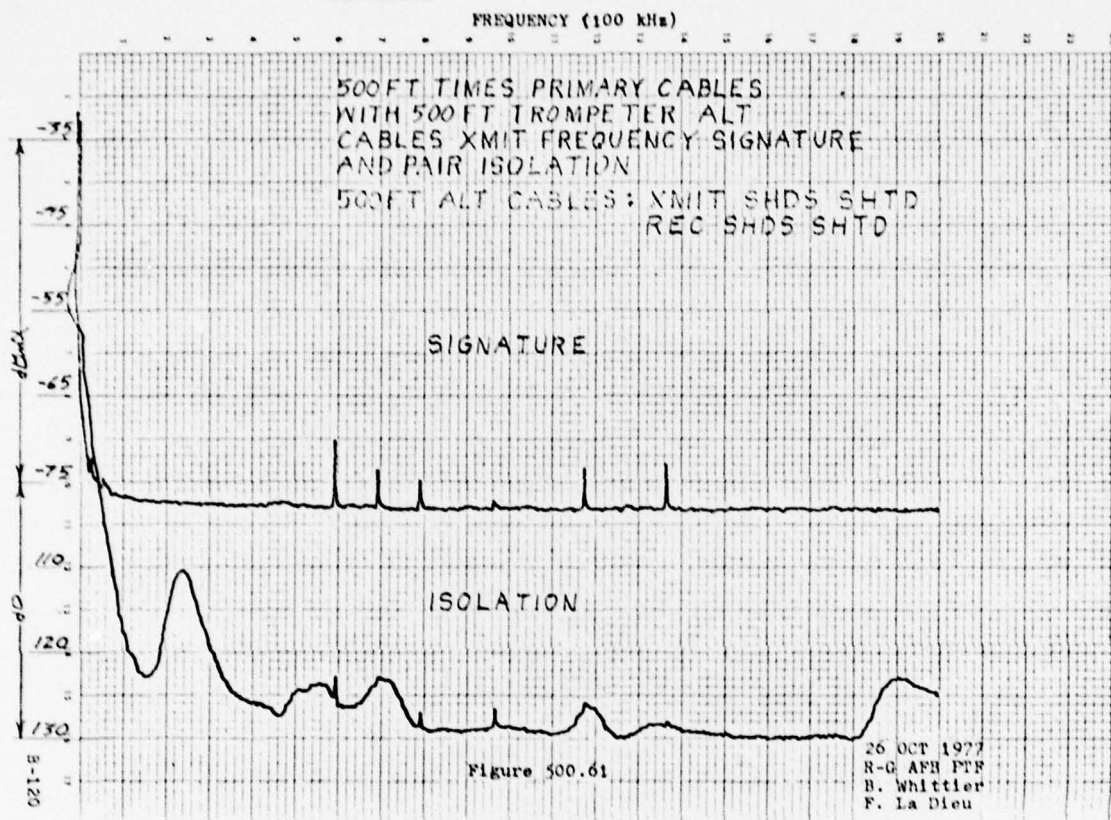
FAA-RD-78-83

NL

2 of 5

AD  
A058 797







ABSTRACT

THE ROLE OF INDUCTANCE IN LIGHTNING PROTECTION

BY  
J.A. Plumer

Lightning Technologies, Inc.  
560 Hubbard Avenue  
Pittsfield, Massachusetts 01201

Presented at  
Federal Aviation Administration/  
Georgia Institute of Technology  
Workshop on Grounding and Lightning Protection

PRECEDING PAGE BLANK

## ABSTRACT

While much has been written about the need to provide low resistance paths for lightning currents, it is equally important to provide paths of low inductance. This paper shows how to calculate the inductance of typical paths, how inductance causes problems, and how inductance may also be used to advantage.

## The Role of Inductance in Lightning Protection

by  
J.A. Plumer  
Lightning Technologies, Inc.  
560 Hubbard Avenue  
Pittsfield, Massachusetts 01201

### Introduction

Much has been written about the role of grounding in lightning protection, and the desirability of having lightning grounds provide a low resistance to the earth. A low-resistance path is preferred, of course, for two reasons:

1. to provide a direct path for lightning currents to flow into the earth, and
2. to minimize voltages that arise during lightning current flow along this path.

Provision of a low *resistance* ground by itself, however, will not assure that the above two objectives will be met because significant voltage rises and impedances to lightning current flow may occur along low resistance ground paths if the *inductance* of these paths is not also made low.

Emphasis upon low resistance ground paths also appears in literature related to electrical bonding, with the criteria for an electrical bond designed to carry lightning currents being given in terms of the bond resistance only. Very often, no restrictions are placed upon the inductance of a bond, with the result that lightning currents encounter excessive inductance and seek alternate paths; sometimes with destructive results.

### What Is Inductance?

Inductance is the property of a conductor that allows energy to be stored in a magnetic field.

Surrounding any electric current is a magnetic field. Since this magnetic field is capable of doing work it represents stored energy. The amount of energy that is stored in a magnetic field depends on the number of electric current paths in the neighborhood and the intensity of the current in these paths. The simplest situation, of course, is a single conductor "by itself" as shown in Figure 1.



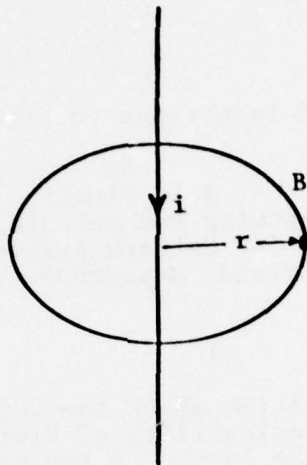


Figure 1 - Magnetic Field around a Single Conductor.

The magnetic field *intensity*,  $B$ , at any point a distance  $r$  away from the conductor is proportional to the current amplitude and diminishes inversely with distance from the outside surface of the conductor as follows:

$$B = \frac{\mu I}{2\pi r} \quad (1)$$

where:

$B$  = magnetic flux density (webers/meter<sup>2</sup>)

$\mu$  = permeability of medium (henrys/meter)

=  $4\pi \times 10^{-7}$  H/m for air

$i$  = current in the conductor (amperes)

$r$  = radial distance from the conductor (meters)

The total magnetic field around this wire is equal to the integral of the flux density from the surface of the conductor (where the flux density is very intense) out to where its value is insignificant. This may be expressed per meter of conductor length as:

$$\phi = \int_{r_1}^R \frac{\mu i}{2\pi r} dr = \frac{\mu i}{2\pi} \int_{r_1}^R \frac{dr}{r} \quad \text{webers/meter}$$

where:

$\phi$  = magnetic flux linkages (webers)

$r_1$  = the radius of the conductor

$R$  = a large distance away from the conductor, where  $B$  is very small

For example, the magnetic flux surrounding an AWG 4/0 ground conductor with a radius,  $r_1$ , of 0.66 cm is:

$$\begin{aligned}\phi &= \frac{\mu i}{2\pi} \ln\left(\frac{R}{r_1}\right) = 2 \times 10^{-7} \ln\left(\frac{1000\text{m}}{0.0066\text{m}}\right) \quad \text{webers/meter} \quad (3) \\ &= 2 \times 10^{-7} (11.93) = 2.39 \times 10^{-6} i \quad \text{webers per ampere of} \\ &\quad \text{current, per meter of} \\ &\quad \text{conductor length}\end{aligned}$$

The *inductance*,  $L$ , of a conductor is defined as the ratio of the magnetic field surrounding a conductor to the current that produces it and is measured in *henrys*. Thus:

$$L = \frac{\phi}{i} = \frac{\text{webers/meter}}{\text{ampere}} = \text{henrys/meter} \quad (4)$$

thus,

$$\text{henrys} = \frac{\text{webers}}{\text{ampere}} \quad (5)$$

and the inductance of the 4/0 conductor mentioned above is:

$$\begin{aligned}L &= \frac{2.39 \times 10^{-6} i}{i} = 2.39 \times 10^{-6} \quad \text{henrys/meter} \quad (6) \\ &= 2.39 \quad \text{microhenrys/meter}\end{aligned}$$

#### Lightning Currents vs. Inductance

As with other energy-storage situations, it is not possible to store the energy in the magnetic field instantaneously. The current and associated field must build up from zero over a finite period of time. The rate at which current can build up ( $\Delta i / \Delta t$ ) is directly proportional to the electrical force (voltage,  $e$ ) behind the current, and inversely proportional to the inductance (capacity to store energy) of the conductor, or:

$$\frac{\Delta i}{\Delta t} = \frac{e}{L} \quad \text{amperes/second} \quad (7)$$

where,

$e$  = the driving voltage (volts)

$t$  = time (seconds)

If, as in the case of a lightning strike, the rate of energy delivery to the conductor is determined by an outside source, then the voltage along the conductor will automatically increase to a level sufficient to allow the lightning current to enter the inductor at the predetermined rate.

Thus,

$$e = L \frac{\Delta i}{\Delta t} = L \frac{di}{dt} \quad \text{volts} \quad (8)$$

Equation 8 is very important because it shows that voltage can arise along a conductor which has no resistance, and that this voltage is proportional to both the inductance and to the rate of change of current flowing in it.

The high amplitude strokes associated with a lightning flash have very fast rates of change. These rates, (also called rate of *rise*) have been recorded by many investigators and summarized by Cianos and Pierce (Reference 1) on Figure 2. These are the rates at which lightning currents may be injected into a ground conductor.

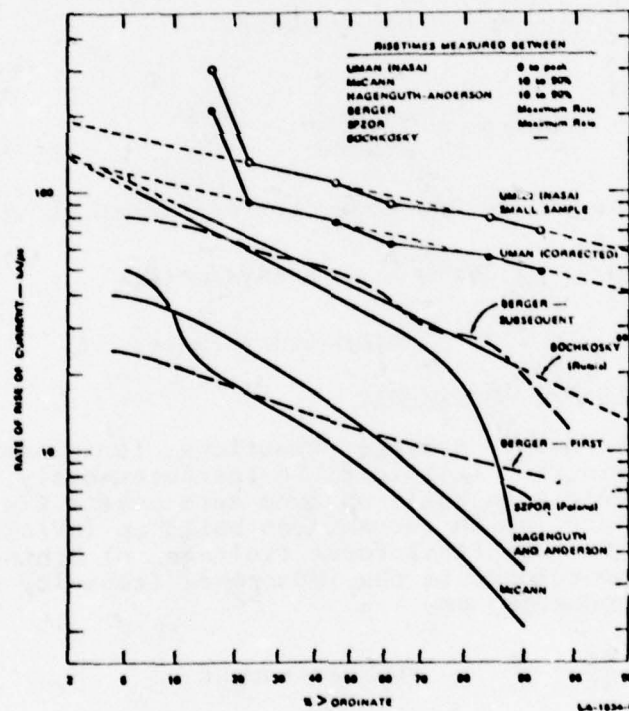


Figure 2 - Statistics of Rate of Current Rise.

It is good practice to design for a maximum expected rate, such as 100 kiloamperes per microsecond, which would be produced by a "severe" stroke occurring only 5% or so of the time. In fundamental units this is  $10^{11}$  amperes per second. A lightning current entering the 4/0 conductor discussed earlier and rising to its peak at a rate of  $10^{11}$  amps/sec would create a voltage of (from equations 3 and 8) :



$$e = L \frac{di}{dt} \quad \text{volts} \quad (9)$$

$$= (2.39 \times 10^{-6} \text{ henrys/meter})(1 \times 10^{11} \text{ amps/sec})$$

$$= 239,000 \text{ volts per meter of conductor length}$$

This voltage would appear along the conductor while the lightning current is changing. When the current reached its peak, it would cease to change and for a moment the inductive voltage would be zero. Then, as the stroke current decays, the inductive voltage would increase again but in the opposite direction as the magnetic field diminishes and energy begins to leave. Using a  $(1-\cos)$  expression to represent a typical stroke wavefront, the stroke current and the inductive voltage that it would produce along the 4/0 ground conductor would appear as shown in Figure 3.

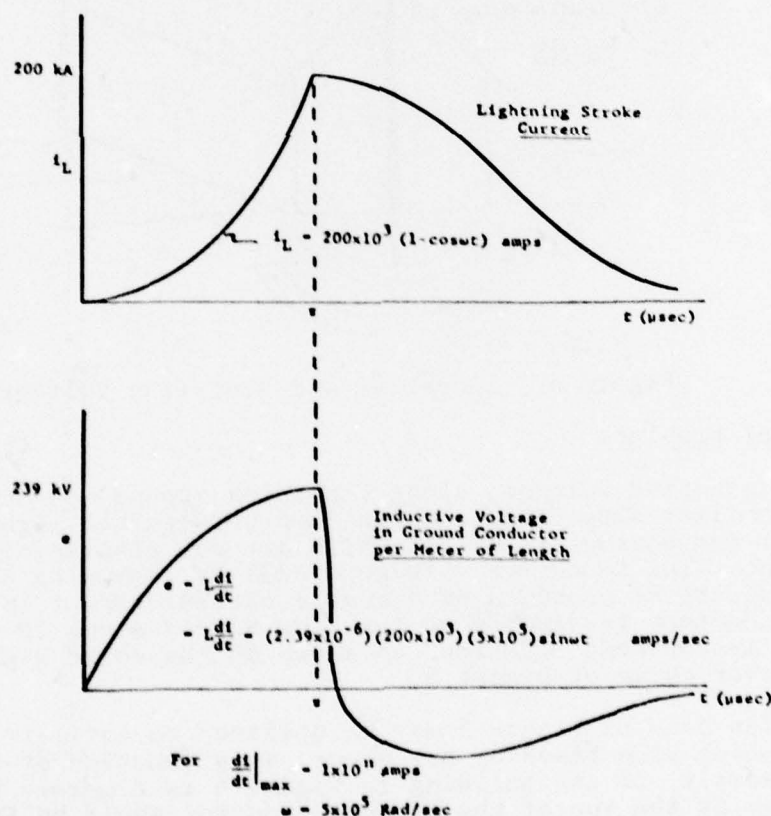


Figure 3 - Severe Lightning Stroke and Inductive Voltages in Ground Conductor

If there is resistance in the ground path, there will also be a resistive voltage rise in accord with ohms law. In most cases the resistance will be associated with the earth connection (ground rod), whereas the inductive voltage will be distributed along the entire ground conductor. This situation is shown in Figure 4.

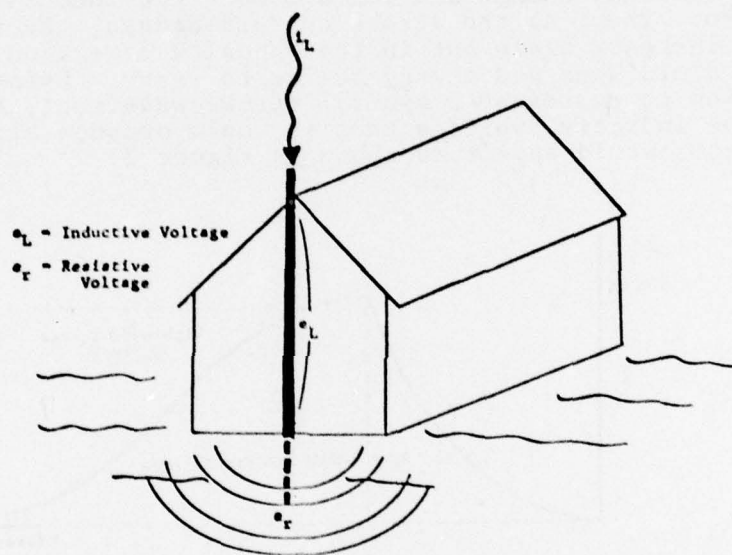


Figure 4 - Inductive and Resistive Voltages.

#### Typical Problems

Inductive voltages along lightning ground conductors cause the familiar side-flashes which jump between the lightning conductor and nearby conductors which are not also carrying lightning current. The inductive voltage of 239 kV, shown by the foregoing analysis to be produced by a severe stroke current in one meter of conductor, is capable of sparking across about 25 cm of air in its 3 microsecond lifetime, as shown on the solid high voltage sparkover curve of Figure 5.

The data of Figure 5 may be utilized to estimate the distances over which side flashing may occur, as a function of conductor length. For example, if the building in Figure 4 is 6 meters high, the voltage at the top of the ground conductor would be (assuming the severe stroke analyzed previously occurred):

$$e_{\text{top}} = (6 \text{ m}) (239 \text{ kV/m}) = 1434 \text{ kV} \quad (10)$$

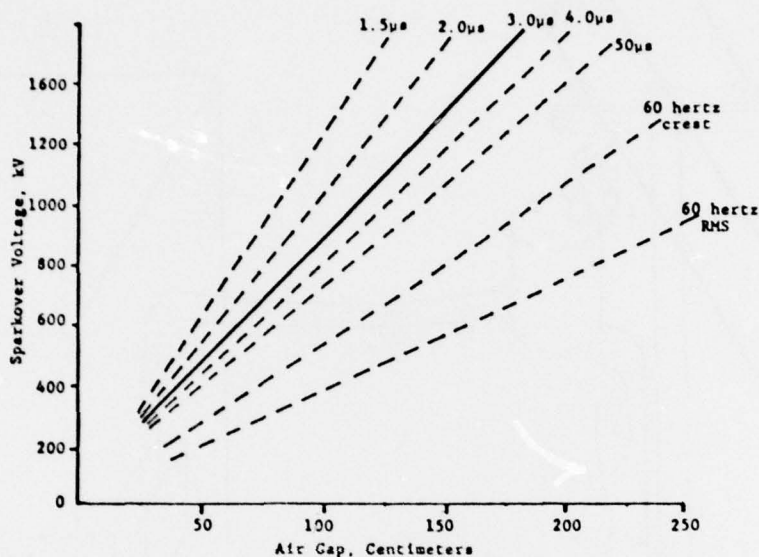


Figure 5 - High Voltage Sparkover Voltage vs. Air Gap Length for Voltages of Various Risetimes.

From Figure 5, this voltage would be sufficient to spark across 150 cm of air. Thus, conducting objects such as water pipes and electric wiring in the upper portion of the building would be subject to side-flashes. When these occur, a portion of the lightning current would leave the ground conductor and flow to earth via the path formed by the side flash. Since most other conductors are not designed to carry lightning currents, damage frequently results.

Inductive voltages are also a frequent cause of electrical surges which can damage electrical or electronic equipment. A very common example of how this occurs is shown in Figure 6.

The maximum value of surge voltage that appears in the building is usually limited by sparkover of terminal boards etc. to about 6 kV. Thus, the lightning arrester protects the transformer but does not protect equipment connected to the transformer secondary. If the power line is protected by an overhead ground wire (often called a shield wire) there will be little difference in the surge produced in the secondary because lightning current must still flow to earth via the pole ground wire. The surge may be reduced, but not eliminated, by bringing the secondary into the building via an underground conduit. Thus, surge suppression must be applied in the building to eliminate the 6kV surge.



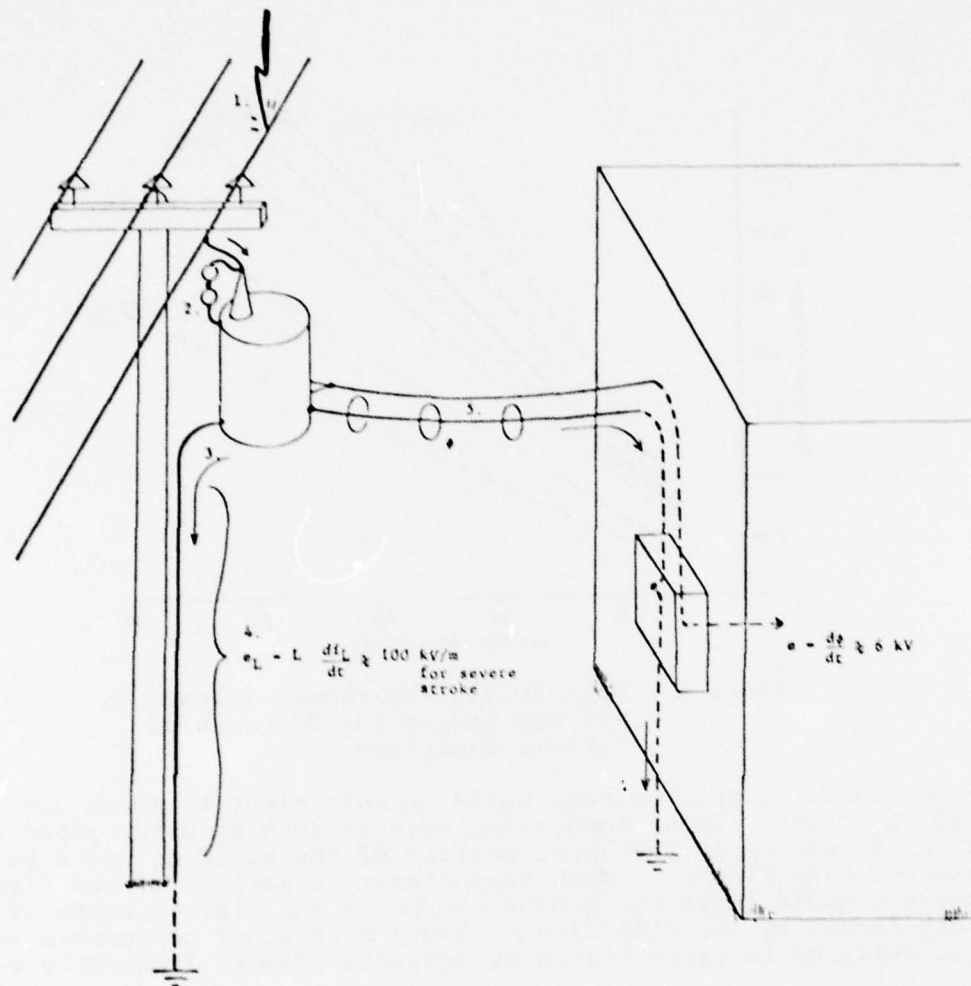


Figure 6 - Source of Surge in Power Distribution Circuit.

1. Lightning strikes power line
2. Arrester sparks and protects transformer
3. Lightning current flows to ground
4. Inductive voltage in ground wire raises transformer to high voltage
5. Some lightning current enters neutral and magnetic field couples surge into secondary circuit.

Inductance may cause hazardous voltage rises in secondary circuits as well as in conductors dedicated to carrying lightning currents. A common example in which inductance greatly diminishes the effectiveness of a surge suppressor is shown in Figure 7.

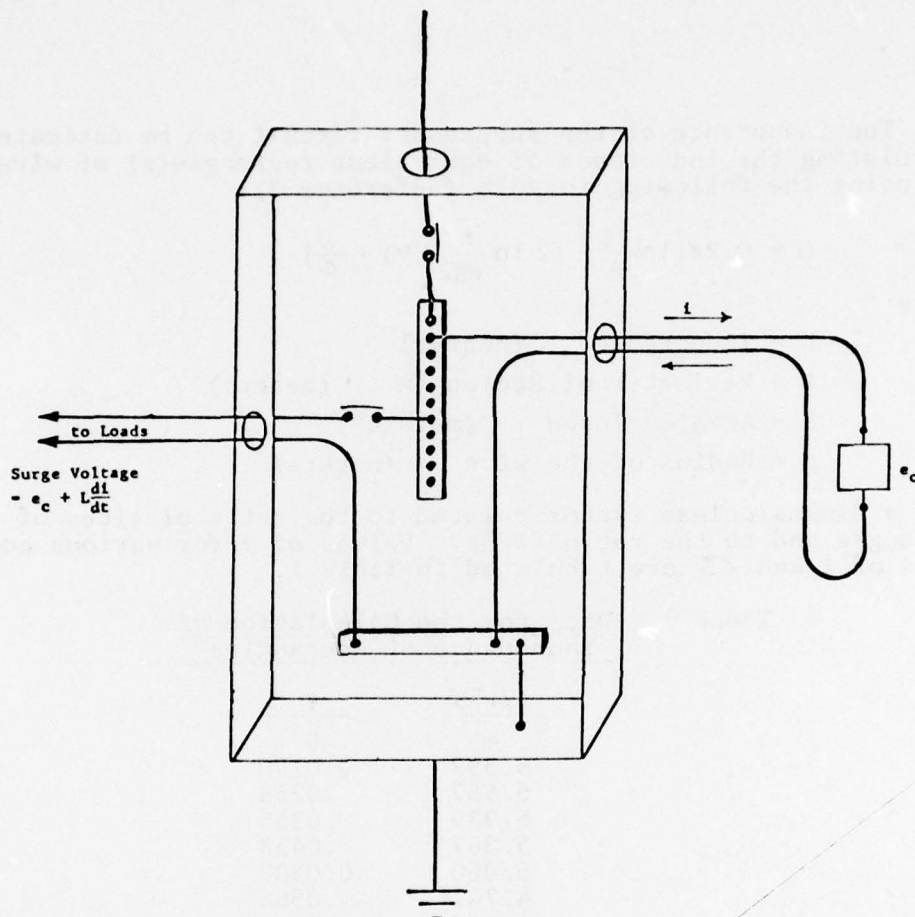


Figure 7 - Suppressor Effectiveness Diminished by Long Leads.

If the maximum rate of rise of current induced by lightning in secondary power distribution systems, due to the mechanism of Figure 6, is taken as 500 amps/ $\mu$ s as implied by Crouch et al (Reference 2), the voltage produced by this current along the suppressor leads would be:

$$\begin{aligned}
 e &= L \frac{di}{dt} & (11) \\
 &= (1 \times 10^{-6} \text{H})(5 \times 10^8 \text{ amps/sec}) \\
 &= 500 \text{ volts per microhenry of inductance}
 \end{aligned}$$

The inductance of the suppressor circuit can be estimated by calculating the inductance of equivalent rectangle(s) of wire in air using the following formula (Reference 3):

$$L = 0.2\ell \left[ \ln \frac{2\ell}{\rho} - \left( 2 \ln \frac{\ell}{\sqrt{S}} + \Psi \right) + \frac{1}{4} \right] \quad (12)$$

where:

- L = Inductance (henrys)
- $\ell$  = Perimeter of Rectangle (meters)
- S = Area enclosed (meters<sup>2</sup>)
- $\rho$  = Radius of the wire (meters)

$\Psi$  is a dimensionless factor related to the ratio of sides of the rectangle and to the ratio  $\ell/\sqrt{S}$ . Values of  $\Psi$  for various combinations of  $\ell$  and  $\sqrt{S}$  are tabulated in Table 1.

TABLE 1 - Data for the Calculation of Inductance of Rectangles

$\ell/\sqrt{S}$	$\Psi$
$\infty$	0
9.392	0.0140
6.957	.0258
5.939	.0355
5.367	.0438
5.000	0.0507
4.747	.0565
4.427	.0653
4.243	0.0714
4.131	.0755
4.064	.0782
4.025	.0798
4.006	.0807
4.000	0.0809

where  $\beta$  = the ratio of sides of the rectangle.

For example, if the suppressor leads of Figure 8 are each 1.0 m long and average 0.02 m apart, and if the wire has a radius of 0.13 cm (AWG #10) the inductance of the loop thus formed would be calculated as follows:

$$S = (0.02\text{m})(1.0\text{m}) = 0.02\text{m}^2 \quad (13)$$

$$\ell = 2(1.0\text{m}) + 2(0.2\text{m}) = 2.04\text{m} \quad (14)$$

$$\frac{\ell}{\sqrt{S}} = \frac{2.04}{\sqrt{0.02\text{m}^2}} = 14.42 \quad (15)$$



From Table I,

$$\Psi \approx 0.01$$

and, from eq. 12,

$$L = 0.2(2.04) \left[ \ln \left( \frac{2 \times 1}{0.0013} \right) - (2 \ln 14.42 + 0.01) + \frac{1}{4} \right] \quad (16)$$

$$= 2 \mu\text{H}$$

From equation 11, the inductive voltage along this 2  $\mu\text{H}$  suppressor circuit would be 1,000 volts.

The surge voltage appearing across the distribution circuits (bus-to-ground) in Figure 7 would be the sum of the suppressor clamp voltage ( $e_c$ ) and the inductive voltage in the leads. For example, if the suppressor in Figure 7 were capable of clamping a surge to 600 volts, the surge voltage appearing across the power distribution circuits would be 1600 volts and protection thought to be achieved by installation of the suppressor is not obtained.

Situations like the one just described appear very often because the role of inductance in lightning protection is not well understood by many installers of protective devices. The amount of inductance associated with each installation should be estimated beforehand and if significant, the installation rearranged to reduce it and its associated inductive voltage to an acceptable level. Equation 12 may be utilized to estimate the inductance of circuits that form rectangles, but if one dimension is much longer than the other (i.e. 10:1) equation 12 may be simplified by elimination of the  $\Psi$  turn, as follows:

$$L \approx 0.2\ell \left[ \ln \frac{2\ell}{\rho} - \ln \frac{\ell}{\sqrt{S}} + \frac{1}{4} \right] \quad (17)$$

$$\approx 0.2\ell \left[ \ln \frac{2\sqrt{S}}{\rho} + \frac{1}{4} \right] \quad (18)$$

from which the inductance of the loop analyzed previously would calculate to be 2.3  $\mu\text{H}$ , an acceptable approximation.

#### Ways to Minimize Inductance

Clearly, the way to minimize inductive voltages is to minimize the inductance of conductors and circuits that may conduct lightning currents. From the discussion thus far, it should be clear that there are at least two basic ways to accomplish this:

1. Keep paths as short as possible
2. Minimize circuit loop areas

There is also a third approach: provision of multiple, parallel current paths. This should be clear when it is recalled that inductors combine in parallel as do parallel resistors (by the inverse sum of reciprocals) resulting in an equivalent lower than any of the individual inductances. The effect can also be visualized by consideration of the magnetic flux associated with several conductors, as shown in Figure 8.

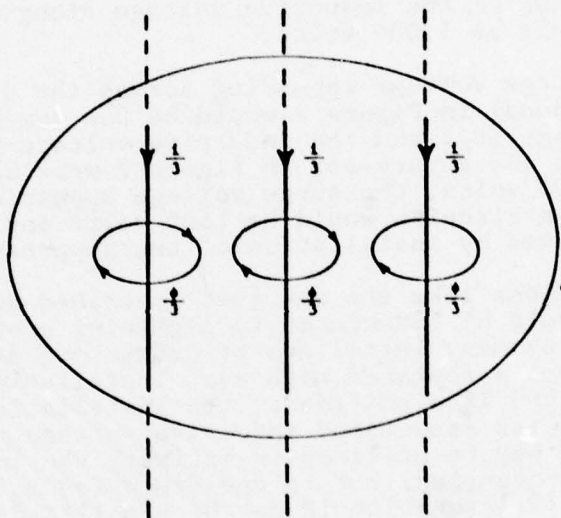


Figure 8 - Magnetic Flux Associated with Multiple Conductors.

In this case, a portion of the magnetic flux produced by the current in each conductor opposes and cancels a portion of the flux produced by currents in the other two conductors in the area between the conductors, such that the net magnetic flux surrounding the total current is outside of the group of conductors. Integration of this flux effectively begins a large distance,  $r$ , from the center of current flow. Thus, by equation 3, the total flux surrounding the group of conductors is less than that which surrounds the same amount of current flowing in a single conductor.

Several important "Do's and Don'ts" based on these principles are shown in Figures 9 and 10.

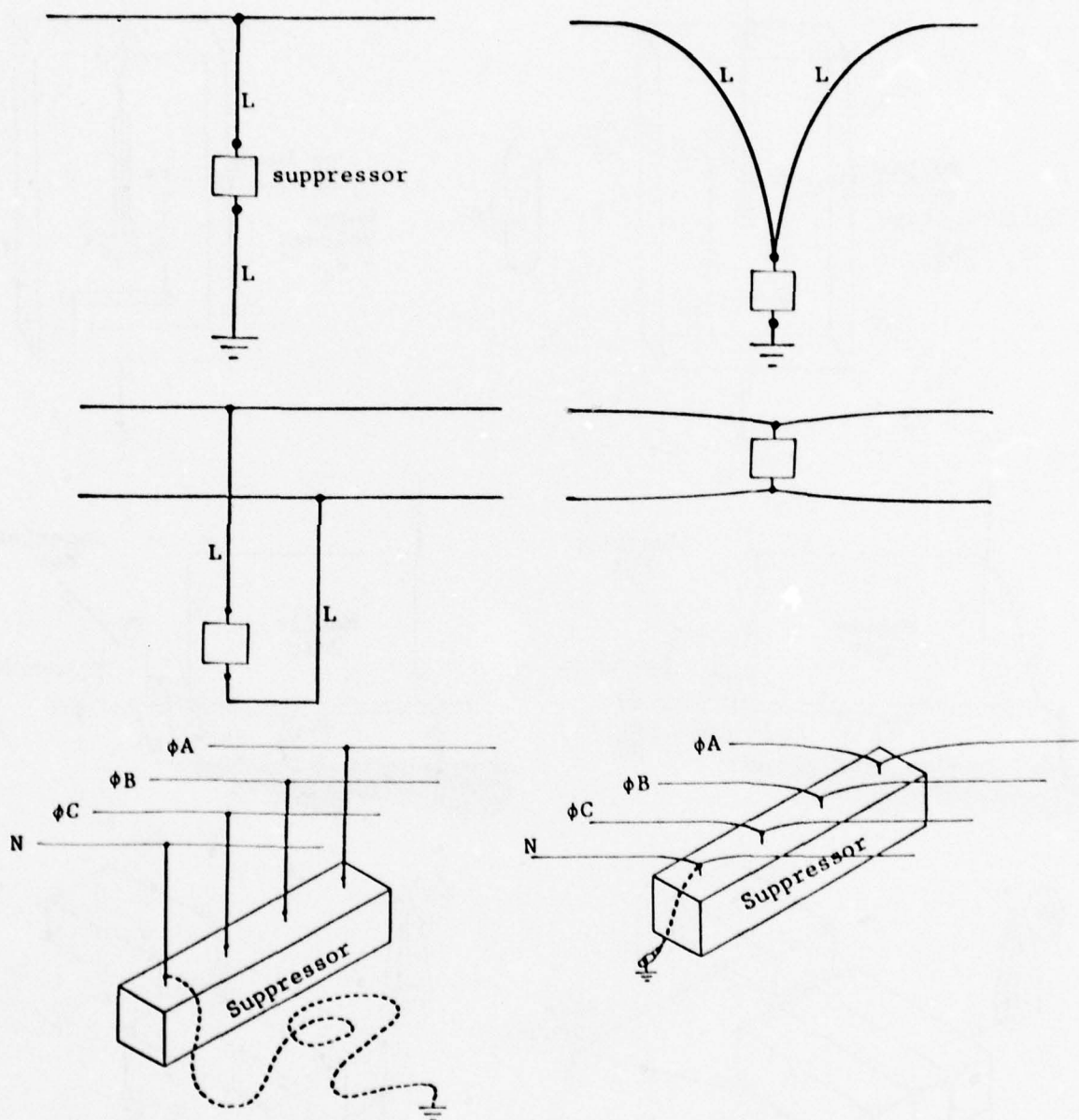


Figure 9 - Don't Have Surge Currents Flow through Inductance in Suppressor Leads

Do Keep Inductance in Suppressor Leads Low. If Long Leads Must be Used to Reach Suppressor, Bring the Circuit to the Suppressor and Keep Ground Leads Short.



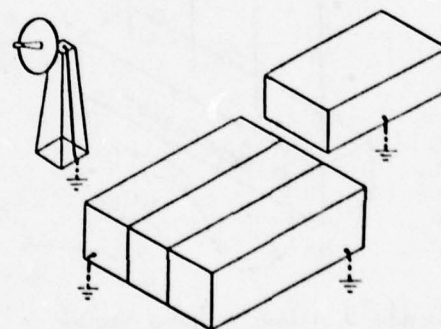
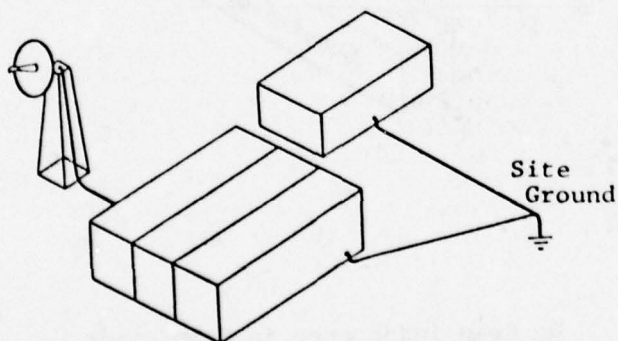
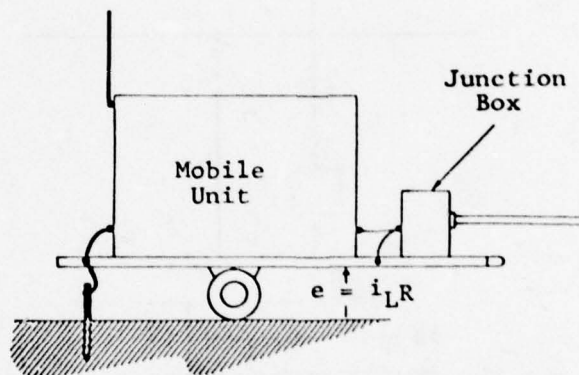
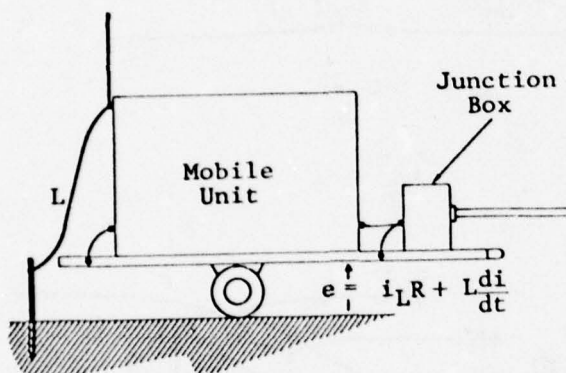
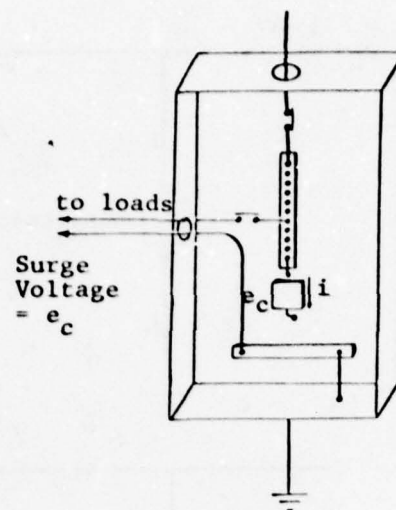
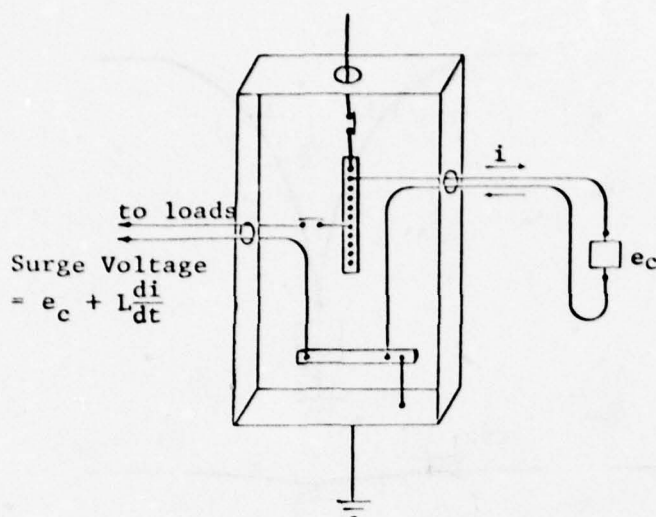


Figure 10 - Don't Create Unnecessary Loops or Have Long Ground Wires.

Do Ground Structures Directly at Their Bases.

### How Inductance Can Help

The discussion thus far has shown how inductance aggravates lightning protection problems and how it may greatly diminish the protection expected from protective devices such as surge suppressors. There are also situations where inductance may be intentionally included in a circuit to enhance protection. In most of these cases, inductance is used to help isolate a vulnerable component from an incoming surge. An example is shown in Figure 11.

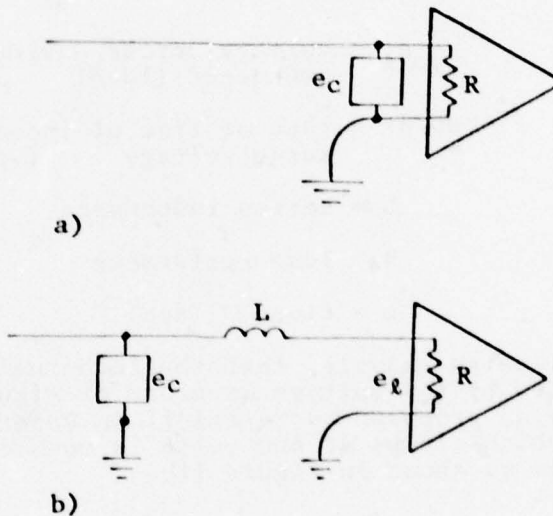


Figure 11 - Use of Inductance to Improve Protection.

In Figure 11a, a surge suppressor is shown connected directly across the terminals of a solid-state device or load to be protected. Here the surge voltage which enters the device is limited to the clamping voltage,  $e_c$ , of the suppressor. Since many solid-state devices operate at low voltages, it is sometimes difficult to find a suppressor capable of clamping the surge to such a low level (i.e. several volts) and sustaining the high (i.e. several thousand amperes) surge currents that may then flow to ground via the suppressor (suppressors capable of sustaining the high currents frequently have high clamping levels). A solution is to select a suppressor that can sustain the full surge current, and separate it with series inductance from the device to be protected as shown in Figure 11b. In this case surge current may begin immediately to flow to ground via the suppressor, but the flow of surge current to the load is delayed by the inductance. If the surge is of short duration the surge voltage across the load (represented by a resistor in Figure 11) may never reach the suppressor clamping level.

If the surge is of long duration the load voltage,  $e_l$ , may eventually reach the suppressor clamping level, but it will be delayed in time from when it appears at the suppressor, thus giving the suppressor ample time to operate and preventing an overshoot at the load.

The amount of surge reduction and/or delay afforded by the series inductance may be calculated by the equation:

$$e_l = \frac{dv}{dt} \left[ t - \frac{L}{R} (1 - e^{-\frac{R}{L}t}) \right] \quad (19)$$

where:

$e_l$  = voltage across device to be protected (load) (volts)

$dv/dt$  = rate of rise of incoming surge voltage (volts/sec)

$L$  = series inductance (henrys)

$R$  = load resistance (ohms)

$t$  = time (sec)

Assume, as an example, that the incoming surge voltage may be represented by the voltage waveform of Figure 12 rising to a crest of 6kV as proposed by Martzloff in Reference 4, and that a suppressor which clamps at 600 volts is connected across the incoming line as shown in Figure 11b.

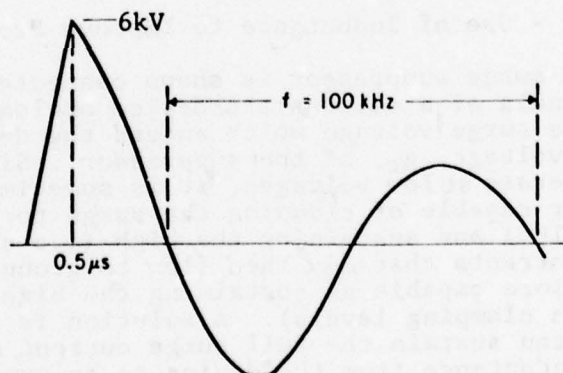


Figure 12 - Voltage Surge Waveform.



The waveform of Figure 12 has a rate of rise of:

$$\frac{dv}{dt} = \frac{6,000 \text{ volts}}{0.5 \times 10^{-6} \text{ sec}} = 12 \times 10^9 \text{ volts/sec.} \quad (20)$$

The clamping level would be reached at time,  $t_c$ , of:

$$\begin{aligned} t_c &= \frac{e_c}{dv/dt} = \frac{600 \text{ volts}}{12 \times 10^9 \text{ volts/sec}} \\ &= 5 \times 10^{-8} \text{ seconds} \\ &= 0.05 \text{ } \mu\text{sec.} \end{aligned} \quad (21)$$

If the load,  $R$ , is represented by a 100 ohm resistor and the inductance,  $L$ , is 100 microhenrys, then the surge voltage appearing across the load would be, from equation 19:

$$\begin{aligned} e_l &= 12 \times 10^9 \left[ 0.05 \times 10^{-6} - \frac{100 \times 16^{-6}}{100} \left( 1 - e^{-\left( \frac{100}{100 \times 10^{-6}} \right) (0.05 \times 10^{-6})} \right) \right] \\ &= 14.75 \text{ volts} \end{aligned} \quad (22)$$

After clamping occurs at 0.05  $\mu\text{sec}$ , the surge voltage entering the series L-R circuit appears as a square wave with amplitude of 600 volts and duration approximately 2.5  $\mu\text{sec}$ . The voltage across the load now depends on the time constant,  $T$ , of the series inductance and load resistance, or:

$$T = \frac{L}{R} \quad \text{seconds} \quad (23)$$

and after clamping occurs the voltage across the load resistance would increase according to the relation:

$$e_l = e_c (1 - e^{-t/T}) \quad (24)$$

where:

$e_c$  = suppressor clamping voltage (volts)

$T$  = time constant =  $L/R$  (seconds)

In the present example the original surge of Figure 12 would last for about 2.5  $\mu\text{sec}$  before falling off. At this time,

$$\begin{aligned} e_l &= 600 \left( 1 - e^{-\frac{2.5 \times 10^{-6}}{1 \times 10^{-6}}} \right) \\ &= 550 \text{ volts} \end{aligned} \quad (25)$$

After 2.5  $\mu$ s the original surge voltage would fall below the clamping level so the load would never experience the full 600 volts. If a larger inductance were used (or if the load resistance were lower) the time constant would be greater and the portion of surge voltage reached at the load would be even less. If circuit performance requirements limit the amount of inductance that can be placed in series with the incoming line, a second suppressor with a lower clamping voltage can be placed directly across the load and the inductance selected to limit the surge current to a level that can be withstood by the low voltage suppressor.

### Conclusions

1. Inductance is the cause of the familiar "side flash" and many other adverse effects from lightning strikes. Common inductors are made up of coils of wire, but even the inductance of a single turn or a straight wire may be excessive when lightning currents are involved.
2. Achievement of low inductance in lightning grounding systems is at least as important as achievement of grounds with low resistance to earth, and a low resistance ground might not necessarily be a low inductance ground.
3. Low inductance is achieved by:
  - Use of multiple short, parallel paths
  - Use of wide conductors such as the walls of metal buildings, instead of individual wires, to conduct lightning currents to ground
  - Avoidance of loops and round-about routing of ground conductors
4. Inductance may be utilized to *improve* lightning protection in certain situations, especially where it is desired to isolate a sensitive device from an incoming surge, or where it is desired to keep lightning currents out of a certain path.

#### References

1. N. Cianos and E.T. Pierce, "A Ground-Lightning Environment for Engineering Use", Technical Report 1, Stanford Research Institute, August 1972.
2. K.E. Crouch, F.A. Fisher and F.D. Martzloff, "Transient Control Levels - A Better Way to Voltage Ratings in Power Converter Applications", IEEE Industry Applications Society Conference Record, October 1976, Figure 5 and Table I, p. 942.
3. F.W. Grover, "Inductance Calculations", Dover Publications, New York, 1962, pp 61-62.
4. F.D. Martzloff, "A Guideline on Transient Overvoltages in Low Voltage AC Power Circuits", General Electric Report No. 77CRD221, October 1977, p. 4.



CONDITION FOR EVALUATION OF THE PROTECTING ZONE  
OF THE LIGHTNING ROD

BY  
A. D. Vorgučić

School of Electrical Engineering  
Georgia Institute of Technology  
Atlanta, Georgia

Presented at  
Federal Aviation Administration/  
Georgia Institute of Technology

Workshop on Grounding and Lightning Protection

PRECEDING PAGE BLANK

## ABSTRACT

The height of a lightning rod is not the only determining parameter of the protecting zone. More complete evaluation of the protecting zone requires knowledge of the value of lightning current, which depends on physicogeographic properties of a given area.

## I. Introduction

The lightning rod, which should protect a specified ground area from lightning strokes by causing all strokes to hit the rod, was introduced by Benjamin Franklin in 1753. Its use spread rapidly throughout the United States and Europe. During the more than 200 years since its introduction, many theories and hundreds of papers were presented to define the zone protected by the lightning rod. This large number of theories was occasioned doubtlessly by the fact that the principal processes associated with lightning were not well known. But each of these theories, coupled with experience obtained from observation and experimental evidence, contributed to the fund of collected knowledge. The conformation and extent of the zone protected by the lightning rod was determined principally from experience. But this evidence differed from place to place as evidenced by the variability in national electrical codes relative to lightning protectors. In this paper, we will reexamine the protective zone of the lightning rod and present a new perspective of the protective zone related to lightning rods and tall structures based on the striking distance found by Golde.<sup>[1]</sup>



## II. Protective Zone of the Lightning Rod - A Brief Historical Development

In lightning protection, a very important matter was what was the nature of the space protected by the lightning rod. It has been assumed that the protected space is either conical or cylindrical. The base of the cone or cylinder is a circle having a radius which depends on the height of the lightning rod and experience of the observer. The appropriate was often changed. For example, in French Instruction from the last centry, Gay-Lussac first said, "A lightning conductor protects effectively against a lightning stroke a circular space about it, the radius of which is twice its heighth." This ratio in subsequent editions of the Instruction was reduced from 2 to 1.75. Various definitions of the protected space proposed in the 19th century were collected by Sir Oliver Lodge and are shown in Fig. 1.<sup>[2]</sup> As seen, the conformation of the protected zone included cones and cylinders with considerable variations in

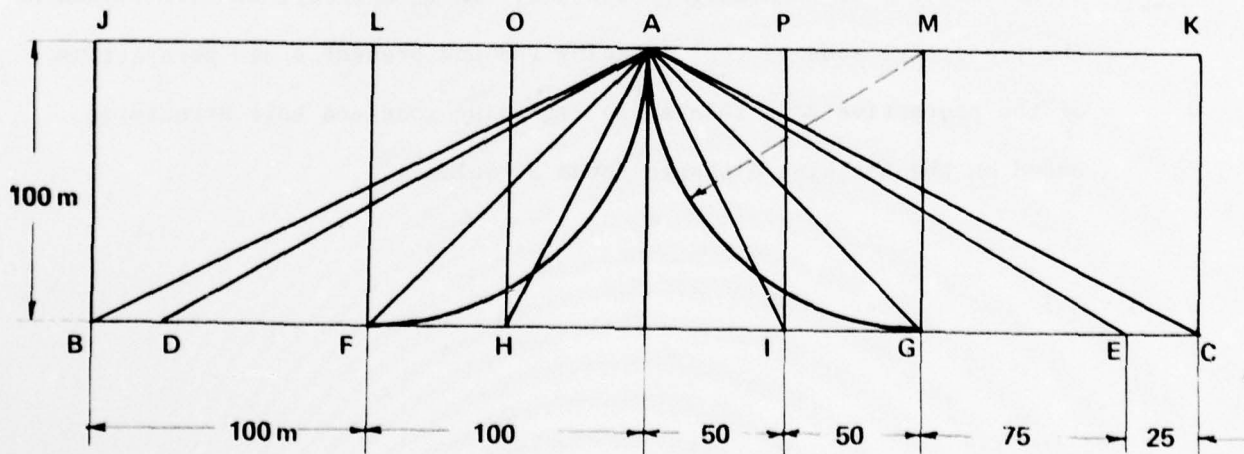


Fig.1. Zones of protection by vertical lightning rod (after O.J.Lodge)

JBCK cylinder	Gay Lussac 1823	FAG cone	Adams 1881
BAC cone	De Fonveille 1874	OHIP cylinder	hypotesis
DAE cone	Paris Commission 1875	FAG special cone	Preece 1881
LEGM cylinder	Chapman 1875	HAI cone	Melsens

the radius. Current practice in many countries indicates that the protective zone is defined either by an angle from the vertical or by a radius which depends on rod height. For example, in the South African electrical code the single mast protective angle is specified as  $45^\circ$  while with two masts the protective angle between them is  $60^\circ$ . In U.S. Code of 1945, the base-to-height ratio is 1 for important cases of protection and 2 for less important cases.

One of the first theoretical determinations of the protected zone was based on the "principle of the shortest distance." At this time, it was assumed that the lightning stroke seeks out the point of the earth's surface which is nearest to the place at which it exits the cloud. It was assumed that the exit points for all earth-bound lightning discharges lie in a place (WW on Fig. 2) which is parallel to the surface of the earth (EE).<sup>[3]</sup> In Fig. 2 it is easy to see that the protected range CC

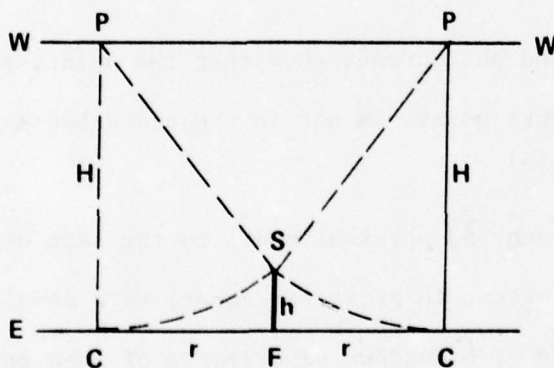


Fig.2. One of the first derivation of the radius of protection zone of the lightning rod.

of the lightning rod RS is obtained by finding the points P and P'. All strokes leaving the cloud at points in a circle with the diameter PP' under this assumption seek out the point S. All those strokes leaving the cloud outside the circle of diameter PP' will strike points outside of the protected surface (circle with diameter CC'). This radius of the protected zone according to this consideration was

$$r = (2H - h)^{\frac{1}{2}} \quad (1)$$

To evaluate the values of this radius Walter<sup>[3]</sup> used the findings of the Hamburg Fire Insurance Office on buildings damaged by lightning strokes over a period of 20 years. Significantly he found that the protected zone is much smaller than the radius in Eq. 1. He concluded that the basic assumption, that when the lightning leaves the cloud it is directed to the nearest point on the earth's surface, must be false. From other observations he concluded that the altitude at which the lightning definitely seeks the tower is  $H \approx h$ ; very near the top of the tower. After some experiments which he conducted in 1932 he found the radius of the base of protected cone to be  $r = 1.5h$ .

Peek<sup>[4]</sup> was the first investigator with systematic model tests. He found that the attractive range depends on the altitude of the high voltage electrode. According to Peek the "protective ratio" varied between 2 and 4.

Many direct observations and photographs show that the point, from which the lightning seeks the stroke point, is not in the cloud but is much nearer to the stroke point.<sup>[5]</sup>

The optimum solution approach and physical model to the last steps of the leader (which are very important in protected zones) were developed by Golde<sup>[1,2,6]</sup>, using the results of breakdown experiments of long spark gaps excited by an impulse generator. Using the supposition that the last step of leader moving toward the ground could be compared with long sparks, he defined the last discharging distance. In the initial discharge the negative leader moves from the cloud toward earth in steps. The velocity of the leader propagation can be taken as  $1.5 \times 10^5$  m/s. The interval between steps is about 100  $\mu$ s. The main stroke, which builds up from the



earth toward the cloud, is initiated by the electrical field from the down-coming leader. The distance between the tip of the leader and the stroke point is termed "the striking distance." The main stroke, which propagates with much greater velocity than the leader originates at the stroke point.

The electrical field strength above ground, due to the charge along the leader channel, was evaluated by Golde and is given in terms of the tip heights in Fig. 3. The critical field strength which can initiate the main stroke from the earth is larger for negative impulses than for positive

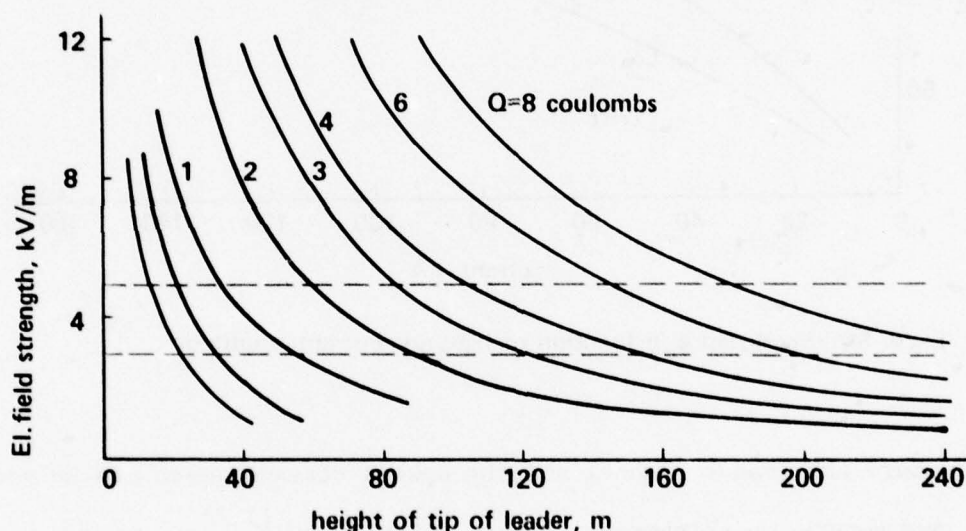


Fig.3 Electric field in function of tip height for different charge on leader channel

impulses, and is described by the horizontal lines in Fig. 3. The crossing points of these lines with the charge curves, define the critical distances between the tip of the leader and the point which would be struck. The charges in the leader channel are neutralized during the return stroke process. The magnitude of the lightning current depends on this charge. From the integration of current oscillograms it is concluded that an average

lightning current of 25 kA corresponds to a charge of 1 C. Figure 4 illustrates the relationship between the striking distance and the lightning current magnitude for both positive and negative impulse<sup>[1]</sup>. The

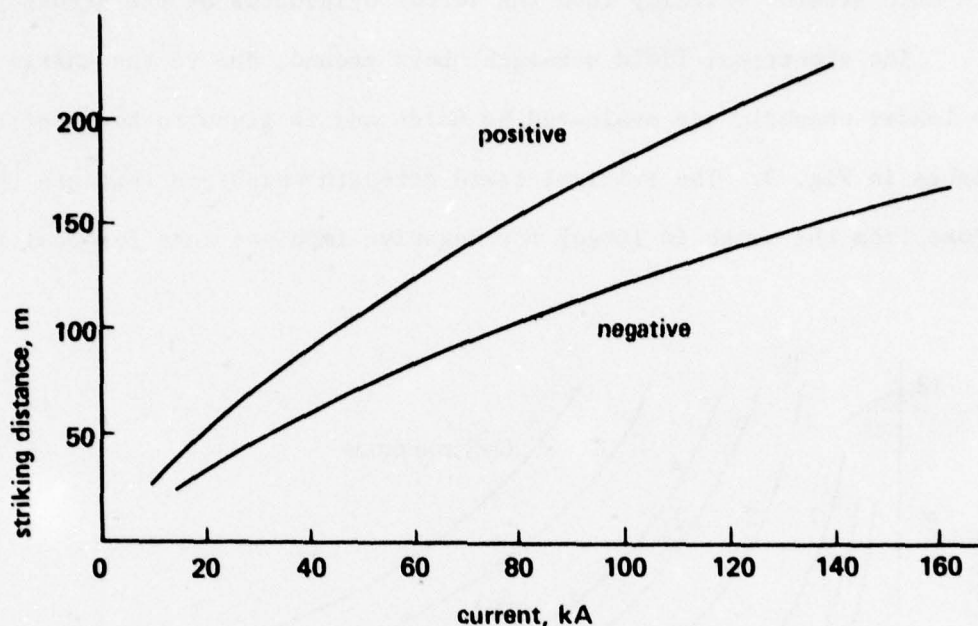


Fig.4. Striking distance in function of lightning current amplitude

point where the leader channel and the upward streamer meet can be seen in some photographs which thereby support this theory.<sup>[1,5]</sup>

From foregoing considerations it follows that the striking distance to a lightning rod cannot be described by just one value. Golde introduced a new concept of the attractive effect and protected zone of a vertical lightning rod, which is depicted in Fig. 5. He wrote, "Assume a vertical lightning rod of the height  $H$  and a striking distance  $D$ , according to the charge on the leader channel. When the tip of a leader, approaching from any angle, penetrates into the zone shaded horizontally it will be attracted by the lightning rod; if it penetrates into the zone shaded vertically, it

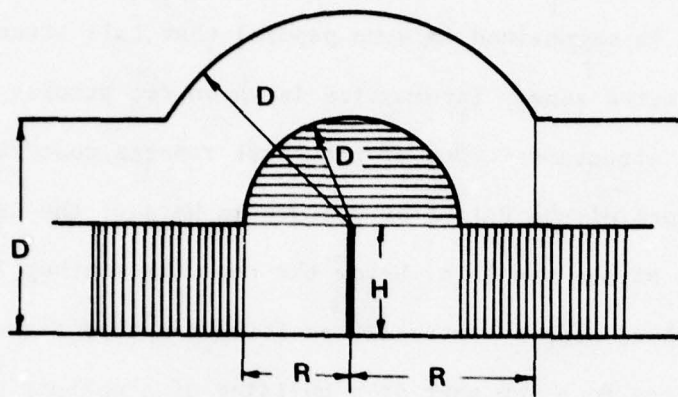


Fig.5. Attractive effect of  
vertical lightning rod (Golde)

will be attracted to earth. The protective zone of a freestanding vertical lightning rod might thus be described by a cylinder about the rod, the radius  $R$  of the cylinder being given by:

$$R = (2DH - H^2)^{\frac{1}{2}} \quad \text{if } D > H \text{ or}$$

$$R = D \quad \text{if } D < H \quad .'' [1]$$



### III. Cases of Toll Structures

It seems (and it is maintained in some papers) that tall structures have no associated protected zone. Information is known for strokes near and to the side of tall structures. One of the first reports concerned a stroke to a lower platform of the Palace of Culture in Warsaw; the height of which is 230 m. The stroke was 95 m. below the top. In another instance, lightning struck the ground near a vertically positioned Apollo rocket. A weak lightning discharge to a low part of a building of a nuclear power station in Sweden damaged a computer center.<sup>[7]</sup> This low part was between two taller parts of the building which were protected against lightning.

In 8 years of observation of lightning strokes on the 540 m.-high Ostenkino TV tower in Moscow, there are 185 photos of lightning strokes on the tower and 16 photos of strokes to the ground at originating distances of from 200 to 500 m. from the tower. About 8% of all the lightning strokes on the tower were below the top from 60 to 220 m.<sup>[7]</sup> It was concluded that very tall structures provide a very small protected zone. It was also reported increasing of the density of upward lightning in nearness of the tower from 2-2.5 to 4 1/km<sup>2</sup> in a year.

#### IV. Evaluation of the Protecting Zone of the Lightning Rod

If we accept the "striking distance" developed by Golde<sup>[1]</sup>, it is possible to evaluate the protected zone of high lightning rods and also explain the lateral strokes in the proximity of tall structures. According to Fig. 6, if the leader approaches a very long vertical rod or a tall structure, it will be struck at a point and that the shortest distance from the leader tip is equal to the striking distance. The striking distance depends on the charge in the leader channel and the lightning current magnitude

$$r = f(I)$$

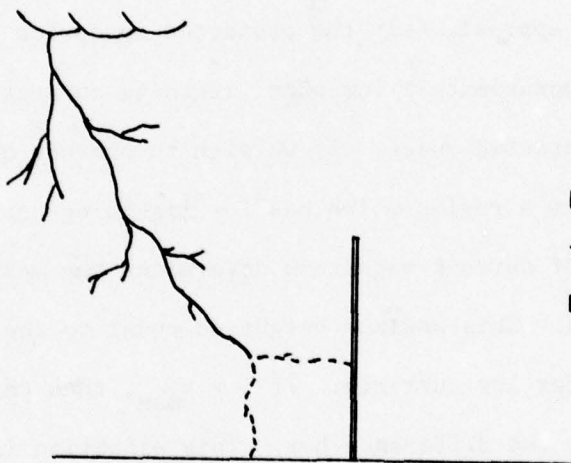


Fig.6. Leader approaching to the tall structure seek the striking point.

The radius  $r$  of the protection zone for each current is equal to the striking distance. Figure 7 shows the protective zones of a tall structure for three values of lightning current magnitude.

According to the principle of "minimal distance" the protected space is inside the cone which has a circularly shaped envelope, with radius approximately equal to the striking distance as is shown in Fig. 7.

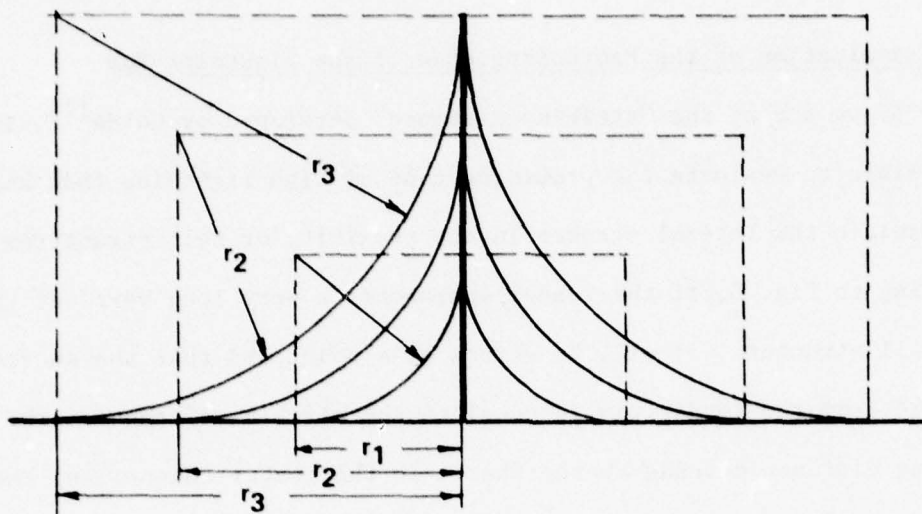


Fig.7 Protective spaces in function of lightning current magnitude.

Now we can evaluate approximately the protected space for each current and also predict approximately for what lightning current is an object protected in the protected space. If we wish to protect objects with a tall lightning rod in a region which has low lightning current magnitude, then the value of current magnitude determines the maximum height of the lightning rod. This maximum height is equal to the striking distance  $r$  which is small for low currents. If  $h > r_{\text{max}}$ , then this rod is longer than necessary by the difference  $h-r$ . This situation is shown in Fig. 8 where the protected zone for one current is depicted with its striking distance which in this case is independent of the length of the rod (only if  $h > r$ ).

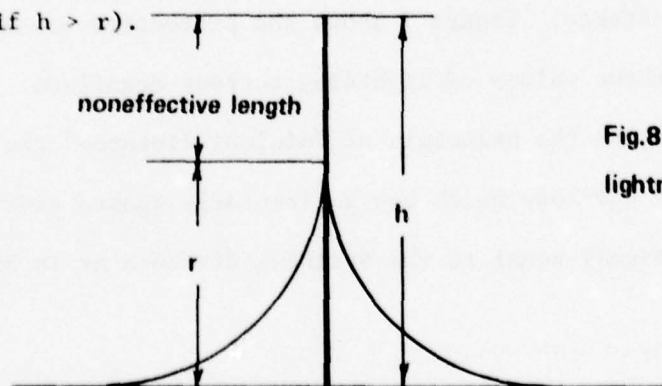


Fig.8 Case of the long lightning rod.



## V. Lightning Current Magnitude

For evaluation of the protected zone of a lightning rod or tall structure, it is necessary to know the value of lightning current magnitude. There is a broad range of lightning current magnitudes, from some hundreds of amperes to 200 kA. One instance of a 460 kA lightning current magnitude is also included. The physico-geographic properties of a region have a great influence on the development of dynamic atmospheric phenomena and on values of lightning current impulse parameters.<sup>[8]</sup> In Fig. 9 are shown curves of probability of various lightning current magnitudes given by some authors.<sup>[9]</sup> These probabilities are not consistent because they also depend on the topographic properties of the observed region. In one region the values of lightning current parameters are dependent on altitude.

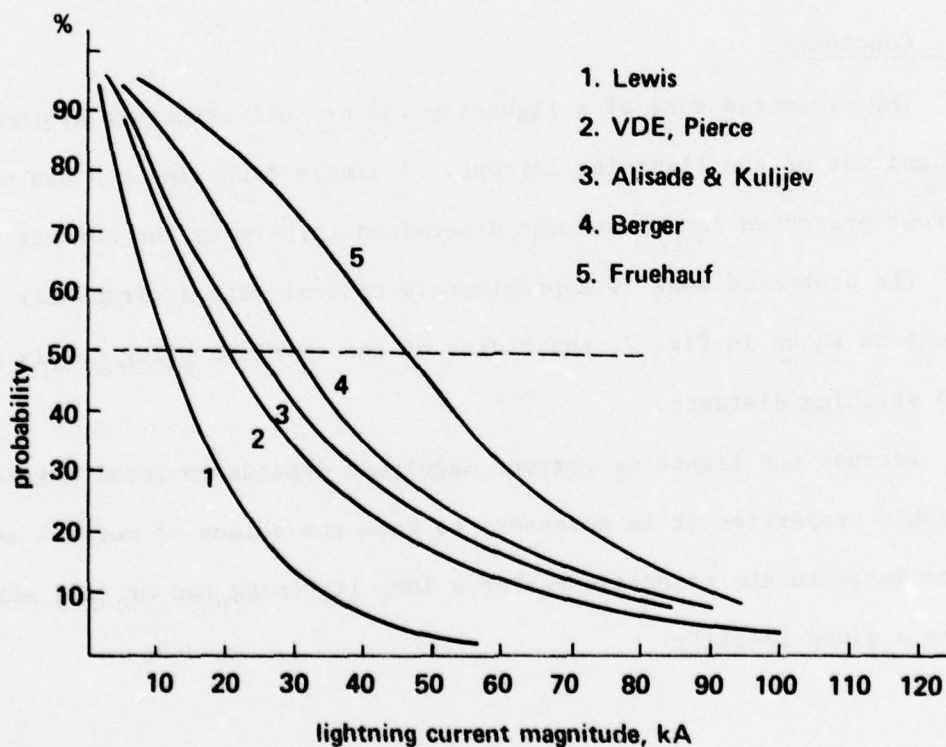


Fig.9 Probability of lightning current magnitude

Table 1 summarizes parameters the values of lightning current  $I_m$  and values of  $di/dt$  in Azerbaidjan (USSR). [8]

TABLE 1

Altitude	$I_m$ (kA)	$di/dt$ (kA/ s)
$H < 400$ m	48	21 (low land)
$400 \text{ m} < H < 900$ m	39	19 (hills)
$900 \text{ m} < H < 1400$ m	31	13 (mountains)
$1400 \text{ m} < H$	22	7 (high mountains)

#### VI. Conclusion

The protected zone of a lightning rod or tall structure depends on the magnitude of the lightning current. A single lightning rod has many different protected zones each one determined largely by the current magnitude. The protected zone is approximately conical with a circularly shaped envelope as shown in Fig. 7, the radius of the envelope being nearly equal to the striking distance.

Because the lightning current magnitude depends on local physico-geographic properties it is necessary to know the values of current magnitude to evaluate the effectiveness of a long lightning rod or tall structure in a given locality.

## VII. References

- [1] Golde, H. R., Lightning Protection, Edward Arnold, London, 1973.
- [2] Golde, H. R., The Lightning Conductor, J. of Franklin Inst., 283, No. 6, 1967, p. 451-477.
- [3] Walter, B., Veber Blitzschutz durch "Fernblitzableiter," Z. für techn. Physik, 14, No. 3, 1933, s. 118-126.
- [4] Peek, W. F., Dielectric Phenomena in High-Voltage Engineering, McGraw-Hill Book Co., New York, 1929.
- [5] Walter, B., Von wo ab steuert der Blitz auf seine Einschlagstelle zu?, Z. für techn. Physik, 18, 1937, s. 105-109.
- [6] Golde, H. R., Teoretische Betrachtungen ueber den Schutz von Blitzableitern, ETZ-A, 82, 1961, s. 273-277.
- [7] Lundquist, S., Uticaj munje sa posebnim naglaskom na zastitu nuklearnih elektrana, predavane u Inst. M. Vidmar, Ljubljana, 1977.
- [8] Alisade, A. A., Kulijev, D. A., Forschungsergebniss der Gewitterteatigkejt und Kenngrossen des Blitzes auf dem teritorium Azerbaidjans, X Internationales Blitzschutzkonferenz, Budapest, 1969.
- [9] Vorgucic, A., Uticaj parametara impulsa struje groma na otpornost uzemljenja, Elektrotehnika, br. 7-8, 1975, s. 10E-14E.



EMP PROTECTION OF  
MINUTEMAN LAUNCH FACILITIES

BY  
A. E. Brockschmidt Jr.

BOEING AEROSPACE COMPANY  
Seattle, Washington

Presented at  
Federal Aviation Administration/  
Georgia Institute of Technology

Workshop on Grounding and Lightning Protection

PRECEDING PAGE BLANK

#### ABSTRACT

The design of fail safe EMP protection systems for MINUTEMAN Launch facilities and high-reliability hardware required is discussed. EMP threats resulting from local and exo-atmospheric nuclear bursts require close attention to design of high current grounds and of devices for suppression of high energy repetitive pulses with rise times of several nanoseconds.

The system approach to protection is discussed, and specific examples of ESAS, zeners, transformers, grounding methods, and filters are detailed.

Test data and test methods on systems and devices are presented as examples of performance capabilities, as many EMP methods are also applicable to lightning protection.

#### EMP SOURCES

EMP is considered a major threat to weapon systems and has been specifically protected against starting about 1970 in the Minuteman Program. Much effort has been expended and extensive hardware deployed to upgrade the system EMP hardness.

Minuteman facilities are primarily threatened by two sources of EMP generation. These sources are radiated fields generated by Compton electrons and positive ions, freed by interaction of gamma rays with the atmosphere. Compton currents are also generated in solids by interaction with gamma rays, the worst case being electrons freed from wiring insulation and causing pulses on the line. The radiated fields can be generated by either high altitude or ground bursts. A single high altitude nuclear burst can cast an effective EMP blanket over the entire United States. Since the launch facilities are designed with wartime nuclear scenarios in mind, protection is provided for many closely spaced and repetitive EMP pulses. A secondary function of the EMP limiters is to suppress lightning transients and EMI noise.

#### TYPICAL THREATS AND LIMITING REQUIREMENTS FOR MINUTEMAN EMP LIMITERS

The ability of EMP to damage electronic equipment is well known, and long range civilian damage has even been experienced. It has been said that some of the first transistorized garage door openers in Hawaii quit working after nuclear testing in the South Pacific. In addition to permanent damage, protection from temporary system upset and resetting due to EMP pulses being superimposed on signals must be provided. Specifications for limiters include definition of input voltage, waveform source and load resistances, repetitive input waveform rate and duration, and allowable output voltages. Requirements for individual limiters are determined by a complete system analysis, taking into account existing system losses and attenuation, damage threshold for protected equipment, and pickup sources. A typical example of a specification for a single limiter is shown in Figure I. The input threat voltage for an EMP event resulting from a single high altitude burst is roughly equivalent to lightning surges for the case of high altitude bursts, but also includes high frequency content up to 20 MHz. The maximum voltage developed due to a high altitude burst on a line is usually limited by wire insulation breakdown. For a ground burst, where Compton currents occur, the peak voltage may be reached before wiring insulation can breakdown. An examination of the Figure I waveshape shows that the energy content of the "pulse generator" is on the order of 100's of kJ, and charge of near 10's of coulombs. Hardware designed to suppress this amount of energy and survive for hundreds of closely spaced pulses would be prohibitively expensive; therefore, requirements usually specify survival for a limited number of pulses, with a failure mode (short, or open line) which will maintain the limiting function of the hardware.



### EMP PROTECTION METHODS

Figure II shows a typical launch facility. Numerous schemes and methods are used to prevent damage and upset from radiation, EMP fields, and compton currents. Typical of the methods used are:

1. Design of critical circuits with components capable of surviving large voltage/current pulses.
2. Circumvention - The detection of EMP with a special antenna and shutdown of circuits for the duration of the pulse.
3. Shielding - Primary electromagnetic shielding is accomplished by the presense of a  $\frac{1}{2}$ " steel liner surrounding the launch facility. The main launch tube closure door and the personnel access door both are provided with EM tight seals. All electrical and mechanical penetrations of this liner are made EM tight by circumferentially welded attachments of limiters or conduits. Most ESA's are housed in an electro-magnetic tight vault, providing a second level of shielding; and limiters are packaged in an electro-magnetic tight vault, providng additional shiedling. Figure III shows typical electro-magnetic shielding methods.
4. Limiters, consisting of spark-gap surge arrestors (ESAS), avalance diodes, grounding methods, filtering, and isolation.

This paper is primarily concerned with the limiters used for Minuteman protection.

The protection of the system for EMP (and other threats) is several layers deep, consisting in some cases of nearly identical limiters in series, each capable of independent attenuation of the EMP pulses. There are some critical circuits where a primary limiter is followed by a secondary limiter containing a backup ESA with a firing voltage higher than the maximum expected output of the primary limiter.

### GROUNDING REQUIREMENTS

The voltage drops across all bonding and grounding paths contribute to the output voltage of the limiter. The desire to group surge arrestors within a single piece of hardware (for ease of maintenance and reduction of production costs) has resulted in as many as eleven surge arrestors sharing the same ground point with the other components of the limiters. In some cases this requires a ground that will carry 30 - 40 KA with a voltage drop well below 2 volts peak at frequencies of 20 MHz.

### GROUNDING METHODS

The problem of an earth ground to conduct several megamps is trivial when the existing "ground rod" is considered. The steel liner (used as the reference point for threat voltages) and concrete shell of the launch facility itself functions as a 12 ft. to 24 ft. diameter, 80 ft. deep ground rod, with an array of radial conduits below the water table. A high usage of ammonium nitrate fertilizer by farmers

### GROUNDING METHODS (Cont)

in the vicinity of most launch facilities results in very conductive soil, so that resistance to earth of a few tenths ohm is typical. Within the launch facility, surge arrestors and limiters are mounted on structural supports welded to the steel liner. The need to support limiting equipment for high G mechanical shock loads results in a massive structure with many feet of weld having a very low resistance and inductance. See Figure IV for a typical attachment. Grounding effectiveness is further enhanced since all protected equipment is enclosed in the "ground rod".

Grounding methods include ground straps, individually grounding of ESA's to primary structure, faying surface contact, and welding. Multiple grounding paths connect all equipment in the launch facility. These paths include the liner, copper sheet ground straps, cabling shield braid, woven steel mesh, and power grounds. For the limiting equipment, the highest impedance grounds used are 6" long X 6" wide copper braid ground straps, which are used on 30 KA grounds and achieve 35 microohm, 2.3 microhenry bonds, including contact resistance at each end. These straps are held at each end by 4 -  $\frac{1}{4}$ " diameter bolts. A large improvement over use of a ground strap was achieved by utilizing the faying surface of the mechanical support. An example is alodined aluminum chassis held to  $\frac{3}{4}$ " thick nickel-plated steel mounted with 20 -  $\frac{1}{2}$ " bolts and a controlled bolt torque of 100 ft.-lbs, which has a bond resistance of less than 20 microohms and a bond inductance near zero.

### 60 HZ POWER LIMITERS - SYSTEM CONSIDERATIONS

Both EMP fields and compton currents are present on the 60 Hz power lines to the launch facility. High altitude bursts can induce megavolts onto the 6 or 13 KV land lines, but insulator breakdown, transformer breakdown, and the primary arrestors limit this value to  $10^5$  of KV. The launch facilities have underground diesel generator sets which can be switched on line when the commercial 60 Hz power lines have been destroyed. Surge arrestors and limiters thus are required to survive and be able to transfer 60 Hz power after the EMP pulse. Nuclear ground bursts can destroy the diesel-generator, and concurrently, generate compton currents on the power cables in the conduit which connect the diesel generator and launch facility. The launch facilities are capable of operation on batteries by way of a DC/60 Hz/400 Hz motor-generator set, so that even with all 60 Hz power lines destroyed, limiting is still required.

Typical limiting requirements are:

<u>Frequency Range</u>	<u>Maximum Peak EMP Output</u>	
	<u>For 60 Hz Lines</u>	<u>For Signal Lines</u>
DC - 10 KHz	100 $\zeta$ v - peak	10 $\zeta$ v - peak
10 KHz - 100 KHz	$\approx$ 100 v - peak	10 v - peak
100 KHz - 100 MHz	SEVERAL v - peak	SEVERAL v - peak

## 60 HZ POWER LIMITERS - SYSTEM CONSIDERATIONS (Cont)

These requirements assure that neither conducted pulses or fields radiated from 60 Hz lines can affect critical circuits. Some 60 Hz lighting and control circuits extend outside the shielded areas of the launcher where gamma ray initiated compton currents can cause pulse amplitudes on these lines of 10's of KV levels. These threats also require limiting.

## 60 HZ POWER LINE LIMITERS, DESIGN EXAMPLES

Three basic types of limiting arrangements have been used for power lines:

- A. ESA followed by LC filter
- B. ESA followed by saturable transformer and resonating capacitor
- C. ESA followed by balanced transformer and rectifier circuits

## DETAILS OF LIMITER TYPES

- A. This is the simplest type limiter, shown in Figure V.a), but not necessarily the most effective or least expensive. ESA's are primarily selected for response time and energy handling capabilities, with high mechanical strength also required. EMI type filters are sometimes ineffective for EMP if they contain single-line iron-core inductors, as pulse currents in addition to 60 Hz currents can saturate the cores of the first inductor. Where a number of filters are in the same low power circuit so that ESA power follow current is limited by the filter resistance, an ESA without internal power follow limiting resistance can be used. As experience was gained with EMP limiters, fewer of this type limiter were designed and deployed.
- B. This design type can be expanded to nearly any level commercial power system. Figure V.b) shows the components of the limiter and the equivalent circuits. Existing transformers in power systems can be incorporated into such a limiter if the leakage inductance, interwinding capacitance, and turns ratio is known. The 3Ø transformer specified for launch facility limiter usage controlled the core size, specified low interwinding capacitance (which required .5" separation between windings), limited leakage inductance of secondary, required an internal shield, and specified normal power transformer parameters. This type circuit can be analyzed by simple hand calculations. Fuse F (in the form of a No. 10, 200°C wire or larger) is both an inductance and fuse. E<sub>1</sub> was selected so as to always fail short initially for high coulomb pulses, but long term heating from repetitive pulses can melt the hermetic seal on the gap, admitting air, which raises the firing voltage. The fusing function (#10, 200°C wire fuses approximately in 8 ms @ 20 ka) assures a fail-safe failure mode, so that repetitive multi-kj surges cannot blow E<sub>1</sub> open. The inductance of F plus the capacitance of E<sub>1</sub> and the wiring typically



#### DETAILS OF LIMITER TYPES (Cont)

##### B. (Cont)

slows the EMP voltage rise at  $E_1$  from 5 KV/nanosecond to less than 350 V/nanosecond.  $E_1$  fires at less than 5 KV for this rate of rise, and  $L_3$  and the wiring capacitance to ground lowers the voltage at the splice to 3 KV peak.

At high frequencies, (10-100 MHz), the circuit can be reduced to the circuit of Figure VI.a, and calculations to determine output voltage made as shown. At low frequencies, where a worst case assumption of a surviving ESA, a short ESA, and an open "fuse" (Figure VI.B) is made so that 10 KV is impressed across a primary winding, the circuit can be analyzed in the same manner as a pulse XFMR circuit, with the ringing frequency and peak voltage overshoot of the output determined by the resonance of  $L_1$  and  $C_1$ , and the maximum energy transferred determined by core size and saturation characteristics. For a commercial installation where a plant is supplied by a high voltage line with numerous distribution XFMRs, the EMP protection afforded by an existing system can be analyzed using the above procedure by considering the primary arrestor, XFMR parameters, secondary arrestors, and the capacitance of any EMI filters or power factor correction capacitors.

- C. Power supplies, incandescent lighting, and other circuits using or able to operate on DC power have been well protected over the entire 100 MHz EMP threat band width by a circuit as shown in Figure VII. The interesting feature is that this arrangement can function equally well with single  $\phi$  or 3 $\phi$  systems with the EMP source on either side of the XFMR. An ESA is required only to protect the XFMR or capacitor dielectrics or the diode junctions from reverse breakdown. The only magnetic coupling present is that due to leakage current of the diodes and imbalance of the bifilar windings. By controlling the interwinding capacitance  $C_2$  and using a feed-through capacitor ( $C_1$  and  $C_3$ ), high frequency coupling between windings is controlled. The use of a feed-through capacitor makes certain that the frequency of any energy coupled through the XFMR due to

## DETAILS OF LIMITER TYPES (Cont)

### C. (Cont)

an imbalance between diodes or windings will be below the resonant frequency of the XFMR winding and capacitor. The short-circuit current of small XFMR's can be controlled to limit power follow current through the ESA, allowing use of an ESA without a current limiting resistor.

## SIGNAL LINE LIMITERS - SYSTEM CONSIDERATIONS

Signal lines can be threatened by common current pulses of the same magnitude as seen on power lines. The limiter design problem is eased by not having 60 Hz power follow to deal with in ESA selection. The use of avalanche diodes is often necessitated by having to limit the EMP voltage to just above signal levels without attenuating those signals. The selection of avalanche diodes is usually governed by capacitance and repetitive pulse considerations rather than single pulse withstand capability. Local signal lines partially shielded from gamma rays, such as area security system lines, have much lower level threats and are easily handled by ESA, diode, and filter combinations. EMI type filters having ferrite beads at the front end of the filters usually cannot be used for EMP limiting due to saturation effects. Typical limiting requirements are shown with 60 Hz limiting requirements (Page 4).

## DESIGN EXAMPLES - SIGNAL LINES

Three main types of limiters are used on Minuteman signal lines:

1. ESA followed by LC filter
2. ESA followed by inductor, avalanche diode, and LC filter
3. Balanced ESA, XFMR, zener diodes, LC filter

### Variations:

Balanced ESA, resonant XFMR, resistor, LC filter  
Balanced ESA, XFMR, second ESA, LC filter

- A. This type filter is straight forward, and is used primarily on voice/audio lines. Design is by selecting an ESA able to respond to the pulse rate of rise, and selecting or designing a filter (even a  $\pi$  type EMI filter will work on low threat circuits) with a peak voltage rating as high as the gap breakdown and with the desired frequency response at the source and load impedances of the EMP threat.
- B. This type is primarily used for capacitance sensitive signal lines. Figure VIII shows a typical example, where the signal is a verification pulse on a security line, the voltage levels being important but waveshape deformation allowable. Inductor  $L_1$  is sized to limit current through the diode to enable the diode to survive repetitive pulses. The junction capacitance of the diode is controlled and functions with  $L_2$  and C to limit high frequencies.  $L_2$  is designed primarily to have a resonant frequency of 20 MHz or above (i.e. distributed capacitance very low, a few pf). The resistance in the circuit is sized for critical damping, to prevent oscillation when the diode switches off.

#### DESIGN EXAMPLES - SIGNAL LINES (cont)

- C. The third and most critical type of line requiring limiting is for digital communication lines, which are used for reporting missile status and controlling missile launch. The two binary systems in use are audio frequency phase modulated systems, both of which are sensitive to any phase delay introduced by the limiters. These lines are also subject to high energy pulses of nearly the same magnitude as the power lines. Due to these phase delay requirements, balanced lines are used. These required dual-gap ESAs to prevent unbalanced EMP currents from destroying downstream balanced XFMRs. Typical designs are shown in Fig. IX. Circuit a) shows a balanced line with a dual ESA. The common mode XFMR cancels signals common to both lines,  $D_1$  and  $D_2$  clip low frequencies in the pass band, and the LC filters suppress high frequencies coupled through by leakage capacitances of the XFMRs. Circuit b) uses a capacitor to resonate with the XFMR secondary to limit the low frequency peaks, and a Pi filter to attenuate high frequencies, and the resistor to dampen ringing. Backup using MF and UHF communication channels is available to launch a missile and these can also be affected by a large EMP signal getting past the limiter. Circuit c) is for an MF antenna line.  $T_1$  is a matching XFMR protected by dual ESAs. ESA  $E_3$  clips the peaks resulting from  $T_1$  ringing when saturation of  $T_1$  occurs from an EMP pulse. The lossy line and capacitor attenuate the high frequency EMP signals with minimal effect on MF radio signals. Circuit d) is an example of an ESA protected 5th order maximally flat phase delay filter,  $D_1$  functions as a capacitor in addition to clipping EMP noise frequencies in the passband.

#### HARDWARE DESCRIPTION - GENERAL

In addition to meeting the requirements for EMP, the hardware is also designed for stringent humidity, vibration, thermal shock and mechanical shock. The heavy structure required for mechanical shock is an advantage for dissipating energy (as high as 1000 watts for 10 minutes) in repetitive pulse situations.

- A. ESAS - The 60 Hz primary power ESA is a good example. This ESA is essentially the same electrical hardware as the Joslyn 1456-01 ESA used at many FAA and commercial facilities. The Fig. X shows the differences which enable the device to handle 60 kj at high current levels rather than 10 kj which is typical for the commercial part. Other examples of ESAs used are shown in Fig. XI, including the original carbon-block type lightning protectors deployed in 1962.
- B. Avalance Diodes - 50 w, IN 3300 series diodes have usually been chosen for use due to their high current rating and ability to absorb energy from repetitive pulses. Smaller diodes are used on secondary and communication XFMRs and are of many types and manufacture. The IN 3300 series is also used, with a specified junction capacitance, as a combination filter capacitor and limiter. Junction capacitance is in the 1,000 - 10,000 pf range, depending on manufacturer and voltage.



#### HARDWARE DESCRIPTION - GENERAL (Cont)

C. Transformers - The discussion on 60 Hz power filters shows examples of power transformers. Signal line transformers are simply military quality line matching XFMRs with internal shields.

D. LC Circuits - Inductors: Inductors used vary in size from a 40 turn, #2/0 wire, air core inductor (Figure XIIa), to ferrite beads. Figure XIIb shows an air core inductor constructed to have a distributed capacitance of 2 pf. Most air core inductors were housed in conductive cases which function as shorted turn. At frequencies in the stop band, this shorting effect lowers the Q to low values (5 and below) which prevents circuit ringing. Series and parallel resistors are also used to prevent circuit ringing.

Capacitors: Extended foil capacitors are used where wound capacitors are necessary. When voltage, environmental and passband loss considerations allow, ceramic feed through capacitors are used because the high dissipation helps prevent filter ringing and reflection. Most capacitors are specified to allow eigen-resonances and require testing with sweep measurements before and after burn-in. In high-reliability wound capacitors, the eigen-resonances are unavoidable with ecologically allowed impregnates (unless a controlled internal resistance in the milliohms is employed), and losses must be designed into the filter to avoid EMP passing through the filter at these resonant points. Figure XIII shows a typical feed through capacitor ( 2.5 uf 120v AC) and its 50 ohm insertion loss curve.

E. Semiconductor Limiters, Silicon Carbide and Metal Oxide Varistors - MOV devices are presently used only on one secondary protection limiter, due to lack of reliability data and history when the present Minuteman designs were deployed. Future weapon system EMP suppression will undoubtedly make use of these devices.

Silicon carbide is used in a number of ESAs in series with the spark-gap to limit power-follow current. The energy handling capability of these devices has increased over the past few years as controls on binders, mixes and size has been improved. Maximum single pulse energy absorption achieved in Minuteman ESAs is 20 kj per cubic inch.

#### TEST DATA

Figures XIV and XV show the schematic of pulsers used to test EMP filters. Many other pulsers are used to test for intermediate frequency and energy consideration. Final performance for specific EMP threats is obtained by calculating the non-linear transfer functions of the limiters using the test data, and applying the EMP threat pulse to this model. The resulting printout contains the expected output waveform of the EMP limiter for a nuclear event.

Figure XVI is an example of test data for the 60 Hz primary power filter previously discussed.

#### TEST DATA (Cont)

Figure XVII shows the voltage/current waveform for a typical ESA subjected to a high kj pulse , and power follow current before and after this test.

Figure XVIII is an example of a silicon carbide block used in a typical ESA which "punched-through", indicating failure in a fail-safe (short) mode.

Figure XIX is an example of limiting achieved by using the bifilar type 60 Hz XFMR limiter.

Figure XX shows signal line test data for an LC type limiter and balanced line filter.

Figure XXI. Grounding method test data is detailed.

#### COMPARISON TO LIGHTNING THREATS

The primary difference between lightning and EMP threats is the high frequency (greater than 1 MHz) content of EMP pulses. Voltage levels on long land lines are often limited by line arcing, so that voltage levels are similar. EMP can have a long tail current similar to lightning, and lightning strokes have been photographed within the nuclear cloud. The methods to suppress EMP can be used for lightning protection, and in many instances the LC filter portion of the limiters could be deleted if lightning protection only is desired.

#### COMPARISON OF WEAPON SYSTEMS HARDWARE TO COMMERCIAL HARDWARE

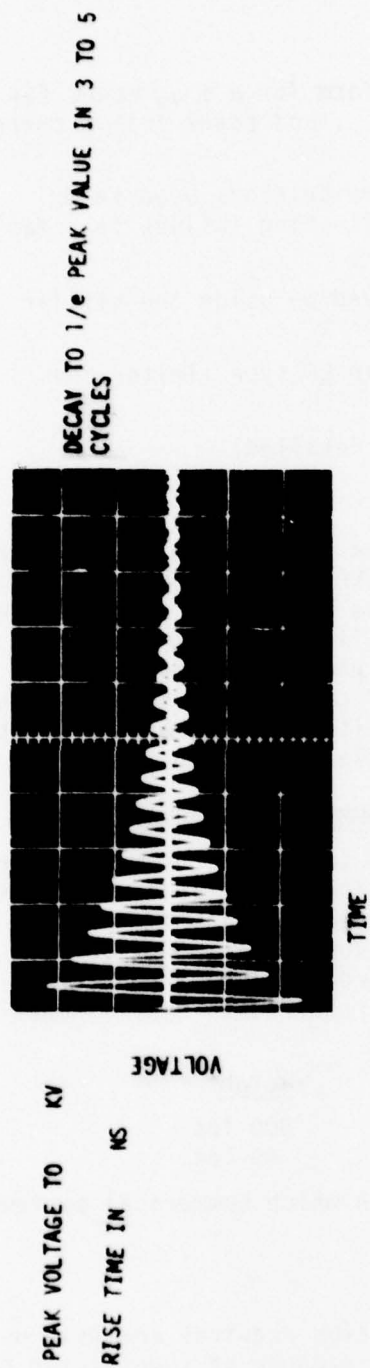
The size and cost between hardware designed to meet Minuteman requirements and commercial needs is illustrated in the following table. Unit X is a 4 wire, 208V 3Ø 200 AMP power line filter used for Minuteman. Unit Y is a 280V, 3 wire, 1Ø filter used on satellite communication systems. The limiting requirements for each filter are similar. The primary difference is that the Minuteman filter is required to handle repetitive pulsing, and severe shock and vibration.

	<u>Cost</u>	<u>Size</u>	<u>Weight</u>
Unit X	\$X	34" X 54" X 10"	800 lbs
Unit Y	\$.1X	11" X 21" X 5"	46 lbs

This is to illustrate the relative ease with which commercial systems can be provided with EMP protection.

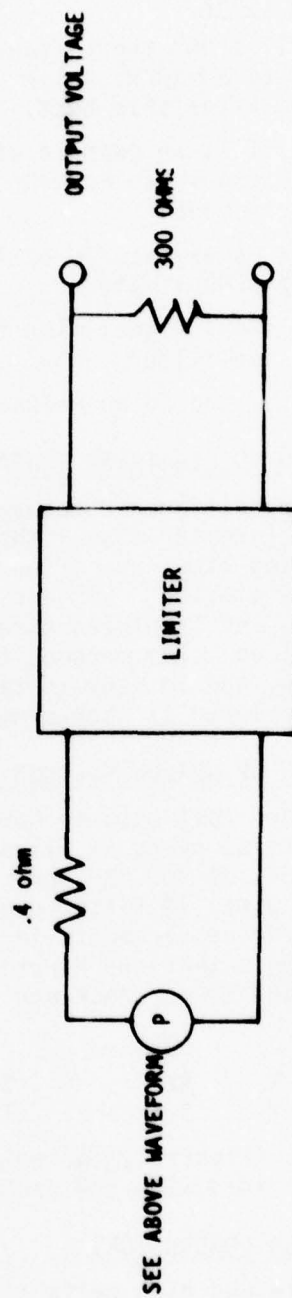
#### SUMMARY AND CONCLUSIONS

Large scale and high reliability EMP protection requires analysis on a system level. Few individual devices are capable of suppressing EMP pulses, and the interaction of different devices must be studied. Hopefully, by the grace of God, the occasion will never arise where EMP protection is tested in combat, and EMP limiting hardware will only be needed to fulfill a lightning protection role.



# TYPICAL EMP THREAT PULSE WAVEFORM

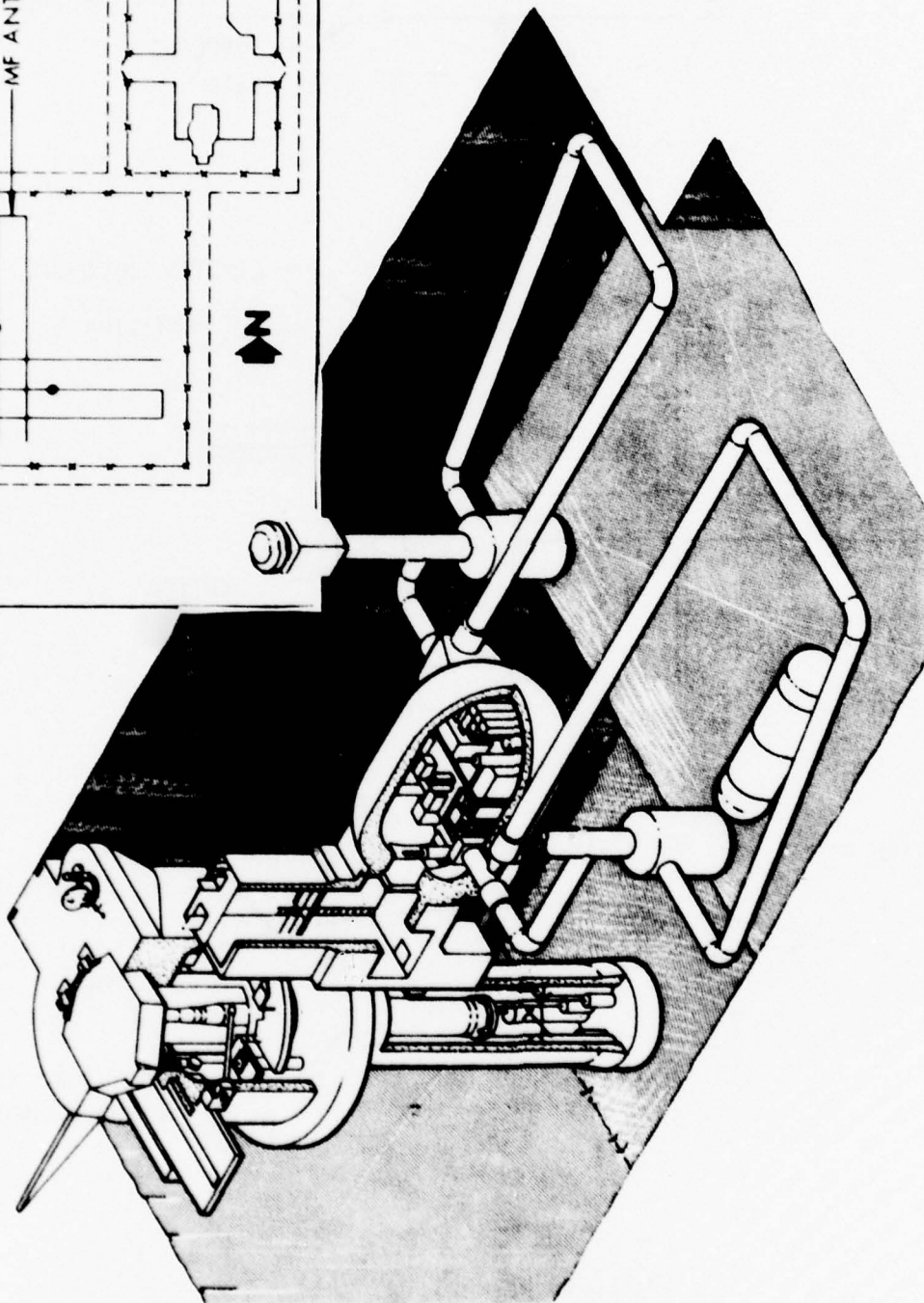
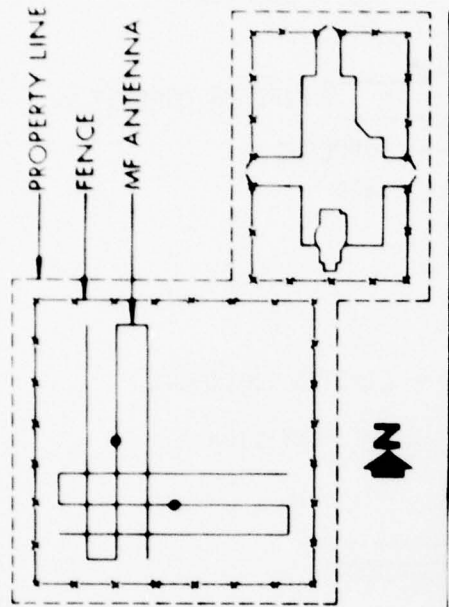
minimum frequency = 1 KHz  
maximum frequency = 20 MHz



TYPICAL EMP PULSE AND TEST SETUP

FIGURE 1





LAUNCH FACILITY

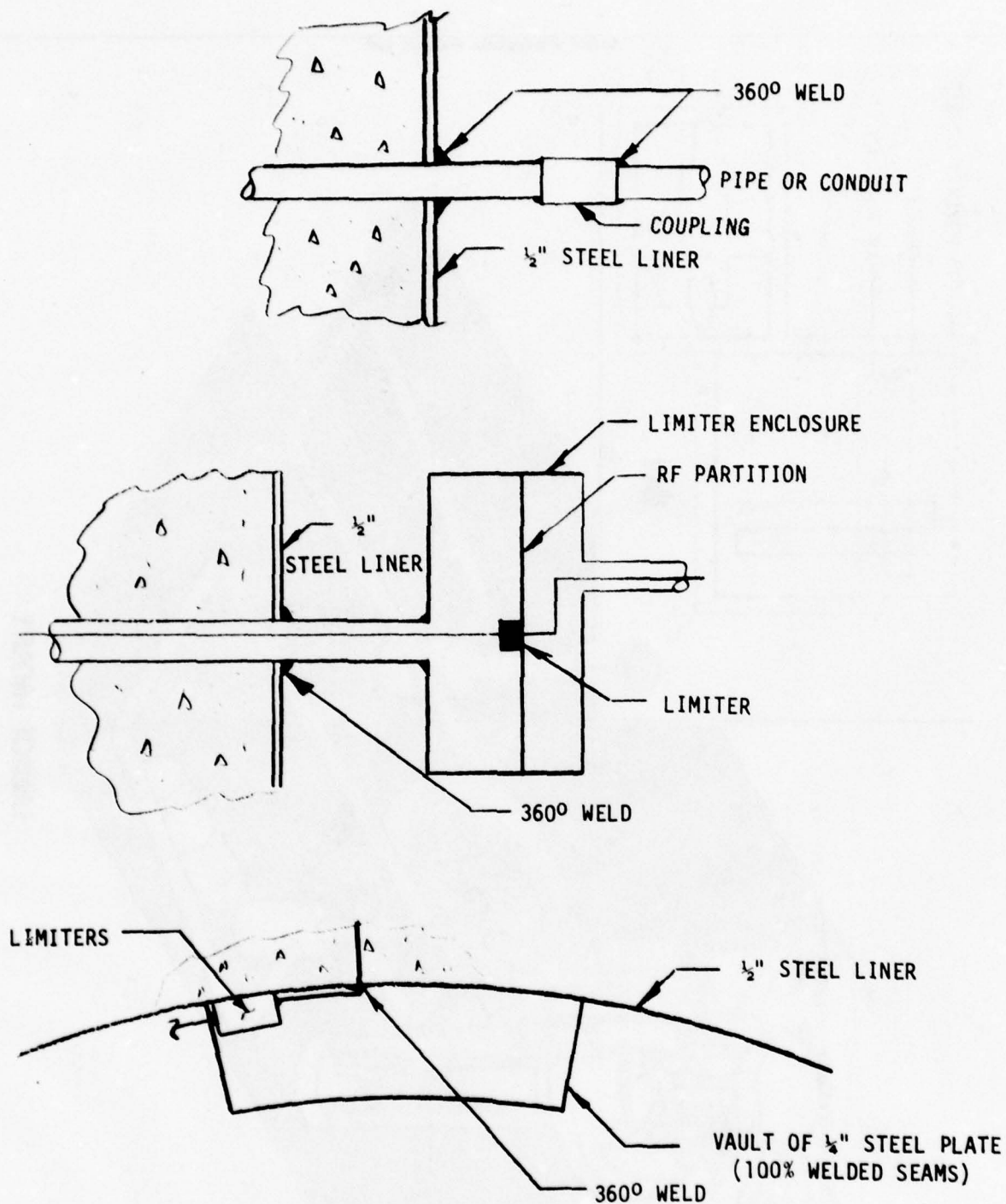
FIGURE II

FOR TRAINING  
PURPOSES ONLY

NA-69.1.3A

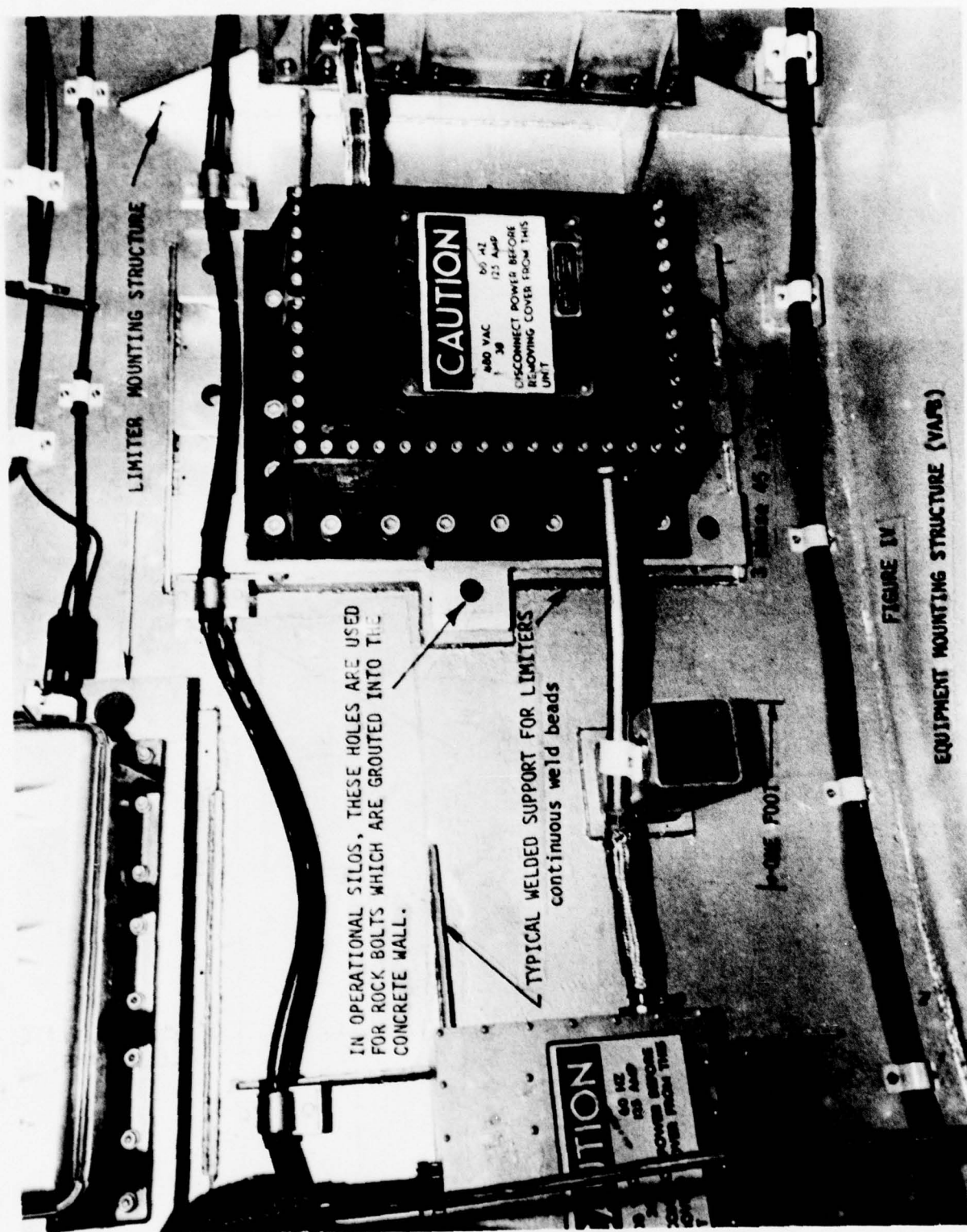
6-25-64

BLACK OF 1

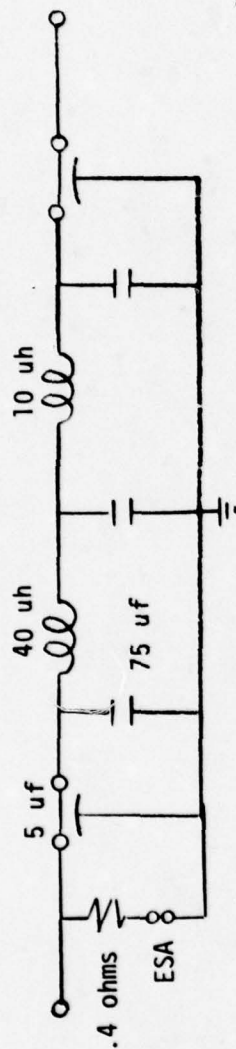


# SHIELDING METHODS

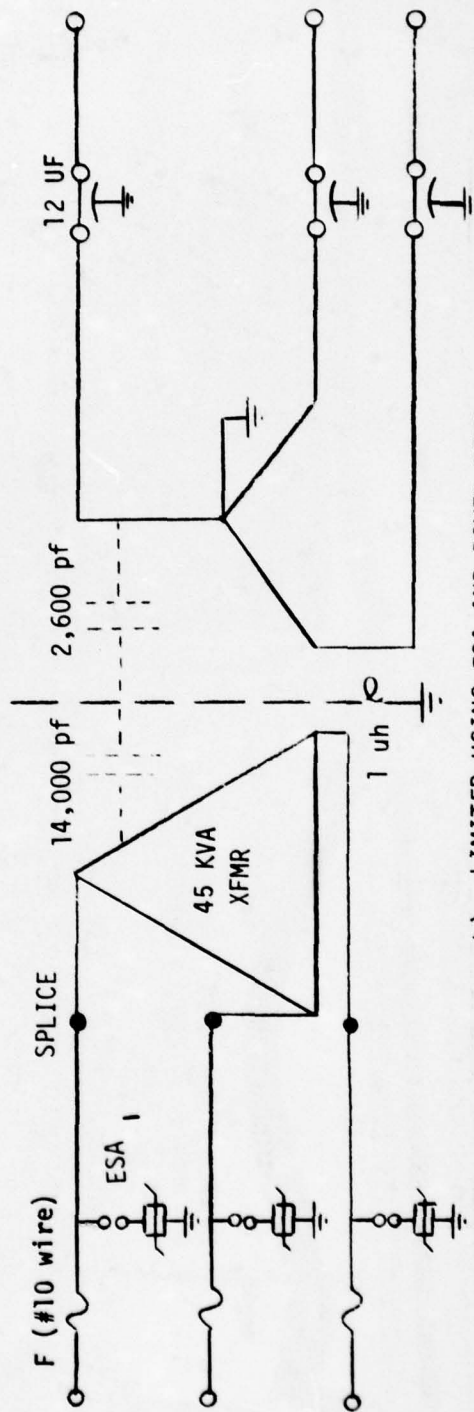
FIGURE III





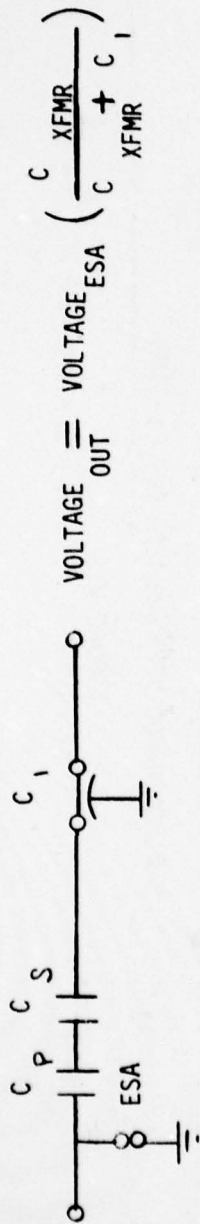


a) 200 AMP 60 HZ POWER FILTER  
ESA WITH LC FILTER



b) LIMITER USING ESA AND POWER XFMR

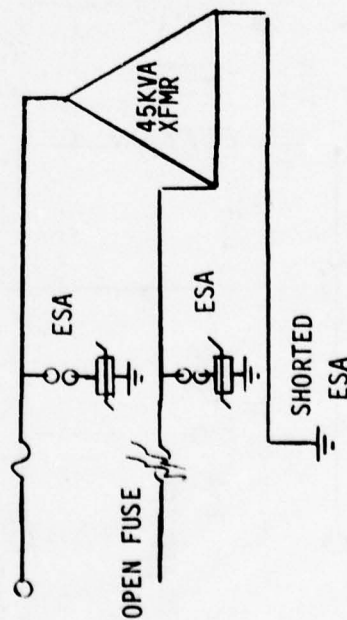
FIGURE V



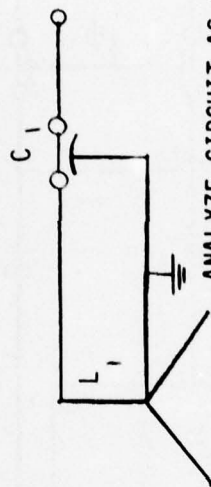
$$\text{VOLTAGE}_{\text{OUT}} = \text{VOLTAGE}_{\text{ESA}} \left( \frac{C_{\text{XFMR}}}{C + C_I} \right)$$

$$C_{\text{XFMR}} = \frac{C_S C_P}{C_S + C_P}$$

a) HIGH FREQUENCY EQUIVALENT CIRCUIT

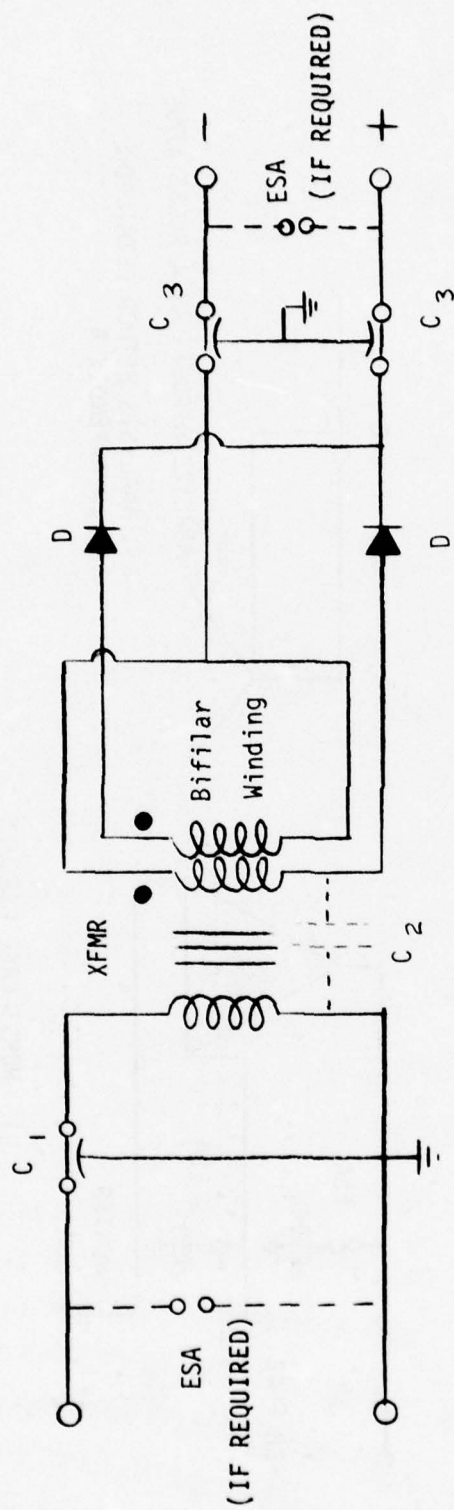


b) WORST CASE CIRCUIT



ANALYZE CIRCUIT AS A PULSE XFMR  
ANALYSIS METHOD DETAILED  
IN APPENDIX A

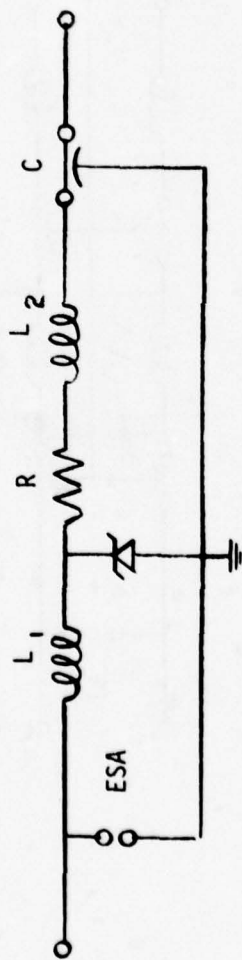
FIGURE VI



BIFILAR WOUND XFMR AND ESA EMP LIMITER

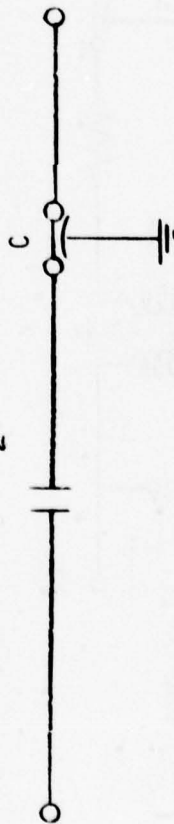
FIGURE VII





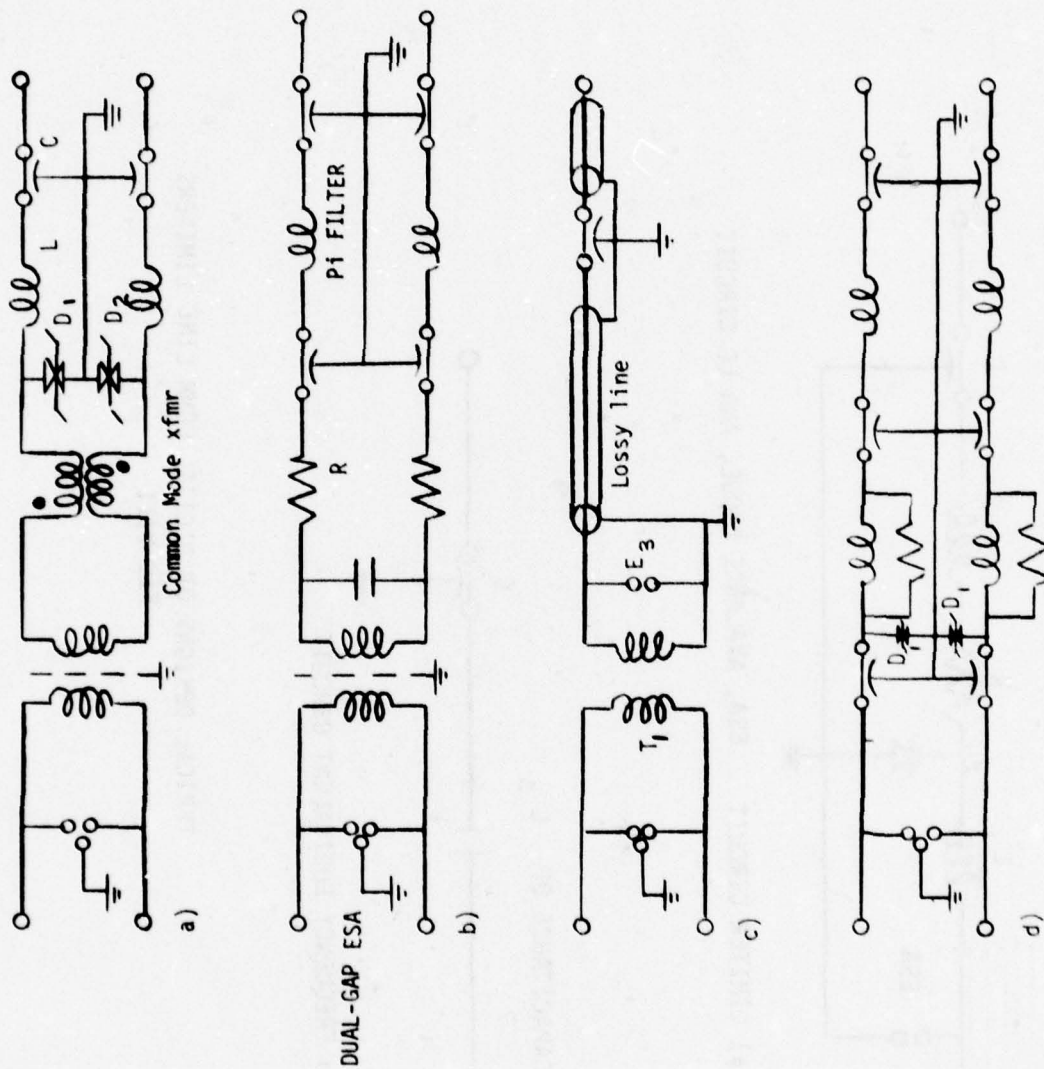
a) LIMITER CIRCUIT ESA, AVALANCE DIODE, AND LC CIRCUIT

DISTRIBUTED CAPACITANCE OF  $L_2$

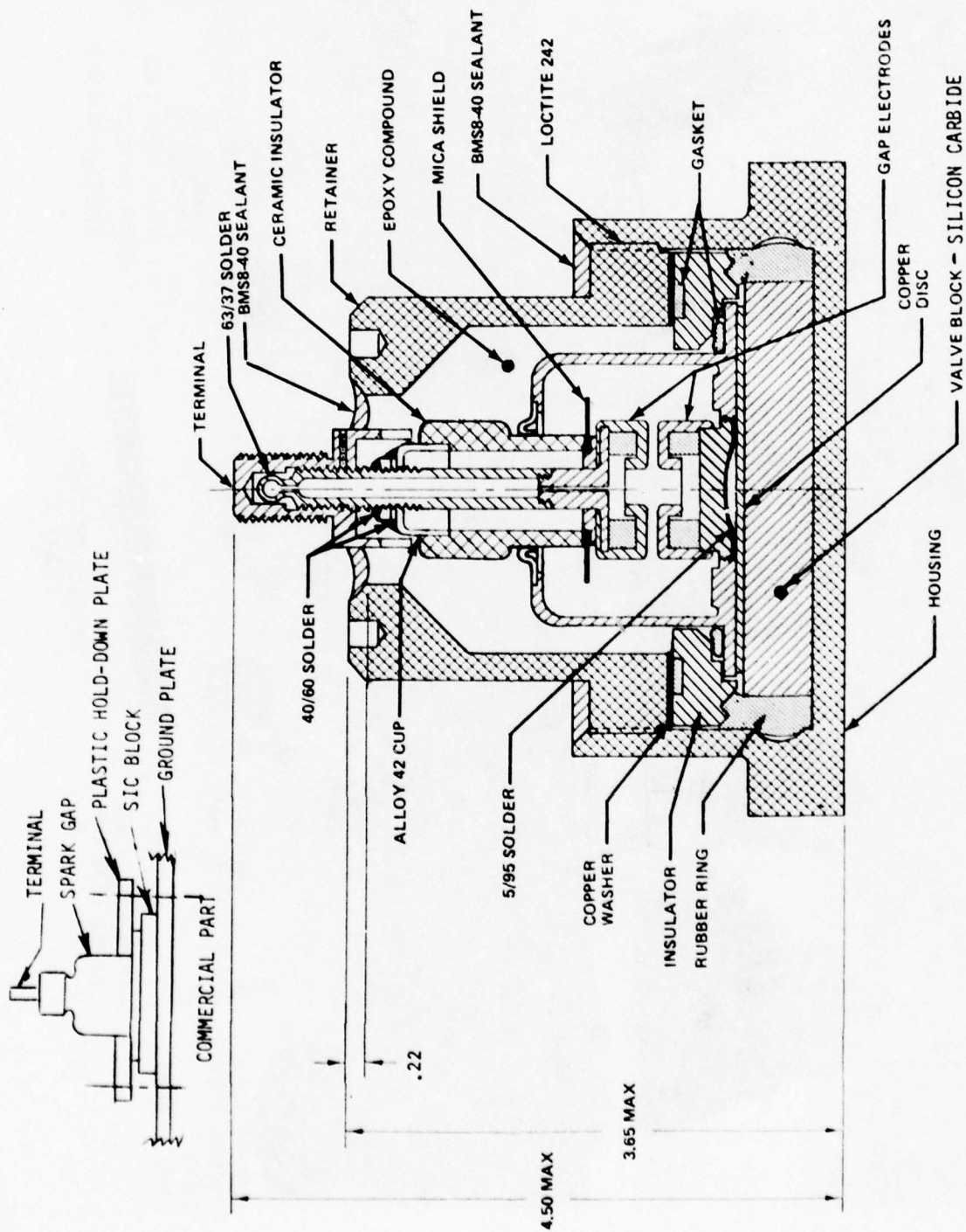


b) HIGH FREQUENCY EQUIVALENT CIRCUIT

TYPICAL DESIGNS OF DIGITAL COMM LINE LIMITERS  
FIG VIII



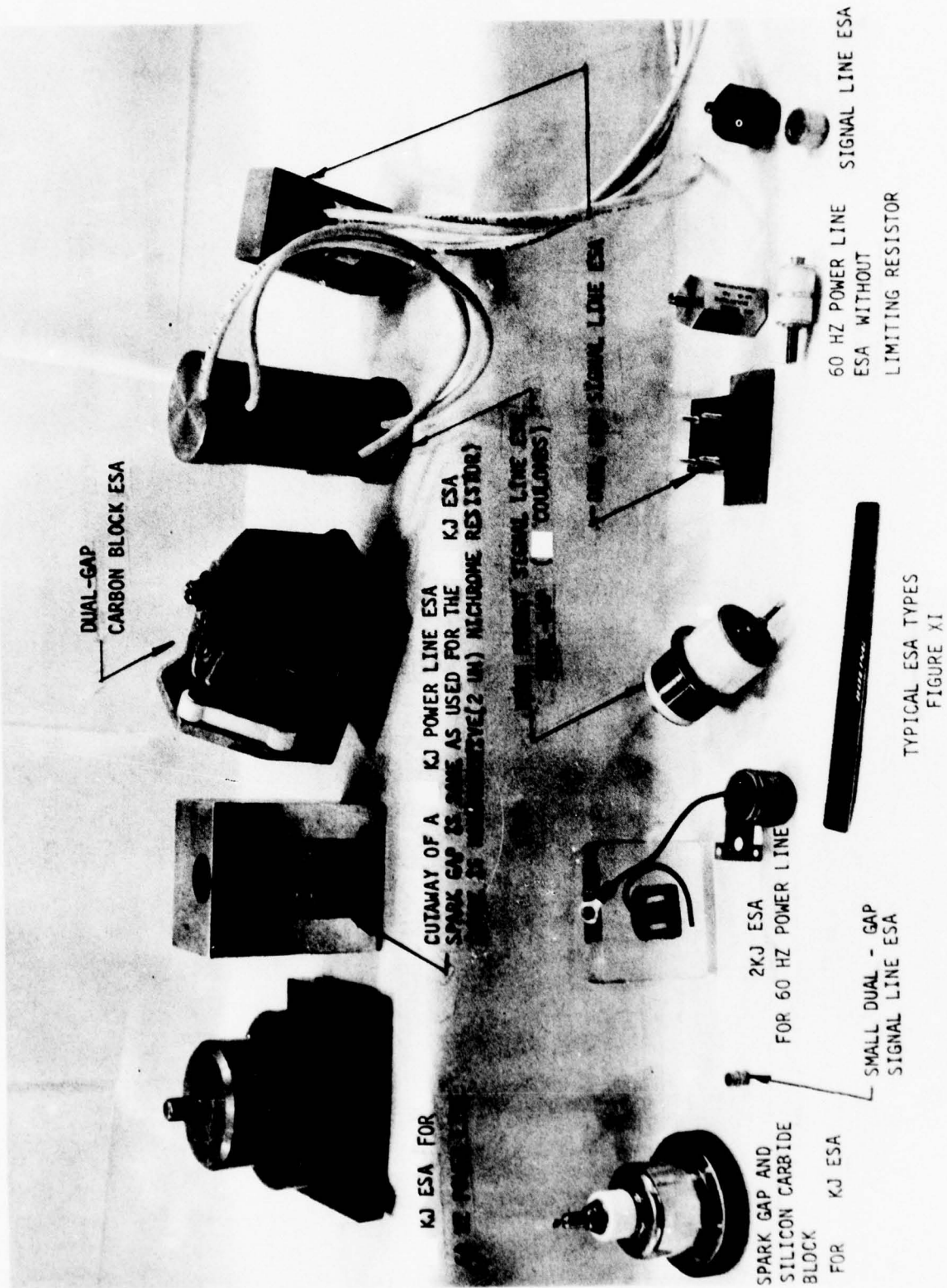
TYPICAL SIGNAL LINE LIMITER CIRCUITS  
FIGURE IX



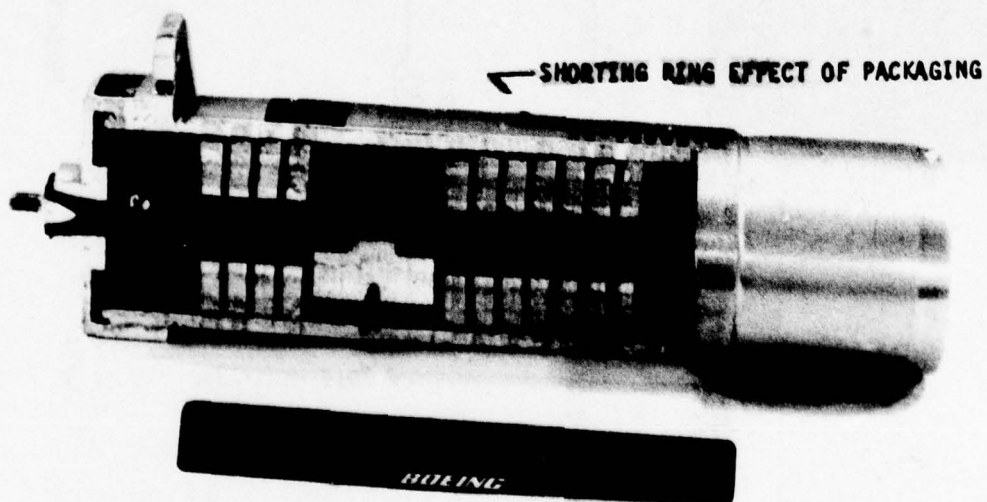
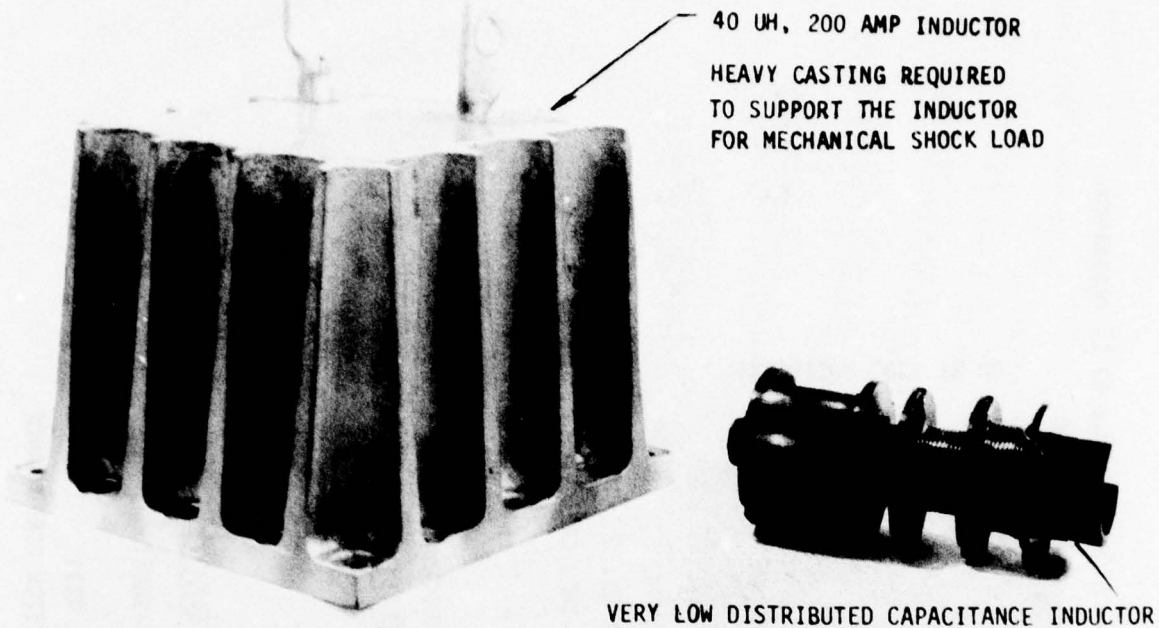
ESA CROSS SECTION, HIGH ENERGY ESA

FIGURE X





TYPICAL ESA TYPES  
FIGURE XI



TYPICAL INDUCTORS  
FIGURE XII

EIGEN-RESONANCES, due to LC resonances

30  
40  
50  
60  
70  
80  
90  
INSERTION LOSS IN db

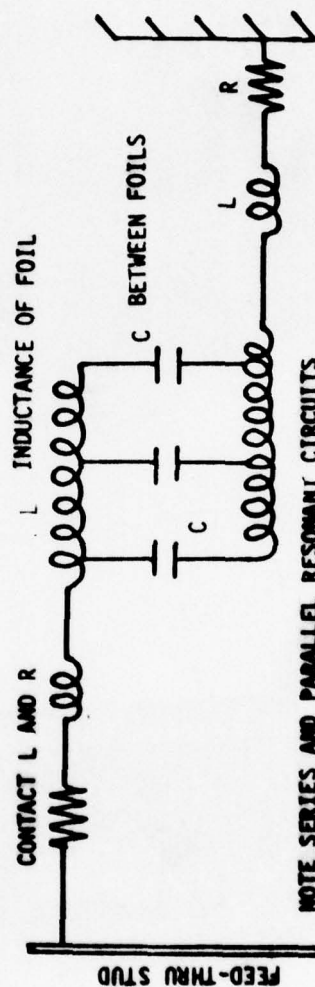


SERIES RESONANCES

UPPER CURVE IS SWEPT FREQUENCY, 0 - 10 MHZ

LOWER CURVE IS SWEPT FREQUENCY, 0 - 100 MHZ

50 OHM INSERTION LOSS FOR EXTENDED FOIL FEED-THRU CAPACITOR - 2.5 UF

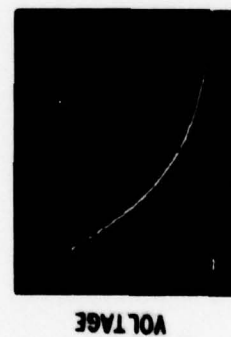
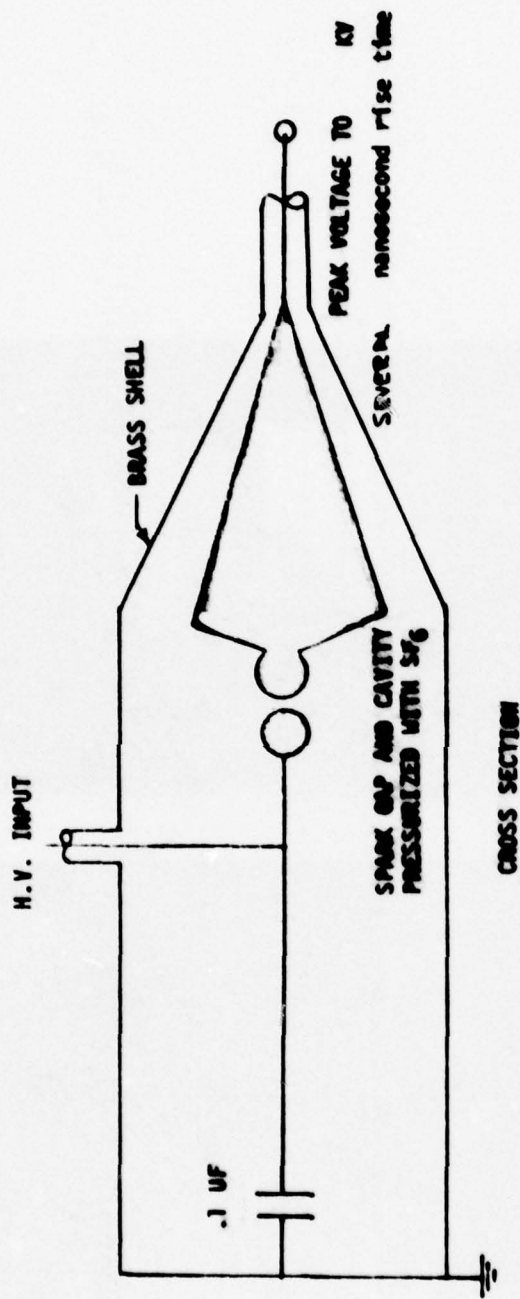


NOTE SERIES AND PARALLEL RESONANT CIRCUITS

FIGURE XIII

FEED-THROUGH CAPACITOR PERFORMANCE



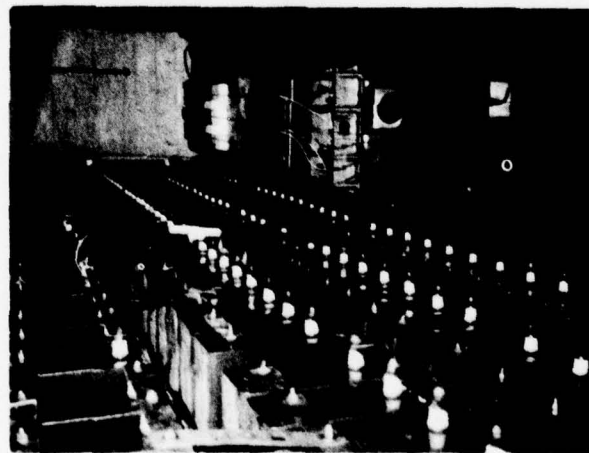
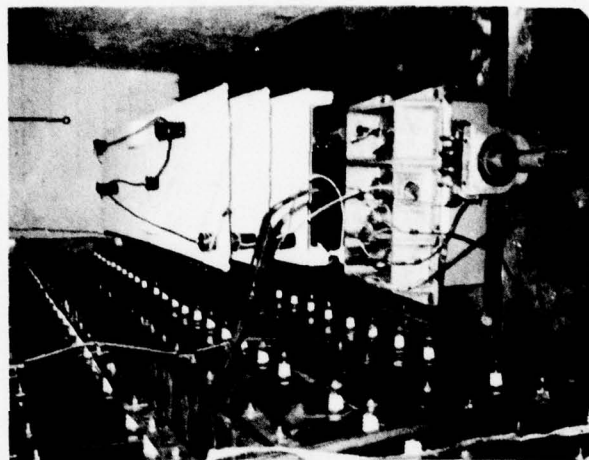
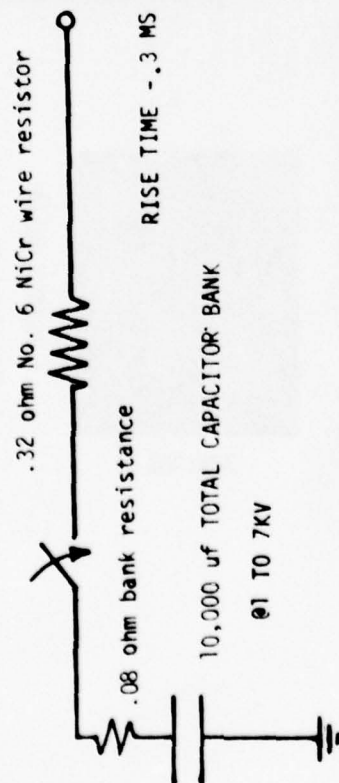
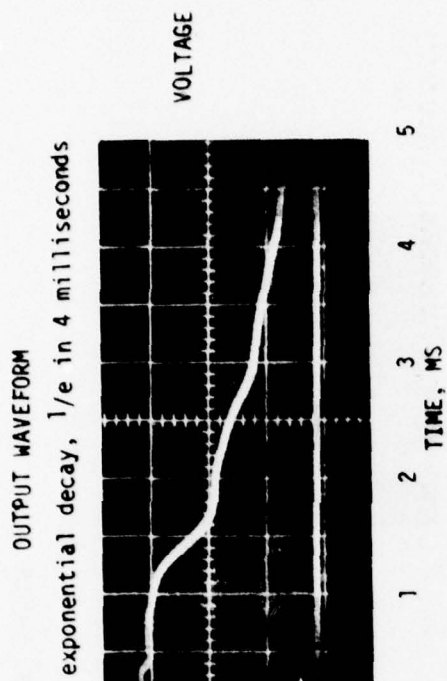


2 US/DIV SWEEP  
OUTPUT INTO 50 OHMS



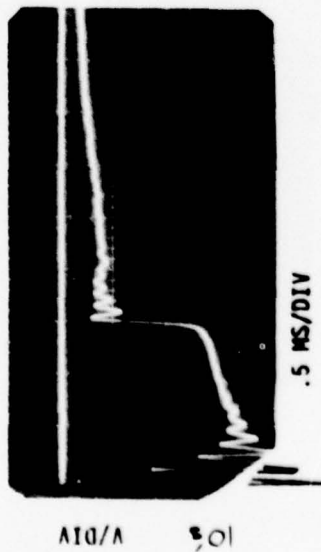
100 NS/DIV SWEEP  
OUTPUT INTO POWER LINE ESA

HIGH FREQUENCY M<sup>2</sup> PULSER  
FIGURE XIV



HIGH ENERGY M2 PULSER

FIGURE XV



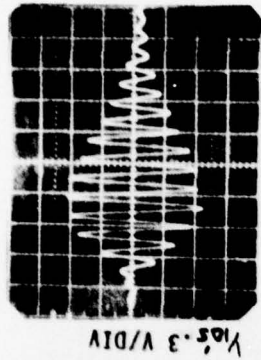
CIRCUIT RESPONSE, DRIVEN AS  
IN FIGURE VIIb BY PULSER OF  
FIGURE XV.

TYPICAL PULSE XPR  
RESPONSE

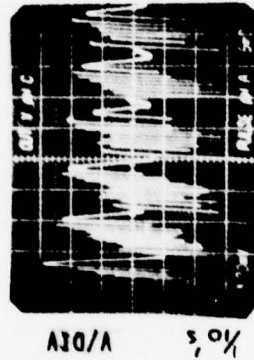
SEE APPENDIX A FOR ANALYSIS



1 MS/DIV

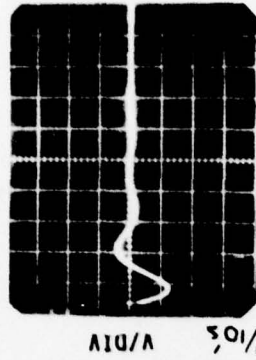


.5 US/DIV



5 MS/DIV

CIRCUIT RESPONSE, DRIVEN AS  
IN FIGURE VIIb BY PULSER OF  
FIGURE XIV



50 US/DIV

CIRCUIT RESPONSE, ALL INPUTS  
DRIVEN BY PULSER OF  
FIGURE XIV

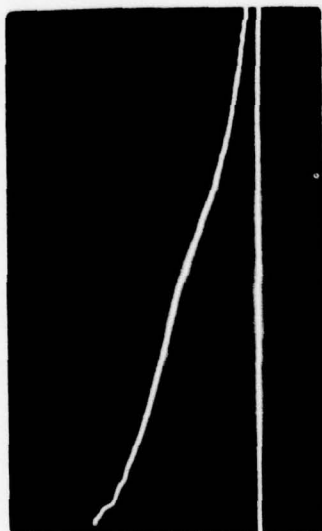
GROSS NON-LINEAR RESPONSES  
DUE TO NON-DRIVEN ESA FIRING  
AND XPR GOING IN AND OUT OF  
SATURATION

LIMITER PERFORMANCE EVALUATION

FIGURE XVI



ESA VOLTAGE



00V/DIV

2MS/DIV

ESA CURRENT



KA/DIV

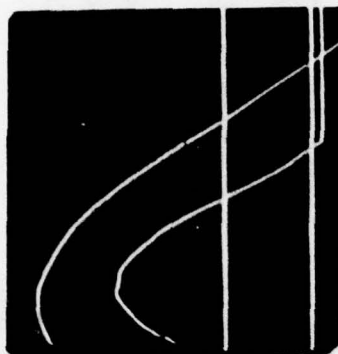
1MS/DIV

$$\text{ENERGY} = \int V I dt = \text{KJ}$$

HIGH ENERGY ESA PERFORMANCE  
DRIVEN BY PULSER OF FIG XV

LINE VOLTAGE

(277 VAC)

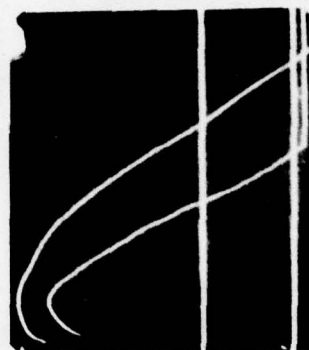


17A/DIV

60 HZ POWER FOLLOW BEFORE 70 KJ TEST

LINE VOLTAGE

(277 VAC)

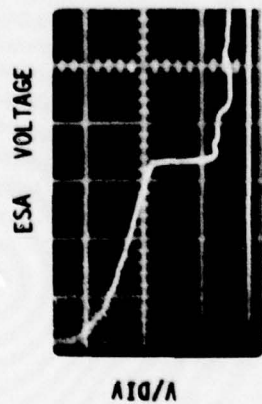


17A/DIV

60 HZ POWER FOLLOW AFTER 70 KJ TEST

ESA HIGH ENERGY TEST DATA

FIGURE XVII



2MS/DIV

FAIL-SHORT AT 6 + MS  
VOLTAGE CLAMPED AT 200V

ENERGY ABSORBED BY SIC ESA

$$= \int V I dt = KJ$$



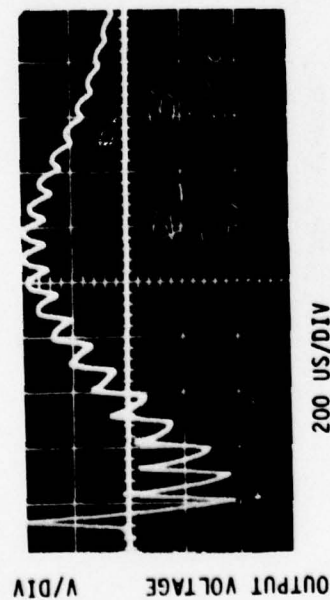
1MS/DIV



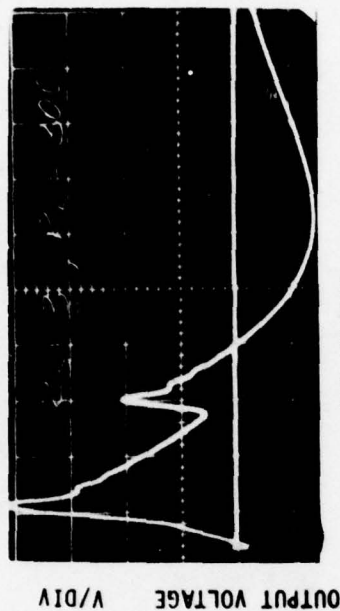
60 HZ POWER FOLLOW AFTER HIGH ENERGY TEST

SILICON CARBIDE PUNCH-THRU FAILURE MODE DATA

FIGURE XVIII



OUTPUT WITH 10KHZ INPUT



OUTPUT WITH 100 KHZ INPUT

INPUT VOLTAGE WAVEFORM PER FIG I

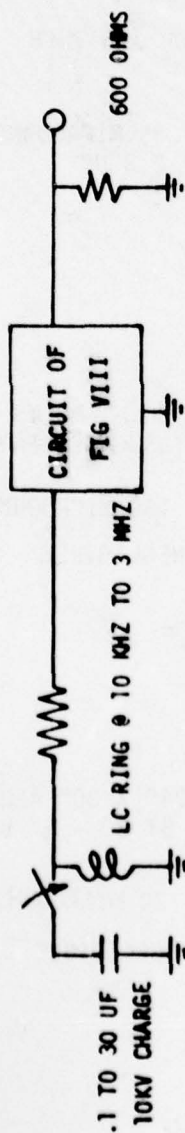
PEAK INPUT VOLTAGE = 10KV

NOTE THAT FUNDAMENTAL FREQUENCY OF BOTH WAVEFORMS IS DETERMINED BY XFMR AND OUTPUT CAPACITOR RESONANCE

60 HZ BIFILAR XFMR LIMITER TEST DATA  
CIRCUIT OF FIGURE VII

FIGURE XIX





OUTPUT VOLTAGE 3 MHZ INPUT



OUTPUT VOLTAGE 40 KHZ INPUT

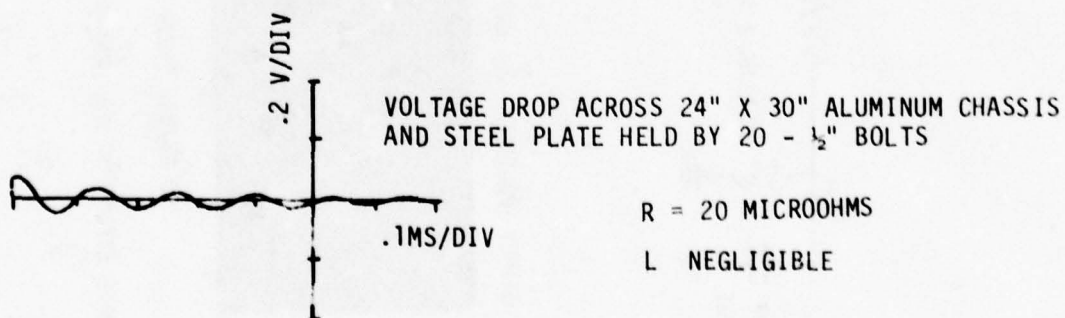
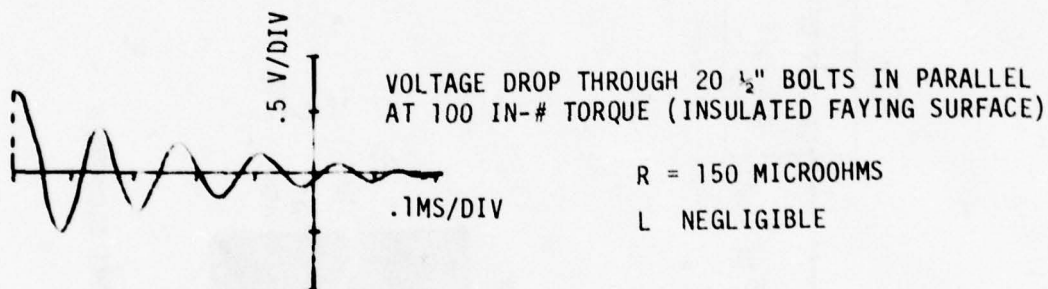
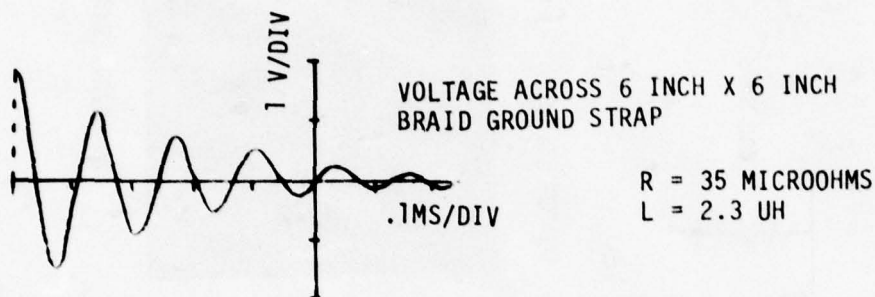
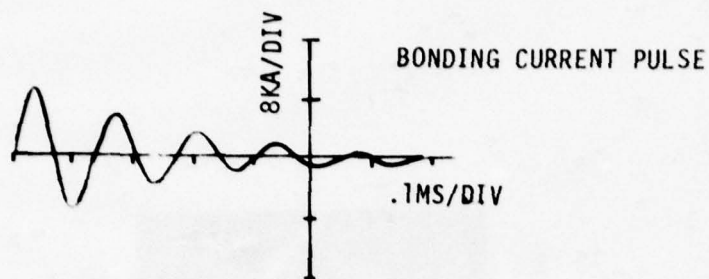


NOTE EFFECT OF NON-LINEAR CIRCUIT ELEMENTS

20 US/DIV SWEEP

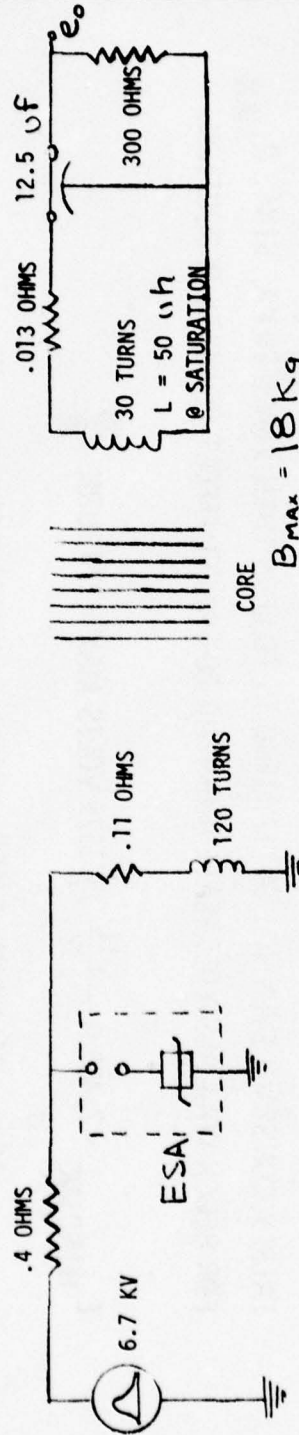
SIGNAL LINE LIMITER TEST DATA, CIRCUIT OF FIG VIII

FIGURE XX



GROUNDING PERFORMANCE DATA  
FIGURE XXI

# TYPICAL POWER SYSTEM WORST CASE ANALYSIS AT LOW FREQUENCY



$B_{max} = 18 \text{ Kg}$   
 $AREA = .00968 \text{ meters}^2$

$L = 25.5 \text{ mh OPEN CIRCUIT}$

L VALUES FROM VENDOR DATA



WCA  
(CONT)

$$N \frac{d\phi}{dt} = 30 \frac{d\phi}{dt} = L \frac{di}{dt} = E_{esa} - I_{MAX} (R_W) = E_{WINDING}$$

$$= ESA = I_{MAX} (.11) = E_{esa} - I_{MAX} (.11)$$

$$I_{MAX} = \frac{E_{ESA}}{.32} ; .32 = \text{EQUIVALENT LOOP RESISTANCE AT } E_{ESA} \text{ MAX.}$$

$$E_{WINDING} = E_{ESA} \left(1 - \frac{.11}{.32}\right)$$

$E_{ESA}$  MAX FOR WORST CASE = 2400 VOLTS, ACCOUNTS FOR BLOCK SPEC OF 3000 V @ 20 KA LESS REDUCTION IN CURRENT DUE TO ESA IN CIRCUIT. NOTE:  $\frac{di}{dt}$  WILL REMAIN FAIRLY CONSTANT EVEN IF ESA LIMITING IS TO LESS THAN 3 KV @ 20 KA, SINCE  $R_{MAX}$  FOR BLOCK WILL ALSO DECREASE AND TEND TO CANCEL EFFECT OF VOLTS REDUCTION.

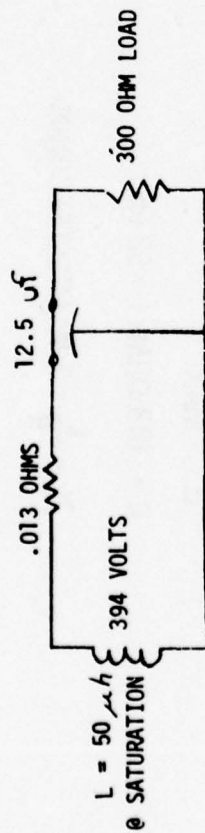
$$E_{WINDING} = 2,400 \left(1 - \frac{.11}{.32}\right) = 1575 \text{ VOLTS MAX} = 120 \text{ TURN } \frac{d\phi}{dt}$$

$$d\phi/dt = 13.125 \text{ W-M}^2/\text{SEC}$$

$$e_{OUT} = (13.125) (30 \text{ TURNS}) = 394 \text{ V (CORE SATURATION REACHED)}$$

APPENDIX A SHT 2

THE BOEING COMPANY  
SEATTLE WASHINGTON



F (RESONANCE) = 6 TO 8 KHZ

DAMPING FACTOR FOR  $R_L = 300 \Omega$ ;  $= \left( \frac{.013}{50 \mu h} + \frac{1}{(12.5 \mu F \times 300)} \times \frac{1}{(4 \pi F)} \right) = .003$   
 NEGLECTING DISSIPATION OF  
 FEED-THRU CAPACITOR

$$D; \text{ FOR } R_L = 4 \Omega \approx .15 = \frac{1}{(12.5 \mu F) 4} \times \frac{1}{(4 \pi F)}$$

FROM STD CURVES  
 OVERSHOOT FOR  $300 \Omega$  CASE

190 %  $e_p = 354 \text{ v @ } 8 \text{ KHZ}$  (WOULD BE REDUCED BY  
 DISSIPATION OF FEED THRU CAP)  
 FOR  $4 \Omega$

130% OVERSHOOT,  $e_{\text{peak}}$  OF 8 KHZ = 120 v

APPENDIX A SHT 3

THE **BOEING** COMPANY  
 SEATTLE WASHINGTON

# DURATION AND SHAPE OF OUTPUT VOLTAGE PULSE

$$\phi_B = BA = 1.8 \times .00968 = .017 \text{ WEBERS (B}_s = 18 \text{ Kg FROM CORE CATALOG)}$$

$$\text{FOR PRIMARY, } N\phi = .017 (120) = 2.04 \text{ WEBER-TURNS} = \text{VOLT-SEC}$$

$$V_{IN} = 1600 \text{ V}$$

$$V_{IN} \times (\text{time TO } B_{MAX}) = N\phi = 2.04$$

$$\text{time TO SATURATION} = \frac{2.04}{1,572} = 1.3 \text{ ms.}$$

DURATION OF PULSE OUT IS INVERSELY PROPORTIONAL  
TO AMPLITUDE OF PULSE ( $V_1 t_1 = V_2 t_2$ )

EXPONENTIAL DECAY OF PULSE IS BY

$$e_o = e_{MAX} (e^{-Rt/L})$$

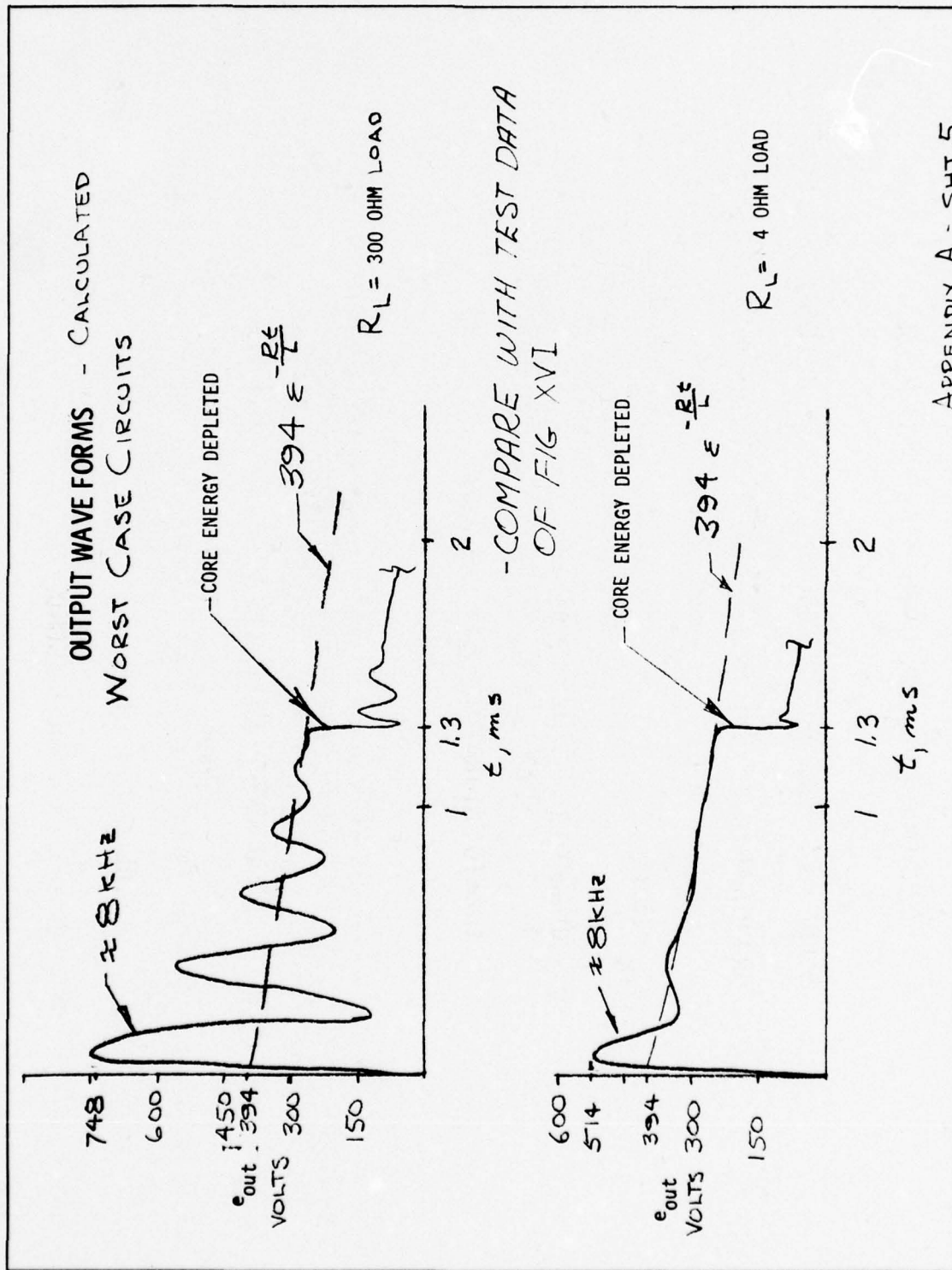
$$R = .013 \text{ OHM, } L = 50 \text{ vH}$$

$$\tau = \frac{L}{R} = 3.92 \text{ MILLISECONDS}$$

APPENDIX A SHT 4

THE **BOEING** COMPANY  
SEATTLE WASHINGTON





APPENDIX A - SHT 5

LONG TERM RELIABILITY STUDY  
OF THE TRANSORB<sup>TM</sup>

BY

O. MELVILLE CLARK

GENERAL SEMICONDUCTOR INDUSTRIES, INC.

TEMPE, ARIZONA

Presented At

Federal Aviation Administration/  
Georgia Institute of Technology

Workshop on Grounding and Lightning Protection

## ABSTRACT

Silicon avalanche suppressors designed specifically for transient protection have been in service for more than seven years. Applications for these components began with telecommunication protection and subsequently broadened over a large spectrum including submarines to satellites. Good engineering design along with stringent production tests have yielded products that have well satisfied the market in terms of reliability. History of performance has been very good, but unfortunately only qualitative and lacking exhaustive tests to accurately and quantitatively define life expectancy. NASA has recently funded a thorough, in-depth study on reliability of the TransZorb<sup>tm</sup> for developing engineering guidelines for using transient voltage suppressors. This two part test program has generated more than ten million device test pulses in which the components were pulsed in increments of 25% of the peak current (Ipp) from 25% to 150% of the maximum rating. From the extensive data gathered, a meaningful analysis was performed by the Reliability Analysis Group in the college of Engineering at the University of Arizona. The results of the test program and subsequent mathematical analysis yielded reliability curves which define the Mean number of Peak Pulses Before Failure (MP<sup>2</sup>Bf). Devices used in this study included the 6V, 33V, 91V, and 190V types to obtain adequate representation from the broad range of voltage distribution.



## INTRODUCTION

Technology in the semiconductor field has evolved into a very sophisticated process. Active semiconductor junctions can be packed into extremely tight geometries to the extent that in excess of 5800 transistors can be put on to a single silicon chip. The decreasing size of semiconductor elements has subsequently resulted in components which are quite vulnerable to transient voltages. Most CMOS structures have destruct levels in the microjoule region.<sup>(1)</sup>

Environments have been reasonably well defined quantitatively, with close proximity lightning producing static electric fields in excess of 100 volts per meter<sup>(2)</sup>, also with inductive transients aboard aircraft producing transient voltages of 800 volts<sup>(3)</sup> and with shipboard transients having magnitudes of 2500 volts peak.<sup>(4)</sup>

The TransZorb<sup>tm</sup> transient voltage suppressor was developed specifically to protect semiconductors from the destructive effects of transient voltages. To develop a meaningful definition of the long term reliability of the TransZorb, NASA awarded a contract to General Semiconductor Industries, Inc. to perform this study. This testing and evaluation effort was performed over a period of approximately two years involving in excess of 12-1/2 million test pulses. This report summarizes the results of the work performed under NASA Contract Nos. NAS8-30811 and NAS8-31547.

From this study was developed a meaningful definition of reliability in terms of the Mean Number of Peak Pulses Before Failure (MP<sup>2</sup>BF) for a broad spectrum of transient voltage suppressor types. This measure of reliability is in contrast to that to which we are ordinarily accustomed which is the Mean Time Before Failure (MTBF). The Mean Time Before Failure is virtually meaningless to a transient suppressor without knowledge of the number of transients and the magnitude of the transients to which the device was subjected. The MP<sup>2</sup>BF measure of reliability is meaningful to a transient voltage suppressor as this component operates in a stand-by mode in the circuit until a transient voltage appears. The device used in this

TransZorb<sup>tm</sup> - registered trademark of General Semiconductor Industries, Inc.

study was the TransZorb<sup>tm</sup> as manufactured by General Semiconductor Industries. The results of this study are not applicable to silicon suppressors manufactured by other suppliers because of the differences in design, construction, processing and test methods.

#### TEST METHODOLOGY

The devices tested for establishing MP<sup>2</sup>BF included 1200 TransZorbs with 300 parts used in each of four categories, including the 6.8V, 33V, 91V and 190V device types. The components within a given voltage category were sub-divided into groups of 50 each which were tested at 25°C ambient. The TransZorbs were pulsed over a broad range of Peak Pulse Current (Ipp) levels. The lowest pulse level was at 25% of the rated Ipp with subsequent pulsing at increasingly higher levels in increments of 25% up through 150% of the rated Ipp. The specific peak pulse current values are shown in Table I. All

TABLE I  
TRANSZORB<sup>TM</sup> PULSE EXPOSURE

Group	Sample Size	% Rated Ipp	Peak Pulse Current in Amperes			
			1N5629A 6.8V	1N5645A 33V	1N5656A 91V	1N5665 190V
1	50	25	35.75	8.25	3.0	1.45
2	50	50	71.5	16.5	6.0	2.9
3	50	75	107.2	24.75	9.0	4.35
4	50	100	143.0	33.0	12.0	5.8
5	50	125	178.7	41.25	15.0	7.25
6	50	150	214.5	49.5	18.0	8.70

electrical parameters were measured on the devices prior to test with parameters measured at pulse test levels of 500, 1500, 2000, 4000, 5760, 13,260, 15,760, 18,260, 20,760, and 25,760.

The components were selected for this study with a conscious effort to make each lot a homogenous group of several production runs. No additional pre-screening (i.e. burn-in at high temperature, storage, etc.) was performed to select out only the very best devices. Components used in these tests were considered representative of typical production lots.

The silicon transient suppressors were placed on pulse tests using automatic surge testing equipment with the capability of accommodating 50 components for a single test series. The equipment was constructed with individual test stations having the capability of recording the number of pulses administered to the components on test. Devices were pulsed at intervals of one minute. When the suppressor became inoperative, either open or short, the pulse counter was automatically disengaged from the test circuit thus displaying the number of pulses which the device incurred prior to failure.

The  $I_{pp}$  was adjustable over a wide output range to accommodate all pulse levels required in this study. The waveform of the test current pulse is a 10 X 1,000 (10 micro-seconds rise to peak with 1,000 micro-seconds to decay exponentially to one-half crest value). This waveform is shown in Figure 1.

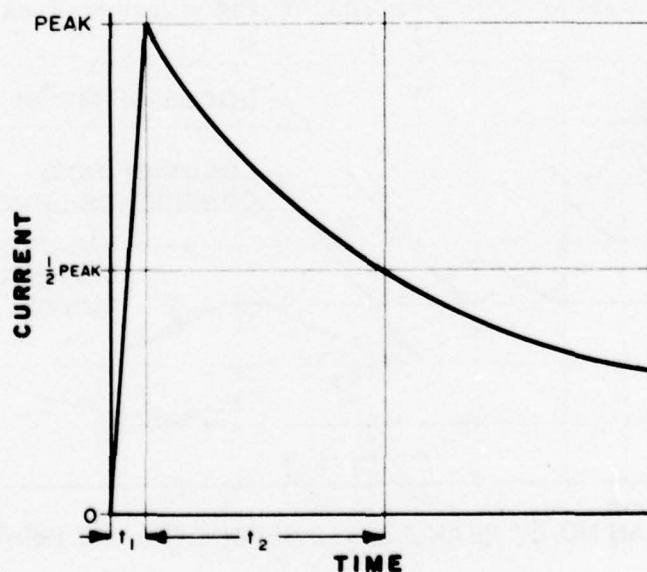


Fig. 1: Test Current Pulse Wave Form



The electrical parameters which were measured prior to surge testing included the Breakdown Voltage (BV) at the specified Test Current Level ( $I_t$ ), Reverse Leakage Current ( $I_r$ ) at the Reverse Standoff Voltage ( $V_r$ ), and Clamping Voltage ( $V_c$ ) at the 100% Peak Pulse Current ( $I_{pp}$ ) level. These parameters are characteristic of silicon transient voltage suppressors.

### RELIABILITY ANALYSIS

The evaluation of data gathered during the life tests and subsequent analysis of the test results on this study contract were performed by Professor E. B. Haugen and his staff at the University of Arizona in Tucson. The goal of this study was to obtain a meaningful reliability curve for each of the TransZorb<sup>tm</sup> voltage types tested and for the development of a meaningful  $MP^2BF$  curve for those voltage categories. An idealized curve plotting the percent of rated peak pulse current versus the mean number of peak pulses before failure is shown in Figure 2. With a sufficient number of pulses, it should be possible to extend this curve for each of the device types selected in this test. However, there were insufficient failures at the 75% peak pulse level and below to generate meaningful data and subsequently this portion of the curve was extrapolated.

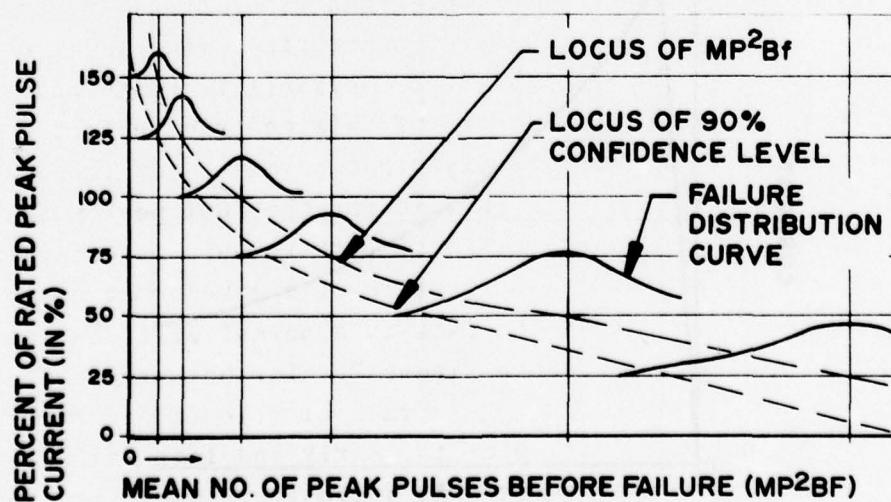


**Fig. 2:** Loci of Mean No. of Peak Pulses to Failure and 90% Confidence Level for Ideal Case

The pulse levels at which failures occurred extended over a very broad range as illustrated in Table II. This table lists the data for the 6.8V types indicating the first failure occurring at 834 pulses with the last failure occurring at 20,540 pulses. For the higher voltage types, the devices failed at earlier pulse levels as shown in Table III. For the 91V type the first failure occurred at 496 pulses with the last failure occurring at 9,895 pulses. This illustrates the generally higher reliability of lower voltage pn junctions.

The mean number of pulses to failure and standard deviation for the 6.8V type are shown in Figure 3 which portrays the failure distribution curve along with a histogram of the failed devices. For the most part, the histogram compares reasonably well to a distribution curve with exception of the four early failures. The failure statistics, including the number of pulses to failure and the standard deviation for the 91V TransZorb<sup>tm</sup> are shown in Figure 4. Here again, a reasonably good fit of the histogram to the distribution curve is illustrated with the exception of two components which lie outside of the distribution on the high side. In contrast to the 6.8V and the 91V types the failure statistics for the 190V type are shown in Figure 5. There appears to be three separate populations within this group and definitely no fit of the histogram to the distribution curve. At the beginning of this test effort, the 190V had been considered less reliable than other types and concurrent with the NASA tests new designs were constructed using a different technique yielding higher reliability. Reliability tests on this new structure were not performed as part of this contract effort.

Fit of the data to a normal distribution curve for the 6.8V failures is shown in Figure 6. This is for the 100% peak pulse current failures as mentioned previously, there were insufficient failures at the 75% peak pulse current level and below to perform reliability analysis. Fit of the data to a normal distribution curve for the 91V TransZorb is shown in Figure 7. For both the 6.8V and 91V types, the fit of the data to a normal distribution curve appears to be linear, with the exception of the early and late failures.

The results given in Figures 8-11 inclusive, summarize the MP<sup>2</sup>BF at the various levels of Ipp from 25% of Ipp max up to 150% of Ipp

TABLE II

PULSE LEVEL AT WHICH FAILURE OCCURRED

DEVICE TYPE: 6.8V TRANSZORB™

(1N5629A)

---

FAILURE SEQUENCE	PULSES INCURRED	FAILURE SEQUENCE	PULSES INCURRED
1	834	26	9637
2	2054	27	9776
3	2581	28	9824
4	2767	29	10079
5	4201	30	10136
6	5762	31	10175
7	5806	32	10254
8	5899	33	10263
9	6214	34	10287
10	6658	35	10641
11	7206	36	11112
12	7591	37	11618
13	7853	38	11693
14	7861	39	11999
15	7922	40	12611
16	8380	41	12761
17	8454	42	12945
18	8603	43	13020
19	8842	44	13870
20	8883	45	14629
21	8966	46	15006
22	9209	47	15425
23	9387	48	20102
24	9453	49	20540
25	9454		

 $n = 49$      $\bar{x} = 9100$



TABLE III

PULSE LEVEL AT WHICH FAILURE OCCURRED

DEVICE TYPE: 91V TRANSZORB™

(1N5656A)

FAILURE SEQUENCE	PULSES INCURRED	FAILURE SEQUENCE	PULSES INCURRED
1	496	24	2227
2	547	25	2569
3	637	26	2607
4	678	27	2610
5	745	28	2627
6	852	29	2681
7	942	30	2683
8	1114	31	2687
9	1233	32	2708
10	1246	33	2822
11	1309	34	2965
12	1311	35	3173
13	1342	36	3177
14	1361	37	3195
15	1371	38	3410
16	1392	39	3469
17	1411	40	3664
18	1592	41	3785
19	1698	42	5081
20	1780	43	5209
21	2118	44	5495
22	2122	45	9698
23	2150	46	9895

$n = 46 \quad \bar{x} = 2562$

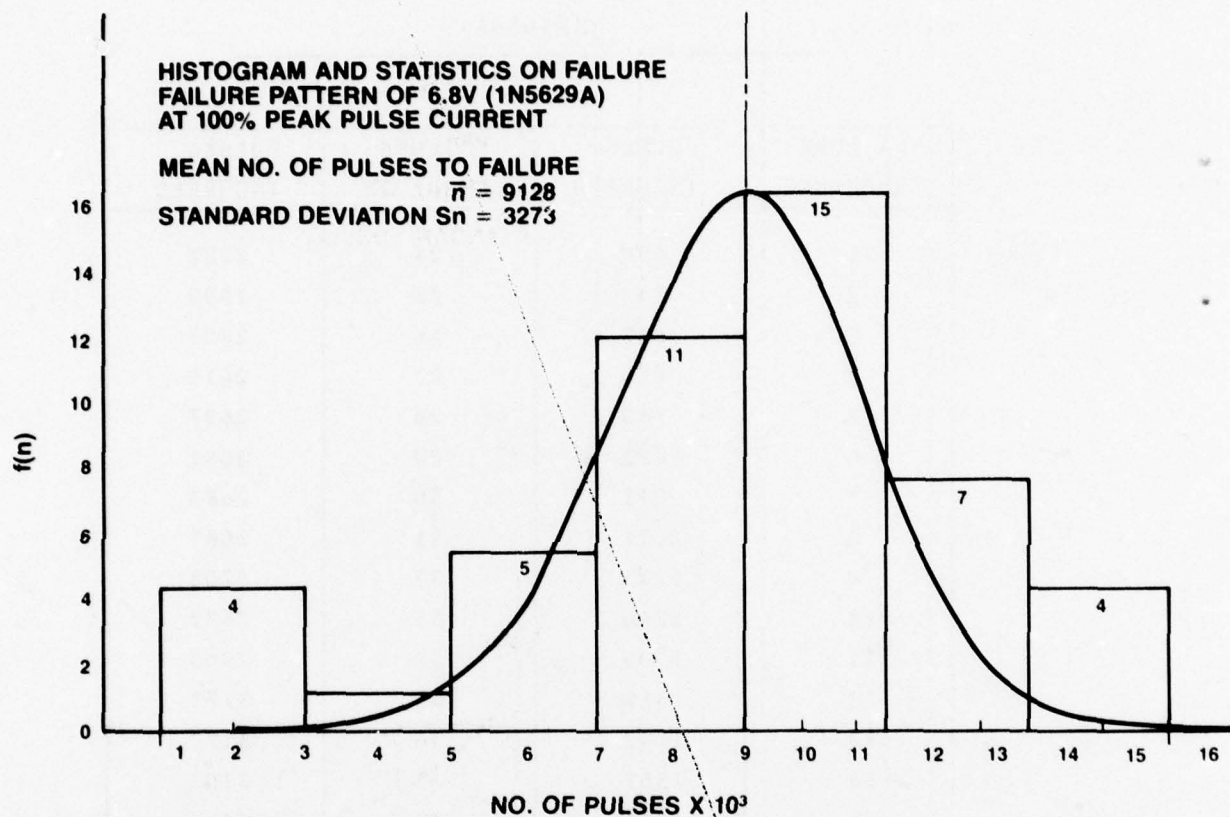


Fig. 3: Failure Statistics for 6.8V (1N5629A)

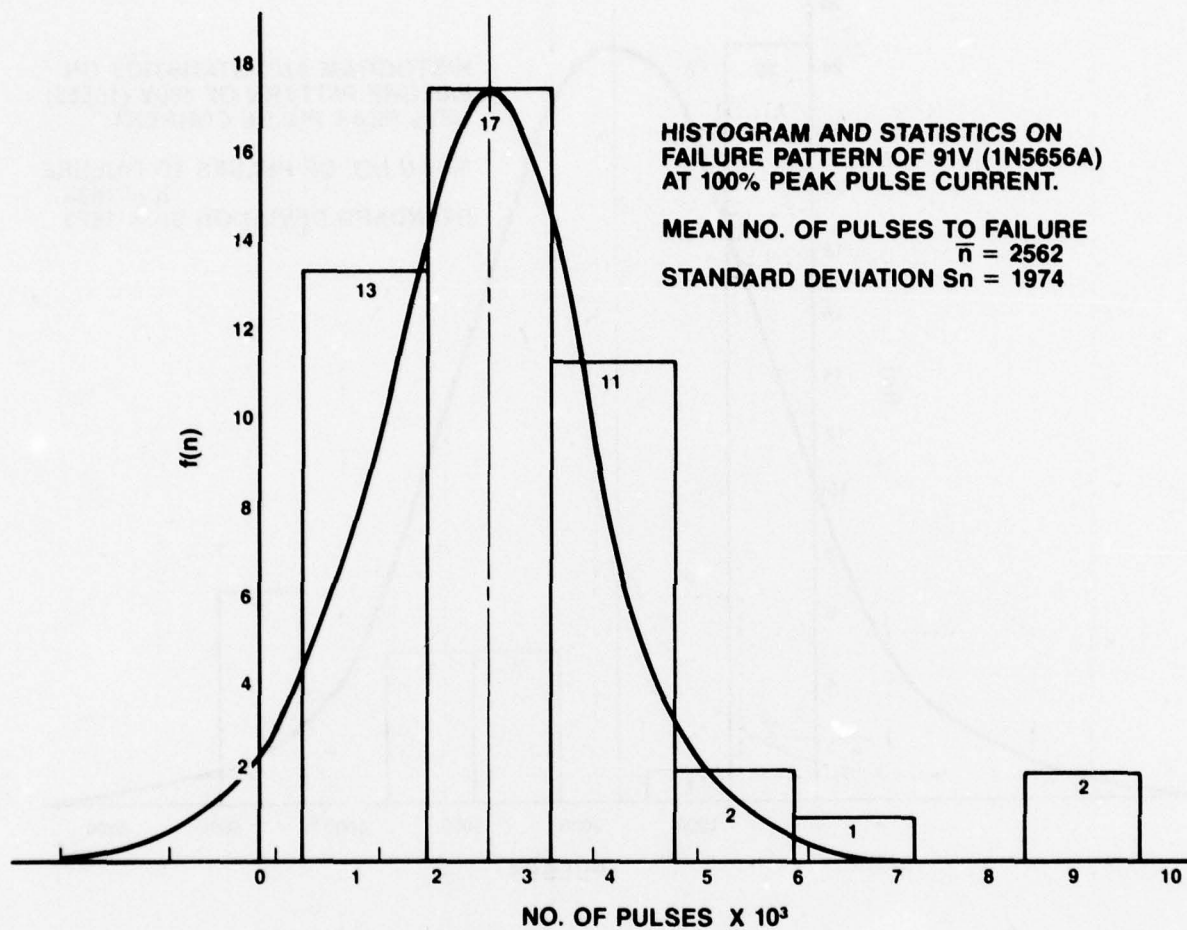


Fig. 4: Failure Statistics for 91V (1N5656A)



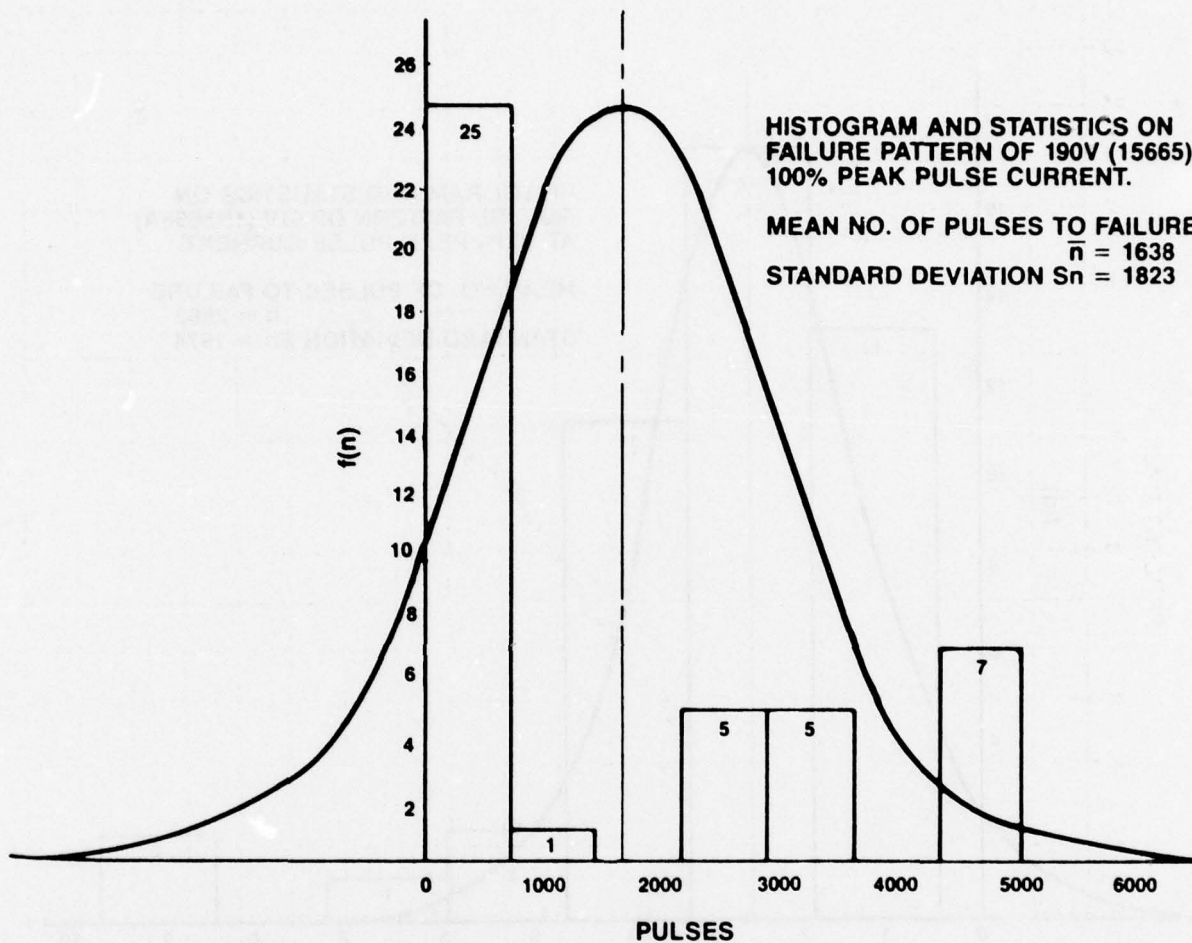


Fig. 5: Failure Statistics for 190V (IN5665)

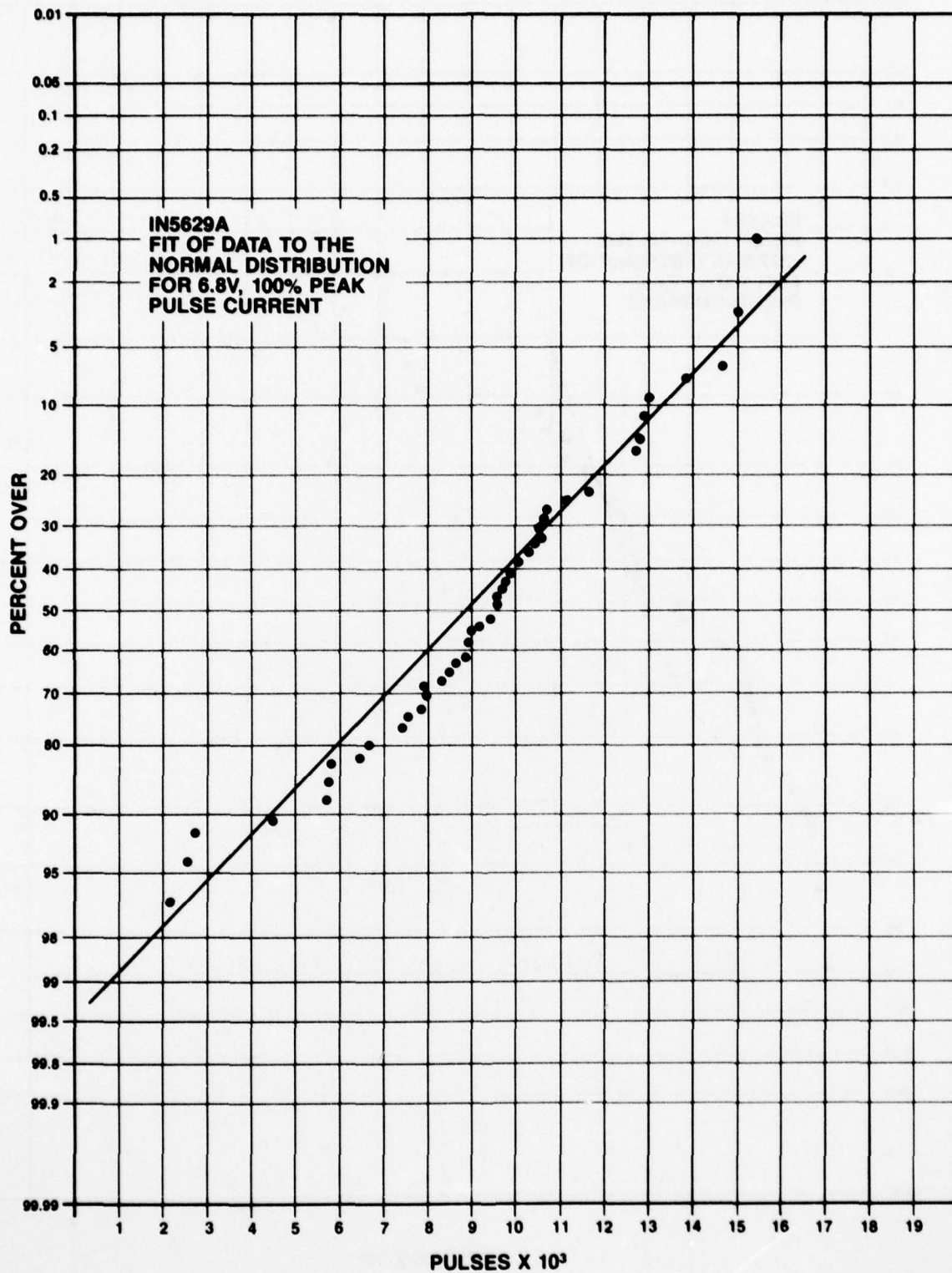


Fig. 6: Fit of Data to Normal Distribution Curve for 6.8V  
(IN5629A) TransZorb™

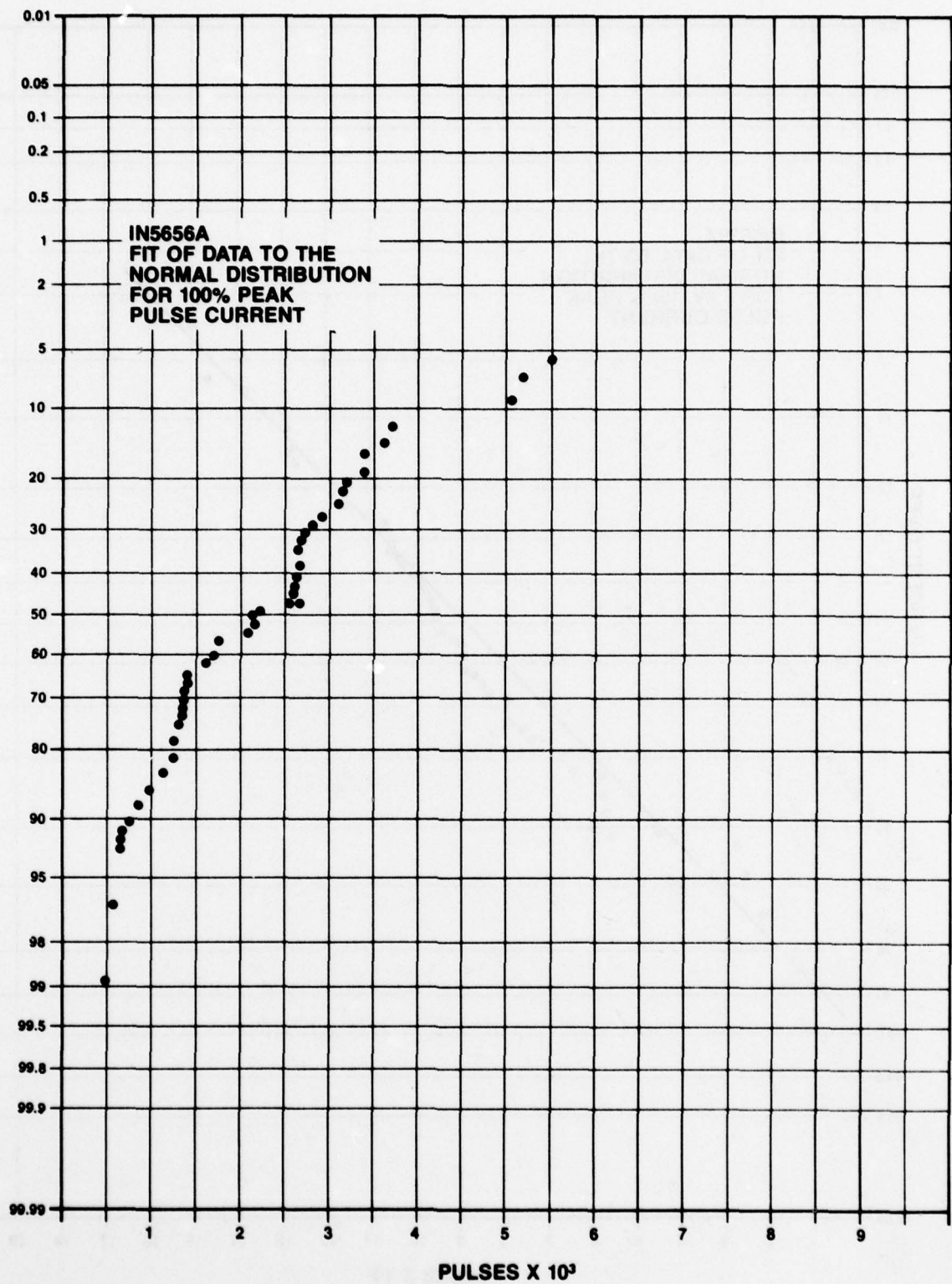


Fig. 7: Fit of Data to Normal Distribution Curve for 91V  
(IN5656A) TransZorb™



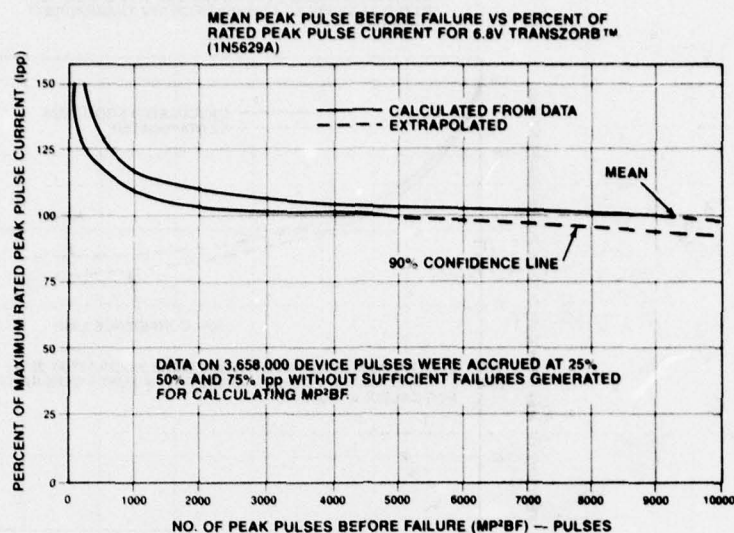


Fig. 8: Summary for 6.8V TransZorb™ (1N5629A)

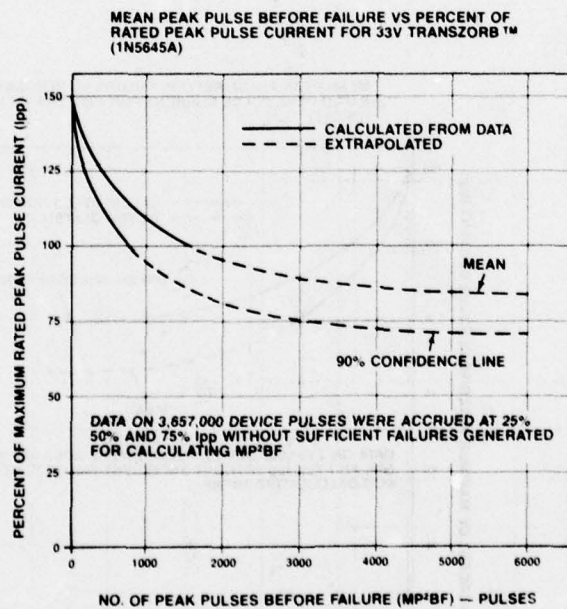


Fig. 9: Summary for 33V TransZorb™ (1N5645A)

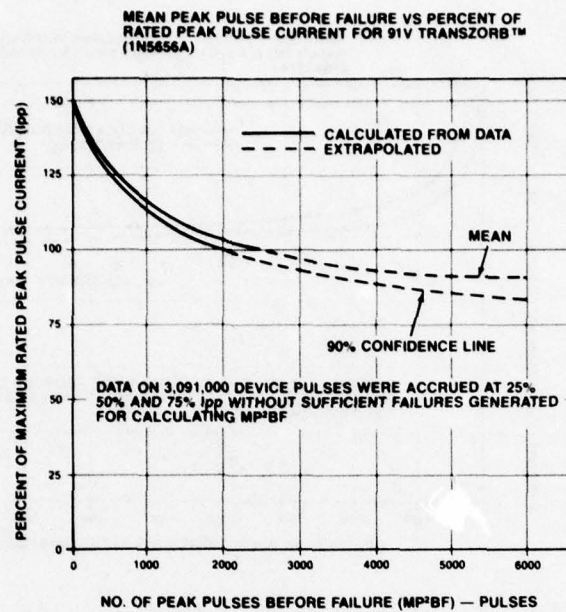


Fig. 10: Summary for 91V TransZorb (1N5656A)

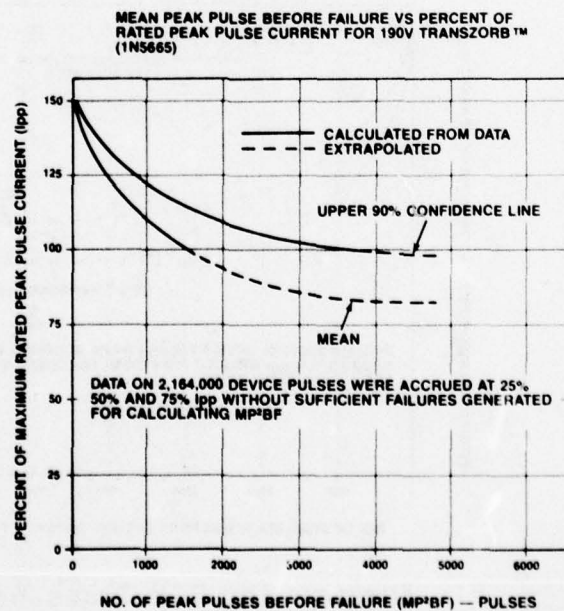


Fig. 11: Summary for 190V TransZorb (1N5665)

max for all devices tested. These curves display both mean and 90% confidence levels for each device type. The solid line in the curves is derived from the data and the dotted line represents extrapolated data. The extrapolations were necessary due to insufficient failures to generate accurate calculations.

#### FAILURE ANALYSIS

All devices which failed during the course of this test failed catastrophically in the shorted mode. From previous experience, devices which fail under pulse test conditions fail in the shorted mode. This was expected. There appeared to be two basic reasons for failure. One was attributed to overstressing the components in excess of their rated values where devices failed short under relatively few pulses. The other appears to be a "wear-out" which manifests itself near the maximum peak pulse current levels after long term pulsing. This "wear-out" appears to be due to a very gradual change in the intermetallic bonding material between the silicon junction and the silver heat sinks. This change in the bonding results in gradual separation beginning at the periphery. This reduction in bonding area subsequently reduces the heat sinking capability of the silicon junction thus increasing the temperature under pulsing to a level which would produce subsequent shorting.

A sample of devices from each voltage category were dissected and the junctions were removed and subsequently analyzed for the physical nature of failure. An example of a 6.8 volt shorted silicon die is shown in Figure 12. Figure 13 shows an example of a shorted 33 volt silicon junction. This particular junction had significant heat generated to result in cracking of the die. This is not unusual in a failure of this type of component. Figure 14 represents a typical 91 volt shorted silicon junction. Here again the die was fractured due to the heat generated. Although it is not readily apparent in the photographs shown, a well-defined melted area in the silicon exists in the region of the short. This melting is the result of preferential funneling of the current through one small region of the junction during the current.



pulse and subsequently increasing the temperature to the melting point of silicon which is about  $1420^{\circ}\text{C}$ .

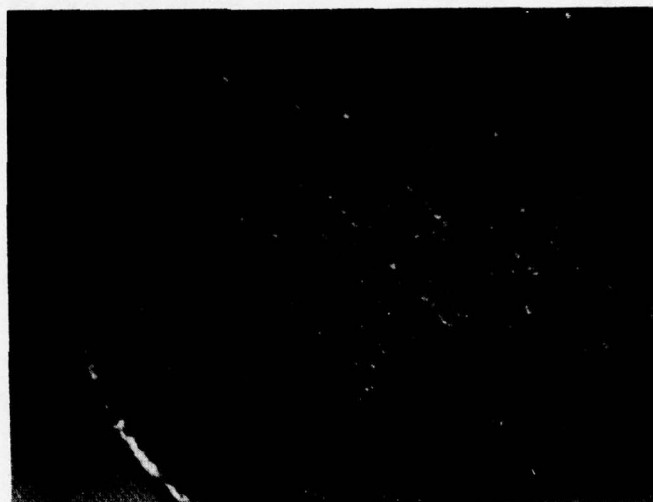


Fig. 12: Shorted 6.8V Silicon Junction

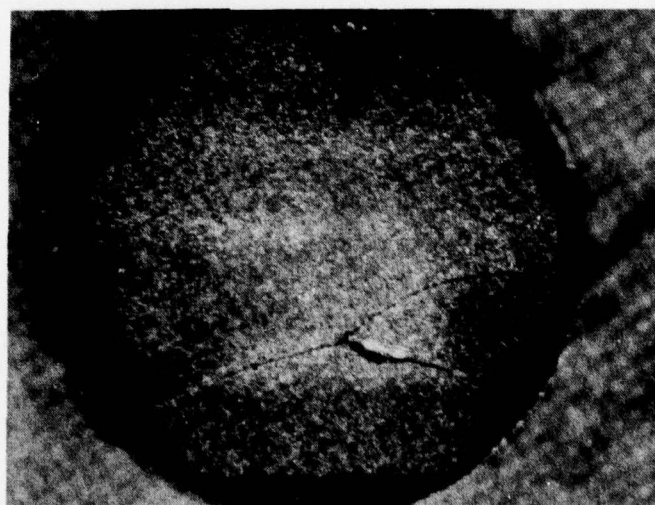


Fig. 13: Shorted 33V Silicon Junction

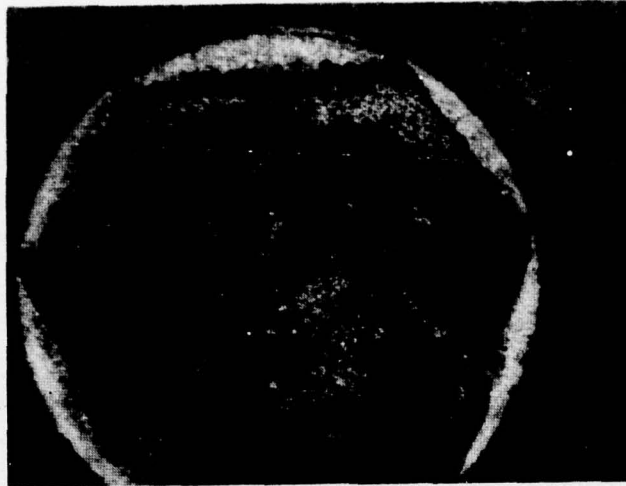


Fig. 14: 91V Shorted Silicon Junction

Transient suppressors which fail short in most instances melt through the silicon junction. The shorted areas appear to be distributed randomly across the surface of the junction. Shorts occur both at the periphery and internally.

The reasons for failure at a specific location can be many and varied. Latent failure points could be due to defects caused by micro-fractures, dislocations, the presence of some impurity, or a variety of other possible reasons.

#### SUMMARY AND CONCLUSION

The silicon transient suppressor was introduced 10 years ago on the market with most applications in environments where transient voltages are random in both incident and amplitude. Although field history has been excellent, a quantitative measure of reliability is required which is described in this report. A high degree of reliability of the silicon transient suppressor is required to define the necessary engineering criteria for remote applications such as space where replacement of defective components such as those destroyed by a transient is virtually impossible.

This effort represents the first long-term reliability test on a transient volt suppressor. (A long-term test of the life testing equipment could be considered as a secondary benefit).

Some electrical parameters of devices tested were quite stable, including the Breakdown Voltage (BV) and Reverse Leakage Current (Ir). The magnitude of Ir, which is often considered an important parameter in reliability, does not seem to be an influencing factor for the TransZorb<sup>tm</sup> as long as the components originally met the electrical specifications when selected for the test. Both the mean values and the standard deviations of the Reverse Leakage Current were stable throughout the testing program. The MP<sup>2</sup>BF curves in Figures 8-11 inclusive, represent the anticipated life expectancy of the four TransZorb types over a wide spectrum of transient exposure. The 6.8V device seems to have the highest reliability at 100% Ipp with an MP<sup>2</sup>BF extending an excess of 9,000 pulses and the 90% confidence level extending to almost 5,000 pulses at 100% of the peak pulse level. The 33V TransZorb has an MP<sup>2</sup>BF level of slightly over 1,500 pulses and a 90% confidence of approximately 750 pulses. The 91 volt TransZorb by comparison with the 33V type appears to have a higher reliability. These slight inconsistencies are characteristic of semiconductor devices. The MP<sup>2</sup>BF of the 91V type is in excess of 2,500 pulses and with a 90% confidence level of slightly over 2,000 pulses. The data gathered for the 190 volt type is not applicable to TransZorbs manufactured and sold today because of improved reliability from design changes. The improvement was made concurrently with these tests because of suspected lower reliability compared to lower voltage types. This reliability study confirmed these earlier assumptions. At the time of this writing, a subsequent test on the modified 190 volt types has not been completed but is anticipated to yield the approximate reliability of the 91 volt types.

It is shown in the curves of the MP<sup>2</sup>BF versus the percent of related peak pulse current that if devices are operated at peak pulse current levels below 75%, the component has an apparent unlimited lifetime. In applications where the maximum pulse anticipated can be accurately defined, adjustment of the suppressor parameters to accomodate operation at below 75% peak pulse current should insure adequate reliability. However, please bear in mind that if



the distribution of transients is random, the number of transients approaching the peak capability of the TransZorb<sup>tm</sup> is usually represented by far less than 25% of the number of total pulses occurring as evidenced by the probability distribution of the peak current for lightning strokes as shown in Figure 15.

When a silicon transient voltage suppressor fails, it appears that in all cases it will fail in the shorted mode. During the process of failure, a relatively small area, of the order about .030 inches or smaller is heated sufficiently to melt the silicon producing the short. For those applications in which shorted mode failure is undesirable, it is possible in some instances to place a fuse in series with the TransZorb which will subsequently open when the TransZorb shorts and then draws a significant amount of current. These applications lie primarily in areas involving power distribution and would perhaps not be feasible for communication lines.

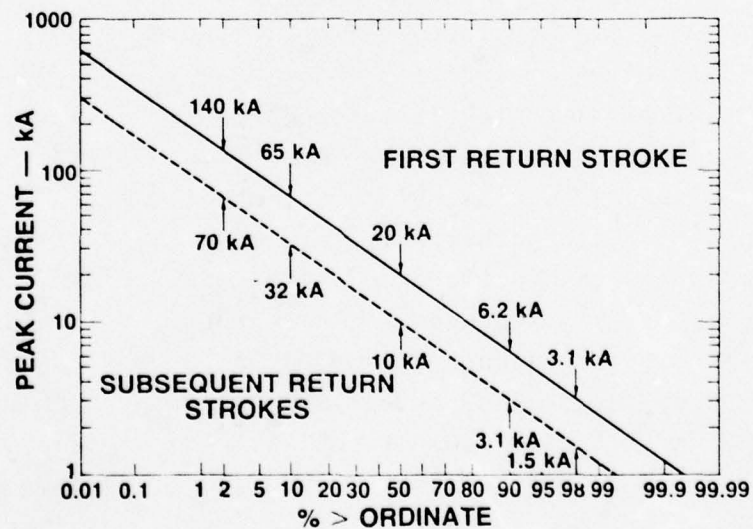


Fig. 15: Distribution of Peak Currents for First Return Stroke (2)

AD-A058 797

GEORGIA INST OF TECH ATLANTA

F/G 4/1

FEDERAL AVIATION ADMINISTRATION-GEORGIA INSTITUTE OF TECHNOLOGY--ETC(U)

MAY 78

UNCLASSIFIED

FAA-RD-78-83

NL

3 of 5

AD  
A068 797



#### REFERENCES

- (1) IEEE Electromagnetic Compatibility Symposium Record;  
IEEE75CH1012-4MONT, Effects of EMP Induced Transients  
on Integrated Circuits, E. Van Keuren, R. Hendrickson  
and R. Magyarics (May 1975).
- (2) A Ground Lightning Environment for Engineering Usage;  
N. Cianos and E. T. Pierce, Stanford Research Institute,  
McDonnell Douglas Contract No. LS-2817-A3 (1972).
- (3) Inductive Switching Transients on the KC-135 Airplane  
A.C. and D.C. Electrical Systems, The Boeing Company  
Report No. T6-2408, C. B. Tenning.
- (4) Mil-Std-1399



PROTECTING FACILITIES AND/OR EQUIPMENT FROM  
INDUCED LIGHTNING AND POWER LINE SWITCHING TRANSIENTS

by

Richard Odenberg

Transtector Systems

Monterey Park, California

Presented at

Federal Aviation Administration - Georgia Institute of Technology  
Workshop on Grounding and Lightning Protection

May 1978

## ABSTRACT

- Part 2 of Protecting Facilities and Equipment from Induced Lightning and Power Line Switching Transients
- Review of the five major requirements for electronic equipment and facility protection
- Details of selection and placement of protection equipment based on sensitivity of equipment to be protected and energy levels in the transients or power line surges

The paper will discuss the use of components, circuits, and systems.

## INTRODUCTION

The entire electronic industry was more than elated when the semiconductor made its appearance in the marketplace. At last the scientific community had produced a device that would eliminate the need for costly replacement of electronic components that had reached the end of their useful life. In theory, the semiconductor that is correctly manufactured and properly installed should operate into infinity. In the practical applications, however, the semiconductor, to a greater degree, and the integrated circuit, to a lesser degree, have performed with a level of reliability below that which was expected.

This constant erosion of solid-state semiconductors and integrated circuits is of prime concern to users and manufactureres of electronic equipment containing these components. The degeneration of these electronic components and circuits is attributed directly to an often misunderstood phenomenon known as "transient voltage." Observation by hybrid generation recording equipment allows the exact definition of transients as high-speed, DC voltage superimposed on the positive side of the sine wave of the AC power supply. It is important to note at this point that these high-speed overvoltages which cause the disruption of operation or destruction of these electronic devices are not restricted to



AC power lines but may enter delicate circuitry by any pathway provided, i.e., coaxial cables, dedicated telephone lines, etc.

Various attempts have been made to eliminate the destructive transient from the AC power supply. However, the sheer number of transient generating sources makes this approach infeasible economically and from a practical standpoint virtually impossible. Isolation of the vulnerable electronic components from these destructive overvoltages is, therefore, the solution of choice.

#### Causative Factors

There are three specific reasons for the change in voltage suppression requirements: 1) the increased effect of induced lightning on solid-state components (also enhanced by a changing world weather pattern), 2) more and more sophistication in semiconductor technology, simply smaller and smaller devices, and 3) the very monumental effect of switching transients/surges caused by a degenerating supply of commercial power. As the demand upon power companies increases at a geometric rate, the ability to produce power does not increase at the same rate. Therefore, loads are constantly being switched from one line to another causing "surges" (which, in turn, cause high-speed, short-duration transients to proceed down the power line). As little as 1 nanojoule ( $1 \times 10^{-9}$ ) of energy applied to the semiconductor can cause a shut down of operations. Figure 1 shows how little energy can either upset

or destroy a transistor, I.C., or semiconductor. This data was developed for transients in the microsecond region. Just think, if they were 1 millisecond long (a thousand greater) what damage they might do. Figures 2 and 3 show what can happen when the transient or surge hits the semiconductor. By definition, a transient is less than 8.3ms, and a voltage surge is greater than 8.3ms. Transients are also related to high impedance sources and can range from a few millivolts to 20K volts. Voltage surges are produced from low impedance sources. In general, the maximum voltage seen is 2 to 3 times the nominal operating voltage. The failure of the power diodes in Figure 2 was due to a voltage surge. The failure in Figure 3 was due to a transient. Figure 4 shows a 1/4 x 1/4 inch I.C. with 20,000 components on it.

In plant operations, circuit breaker switching, load disconnects, ON-OFF cycling of large motors, and operation of protective devices will introduce transients into the AC power system. Figure 5 shows locations to place transient suppressors. Figures 6 and 7 list the sources of these transients.

#### Remedy

After many years of testing and field evaluation of different devices, i.e., gas tube and metal oxide varistors, it was found that the systems approach was the only way to meet all of the technical requirements for protecting solid-state equipment. These facts came out when, in many applications (hospital, air traffic, etc.), human lives were at stake. The FAA saw this in the late '60's and moved to put in solid-state

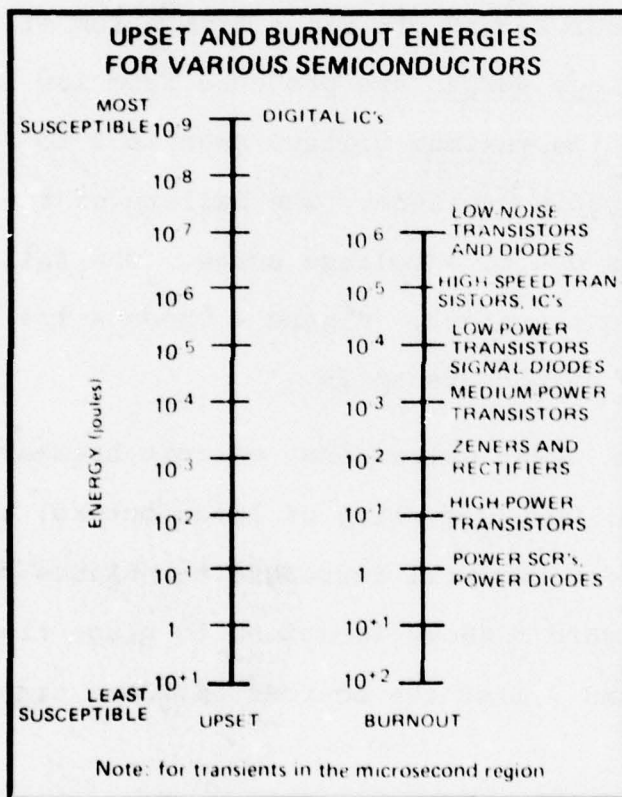


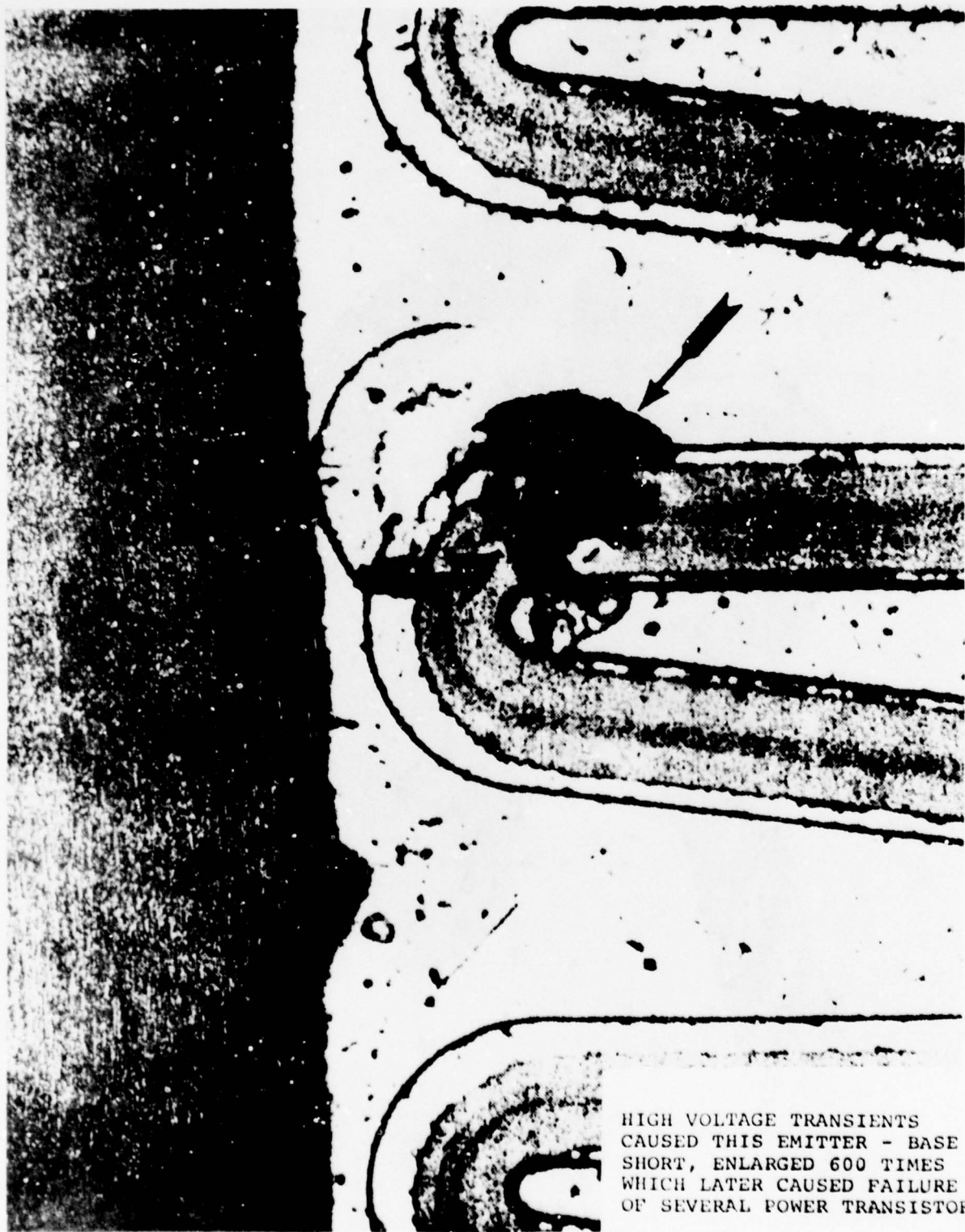
Figure 1





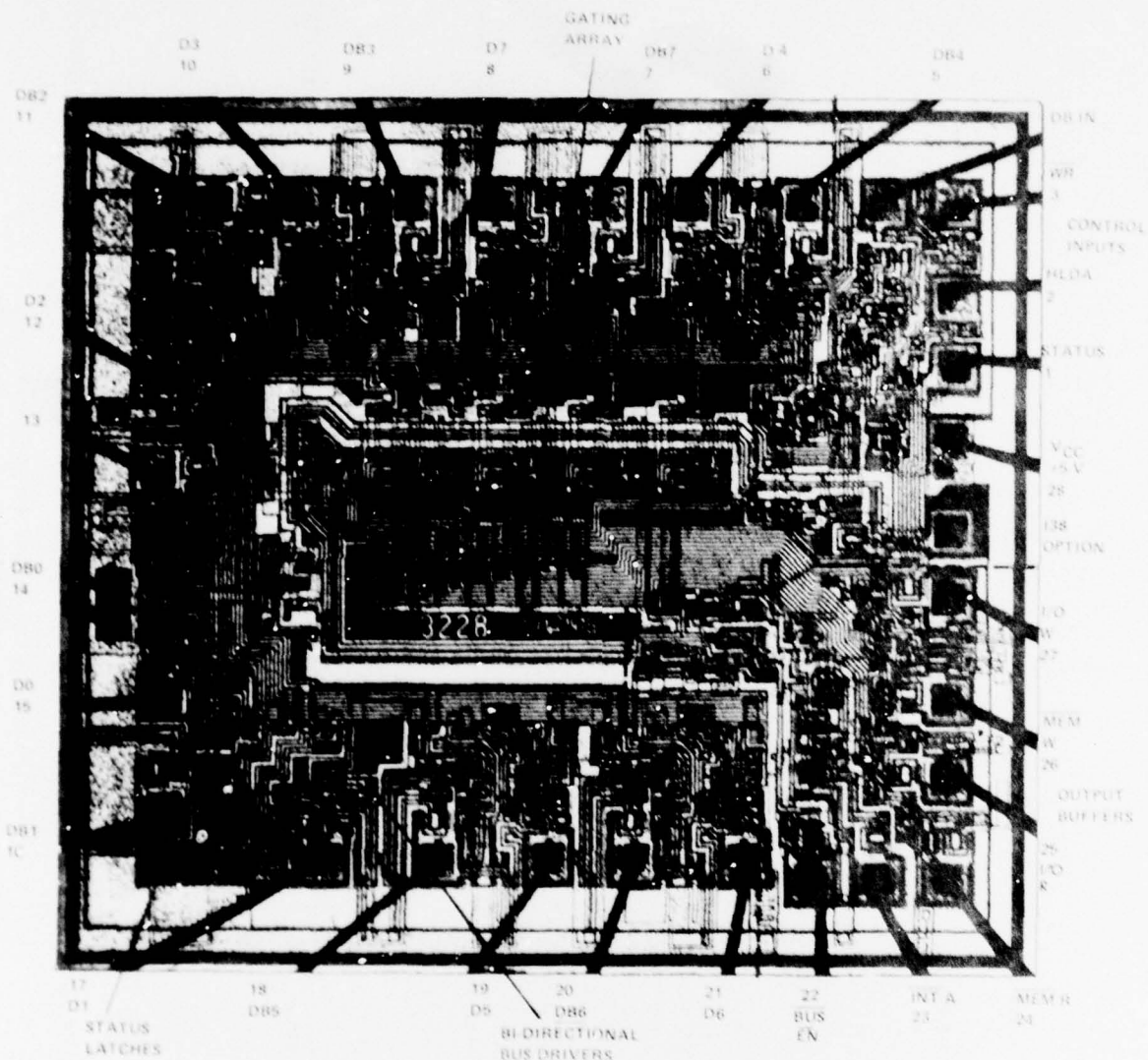
A voltage detector on 480 VAC  
detected a 2100 volt surge,  
causing these power diodes to  
short and then explode.

Figure 2



HIGH VOLTAGE TRANSIENTS  
CAUSED THIS EMITTER - BASE  
SHORT, ENLARGED 600 TIMES  
WHICH LATER CAUSED FAILURE  
OF SEVERAL POWER TRANSISTORS

Figure 3

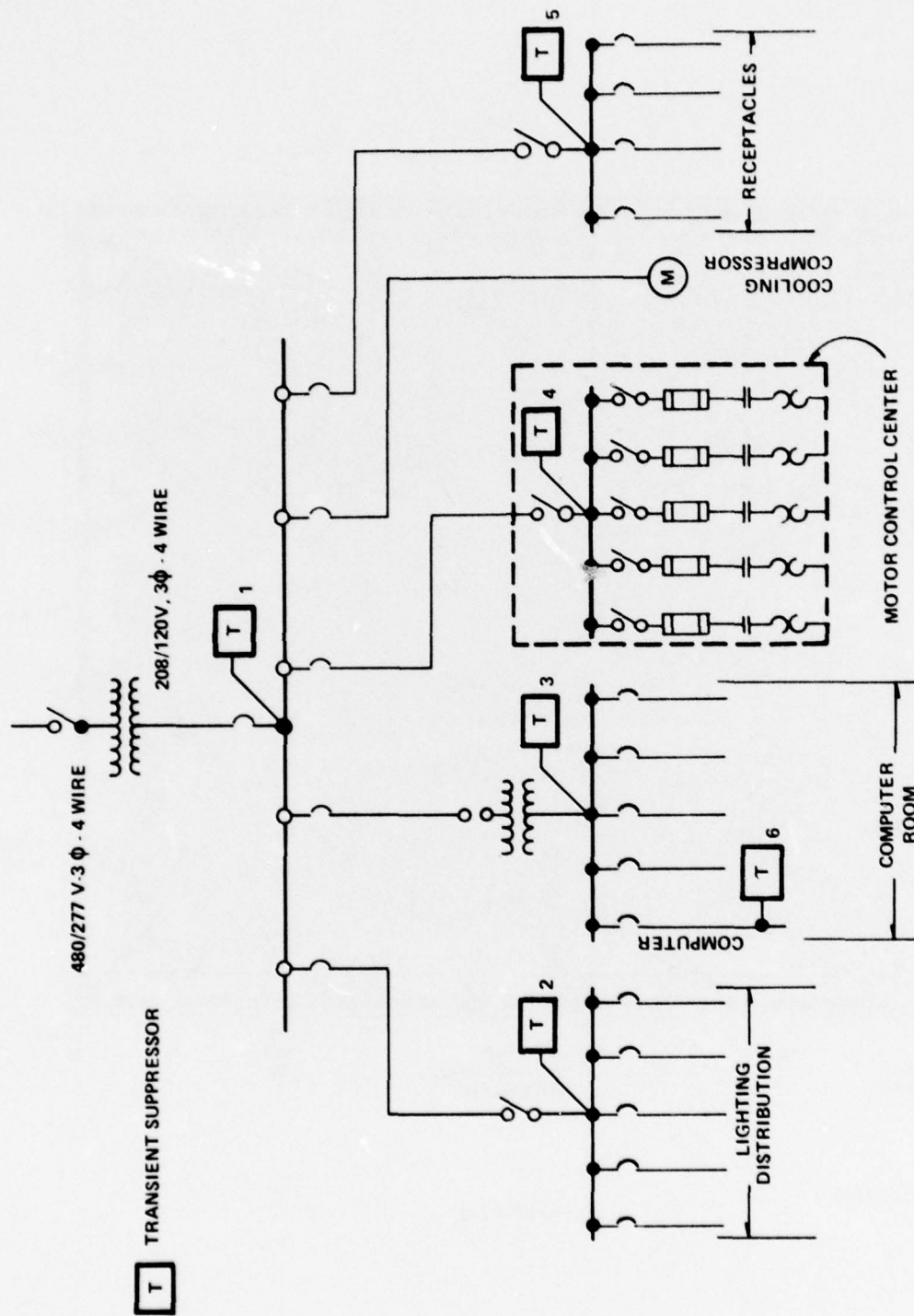


□ ACTUAL SIZE

Intel MD8228

Figure 4





APPLICATION OF TRANSIENT SURGE SUPPRESSORS  
TO TYPICAL ELECTRICAL DISTRIBUTION SYSTEMS

Figure 5

### TRANSIENTS GENERATED FROM OUTSIDE FACILITIES

1. Power Company Switching
2. Power Line Insulator Arcing
3. Other Users On Same Power Distribution
4. Lightning

Figure 6

### TRANSIENTS GENERATED INSIDE FACILITIES

1. Air Conditioning Systems
2. Refrigeration Systems
3. Fluorescent Lights Ballasts
4. Elevators
5. Copy Machines to Printing Presses
6. Contactors
7. Other Process Equipment, i.e. Punch Presses, SCR Drives

Figure 7

surge protection then. In addition, in the early '70's UPS Systems were put in also. In applications where human life is at stake, one must consider technically nothing less than absolute transient suppression. Where equipment damage, only, is involved, then the cost factors must be considered as a trade-off to the other economics such as maintenance of equipment and downtime.

ISOLATION TRANSFORMERS were originally thought to provide some measure of protection from transients. However, further scientific studies have shown that these devices when operating at near saturation levels act as virtual accelerators for the transient voltage. Regulator overshoot or failure, the purpose for which these devices were designed, is controlled quite adequately, but without additional protection the destructive transient problem may be compounded.

Two basic designs for stored energy systems that isolate the semiconductors and integrated circuits from transients entering these devices over the AC power lines are currently in wide use. These are the Motor-Generator set and the solid-state Uninterruptible Power System (UPS).

THE MOTOR-GENERATOR SET, while less costly than a solid-state UPS, does have certain inherent problems associated with dispersion of the kinetic energy stored in the flywheel portion of the set. Operational reliability, space, noise, mean-time-to-repair, and routine maintenance



of the rotating portion of the motor-generator add to the operation cost.

THE SOLID-STATE UPS is a more reliable source of uninterruptible power. Basic considerations must be given to the economics of these devices due to the high initial cost in comparison to other stored energy systems.

The designers of the UPS have taken great care to insure proper operation of their equipment as it relates to the device for which it is providing constant power. An investigation of the solid-state circuitry in the control portion of the UPS will show very careful consideration given to providing bypass switch-gear that allows an electrical noise-free transfer from the UPS to the backup power system in case of UPS failure.

The control portion of the UPS is made up of solid-state integrated circuits. Transients cause damage to these circuits due to the fact that the UPS is fed by an unfiltered AC power line. Additionally, the alternate power source is usually the same unfiltered AC power line that feeds the UPS. In the case of UPS failure where the UPS is interfaced with computer hardware, the switch to alternate power allows for a direct pathway by which transients will enter the computer circuitry.

It should be noted here that it is not necessary for the UPS to fail before the computer is connected to the

unfiltered AC power line. The static load transfer switch-gear is devised from noise-free electronic switches (SCR's). These SCR's can be caused to misfire by transients, thus, resulting in an unnecessary and potentially damaging transfer to the unfiltered AC power source.

It is clear that there is an enormous need for a dynamic transient protection device that will identify these high-speed overvoltages and shunt them to ground. This device must incorporate both an extremely fast response time in order to provide adequate protection for logic and memory circuitry as well as a design that allows simultaneous transient suppression on all phases of the power source.

The five major considerations in protecting facilities and equipment against high-energy and high-speed voltage transients are listed on the next page. Once all five factors have been considered, one must look at where the voltage will be at maximum power dissipation. For example, dissipating 10 joules, a Transtector Transient Suppressor (ACPl00C) will not allow the voltage to exceed 300 volts peak. Where a metal oxide varistor would dissipate 10 joules, the voltage would rise to 2500 volts peak. If this happened on 120 VAC service, your equipment would fail using the metal oxide varistor.

FIVE MAJOR CONSIDERATIONS IN PROTECTING FACILITIES  
AGAINST HIGH-ENERGY AND HIGH-SPEED ABNORMAL VOLTAGES

1) Response Time - High-speed/low nanoseconds is a must. This is important because of the high-speed rise time of the induced transients or surges.

Lightning ..... 600V to 1000V/Microsec.

Power Line Surges ..... 100V to 300V/Microsec.

EMP (Electromagnetic Pulse) ..... 5KV/Nanosec.

2) Suppression (Power) Capability - 100,000 to 1,500,000 watts and capability of suppressing 15,000 to 50,000 amps induced on the AC service line.

3) Voltage Suppression & Clamping Ratio - Low threshold and less than 1:1.5 clamping ratio. The device is to turn on and start suppressing at 120 percent of nominal line, and at maximum power not to exceed 150 percent of nominal line; a clamping ratio of 1:1.5. If a protector does not begin to suppress at low voltage threshold, it will allow the low level surges through to damage equipment.

4) High Reliability - The device should be totally solid-state, with redundant circuitry, and be failsafe.

5) Operation - Automatic or resettable. If the nature of a system precludes an interruption in service (that is, if one cannot afford to be shut down), an automatic device is required.

These principles were considered in the design of



Transtector's Model ACP1000 and ACP10,000 AC Voltage Surge Suppressors.

DESCRIPTION OF ACP10,000 & ACP1000  
VOLTAGE SURGE SUPPRESSORS

General

The AC Voltage Surge Suppressors are high-speed and high-current, solid-state devices designed to protect solid-state electronic equipment and systems from transient overvoltages. They perform their function by limiting the magnitude of the transient overvoltage present on the AC power lines at a specific peak threshold voltage. Such transient voltages occur due to the fuse clearing/phase switching between power sources, e.g., equipment start-ups or shut-downs, switching loads, and induced lightning. The ACP series is designed specifically to operate on either single, two, or three-phase Delta or Wye services.

Operation

The suppressors operate when the instantaneous voltage rises above 120 percent of the nominal peak voltage. The power dissipated in the suppressor is a function of the energy in the transient only. The suppressor does not handle available fault current of the power line, as do crowbar-type circuit protectors, when dissipating the transient energy. The ambient temperature of the suppressor rises as does the suppressor voltage level. When the line voltage is below 120

percent, the device draws a maximum power of 1 watt per phase. The elements employed are 100 percent solid-state using redundant techniques and component ratings and construction to assure good reliability.

#### Functional

When a transient overvoltage is sensed at the suppression voltage level (on any or all phases), the suppressor on that phase conducts in approximately 5 nanoseconds, attenuating the transient voltage and dissipating its energy. It continues to suppress until the voltage drops below the clamping level. When the transient voltage is no longer on the line or is below the clamping voltage, the suppressor automatically recovers, ready for the next transient. The suppressor is bi-polar, suppressing transients either on the positive or negative side of the sine wave. It is also bi-directional and will suppress transient voltages generated by the load as well as the source.

## ACP10,000-120W - 2500 JOULE SUPPRESSOR

(FOR 120, 240, or 480 VAC SERVICE)

### Mechanical

The controls and power electronics are located in a Nema 12, free-standing enclosure, 6' x 3' x 1-1/2'. The unit weighs approximately 800 pounds. (Figures 8 and 9)

### Electrical

All functional devices are silicon solid-state. No MOV (metal oxide varistors) or gas discharge tubes are used in the circuits due to their short life expectancy and lack of adequate protection for solid-state electronic equipment. In order to suppress such large currents in the nanosecond to microsecond region, there are several stages of suppression in the ACP10,000. The first stage has the capability of suppressing at 150,000 watts per phase before the second stage comes on automatically and suppresses up to the maximum rating of 1.5 megawatts. It is very important to realize that this device does not short or distort the AC line; it strictly clips the transient "off" and then automatically resets upon removal of the transient. (Summary Spec., Figure 10)

The dynamic impedance for the suppressor, when no transients are suppressed, will be in the hundreds of thousands of ohms. But, when a major surge occurs, it could be as low as .1 ohms which gives you a substantial suppression capability of the power line.



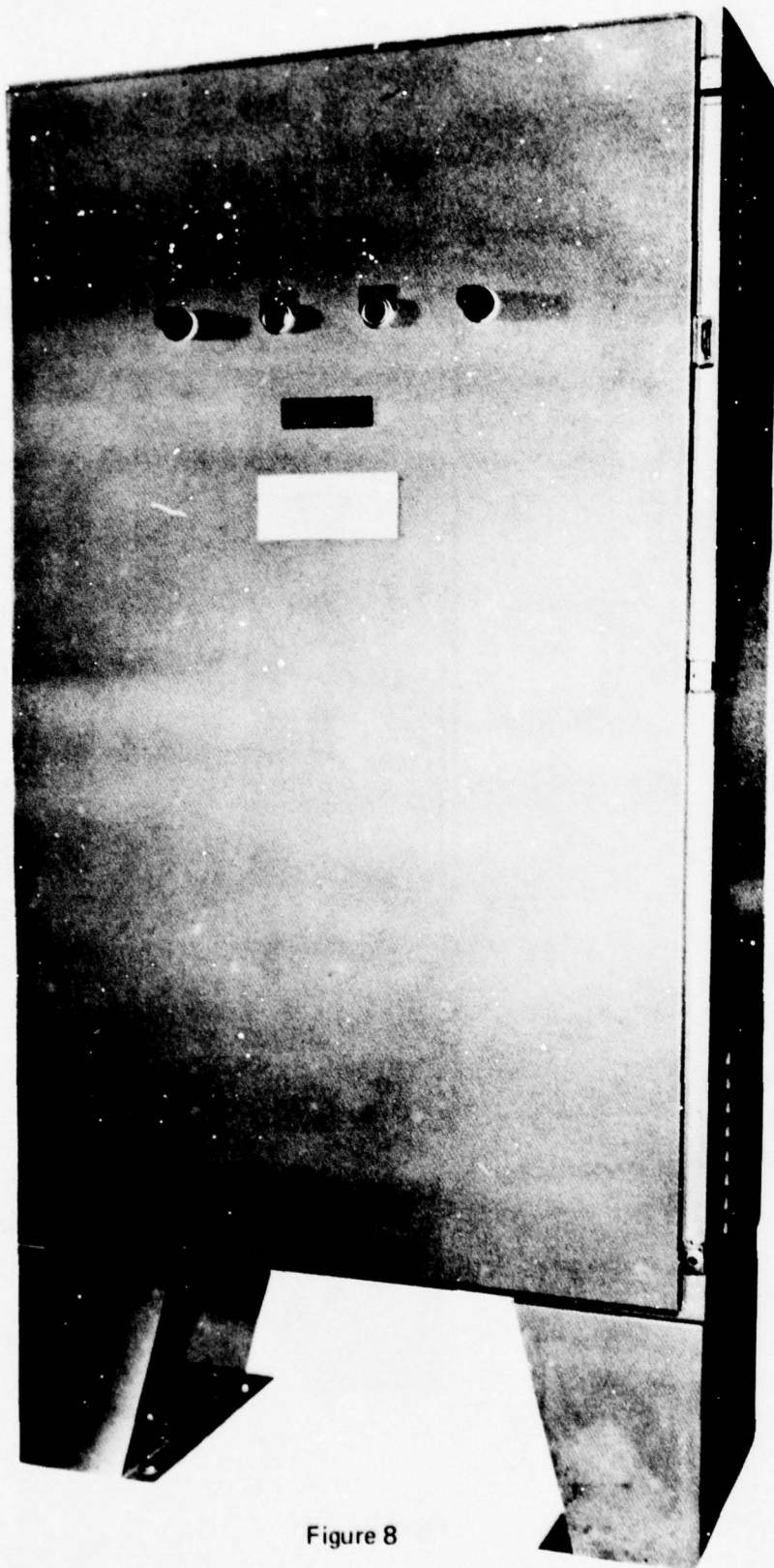


Figure 8

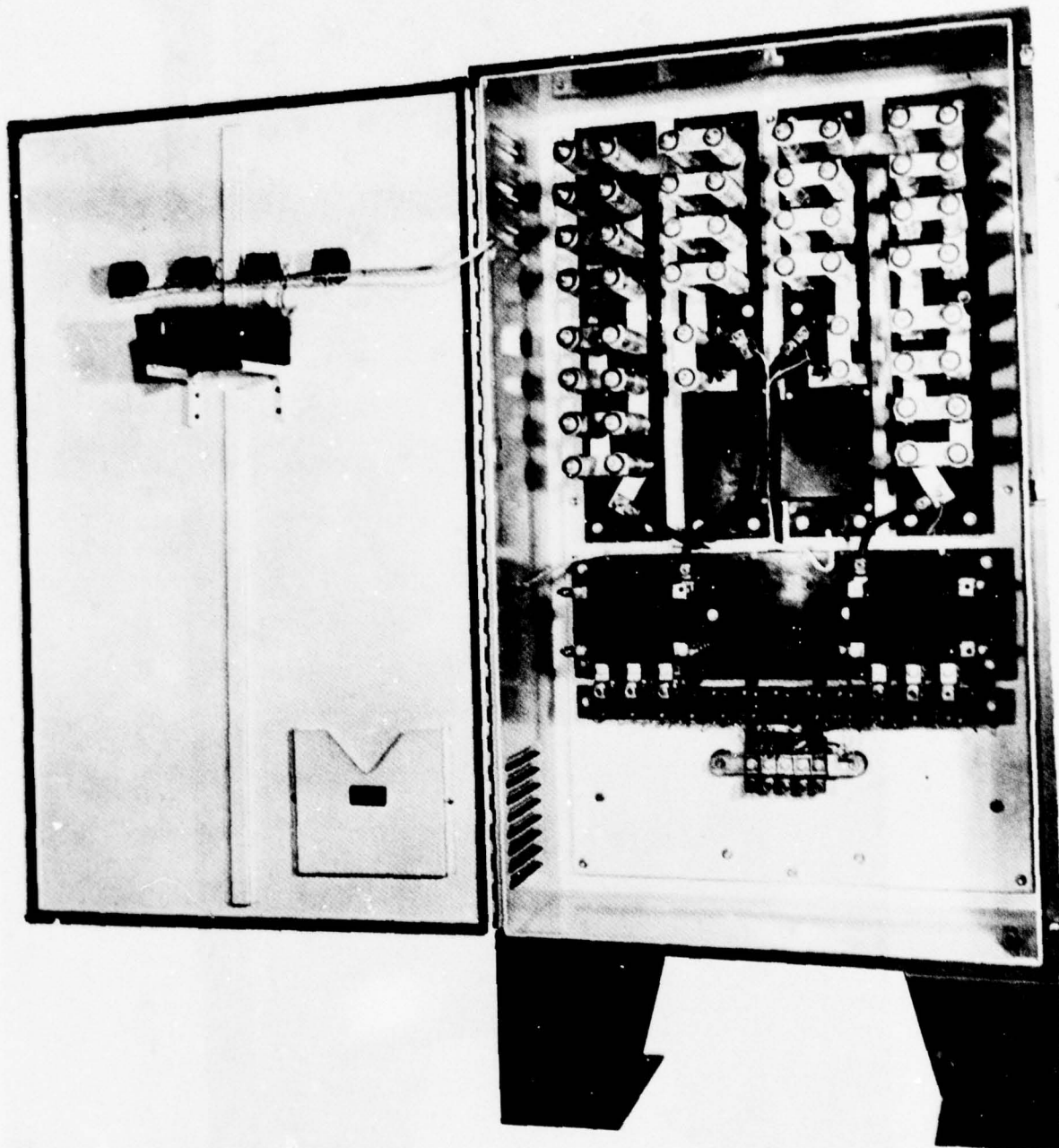


Figure 9

SPECIFICATION: ACP10,00C-120W

1.0	GENERAL:	
1.1	Voltage .....	120/208 VAC
1.2	Frequency .....	50/60 or 400 Hz
1.3	Phases .....	3 $\phi$ Wye
1.4	Max. Number of (150Amp) Branch Circuits Protected...	6
2.0	Suppression Voltage Level .....	200 Volts Peak
3.0	Maximum Suppression Voltage Level.....	400 Volts Peak
4.0	Peak Power Dissipation (lms) .....	1.5 Meg Watt
5.0	Response Time - 1st Stage .....	5 Nanosec. Max.
	2nd Stage .....	10 Microsec Max.
6.0	Maximum Energy Dissipation .....	2500 Joules
7.0	Standby Power .....	7.5 Watts Max.
8.0	Duty Cycle .....	.01%
9.0	Operating Temperature .....	0°C to +50°C
10.0	Storage Temperature .....	-20°C to +85°C
11.0	Mechanical Details - Weather Proof.....	Dwg 629 RECC

Figure 10



The ACP10,000 has additional features which are:

1) Transient Simulate Test - This test triggers the suppressor by pressing a test simulate button which gates on the circuitry (note: it does not disturb the line at all) and, if the suppressor triggers, it turns on lights on the front panel. The suppressor is then reset by pressing the "reset" button. This test procedure is done on a regular basis at the site to verify the unit is still functioning properly.

2) Digital Transient Counter - The counter is mounted in the front of the enclosure for ease of reading and safety. It counts the number of surges the protector suppresses if the surges are 500 nanoseconds or greater. This means that the counter does not count all of the transients suppressed (i.e., the ACP10,000 responds in the 5 nanosecond region). The counter must also detect a minimum of 1000 nanojoules of energy before it will count.

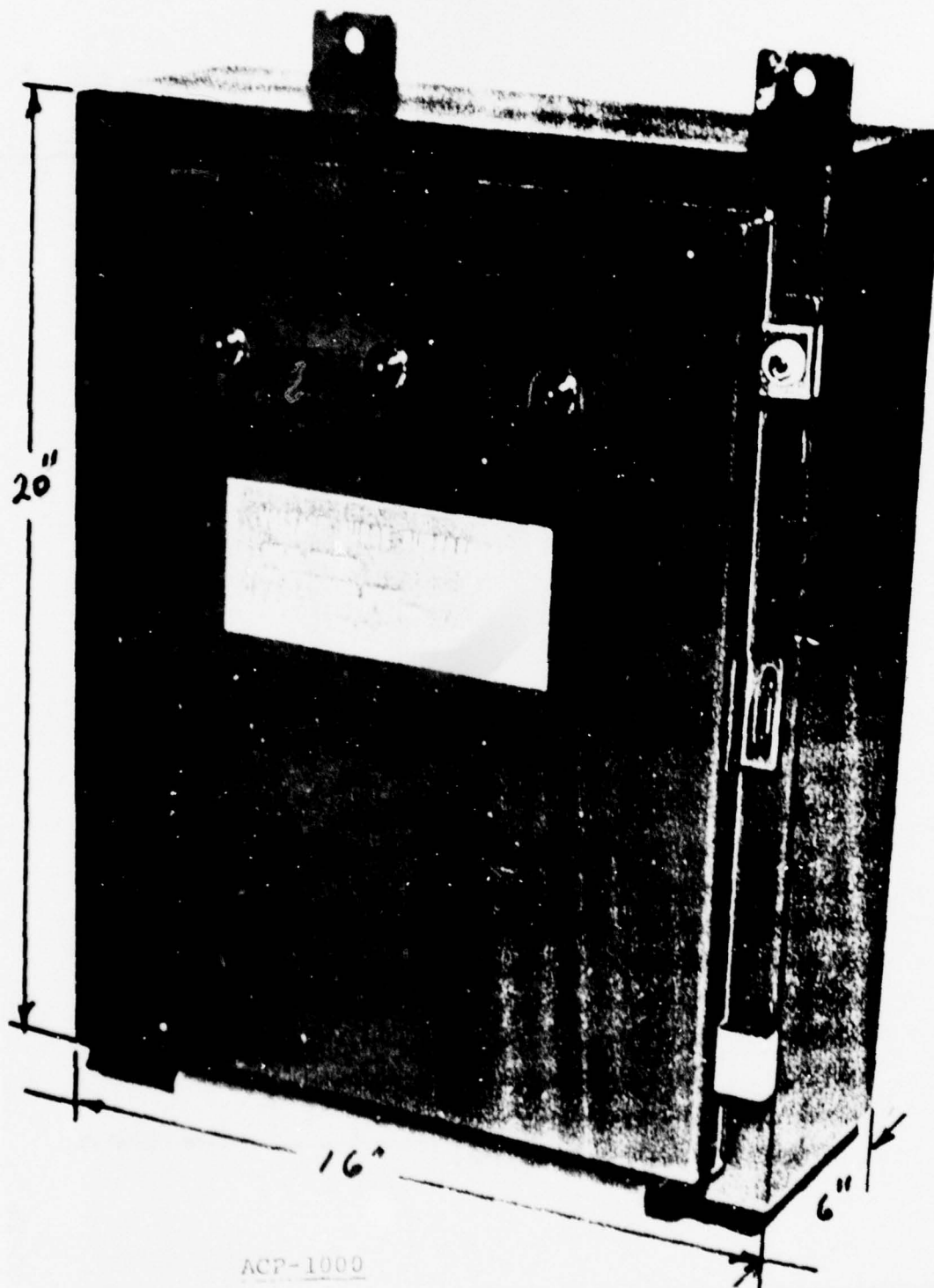
ACP1000 - (MANUFACTURED FOR 120, 240, or 480 VAC SERVICE)

#### Mechanical

The controls and power electronics are located in a Nema 12 enclosure, 20" x 16" x 6". It weighs approximately 45 pounds. (Figures 11 and 12)

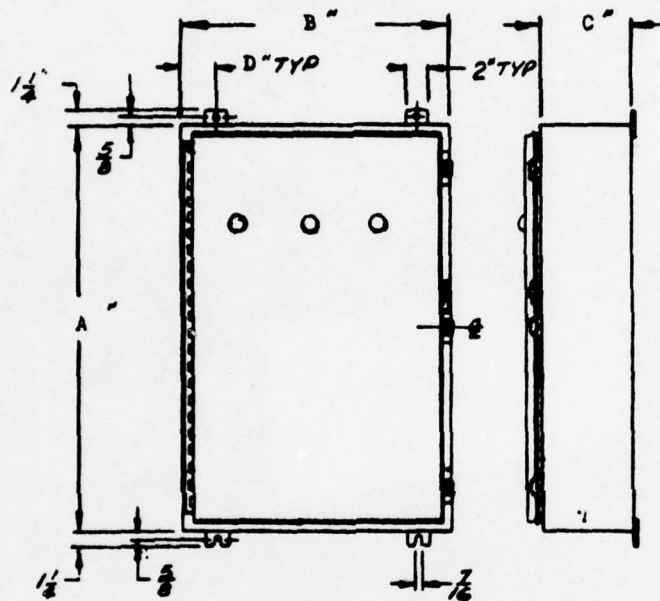
#### Electrical

The unit functions basically like the ACP10,000 except that it has the power capability of 105,000 watts total



ACP-1000

Figure 11



ACP1000	A	B	C	D
-120D -120W -120T	20	16	6	3
-120S	16	12	6	1 1/2

NEMA TYPE 12

Dimensions in inches.

Figure 12



(1 x 1000 microsecond pulse) 35,000 watts per phase. This is equivalent to suppressing an 8 x 20 microsecond lightning-induced strike of 25,000 amps. This device has the same response time as the ACP10,000 of 5 nanoseconds. See Summary Spec., Figures 13 thru 15. Electrical installation and wiring diagrams are shown in Figures 16 thru 21 for each service's voltage and phase configuration.

#### Tests of The ACP1000 Surge Suppressor

Tests were performed by a governmental testing laboratory to verify the functional parameter of the ACP1000-120W (208/126 3Ø, 4W system). Figure 22 shows the test setup. Note that the wire length to the measuring instrument was approximately 42". The results are out of spec, but this was due to the measurement made at the ACP1000 terminals (Figure 23). Figure 24 is the graph of data. This shows lead lengths are extremely important to fast response and low clamping level. Figure 25 shows oscillograph of the 35-joule transient unsuppressed and then suppressed. In conclusion, this protector can suppress 35 joules of energy (delivered in 30 microseconds) with a clamping ratio of 1:5.1.

SPECIFICATION: ACP1000-120

1.0 GENERAL:

- 1.1 Voltage..... 120 VAC
- 1.2 Frequency..... 50/60 or 400 Hz
- 1.3 Phases..... 1 $\phi$ , 2 $\phi$  or 3 $\phi$   
(See P/N)
- 1.4 Electrical Service

<u>Part Number (P/N)</u>	<u>Suppressor Connection</u>	<u>Service</u>
ACP1000-120D	Line to Line	3 $\phi$ 3 Wire DELTA
ACP1000-120W	Line to Neutral	3 $\phi$ 4 Wire WYE
ACP1000-120S	Line to Neutral	1 $\phi$ 2 Wire
ACP1000-120T	Line to Neutral	2 $\phi$ 3 Wire

- 2.0 Suppression Voltage Level..... 200 Volts Peak
- 3.0 Maximum Suppression Voltage Level..... 300 Volts Peak
- 4.0 Peak Power Dissipation (lms)..... 35,000 Watts/Phase  
105,000 Watts Total/  
for 3 phases
- 5.0 Response Time..... 5 Nanosec. Max.
- 6.0 Standby Power..... 10 Watts Max./Phase
- 7.0 Duty Cycle..... .01%
- 8.0 Operating Temperature..... 0°C to +50°C
- 9.0 Storage Temperature..... -20°C to +85°C
- 10.0 Mechanical Details..... SK1872 Dwg.
- 2 $\phi$ , 3 $\phi$ , Suppressor..... 20"H x 16"W x 6"D
- 1 $\phi$  Suppressor..... 16"H x 12"W x 6"D
- 11.0 Electrical Installation..... Dwg. 1091

Figure 13

SPECIFICATION: ACP1000-240

1.0 GENERAL:

- 1.1 Voltage..... 240 VAC
- 1.2 Frequency..... 50/60 or 400 Hz
- 1.3 Phases..... 1 $\phi$ , or 3 $\phi$   
(See P/N)
- 1.4 Electrical Service:

<u>Part Number (P/N)</u>	<u>Suppressor Connection</u>	<u>Service</u>
ACP1000-240D	Line to Line	3 $\phi$ , 3 Wire DELTA
ACP1000-240W	Line to Neutral	3 $\phi$ , 4 Wire WYE
ACP1000-240S	Line to Neutral	1 $\phi$ , 2 Wire

- 2.0 Suppression Voltage Level..... 400 Volts Peak
- 3.0 Maximum Suppression Voltage Level..... 600 Volts Peak
- 4.0 Peak Power Dissipation (1ms)..... 35,000 Watts/Phase  
105,000 Watts Total/  
for 3 phases
- 5.0 Response Time..... 5 Nanosec. Max.
- 6.0 Standby Power..... 10 Watts Max./Phase
- 7.0 Duty Cycle..... .01%
- 8.0 Operating Temperature..... 0°C to +50°C
- 9.0 Storage Temperature..... -20°C to +85°C
- 10.0 Mechanical Details..... Dwg. SK1872
  - 3 $\phi$  Suppressor..... 20"H x 16"W x 6"D
  - 1 $\phi$  Suppressor..... 16"H x 12"W x 6"D
- 11.0 Electrical Installation..... Dwg. 1091

Figure 14



SPECIFICATION: ACP1000-480

1.0 GENERAL:

- 1.1 Voltage..... 480 VAC
- 1.2 Frequency..... 50/60 or 400 Hz
- 1.3 Phases..... 1 $\phi$ , or 3 $\phi$   
(See P/N)
- 1.4 Electrical Service:

<u>Part Number (P/N)</u>	<u>Suppressor Connection</u>	<u>Service</u>
ACP1000-480D	Line to Line	3 $\phi$ 3 Wire DELTA
ACP1000-480W	Line to Neutral	3 $\phi$ 4 Wire WYE
ACP1000-480S	Line to Neutral	1 $\phi$ 2 Wire

- 2.0 Suppression Voltage Level..... 800 Volts Peak
- 3.0 Maximum Suppression Voltage Level..... 1000 Volts Peak
- 4.0 Peak Power Dissipation (lms)..... 35,000 Watts/Phase  
105,000 Watts Total/  
for 3 phases
- 5.0 Response Time..... 5 Nanosec. Max.
- 6.0 Standby Power..... 10 Watts Max./Phase
- 7.0 Duty Cycle..... .01%
- 8.0 Operating Temperature..... 0°C to +50°C
- 9.0 Storage Temperature..... -20°C to +85°C
- 10.0 Mechanical Details..... Dwg. SK1872
- 11.0 Electrical Installation..... Dwg. 1091

Figure 15

SERVICE VOLTAGE (VRMS)	V <sub>1</sub>	V <sub>2</sub>	V <sub>3</sub>
240/120	115	115	230

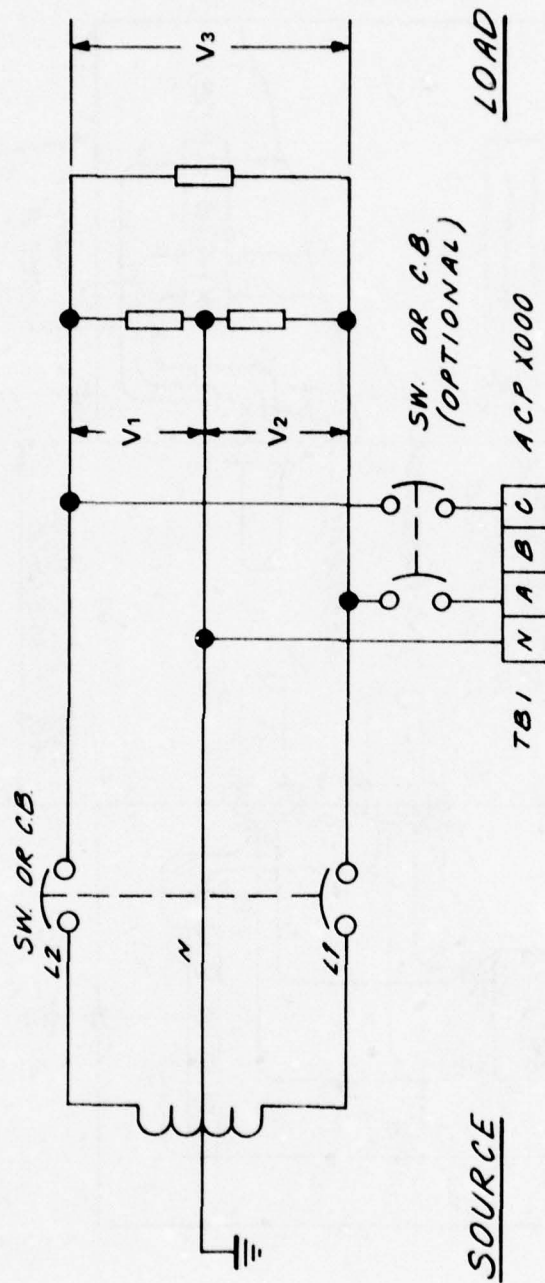


Figure 16

- 219 -

**ELECTRICAL WIRING DIAGRAM: (240/120 1Ø 3 WIRE) TRANSTECTOR – ACP X000-120T**

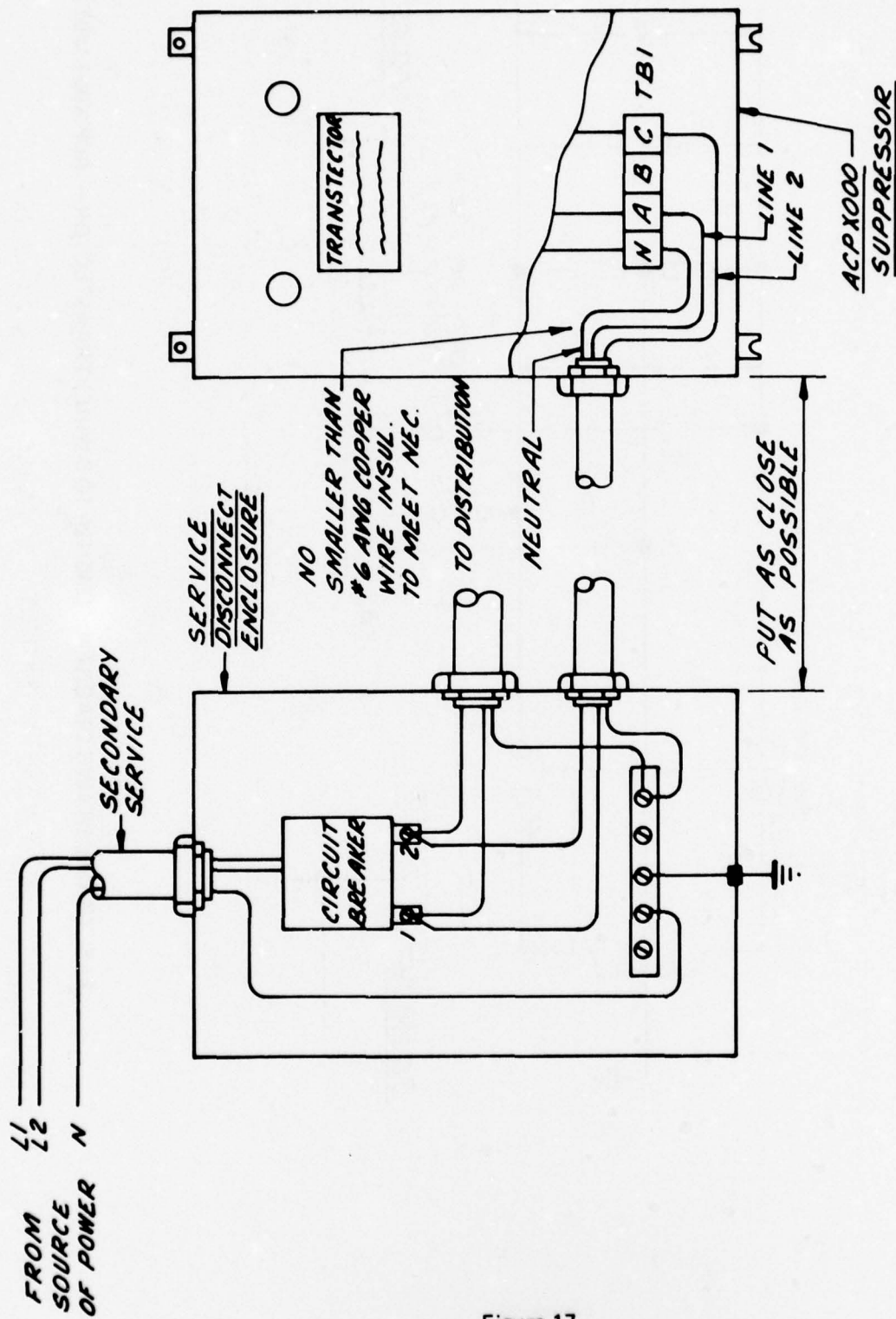
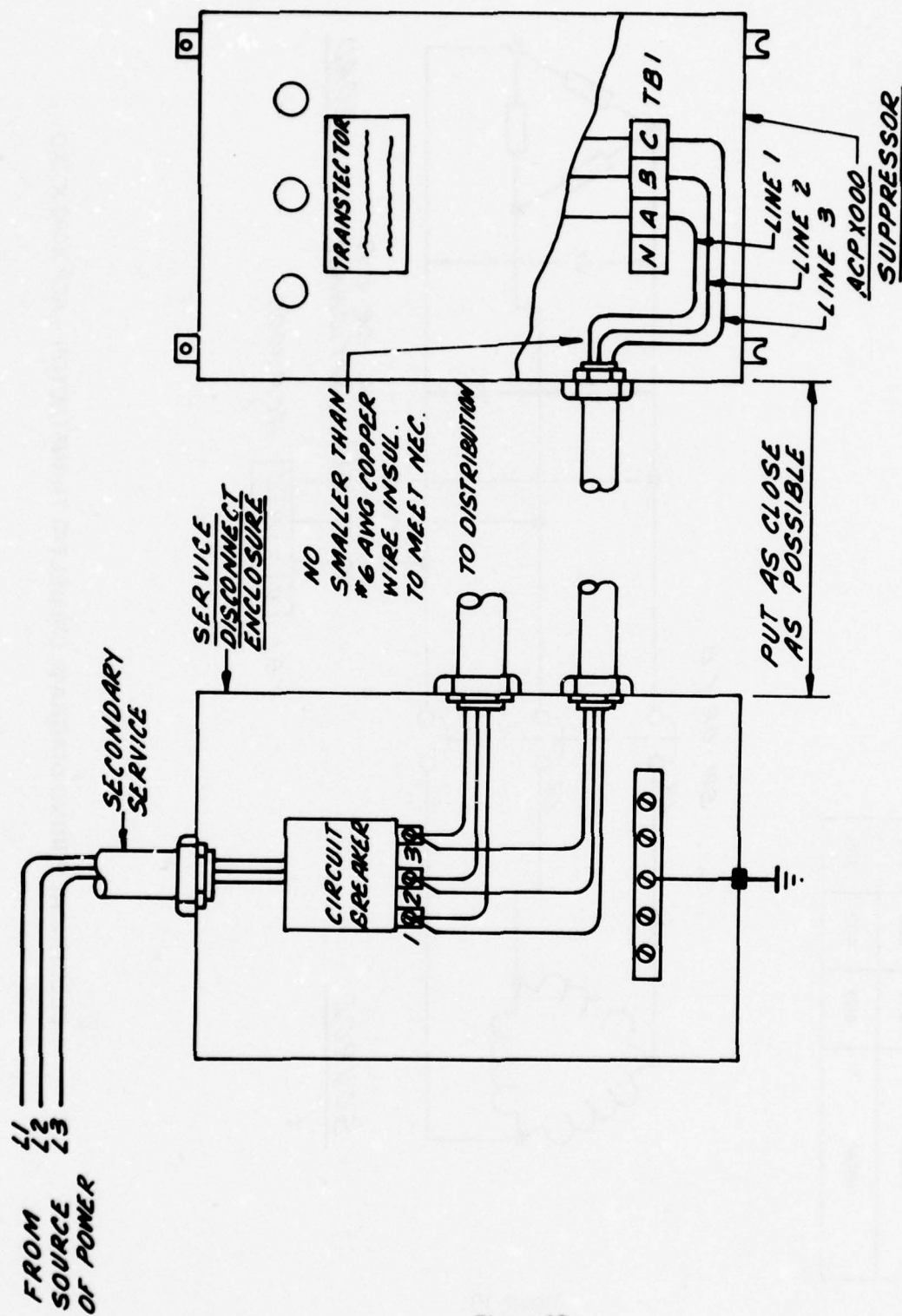


Figure 17

INSTALLATION DIAGRAM: 240/120, 1 $\phi$ , 3 WIRE TRANSTECTOR — ACP X000-XXXT





INSTALLATION DIAGRAM: (3Φ DELTA) TRANSTECTOR - ACP X000-XXD

Figure 18

SERVICE VOLTAGE (VRMS)	V <sub>1</sub>	V <sub>2</sub>	V <sub>3</sub>
240V	230	230	230
480V	460	460	460

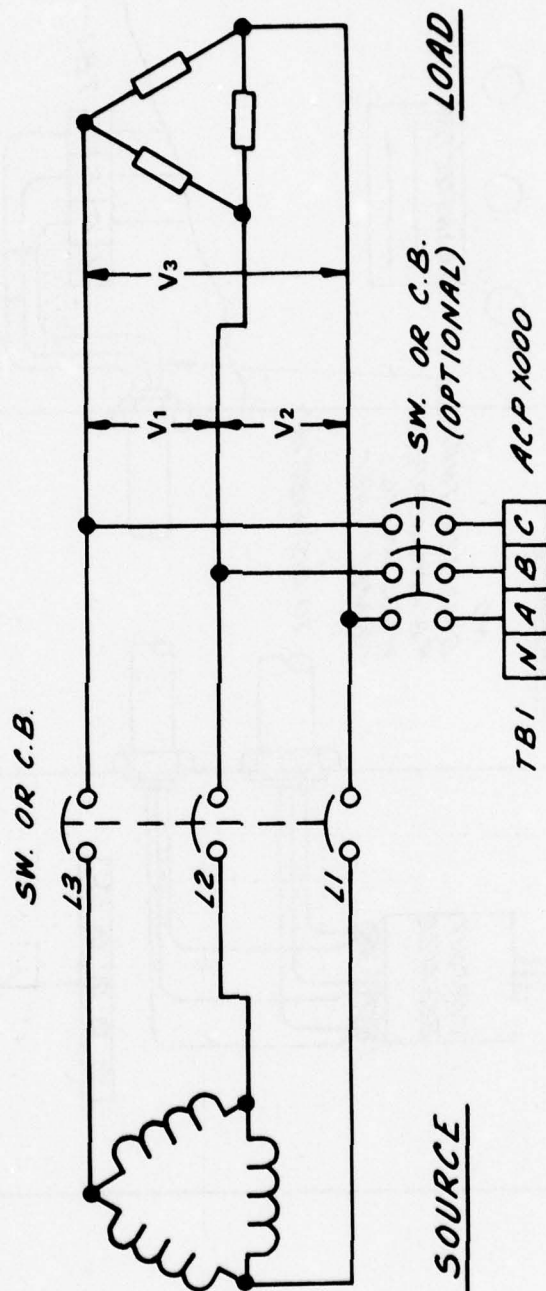
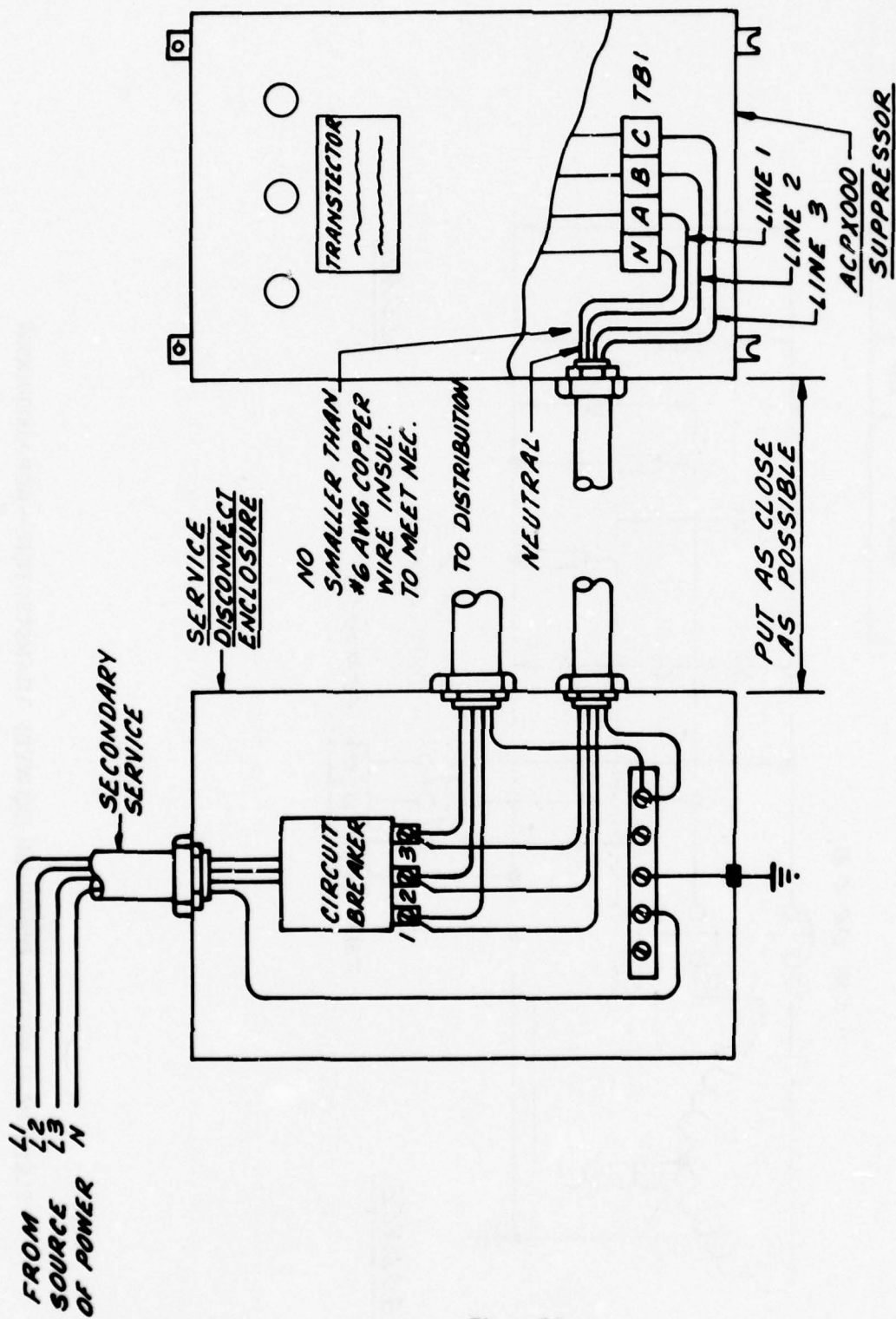


Figure 19

ELECTRICAL WIRING DIAGRAM: (3Φ DELTA) TRANSTECTOR - ACP X000-XXXX







INSTALLATION DIAGRAM: (3Φ WYE) TRANSTECTOR – ACP X000-XXXW

Figure 21



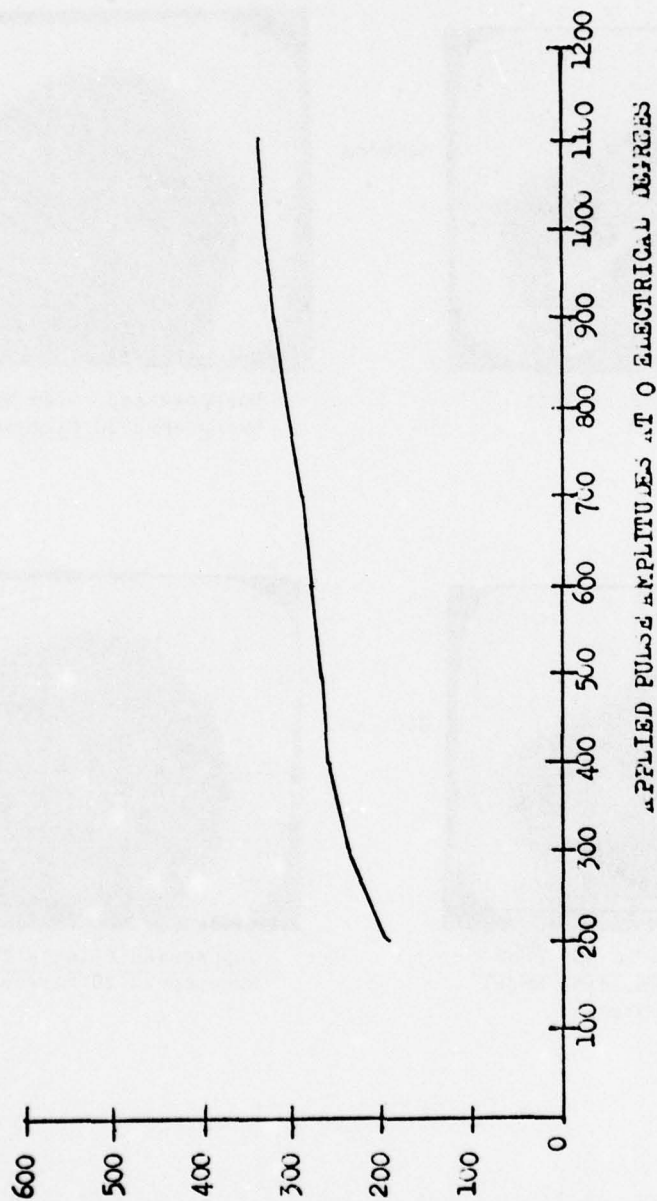
**Table** Clamping Voltage Levels of Transistor Systems, Model Apc-1000-120W Suppressor  
Pulses of 30 Microseconds Duration Applied at 0 and 90 Electrical Degrees.

0 Degrees				90 Degrees			
APPLIED PULSE PEAK VOLT AMPLITUDE	CLAMPING LEVEL			APPLIED PULSE PEAK VOLT AMPLITUDE	CLAMPING LEVEL		
	$\phi$ A	$\phi$ B	$\phi$ C		$\phi$ A	$\phi$ B	$\phi$ C
200	200	200	200	200	200	200	200
300	240	225	220	300	225	210	220
400	260	240	245	400	240	220	225
500	270	260	260	500	245	225	230
600	280	270	265	600	260	240	245
700	290	285	280	700	265	250	260
800	310	300	290	800	270	265	270
900	325	315	305	900	285	280	290
1000	335	325	325	1000	300	285	305
1100	340	335	340	1100	315	305	320

**Note:** The maximum energy stored in pulse generator for 1100 volt pulse for 30 microseconds duration is 35 joules. Pulse rise time approximately 15 microseconds.

Figure 23





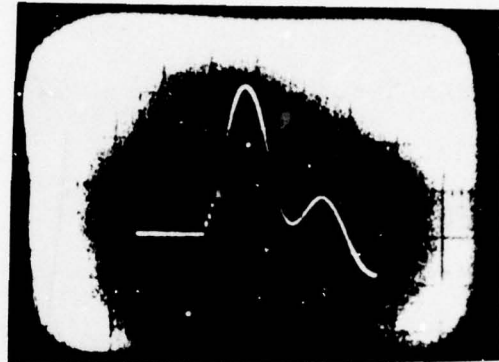
Voltage clamping levels for section A of Transtector ACP-1000-120W  
for 30 microsecond duration impulse voltage transients. 35 Joules

Figure 24

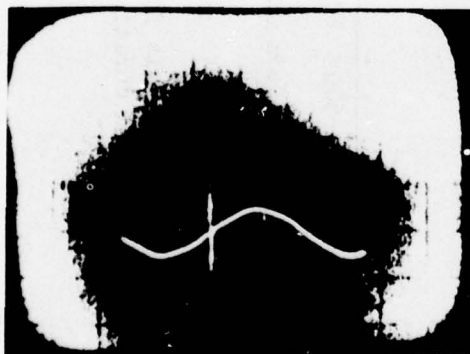


Approximate 1100 Peak Volt  
Unsuppressed Pulse

340V/cm

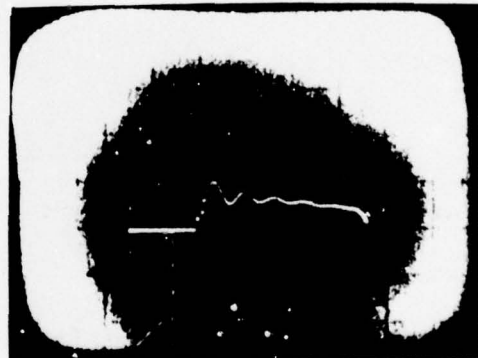


Unsuppressed Pulse With Oscilloscope  
Sweepsepd 20 Microseconds/cm



Pulse Suppressed to 355 Peak  
Volts Using Transtector Model  
ACP-1000-120 Suppressor

340V/cm



Suppressed Pulse With Oscilloscope  
Sweepsepd 20 Microseconds/cm

Figure 6. Suppression of a 1100 Peak Volt 30 Microsecond  
Duration (35 Joule) Pulse Using Transtector  
Systems ACP-1000-120W Suppressor.

Figure 25

## APPLICATIONS

### FAA/ARTCC - Longmont, Colorado

Early in 1971, several of the slower-responding (10 microsecond) models of the ACP10,000 were installed in FAA Air Route Traffic Control Centers. The Longmont, Colorado, ARTCC had the ACP10,000-120W installed as shown in Figure 26. It protected the seven critical 150-amp, 120/208 3-phase, 4-wire circuits. These circuits feeding the IBM 360's had numerous problems with outages due to induced lightning and switching surges on the power line. It also protected the computers from a more common problem of fuse arching. An FAA study showed that if a 150 amp fuse blew, the transient generated was a pulse of 2000 amps for 2 milliseconds. It would travel down other branch service legs and damage equipment.

After installation of the ACP10,000, the records showed no outages due to overvoltage surges or transients. During a 3-1/2 year period, a total number of transients suppressed was 597,332. The counter used had a maximum response time of 5 milliseconds. Because of the slow counting time, many of the high-speed transients were suppressed but not detected.

### East Coast Satellite Tracking Station - Blossom Point, Maryland

In December of 1974, Transtector Systems received an urgent message from a well known national corporation. In an insuing meeting, the management of Transtector was advised





that this major corporation managed a satellite tracking station for a U.S. Government agency and that, for some time, they had been having serious problems with most of their electronic equipment and instrumentation at the tracking station (Figure 27). The problems were due to induced lightning strikes and high-energy switching transients on the AC power line feeding the site. They had on many occasions suffered great economic losses and, even worse, could have lost "satellites down range." After evaluation of other methods of protection, the corporation asked if there was anything Transtector could do to solve the problem. Technical review and analysis of the information provided to Transtector showed: 1) lightning transients were being induced on the 7200 VAC power line feeding the complex, 2) power and load switching by other users on the same feed was causing numerous outages, and 3) high-energy lightning was entering the 480 VAC lines to the 48' radar antennas and damaging the solid-state motor drives for the antennas.

The commercial power to the facility (Figure 27) came from overhead lines at 7200 Vrms (Delta) and was fed, in buried conduit, several hundred yards to a 500 KVA transformer. The output of the transformer was 120/208 volts, 3-phase, 4-wire which provided power to the total facility. A step-up, 100 KVA transformer provided 480 volts, 3-phase, 3-wire to the two 48' tracking antennas. The power was run in buried conduit (6" x 6" wireways) approximately 600 yards to the antennas.

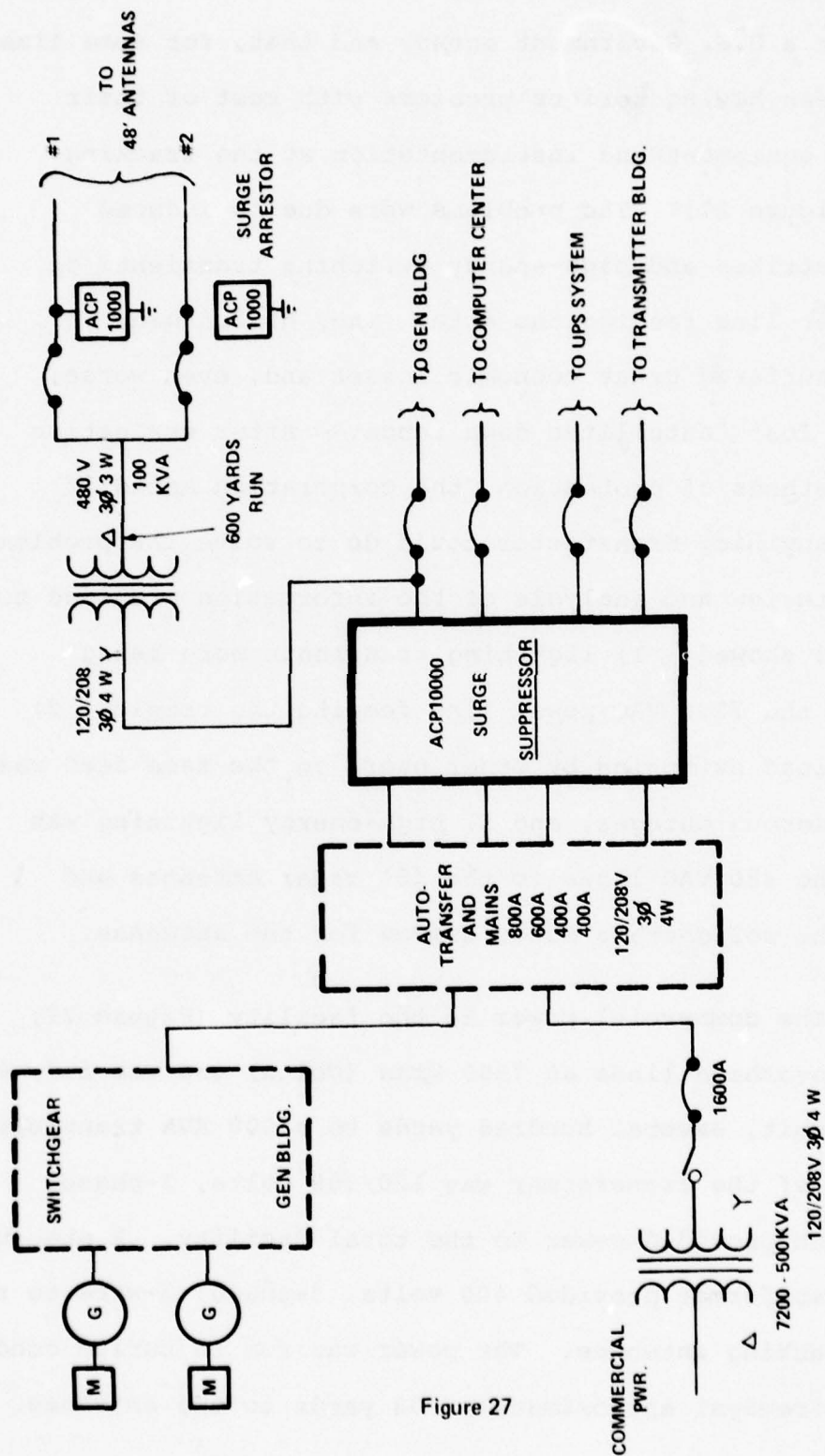


Figure 27



At the antenna end of each feed, an ACP1000-480D, AC Lightning Surge Suppressor, was installed (Figure 28).

The 120/208 volts entered the Power Distribution Building (Figure 27) where the ACP10,000-120W Lightning Surge Suppressor was located, on the load side of the switching gear. This location was important as, during testing of the ACP10,000, there were as many as 60 transients produced during transfer to a motor-generator and back to commercial power, which the suppressor promptly suppressed. In addition, short lead lengths and large cable-size wires were used. The Power Distribution Building houses the switch-gear and main distribution system for the complex. Attached to the Power Distribution Building is the Generator Building which houses the two 250KV motor-generators for back up when power fails.

The 120/208 volt power ran to the Operations Building, approximately 50 feet away, and other locations within the complex. In the Operations Building, main power distribution panels were provided for all systems including the UPS (Uninterrupted Power System) which fed the computer, control systems, and communication equipment.

The problem was solved by Transtector Systems recommending that the total site be protected by Transtector's Model ACP10,000-120W, Figure 8, (1.5 million watt transient suppressor) placed at its 1600-amp main power feed and an ACP1000-480D, Figure 11, (105,000 watt transient suppressor) placed at each 48' antenna to protect the antennas' SCR

CHATSORTH  
CHATSORTH, CALIFORNIA

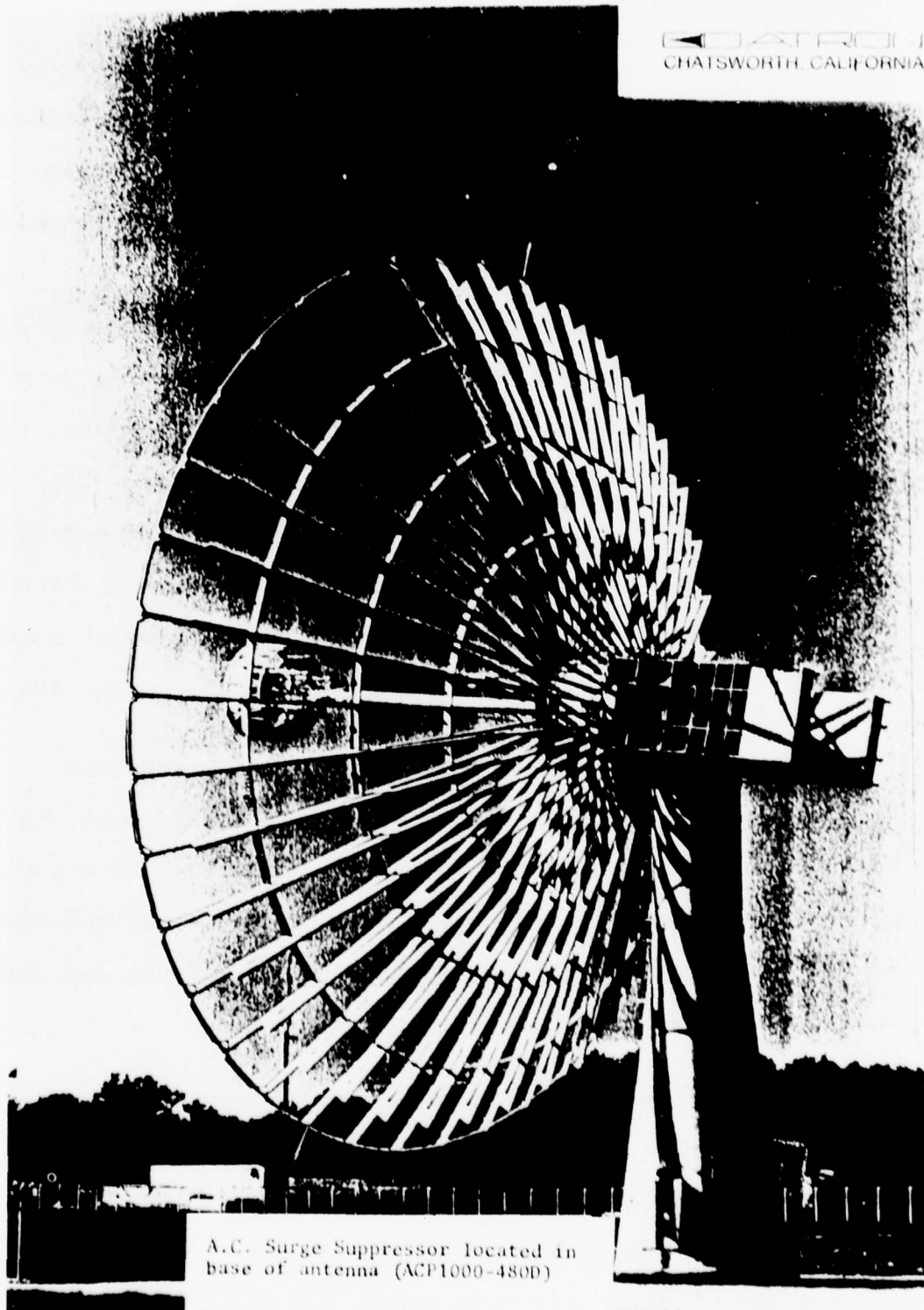


Figure 28

solid-state motor drives and controls. In May of 1975, the products were delivered and installed under the supervision of Transtector Systems' installation engineers.

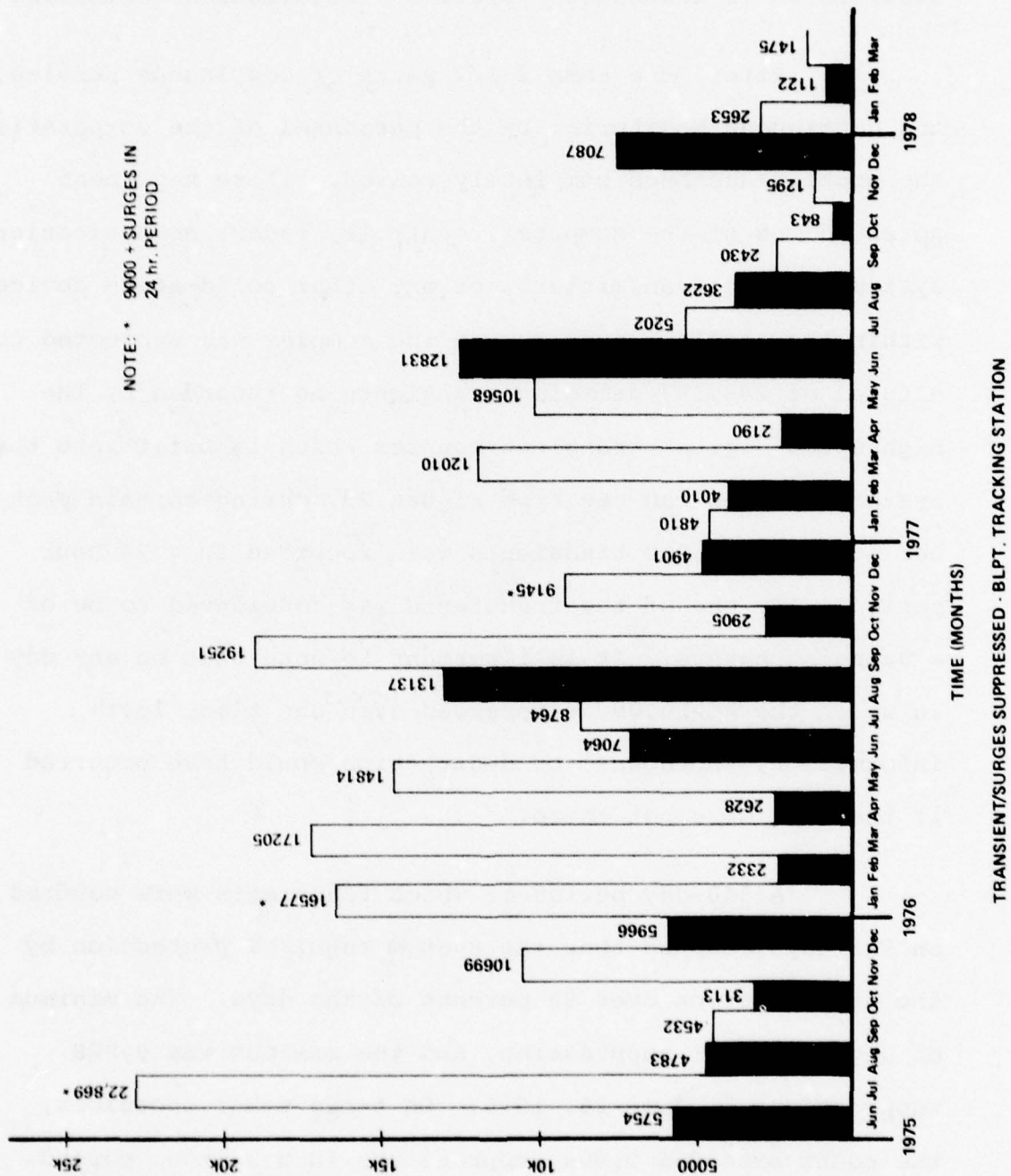
After more than 2-1/2 years of continuous service, and continuous monitoring by the personnel of the corporation, the problem has been completely solved. There have been no shutdowns of the computer, controls, radar, communication systems, radio transmitters, or any other solid-state devices within the complex, even though the complex was subjected to a total of 248,587 damaging transients as recorded by the high-speed digital transient counter which is built into the system. As one can see from Figure 29, during certain peak periods, over 9,000 transients were recorded in a 24-hour period. Any one of the transients was considered to be of a damaging nature. It is important to note that on any day in which the ACP10,000 suppressed even one time, lost information, shutdowns, or destruction could have occurred if the unit were not there.

A 550-day period, of which transients were counted on 511 days, showed that the system required protection by the suppressor on over 93 percent of the days. The minimum on any day was 1 suppression, and the maximum was 9,028 suppressions on June 26, 1975. On three other occasions, the count exceeded 9,000 suppressions in a 24-hour period. The average suppressions per day required for the 18-month period was 10.8.



Figure 29

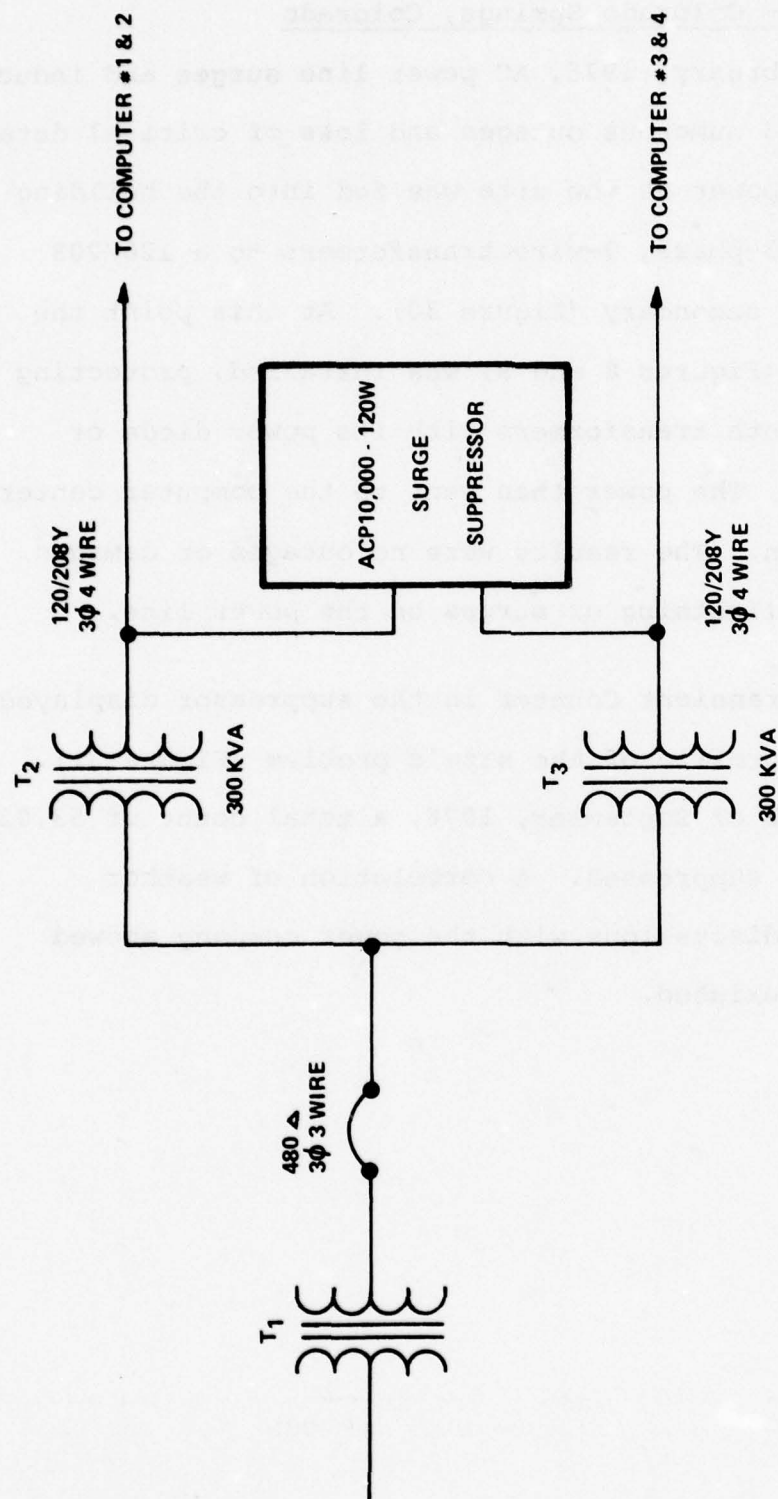
VOLTAGE SURGES/TRANSIENTS (SUPPRESSED) > 1 JOULE



Air Force Site - Colorado Springs, Colorado

In February, 1976, AC power line surges and induced lightning caused numerous outages and loss of critical data. The commercial power at the site was fed into the building to two 480 VAC 3-phase, 3-wire transformers to a 120/208 3-phase, 4-wire secondary (Figure 30). At this point the ACP10,000-120W (Figures 8 and 9) was installed, protecting the output of both transformers with its power diode or logic circuits. The power then went to the computer center for distribution. The results were no outages or damaged equipment from lightning or surges on the power line.

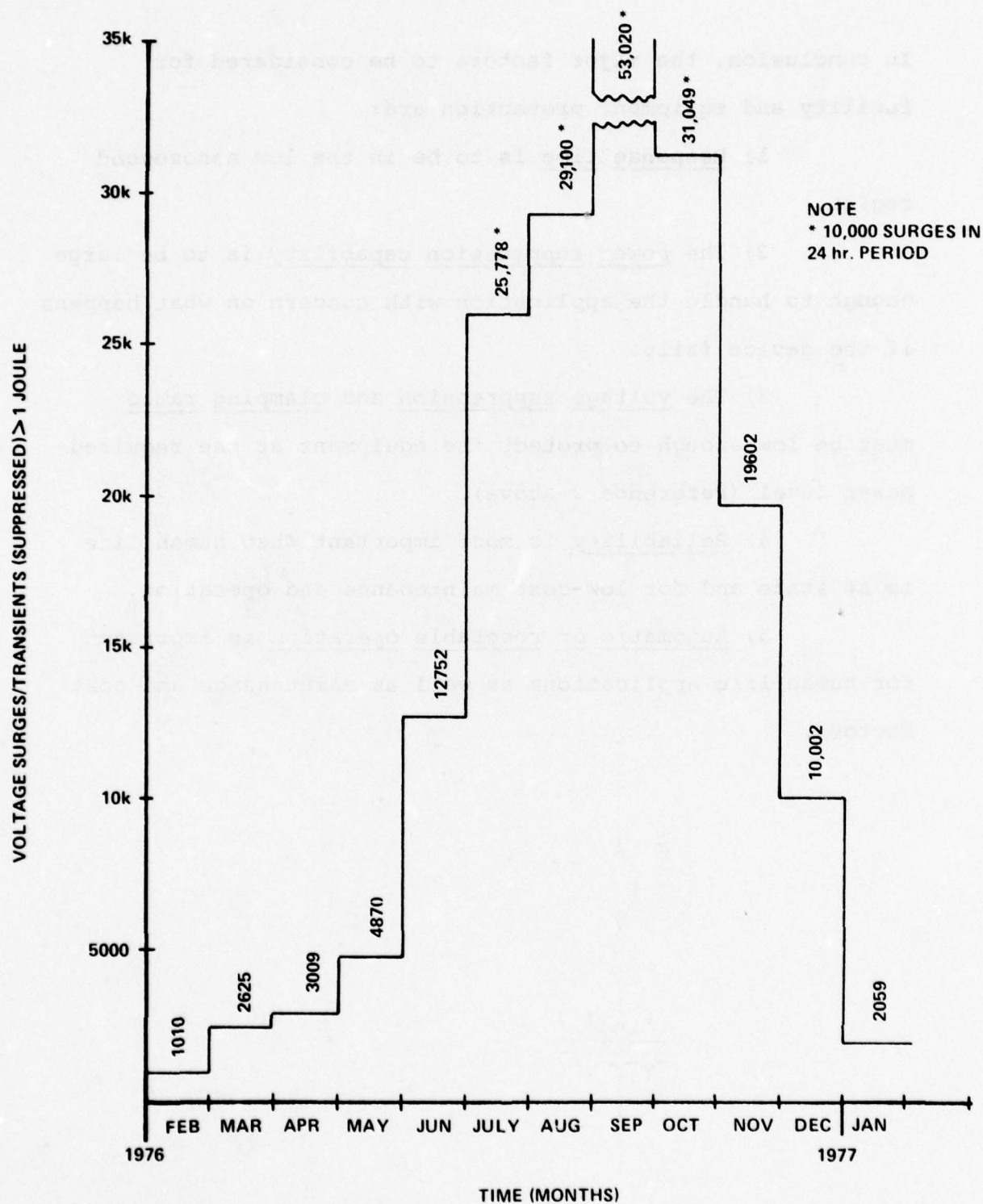
The Transient Counter in the suppressor displayed an interesting profile of the site's problem (Figure 31). During the month of September, 1976, a total count of 53,020 transients were suppressed. A correlation of weather conditions and discussions with the power company showed this condition existed.



ADC POWER DISTRIBUTION SYSTEM

Figure 30





TRANSIENT/SURGES SUPPRESSED - AIR FORCE SITE

Figure 31

## SUMMARY

In conclusion, the major factors to be considered for facility and equipment protection are:

- 1) Response time is to be in the low nanosecond region.
- 2) The power suppression capability is to be large enough to handle the application with concern on what happens if the device fails.
- 3) The voltage suppression and clamping ratio must be low enough to protect the equipment at the required power level (Reference 2 above).
- 4) Reliability is most important when human life is at stake and for low-cost maintenance and operation.
- 5) Automatic or resetable operation is important for human life applications as well as maintenance and cost factors.

A Study of  
Lightning Transients in  
Telephone Cables

by

K.E. Crouch

Lightning Technologies, Inc.

560 Hubbard Avenue

Pittsfield, Massachusetts 01201

and

B.I. Wolff

General Electric Company

Semiconductor Products Dept.

Syracuse, New York 13201

Presented at

Federal Aviation Administration/

Georgia Institute of Technology

Workshop on Grounding and Lightning Protection



## ABSTRACT

Protection of electronics connected to telephone cables against lightning requires knowledge of transient current and voltages. Basic lightning statistics are combined with a computer-solved simulation to predict lightning-induced currents and voltages on typical telephone cables. The results indicate that currents exceeding one kiloampere would rarely occur.

## 1.0 Introduction

For many years carbon gap and more recently, gas tube protectors have been utilized to protect telephone switching centers from transients induced in telephone cables. These protectors have usually provided adequate protection to the equipment found in most systems.

The newer switching equipment now appearing in some systems is inherently more sensitive to lightning-induced transients than their more rugged predecessors, however, and gap-type protectors have not always prevented damage to this equipment. This has led to a re-examination of protection technology and has identified a need for protectors with lower clamping voltage characteristics and higher reliability than that provided by the gap-type protectors.

Specifications for telephone protectors usually include tests to verify the ability of a protector to withstand a specified transient, but these tests are designed to verify the spark gap capability and do not necessarily represent transients that are actually induced in the system by lightning. This study was performed to determine the expected waveforms and amplitude of lightning-induced voltages appearing in telephone cables.

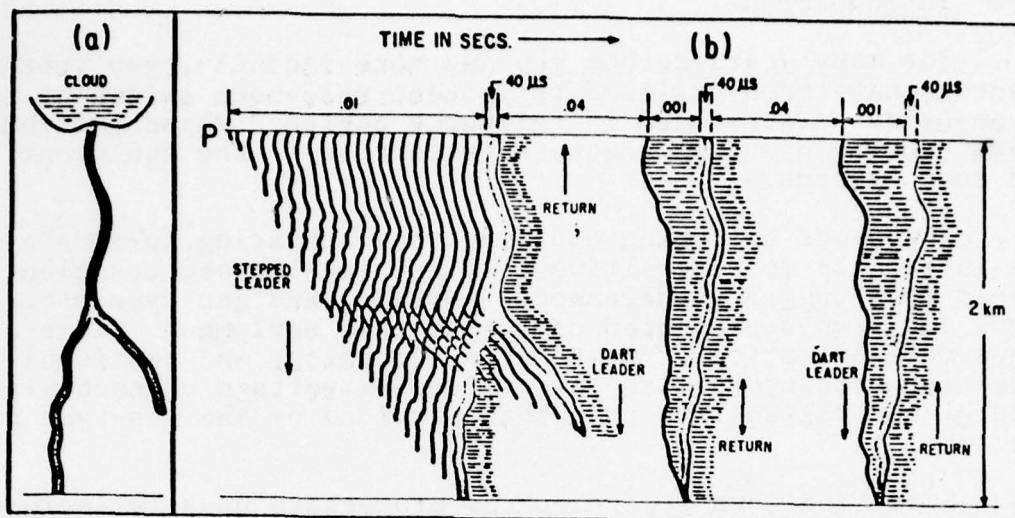
The analytical techniques that were applied for predicting the lightning-induced transients were first proven successful in predicting the lightning-induced voltages in launch umbilical cables at NASA's Kennedy Space Center (Reference 1).

## 2.0 Lightning-Induced Transients in Telephone Cables

To understand how lightning may induce transients on telephone cables it is necessary first to review pertinent characteristics of natural lightning and then to examine the mechanisms that relate this environment to the cables.

### 2.1 Characteristics of Lightning

A lightning *flash* consists of one or more rapid discharges from an electrically charged cloud to the earth or to another oppositely charged cloud. A flash begins as a series of long electrical sparks called the stepped leader extending outward from an electrically charged cloud to ground, or to another cloud channel, to the opposite polarity. This process is illustrated in Figure 1.



This flash contained three separate discharges or *strokes*. Many studies have been made to measure lightning stroke currents. A typical measurement made of a lightning flash to the Empire State Building is shown in Figure 2.



In this case, the flash started from the building and the leader progressed upward to the cloud, resulting in a relatively long duration low amplitude current of about 250 amperes. At 0.2515 second, the first return stroke occurred, with a peak of 15 kiloamperes (kA). Three more strokes were recorded, one of which exceeded 20 kA.

Flashes that are initiated from the cloud deliver similar stroke currents but do not exhibit the low amplitude currents prior to the first stroke. Stroke current amplitudes such as those of Figure 2 occur most frequently, but a few measurements of stroke currents exceeding 100 kA have been made. A comprehensive statistical summary of stroke amplitudes and other characteristics measured by many researchers has been compiled by Cianos and Pierce (Reference 2).

The lightning characteristics of most importance to the induced voltage problem are the *peak amplitude*, *rate of rise* and *duration* of the stroke currents. The first two influence the electric and magnetic fields which induce voltages in the cable conductors and the third determines the energy content of the induced transients.

Figure 3 shows statistical distributions of the peak current amplitude of lightning strokes in a flash. There are two curves shown, one for the first return stroke and one for subsequent strokes.

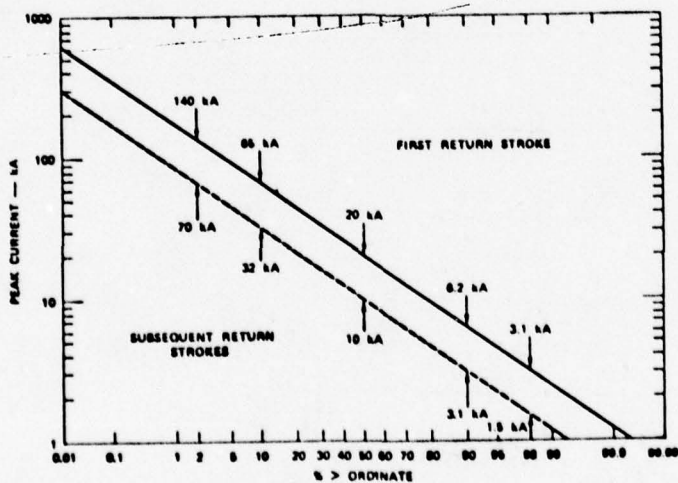


Figure 3 - Distribution of Peak Currents for First Return Stroke and Subsequent Strokes  
(from Cianos & Pierce-Fig. 24)

For engineering analysis, Cianos and Pierce have determined that the amplitude of subsequent strokes may be considered to be half that of the original stroke. Figure 4 shows the statistical distribution of rate of rise.

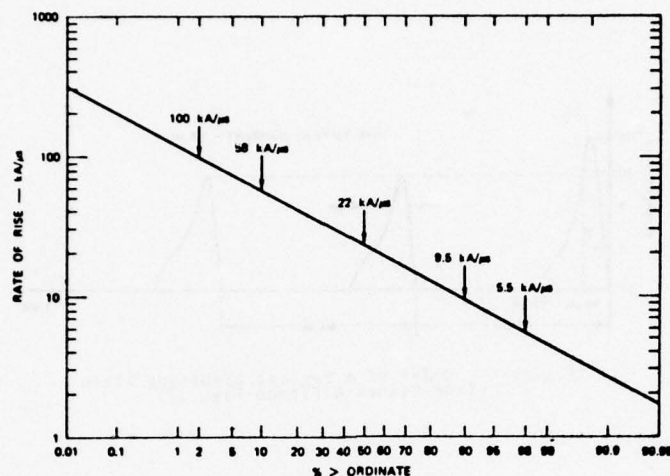


Figure 4 - Distribution of Rates of Rise  
(from Cianos & Pierce-Fig. 27)

Figure 5 shows statistical distributions of the time to stroke current half value.

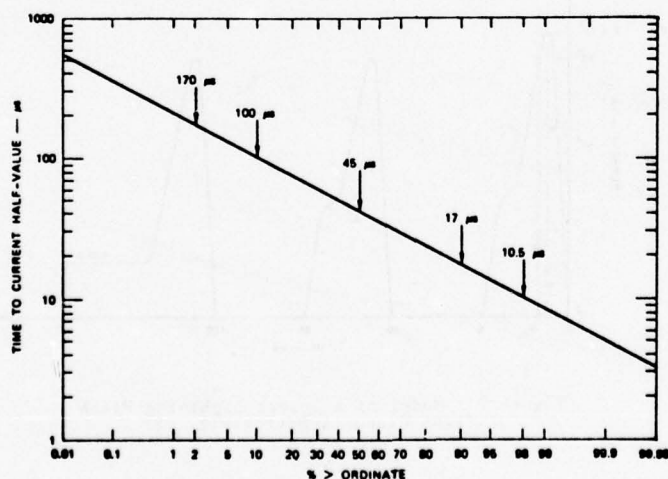


Figure 5 - Distribution of Time to Current Half Value  
(from Cianos & Pierce-Fig. 28)

For the purposes of analysis, it is helpful to have models of *typical* and *severe* lightning flashes. Cianos and Pierce suggest the models shown in Figures 6 and 7.

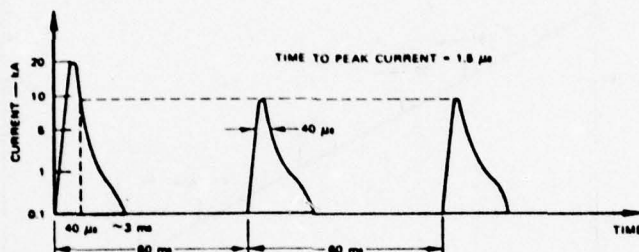


Figure 6 - Model of a Typical Lightning Flash  
(from Cianos & Pierce-Fig. 32)

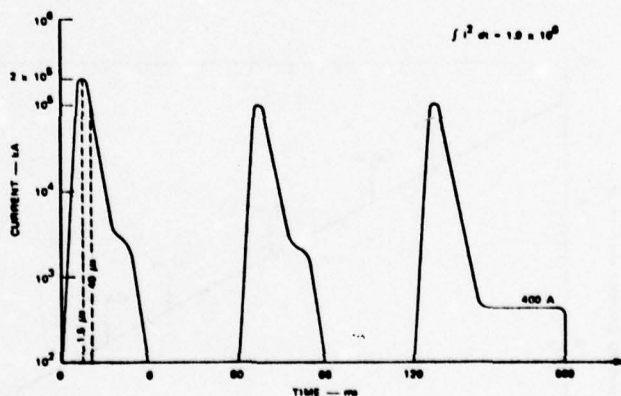


Figure 7 - Model of a Severe Lightning Flash  
(from Cianos & Pierce-Fig. 35)

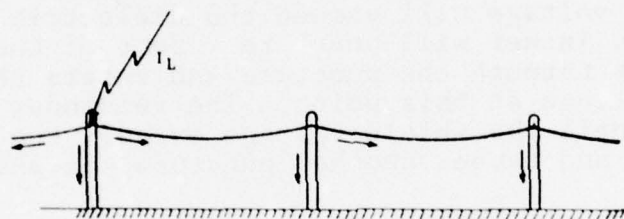
The continuing current portions of the models have little effect on telephone systems and can be neglected.



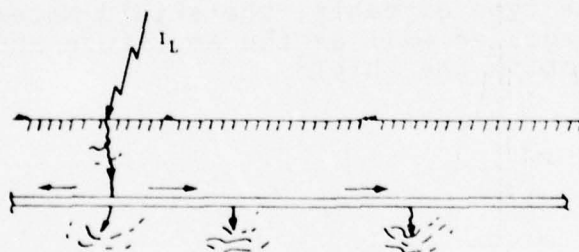
### 3.0 Lightning Induced Voltages in Cables

Most telephone system cable plant (distribution system) is contained in shielded cables, either suspended from poles or buried in the ground. Some sections of open wire transmission are still used, but most of these are remote from central offices and protectors are usually installed where the open wire enters the shielded cables. A shielded telephone cable consists of many twisted pairs (tip and ring) contained within an insulating jacket covered with a continuous metal foil shield. Another insulating jacket covers the shield.

Lightning currents may enter the cable shield either by directly contacting the suspended cable or seeking the cable in the resistive ground, as illustrated in Figure 8.



a) to an aerial shielded cable  
(cable grounded at each pole)



b) to a buried shielded cable

Figure 8 - Methods of Lightning Current Entry

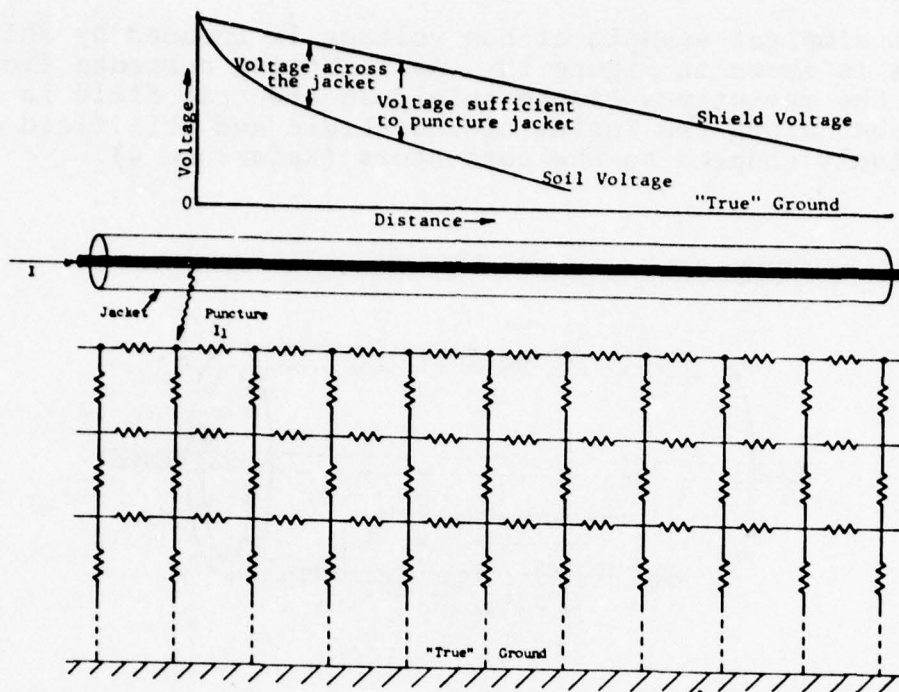
Many suspended cables share poles with power lines and would not get struck directly. Even so, part of the lightning stroke current will go on the telephone cable on its way to other grounds. For this analysis, the worst case will be considered, in which the lightning stroke directly contacts the shielded cable.

At the stroke attachment point, current divides and goes in both directions along the shield. If the strike occurs at a pole, some of the current goes directly into ground. Some of the current will leave the cable and go to earth at each grounded pole along the line. Studies (Reference 3) have shown that all of the lightning current has left the cable after passing 10 grounded poles in high conductivity soils and 20 grounded poles in soils of low conductivity.

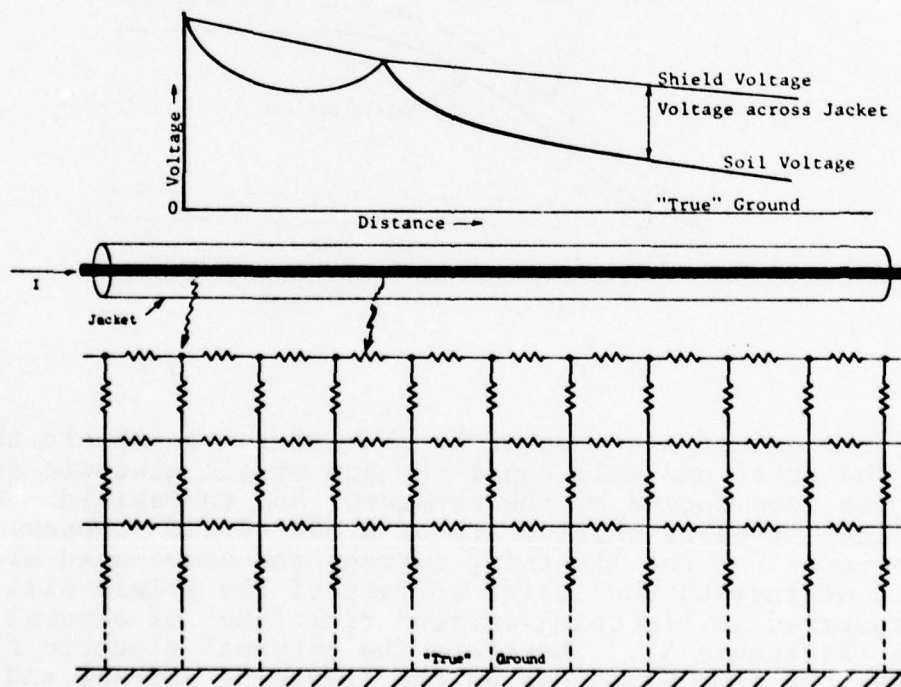
Stroke currents leave buried cables in a similar fashion but due to a different cause. A voltage will appear along the cable shield as the lightning current passes through it since it has an impedance. This voltage will be impressed across the jacket between the shield and the soil, as shown in Figure 9. At some point, the shield voltage will exceed the dielectric strength of the jacket and the jacket will puncture. Some of the lightning current then flows through the puncture and enters the soil, equalizing the voltage at this point. The remainder continues down the shield until the shield voltage exceeds the jacket insulation capability and causes another puncture, as shown in Figure 9.

Lightning currents are not harmful to the shield itself. However, these currents induce surge voltages on the conductors contained within, and these surge voltages can be harmful to sensitive equipment in the telephone system.

The surge voltage that appears at the end of the shielded cable depends on the type of cable, the shield material, its thickness and coverage, as well as the amplitude and waveshape of the lightning current in the shield.



Conditions after One Puncture of a Cable Jacket has Occurred



Conditions after Two Punctures have Occurred

Figure 9 - Mechanism of Jacket Puncture



The simplest example of how voltage is induced by shield currents is shown in Figure 10. As lightning currents flow through the resistance of the shield an electric field is established along the inside of the shield and this field is capacitively coupled to the conductors (Reference 4).

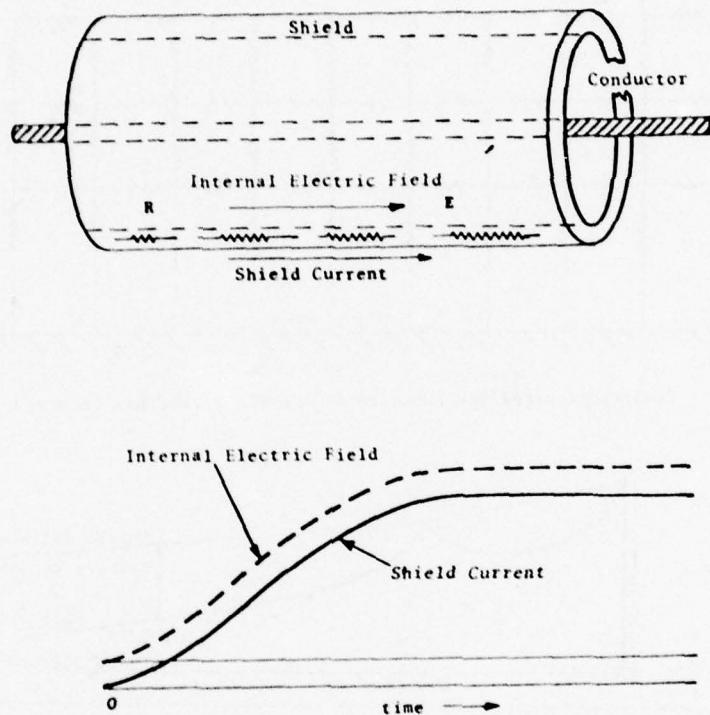


Figure 10 - Coupling Mechanism

If one end of a conductor is shorted to the shield, the voltage at the other end will equal the sum of all electric fields around the loop formed by the conductor and the shield. Since most telephone cable shields are of 0.005"-0.010" copper, the time it takes for the lightning current and associated electric field to diffuse to the inside surface of the shield will be short compared to lightning current rise times of several microseconds (Reference 5). Therefore the internal electric field will have the same waveshape as the lightning current and will be related to it by Ohm's Law:

$$E = IR \quad (1)$$

where

E = Internal electric field (volts/meter)

I = Lightning current in shield (amperes)

R = Shield resistance (ohms/meter)

The voltage surge thus induced will propagate as a traveling wave in either direction away from the region where it was induced. The cable acts as a transmission line, in which the surge voltage and surge current are related to each other by the surge impedance,  $Z_o$ .

Surge impedance is defined as the instantaneous ratio of surge voltage to surge current at a particular point on a cable conductor. It can also be expressed in terms of the inductance, L, and capacitance, C, per unit length of the cable as:

$$Z_o = \sqrt{\frac{L}{C}} \text{ (ohms)} \quad (2)$$

The velocity, v, with which a surge propagates along the conductor is also a function of the inductance and capacitance per unit length as follows:

$$v = \sqrt{\frac{1}{LC}} \text{ (meters/second)} \quad (3)$$

The inductance and capacitance per unit length of a conductor depend upon the relative permeability  $\epsilon_R$ , and relative permittivity (dielectric constant),  $\mu_R$ , of the medium. If the insulation is air,  $\epsilon_R$  and  $\mu_R$  are both unity and the velocity of propagation is equal to the speed of light,  $3 \times 10^8$  meters/second, or about 1000 feet per microsecond.

If the cable dielectric is not air and the relative permeability is unity, the inductance and capacitance are given by:

$$L = \frac{\sqrt{\epsilon_R} Z_o}{3 \times 10^8} \text{ (henries/meter)} \quad (4)$$

and

$$C = \frac{\sqrt{\epsilon_R}}{3 \times 10^8 Z_o} \text{ (farads/meter)} \quad (5)$$

The most common cable dielectric is polyethylene with  $\epsilon_R = 2.3$ .

Tests conducted on typical telephone cables have found surge impedances of 80 ohms between any of the conductors and the shield, and shield resistances of between 5 and 6 ohms per mile have been measured (Reference 6).

Using these values, an analytical model of a telephone cable was defined for use in calculating worst case lightning induced currents and voltages appearing at one end of the cable. This model is shown in Figure 11. An average cable span between poles of 165 ft. and a ground on every fourth pole, or every 660 ft., was assumed. The values of the lumped L, R and C components of the model are derived from the conductor resistance and cable surge impedance by equations 4 and 5.

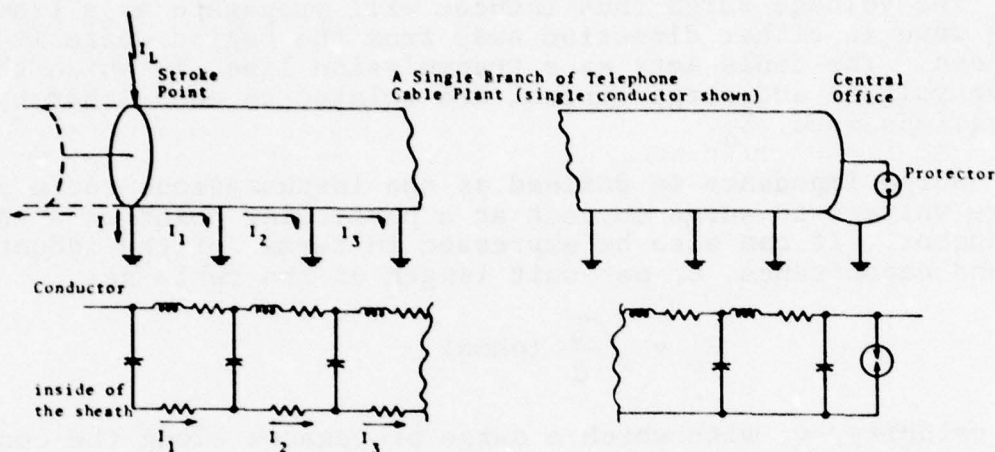


Figure 11 - Analytical Model of a Telephone Cable

The model with values of all elements assigned is shown in Figure 12.

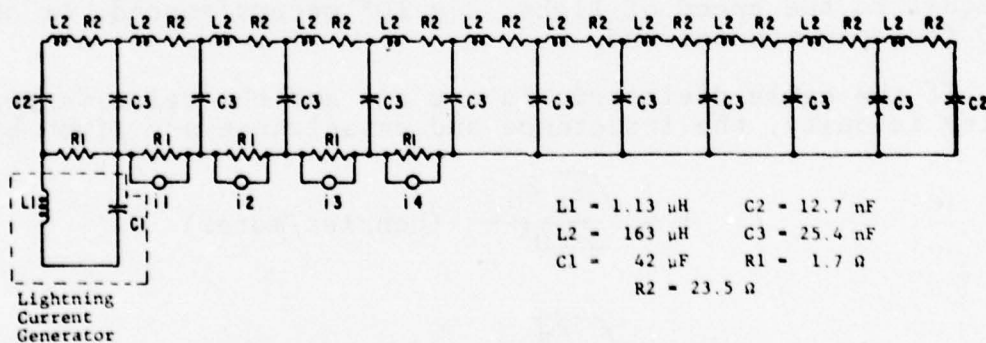


Figure 12 - Computer Model of the Telephone Cable

The number of transmission line sections represented were selected to fit the maximum size limits of the Electronic Circuit Analysis Program (ECAP) available in the General Electric time sharing computer library (Reference 7).



Each pi section of the model represents 1320 feet (1/4 mile) so the total length of the line is 2.75 miles. The severe lightning current,  $i_0$ , is generated analytically by capacitor C1 discharging into the first line section through waveshaping elements, L1 and R1, shown in the dashed area of the figure. The waveshape of the applied lightning current is shown in Figure 13. The reduced shield currents  $i_1$ ,  $i_2$ ,  $i_3$  and  $i_4$  are dependent current sources in the model. These currents passing through the shield resistances in the first five sections produce the electric fields inside the shields.

Typical induced voltages and currents calculated by the model are presented in Figures 14, 15 and 16. Figure 14 shows the voltage arriving at the central office end of the struck cable. This output assumes that the cable will support such a voltage level without sparkover.

Figure 15 shows the short-circuit current available at the central office. This result was obtained by replacing the final capacitor in Figure 12 with an 0.1 ohm resistor and calculating the current in that element.

Figure 16 shows the short-circuit current at the central office when the cable is shorted at the lightning strike. This condition represents a protector or insulation breakdown at the striking point. For this analysis, the condition was simulated by replacing the initial capacitor by an 0.1 ohm resistor.

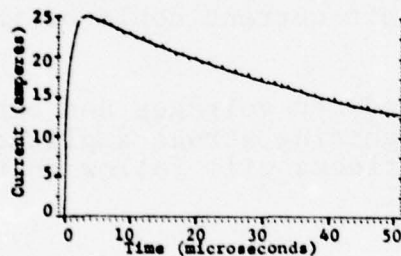


Figure 13 - Applied Lightning Current Waveform (2x50  $\mu$ s)

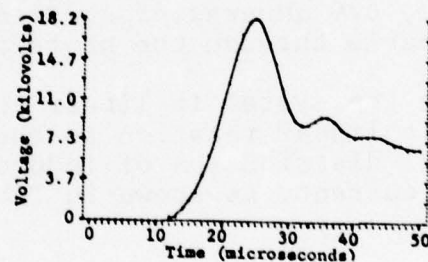


Figure 14 - Open Circuit Voltage at the Central Office 2.75 Miles Away from a 100 kA Strike (No breakdown of conductor insulation or protectors).

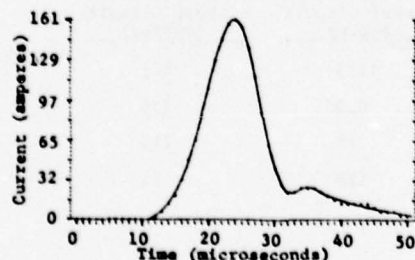


Figure 15 - Short Circuit Current Available at the Central Office 2.75 Mile Line - 100,000 Ampere Stroke (No Cable or Terminal Block Breakdowns)

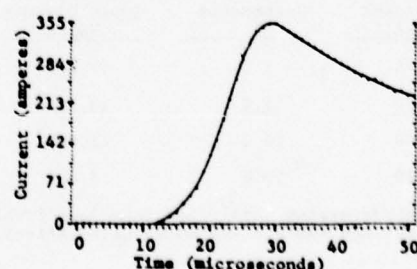


Figure 16 - Short Circuit Current Available at the Central Office 2.75 Mile Line - 100,000 Ampere Stroke (Protectors at Both Ends of the Cable).

Figure 17 shows the short circuit current that would enter the cable if a protector were present at the stroke point. This corresponds to the situation where lightning strikes the central office directly.

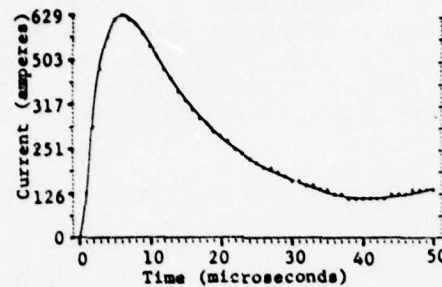


Figure 17 - Short Circuit Current Available to a Protector at the Stroke Point  
2.75 Mile Line - 100,000 Ampere stroke (protectors at Both Ends of the Cable).

This analysis shows that if a severe (100 kA) lightning flash strikes a cable 2.75 miles from a central office, a voltage surge reaching a peak of 18,400 volts can be transmitted by the cable plant to the office and 355 amperes of short circuit current can be available when a sparkover occurs. If the central office was struck, 629 amperes of short circuit current could be injected into the cable through the protector.

Since the system is linear the induced voltages and currents will bear a linear relation to the lightning stroke amplitude. The statistical distribution of induced effects will follow that of the lightning current, as shown in Table I.

Table I - Probability of Occurrence

Lightning Stroke Peak Current (kA)	Probability of Occurrence (%)	Induced Voltage (Open Circuit Volts)	Induced Current At the Stroke (Short Circuit Amperes)	Induced Current 2.75 miles From the Stroke (Short Circuit Amperes)
175	1.0	32,200*	1103	621
<u>100</u>	<u>5.0</u>	<u>18,400*</u>	<u>630</u>	<u>355</u>
60	15.0	11,040*	378	213
20	50.0	3,680	126	71

\* above system insulation breakdown level  
Underlined numbers are model calculations

The lightning current statistics of Table I are taken from Figure 3.

All of the induced voltages predicted in Table I would cause the protectors to spark, reducing the voltage to the clamping level of the protector. The protector must then conduct the induced current. Thus a protector may sustain a 126 ampere surge for strokes of average intensity, but up to ten times this much on rarer occasions.

To determine the induced currents caused by lightning strikes closer to the central office, the model was modified and calculations repeated. The calculations were made for two conditions. No breakdown at the stroke point, and a breakdown at the stroke point. The results are summarized in Table II.

Table II - Peak Lightning Induced Currents in Various Lengths of Telephone Cable (100 kA Lightning Stroke)

Distance Central Office to Stroke in Miles	Peak Induced Currents		
	No Stroke Breakdown	Breakdown at Stroke	
	Central Office Amperes	Central Office Amperes	Stroke Point Amperes
2.75	161	355	630
1.50	325	637	630
1.00	420	799	734
0.50	347	1120	1110
0.25	276	1480	1480

The response of only one wire in a cable has been considered in these calculations. The mutual capacitive and inductive coupling between several wires in a cable are quite complex and cannot be represented in the present computer model. In general, the voltage induced on any one wire in the cable will be the same as that induced on all others, provided they have similar loads attached. If all wires have protectors attached that are removing currents, and all protectors have the same electrical characteristics, then all currents will be approximately equal. For a 6-pair cable, if each wire carried the 1480 amperes predicted by the computer analysis, they would deliver 17,760 amperes to the central office protectors or 70% of the total current with only 30% left on the cable sheath. For a 100-pair cable, approximately 150 kA would be carried by the wires which is greater than the total stroke. By assuming that the wire currents will remain proportional to the ratio of wire resistance to sheath resistance and reduced a constant amount by the cable inductance, a prediction of individual wire currents can be made. These predictions are shown in Table III.

TABLE III - Peak Lightning Induced Currents in Short Lengths of Multiple Wire Telephone Cable (100 kA Lightning Stroke)

Distance from Central Office to the Stroke in Miles	Peak Induced Current Breakdown at Both Ends of Cable	
	6-Pair Cable	12-Pair Cable
	Amperes	Amperes
0.25	852	463
0.50	712	453



The cables entering telephone central offices are usually quite large, 600 to 1200 pairs, and the lightning-induced currents on each wire would be much lower, 1 to 2 orders of magnitude. The induced currents on each wire in longer multiple wire cables will also be lower, due to parallel paths.

An induced current of 850 amperes due to a 100 kA lightning stroke 0.25 miles from the central office represents an upper limit since a stroke closer than 1000 ft. of cable would be a stroke that hits the central office directly and results in a 630 ampere induced current.

It is interesting to compare the predictions of this study with the findings of other investigators. The most extensive measurements of cable plant surge voltages have been conducted by Bodle and Gresch (Reference 8) and Bennison et al (Reference 9). Both of these studies conclude that voltage surges on paired, shielded cables will not exceed 1000 volts for 99% of the surges. Other studies (References 10 and 11) also support such conclusions. However, some field experience on rural telephone lines indicates that voltages in excess of 1000 volts are indeed present (Reference 12). The Bodle and Gresch, and Bennison et al, studies were made either with protection on the monitored wires or on other wires in the cable bundle, and it is possible that protector operations to remove energy from the cable affected their results.

TRANSIENT INTRUSION  
INTO  
CABLE TELEVISION SYSTEMS

BY  
Warren L. Braun, P.E.

ComSonics®, Inc.  
Harrisonburg, Virginia

Presented at  
Federal Aviation Administration/  
Georgia Institute of Technology  
Workshop on Grounding and Lightning Protection

## ABSTRACT

Cable television system reliability is deteriorated by outer conductor sheath current inherited via ground bonding interconnect to power/telephone facilities as required by pole attachment agreements. A quantitative analysis of the ensuing transient sheath currents is provided together with practical solutions to the problem. A summary of applicable field experience is provided.



TRANSIENT INTRUSION  
INTO  
CABLE TELEVISION SYSTEMS

AUTHOR: Warren L. Braun, P.E.

ABSTRACT

Cable television system reliability is deteriorated by outer conductor sheath current inherited via ground bonding interconnect to power/telephone facilities as required by pole attachment agreements.

A quantitative analysis of the ensuing transient sheath currents is provided together with practical solutions to the problem.

A summary of applicable field experience is provided.

In a previous paper<sup>1</sup> the author has determined that approximately 33% of the failures of cable television equipment were due to transient overvoltage. At the time the paper was written, June 1973, there was little documented evidence to identify the source of such transient overvoltage. By an internal monograph<sup>2</sup>, the author identified the principal source of the problem to be the fault current flowing through the CATV external sheath/strand of the CATV plant, induced via the requisite bonding practices currently in effect. This was further confirmed by the Herman, Shekel paper<sup>3</sup> which outlined the magnitude of the steady state sheath currents which could

- 
- <sup>1</sup> - THE CASE OF THE MISSING HEADROOM - Warren L. Braun, P.E., 1973 NCTA Convention paper.
  - <sup>2</sup> - CATV SYSTEM GROUNDING CONCEPTS FOR IMPROVED SAFETY AND RELIABILITY - Warren L. Braun, P.E., 1970.
  - <sup>3</sup> - "Longitudinal Sheath Currents in CATV Systems" - James C. Herman/Jacob Shekel, presented at the 24th Annual NCTA Convention, April 13-17, 1975, New Orleans, Louisiana.

flow through the CATV sheath/strand system as a consequence of the common bonding practices. This paper demonstrates that the efficiency of CATV grounding practices are relatively inconsequential as the resistance of the grounding system was much larger than that inherited by the common bond.

In a paper by Bilodeau<sup>4</sup> the author's concept of deliberate decoupling of the common bond was noted with considerations for safety set as the limitation for the total isolation of such bonds. In an attempt to determine the magnitude of the common bond problems, the author totally decoupled the common bond between utilities and the CATV ground, ie., no common bond in a Louisiana cable television system in 1969 for a period of one year. In the interim, the CATV system was provided with an elaborate set of excellent independent grounds, such that the potential difference between the two plants would be kept to a minimum so there would be no residual safety hazard. The improvement of the equipment reliability was dramatic, improving nearly an order of magnitude. Unfortunately, the utilities determined that there could be a safety hazard under severe fault current conditions, and the separate system of grounding had to be abandoned.

Recently this concept was resurrected in a technical article of the TV COMMUNICATIONS journal<sup>5</sup> suggesting the use of these separate ground procedures to relieve the common bond induced current problem. The hue and cry from the utility industry safety groups made it quite clear that the utilities are not any closer to accepting such approaches to the problem than when proposed by the author eight years ago.

Recently the author has found an enlightened utility group receptive to a partial solution to this problem, which method of ground and bonding would provide a higher degree of isolation than had been previously achieved. If we will consult Figure 1, it will be noted that this method of grounding provides a substantial dynamic impedance between the interconnection of two separate grounds at the base of the pole, in lieu of the bond at the aerial interconnect conventionally specified. This provides approximately 33 ohms of dynamic impedance isolation at 1 MHz between the CATV system and the utility ground, which substantially reduces the high frequency components of the ground fault currents which in turn reduces the damage which the CATV equipment would otherwise suffer. It is this type of enlightened understanding of the cable television problems which we trust will continue over the next few years.

---

<sup>4</sup> - "System Grounding: An Important Protection" - Robert Bilodeau, pp. 76-80, TV COMMUNICATIONS, April 1970.

<sup>5</sup> - "Thoughts on Bonding and Grounding: How to Avoid Those 'Unexplained' Outages" - Roy Ehman, TVC MAGAZINE, pp. 44-46, February 1978.

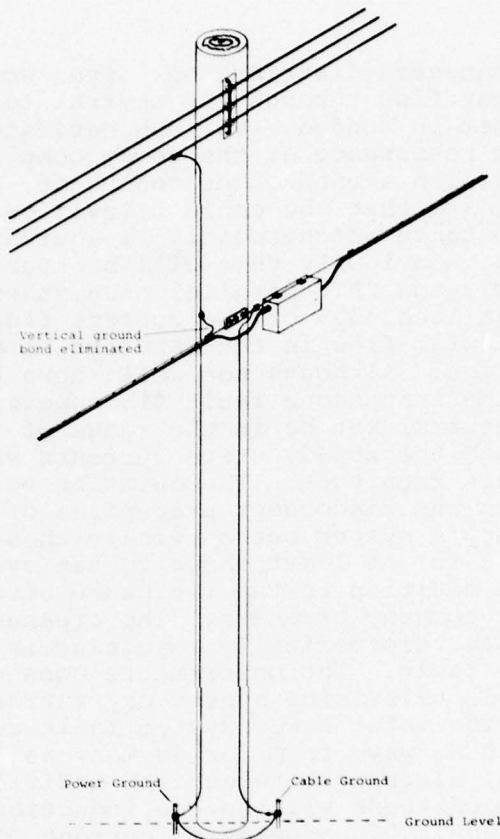


FIGURE I

#### ANALYSIS OF THE PROBLEM

It is unfortunate that this problem is not amenable to a simple solution. However, the understanding of the totality of its complexity allows us to make some reasonable estimates of the problem in terms of its absolute magnitude which can be expressed in terms of probability.

Worst case conditions may provide an appreciation of the dilemma faced by the serious researcher. This type of analysis is provided here. It is known, but not fully appreciated that CATV system bonds are made to power company grounds without regard to the substation from which the power company neutral originates. This may, and on occasion does, interconnect neutrals between two different power company substations. If one substation suffers a single phase overcurrent disconnect the entire phase to phase imbalance current will in all likelihood flow through the neutral return,



assuming "Y" connected distribution. Even worse, the entire fault current may flow through the neutral to which the cable television system is bonded. Various estimates have been provided as to the resistance of the power company neutral and the cable television strand/outer conductor, however, most estimates<sup>6</sup> indicate that the cable television bond interconnect provides a resistance which roughly is equivalent to the power company neutral. Obviously this will be true only where the conductors, power and CATV parallel each other. In this specialized case at least 50% of the current flowing in the power company neutral will flow in the CATV system external sheath/strand combination. Although not well known to the cable television field, the instantaneous fault disconnect currents in the power company neutral can be in the range of 10,000-30,000 amperes, although the steady state currents will be very much smaller than this magnitude. The duration of these currents will depend upon the disconnect properties of the breakers in the power company's system but generally these devices will remain connected for at least three to ten cycles of the 60 Hz power supply in addition to the reclosure attempts designed into most power company breakers. The breakers may cycle as many as 3-5 times before finally remaining in the open position on a continuing fault. The unfortunate consequence of this is that the cable television system may suffer a strand current of 50% of the total power system fault current for 6-10 cycles of the 60 Hz wave form for as many as 3-5 periods with 100 ms (or more) elapsing between such individual periods. The consequence of these will be the induction of the currents in order of 5,000-15,000 amperes of current flowing through the strand/sheath of the CATV system. The current flowing on the inside of the coaxial sheath arrives there via the current penetration through the wall thickness, which magnitude follows the "skin effect" phenomenon. A short review of the pertinent relationships is provided in the appendix.

For typical aluminum sheathed cable, the magnitude of inner coaxial currents are shown to be as is shown here in Figure II, for 0.5" coaxial cable, expressed as a percentage of the external sheath currents.

---

<sup>6</sup> - Herman & Shekel paper - ibid.

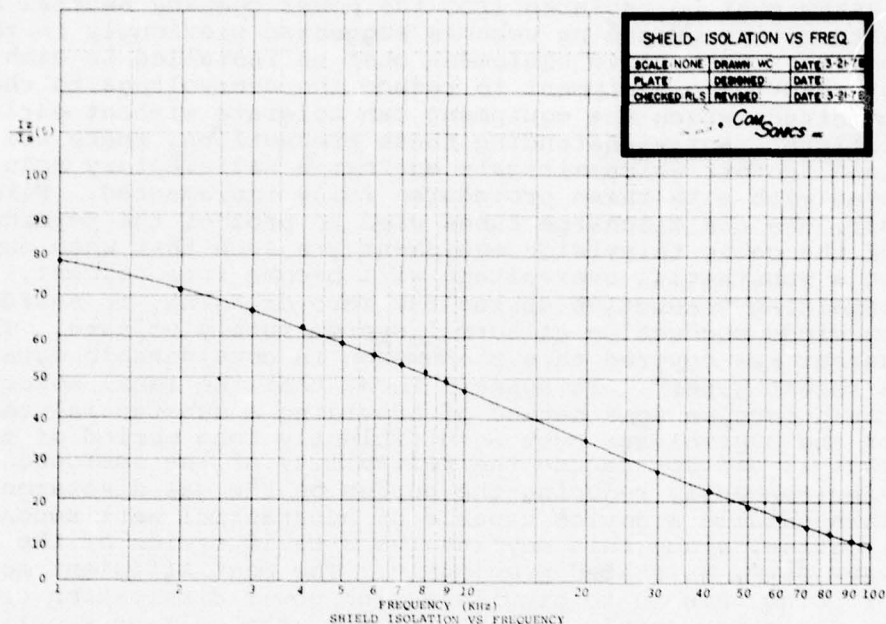


FIGURE II

The full magnitude of this interior sheath current will provide the appropriate  $I_z$  drop, which will appear in series with the CATV simplex supplied cable powering voltage.

Data taken in 1968 and 1969 on surge voltages<sup>7</sup> induced in coaxial cable systems during thunder storms indicates less than 1% of the transients induced exceeded 1000 volts. By contrast, the author's experience with power fault current system overvoltage failures clearly indicate that a voltage of at least 3000 volts peak is quite common. Due to the magnitude of the surge overvoltage, the cable television

<sup>7</sup> - E. Bennison, A.J. Ghazi, and P. Ferland, "Lightning Surges in Open Wire, Coaxial and Paired Cables". PROCEEDINGS OF THE IEEE, 1972 International Conference on Communications, Philadelphia, June 19-21, 1972.

system must be isolated from the power company neutral by alternative grounding schemes suggested previously in this paper or protective equipment must be installed in each piece of electronic equipment to reduce the overvoltage to that magnitude which the equipment can tolerate without early failure. Notwithstanding these precautions, there are certain factors which mitigate against a satisfactory solution even with both these procedures fully implemented. First off, the gas discharge tubes used to protect the terminals of the cable television equipment are such that when exposed to a substantial overvoltage will become incandescent, remaining conductive during the zero crossing, to selfdestruct by diode conduction at normal system supply voltage. The author has covered this phenomenon in considerable detail in a recent paper<sup>8</sup>. It appears then, that the ideal solution would involve some method of providing a substantial reduction of the overvoltage over a sufficiently long period of time that it did not reduce the reliability of the semiconductors simultaneously reducing the burden on the gas discharge tubes. This entails a device capable of substantial watt second dissipation, since this may involve 3 to 10 cycles of the 60 Hz wave form, as stated previously. The most efficient method of doing this is to provide a high power dissipation crowbar in the power supply network ahead of the voltage supplied to any of the semiconductors. The author's firm markets such devices which are capable of providing this type of protection. As has been stated recently<sup>9</sup>, this type of device can be quite successful<sup>10</sup> to provide an adequate degree of protection for the electronic equipment that has been exposed to this equipment.

All of this does not adequately protect the passive devices which may be exposed to this flux. As the author has stated previously<sup>11</sup> the various gas discharge devices must be of such a watt second capability so as to avoid the "incandescent

---

<sup>8</sup> - SYSTEM RELIABILITY - THE TRUTH IS, Warren L. Braun, P.E., paper presented at the SCTE CATV Reliability Conference, February 5-6, 1976, Philadelphia, PA.

<sup>9</sup> - POWER AND LIGHTNING SURGES IN COAXIAL DISTRIBUTION SYSTEMS, James R. Palmer, C-COR Electronics, Inc., paper presented at the 2nd Annual Conference on CATV Reliability, February 23-24, 1977, Atlanta, GA.

<sup>10</sup> - "Thoughts on Bonding and Grounding.....", *ibid.*

<sup>11</sup> - SYSTEM RELIABILITY....., *ibid.*



cathode" operation during periods of excessive overvoltage. This can be achieved by utilizing devices which either have greater thermal capacity<sup>12</sup> or be of such a design as to not ignite until much higher voltages are experienced<sup>13</sup>. Either solution has merit, however, the latter solution requires a special consideration in the design of the transformers used in the cable television amplifiers, specifically those which have a B-H characteristic saturating at 3X supply voltage. Upon application of this suitable combination, equivalent reliability can be achieved.

In summary, the author has found that high watt second crowbar apparatus used in conjunction with gas discharge tubes of substantially improved watt second capability provide adequate protection for CATV amplifiers, especially when utilized in conjunction with improved grounding methods. Alternatively, a higher voltage gas discharge tube used in conjunction with an amplifier transformer which saturates at a voltage such that the electronic apparatus following is not damaged may be employed. The latter solution requires a particular attention to over design of the rectifier and regulator apparatus to be able to withstand the overvoltage which would exist up to the clipping point of the transformer magnetics. Again, either of these solutions are appropriate.

For retrofit, the solution comprised of protective apparatus is perhaps the only realistic answer. In retrofit it is essential to provide  $dv/dt$  filtering networks such that the voltage rate of rise is brought within the safe limits of the devices to be used for crowbar protection. These devices cannot tolerate the rates of rise experienced in most CATV systems, which  $dv/dt$  rates often are 10X those which can be tolerated by the devices used to protect. The author's company manufactures the protective devices required to survive under these conditions under the trade name of the Mark V ARMOR Transient Protection System.

---

12 - SYSTEM RELIABILITY....., *ibid.*

13 - PROTECTING CATV TRANSMISSION EQUIPMENT FROM SURGES, Robert A. Sherwood, GTE Sylvania, Inc., paper presented at the 2nd Annual Conference on CATV Reliability, February 23-24, 1977, Atlanta, GA.

#### SUMMARY

It has been shown that the transient overvoltage induced in the cable television system or equivalent type of networks arrive via the common bond inherited from the power company neutral bonding interconnection. Under these conditions the transient overvoltage presented to the cable television equipment is vastly in excess of the capability of the current transient protective equipment. Suitable devices for protection from this type of transient are found to be available and economically viable.

## APPENDIX

The current flowing on the exterior of the CATV coaxial cable sheath also flows on the interior of the same cable, reduced in magnitude by the following equation:

$$\frac{\text{Current at depth } I_z}{\text{Current on exterior } I_s} = e^{-\frac{z}{\delta}} \quad 1$$

Where:  $z$  = thickness of material, ie., outer wall thickness in Cm.

$\delta$  = "Skin effect" depth in Cm.

$\delta$  is also identified as the depth at which the surface current has been reduced to 36.8% of that value at the surface.

$\delta$  is further defined as follows:

$$\delta = 5033 \sqrt{\frac{\rho}{\mu f}} \quad 1$$

Where:  $\delta$  = skin depth in Cm.

$\rho$  = resistivity of conductor in ohms per  $\text{Cm}^3$

$f$  = frequency in Hz

$\mu$  = magnetic permeability of conductors.  
( $\mu$  of air = 1.0)

Further references provide a plot of "Skin depth" as a function of frequency<sup>2</sup> and conductor thickness<sup>3</sup>. The Figure II plot was derived from these methods.

As can be determined from these plots, power transients have no difficulty invading the CATV plant into the upper kilohertz region.

---

<sup>1</sup> - TERMANS ELECTRONIC AND RADIO ENGINEER, Fourth Edition, pp. 22-23.

<sup>2</sup> - RADIO ENGINEERING, Sandeman, II: 13.1, pp. 37-39.

<sup>3</sup> - TRANSMISSION LINES, ANTENNAE AND WAVE GUIDES, King, Mimno & Wing, p. 13.



THE TRANSIENT RESPONSE OF A TWO-WIRE TRANSMISSION LINE  
INSIDE A MISSILE DUE TO ELECTROMAGNETIC PULSE AND LIGHTNING

by

Abul Rashid  
General Dynamics Convair Division  
San Diego, California

Presented at

Federal Aviation Administration - Georgia Institute of Technology  
Workshop on Grounding and Lightning Protection

May 1978

PRECEDING PAGE BLANK

## ABSTRACT

A missile is represented by a shorted dipole antenna. The frequency spectrum of the current induced on the dipole is expressed in terms of the frequency spectrum of the incident EMP and lightning discharge. The behavior of the currents and their relationships to the impedances and incident fields are described. The electric field inside the missile is expressed in terms of the incident field, the thickness of the missile skin, and the conductivity of the skin. The frequency spectrum of the load currents on a two-wire transmission line is expressed in terms of the frequency spectrums of the transmission line parameters, and the incident EMP and lightning discharges. Waveforms of currents are numerically calculated and represented in graphical forms.

# THE TRANSIENT RESPONSE OF A TWO-WIRE TRANSMISSION LINE INSIDE A MISSILE DUE TO ELECTROMAGNETIC PULSE AND LIGHTNING

Abul Rashid  
Senior Design Engineer  
General Dynamics Convair Division  
San Diego, California

## INTRODUCTION

The operational electromagnetic environment of a present-day missile may consist of the fields produced by nuclear explosion and lightning. Consequently, the electronic system of a missile must be compatible with these electromagnetic fields. Such compatibility depends upon the shielding effectiveness of its structure, layout of interconnecting cables, cable shielding, and sensitivity of equipment within the missile.

There have been numerous studies of the effects of nuclear radiation upon electronic circuitry. Haynes, et al., <sup>(1)</sup> presented results of an investigation of a dipole model for transient analysis of electromagnetic field coupling into long cables. The dipole model representation of a cable is the worst-case representation and may never be practically realized. One result of relying upon such a model would be expensive overdesign of a missile system.

The most cost-effective design would be one in which the design is based upon realistic representation of a field-to-wire coupling model. Current missile wiring practice is to not use the missile skin as a return path; instead, two separate wires are used for each transmission of information from item of equipment to another.

Mathematical formulas are available in the literature to calculate the response of a two-wire transmission line to a plane-wave field. These formulas are combined with formulas for an electrical field within a cylindrical enclosure in terms of the incident field and the conductivity and thickness of the structure to develop a mathematical model to calculate both the frequency and time-dependent load currents of a two-wire transmission line inside a missile. A mathematical model representing the response of a two-wire line is developed for both lightning and electromagnetic pulse (EMP) excitation of a missile and is presented in this paper.

## RESPONSE OF A TWO-WIRE TRANSMISSION LINE

The time and frequency domain representations of an EMP and lightning may be shown to be:<sup>(1,2)</sup>

$$E(t) = C [ \exp (-At) - \exp (-Bt) ] \quad (1)$$

and

$$E(w) = C \left\{ \left[ \frac{A}{A^2 + w^2} - \frac{B}{B^2 + w^2} \right] + j \left[ \frac{w}{B^2 + w^2} - \frac{w}{A^2 + w^2} \right] \right\} \quad (2)$$



for EMP

$$C = 5.2 \times 10^4, \quad A = 1.5 \times 10^6, \quad \text{and } B = 2.6 \times 10^6$$

for lightning

$$C = 6.8 \times 10^5, \quad A = 1.3 \times 10^6, \quad \text{and } B = 10^6$$

Consider the incidence of an EMP or lightning strike upon a missile that, for the purpose of analysis, is represented as a hollow cylinder, as shown in Figure 1. Harrison and King<sup>(3)</sup> derived Eq. 3 to calculate the electric field within a hollow cylinder in terms of the external field.

$$\frac{E_z(w, a_1)}{E_z(w, a_2)} = \sqrt{\frac{a_2}{a_1}} \left\{ \frac{1}{\cos [K_m (a_2 - a_1)]} \right\} \quad (3)$$

and

$$E_z(w, a_2) = \frac{2 l_e}{\pi Z_{in}} \frac{E_z^i}{\sigma a_2^2} \left( \frac{K_m a_2}{2} \right) \cot [K_m (a_2 - a_1)] \quad (4)$$

where:

$E_z^i$  is the incident electric field

$a_2$  is the outer radius of the cylinder

$a_1$  is the inner radius of the cylinder

$$K_m = (1-j) \sqrt{\frac{w \mu \sigma}{2}} \quad (5)$$

where:

$w = 2\pi f$ ,  $f$  is the frequency in Hz.

$\sigma$  = conductivity of the skin.

$l_e$  = effective length of cylinder acting as a shorted dipole antenna.

$Z_{in}$  = input impedance of the cylinder

From Eq 3 and Eq 4, we have

$$E_z(w, a_1) = \frac{2 l_e}{\pi} \frac{1}{\sigma a_2^2} \frac{E_z^i(w)}{Z_{in}(w)} \left( \frac{K_m a_2}{2} \right) [\sin K_m (a_2 - a_1)]^{-1} \quad (6)$$

Now, consider a two-wire transmission line located just inside the cylinder, as shown in Figure 1. It is desired to calculate the load currents of this line when it is excited by a transient field whose frequency spectrum is described by Eq 2. Harrison, et al.,<sup>(3)</sup> derived the following formula to calculate the load current of a two-wire transmission line due to an incident plane wave as:

$$I(w, h) = -j \frac{2}{\gamma D} E_z(w, a_1) \sin \left( \frac{K_1 b}{2} \right) [Z_c \sinh 2 \gamma h + Z_h (\cosh 2 \gamma h - 1)] \quad (7)$$

$$I(w, h) = -j \frac{2}{\gamma D} E_z(w, a_1) \sin \left( \frac{K_1 b}{2} \right) [Z_c \sinh 2 \gamma h + Z_h (\cosh 2 \gamma h - 1)] \quad (8)$$

where  $2h$  is the length of the line

$$\gamma = \sqrt{ZY} \quad (9)$$

$$Z = Z^i + j w l^e \quad (10)$$

$$z^i = \frac{1}{\pi a_1} \sqrt{\frac{w\mu}{2\sigma}} (1 + j) \quad (11)$$

$$l^e = \frac{\mu}{\pi} \ln \left( \frac{a_2}{a_1} \right) \quad (12)$$

$$Y = j \frac{K_1^2}{w l^e} \quad (13)$$

$$K_1 = \frac{2\pi}{\lambda} \quad (14)$$

where

$b$  = spacing between wires

$Z_h$  = load impedance at  $z = h$

$Z_{-h}$  = load impedance at  $z = -h$

$$Z_c = \sqrt{\frac{Z}{Y}} \quad (15)$$

$$D = Z_c (Z_h + Z_{-h}) \cosh 2 \gamma h + (Z_h Z_{-h} + Z_c^2) \sin h 2 \gamma h \quad (16)$$

It may be seen from Eq 4, 7, and 8 that the load currents of a two-wire transmission line within a missile depends upon the input impedance of the missile structure. The length of current missiles is very small compared to the wavelengths of the frequency contents of an EMP. Under this condition, the input impedance of the dipole-represented missile<sup>(4)</sup> is:

$$Z_{in}(w) = 20 (2\pi/\lambda)^2 - j 120 (2\pi l/\lambda)^{-1} (\log 2 l/a - 1) \quad (17)$$

where

$l$  is the half-length of the missile

$a$  is the radius of the missile

$\lambda$  is the wavelength

Eq 7 and 8 may be used to calculate the frequency domain response of a two-wire transmission line within a missile. The time domain response of the line may be obtained by taking the Fourier integral of Eq 7 and 8. Such an integration may be evaluated numerically.

The above equations have been used to calculate the two-wire transmission line responses within a missile due to EMP and lightning for the following values of the missile:

$l = 110$  inches

$a_2 = 0.104$  inch

$a_1 = 0.049$  inch

Figures 2 through 8 present results of these calculations for EMP; Figures 9 through 14 are results for lightning. The plots show the frequency spectrum of both EMP and lightning, the impedance, and load currents, the electric field within the missile, and the time domain response of the load current. The time waveform calculation shows that the rise time of the load current is much higher than the rise time of the incident pulse.

#### ACKNOWLEDGMENT

The author is indebted to Michael F. Derr for his assistance in preparing this paper.

#### REFERENCES

1. Haynes, W. H. and Wilkerson, C. L., "Investigation of a Dipole Model for Transient Analysis of Electromagnetic Field Coupling into Long Cables," *IEEE Trans. on Electromagnetic Compatibility*, Vol EMC-12, No. 3, August 1970, pp 112-117.
2. Robb, J. D., et al., "A Joint Study on Lightning Effects for the B-1 Program," coordinated by E. S. Hughes, 1972 Lightning and Static Electricity Conference, AFAL-TR-72-325, December 1972, p 512.
3. Harrison, Jr., C. W., and King, R. W. P., "Response of a Loaded Electric Dipole in an Imperfectly Conducting Cylinder of Finite Length," *J of Research*, National Bureau of Standards — D. Radio Propagation, Vol 64D, No. 3, May-June 1960.
4. Harrison, Jr., C. W., and Houston, M. L., "The Response of a Terminated Two-Wire Line Buried in the Earth and Excited by a Plane-Wave RF Field Generated in Free Space," *IEEE Trans. on Electromagnetic Compatibility*, Vol EMC-11, No. 4, September 1969.
5. Tai, C. T., "Characteristics of Linear Antenna Elements," *Antenna Engineering Handbook*, H. Jasik, ed., McGraw-Hill Book Co., 1961, p 3-2.

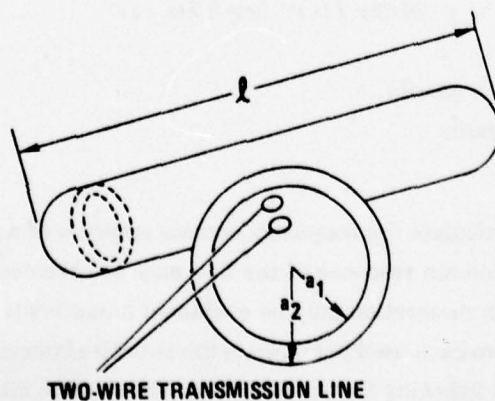


Figure 1. Hollow cylinder representation of a missile.



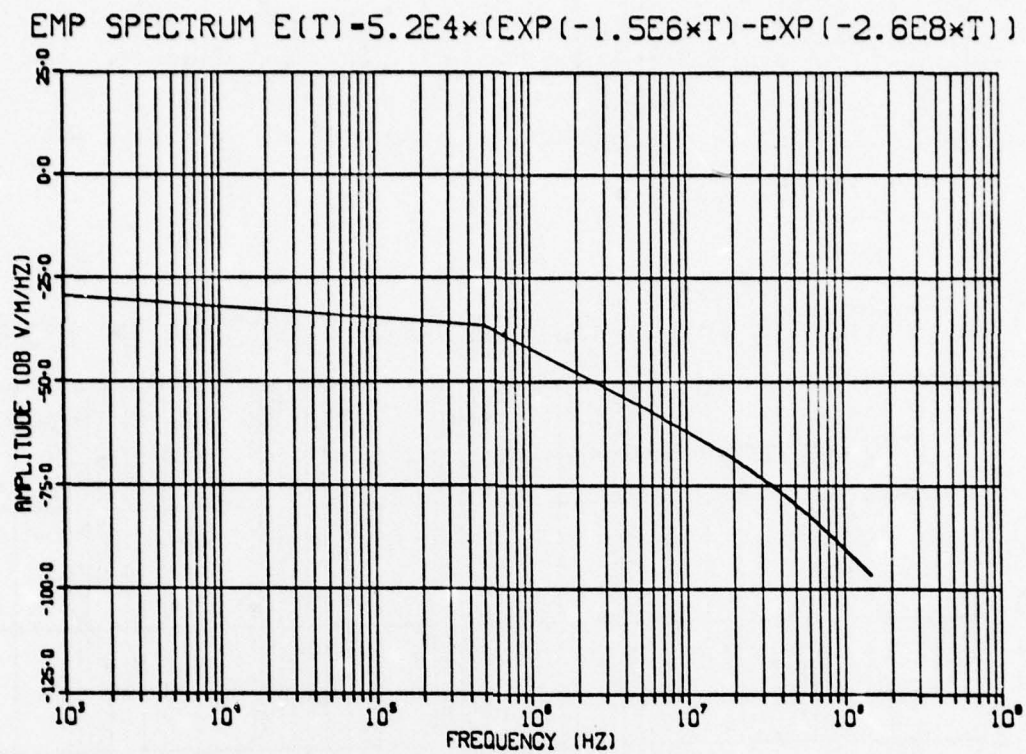


Figure 2. EMP frequency spectrum.

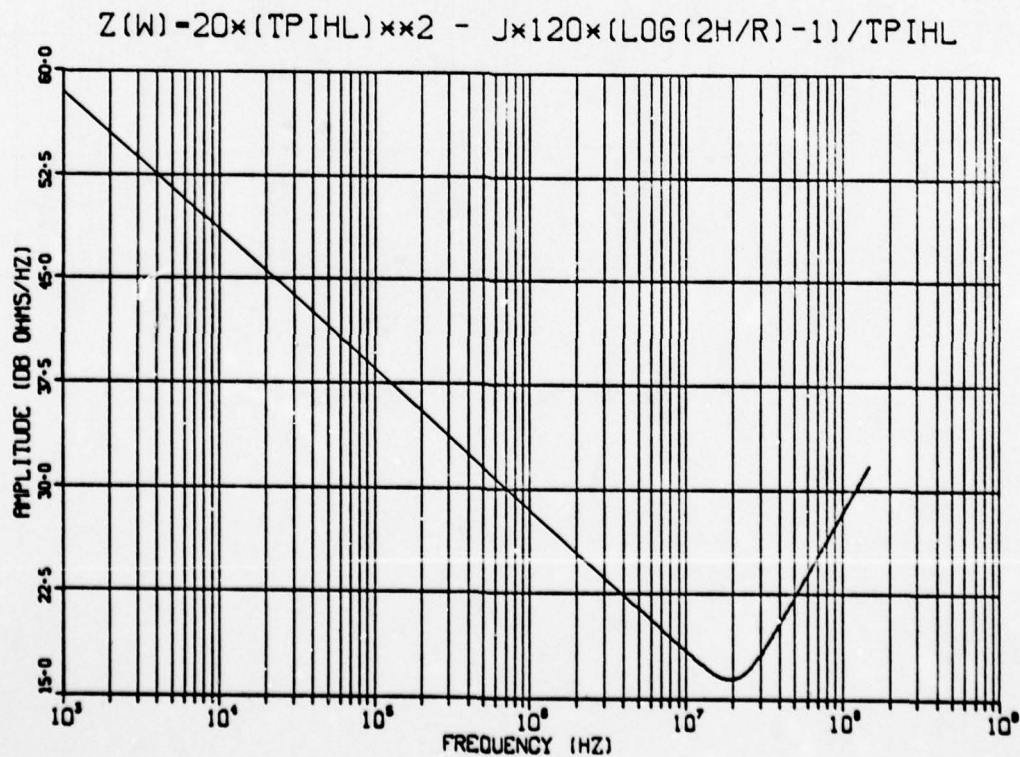


Figure 3. Impedance of the missile.

### 3 INTERNAL HULL VOLTAGE AS A FUNCTION OF FREQUENCY

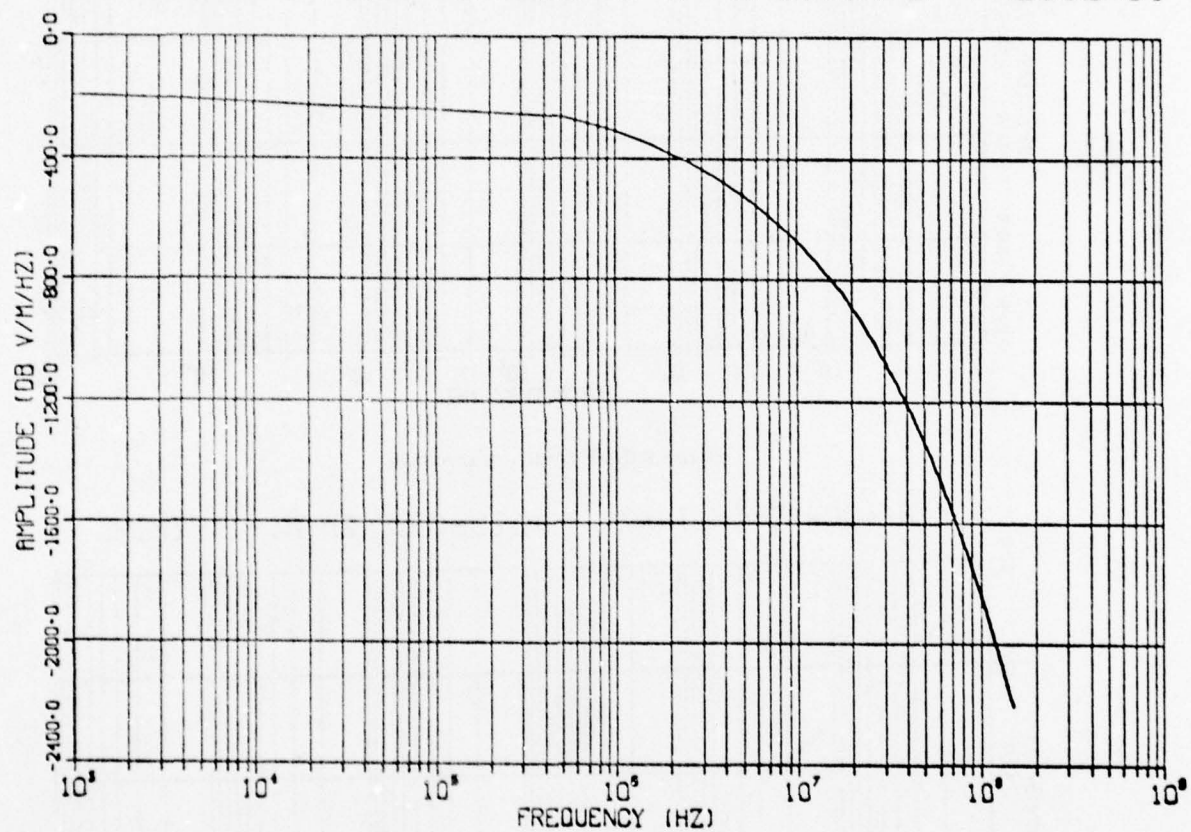


Figure 4. Electric field intensity within missile.

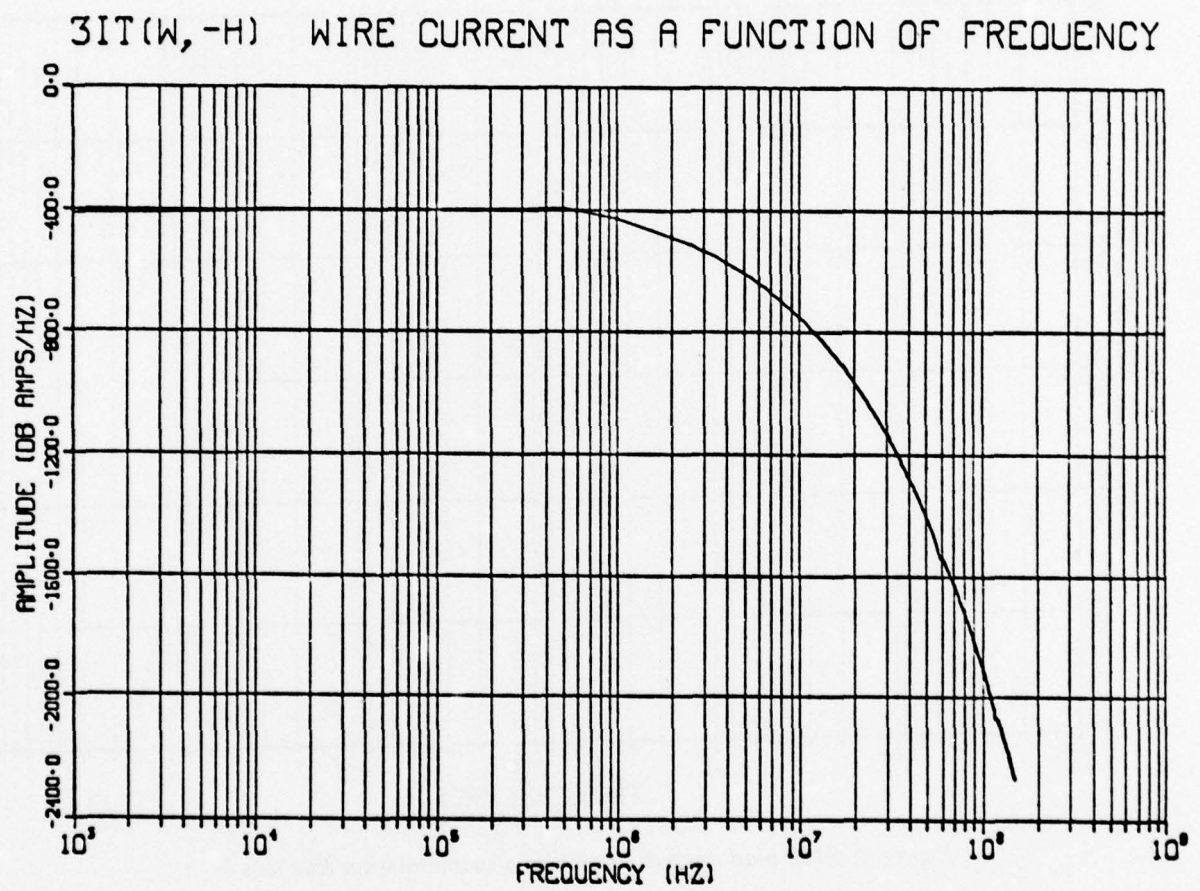


Figure 5. EMP load current spectrum of transmission line at  $z = -h$ .



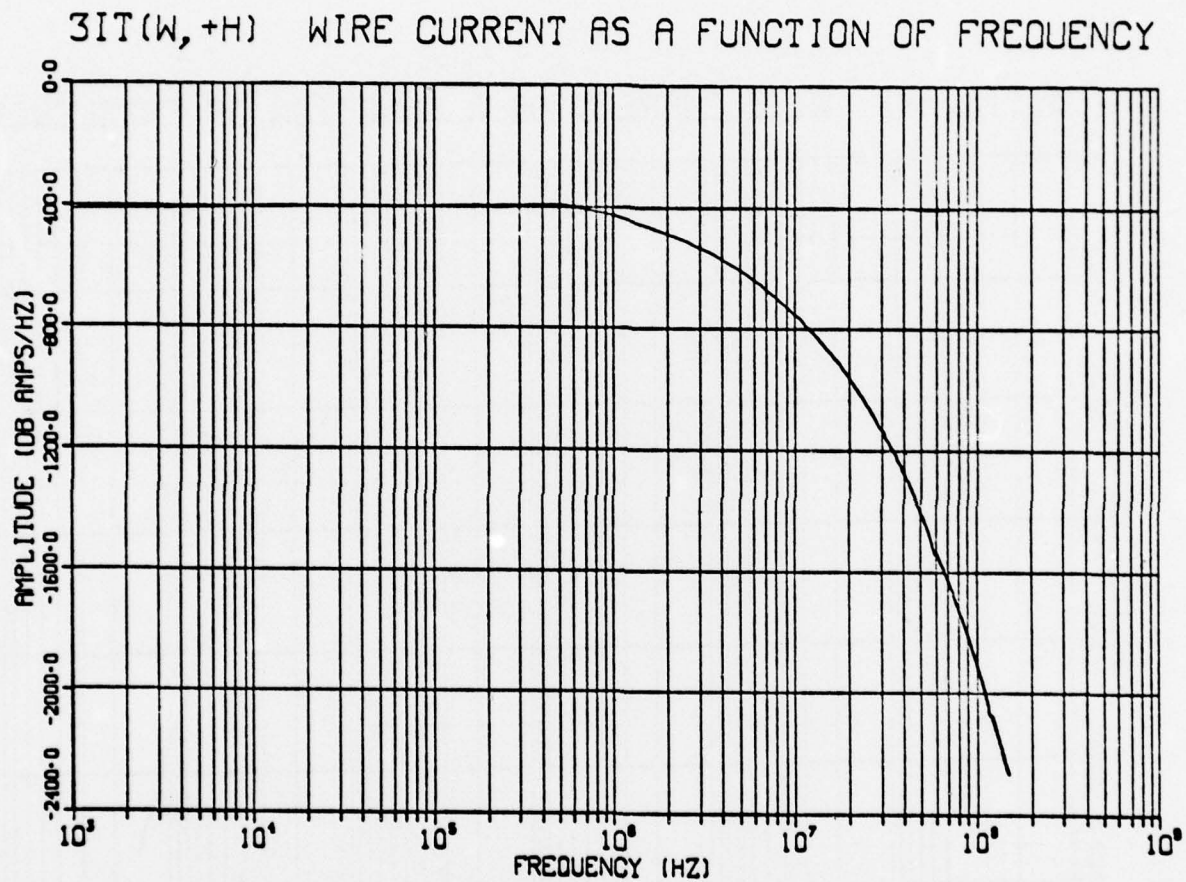


Figure 6. EMP load current spectrum of transmission line at  $z = h$ .

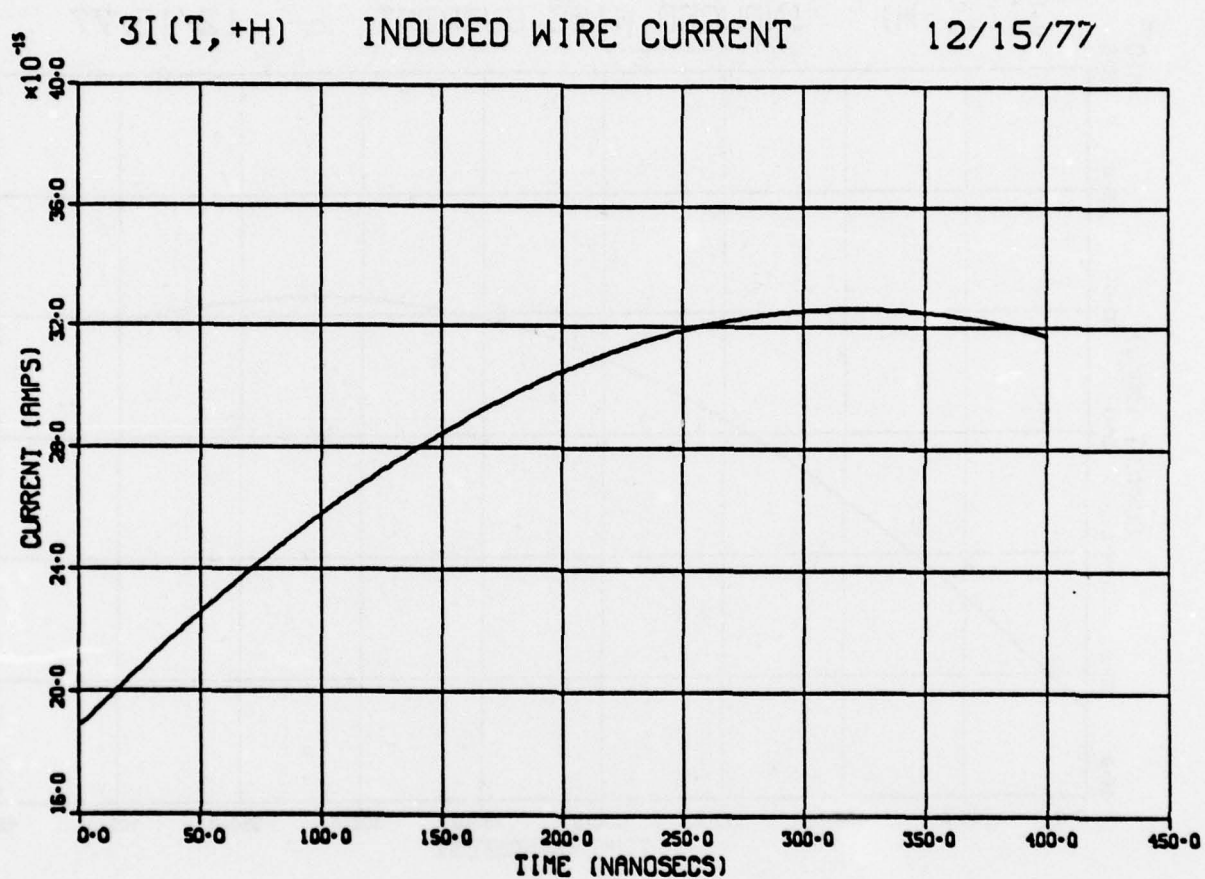


Figure 7. EMP load current waveform of transmission line at  $z = -h$ .

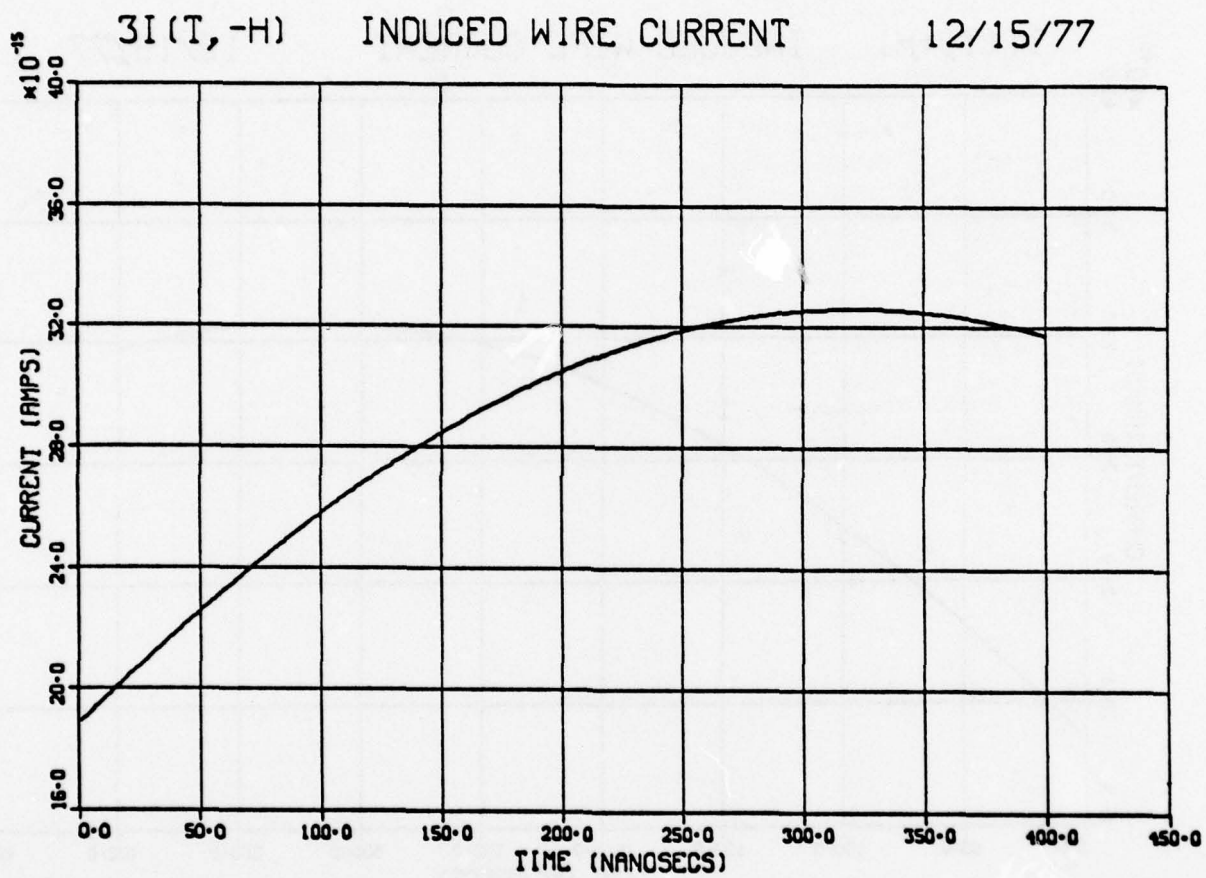


Figure 8. EMP load current waveform of transmission line at  $z = h$ .



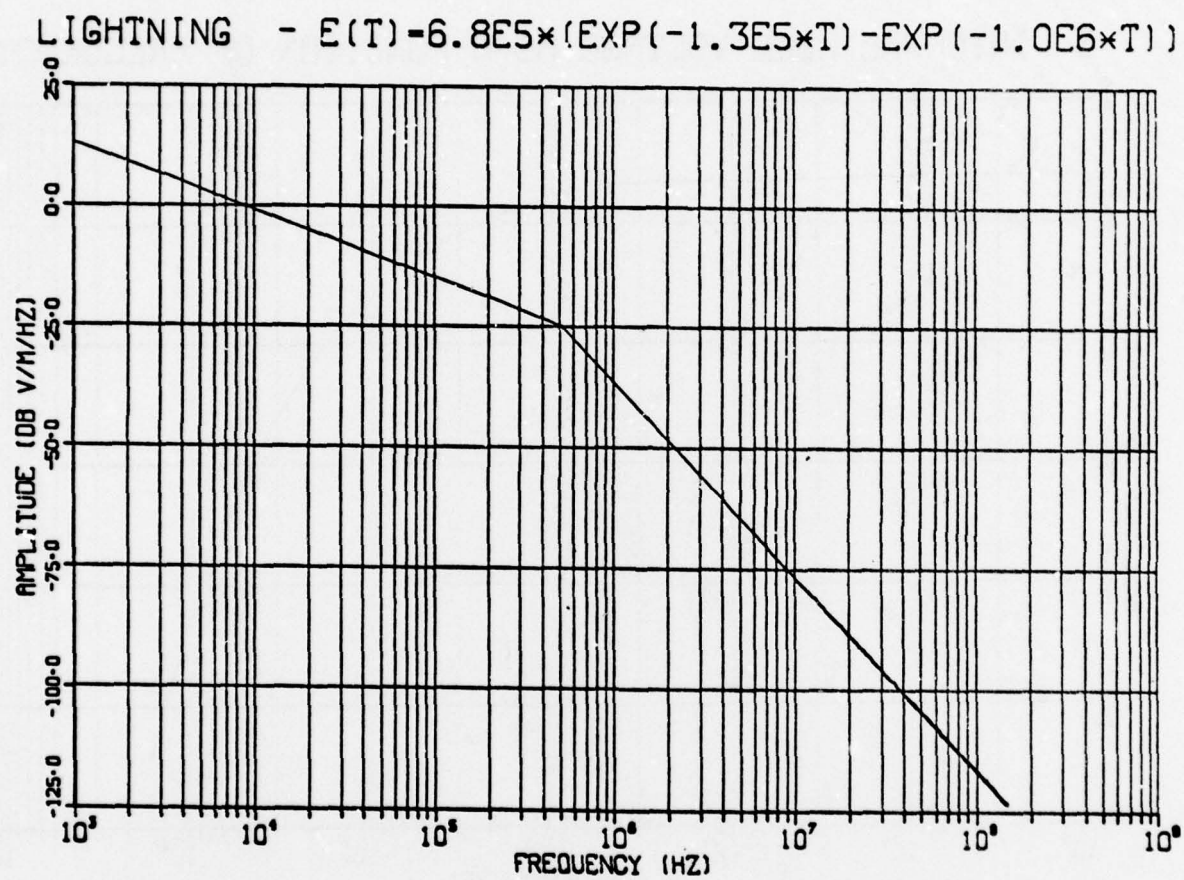


Figure 9. Lightning frequency spectrum.

### 3 INTERNAL HULL VOLTAGE AS A FUNCTION OF FREQUENCY

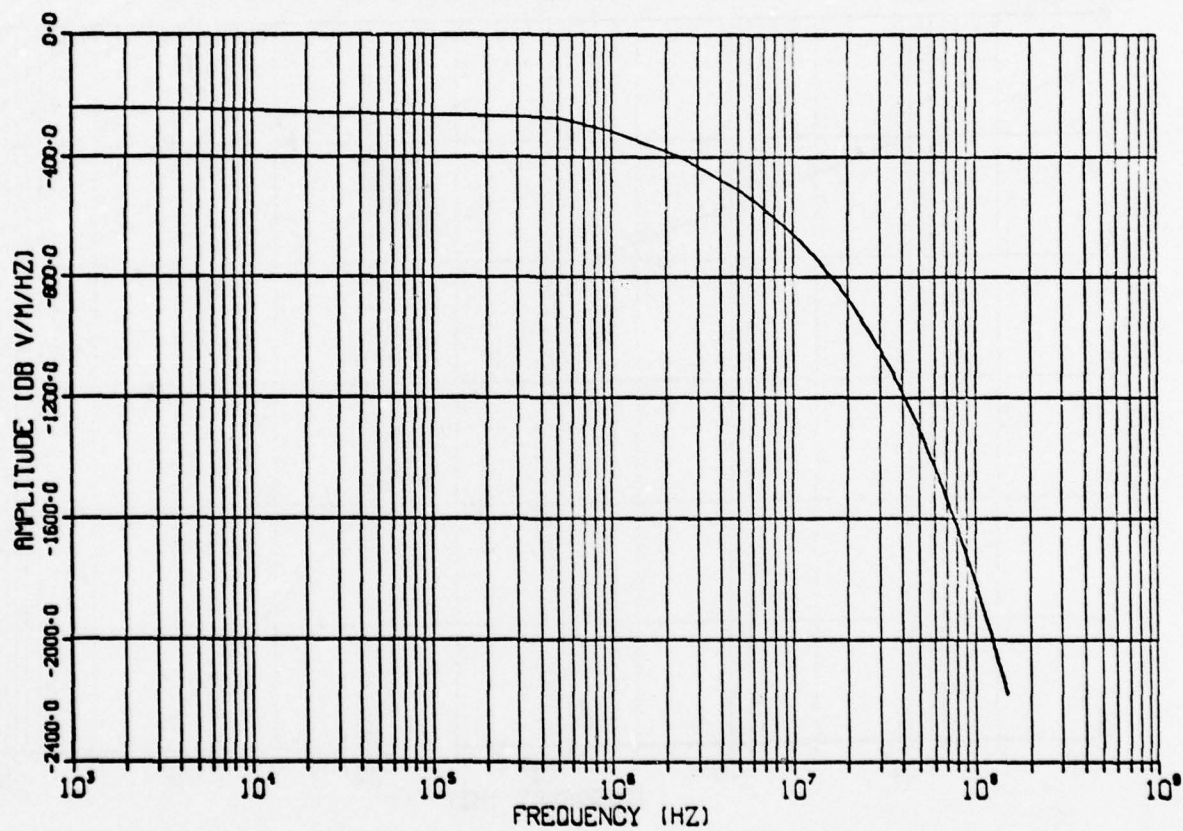


Figure 10. Electric field intensity within missile due to lightning.

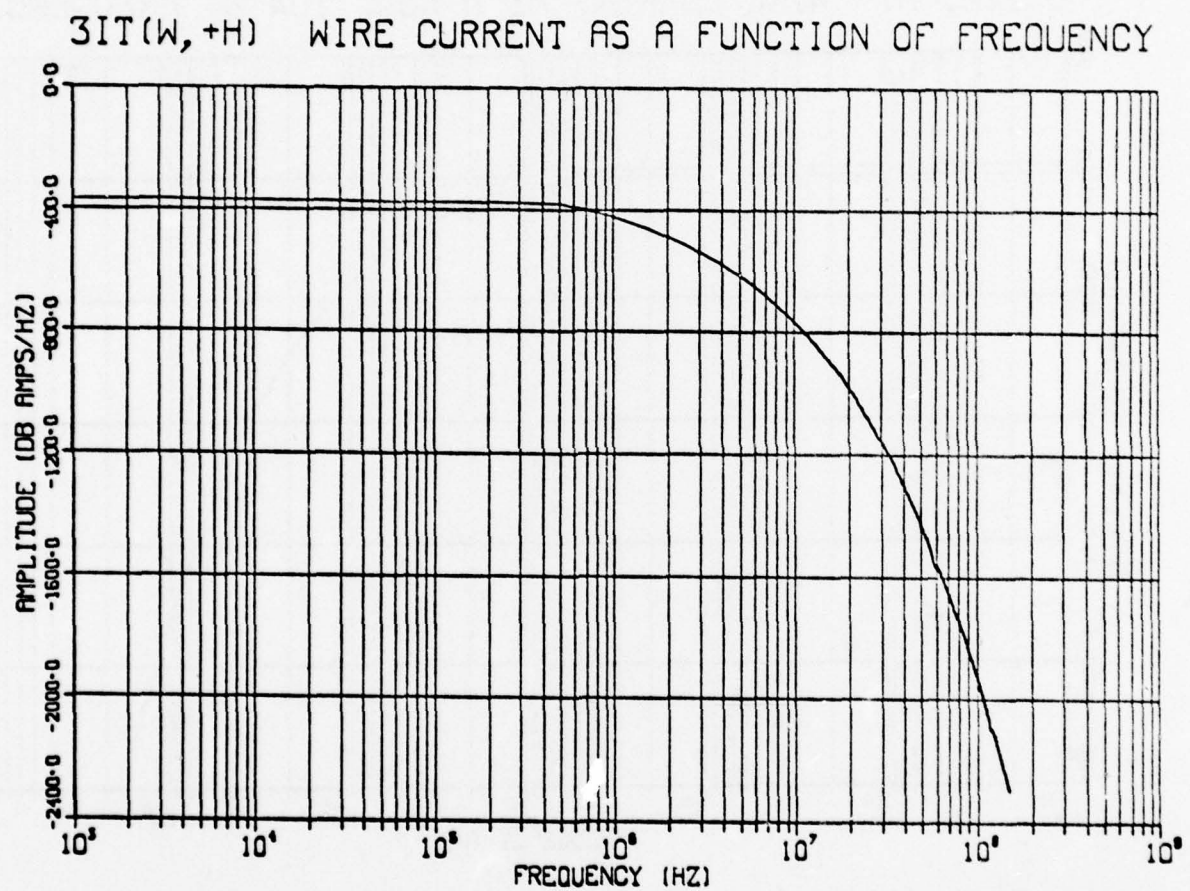


Figure 11. Lightning load current frequency spectrum of transmission line at  $z = -h$ .



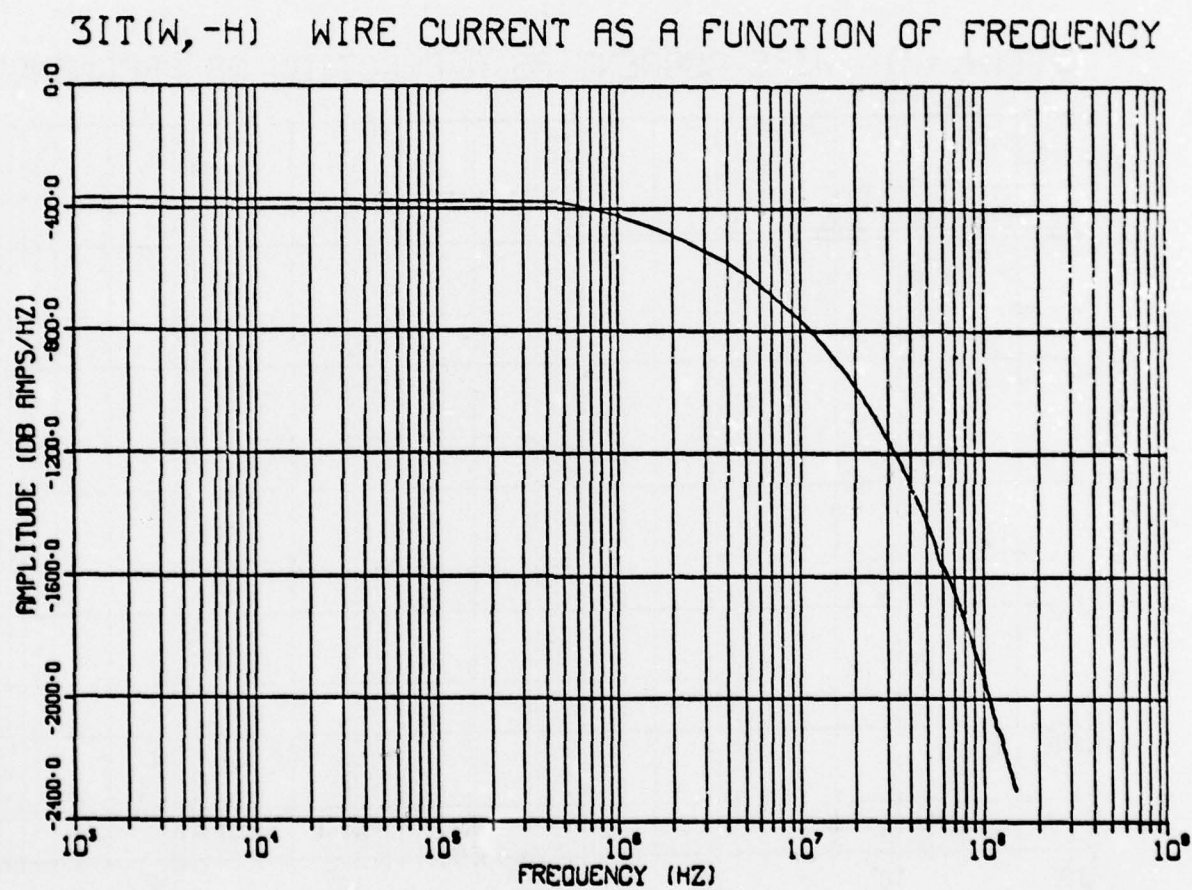


Figure 12. Lightning load current frequency spectrum of transmission line at  $z = h$ .

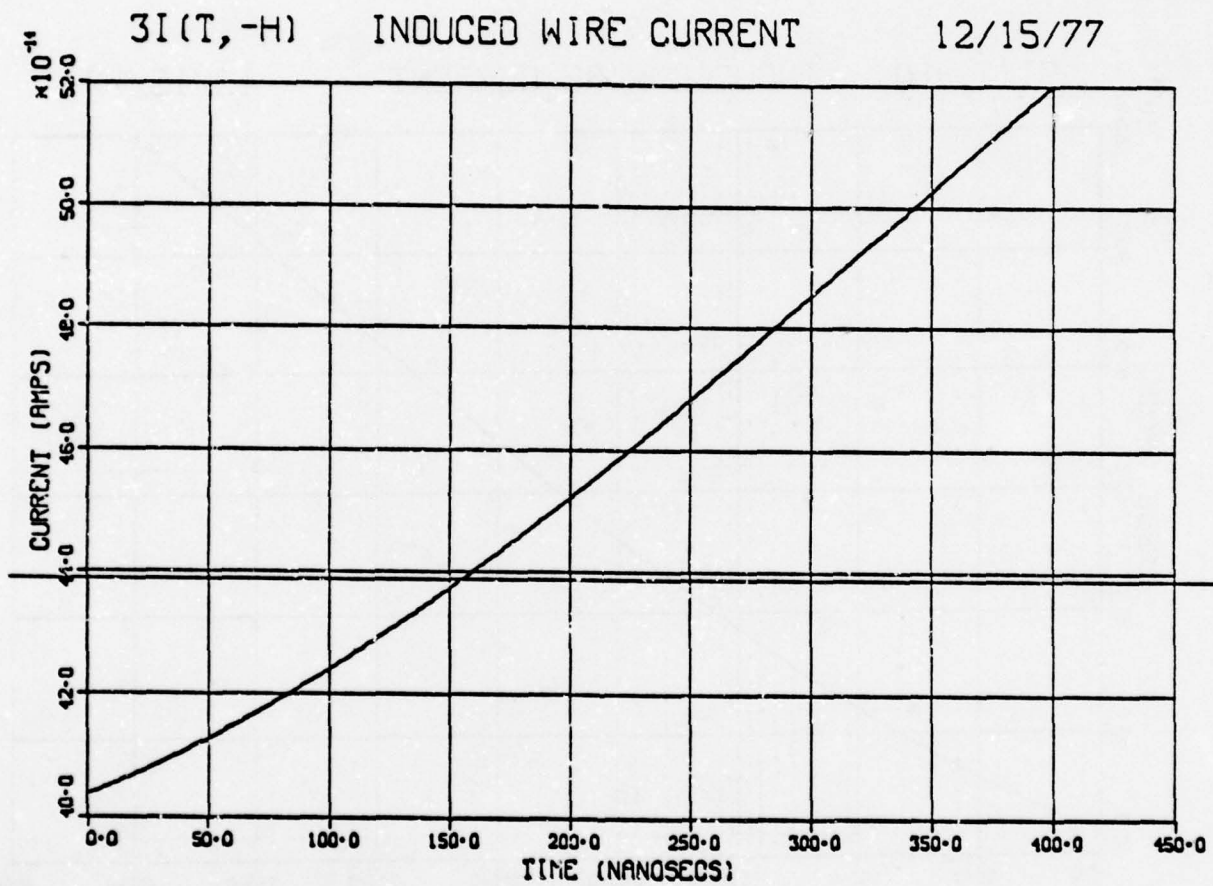


Figure 13. Lightning load current waveform of transmission line at  $z = -h$ .

AD-A058 797

GEORGIA INST OF TECH ATLANTA

F/G 4/1

FEDERAL AVIATION ADMINISTRATION-GEORGIA INSTITUTE OF TECHNOLOGY--ETC(U)

MAY 78

UNCLASSIFIED

FAA-RD-78-83

NL

4 of 5

AD  
A058 797





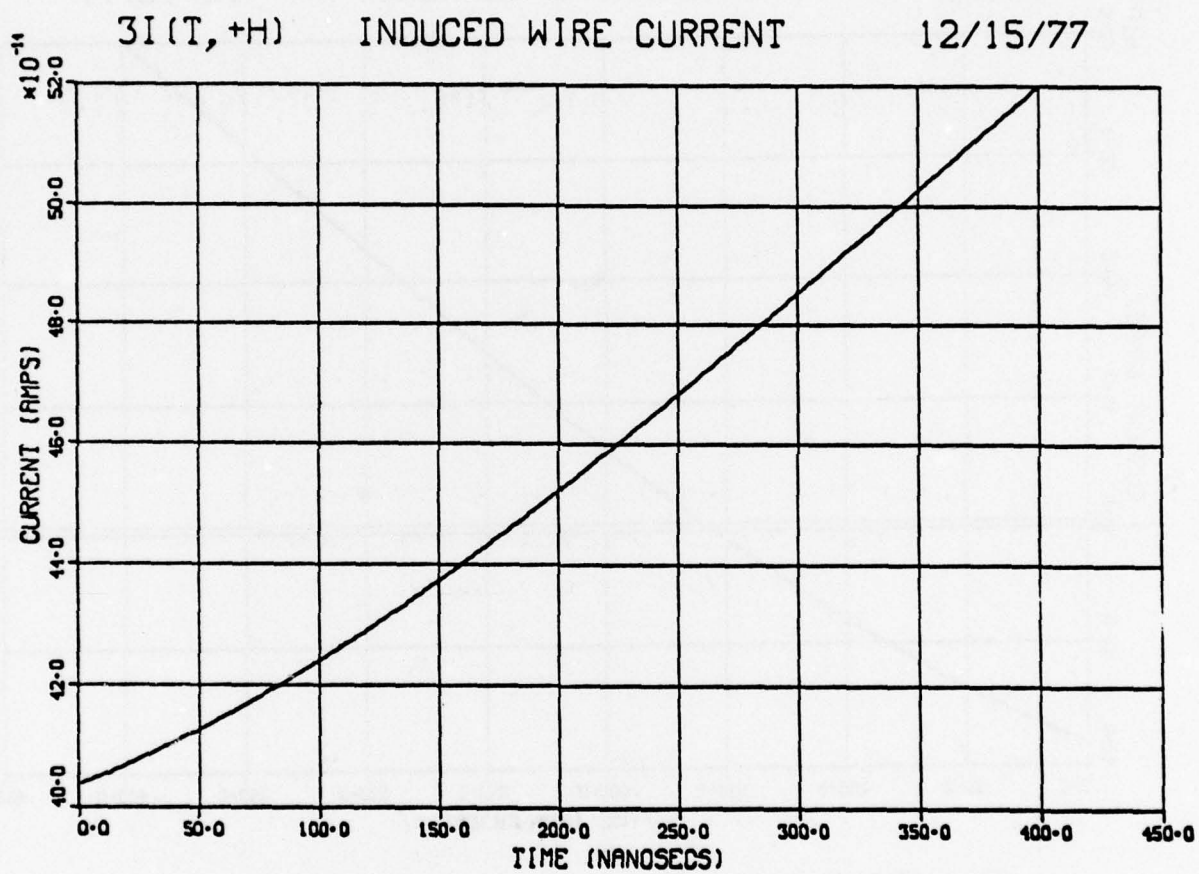


Figure 14. Lightning load current waveform of transmission line at  $z = h$ .

**LABORATORY SIMULATION OF NEAR-BY  
LIGHTNING INDUCED ELECTRICAL TRANSIENTS**

**By**

**J. E. Lee, W. G. Butters, and R. J. Lauber**

**LIGHTNING SIMULATION LABORATORY  
MCDONNELL AIRCRAFT COMPANY  
ST. LOUIS, MISSOURI**

**Presented at  
Federal Aviation Administration/  
Georgia Institute of Technology  
Workshop on Grounding and Lightning Protection**

### ABSTRACT

This paper describes the continued development of a test technique for simulating lightning induced voltages on aircraft cable runs. The goal of the R&D Program is to adequately reproduce the induced voltages generated by all aspects of lightning environment (i.e., near miss, pre-strike, direct strike voltage and return stroke current). The major area discussed in this paper is the near miss condition.

A test approach is discussed that produces a well-controlled transient electromagnetic (EM) wave. This wave irradiates the test specimen and induces voltages which can be adjusted by changing the magnitude and frequency content of the incident EM wave.

*The electromagnetic wave is produced by simulators that are similar to those used for nuclear EMP studies but which have been specially designed to create the lightning type waveform. Shielded Marx surge generators are used to produce the high voltage driving pulse applied to the Lightning Electromagnetic Pulse (LEMP) bounded-wave simulator.*

Preliminary results using this newly developed technique show that extreme care must be taken in conducting ground-based tests of aircraft electrical circuits. With proper care, voltages induced in certain test specimens can be related quantitatively to the laboratory generator output parameters.



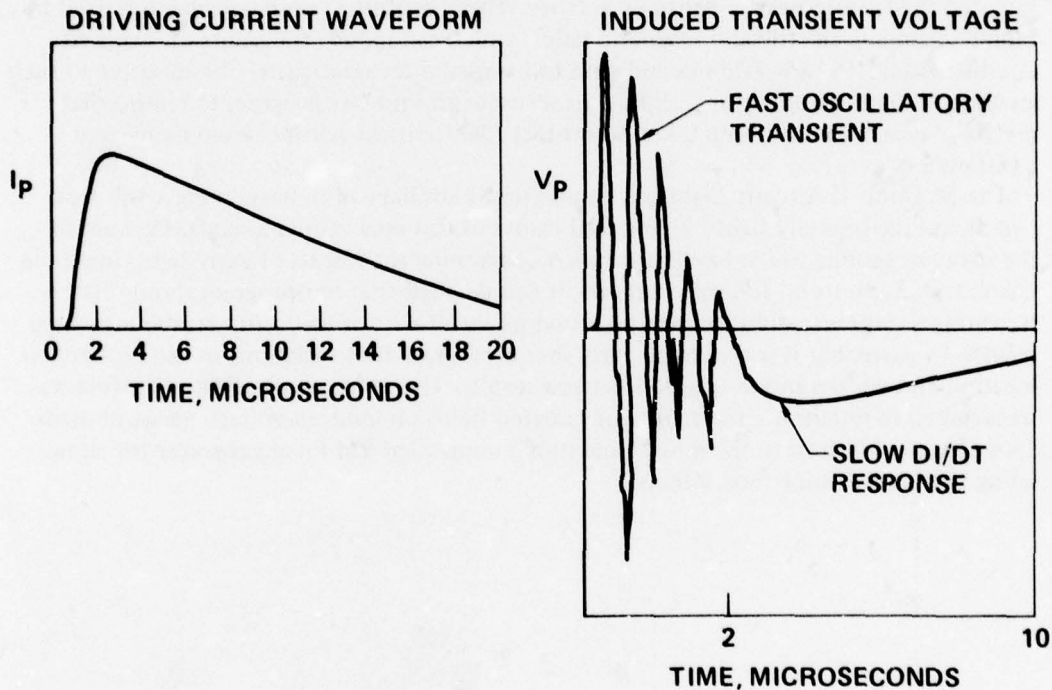
## 1.0 INTRODUCTION

Aerospace vehicles operating in a thunderstorm environment are often exposed to radiated fields from nearby lightning activity. These lightning events are characterized by rapidly changing electric and magnetic fields, which can induce transients on exposed aircraft wiring.<sup>1,2</sup> New avionics and data transmission techniques may be sensitive to such an environment and therefore, require an accurate ground test program to ensure that adequate measures have been taken to protect flight critical avionics from damage or malfunction.

The McDonnell Aircraft Lightning Simulation Labs have been developing a full-scale test technique to study lightning induced transients on operational aircraft. Because of the many questions which have been raised concerning the results of early lightning simulation test attempts on full-scale aircraft, it was decided that our program should first resolve the very difficult questions surrounding the effects of test setup on the measured results. In particular it was noticed early in our program that variations in test equipment location and configuration could affect test results. Therefore, a concentrated effort was undertaken to determine the effects of radiated fields on induced voltage measurements. This effort led in turn to the development of a controlled EM Field generator for simulating natural lightning field effects.

## 2.0 BACKGROUND

Most of the early work in lightning simulation testing for induced coupling effects has concentrated on the return stroke current pulse as the most significant factor of the lightning environment. Tests on full-scale aircraft have used various current waveforms passed through the aircraft structure to produce transients on internal wiring.<sup>3,4,5</sup> These return stroke current tests are conducted by driving a scaled down (magnitude) lightning current waveform through the aircraft under test. The voltages induced on the aircraft wiring are then extrapolated to full threat level by a multiplication factor, calculated as the ratio of the threat level value to the test current value. Figure 1 shows the waveform generally used and the typical transient response.



GP78 R333 17

Figure 1. Lightning Induced Transients

A number of workers in this field have observed that the transients produced on aircraft wiring by such tests generally exhibit two principal components. The first component is a fast damped oscillatory transient rising to peak near time zero (when the driving waveform is initiated) and decaying rapidly to zero. The total duration of this component is seldom more than a few microseconds and the oscillatory frequency can generally be related to the particular circuit under test. This transient is particularly noticeable on high impedance circuits.

The second component of the transient is a slower waveform which can be related directly to the driving current waveform. This component is observed only when the test circuit is susceptible to magnetic (or IP) coupling and is not generally observed when measuring wire to wire (differential) responses in shielded circuits.

The nature of the fast component (damped oscillatory train) has led some workers to consider it entirely as an artifact of the test system.<sup>4,6</sup> Others have interpreted it as a direct response to the driving current waveform and have scaled it upward by the multiplication factor. Earlier MCAIR work reported in Reference 7 showed that the fast transient is real, and is, in fact, observed by simply pulsing the structure with a voltage pulse with no return stroke current flowing at all (system isolated from ground).

Although it is clear from such tests that the fast transient is not produced solely by return stroke currents, the true source of the transient remain to be quantitatively identified and characterized, even in the laboratory. When that is done it will still remain to determine the relationship between the laboratory and flight environments and establish the correct scaling factor or factors.

**INSTRUMENTATION.** Insights into the effects of radiated electric fields on induced voltages was obtained during an R&D test performed for the Naval Air Systems Command.<sup>8</sup> That program required the development of highly reliable and accurate electric field (E-field) sensors and instrumentation capable of measuring the magnitude and waveforms of transient electric fields. Most conventional E-field sensors disturb the field being measured and thus somewhat affect the overall test. This problem was minimized by combining a capacitive E-field sensor with a high bandpass fiber optic transmission system. The shape of the sensor is spherical, thus giving very little disturbance of the measured E-field. Figure 2 shows a photograph of the sensor and a schematic equivalent circuit. The sensor is basically a dipole antenna which is designed to withstand high intensity electric fields without corona discharge and which has a wideband response (able to measure from kilohertz to megahertz frequencies).

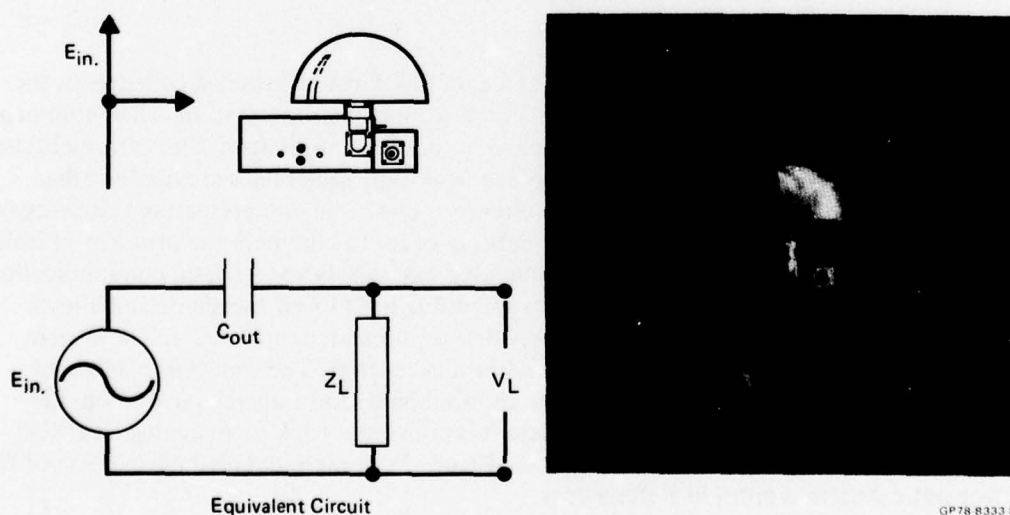


**Figure 2. Spherical Sensor with Fiber Optic Transmitter**



Figure 3 shows a complete block diagram of the general setup of test instrumentation for transient data recording. Data is recorded in both the frequency and time domain. The data is stored on magnetic tape using a HP/9825 minicomputer.

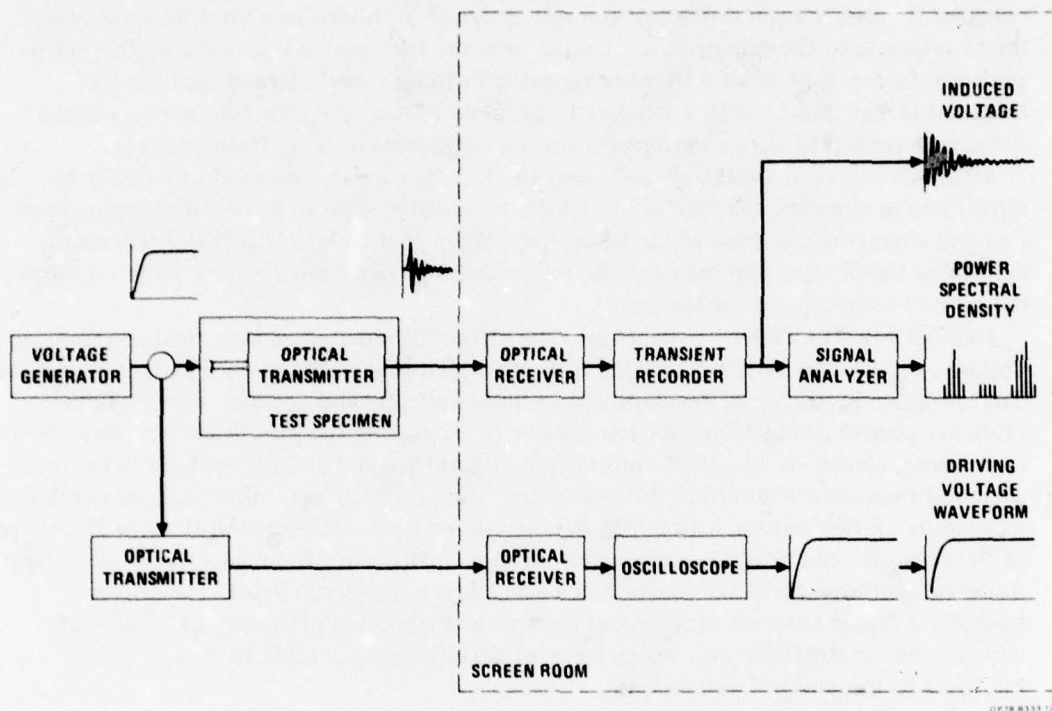


Figure 3. Test Instrument Option

To obtain information from the cylinder a data link must be established between the test specimen (cylinder) and the measurement/recording instrumentation. The equipment is placed in an RFI shielded enclosure to prevent induced transients in the instrumentation. It has been noted that even when well shielded coax type signal lines are used for data transmission into the shielded room, interference is produced and premature triggering of instrumentation often occurs, giving false data. In order to eliminate the problem of isolation from transients, fiber optics systems are used exclusively for all data, communications and control. The fiber optic system is not susceptible to induced transients and allows complete high voltage isolation of the test article as illustrated in Figure 4. The system consists of a transmitter, fiber transmission line and receiver. The transmitter takes an analog electrical input signal, converts it to infrared light, and transmits it through the fiber transmission line to the receiver, where it is converted back to an analog electrical signal to be fed into a transient recorder (see Figure 3). A more detailed description of the fiber optic system is given in Reference 6.

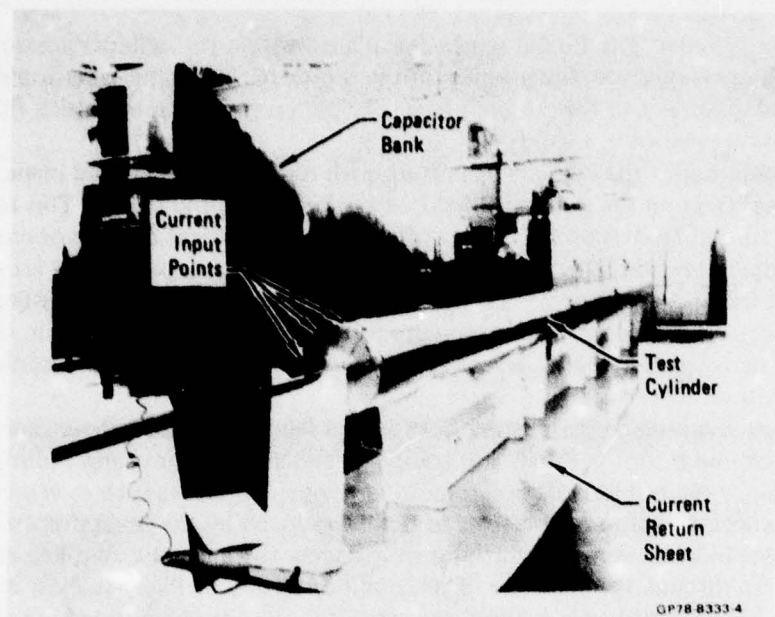


Figure 4. Simulated Fuselage

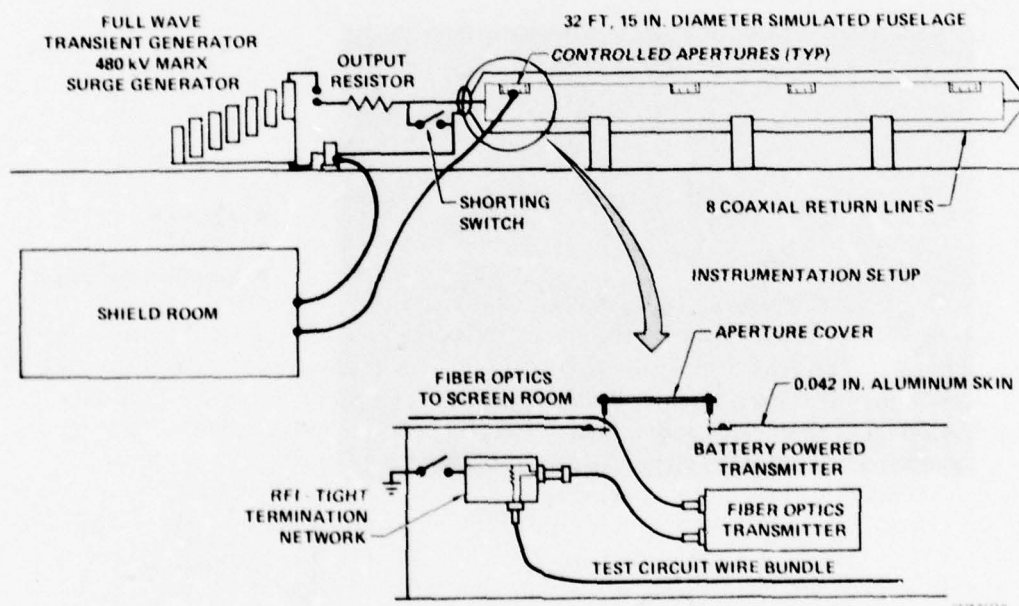


Figure 5. Test Setup for CRAD Test

**TEST PROGRAM.** Figure 5 shows the basic test configuration used during the Navy R&D program. The 32-foot long cylinder was used as the test specimen and was equipped with interchangeable aperture covers. The cylinder was tested in several ground return configurations as explained in Reference 7. However, the most important information of concern here is that which was obtained with the planar ground return. As shown in Figure 5, a 400 kV Marx surge generator was used to apply a  $2 \times 50 \mu\text{sec}$  current wave-

form to the cylinder. The E-field sensor was placed within the cylinder adjacent to a 12-inch square open aperture; the position of the sensor remained the same while the cylinder was rotated in respect to the ground plane. The data resulting from pulsing the different orientations are shown in Figures 6, 7, 8 and 9.

The orientation of the cylinder's aperture with respect to the ground plane had a tremendous effect on the internal E-field, as can be seen in the figures. This test result prompted further studies on the effects of generator placement and the orientation of transmission and return lines with respect to various apertures on the test article. It was found that the magnitude of voltages induced on wire pairs in the cylinder could vary over a wide range depending on the test configuration and aperture orientation. (Since shielded wire pairs were generally being used, only the fast oscillatory transient described earlier was being observed.)

These test results carry serious implications for laboratory tests where generator placement and ground return paths are arbitrarily set and adjusted or changed during the course of a test. Since the test aircraft is certain to have open apertures such as canopies, radomes, wheel wells, etc., the effects of fields produced by the generator driving voltage may produce induced voltages which far overshadow the magnetic coupling effects of the current pulse through the structure. This condition would be likely to exist especially when very low current levels are used and when the circuits being tested are reasonably well shielded from magnetic flux coupling.

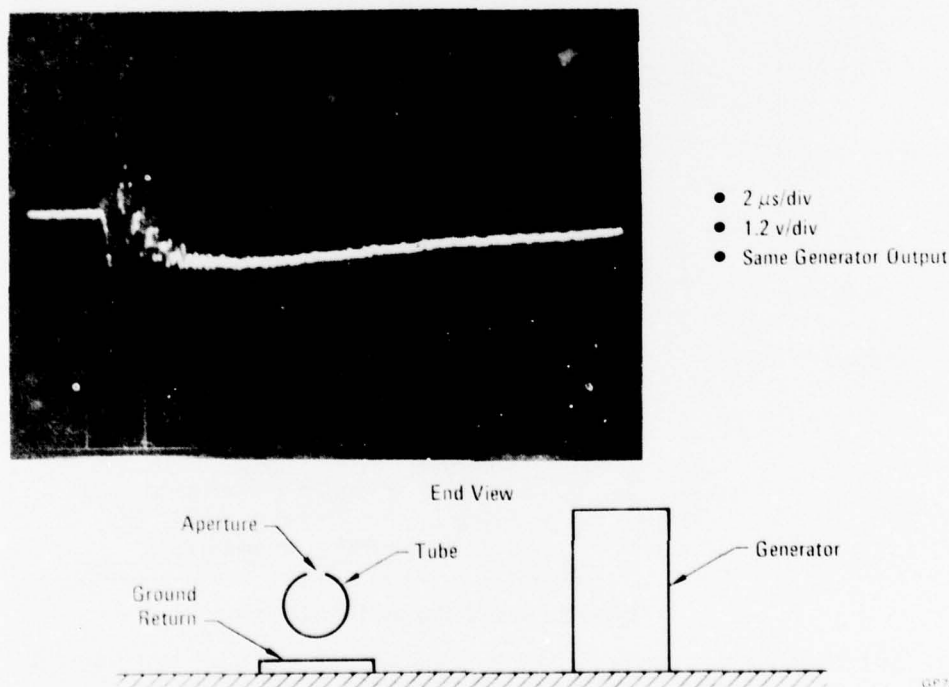
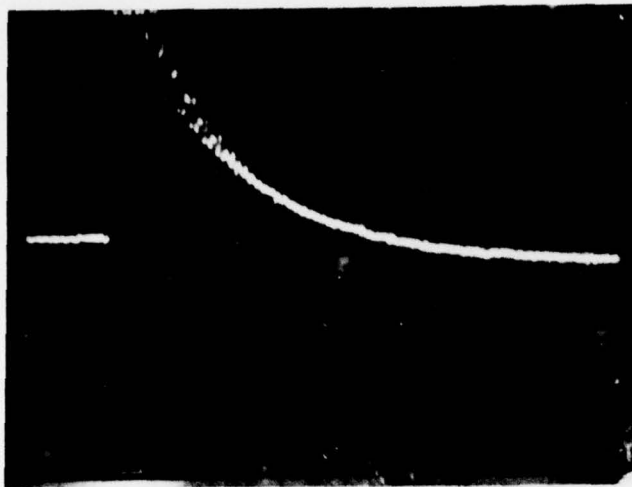


Figure 6. E-Field Sensor  
Open Aperture Away From Current Return





- $2 \mu\text{s}/\text{div}$
- $1.2 \text{ v}/\text{div}$  (Saturated Upper Signal Limit)
- Same Generator Output

End View

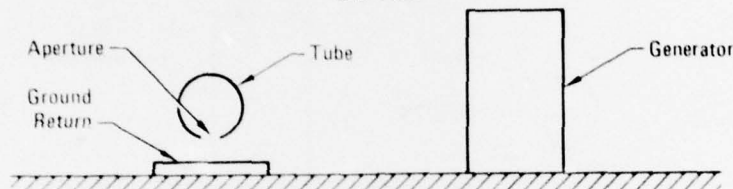
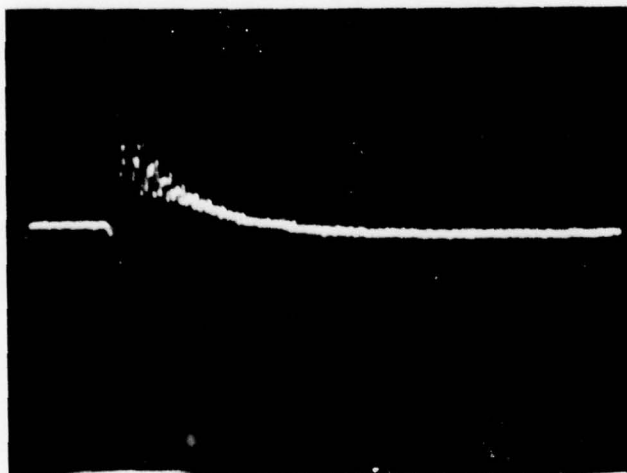


Figure 7. E-Field Sensor  
Open Aperture Toward Current Return

GP78 8333-12



- $2 \mu\text{s}/\text{div}$
- $2.5 \text{ v}/\text{div}$
- 340 KV Generator
- $9000 \text{ amp} \pm 100 \text{ amps}$

End View

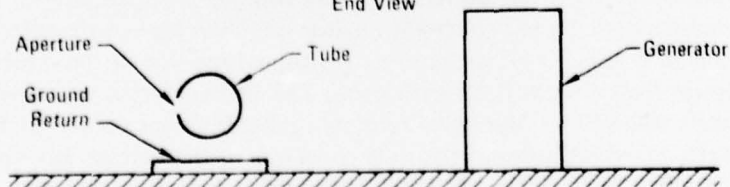
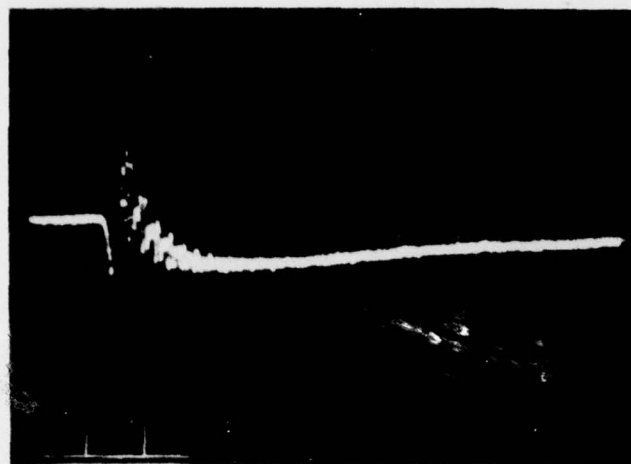
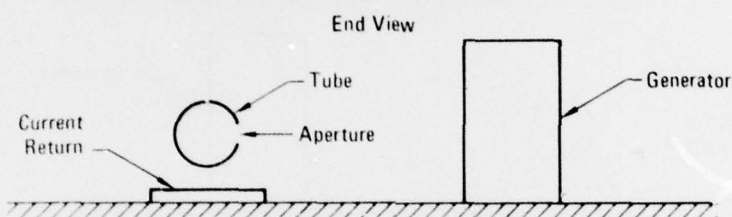


Figure 8. E-Field Sensor  
Open Aperture Away From Generator



- 2  $\mu$ s/div
- 1.2 v/div
- Same Generator Output



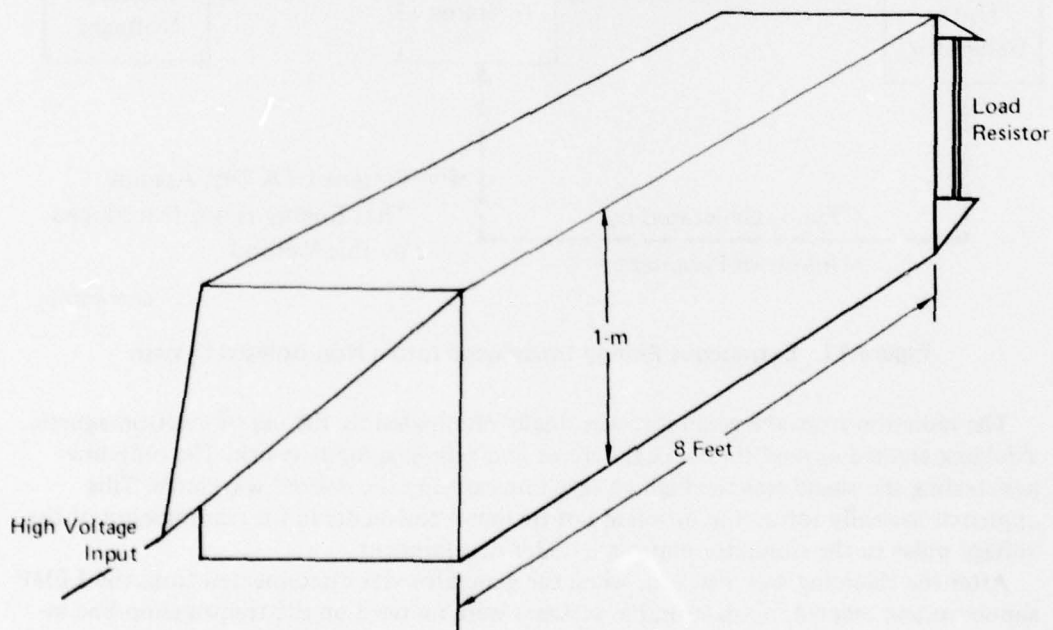
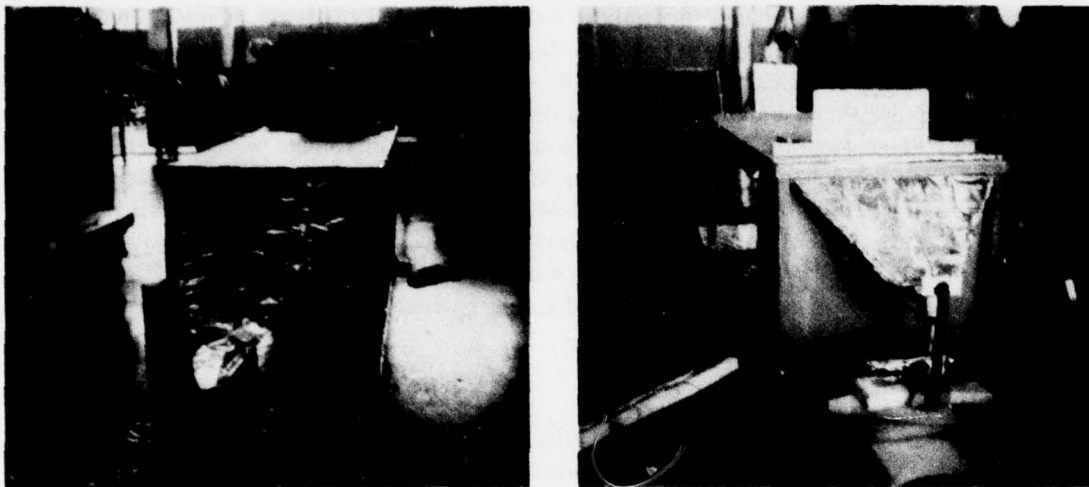
**Figure 9. E-Field Sensor  
Open Aperture Toward Generator**

**LIGHTNING ELECTROMAGNETIC PULSE (LEMP) SIMULATION.** Based upon the previous discussion, a logical question might be raised concerning the relative effects of radiated fields associated with an actual lightning strike compared to the effects of the return stroke currents. Nanevich<sup>9</sup> and Pierce<sup>1</sup> both stress the importance of recognizing the possible effects of nearby lightning activity. The magnitude of induced transients observed in the Reference 8 flight test programs were comparable in magnitude to the transients produced by direct strikes to the aircraft. Because of these recommendations and our own laboratory experience, the MCAIR Program is presently focused on the problem of determining the effects of both laboratory and natural radiations on induced coupling behavior. It is felt that until the radiated-field effects are understood and controlled, it is fruitless to attempt experimental studies of direct attachment effects.

One source of a uniform electric field that has been used extensively for laboratory testing is the nuclear Electromagnetic Pulse (NEMP) bounded-wave simulator. High voltage is applied to the simulator plates by an impulse generator, thus producing a fairly uniform transient field over a concisely defined working volume.

A Lightning Electromagnetic Pulse (LEMP) Simulator was therefore constructed for the purpose of investigating transients produced by lightning-type waveforms which, of course, are much slower than nuclear EMP waveforms. The first such system, shown in Figure 10 employed a small 340 kV Marx generator as a pulsed voltage source, and an RLC waveshaping network which allowed the time constants of the voltage waveform applied to the simulator plates to be varied. The fastest rate of rise attainable with this system was 300 kV/ $\mu$ sec, and the peak field strength in the test volume was 100 kV/meter.

as measured by the E-field sensor shown in Figure 2. A schematic representation of the LEMP simulator system is shown in Figure 10.

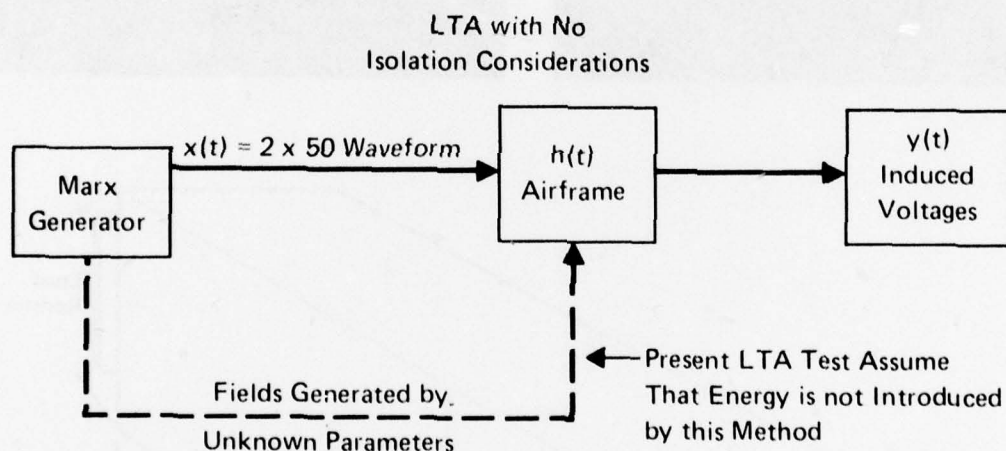


GP78 8333 13

Figure 10. LEMP Simulator



The procedure used with the LEMP Simulator consisted of placing a typical transmission line (length of coaxial cable) in the LEMP simulator, radiating this transmission line with a series of E-field waveforms of varying risetimes and amplitudes, and making simultaneous measurements of the E-field waveform and the induced voltage on the transmission line. After testing had begun it was noted that no matter how the driving voltage waveform was changed, the induced voltage remained the same. It was then discovered that with the high voltage line disconnected from the simulator plates, the same measured field and transient effects were still present. It was thereby determined that the simulator and the test article were being irradiated directly by the radiation from the Marx high voltage generator. Since the switching and erection voltage on the generator was faster than the controlled waveform applied to the simulator plates, the radiation effects from the generator dominated the field environment in the simulator. This finding was important because all induced voltage experiments use some form of high voltage generator to produce the voltage or current pulse used in the test. As shown in Figure 11 unshielded generators may produce induced voltages which are unrelated to the measured driving function.



GP78 8333 2

**Figure 11. Extraneous Energy Introduced Into a Non-isolated System**

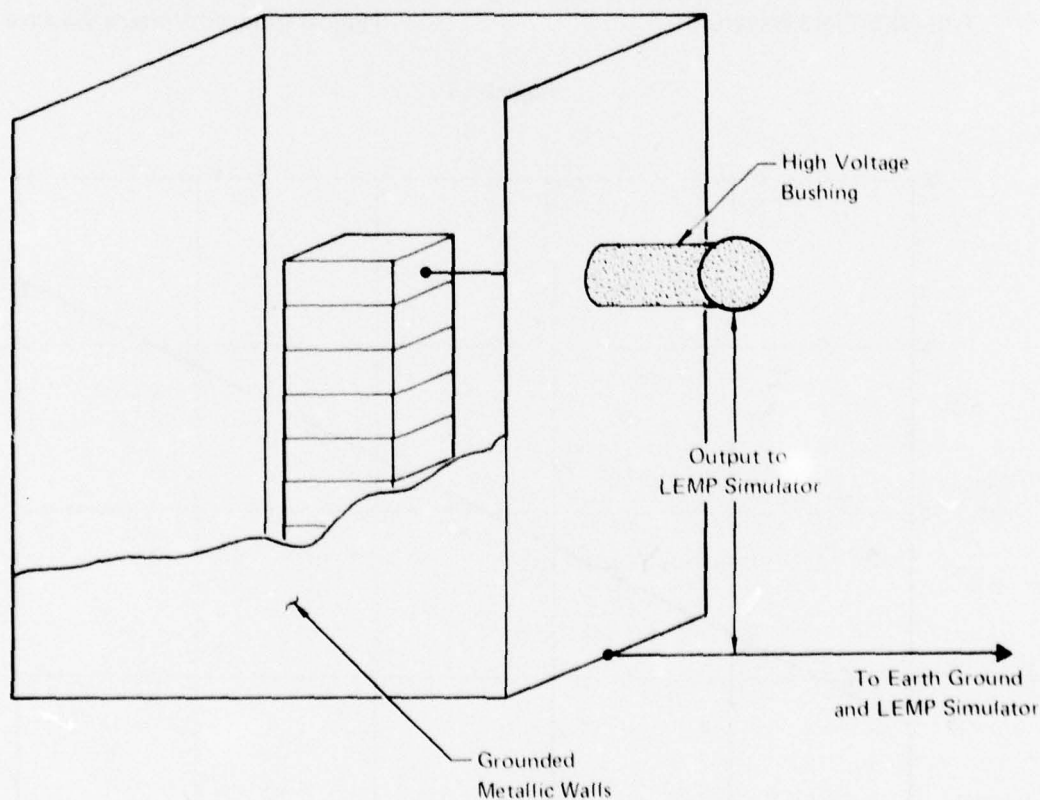
The radiation from the generator was finally eliminated by the use of electromagnetic shielding erected around the Marx generator and waveshaping network. The only line penetrating the shield was the high voltage line carrying the desired waveform. This approach basically solved the problem but further refinements in the transmission of the voltage pulse to the simulator plates are under development.

After the shielding was installed, when the generator was disconnected from the LEMP simulator and erected, no measurable voltages were induced on the transmission line indicating no significant amount of radiation was penetrating the shield. Testing continued using this new test setup as shown in Figure 12. A typical electric field (E-field) waveform and resulting induced voltage waveform shown in Figure 13. Once the extraneous fields were eliminated, it was finally possible to show experimentally the quantitative

relationship between the risetime of the E-field waveform and the peak magnitude of the induced voltage. This relationship is shown graphically in Figure 14. These results indicate that the following relationship exists:

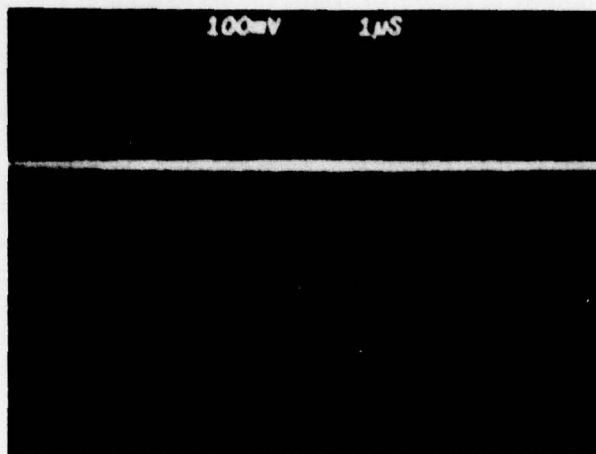
$$|v_i(t)| \propto \frac{dE}{dt}$$

where  $|v_i(t)|$  is the amplitude of the induced voltage, as a function of time. It can be deduced from this information that the test has been properly isolated, and is time invariant and linear. However, further testing is required to prove that the system obeys linear theory, that is, that all parameters affecting the test have been identified. Of course, it also remains to determine the range of the values of  $dE/dt$  associated with natural lightning strikes to aircraft. Test development is continuing at MCAIR with a 1.5 mega-volt shielded Marx generator and a larger model of the LEMP simulator which can contain the aluminum cylinder.



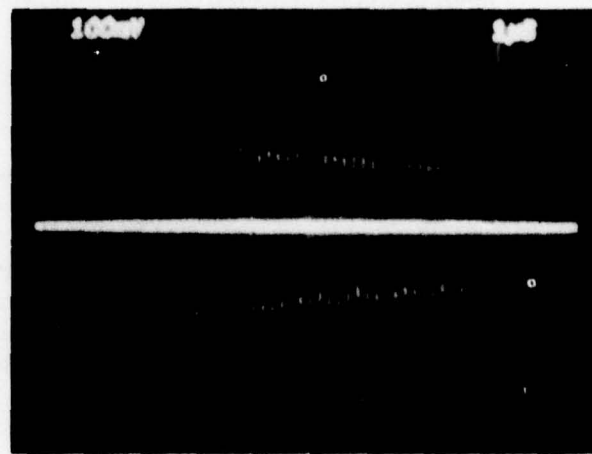
GP78 8333 14

Figure 12. The Shielded Marx Surge High Voltage Generator



50kV/m/Div

Typical E-Field Waveform

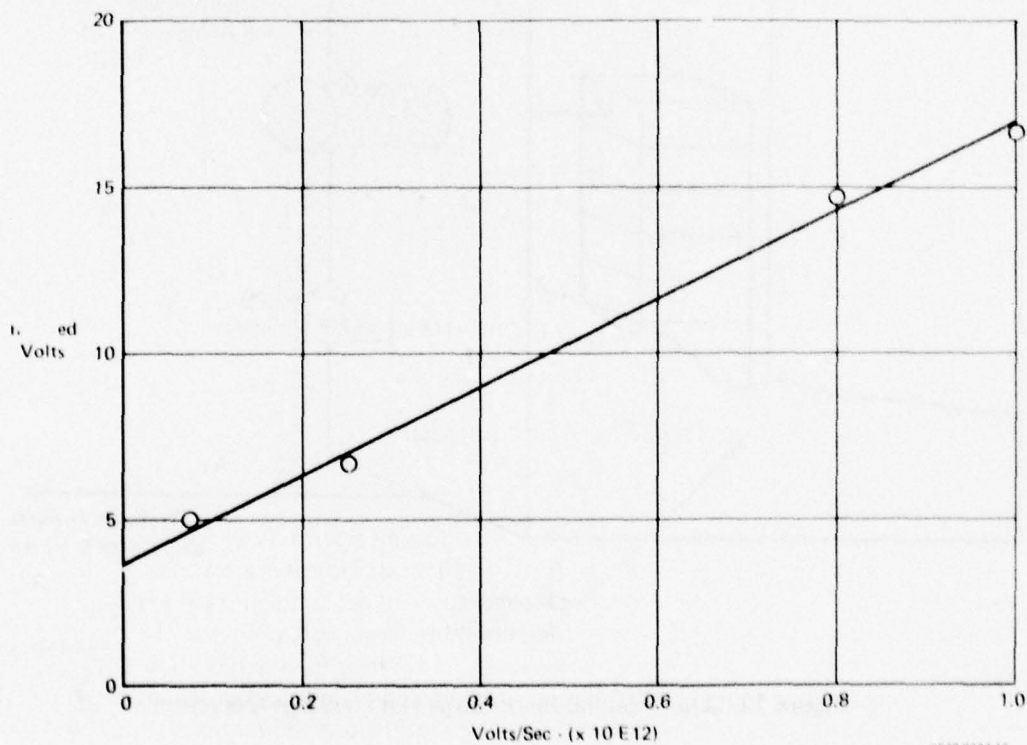


0.14V/Div

Typical Induced Voltage Waveform

Figure 13.

GP78 B333-15



GP78 B333-16

Figure 14. Induced Voltage vs  $\dot{V}$  on RG174 Coaxial Cable



**APPROACH.** The approach to be taken, to achieve the goal of developing a full-scale nondestructive test, consists of four basic steps:

- a) evaluation and development of instrumentation,
- b) computer aids and analytical methods,
- c) development of test techniques,
- d) correlation of simulated data to natural phenomena.

The best test approach would be to generate a lightning stroke in the laboratory. However, this is physically impossible with present technology. The threat level current portion of the lightning stroke is simulated separately from the high voltage portion.

One must realize that all lightning parameters and conditions cannot and need not be simulated simultaneously, and similarly, the system to be tested must be analyzed to determine the type of testing required. One approach to determining test requirements is shown in Figure 15. Whether or not the circuit is to be tested is determined by the impact of a failure on the total system. A flight critical circuit must be tested accurately. Once a test requirement is indicated the type of testing is determined by the input impedance of the circuit.

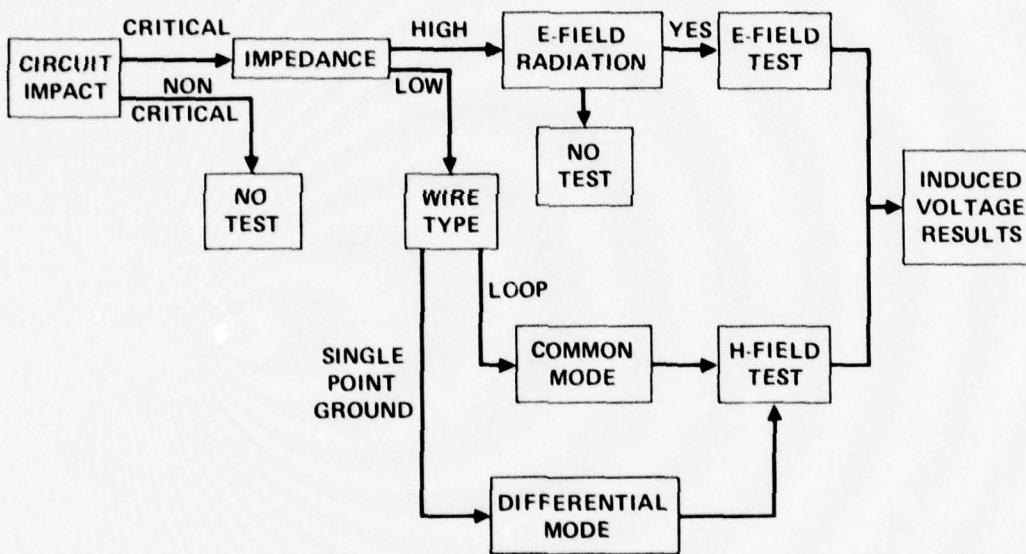


Figure 15. Test Approach

A high input impedance (1 megohm) indicates a test using electric field radiation (such as a near miss test). A low input impedance (such as 50 ohm) indicates a test using magnetic field radiation (such as the LTA). Once it has been determined what type of test the circuit is to be subjected to, a well controlled test must be conducted. This means that all parameters that affect the test must be identified. These parameters should be monitored during the test to make sure that no unsuspected changes occur during the performance of the test. A test performed under these conditions should meet the needs of present solid state avionics, and should lead to the verification of the laboratory test techniques.

**CONCLUSIONS.** More testing is required to determine:

- a) If proper frequency spectrum can be adequately simulated.
- b) If the induced signals on the flight aircraft can be reproduced in the laboratory on the actual airframe.

When testing is completed, enough data will be available to determine the reliability and effectiveness of the test technique. Once this technique has been proven then the laboratory will continue studying the second method of inducing voltages on aircraft wiring, that is the direct stroke attachment.

In summary, what has been discussed is a technique for simulated lightning induced transients from a near miss lightning stroke. Preliminary results show that the technique linear theory and all the parameters adversely affecting the test have been isolated or eliminated.

## REFERENCES

1. E.T. Pierce, G.H. Price, "Electric and Magnetic Fields Due to Close Lightning" S.R.I. Report SR1-P-73401 Aug. 1973
2. M.A. Uman, "Spark Simulation of Natural Lightning" AFAL-TR-72-325 Dec. 1972 (1972 L&SE Conf. Proc.)
3. L.C. Walko, "A Test Technique for Measurement of Lightning Induced Voltages in Aircraft Electrical Circuitry". 1972 L&SE Conf. Proc. USAF (AL)-TR-72-325 Dec. 1972
4. S.D. Robb, "Lightning Electrical Hazards to Flight Vehicles" USAF (AL)-TR-69-269 Dec. 1979
5. R.L. Blount, R.D. Gabbois, D.L. Suiter and J.A. Zill, "ASTP Simulated Lightning Test Report" NASA, Lyndon B. Johnson Space Center JSC-09221 Nov. 1974
6. B.J.C. Burrows, C. Luther and P. Pownall, Culham Laboratory Ukaea, Abingdon, Oxfordshire, England
7. W.G. Butter and D.W. Clifford, "Lightning Induced Electric Transient Testing on Aircraft Wiring System" McDonnell Douglas Corp., St. Louis, Mo. IEEE Symposium Aug. 1977
8. W.G. Butters, "The Effects of Advanced Composites on Lightning Induced Coupling in Aerospace Vehicles" McDonnell Douglas Corp., Final Report; MDC E1708
9. J.E. Nanevich, "Airborne Measurement of the Electromagnetic Environment Near Thunderstorm Cells." S.R.I. International, Menlo Park, CA. IEEE International Symposium Aug. 1977



FLORIDA LIGHTNING ELECTROMAGNETIC-FIELD  
MEASUREMENTS USING AN INSTRUMENTED NASA JET AIRCRAFT

By

J. E. Nanevicz, R. C. Adamo, and E. F. Vance  
SRI International  
Menlo Park, California 94025

and

R. T. Bly, Jr.\*  
ESL, Inc.  
Sunnyvale, California 94086

Presented at:

Federal Aviation Administration/  
Georgia Institute of Technology  
Workshop on Grounding and Lightning Protection

May 1978

\* Formerly with SRI International, Menlo Park, California.

This work was sponsored by National Aeronautics & Space Administration, Houston, Texas and Air Force Flight Dynamics Laboratory, Wright-Patterson Air Force Base, Ohio under contract NAS9-15101 and National Aeronautics & Space Administration, Kennedy Space Center, Florida under contract NAS10-9013.

## ABSTRACT

During the summers of 1976 and 1977, flight test measurements were made of the electromagnetic signals generated by nearby lightning flashes within Florida thunderstorms. The instrumentation carried aboard the NASA Learjet test aircraft was such that it was possible to obtain simultaneous data in both the time domain and in the frequency domain. A brief description of the instrumentation will be presented. The general results of the measurement program will be discussed together with an indication of their implications.

## CONTENTS

### I INTRODUCTION

- A. Background
- B. Jet Aircraft Tests in Florida

### II INSTRUMENTATION

- A. General
- B. Test Jet Aircraft
- C. Static Electric-Field Measurement Instrumentation
- D. Transient Field Sensors and Electronics

### III TYPICAL FLIGHT TEST RESULTS

- A. General
- B. Spectrum Analyzer Data From 1976
- C. Flight Test Data From 1977

### IV CONCLUSIONS AND RECOMMENDATIONS

### APPENDIX



#### ILLUSTRATIONS

1. Locations of Fieldmeter Sensors on NASA Learjet Test Aircraft
2. Lightning Strike--Detail A
3. Lightning Strike--Detail B
4. Detail of Nearby Lightning Event
5. Sample of Data Record from Analog Tape Recorder
6. Lightning-Related Spectrum Analyzer Record
7. Higher Speed Stripout of Lightning-Related Spectrum Analyzer Data
8. Digitizer Record Corresponding to Stroke of Lightning of Figure 7
9. Fourier Transform of Transient Digitizer Record

#### TABLES

1. Instrumented Wires in Interior of Test Jet Aircraft
2. Sensor and Instrumentation Interconnection for Flight of 10 August 1977

## I INTRODUCTION

### A. Background

For the past several decades, aircraft have generally been fabricated using all-metal skins, with the specific materials and dimensions determining by structural requirements. The metal skin material, thickness, and fabrication techniques were usually such that an aircraft could pass lightning stroke currents with relatively minor damage--usually pitting and puddling of the skin at the stroke attachment points. In addition, metal skins shielded the interior electronic systems from interference signals generated by precipitation static, nearby lightning, and direct lightning strikes.

Electronic systems used on early aircraft used high-level analog circuitry that was tolerant of occasional noise pulses of considerable amplitude. Present solid-state digital electronic systems operate at lower signal levels and suffer component damage and upset at much lower levels of noise pulses. Ultimately, it is planned that all avionic systems will be completely digital and will operate at even lower signal levels than are currently used. Experience with digital systems indicates that they are often susceptible to catastrophic upset as the result of a single noise impulse at a level comparable to the system operating level.

Aircraft are currently being fabricated with many of their complex, non-load-bearing surfaces made of fiberglass. In the future, it is planned that for reasons of strength, weight, and cost, large sections of aircraft skin and structure will be made of composite materials. These nonmetallic materials are not suitable for conducting lightning stroke currents and do not provide the RFI shielding that was formerly obtained with metal structures and skin. Accordingly, programs are currently under way to devise techniques, such as coatings, to improve the electrical and shielding properties of composite materials.

Since the skin on an all-metal aircraft is needed for aerodynamic and structural reasons, no additional penalty is imposed in achieving the current conduction capability and electromagnetic shielding that the skin provides. Indeed, it is quite likely that most aircraft are overdesigned in these regards. If, however, in using composite materials it becomes necessary to apply special processes to achieve current-handling ability and shielding, the implementation of these special processes may impose significant penalties--weight, initial cost, and increased maintenance cost. Accordingly, an aircraft designer will require accurate information about the physical processes for which he is endeavoring to provide protection, so that he can avoid overdesigning or underdesigning.

Airplane designers in the past have been very concerned with problems associated with physical damage resulting from direct strikes to the aircraft. As a result, a "standard" stroke has been developed that duplicates in the laboratory the damage observed on actual strikes to aircraft. Tests show that strike damage can be duplicated with considerable accuracy even when certain features of the strike (such as the higher frequency components) are poorly simulated. Thus, the "standard" stroke specifies such parameters as rise time, peak current, and decay time without much regard for processes associated with the formation of the stroke. Nevertheless, this procedure provides a useful simulation of the low-frequency features of the stroke.

However, in developing solutions to the problem of signals coupled into the interior of the aircraft, the high-frequency components of the source are also of great importance as is indicated in the Appendix. Information regarding the high frequency components of lightning is almost entirely confined to data obtained from ground-based measurements. To apply these data to the case of a lightning strokes near an aircraft, it is necessary to perform a substantial number of calculations to properly account for the rate of decay, with distance of the various components of the stroke. Also, it is not clear whether the ground-based measurements adequately account for all of the nonlinear processes involving the presence of the aircraft. As the result of these observations, it was felt that in-flight measurements of lightning source parameters would be highly desirable.

#### B. Jet Aircraft Tests in Florida

In June 1976, it was established that Learjet 705 owned by NASA Ames would be operated in Florida during the peak of the thunderstorm season to investigate the electrostatic characteristics of thunderstorms as they formed in the vicinity of Kennedy Space Center (KSC), giving particular attention to the region of the thunderstorm anvil.

To take advantage of the availability of the test jet aircraft and its static field instrumentation,<sup>1\*</sup> a modest, quick-reaction program was initiated by the Air Force to install suitable instruments on the jet aircraft to permit simultaneous measurement<sup>2,3</sup> of the electromagnetic transients associated with nearby lightning. The instrumentation for the 1976 tests consisted of two spectrum analyzers, each consisting

---

\* References are listed at the end of the paper.



of four fixed-tuned receivers covering the range 10 kHz to 30 MHz, and a Tektronix R7912 transient digitizer. One or the other of these two systems could be flown on the jet aircraft. The sensors in 1976 consisted of: an electric dipole mounted on top of the fuselage, to measure the transient fields associated with lightning; and a 3.6-m long piece of 20 gauge hookup wire running roughly 10.2cm (4 in.) from the aircraft skin on the inside of the aircraft cabin to measure the currents induced in a typical interior wire.

A more elaborate instrumentation system was used in the flight tests of summer 1977 that involved the NASA Learjet 701. Additional sensors were installed on the aircraft, and in some cases both time-domain and frequency-domain measurements were made simultaneously.

In summer 1976, the weather in the vicinity of Patrick AFB, Florida was such that it was possible to find developing isolated thunderstorm cells. Such cells are sufficiently clearly defined that it is possible to fly in close proximity to the cell without risk of inadvertently penetrating a region of extreme turbulence. Accordingly most of the tests in 1976 were conducted with the aircraft essentially at the edge of the outer portion of the cell. Once, when flying between a pair of cells, the aircraft was struck by lightning. On this day, the spectrum analyzer system was installed and operating.

The weather in summer 1977 was atypical of normal conditions. Individual cells formed very infrequently. Furthermore, when single cells could be located, most times they did not develop sufficiently to produce appreciable lightning. Consequently, much of the testing in 1977 was done in the vicinity of extended storm systems containing numerous cells. Close approach and study of a single cell is not possible in such a situation since turbulence in the region between the cells can be severe. Furthermore, restricted visibility makes aircraft maneuvering for successive passes very difficult. As a result, most of the testing in 1977 was carried out with the aircraft substantially farther from individual cells and with other groups of active cells in closer proximity than was true in 1976.

## II INSTRUMENTATION

### A. General

Although results from both the 1976 and 1977 flight tests will be presented here, only the instrumentation system used in the 1977 tests will be described. The 1977 system included all of the instrumentation used in 1976.

### B. Test Jet Aircraft

The Learjet 24B aircraft, owned by NASA Ames and instrumented for use on the test programs, were ideally suited for thunderstorm studies. This aircraft has a service ceiling of 14 Km (45,000 ft), a cruising speed of 239 m/s (464 kn), a rate of climb of 2 Km/min (6,800 ft/min), and can accommodate a two-person crew and three passengers in addition to instrumentation.

The test jet aircraft agility and speed allow considerable data to be collected throughout a large volume of space in the region surrounding a thunderstorm during the entire process of storm formation and development. During this program, measurements were made of the static electric fields in the vicinity of thunderstorms and of the electrical transients produced both outside and inside the aircraft by nearby lightning.

### C. Static Electric-Field Measurement Instrumentation

The presence of an aircraft in an electric field perturbs the field in such a way that the electric fields measured at points on the aircraft surface are different from the free-space electric fields that would exist in the same space if the aircraft were not present. However, the electric-field measurement system installed on the test jet aircraft was designed to readily allow the reconstruction of the free-space field components from four measured aircraft surface fields. To provide redundancy, five compact rotating-vane electric-field sensors were installed on the test aircraft. The locations of these sensors are shown in Figure 1. These locations were chosen to maximize the coupling between the sensors and the free-space field components within the constraints imposed by structure, access, cabling, and aerodynamic considerations.

The relationship between the measured electric-field magnitudes and the four quantities to be determined (i.e., the three free-space field components and the aircraft potential) was determined using scale-model measurement techniques.<sup>1</sup> To provide real-time outputs of the desired quantities, the onboard instrumentation package included an analog signal processor designed to solve the resulting system of linear equations. In addition to the static electric-field readings, the instrumentation system also provides an indication of the static field change resulting from the neutralization of charge during a flash. This change takes place over a period of the order of a second, and it can be used to obtain a rough estimate of the distance from a flash.

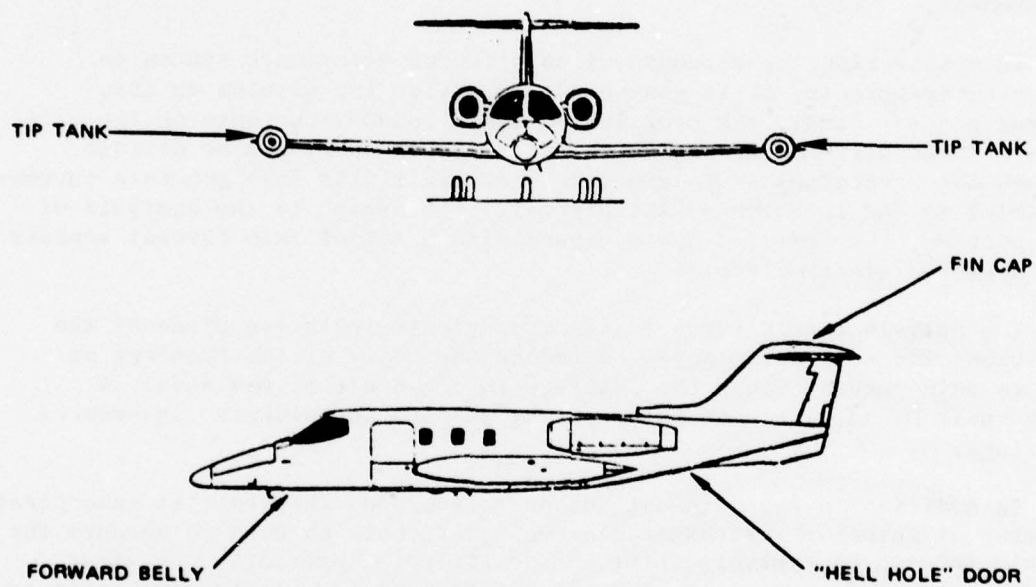


FIGURE 1 LOCATIONS OF FIELDMETER SENSORS ON NASA LEARJET TEST AIRCRAFT



#### D. Transient Field Sensors and Electronics

The propagating field generated at the test aircraft location by lightning was measured by two sensors on the exterior of the aircraft: an E-field antenna located on the top of the fuselage; and an H-field loop antenna mounted in the nose radome.

Although the electric dipole antenna was suitable for measuring the propagating electromagnetic field, it also is influenced by sudden changes in aircraft potential caused by triboelectric charging.<sup>5</sup> A magnetic loop is much less susceptible to triboelectric charging provided it is mounted on an extremity, such as the nose of the aircraft, away from the noise sources.<sup>6</sup> A loop mounted at the nose is also highly decoupled from the currents flowing on the fuselage so that it responds primarily to the propagating H-field, and can be used as a sensor for free-space field measurement.

In considering the response of an airborne electronic system to lightning transients, it is convenient to divide the problem up into several steps. First, the propagating field induces currents on the airframe. These airframe currents, in turn, excite apertures or diffuse through the aircraft skin to generate electric fields that generate currents in wiring in the interior of the aircraft. To assist in the analysis of this problem, the test jet was equipped with a set of skin current sensors that measured airframe fields.

Two half-loop skin current sensors, oriented with the plane of the loop along the roll axis, were located on the belly of the fuselage to measure skin current along the fuselage fore and aft of the wing. A second pair of slot-antenna skin-current sensors were located on each of the wings.

In addition to the external sensors discussed, the test jet incorporated a number of interior instrumented wires\* that could be used to measure the signals induced on typical cables in the aircraft interior. The first instrumented wire, described in Table 1, was installed inside the cabin in the same general manner as in the tests of 1976.<sup>2</sup> This wire sensor was included in the instrumentation complement to provide a common measurement to help tie together the 1976 and 1977 measurement programs.

The remaining instrumented wires shown in Table 1 were installed in the major members of the airframe. Since each wire coupled electromagnetically primarily to currents flowing on the member in which it is installed, the wire current measurements provide a technique for investigating the coupling between airframe skin currents and wiring in the interior of the aircraft.

The spectrum analyzer systems were made up of individual fixed-frequency receiver channels divided into four distinct spectrum analyzer systems.

---

\* Ordinary 20 guage hook-up wire was used for this purpose.

TABLE 1  
INSTRUMENTED WIRES IN INTERIOR OF TEST JET AIRCRAFT

Location	Length-Meters
1. Cabin Wire	3.58
2. Aft Fuselage	7.2
3. Forward Fuselage	3.8
4. Fin Cap	14.34
5. Right Wing	12
6. Left Wing	13

Provisions were included in the overall instrumentation to allow any of the spectrum analyzer systems to be used in monitoring any transient sensor. The output of each spectrum analyzer channel was recorded on one channel of a 14-channel analog tape recorder.

The frequency range covered by the spectrum analyzers was chosen on the basis of several considerations. A substantial fraction of the spectral energy in a lightning flash is contained in the low frequencies (10 kHz): accordingly, much ground-based data has been generated using low-frequency monitors. Therefore, provisions were made for measurements at 10 kHz for comparison with published ground-based data. Experience gained in nuclear EMP analysis indicated that signals coupling through apertures in a shielded system are proportional to  $di/dt$  where  $i$  is the current flowing in the shield as is discussed in the Appendix. This means that the high-frequency processes in the lightning stroke are important in determining the signals induced in aircraft interior wiring. Consequently, the spectrum analyzer system was designed to include provision for measuring signal components up to 30 MHz.

Two transient digitizers were part of the test aircraft instrumentation and could be connected to members of the same set of electromagnetic transient sensors used with the spectrum analyzer system. Each digitizer consisted of a Tektronix R7912 transient digitizer and associated equipment. Each digitizer channel was essentially a wide band (100 MHz or more) oscilloscope, which was triggered by the leading edge of the transient, and wrote the transient signal as a pattern on an array of diode cells. The stored pattern was subsequently read, processed, and stored in the floppy disc memory of a PDP-11 computer, which constituted part of the digitizer system.

Provisions were made for time correlation of the digitizer and spectrum analyzer data. A BCD-encoded time signal was recorded by the PDP-11 computer each time the digitizer was triggered and a continuous IRIG B time-code signal was recorded on one of the analog tape recorder channels used in conjunction with the spectrum analyzer. In addition, digitizer triggerings were marked on the spectrum analyzer record.

All of the low-bandwidth data were multiplexed onto a single channel of the tape recorder. These included outputs from the fieldmeter system, aircraft parameters such as altitude, heading, etc., and the frontal charging current generated by flight through precipitation.

### III TYPICAL FLIGHT TEST RESULTS

#### A. General

The data from the 1976 tests included spectrum analyzer records generated during a direct strike to the aircraft, as well as records from nearby lightning. Data from the 1977 tests include simultaneous transient digitizer and spectrum analyzer records of the same events. During 1977 it was necessary to operate the aircraft at greater distances from the active thunderstorm cells.

#### B. Spectrum Analyzer Data From 1976

##### 1. Direct Lightning Strike

In general, the disturbance associated with the direct strike including the time when signals were induced in the cabin wire, persisted for about 0.5 s. The electromagnetic field at the location of the dipole on top of the fuselage was quite complicated. Bursts of noise (most prominent in the direct, 10 kHz, and 1 MHz channels) were interspersed with short, high-amplitude noise pulses on all channels. The spectral distribution of these short pulses varied from pulse to pulse. In some cases, the highest amplitude response occurred on the 1 MHz channel; on other pulses, the highest response occurred on the 10 MHz channel.

A number of pulses occurred on the cabin wire coincident with pulses on the antenna. Here again, there was no unique relationship between the amplitudes of the current spectral components. Furthermore, the amplitudes of the pulses occurring on the wire were not systematically related to the pulse amplitudes measured on the dipole antenna. This apparent lack of relationship in the behavior of the various spectrum analyzer outputs can be explained as follows:

Signals are induced in the cabin wire primarily by currents flowing along the fuselage of the aircraft; currents flowing along the wing will not induce significant signals in the wire. On the other hand, the field intensity at the external dipole antenna location is relatively independent of the direction of current flow; i.e., a current along the aircraft wing produces relatively the same electric field as does the same current flowing along the fuselage. Thus, it is not unexpected that the relationship between the amplitudes of the spectrum analyzer signals obtained from the two sensors is not immediately obvious.



Details of the spectrum analyzer output obtained near the beginning of the flash are shown as "Detail A" in Fig. 2. Four pulses were induced in the external dipole antenna during this period. Although all four pulses were of roughly the same amplitude in the 1 MHz channel, the amplitudes of the pulses in the 3 and 10 MHz channels varied by more than a factor of two over the same four pulses. In other words, the spectral character of the dipole antenna signal varied substantially from pulse to pulse.

Further examination of Figure 2 indicates that only the last pulse produced a significant reaction in the inside wire. It is interesting to note that the largest deviation from the zero line occurred on the 30 MHz channel and that barely perceptible deviations occurred on the 1 and 3 MHz channels.

A section of a spectrum analyzer record generated roughly 0.05 s after the start of the lightning strike activity (called "Detail B") is shown in Figure 3. The outputs from the antenna spectrum analyzer channels are approximately the same as they were in the last pulse of Figure 2. The signals from the wire-current spectrum analyzer, however, are substantially larger in Figure 3 than in Figure 2. Thus, it is likely that the pulse of Figure 3 is the record of the stroke that produced the main pulse of current along the fuselage.

To give perspective to the induced current data, the magnitudes of the pulses generated in the cabin wire current spectrum analyzer system by the injection of a 1A current-step calibration signal on the wire are shown at the right edge of Figure 3. It is evident that the reaction produced by the lightning strike component of Figure 3 was equivalent to a current step in excess of 1A flowing in the cabin wire.

## 2. Nearby Lightning

Interesting examples of nearby lightning are contained in the data from a 10 August 1976 pass in heavy hail at an altitude of 11.3 km (37,000 ft), under an anvil. Near the beginning of the record, two major pulses occurred in the 10 kHz spectrum analyzer channel. The second of these pulses was accompanied by pulses on all of the other spectrum analyzer channels, including those associated with the cabin wire. Associated with these pulses was a disturbance in the static field record, which indicated a field change of 15 kV/m as the result of the first lightning stroke.

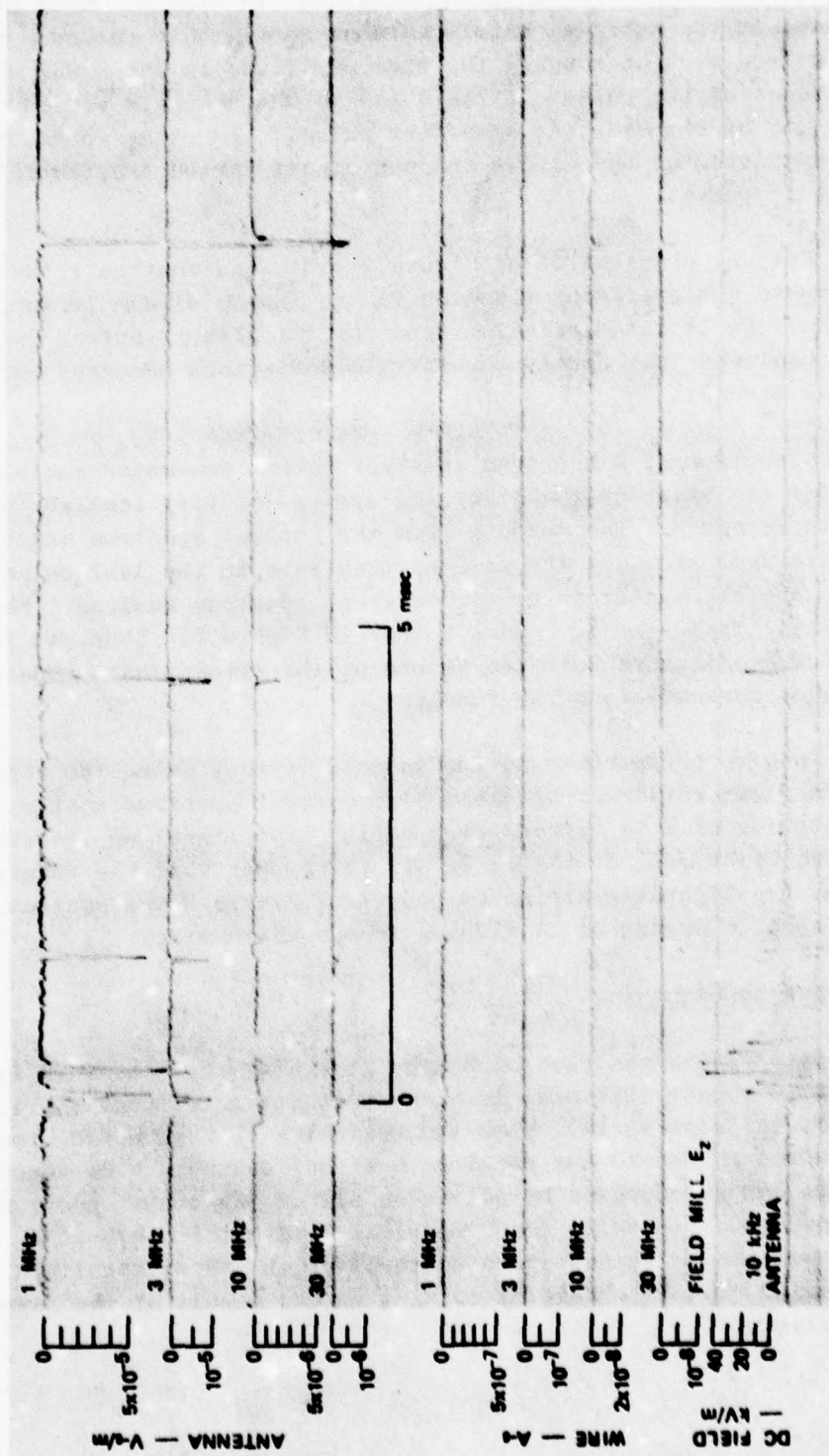


FIGURE 2 LIGHTNING STRIKE — DETAIL A

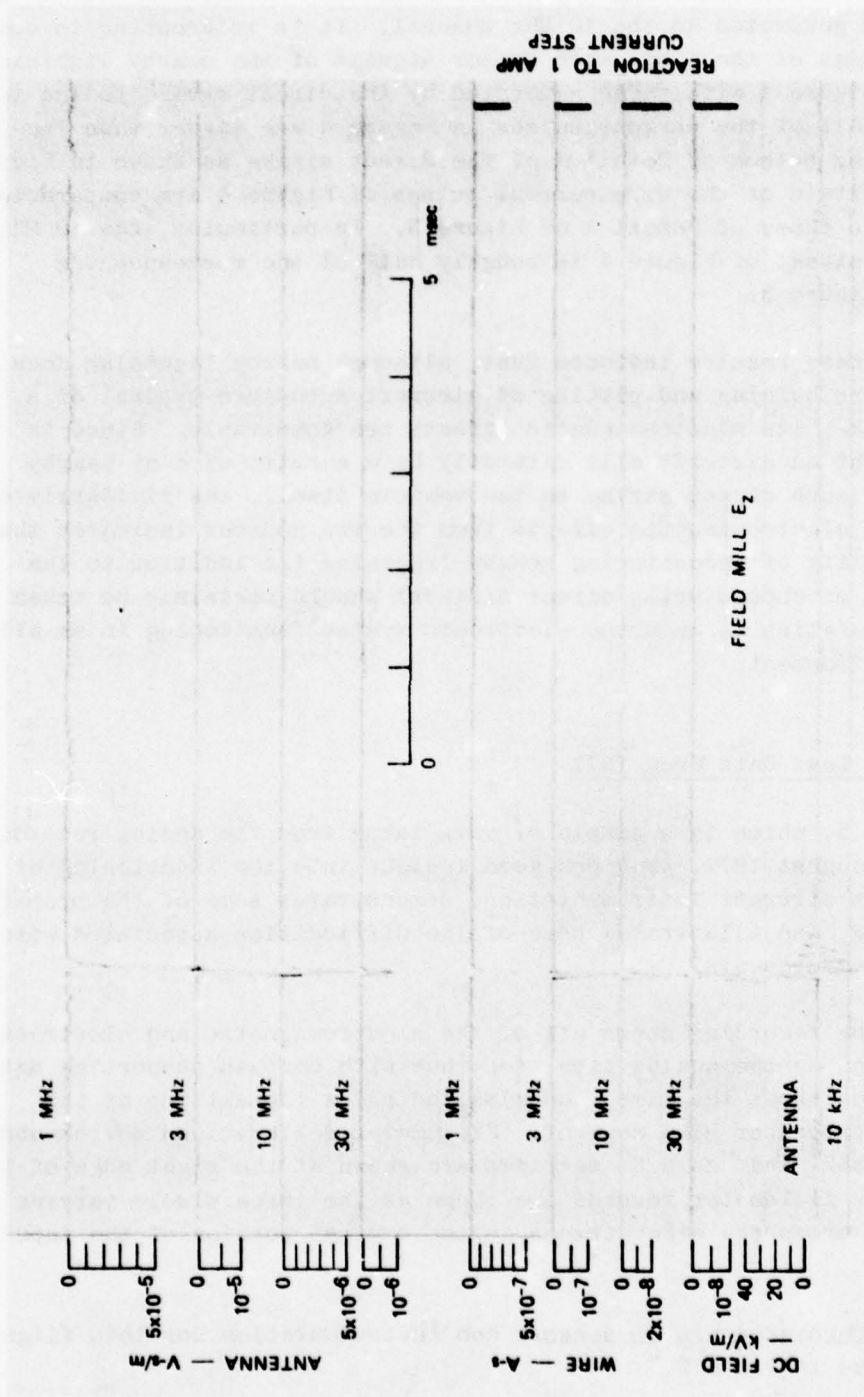


FIGURE 3 LIGHTNING STRIKE — DETAIL B



Details of this lightning stroke are shown in Figure 4. It is evident that substantial signals were induced in the wire in the cabin--the largest was generated in the 10 MHz channel. It is interesting to compare the amplitudes of the cabin wire sensor signals of the nearby lightning stroke of Figure 4 with those generated by the direct strike to the test aircraft. All of the current pulses in Figure 4 are larger than the corresponding pulses of Detail A of the direct strike as shown in Figure 2. In fact, certain of the wire-current pulses of Figure 4 are comparable in magnitude to those of Detail B of Figure 3. In particular, the 10 MHz cabin-wire signal of Figure 4 is roughly half of the corresponding signal in Figure 3.

These results indicate that, although nearby lightning does not cause the burning and pitting of aircraft structure typical of a direct stroke, its electromagnetic effects are comparable. Since in normal flight an aircraft will naturally have a ratio of many nearby strokes for each direct strike to the vehicle itself, the similarity of the induced electromagnetic effects from the two sources indicates that the probability of encountering nearby lightning (in addition to the probability of encountering direct strikes) should certainly be taken into consideration in assuring electronic system functioning in an all-weather environment.

#### C. Flight Test Data From 1977

Figure 5, which is a sample of data taken from the analog recorder tape of 10 August 1977, provides good insight into the functioning of the test jet aircraft instrumentation, demonstrates some of the properties of lightning, and illustrates some of the difficulties associated with lightning measurements.

The tape recording shows all of the electromagnetic and electrostatic data recorded on the analog tape, together with certain supporting data. The top trace shows the time, and also indicates the setting of the fieldmeter-processor gain control. Fieldmeter calibrations corresponding to the "gain 2" and "gain 3" settings are shown at the right edge of the figure. The fieldmeter records are shown as the three widely varying traces that cross the other traces in the central portion of the tape recording.

The interconnection of sensors and instrumentation for this flight are indicated in Table 2.

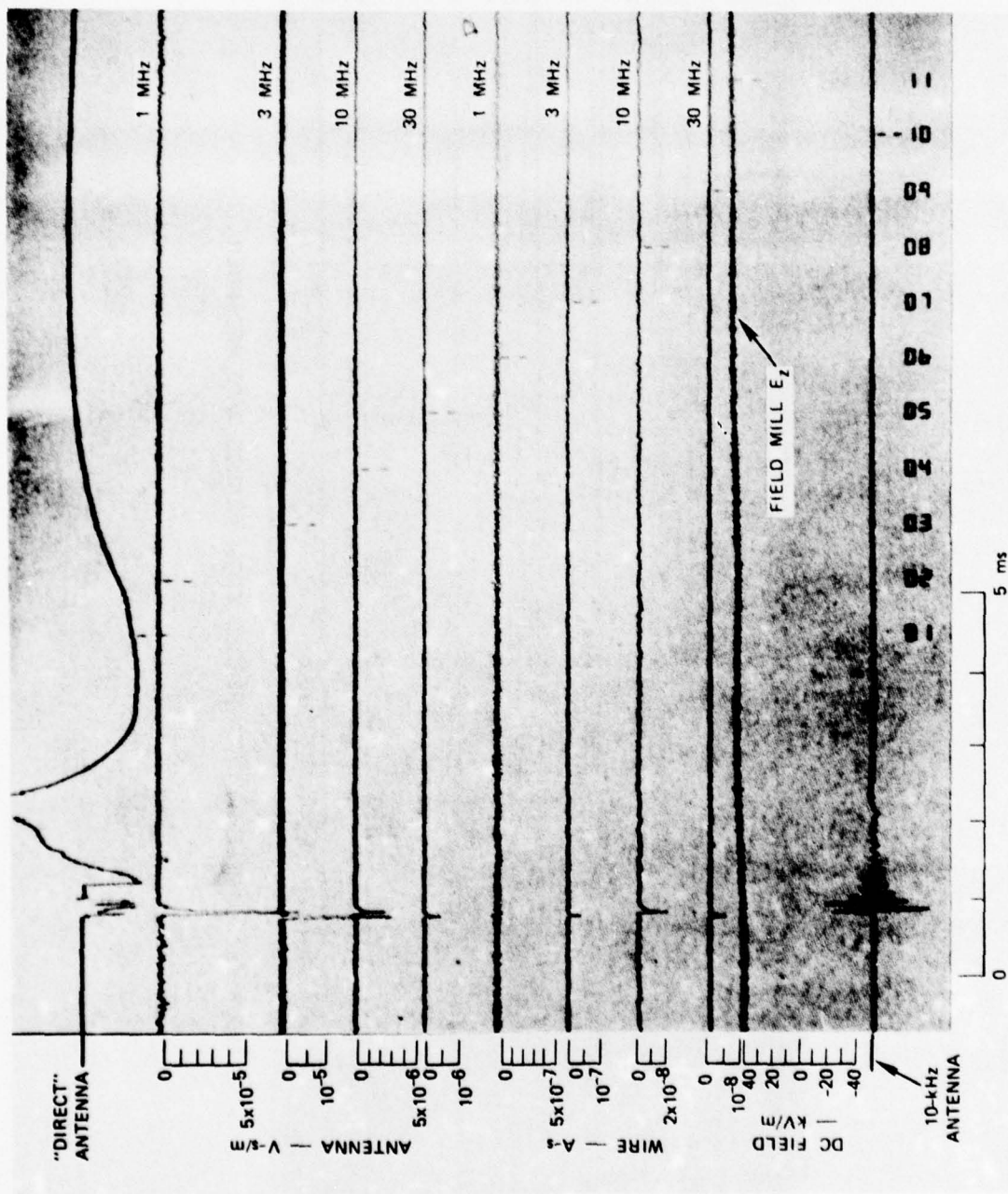


FIGURE 4 DETAIL OF NEARBY LIGHTNING EVENT

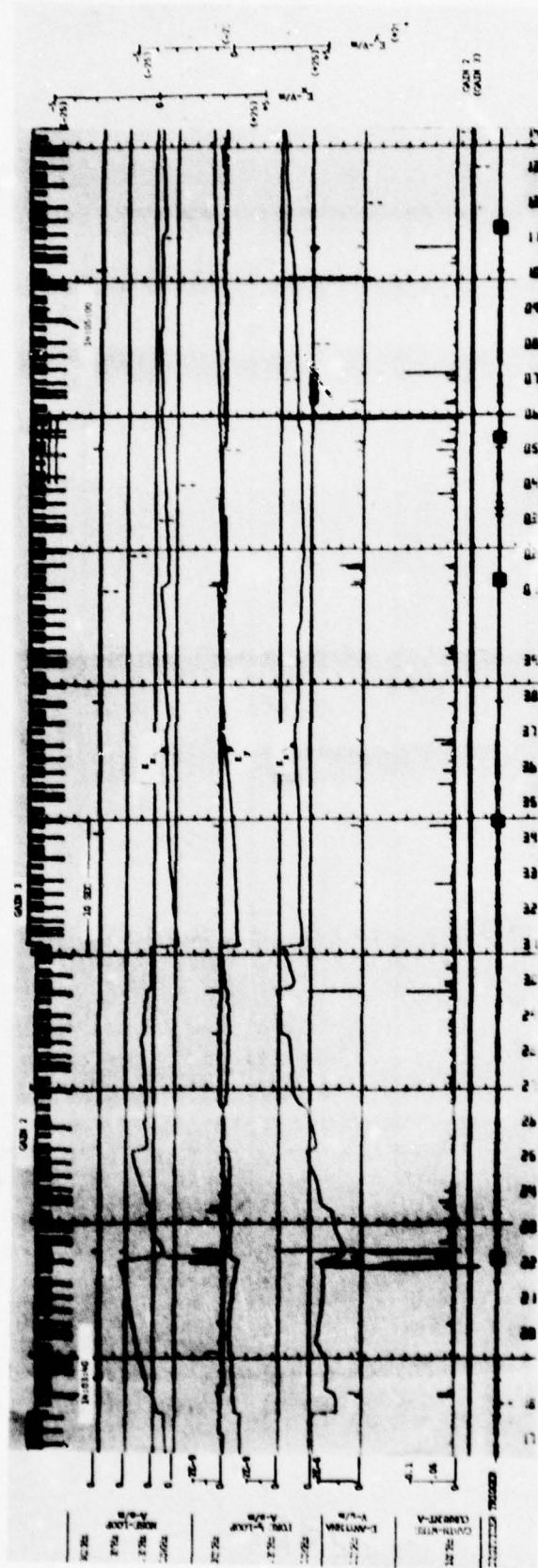


FIGURE 5 SAMPLE OF DATA RECORD FROM ANALOG TAPE RECORDER



Table 2

SENSOR AND INSTRUMENTATION INTERCONNECTION  
FOR FLIGHT OF 10 AUGUST 1977

<u>INSTRUMENTATION</u>	<u>SENSOR</u>
Spectrum Analyzer 1	H-Field Antenna (Nose Loop)
Spectrum Analyzer 2	Forward Fuselage Skin Current (forward 1/2 loop)
Spectrum Analyzer 3	E-Antenna
Spectrum Analyzer 4	Cabin Wire Current
Transient Digitizer 1	E-Antenna
Transient Digitizer 2	--

The outputs of the spectrum analyzer channels are identified on the right side of Figure 5. In general, the record for each channel consists of a zero baseline with upward excursions each time a noise pulse occurs.

The bottom trace in Figure 5 is the voice track filtered to accentuate the 3000-Hz tone bursts generated each time the digitizer was actuated. Five such bursts indicating digitizer actuation occurred in the period covered in the figure.

The electrostatic field changes in the record of Figure 5 indicate the occurrence of lightning flashes. It is important to note that the field component most changed varies from flash to flash which indicates that different charge centers are involved in successive flashes. The magnitudes of the field changes are significant. For example, the flash at time 14:03:50 produced a 2 kV/m field change in  $E_x$  (the component most affected). Since nearby lightning in the 1976 tests produced single-component static-field changes ranging from 15 to 50 kV/m, it is intriguing to speculate as to why the field changes evident in this data are so much smaller, particularly in view of the fact that a review of all of the data taken on the flight shows that the field changes evident in Figure 5, are in fact the largest field changes observed throughout the entire flight.

Examination of the behavior of the various frequency components comprising the pulse generated by lightning indicates that the smaller

quasi-static field-change magnitude observed in 1977 is most likely a result of larger aircraft-to-stroke separation distances. This examination suggests that the 1976 quasi-static field-change magnitudes are consistent with the 4 to 5 km aircraft-to-cell-center closest-approach distances typical of the 1975 and 1976 test aircraft flight tracks. The smaller quasi-static field-changes in Figure 5 are probably a result of doubled aircraft-to-stroke distances. The smaller change amplitudes may possibly be the result of aircraft operations in the critical 5 to 6 km distance from the lightning where the quasi-static signal from an intracloud flash reverses polarity. (See Figure 2 of Section 15 of Reference 8)

It is also interesting to note from Figure 5, that there is appreciable variation from flash to flash in the amount of RF noise generated in the aircraft. For example, the flash occurring at time 14:03:50 produced substantial noise signals in all of the sensors; the flash occurring at 14:03:58.7 produced virtually no reaction in any of the sensors. The static field changes associated with these two flashes differed only by a factor of two. Some of the gross differences in generated noise are a natural result of differences in the radiation source; i.e., was it a cloud-to-ground, or intracloud stroke? Even for a particular stroke type in which a specific amount of charge is neutralized, it is reasonable to expect substantial differences in the character of the RF noise from stroke to stroke because the HF signals are generated, not by the main current flow, but by transient processes leading up to the main discharge.

A further observation of interest in Figure 5 is the nature of the signals that caused the digitizer to trigger. The first triggering is definitely associated with the lightning flash that occurred at 14:03:50, which generated high noise signal levels in all of the sensors. The second and fourth digitizer triggerings, on the other hand, do not appear to be associated with a nearby lightning event since there is no evidence of an electrostatic field change at the times the noise pulses triggered the digitizer. The third and fifth triggerings have associated with them step changes in electrostatic field so that it is likely that they were caused by nearby lightning flashes. In general, an examination of Figure 5 indicates that the digitizer performs the way an oscilloscope normally would if it were set to trigger on low-level signals. It simply generates a sampling of signals that exceed the triggering level.

The record of Figure 5 points out the shortcomings of the two data recording systems when used alone. The spectrum analyzer provides a continuous record of the electromagnetic events that occurred during the flight. The drawback is that it does not provide high-resolution information about the processes that occurred. The transient digitizer,

on the other hand, is capable of generating wide-band, time-domain records of the electromagnetic signals. Unfortunately, these are of short duration so that it is not possible to put them in context in relation to where in a flash they were recorded, or whether the flash under observation was typical of the most severe conditions, or whether the flash was a minor one. By combining the two measurement techniques, as was done in the present program, it was possible to eliminate many of these drawbacks.

A lightning event from the flight of 10 August 1977 recorded both on the spectrum analyzer system and on the transient digitizer illustrates the way in which the two basic measurement techniques complement one another. In addition, the data demonstrate some of the shortcomings of the general system employed on the test jet aircraft.

Figure 6 shows a record generated by lightning events starting at about 15:15:50. In particular, the static field change associated with a flash that occurred at 15:18:59 is evident in the record. The bottom trace in the record indicates that the digitizer was triggered by the electromagnetic transient associated with this flash. The record shown in Figure 6 also shows that there were numerous other electromagnetic pulses at this general time--mostly associated with lightning flashes as evidenced by static field changes--but only the flash at 15:18:59 triggered the digitizer.

Data from the period starting at time 15:18:59 are shown at a faster oscillograph writing rate in Figure 7.

The apparent time delay between the beginning of the digitizer trigger pulse and the lightning event should be ignored. The delay occurs because the trigger pulse was recorded on the voice track, which uses the same head for recording and playback, while the data tracks are played back on separate heads located downstream of the record heads.

An interesting feature of the noise pulse signals in Figure 7 is that perceptible noise starts at roughly 15:18:59.025 and increases intensity until it stops abruptly at 15:18:59.065--probably the time of the return stroke. This behavior is consistent with the observation that HF components of the radiation associated with a lightning stroke are generated by the formative processes occurring prior to the return stroke.

The digitizer record corresponding to the stroke of Figure 7 is shown in Figure 8. Although we cannot be sure, the rise time of the pulse (0.5  $\mu$ s) and its general form are consistent with the transient







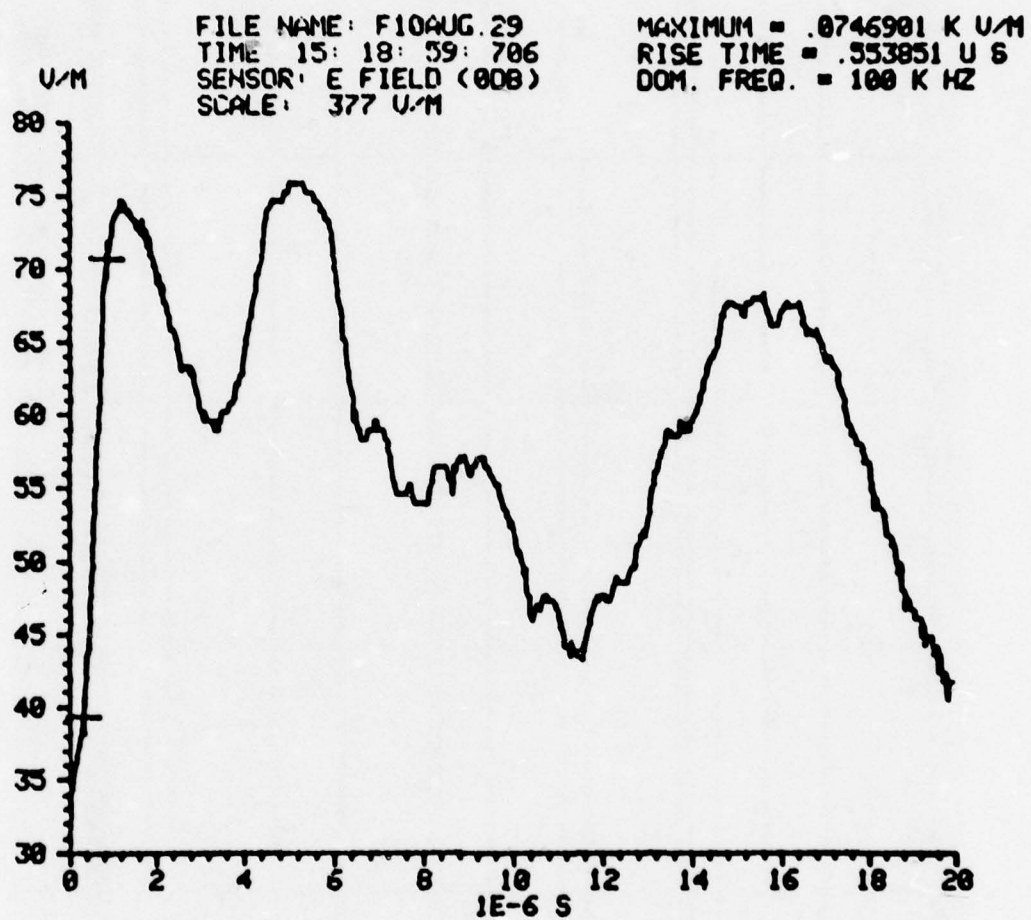


FIGURE 8 DIGITIZER RECORD CORRESPONDING TO STROKE OF LIGHTNING OF FIGURE 7



signal generated by a cloud-to-ground lightning stroke. Note also that the peak field intensity of 75 V/m is suggestive of either a close (i.e., 6 to 8 km) intracloud stroke or a more distant ( $\sim 24$  km) cloud-to-ground stroke. The digitizer was self-triggered by the energetic low-frequency portion of the stroke, and missed the precursor activity.

The Fourier transform of the digitizer record is shown in Figure 9. This plot confirms the earlier observation that the high-amplitude, lower-frequency signals associated with the return current portion of the stroke completely dominate the transient digitizer record so that no spectral components are indicated above a frequency of 3.2 MHz.

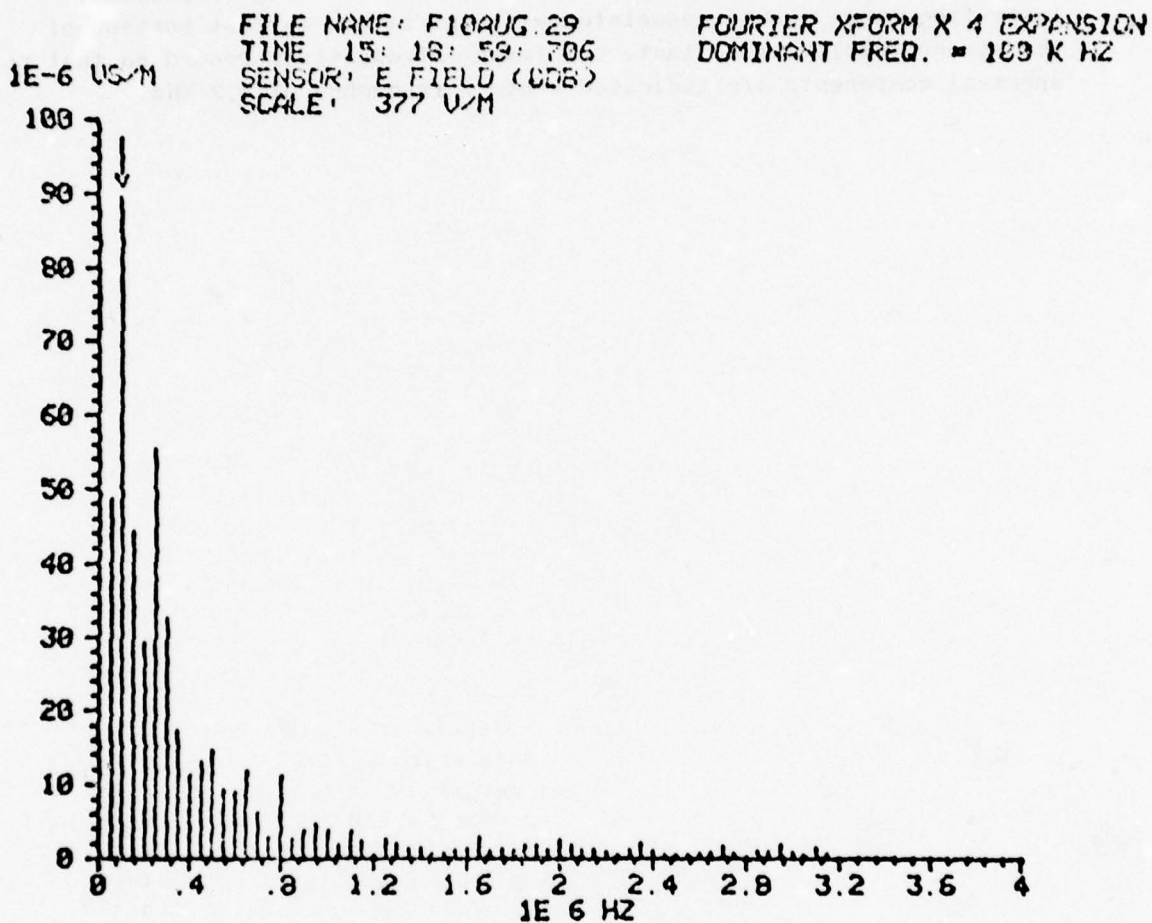


FIGURE 9 FOURIER TRANSFORM OF TRANSIENT DIGITIZER RECORD

#### IV CONCLUSIONS AND RECOMMENDATIONS

A comparison of signals induced in the cabin wire by nearby lightning with signals generated by a direct stroke to the aircraft indicated that the nearby lightning was almost as serious (within a factor of two) a source of interference as the direct stroke. The noise pulse levels were equivalent to those that would be produced by a 1.0 Amp current step in the wire.

The 1976 tests illustrated improvements in the instrumentation system that would permit additional important questions regarding both the noise sources associated with thunderstorm cells and the signals induced in aircraft system to be answered. First, the nature of a typical lightning flash is such that many high-speed events occur over a substantial time period. Thus, the digitizer and spectrum analyzer should be operated together on each flight so that the continuous spectrum analyzer records provide the continuity that puts the transient digitizer records into the proper perspective regarding where during the overall flash the digitizer record was made.

The concept of using a continuously-operating spectrum analyzer in conjunction with a periodically-fired transient digitizer was implemented in the tests of 1977 and proved to be sound and effective because one measurement technique complemented the other.

The scarcity of suitable thunderstorm activity in 1977 caused the measurement program to proceed substantially slower than normal. As a result, it was not possible to carry out measurements using many of the combinations of sensors installed to gain insight into the way in which the airframe is excited and noise pulses couple to the interior. Sometimes a given combination of sensors would be flown on a succession of flights and yield no useful data because the thunderstorm cells being investigated decayed before they produced lightning.

In the data investigated thus far, the spectrum analyzer records indicate that the high frequency noise signals which ultimately couple to the interior of the aircraft are generated primarily at the beginning of the lightning stroke, and that the activity responsible for their generation is quenched at the time of the return stroke. Comparing the spectrum analyzer records with those generated on the transient digitizer system (see, for example, Figure 8) points out a shortcoming associated with the use of oscilloscope-like instruments to record lightning activity. The digitizer was self-triggered by the energetic, low-frequency portion of the stroke and missed the precursor activity responsible for the generation of the HF noise in the spectrum analyzer records. The digitizer also failed to record the overall (i.e., late time) pulse shape. Shedding light on the nature of the high-frequency precursor activity was one of the objectives established for the digitizer system. Such information is needed to properly characterize signals coupling to the interior of the aircraft through apertures and pulse shape information would make possible some differentiation of different kinds of strokes.



If transient digitizers are used in future flight tests, it would be wise to arrange a separate triggering system that uses the onset of high frequency noise--such as the cabin wire current signal of Figure 7--to trigger the sweep. In many strokes, the HF noise persisted in the cabin wire channel for roughly 40 ms before the return-current portion of the stroke. Triggering up to tens of milliseconds before the high-current part of the stroke should provide important insights into the early-time behavior of lightning strokes. It might also be desirable to devote two digitizer channels to a single measurement point to be able to obtain good time resolution of the early time events while at the same time being able to define the overall lightning waveform.

#### REFERENCES

1. R. T. Bly, Jr. and J. E. Nanevich, "Aerial Measurements of the Electric Field in the Vicinity of Florida Thunderstorms: Analysis and Results," Final Report, Contract NAS10-9013, SRI Project 5537, Stanford Research Institute, Menlo Park, CA (June 1977).
2. J. E. Nanevich, R. C. Adamo, and R. T. Bly, Jr., "Airborne Measurement of Electromagnetic Environment near Thunderstorm Cells (TRIP-76)," Final Report, Contract NAS9-15101, SRI Project 5536, Stanford Research Institute, Menlo Park, CA (March 1977).
3. J. E. Nanevich, R. T. Bly, Jr. and R. C. Adamo, "Airborne Measurement of the Electromagnetic Environment Near Thunderstorm Cells," 1977 IEEE International Symposium on Electromagnetic Compatibility, Seattle, WN (August 2-4 1977).
4. J. E. Nanevich, "Analysis of Electrical Transients Created by Lightning," Final Report (in preparation), Contract NAS1-13792, SRI Project 4026-100, Stanford Research Institute, Menlo Park, CA (June 1978).
5. R. L. Tanner and J. E. Nanevich, "An Analysis of Corona-Generated Interference," Proc. IEEE, Vol. 52, No. 1 (January 1964).
6. J. E. Nanevich and R. L. Tanner, "Some Techniques for the Elimination of Corona Discharge Noise in Aircraft Antennas," Proc. IEEE, Vol. 52, No. 1 (January 1964).
7. N. Cianos, E. T. Pierce, "Methods for Lightning Warning and Avoidance," Technical Report 1, Contract 6-73-300H, SRI Project 3057, Stanford Research Institute, Menlo Park, CA (May 1974).
8. R. H. Golde, Lightning, Volume 2 Lightning Protection, Academic Press, New York (1977).

APPENDIX

LEAKAGE THROUGH SHORT CYLINDRICAL CABLE SHIELDS\*

\* Abstracted from E. F. Vance "Transient Tests of Candidate Safeguard Cables," Final Technical Report Contract DAEA18-71-A-0204, SRI Project 1405, Stanford Research Institute, Menlo Park, California (November 1971).



## APPENDIX

### LEAKAGE THROUGH SHORT CYLINDRICAL CABLE SHIELDS

#### A. Experimental Setup

An experimental setup that has been used to make laboratory measurements of the transfer impedance of shielded cables is shown in Figure A-1. A current pulse in the cable shield is produced by charging a 2- $\mu$ F capacitor until a spark-gap switch fires and discharges the capacitor through the cable shield. The discharge current returns to the capacitor through an aluminum tube concentric with the cable. A  $\text{CuSO}_4$  resistor in series with the capacitor has a value approximately equal to the characteristic impedance of the transmission line formed by the test cable and the aluminum tube, so that oscillation of this line is limited (the cable shield being tested and the tube are short-circuited at the instrumentation box). The current in the 3.2-meter-long test cable is measured with a Pearson Model 310 current probe near the instrumentation box. The shields and the coaxial center conductors are short-circuited at the end of the cable where the spark-gap electrode is attached. The core wires are open-circuited inside the instrumentation box.

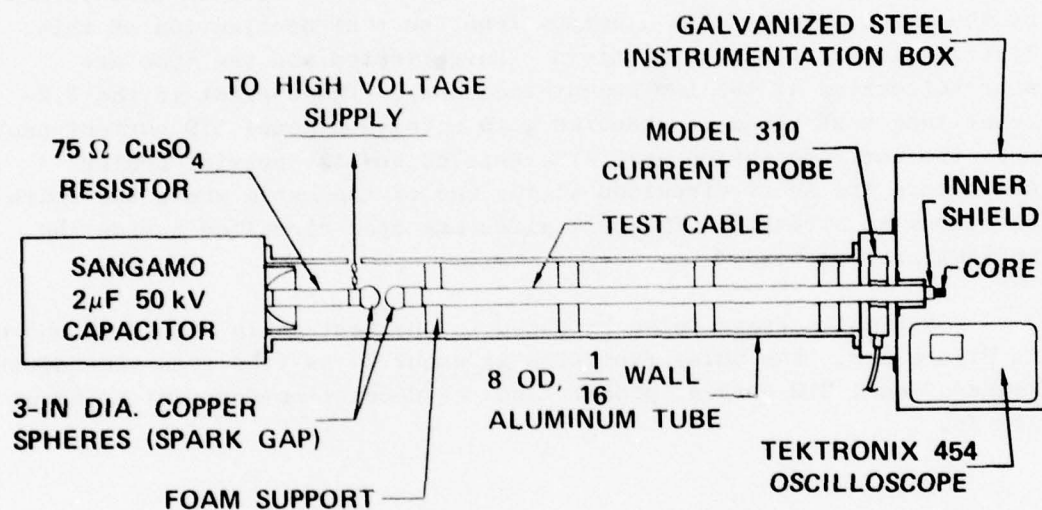
A typical current pulse produced in the test-cable shield is shown in Figure A-2. The pulse rise time is about 20 ns (the rise time of the Pearson Model 310 current probe), and the decay time-constant is about 140  $\mu$ s.

#### B. Cable Characteristics

The work discussed in this appendix was undertaken to determine the shielding effectiveness of two cables with different shield designs.

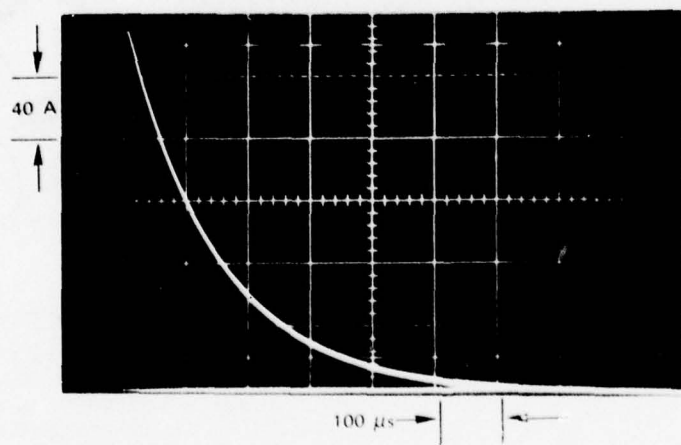
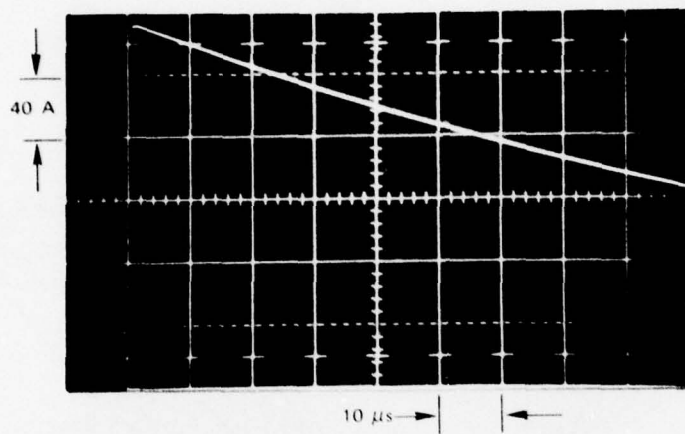
The construction of cable 1 is shown in Figure A-3. This cable is doubly-shielded, with an outer shield of 24-mil-thick copper and an inner shield of 24-mil-thick mild steel. Both shields have continuously welded seams so that they behave electrically as solid-walled shields.

The construction of cable 2 is shown in Figure A-4. This cable is also doubly-shielded, with an outer shield composed of a double layer of counter-spiraled, copper-clad steel straps, and an inner shield of 6.5-mil-thick mild steel with a longitudinal overlapped seam.



TA-7995-120

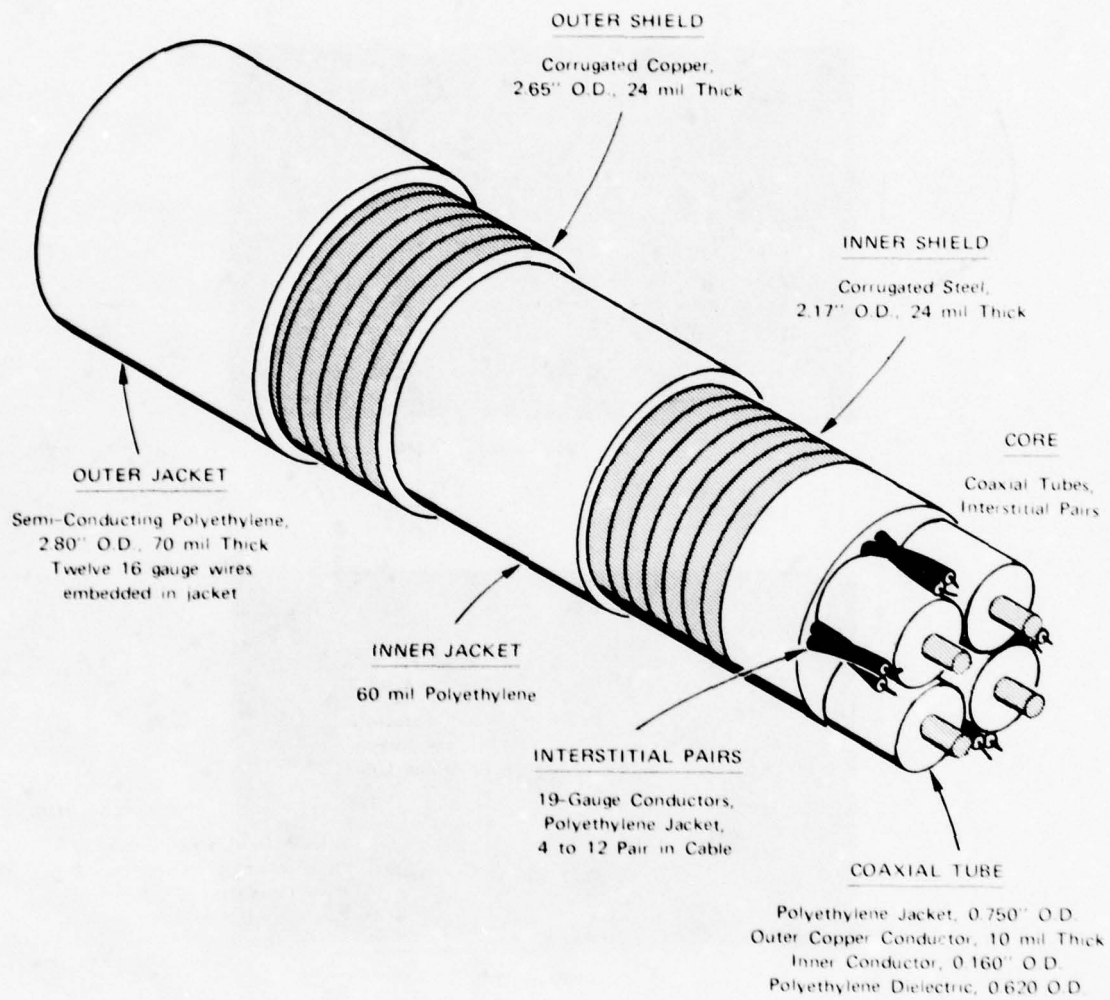
FIGURE A-1 LABORATORY TEST APPARATUS FOR MEASURING TRANSFER IMPEDANCE



TA 1404-3

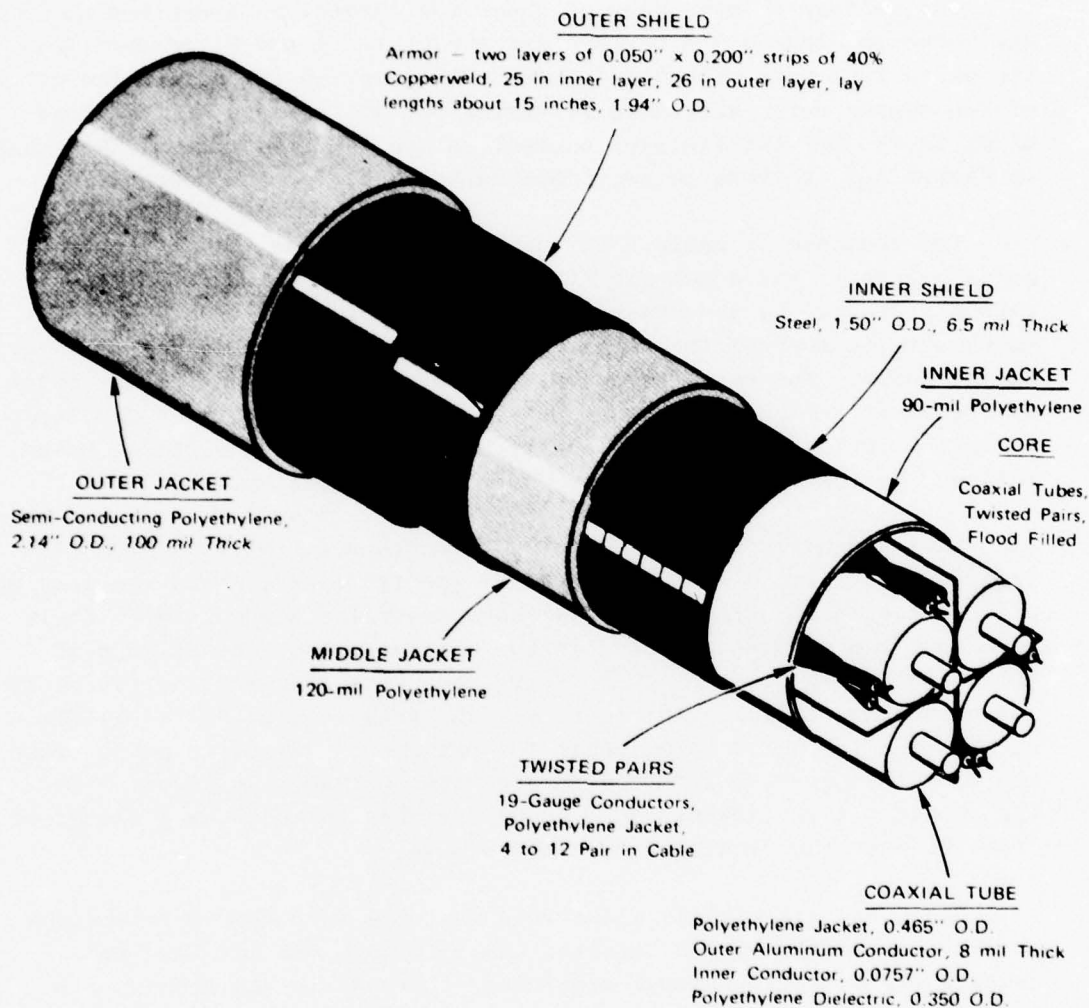
FIGURE A-2 CURRENT WAVEFORM IN CABLE SHIELD





TA 1404 1

FIGURE A-3 CUTAWAY SHOWING CONSTRUCTION OF CABLE 1



TA-1404-2

FIGURE A-4 CUTAWAY SHOWING CONSTRUCTION OF CABLE 2

The tests described here are designed to determine the leakage through the outer shields of these cables.

### C. Test Results

The voltage pulses measured under the conditions described above are shown in Figures A-5 and A-6 for the cables 1 and 2, respectively. The pulse responses of cable 1 shown in Figure A-5 illustrate the effect of the copper outer shield in filtering out the effects of the large  $dI/dt$  in the driving (shield) current, since the rise time of the voltage in Figure A-5 is about 10  $\mu$ s, compared to 20 ns for the current.

The response of cable 2 is quite different from that of cable 1, as is apparent from comparing Figure A-5 and A-6. This difference is caused primarily by the construction of the outer shield of cable 2 which permits some of the large  $dI/dt$  energy to penetrate to the interior of the cable. The penetration of the fast-rising portion of the pulse is apparent in Figure A-6, where it is seen that the voltage developed along the inside of the outer shield has a fast-rising negative pulse, followed by the slower diffusion-controlled positive pulse.

That the outer shield of cable 2 permits penetration of the high frequencies (large  $dI/dt$ ), is apparent in Figure A-7, where the leading edge of the pulse of Figure A-6 is shown greatly expanded. Here it is seen that a damped 24-MHz oscillation dominates the leading edge of the pulse (24-MHz is the quarter-wave resonance frequency of the shorted 3.2-meter-long cable). In Figure A-7 the peak voltage of the 24-MHz oscillation is over 3 volts, while the peak of the diffused pulse after the oscillations have subsided is less than 0.1 volt in Figure A-6. The voltage at the resonance frequency is thus enhanced by a factor of about 30 over the remainder of the response.

These results clearly illustrate the effect of the imperfections on the electromagnetic energy that leaks through the shield. This leakage which occurs through apertures or cracks in the shield, can be represented by a mutual inductance and mutual capacitance between the circuit inside the cylinder and the circuit outside the cylinder. Thus, the voltage induced by the shield current  $I_s$  can be written  $V = j\omega M I_s$  and the current induced by the shield voltage  $V_o$  (or charge  $Q_o$ ) can be written  $I = j\omega C V_o = j\omega C Q_o / C_o$ . Hence if the shield excitation contains high frequencies, these high frequencies tend to dominate the internal conductor response. This dominance was noted in the test results for cable 2 even though its shield had almost 100 percent optical coverage. Similar responses are to be expected for aircraft fuselage and wing wiring due to windows, access plates, and riveted or bolted joints in the skin.



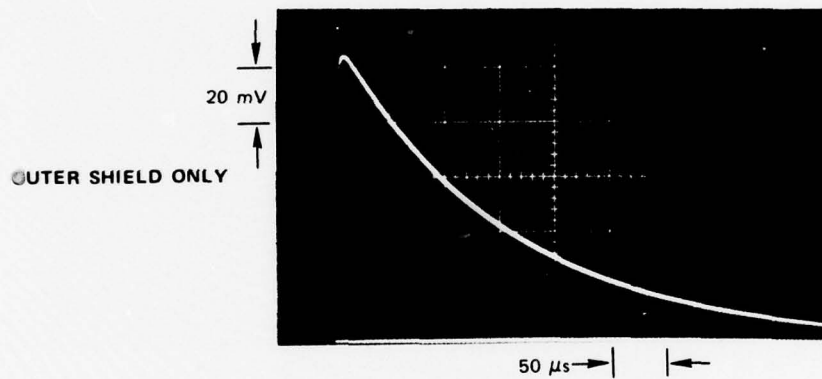


FIGURE A-5 INTERNAL VOLTAGES PRODUCED IN CABLE 1  
BY A 220A PEAK-CURRENT PULSE

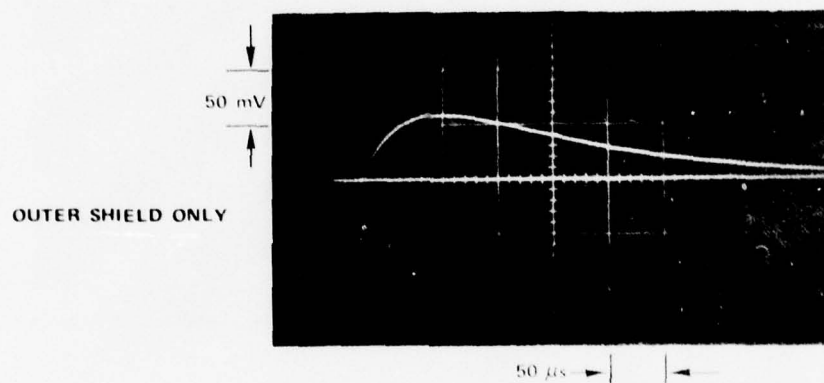


FIGURE A-6 INTERNAL VOLTAGE PULSES PRODUCED IN CABLE 2  
BY A 184A PEAK-CURRENT PULSE

OUTER SHIELD ONLY

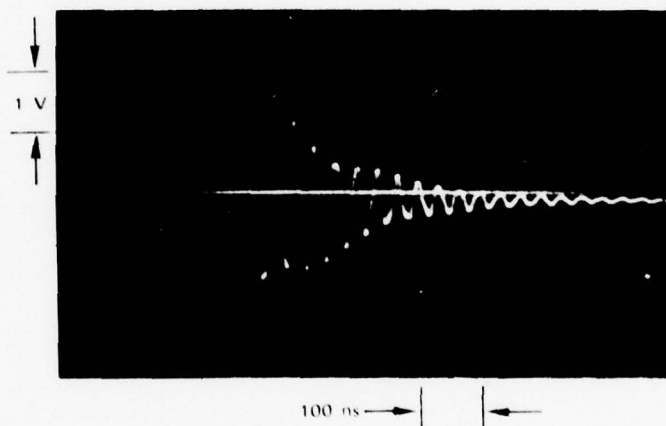


FIGURE A-7 LEADING EDGES OF THE INDUCED-VOLTAGE PULSE OF FIGURE A-6



IN-FLIGHT LIGHTNING DATA MEASUREMENT  
SYSTEM FOR FLEET APPLICATION

BY

G.J. Von Bokern, L.D. Piszker, and R.O. Brick

The Boeing Company  
Seattle, Washington

Presented At  
Federal Aviation Administration/  
Georgia Institute of Technology

Workshop on Grounding and Lightning Protection

## ABSTRACT

The development status of an in-flight lightning strike instrumentation system is presented. The instrumentation is designed to record the transitory properties of the lightning waveform at a time interval centered on the attachment to the host aircraft. The system is intended to be installed on a large number of aircraft to achieve an adequate statistical characterization of the random elements of lightning. A "modular" system is employed whereby sense elements can be added, subtracted or modified to meet a given set of requirements.

## IN-FLIGHT LIGHTNING DATA MEASUREMENT SYSTEM FOR FLEET APPLICATION

G.J. Von Bokern, L.D. Piszker, and R.O. Brick

### INTRODUCTION

An in-flight data measurement system is proposed to advance current knowledge of the aircraft lightning environment.

Aircraft lightning protection design and test criteria have been primarily based on laboratory reproduction of in-service structural damage, supported by data recorded by academic researches at the ground terminal of a lightning discharge. Although a complete knowledge of natural lightning does not exist, adequate design and test criteria have been developed for the protection of aluminum aircraft containing relatively insensitive circuitry.

Recent trends in airplane design require more complete knowledge of the interaction of the aerospace vehicle with the true lightning environment. Increased traffic densities around airports may require more time in holding patterns; hence, more exposure to the altitude region (8,000 to 15,000 feet) in which most strikes to aircraft occur. The greater use of fiberglass, boron and graphite composites, and other non-metals in structure will require re-examination of lightning protection techniques to assure control exists for the electromagnetic field penetration into the interior of the aircraft. The increased reliance on solid-state electronics in the communications, navigation, guidance and flight control systems of advanced technology airplanes implies a need to understand the susceptibility of these circuits to electromagnetic transients associated with a lightning strike.

The ultimate objective is the complete definition of the natural lightning characteristics as related to their effects on aerospace vehicles. This is a long-term goal, however. The immediate objective is the development of an in-flight lightning strike instrumentation to record temporal properties of the lightning waveform at a time interval centered on the attachment to the aircraft. The unit will be designed as a low-cost item that can be installed on a large number of aircraft to achieve an adequate statistical characterization of the random element of lightning.



Fleet wide application of a data logging system implies several constraints normally not applicable to dedicated instrumented aircraft. Cost, maintainence, and reliability must all be considered. It is also highly desirable to construct the unit to be as self sufficient as possible. Normal flight workload dictates that active monitoring of peripheral devices by flight personnel is not usually feasible. Also, since the construction of any aircraft is a fairly controlled procedure, the logistics of mounting and routing extensive sensing configurations is to be avoided.

With these constraints in mind the instrumentation objectives are given as:

- Low Cost
- High Reliability
- Modular Architecture
- Self Sufficient
- Pre- and Post-Trigger Recording
- Reliable Reference (Trigger) Detector

The total system block diagram is given in Figure 1. This system can be broken down into three main subsystems: 1) Sensors, 2) The Front-End and 3) The Data Logger.

#### THE PROTOTYPE SENSOR SYSTEM

A system of five sensors has been selected to obtain information about lightning strikes to aircraft. The sensor system consists of three magnetic field sensors, each in the form of a shorted turn, one relatively long shielded cable, and one flush mounted electric field sensor. The sensor system is intended to provide the following information:

- a) The time history and amplitude of the lightning current.
- b) The main electrical path of the lightning current on the aircraft structure.
- c) The induced voltage in a shielded wire.
- d) The electric field normal to the fuselage at one location.

This information will be determined by analysis of the sensor output signals. A detailed knowledge of the aircraft and sensor frequency response to a direct strike is required.

Figure 2 shows the approximate locations of the sensors in a Boeing 747 aircraft. The exact location and physical make-up (size) of the sensors will be dependent on the model of the aircraft used. Sensors will be installed in the aft and rear sections of the fuselage and in the outboard areas of the wing, but not too close to areas of direct attachment of the lightning flash.

The sensor system is based on frequency domain modeling and tests performed on Boeing 747 and 727 wing structures and components. The models were developed for the case of direct lightning attachment. It is well known that the current density ( $J_s$ ) through any cross section of an aircraft structure will not be uniform. The waveform of ( $J_s$ ) on primary structural elements can be approximated as the sum of signals which are the lightning current and one or more high frequency responses due to resonances in the aircraft structure.

The magnetic field ( $H_s$ ) of the aircraft structure current will couple through apertures in the aircraft skin. If the apertures are electrically small the internal magnetic field ( $H_I$ ) will have the same waveform as the aircraft structural current ( $J_s$ ). The magnitude of ( $H_I$ )/( $H_s$ ) will be less than one. It will also be dependent on location but will be constant over the frequency range of interest.

The three magnetic field sensors in the form of shorted turns and the shielded cable sensor will be installed in areas of the aircraft where internal magnetic fields ( $H_I$ ) are strong.

Figure 3 shows a shorted turn sensor (loop antenna shorted at its ends) installed in the leading edge of the 747 wing. The shorted turn is intended to be one to three meters long. The first resonance of the circuit will be above the frequency range of the front end subsystem (i.e. 20 MHz). The open circuit voltage of the loop follows Faraday's law. If the inductance of the loop is greater than its resistance, the short-circuit current in the

loop has the same waveform as the internal magnetic field ( $H_1$ ). Therefore, by using the appropriate current probe and loop area, the structural current waveform is reproduced directly over the frequency range of interest.

An alternate approach is to measure the structural current directly. Figure 4 shows two possibilities. A skin current probe may be used on the front or rear spars of the wing box or on a longitudinal member such as a span-wise cable channel.

Figure 5 contains a simplified schematic of the shielded cable sensor. The cable will be installed along the front or rear spar in an area where the internal magnetic field is strong. The shield of the cable will be connected to the structure at both ends forming a relatively large shorted turn. The core-wires of the cable will be terminated in the common-mode characteristic impedance of the cable.

The core-wire voltage will be measured directly, and can be related to the current flowing on the cable shield. A knowledge of the transfer impedance and transmission line properties of the shield is required. The waveform of the shield current will be the same as the aircraft structure current except for the high frequency resonances associated with the cable shield itself. Magnetic flux coupling must be the dominant cable driving mechanism. That is, sensitivity to E-field must be minimized.

The data from the three shorted turns (H-field sensors) and coaxial cable will be used to define the gross path of the lightning current path on the aircraft. A large signal on any two sensors, and a relatively small signal on the others should indicate one of six paths (wing tip to wing tip, left/right wing tip to nose/tail, and nose to tail). It appears possible to identify an engine nacelle strike if a large signal is obtained from one of the fuselage magnetic field sensors and the wing sensors exhibit no response.



The E-field sensor will be a standard type blade or plate antenna which is electrically small with respect to the frequencies of interest. The antenna will probably be installed at the central area of the fuselage as shown in Figure 2. The output voltage of the sensor will be either proportional to  $E_N$  or its time derivative.

The data storage sequence is to be initiated by a trigger sense system. Frequently, the success or failure in recording a non-repetitive event depends on the reliability of the trigger pulse to initiate the data storage sequence. For lightning, a reference trigger point is difficult to obtain by conventional "leading edge" level detection. Figure 6 illustrates the wide variability in time and amplitude of the lightning E-field waveform. However, as illustrated, the return stroke (R) is a short duration pulse and is responsible for the maximum low frequency E-field amplitude in all known cases. In light of this, a trigger pulse initiated by the return stroke represents a relatively fixed reference in terms of the total lightning signature. This concept is incorporated in the triggering design. The trigger sense system is based on an aircraft lightning strike detector concept developed by Boeing. The unit is sensitive only to an actual attachment to the aircraft and triggers at the point in time of the return stroke.

The sensor system and cables required to connect the sensors to the data logger will be installed in each type or model of aircraft. Simulated lightning tests will be conducted on the ground to determine the response of the sensors and verify the analytical model of the aircraft responses. Sensors will be modified as required to accommodate the dynamic range of the A/D converters.

#### THE PROTOTYPE DATA ACQUISITION SYSTEM

The electronic data acquisition system is divided into two main components: 1) The front-end subsystem and 2) A remote microprocessor controlled data logging system.

The front-end subsystem consists of a high speed (20 MHz) A/D converter, memory, memory control and a serial communication interface (Figures 7 and 8).

The A/D converter is a multi-threshold parallel conversion type. This design architecture was selected on the basis of high speed (i.e. 20 MHz or greater). It is noted that due to the rapid advancement in solid state technology the availability of a low cost 20 MHz A/D converter is expected within a years time. For the present, sacrifices in bit accuracy due to the discrete multi-threshold design can be tolerated on a feasibility study basis.

The memory is organized into several 1024 X 8 bit segments. Each segment is interleaved to enhance memory access time. For any given sensor, the cycle time can be adjusted to accommodate a wide variety of applications without deviating from the basic system architecture. (Cycle time refers to the rate at which data can be stored into successive address locations in memory). The prototype incorporates four of these memory segments. That is, the initial unit will have 4096 X 8 data locations for each sensor.

The memory controller will direct the flow of data through each of the 1024 address locations contained in each segment. The controller has a limited programmable capability. Its addressing sequence may be altered depending on a series of active status inputs. Address control, halt, increment address, test, and internal address storage (i.e. stack) are incorporated into the controller design.

Data is read out of the logging device via a serial (i.e. two wire pair) link. This is accomplished using an UAR/T (universal asynchronous receiver/transmitter) in a handshake mode with the data logging device. (Handshake refers to interactive communication capability between two system components.) The read sequence is again supplied by the memory controller. The data transfer rate is variable for 100 to 8,000 baud.

In actual operation the front-end subsystem will be in continuous operation sampling the sensor output. The trigger signal will initiate a time out

signal whereby the data recording sequence is halted. In this manner, post- and pre-trigger data is saved.

The front-end subsystem constitutes a data logging system in its own right. Each subsystem is capable of logging 4096 bytes of data to be read out upon command of a peripheral recording device in the air or on the ground. The advantage of incorporating an in-flight logging system is that the front-end units can be interrogated and reset for additional strike data. In this manner the entire subsystem is left fully operational and can be interrogated under more convenient conditions.

The data logger is a micro-processor based system incorporating a standard format mass storage tape cassette. The logger will control the polling of each sensor memory and will also create a real-time output which displays selected lightning strike data to in-flight personnel as well as to the maintenance crew. Also, since the logger is micro-programmable reconfigurations in the sensor arrangement do not necessarily imply hardware changes.

Present state-of-the-art technology for low-cost microcircuitry limits the present sampling period to about 50 ns. However, it is intended that the system be designed to accommodate future increases in the sampling rate as well as modifications to the system's configuration. A "modular" structure will be incorporated to maximize the system's flexibility. It is anticipated that the greatest need for this flexibility is in the data logger design as the logger will be responsible for the polling procedures and priority assignments of the various sensing elements. These sensing elements are the modules which can be added or subtracted from the system in order to satisfy a given set of requirements. Each model can then be tailored to fit a given sensing application. Sampling rate, dynamic range, fast data storage, cost, etc., can be weighted as needed.



Currently, a prototype system is under construction and is scheduled for completion in September 1978. The prototype system will be installed in a 747 wing section laboratory setup. Low-level CW and simulated lightning tests will be conducted to verify the initial design concepts.

#### CONCLUDING REMARKS

The intent of this paper is to inform the lightning community of a current effort to expand the lightning environment data base. This instrumentation is not intended to replace current or future research programs but rather to supplement these tasks. It is anticipated the fleet data logging system will greatly enhance statistical data available on the airborne environment. Also, there are obvious advantages of wide geographic data acquisition on the lightning event as well as in a data logging program not bounded in time. To this end we solicit any suggestions concerning the direction and/or design of the fleet wide lightning instrumentation.

#### BIBLIOGRAPHY

- 1) Uman, M.A.; "Lightning," McGraw-Hill, Inc., New York, 1969.
- 2) Clarence, N.D., and D.J. Malan: Preliminary Discharge Processes in Lightning Flashes to Ground, Quart. J.Roy. Meterol. Soc., 83:161-172, 1957.
- 3) Schonland, B.F.J.; The Lightning Discharge, "Handbuch der Physik," Vol. 22, pp. 576-628, Springer-Verlag OHG, Berlin, 1956.
- 4) J.E. Nanevicz R.T. Bly, Jr., R.C. Adamo, Airborne Measurement of Electromagnetic Environment Near Thunderstorm Cells, "1977 IEEE International Symposium on Electromagnetic Compatibility," Seattle, Washington, August 2-4, 1977.
- 5) Measurements of Lightning Strikes to Aircraft, Project No. 520-002-03X, Report No. DS-68-1, Federal Aviation Administration, January, 1968.

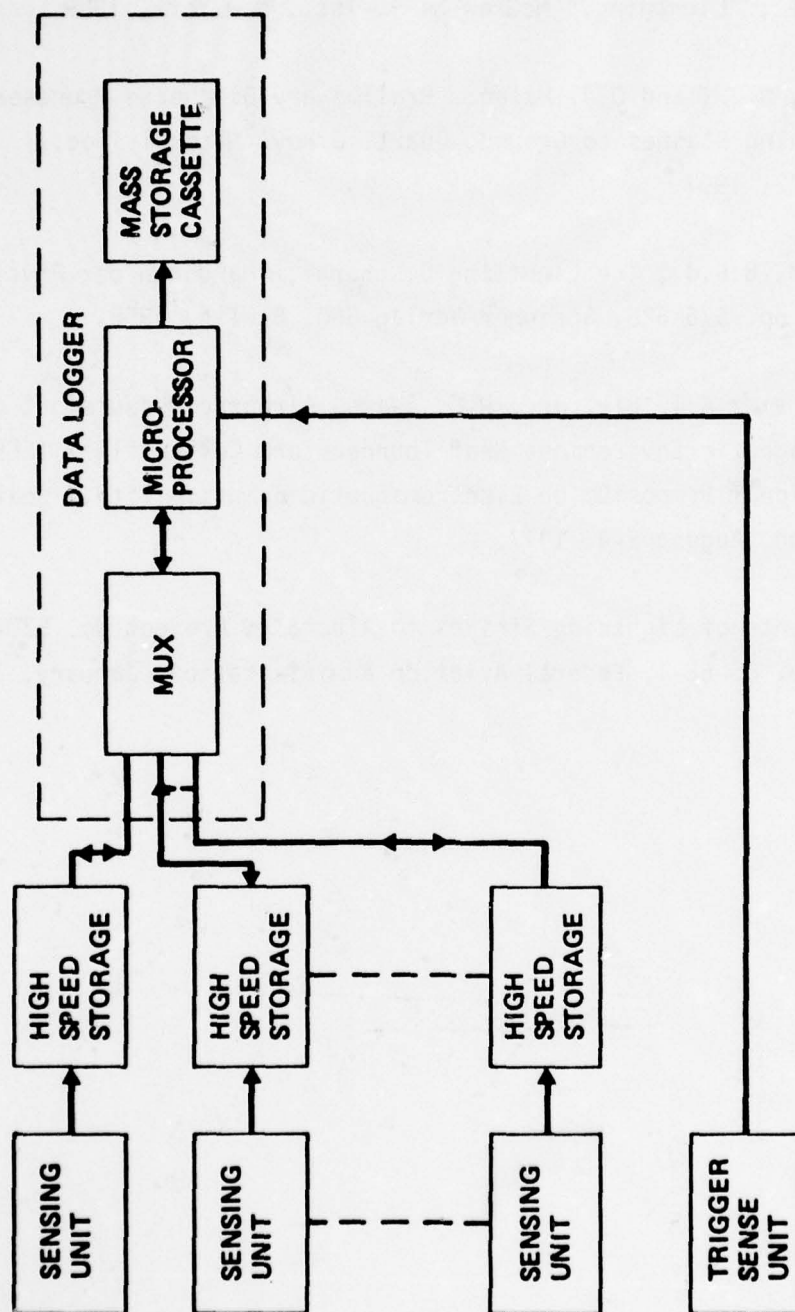


Figure 1. Lightning Strike Instrumentation General Block Diagram



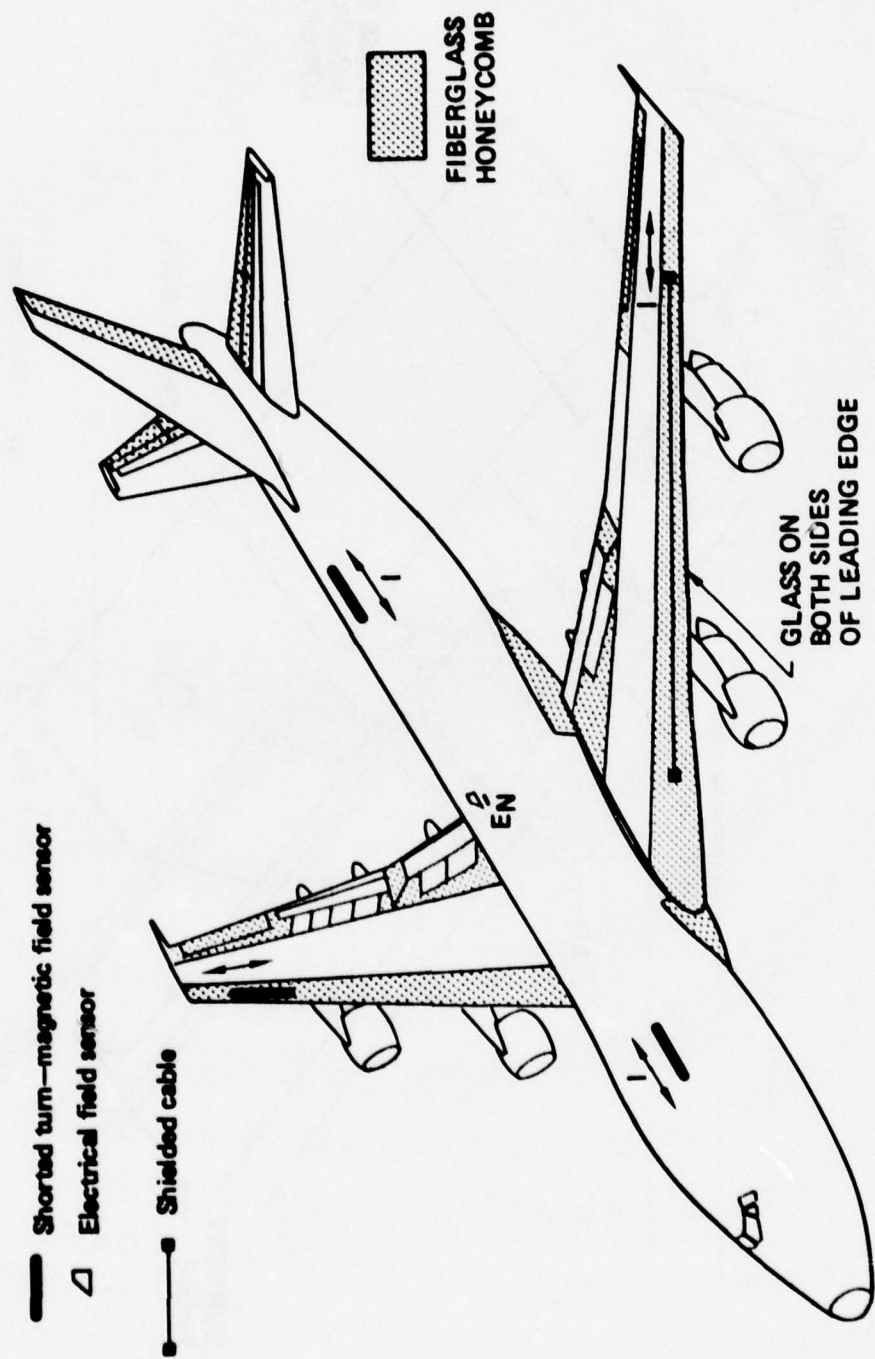


Figure 2. Sensor Locations on a 747 Aircraft—Conceptual

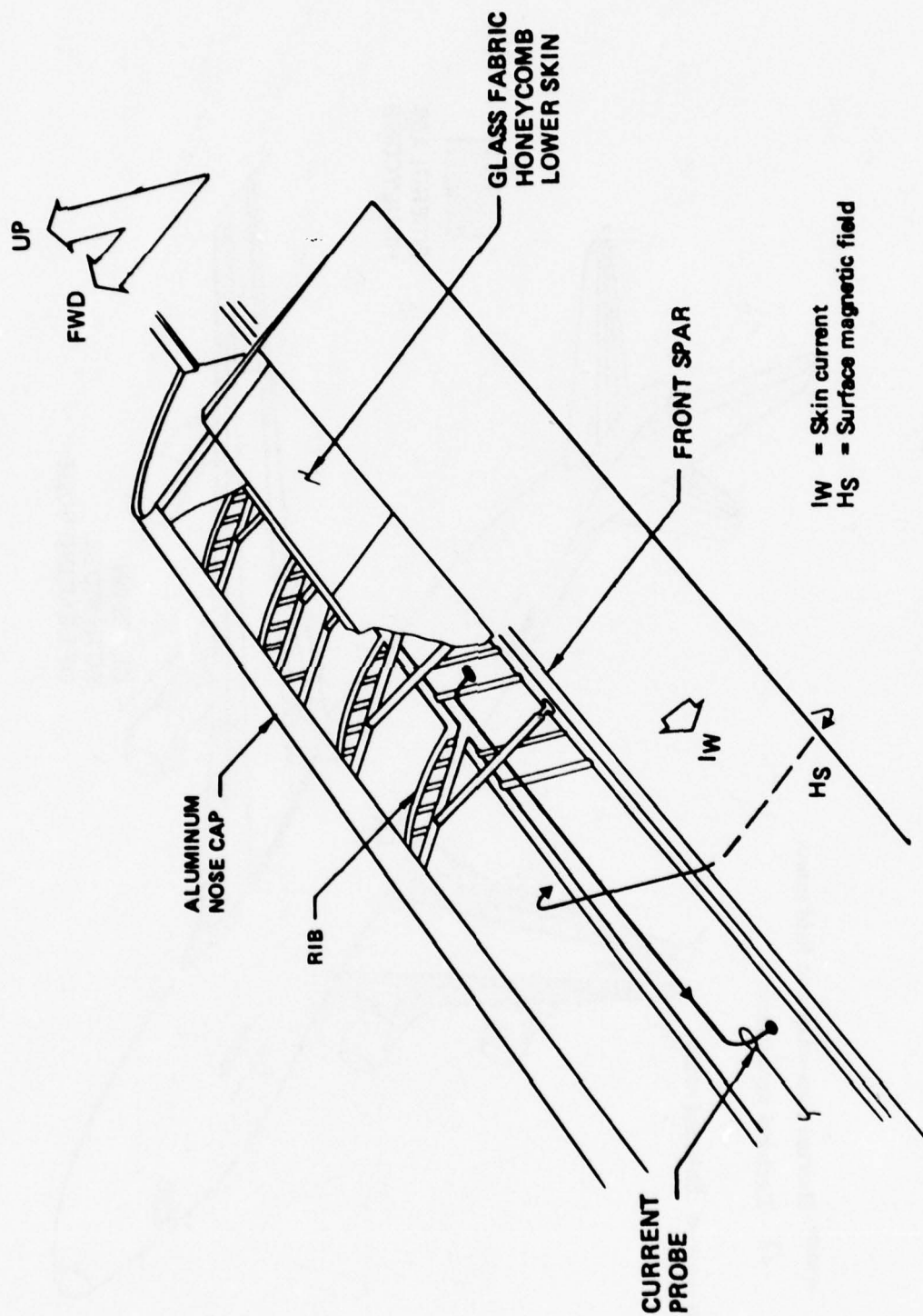
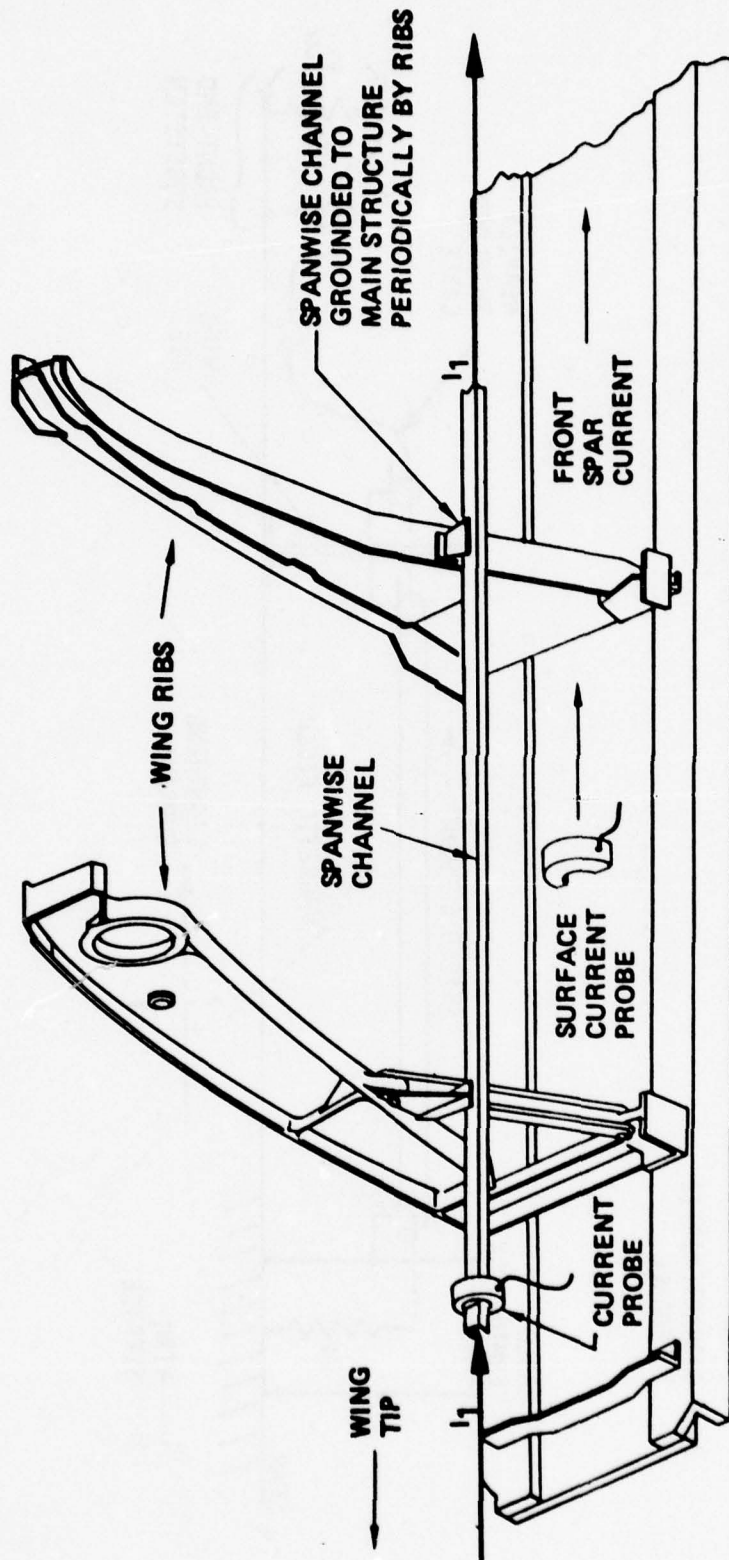


Figure 3. Shorted-Turn Installation—Wing Front Span



$I_1$  = COMMON MODE CURRENT ON SPANWISE CHANNEL = .025 (Iwing)

Figure 4. Current Probe Locations on Wing Structures



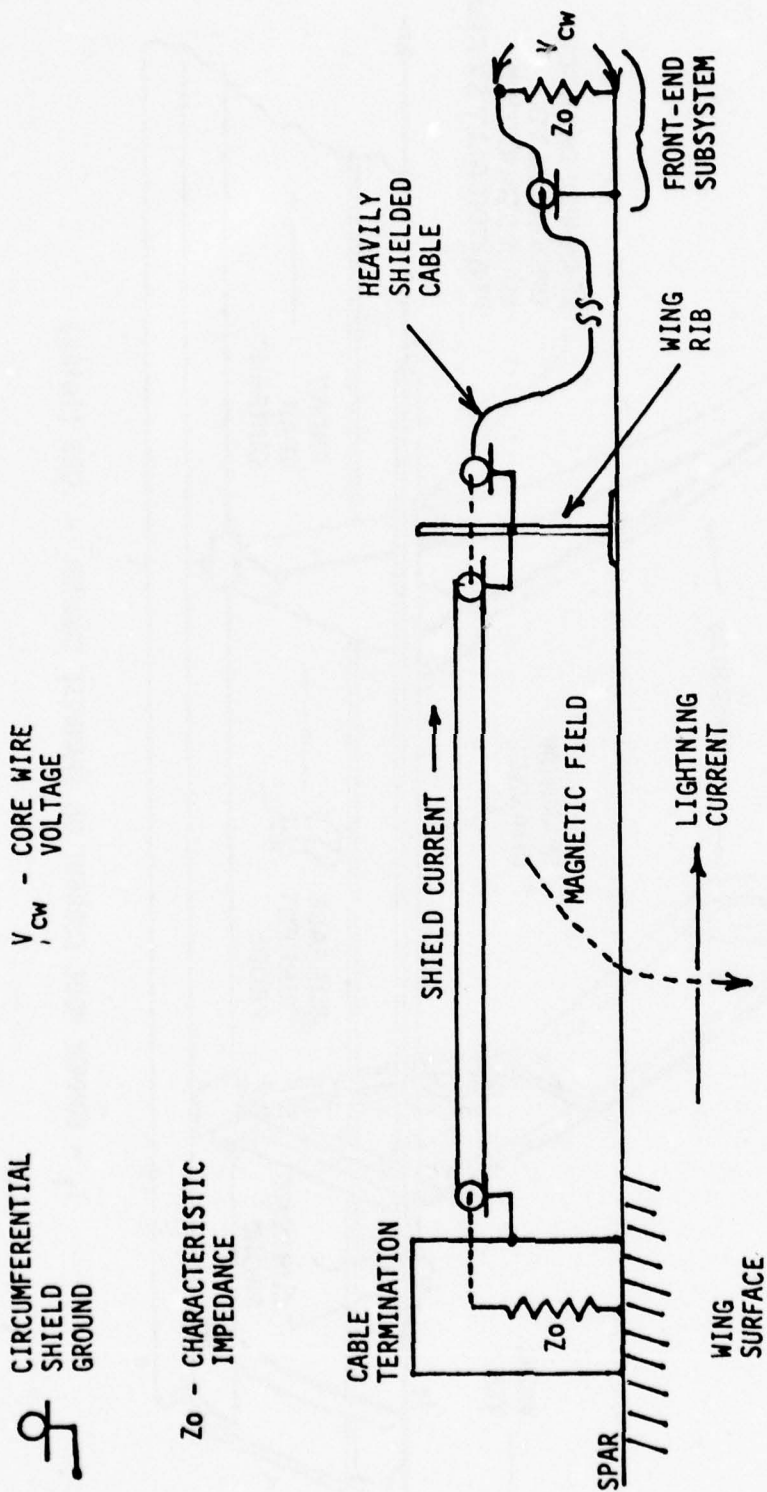


FIGURE 5 SCHEMATIC OF THE SHIELDED CABLE SENSOR

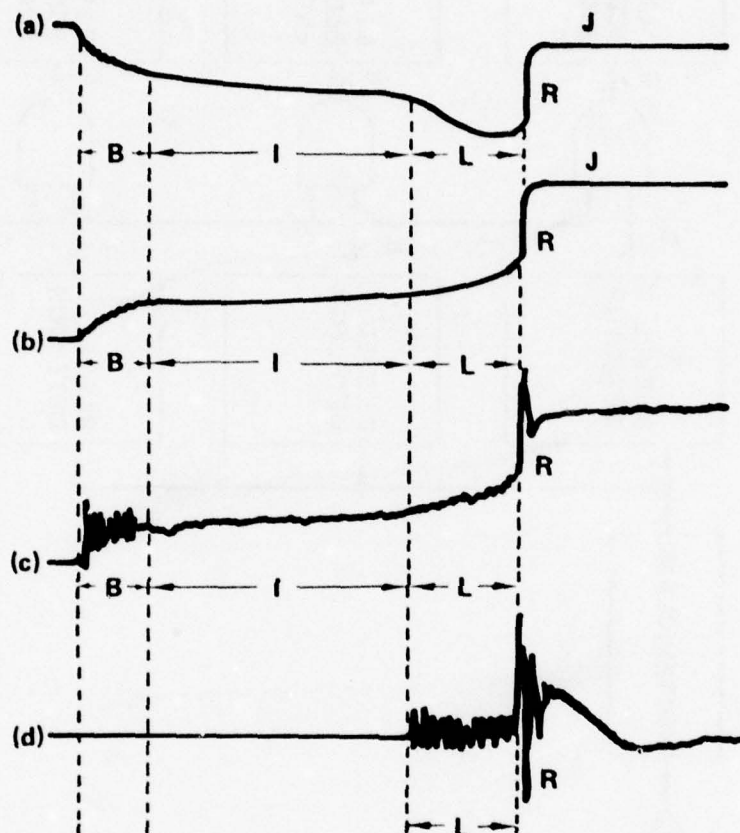


Figure 6. Diagrams of typical field changes of discharges to ground. (a) Electrostatic fields at 2 km. (b) Electrostatic fields at 5 km. (c) Electrostatic, intermediate, and radiation fields at 50 km. The relative amplitude of the R part has been reduced. (d) Radiation fields at 500 km in frequency band 200 Hz to 20 kHz. Durations: B from 2 to 10 ms; I from 0 to 400 ms; L from 4 to 30 ms. (Adapted from Clarence and Malan (1957) and Schonland (1956).)

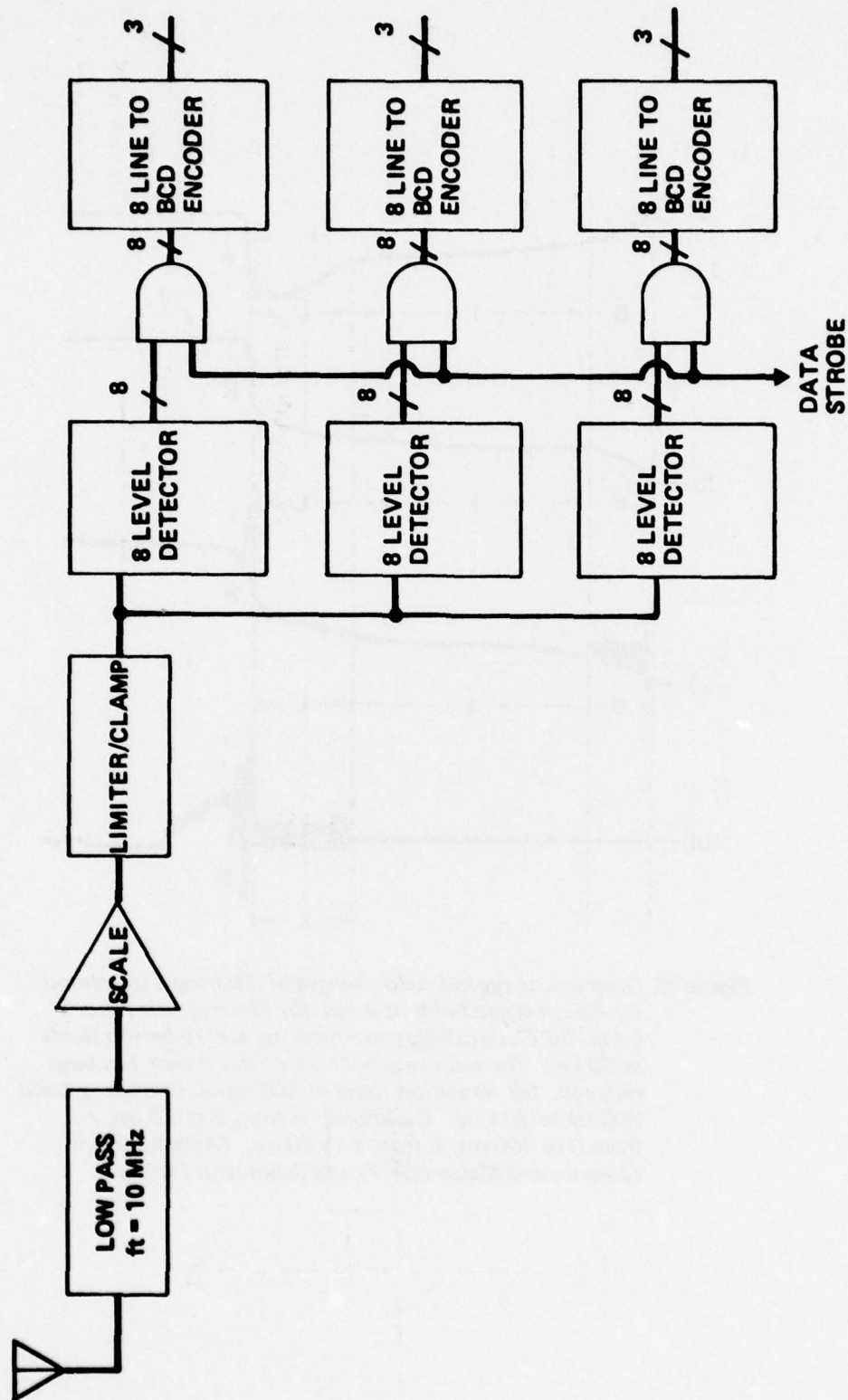


Figure 7. Front End System Diagram—High Speed A/D Conversion (20 MHz)



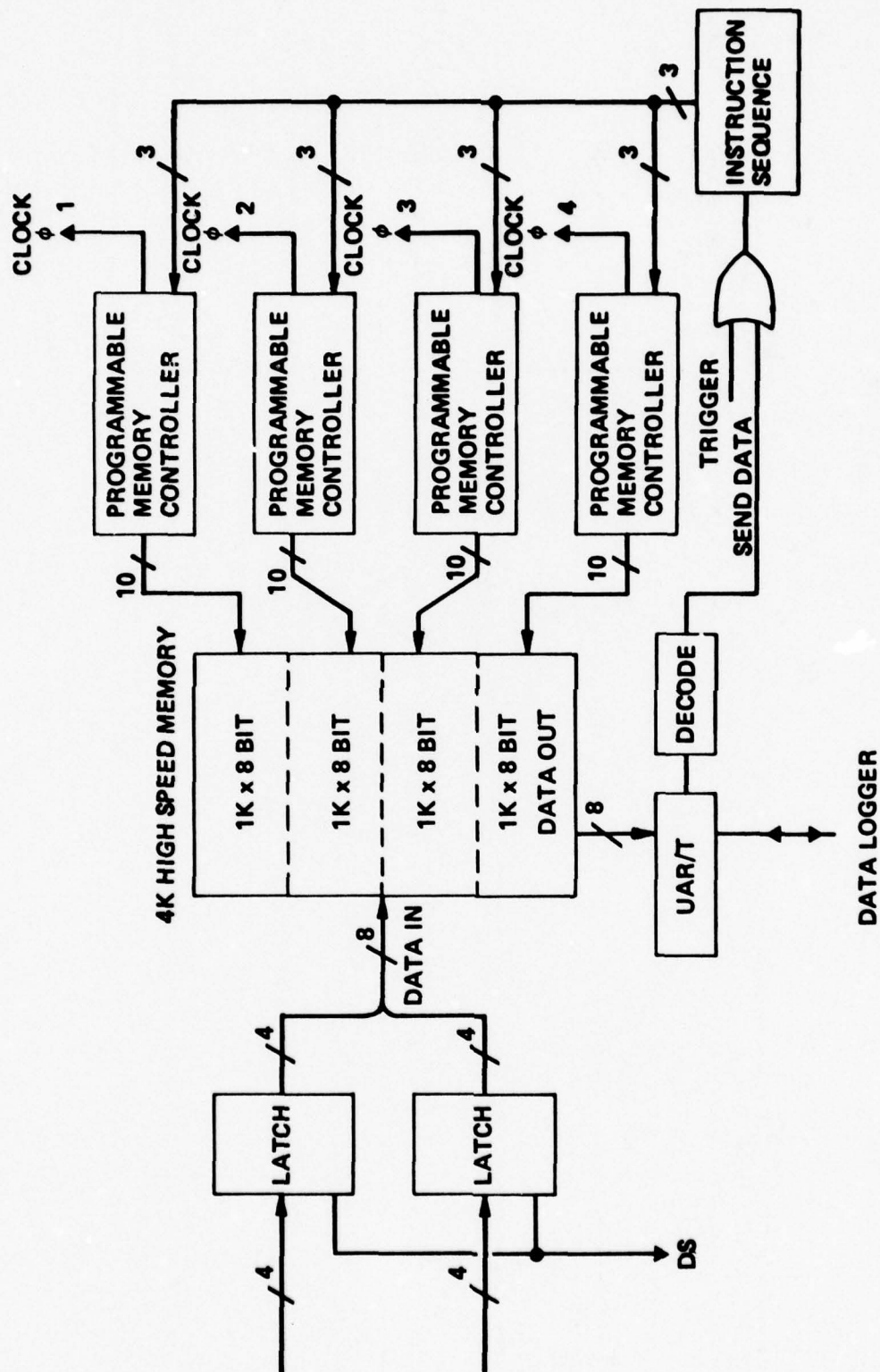


Figure 8. Front End System Diagram—High Speed Memory

THE USE OF CW TEST AND ANALYSIS TECHNIQUES IN  
LIGHTNING VULNERABILITY ASSESSMENT OF AIRCRAFT SYSTEMS

BY  
D. E. Young and L. D. Piszker

The Boeing Company  
Seattle, Washington

Presented at  
Federal Aviation Administration/  
Georgia Institute of Technology

Workshop on Grounding and Lightning Protection

PRECEDING PAGE BLANK

## ABSTRACT

Threat level simulation tests are often impracticable. Therefore, partial tests and analysis are needed to complete vulnerability assessments. Wideband and low-noise coupling information is obtainable using CW test techniques. As an example, comparisons of test and analysis results for a signal cable routed on an aircraft wing are presented.



## THE USE OF CW TEST AND ANALYSIS TECHNIQUES IN LIGHTNING VULNERABILITY ASSESSMENT OF AIRCRAFT SYSTEMS

### Introduction

Vulnerability assessments of aircraft systems to a lightning environment can be made by using test, analysis, or a combination of both. Maximum confidence in the assessment is achieved by the coordinated use of both test and analysis. Tests are required in verifying submodels of the system under assessment.

Electromagnetic modeling is required whenever the external environment cannot be test simulated in all its essential electromagnetic characteristics. This is the situation for nuclear electromagnetic pulse (NEMP) and also for lightning. When the high-level threat environment cannot be simulated, low-level test environments can be created that simulate selected characteristics of the threat environment. The approach that was developed for NEMP vulnerability assessment of aircraft, and which only recently is being applied to the assessment of the effects of lightning, consists of the following tasks:

- 1) Construct an electromagnetic coupling model of the aircraft from configuration data and on-site inspection.
- 2) Identify test requirements.
- 3) Obtain test data to develop and verify the model in the test environment.
- 4) Calculate induced transients using the electromagnetic model with the threat environment.

This approach was used on a recent test of cable samples for a fly-by-wire system concept. Portions of the test and analysis of one of these cable samples demonstrate the use of the assessment approach. The fly-by-wire concept has an electronic control box located in the fuselage and aileron and spoiler actuators on the wings. A sample cable showing the equipment interconnection is displayed in Figure 1. The objective is to estimate the expected voltages on the dummy loads due to a directly attached lightning stroke.

The examples presented in this paper are for an unshielded cable, that is, no overbraid and the shields on each of the twisted shielded pairs were floating. The main objective of the test and analysis was to determine the effects of different shielding configurations on the cable samples.

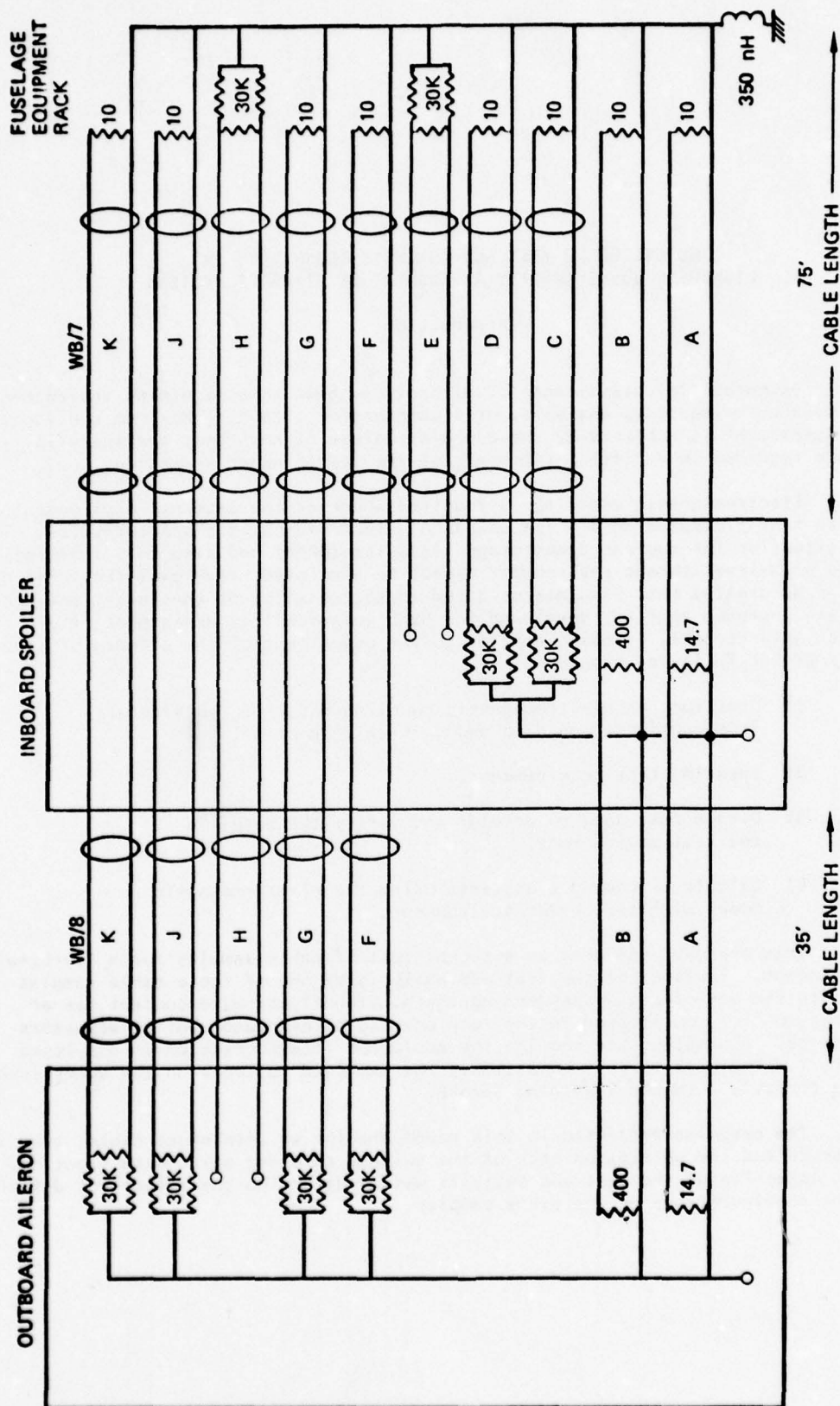


Figure 1. Simplified Circuit Diagram of A Fly-By-Wire Cable

## ELECTROMAGNETIC MODEL DEVELOPMENT

The usual approach in developing the electromagnetic model is to use frequency domain transfer functions for the separate coupling mechanisms. A spectral representation of the threat environment and the test driving source is also required. The coupling mechanisms are generally classified as external models, penetration models, and internal models. The external model is a transfer function of surface current density and charge on the external body (aircraft) due to a unit amplitude source. The penetration models are transfer functions relating the external fields to internal quantities such as cavity fields or induced voltages on internal cables. The final transfer function to the critical element being assessed makes up the internal model. This model is usually a transmission line model of the aircraft wiring which relates the induced cable voltage to a pin voltage at the electronic equipment.

The overall transfer function from source to critical element is obtained by multiplying the three transfer functions together. Multiplying the overall transfer function by the source spectrum yields the spectrum of the induced response at the critical element. The inverse Fourier transform is used to convert the spectrum to time domain voltages and currents. If nonlinearities occur, the transfer function representing that portion of the system which is nonlinear is not valid. The linear transfer functions may still be used, however, to define equivalent circuits on either side of the nonlinear element.

### External Coupling Model

For many sources, such as NEMP and nearby lightning, the aircraft fields can be determined by solving an integral equation for the surface current density. The integral equation satisfies the field boundary conditions on the aircraft and has the incident field as its source. Simpler transmission line models, however, are generally adequate for directly attached lightning because of the boundary conditions of current continuity at the attachment points and the predominant low frequency content of the lightning spectrum.

In the test set-up (Figure 2), the wing and chicken wire groundscreen form a nonuniform parallel plate transmission line. The nonuniformity, due to varying wing width and height, was modeled by subdividing the wing into short uniform sections of transmission line as shown in Figure 3. The inductances at sections 1B and 1C of Figure 3 represent the connection of the chicken wire to the fuselage. The inductance is distributed since the fuselage is at an angle with respect to the wing. The fuselage and right (undriven) wing were also modeled as transmission lines. This was not done in detail since only one resonance is seen below 10 megahertz. Instead, the effect of the fuselage was simulated by a single length of transmission line.



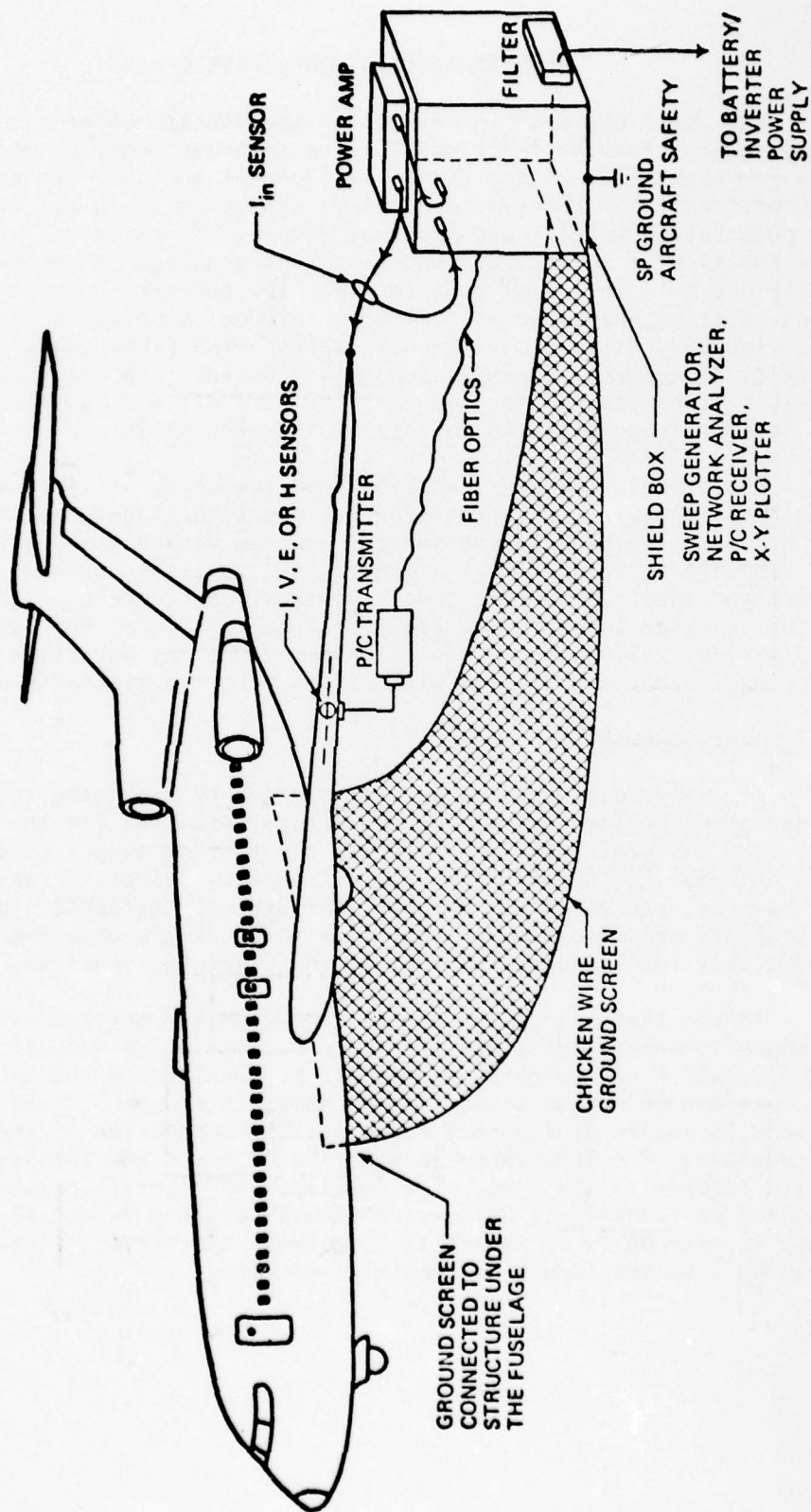


Figure 2. Aircraft Set-Up for CW Testing



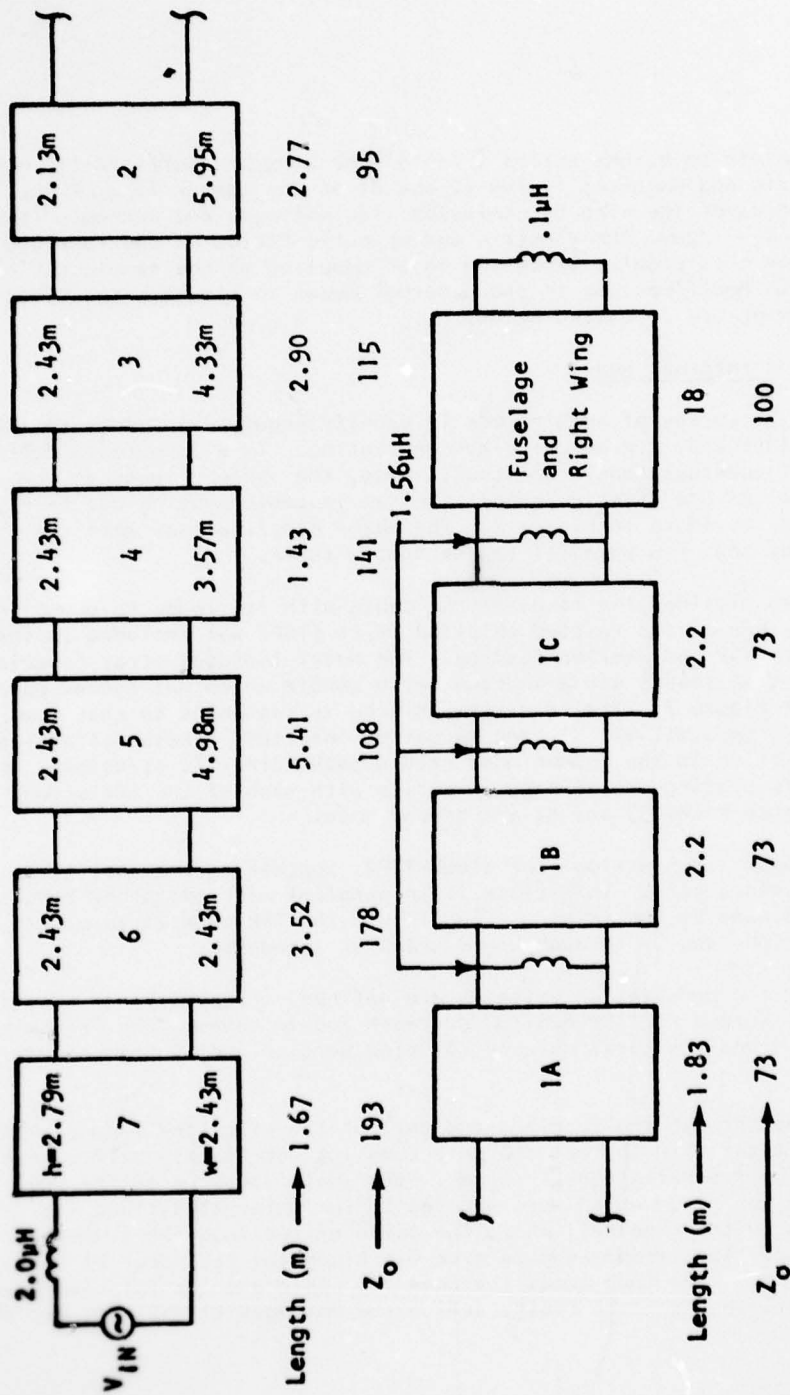


Figure 3. Cascaded Transmission Line Model of 727 Wing

The width to height ratios ( $w/d$ ) of the wing are sufficiently high that the electric and magnetic fields ( $E$  and  $H$ ) at the center line of the wing are given in terms of the wing transmission line voltages and currents ( $V$  and  $I$ ) by  $E = V/d$  and  $H = I/2w$ . The electric and magnetic fields on the fuselage are not required for this problem since the major coupling to the sample cable occurs along the wing. Modifications to the external model to simulate the directly attached lightning are discussed below.

#### Penetrations and Internal Model

On-site survey of an aircraft is usually required in order to identify penetration points and internal wire bundle routing. This is often a difficult task because of numerous bundle branches. Also, the various loads at the bundle terminations are often unknown. The sample cable routing was fairly straightforward, as shown in Figure 2. The major complications were the other aircraft bundles that ran parallel to the sample cable.

A transmission line model of the cable with its loads is shown in Figure 4. Only one of the twisted-shielded pairs (TSP) was included in the model since each TSP had similar loading. The model includes stray capacitance (due mainly to test leads) and a shorted cable bundle which was routed parallel to the cable of Figure 2. The transmission line is segmented so that the penetration voltages,  $V_1$ ,  $V_2$ ,  $V_3$ , and  $V_4$  can be inserted. These voltages are illustrated as being in the common mode return path (aircraft structure) which is equivalent to placing the voltage in series with each of the individual wires. Admittance nodes 33 and 42 are ground nodes.

The upper transmission line block TSP2, represents the core wires of the twisted-shielded pair. This block is in parallel with the other blocks since it is isolated by the shield. Coupling to the TSP core wires occurs by shield terminations and by through braid transfer impedance.

After the penetration voltages are defined, the admittance equations of Figure 4 are solved for the desired currents and voltages. The transmission line admittances and the total network solution were solved by the computer code TRAFFIC.

Routed through the fuselage and part of the wing, the sample cable was inside the metal skin so that the only coupling was by skin diffusion or access panel seams. These penetrations, however, were small compared to the two portions of the cable run which were exposed to the external surface fields. One portion was in the wheelwell where the cable exited from the fuselage and entered the wing. The second exposed area was along the rear spar of the wing below the spoilers. The loop areas (between the cable and aircraft skin) and the external electric and magnetic fields define the voltages  $V_1$ ,  $V_2$ ,  $V_3$ , and  $V_4$ .



### TEST REQUIREMENTS

The primary test requirement is to simulate the mode or modes of excitation of the aircraft which best represents the actual threat environment. This may vary depending upon the type of penetration; e.g., predominantly electric or magnetic coupling. In any case, the external fields may be measured to verify the external fields of the test configuration.

If there are multiple penetrations, it may be desirable to locate a cable or devise a measurement which is sensitive to only one of the penetrations. This is especially true for penetrations which are difficult to model because of geometry or clutter. In a typical shielded cable, for example, one of the secondary penetrations is through braid coupling of the TSP. This measurement could be isolated in a separate test of a short section of cable.

The analytical model is useful in setting up the priorities of the test measurements. Many of the measurements, for example, will have similar responses since they are on the same cable and are excited by the same penetration. Pretest predictions help in eliminating many of these redundant measurements so that a broader sample of responses is obtained. One may also want to prioritize the measurements according to the maximum voltage expected.

Coordination with circuit designers is required to select the pin-to-pin voltages or currents that are most critical for either design effort or are most vulnerable in an existing circuit.



## MODEL VERIFICATION

Swept cw testing is extremely useful in the verification and development of a model. The wideband response obtainable assures that all significant resonances of the system are recorded. Time domain measurements are often limited to the narrow band of either the source or of a single system resonance which may be of lesser importance for the actual threat environment. A block diagram of the swept cw instrumentation is shown in Figure 5.

The tracking generator is the primary energy source and provides a constant amplitude sine wave signal to a 50 ohm load in the 0.1 to 110 megahertz frequency band. The spectrum analyzer system consists of a HP 141T mainframe and display section, a HP 8552B IF section and a HP 8553B rf tuning section. The spectrum analyzer displays in logarithmic form, the amplitude of a signal as a function of frequency.

The tracking generator is swept from one frequency to another by the spectrum analyzer. The sweep signal is a linear ramp voltage generated by the spectrum analyzer. All frequencies between the start and stop frequencies are generated. The instantaneous frequency of the tracking generator output signal is phase-locked to the tuning frequency of the spectrum analyzer so that the frequency deviation between the two is less than one hertz. This permits the spectrum analyzer to measure very small signals by using a narrow band detector. Typically signal levels less than -120 dBm can be detected by the spectrum analyzer in a 100 Hz bandwidth.

The purpose of the power amplifier was to boost the amplitude of the signal applied to the aircraft, thus increasing the dynamic range available for the measurements. The output of the power amplifier is also a swept-cw but varied in amplitude because the impedance of the aircraft transmission was not constant with frequency. The maximum input signal strength was 1 ampere current and 3 watts power.

The output of the magnetic field, electric field, and current sensors were transmitted to the spectrum analyzer by a fiber optics amplifier link. The fiber-optics system consists of a transmitter, a fiber optics cable, and a receiver. The purpose of the fiber optics system is to isolate the sensor from the spectrum analyzer and to prevent test cable interaction. The fiber optics system reduced measurement sensitivity to -100 dBm. The transmitter was designed with a differential, high impedance input circuit so that the fiber optics system could be used as a voltage probe.

The tracking generator, spectrum analyzer, and the fiber optics receiver were placed inside a shield box to protect this equipment from stray electromagnetic fields produced by the aircraft transmission line. An rf filter was installed at the shield box to reduce rf current penetration to test equipment inside the shield box.

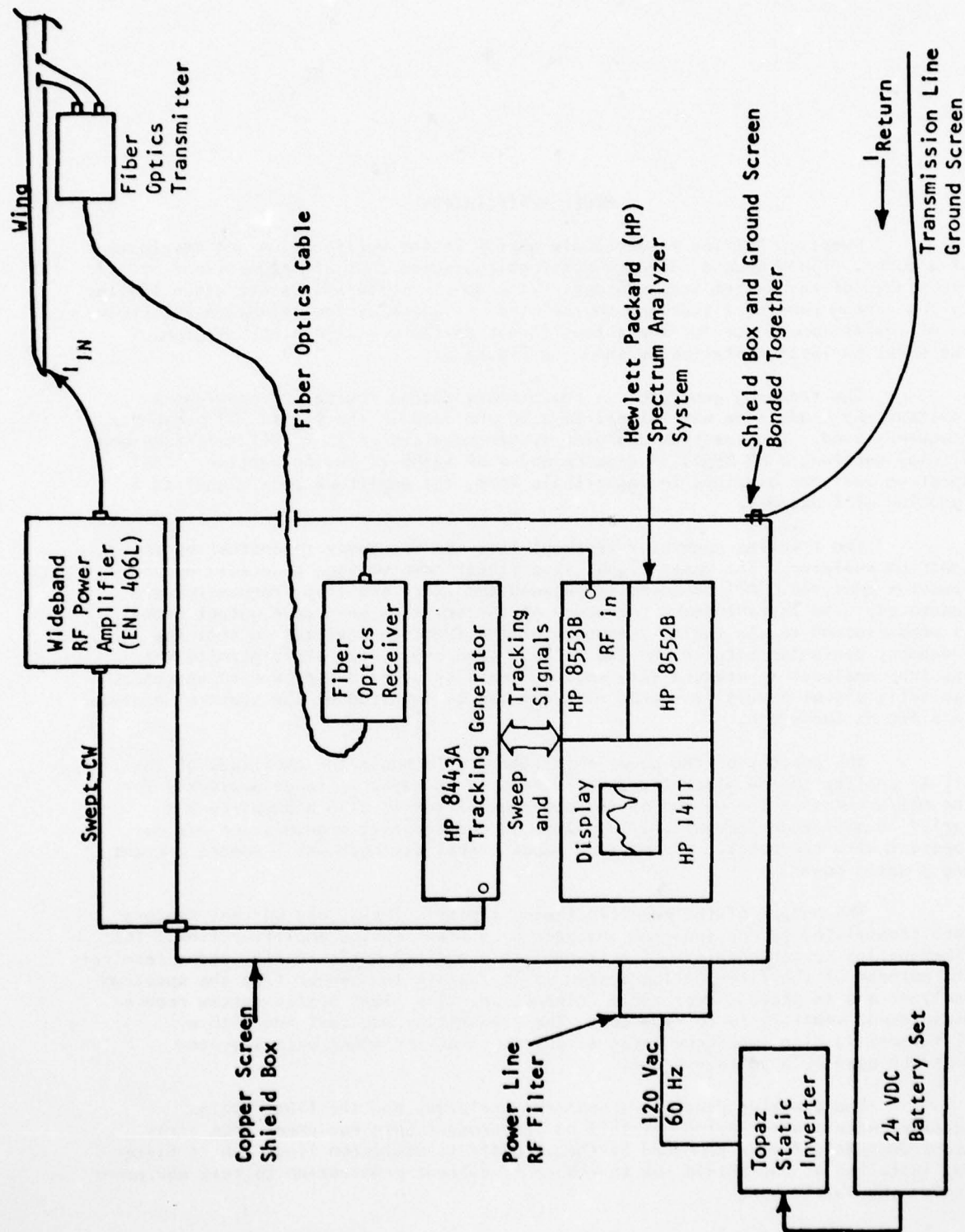


Figure 5. Block Diagram of the Swept-cw Instrumentation System

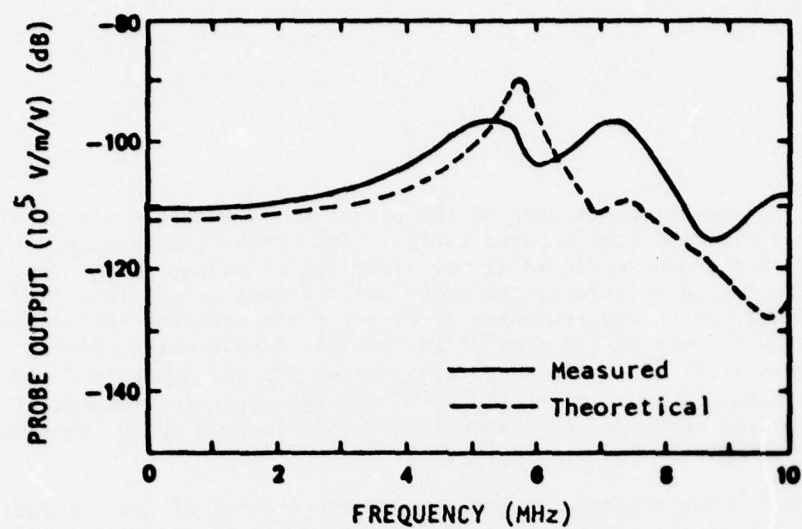
The first measurements were of the electric and magnetic fields along the wing in the vicinity of the exposed cables. The probe responses near the outboard spoiler are shown in Figure 6. To simplify the comparison of test data with theoretical calculations, the probe calibrations were folded into the theoretical calculations. The responses of Figure 6 are transfer functions of sensor output with respect to the wing drive voltage. The electric field sensor has a calibration of 1 volt =  $10^5$  volts-meter and the magnetic field sensor has a calibration of 1 volt =  $490 \times 10^6$  amperes-meter per second. The agreement between the measured and theoretical fields is good up to the wing resonance at 5.6 megahertz and within 10 dB at higher frequencies.

Figure 7 shows several responses which are typical of the voltages at the fuselage end of the cable. These voltage transfer functions roll off rapidly at low frequency, having their first resonance at the cable resonance of 1.2 megahertz. The agreement between the measured and theoretical results is within a few dB at the resonances. Minor modifications were made to the sensitive model parameters to improve the quality of the model. The sensitive parameters were the common mode and differential mode characteristic impedances and the mutual inductance and capacitance to the parallel wire bundle.

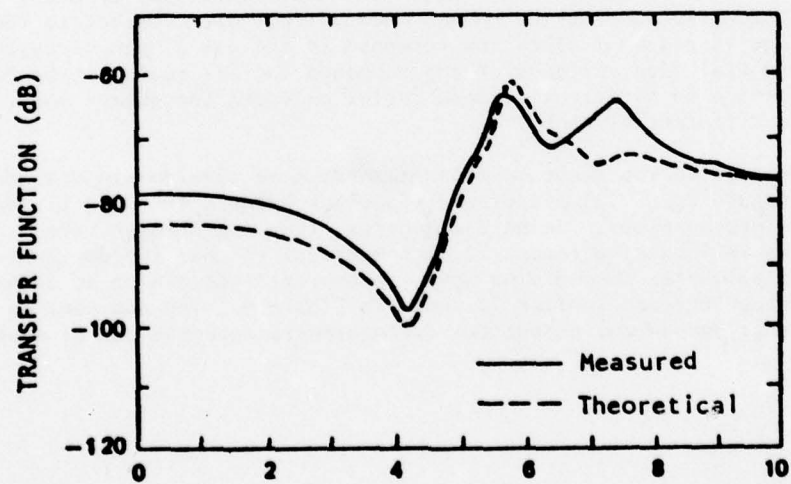
Typical voltage transfer functions at the outboard spoiler are shown in Figure 8. At low frequencies the common mode voltage with respect to the wing drive voltage is constant since the response is the cable open circuit voltage. Differential mode voltages at the outboard spoiler could not be made since the common mode to differential mode ratios exceeded the common mode rejection of the differential probe.

In addition to the swept cw measurements, some time domain measurements were made by discharging a 0.33 microfarad capacitor between the wing tip and the chicken wire ground plane. Below 2 megahertz, the wing-chicken wire transmission line is inductive (about 12 microhenries) so that the dominant wing current is an 80 kilohertz damped sine wave. A typical response on an unshielded twisted pair at the outboard spoiler is shown in Figure 9. The dominant response is the 80 kilohertz damped cosine but the 1.2 megahertz response can also be seen.





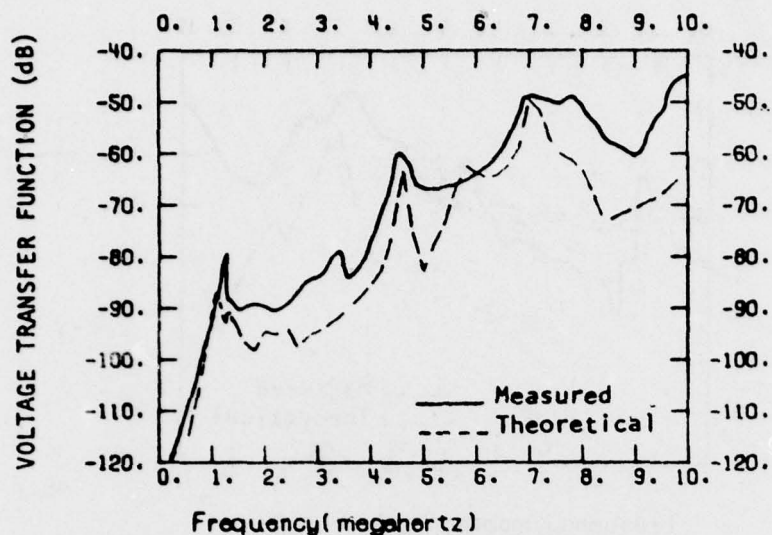
(a) Electric field



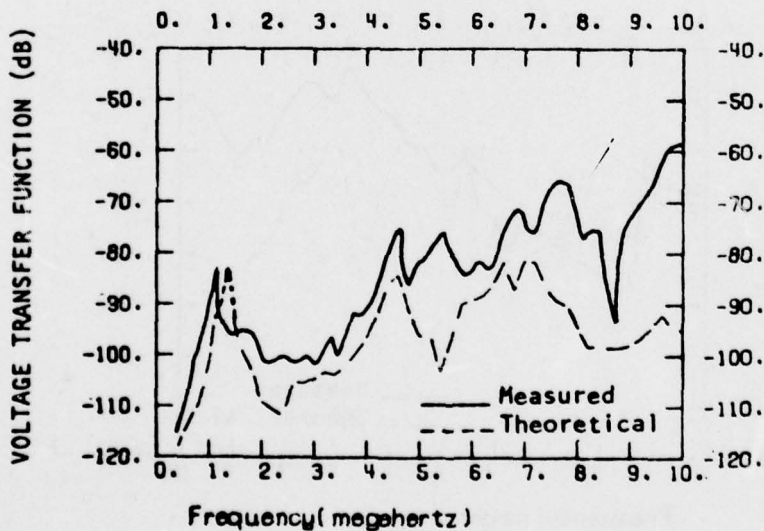
(b) Magnetic field

Figure 6. Electric and Magnetic Fields Near the Outboard Spoiler



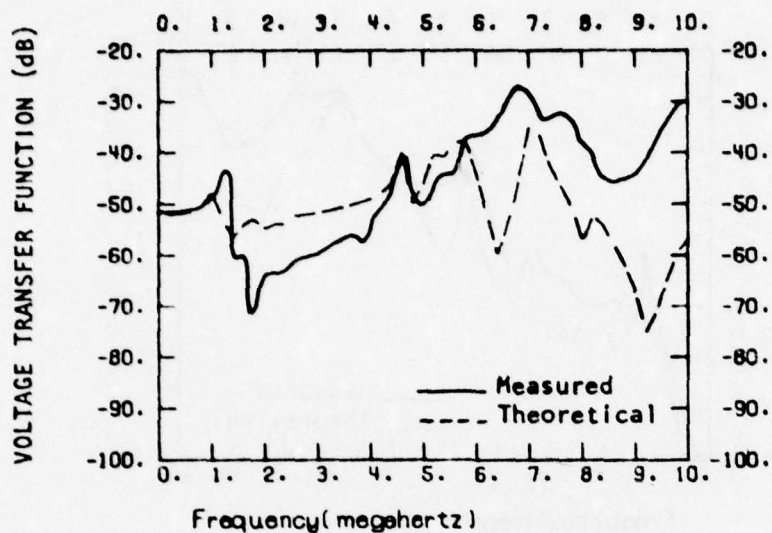


(a) Transfer function for voltage between dc ground and structure at equipment rack (VLI) for an unshielded cable.

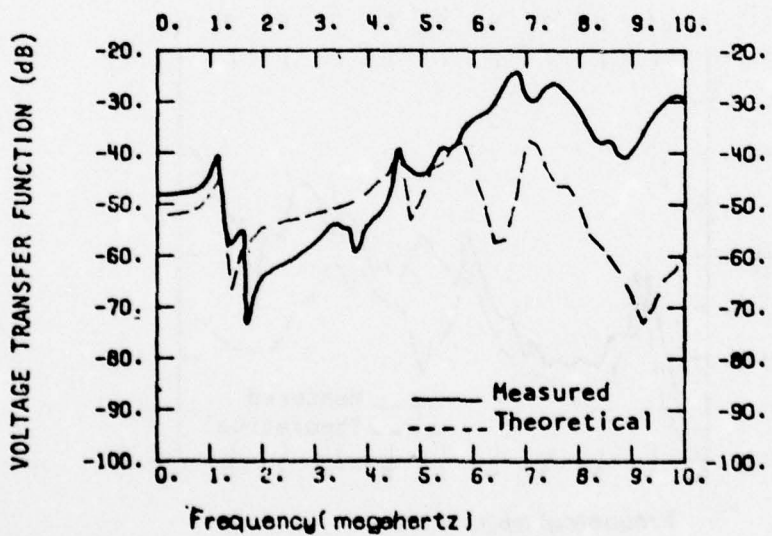


(b) Transfer function for differential voltage on signal line with floating shield at equipment rack (VFR).

Figure 7. Voltage Transfer Functions At the Fuselage

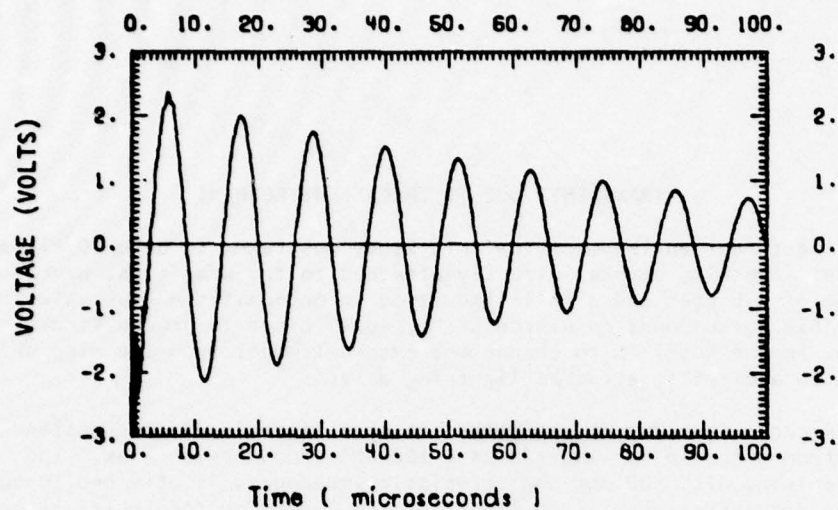


(a) Transfer function for voltage on signal line of unshielded twisted pair at outboard spoiler (VA5).

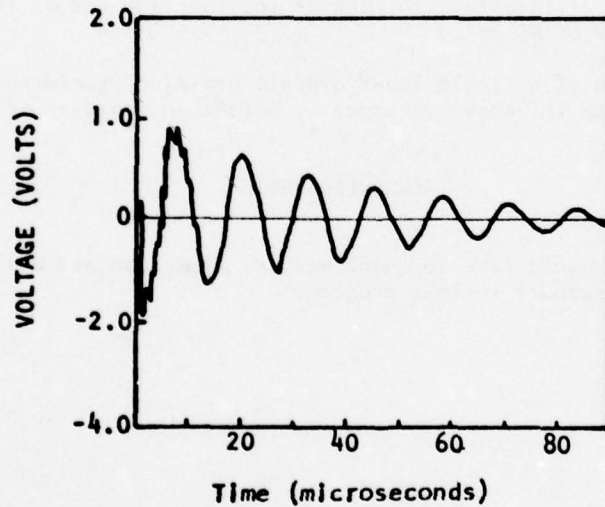


(b) Transfer function for common mode voltage on 30K signal load of twisted shielded pair with floating shield (V5).

Figure 8. Voltage Transfer Functions at the Outboard Spoiler



(a) Theoretical



(b) Measured

Figure 9. Signal Voltage on Unshielded Twisted Pair at Outboard Spoiler (VA5) Due to a 1000 Volt Charged Capacitor.

#### TRANSIENTS DUE TO THREAT ENVIRONMENT

The threat environment for this study was taken to be a 20 kiloampere (peak value) lightning stroke, directly attached to the wing tips; having a rise-time of 0.6  $\mu$ sec and a fall-time (time to one-half the peak value) of 40  $\mu$ sec. This corresponds to Pierce's\* "typical" cloud-to-ground stroke. The only change in the model is to change the external model from the wing-chicken wire drive to a directly attached lightning drive.

A convenient way to model the attached lightning is to consider the aircraft, from wing-tip to wing-tip as a 100 ohm transmission line. The lightning column, with 500 ohm characteristic impedance, is attached to both ends of the aircraft transmission line. If the lightning stroke is assumed to be of infinite length, the lightning transmission line can be reduced to a 500 ohm load on one wing-tip and a 500 ohm drive source on the other wing tip.

Using a typical lightning stroke of 20,000 amperes with a 0.6 micro-second rise time the results of Figure 10 are obtained for an unshielded cable. The common mode voltage at the outboard spoiler has a peak value of 4500 volts. The waveform is predominantly a one megahertz damped sinusoid due to the cable resonance. A typical differential voltage at the fuselage end of the unshielded cable has a peak value of 45 volts.

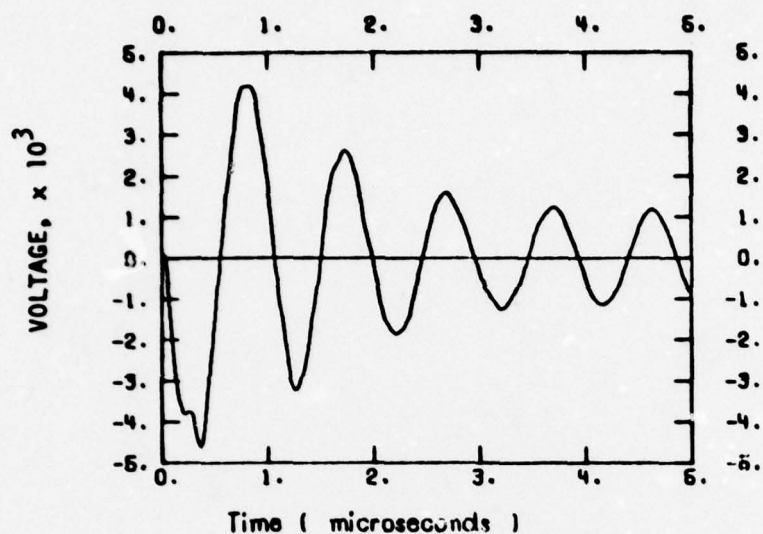
The addition of a single layer overall braid, circumferentially terminated at the ends, can reduce the above voltages by more than 2 orders of magnitude.

#### ACKNOWLEDGMENT

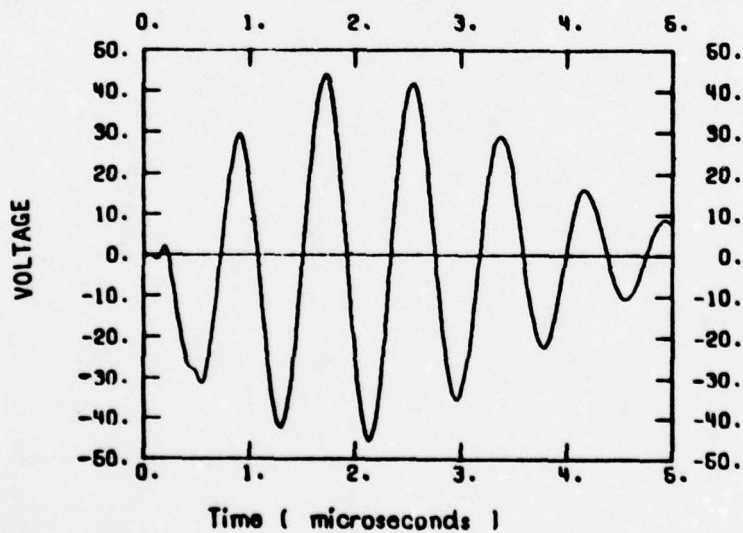
The authors would like to thank Ward H. Zimmerman and William E. Boardman for their continuing support to this program.

\* Pierce, E. T., and N. Cianos, "A Ground-Lightning Environment for Engineering Usage," SRI Technical Report, August 1972.





(a) Outboard spoiler, common mode, on unshielded twisted pair (VA5).



(b) Equipment rack, differential voltage, on shielded twisted pair with floating shield (VFR).

Figure 10. Voltage Due to Typical Lightning Stroke

# **A ONE MEGAJOULE LIGHTNING SIMULATOR**

**By**  
**E.H. Schulte and G.W. Kamerman**

**Lightning Simulation Laboratory  
McDonnell Aircraft Company  
St. Louis, Missouri**

**Presented at**  
**Federal Aviation Administration/  
Georgia Institute of Technology**  
**Workshop on Grounding and Lightning Protection**  
**May 1978**

GP78-4302-1

AD-A058 797

GEORGIA INST OF TECH ATLANTA

F/G 4/1

FEDERAL AVIATION ADMINISTRATION-GEORGIA INSTITUTE OF TECHNOLOGY--ETC(U)

MAY 78

UNCLASSIFIED

FAA-RD-78-83

NL

5 of 5

AD  
A058 797



## ABSTRACT

The McDonnell Aircraft Lightning Simulation Laboratory located at St. Louis, Mo. has developed a one megajoule capacitor bank for lightning damage testing. Using this system, the high peak current, intermediate current, continuing current and restrike components of a natural lightning strike can be simulated in a single test. The system is highly versatile, so that non-standard waveforms can be generated for research and development. This paper describes the test system, its operation and application to simulation problems encountered in the development of advanced aircraft.

## Introduction

The damage inflicted by a direct lightning strike to an aircraft is difficult to quantitatively predict. The damage incurred will be a function of aircraft geometry, attach points, material type and thickness, and construction techniques. Since this situation exists, lightning simulation tests have been developed as design aids and for final hardware qualification. These tests, although generally straightforward in their statement, are difficult to perform without extensive specialized facilities. The MCAIR One Megajoule Lightning Simulator is one of the most advanced facilities of its kind, and incorporates many necessary features for meeting these demanding test requirements.

## Lightning Threat

The credibility of the Lightning Simulation Test is strongly dependent upon the test discharge waveform. The SAE Task Force F<sup>1</sup> and NASA<sup>2</sup> have both developed standardized waveforms for lightning testing (Figure 1). These waveforms represent a severe direct strike and are the result of numerous studies which have attempted to quantitatively describe lightning phenomena.<sup>3, 4, 5</sup> Although they are defined differently, both waveforms embody the important damage mechanisms of a lightning strike. The NASA waveform is defined more rigorously while the SAE waveform lends itself more naturally to simulation.

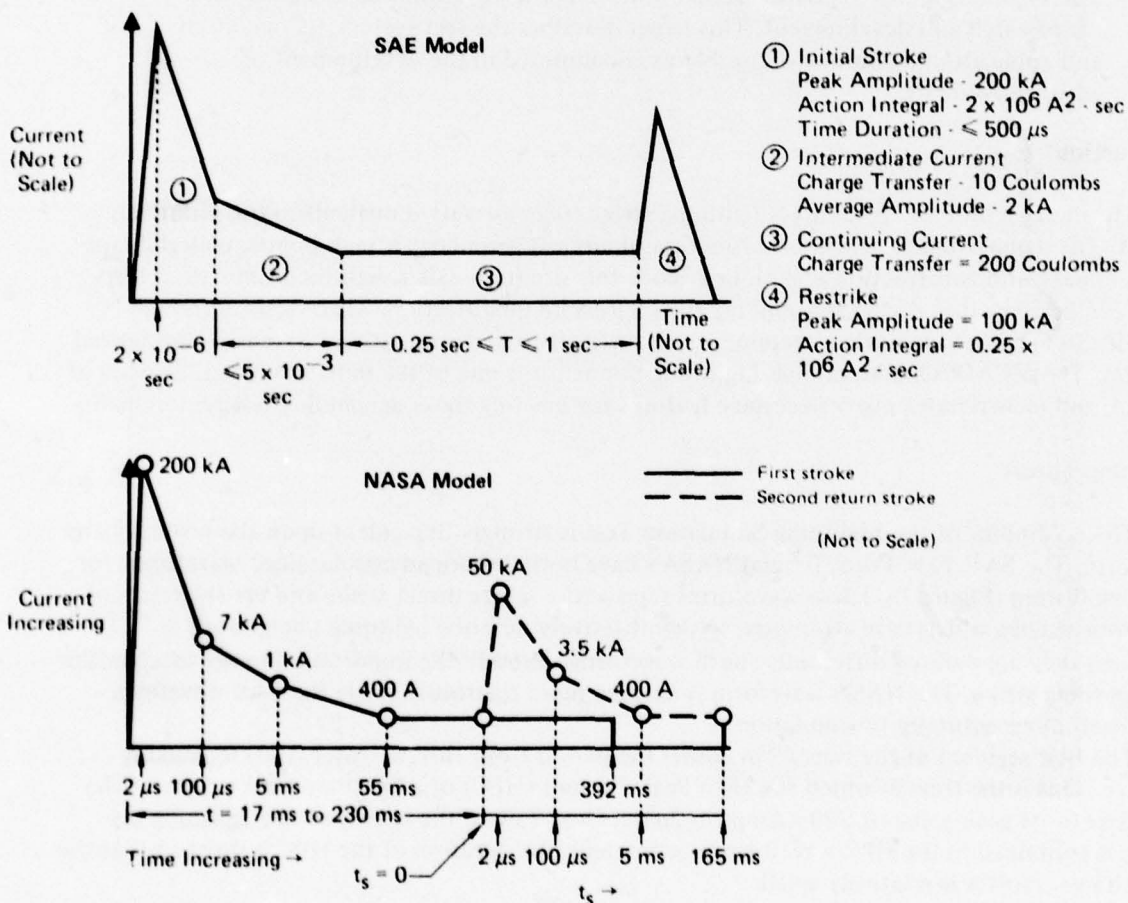
The first segment of the waveform covers the period from current onset ( $t=0$ ) to roughly 100 $\mu$ sec. This is the time in which the High Peak Current (HPC) of a lightning stroke occurs. The HPC rises to its peak value of 200 kAmps in 2 $\mu$ sec. Over 75% of the energy of the lightning discharge is contained in the HPC waveform. Fortunately, the duration of the HPC is short so that the total charge transfer is relatively small.

Because of this small charge transfer, a good conductor seldom experiences more than minimal damage. If, however, the strike is to a material or structure with limited current carrying capacity (e.g. advanced composites, aluminum honeycomb as shown in Figure 2, and electrical wiring) significant damage can result from explosive vaporization or shock heating. The fast rate-of-rise of



current associated with the HPC produces very high intensity, rapidly changing magnetic fields. This causes magnetic stresses in the current carrying members which can lead to structural deformation. Internal arcing (e.g. in fuel cells) can also result from these rapidly changing, high magnitude currents. Shock overpressures from the explosive expansion of the arc channel and vaporized aircraft materials may produce engine stalls or unwanted structural responses. Induced electrical transients may occur in avionics systems from the strong magnetic and electric fields generated during a discharge. Because of the high voltages associated with the HPC, breakdown of dielectrics, such as radomes (Figure 3) is sometimes encountered.

The second segment of the lightning waveform is referred to as the Intermediate Current (IC) and extends from 100  $\mu$ sec to 55 msec. The IC can cause localized heating or burn through of fuel tank skins resulting in the ignition of flammables. It can also cause bulk heating of composites which can result in structural degradation. This problem is intensified by the Continuing Current (CC), the third segment of the waveform. The CC can transfer over 200 coulombs in a time interval from lasting 250 to 400 msec. The high current restrike waveform is similar to the HPC except that it has a lower peak amplitude and energy content.



GP78-8302-12

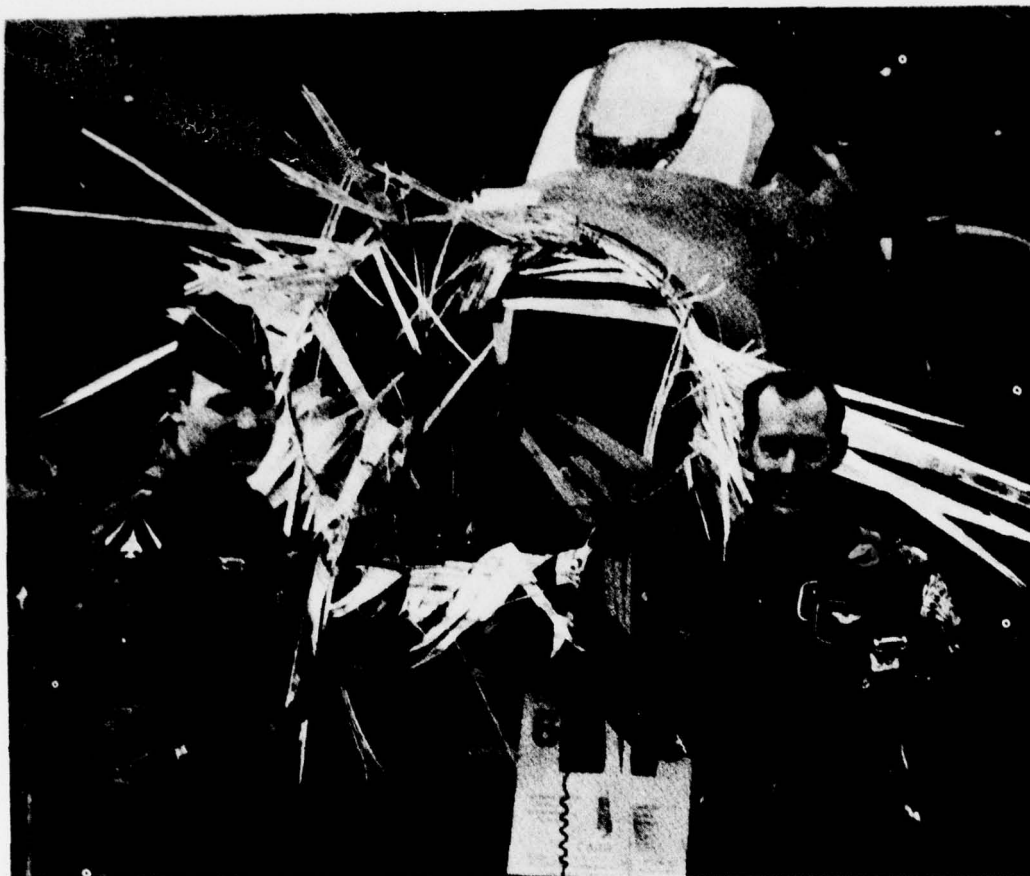
**FIGURE 1**  
**SAE AND NASA IDEALIZED LIGHTNING TEST WAVEFORMS**



Interior View of Unprotected Stressed  
Composite - Aluminum Honeycomb Box Beam  
Section After Simulated 200 kA  
Lightning Strikes

GP78-8302-4

FIGURE 2  
EXAMPLE OF EXPLOSIVE PRESSURIZATION



The RF-4C in the photo was being flown by Capt. Robin Lake, Pilot, and Lt. Denny Watkins, Navigator of the 86th TFW on a routine mission when they sustained substantial damage due to a dual lightning strike. All primary flight instruments were lost after the second strike and the attitude and vertical velocity indicators were fluctuating wildly. After declaring an emergency and taking the necessary precautionary measures, the crew, aided by another RF-4C, made a successful landing. This incident occurred in Europe during April 1970 and the weather conditions at the time of the incident were ceiling 1200 foot overcast, visibility 2 miles, and temperature 6°C. Through the superb airmanship of the crew, a total aircraft loss was averted. (U.S. AIR FORCE PHOTO) Ref. 7

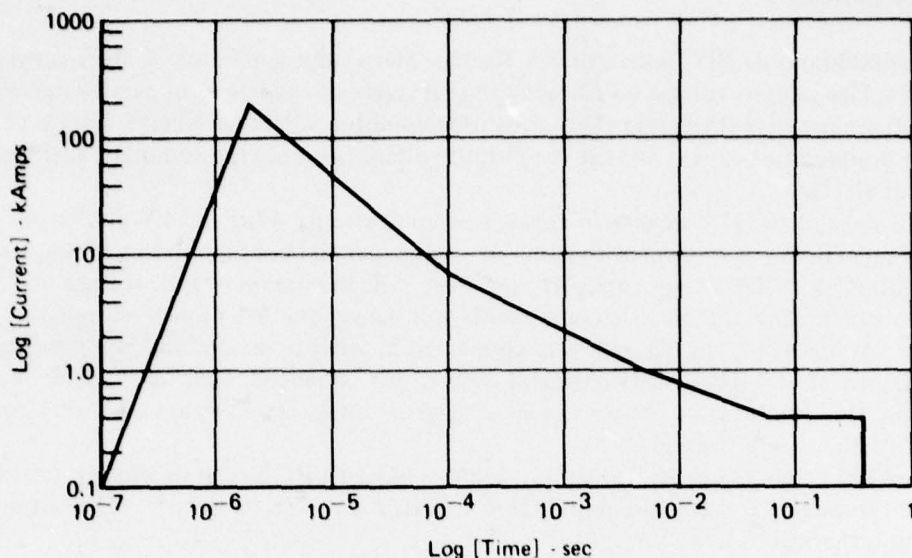
GP78-8302-15

**FIGURE 3**  
**RF-4C AFTER DIRECT NATURAL LIGHTNING STRIKE TO RADOME**

#### Individual Component Testing

As these waveforms demonstrate, lightning currents encompass several orders of magnitude of amplitude and time. This wide spectrum of times and current levels, shown graphically in Figure 4, presents the greatest difficulty in performing realistic lightning tests. For this reason, the lightning test waveform has traditionally been divided into its component parts with each part addressed by a separate test.





GP78-8302-6

**FIGURE 4**  
**DETAIL OF NASA DIRECT LIGHTNING STRIKE MODEL**

By separating the test waveform into these component parts, it has been tacitly assumed that there are no synergistic effects of importance. It is assumed that each component has a damage mechanism associated with it which is a function of the current characteristics, i.e., large  $dI/dt$ , high peak amplitude, large charge transfer, high energy content, etc., that are peculiar to that component. While this has generally been true for metallic aircraft using conventional construction methods, it may not be valid for aircraft utilizing advanced materials and bonding techniques. For example, the damage inflicted to graphite/epoxy (Gr/Ep) composites by a current discharge containing all of the segments of a lightning strike has been found to be different from the damage incurred when these waveform segments are applied individually.<sup>8</sup> Tests have also indicated that the fast rate of rise of the HPC may be required to accurately simulate lightning damage to composites. In addition, some specialized geometries may be less sensitive to the application of the combined waveform than to the individual segments. In these cases, tests using the full test waveform could avoid overdesign weight and cost penalties.

#### One Megajoule Lightning Simulator

The McDonnell One Megajoule Lightning Simulator (Figure 5) can produce a discharge waveform which includes the HPC, IC, CC and restrike in a single test strike (Figure 6). This is done by coupling a 600 kJoule Marx surge generator with a 480 kJoule capacitor bank (Figure 7) and a low energy, high voltage restrike generator. In operation, the high output voltage of the HPC generator closes the spark gap from the output probe to the test sample. The 600 kJ bank discharges the HPC through this gap into the test sample. The 480 kJ bank then discharges into the test sample through the established arc. The restrike generator is triggered separately, and can be programmed to discharge at anytime during the CC.



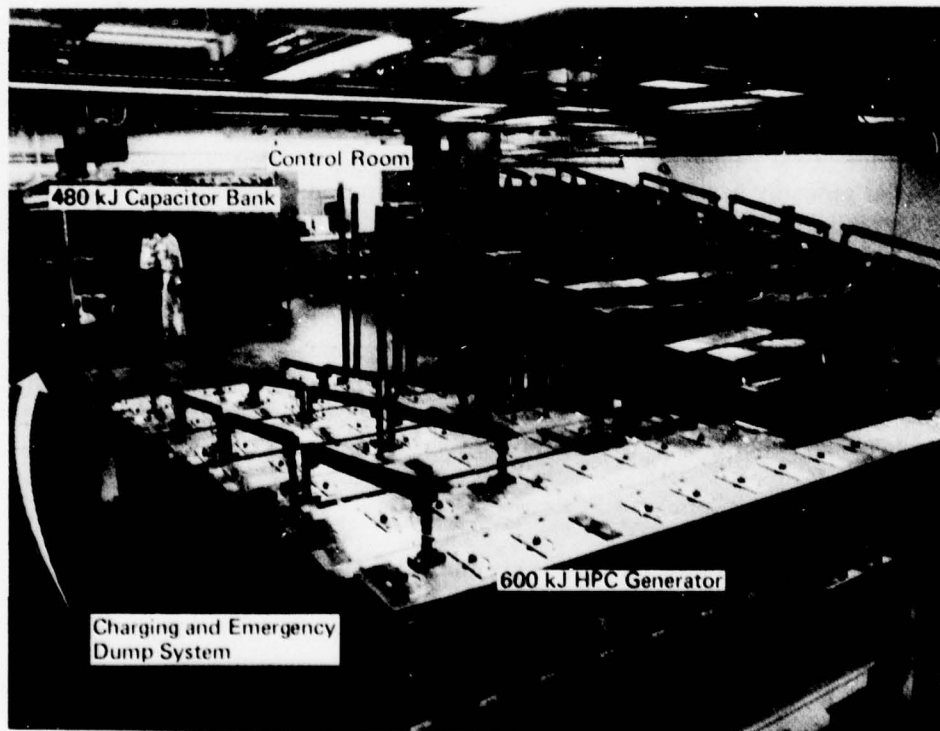
### High Peak Current

The 600 kilojoule HPC generator is a 10-stage Marx surge generator. A Marx surge generator achieves its high output voltage by charging several stages of capacitors in parallel and then discharging them in series (Figure 8). This leads to a condition where the charge voltage of one capacitor is added to the next so that the output voltage becomes the summation of the charge voltages of all stages.

Each stage of the HPC generator consists of up to twenty  $42\mu\text{F}$ , 12 kV discharge capacitors. These 20 capacitors are connected together in a series/parallel configuration yielding a maximum of  $210\mu\text{F}$  with a 24 kV DC charge capability per stage. The maximum output voltage of  $2.4 \times 10^5$  volts allows realistic testing of dielectric components and the production of peak currents of up to  $3.0 \times 10^5$  amps. At discharge, the 10 stages are connected in series by a combination of electronically triggered, pressure regulated spark gaps and capacitively enhanced, open air, variable separation spark gaps. This combination allows a range of charge voltages from as low as 2500V to as high as 24,000V to be reliably triggered.

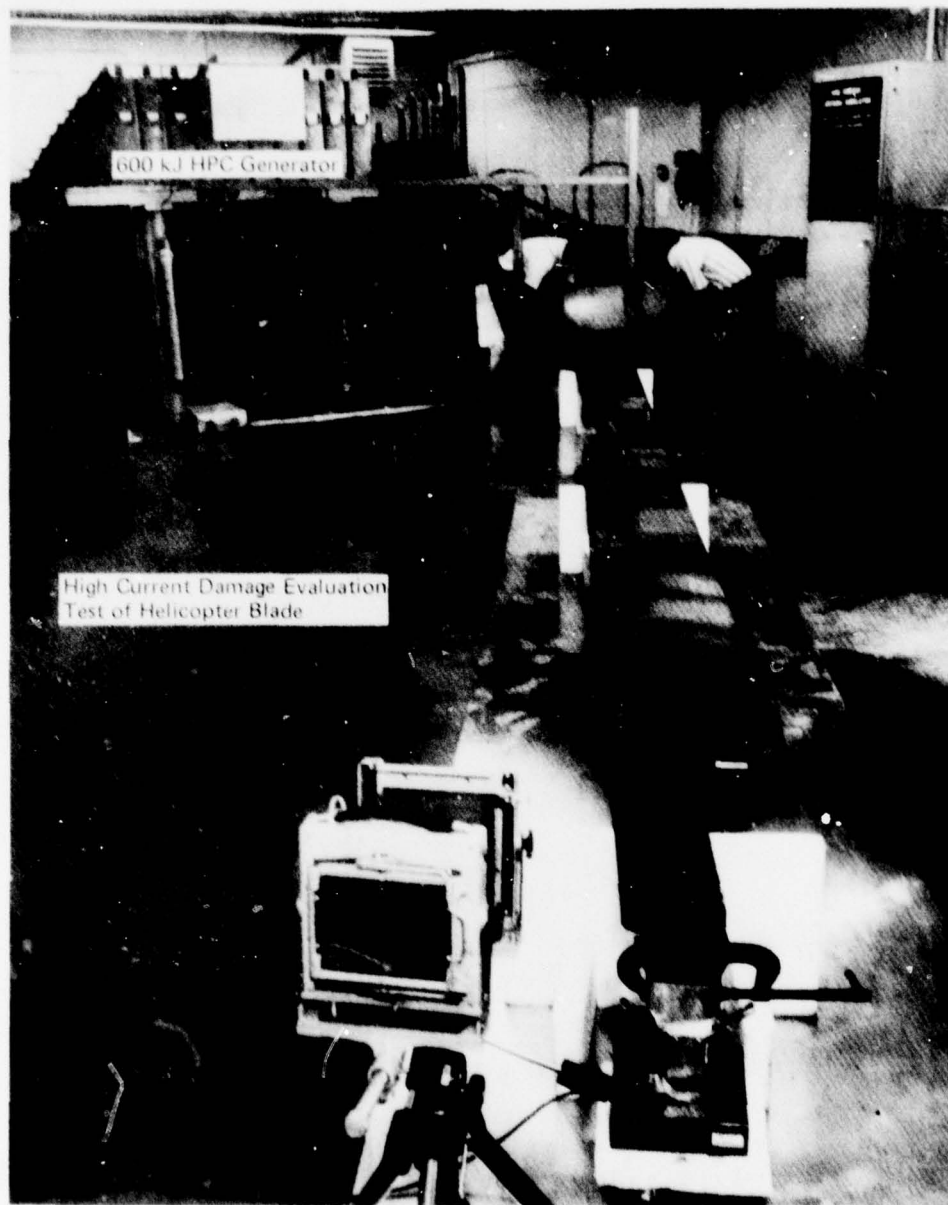
Upon discharge, the generator simply behaves like an LRC circuit in which a capacitor is discharged through a resistor and an inductor by a switch closure (Figure 9). The output current waveform is then given by

$$I(t) = \frac{nV}{\omega L} e^{-\left[\frac{R(t)t}{2L}\right]} \sin \omega t$$



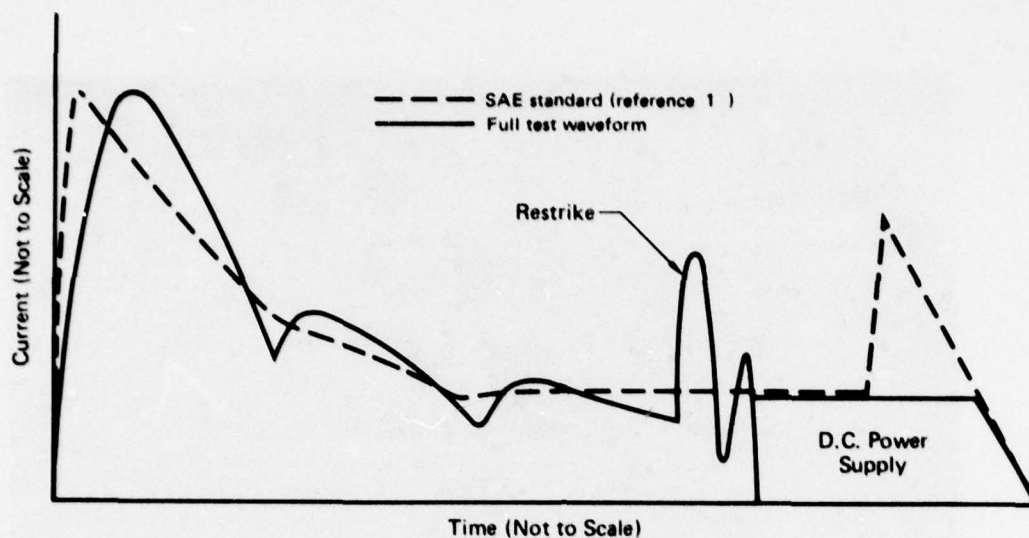
GP78 R302.3

FIGURE 5  
ONE MEGAJOULE LIGHTNING SIMULATION FACILITY



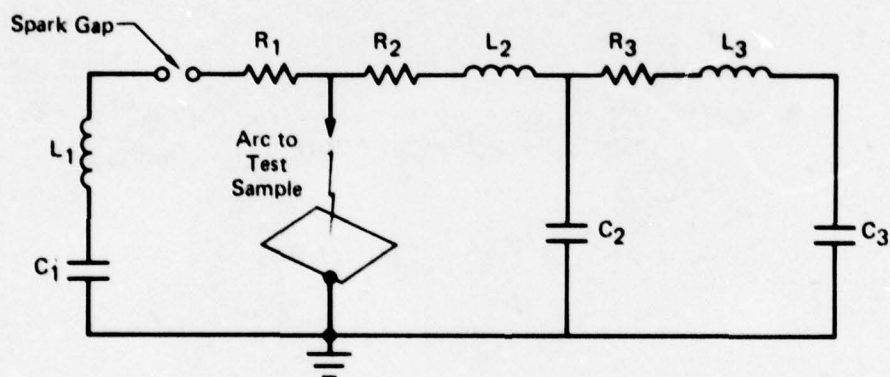
GP7B B302 5

FIGURE 5 (Continued)  
ONE MEGAJOULE LIGHTNING SIMULATION FACILITY



GP76-8302-14

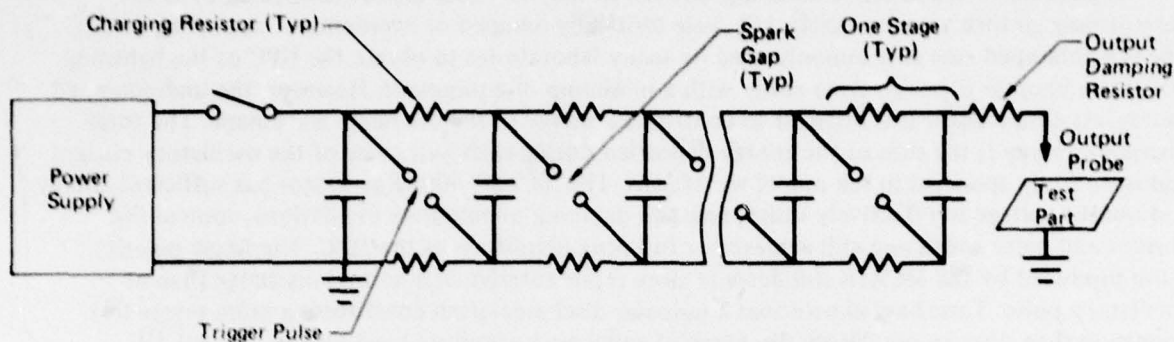
**FIGURE 6**  
**COMPARISON OF SAE AND MCAIR SIMULATED**  
**LIGHTNING TEST WAVEFORMS**



$C_1$  = 600 kJ Capacitor Bank (240 kV), HPC  
 $C_2$  = 90 kJ Capacitor Bank (12 kV), IC  
 $C_3$  = 390 kJ Capacitor Bank (12 kV), CC  
 $C_2 + C_3$  = 480 kJ Capacitor Bank  
 $L_1$  = Inductance of 600 kJ Capacitor Bank System  
 $L_2, L_3$  = Waveshaping Inductors  
 $R_1, R_2, R_3$  = Waveshaping and Current Limiting Resistors

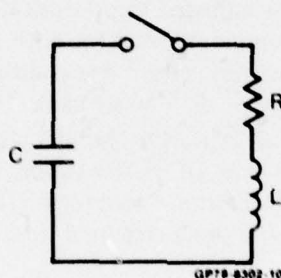
GP76-8302-9

**FIGURE 7**  
**SIMPLIFIED SCHEMATIC REPRESENTATION OF THE 1.08 MJ LIGHTNING**  
**SIMULATOR CONNECTED FOR A 3-COMPONENT LIGHTNING WAVEFORM**



GP78-8302-11

**FIGURE 8**  
**BASIC MARX SURGE GENERATOR CIRCUIT (n STAGES)**



GP78-8302-10

**FIGURE 9**  
**BASIC SERIES LRC CIRCUIT**

where  $n$  is the number of stages, and  $V$  is the voltage of any one stage.  $\omega$  is the resonant frequency of the circuit given by

$$\omega = \left[ \frac{n}{LC_s} - \frac{R^2(t)}{4L^2} \right]^{1/2}$$

$R(t)$  and  $L$  are respectively the bulk circuit resistance and inductance, while  $C_s$  is the capacitance of only one generator stage. The circuit inductance is principally a result of the pulse generator's internal inductance and for all practical test purposes it is unalterable. This limits the rise time of the HPC generator and the resulting discharge is slower than the model waveform's specified value of 2  $\mu\text{sec}$ .

The circuit resistance  $R(t)$  is dominated by the output damping resistor. This resistor can be easily adjusted to regulate the peak current and current decay time. The resistance is expressed here as a function of time to indicate the effect which ohmic heating may have on the output circuit. In most cases, ohmic heating is not an important factor and the resistance is treated as a time independent constant.



Depending on the resistive damping, the circuit may resonate (underdamped case) or the current may go thru approximately 1/2 cycle (critically damped or overdamped case) (Figure 10). The underdamped case is commonly used by many laboratories to obtain the HPC of the lightning waveform because it can be done easily with a minimum of equipment. However, the underdamped case is less desirable for it is difficult to control the energy in the discharge waveshape. The total discharge energy is the sum of the energy deposited during each half cycle of the oscillatory current and is carefully specified in the model waveforms. The MCAIR 600kJ generator has sufficient energy and output voltage to effectively utilize resistive damping to eliminate oscillations, control the current and pulse width and still achieve the full peak amplitude of the HPC. The single polarity pulse produced by the MCAIR simulator is more representative of a natural discharge than an oscillatory pulse. Tests have shown that a unipolar discharge often constitutes a more severe test condition than does an oscillatory discharge of equal peak amplitude and energy content.<sup>10</sup>

#### Intermediate and Continuing Currents

The 480 kJ capacitor bank consists of 160 of the same type 42 $\mu$ F discharge capacitors used in the HPC generator, but connected in parallel. This bank is charged separately from the HPC pulse generator and connected in parallel with it upon discharge. As with the pulse generator, the number of capacitors and the charge voltage can be adjusted to produce the desired output.

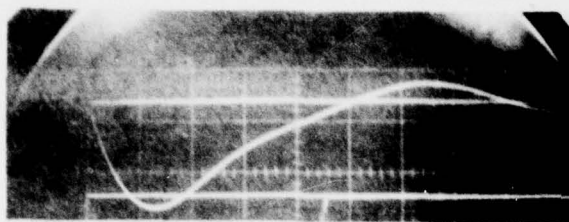
The 480 kilojoule capacitor bank is commonly used for both the IC and CC components of the test waveform (Figure 11). There are, however, certain test conditions which require a continuing current which extends beyond the capacity of the 480 kJ bank. Under these circumstances either the 600 kJ bank is connected in parallel (all capacitors parallel yielding a total charge capacity of 170 coulombs) with the 480 kJ bank or a large DC power supply is connected to deliver the required continuing current portion of the lightning waveform. The One Megajoule Simulator also has the capability to terminate a CC at a predetermined time (Figure 11).

#### Restrike

The Restrike generator is a 5-stage Marx surge generator. Each stage has 0.25 $\mu$ F and a 100 kV DC charge voltage capability resulting in a maximum output voltage of 500 kV. This generator produces a low energy, fast risetime pulse with magnitude of up to 50 kAmp peak with a 1 to 2  $\mu$ sec risetime. This low energy generator can be triggered to discharge at any time during the IC or CC for restrike evaluation. It is particularly valuable in determining induced transients in electrical hardware, swept stroke evaluations of dielectric surfaces and other effects which are directly relatable to rate of change of current.

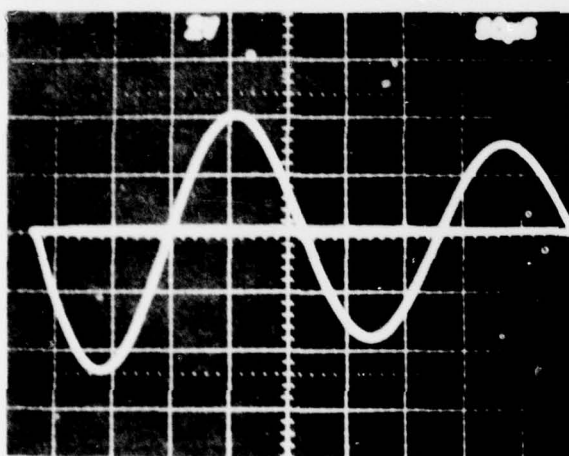
#### Isolation, Switching and Timing of Generators

Whenever generators or power supplies having widely different output characteristics are connected together to produce a single waveform with sequentially occurring components, some method must be employed to switch in the various components and to prevent one generator from affecting the operation of the other(s). The combination of the various waveform components requires precise switching and timing. Standard switching devices (SCRs, transistors, etc.) generally cannot withstand the high-voltage, high-current of the discharge waveform. Mechanically operated devices can generally be made to withstand the high voltage and high current but are too slow acting. This means that mechanical switching must be minimized and that triggered or over-volted spark gaps must be relied on almost exclusively for switching.



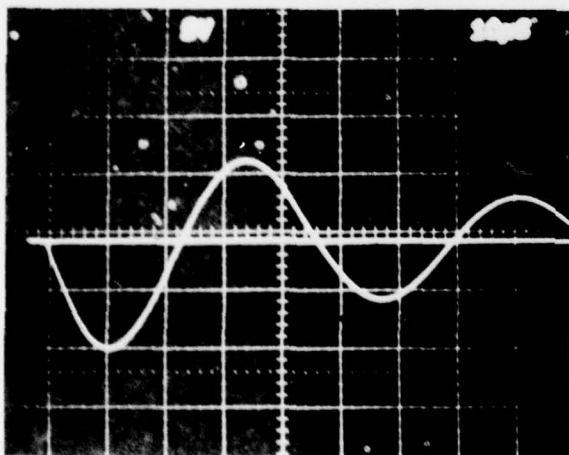
100  $\mu$ sec

Wide Pulse  
200 kA Peak  
Reference 9



230  $\mu$ sec

Wide Oscillatory  
64 kA Peak  
Reference 10

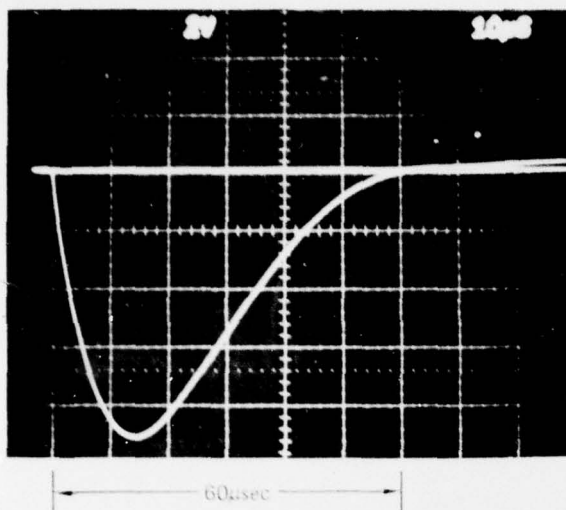


47  $\mu$ sec

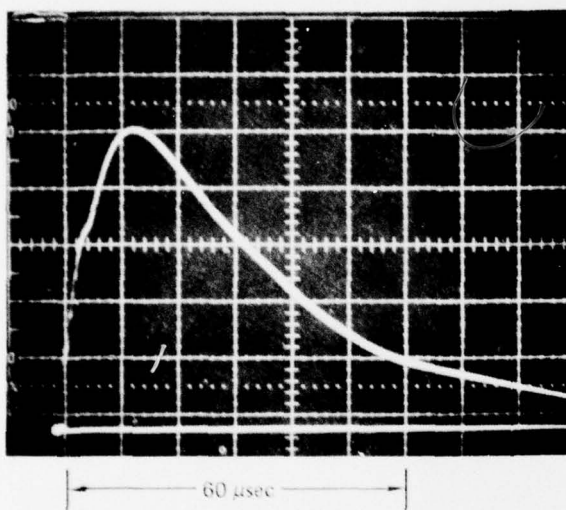
Medium Oscillatory  
125 kA Peak  
Reference 10

GP78-8302 13

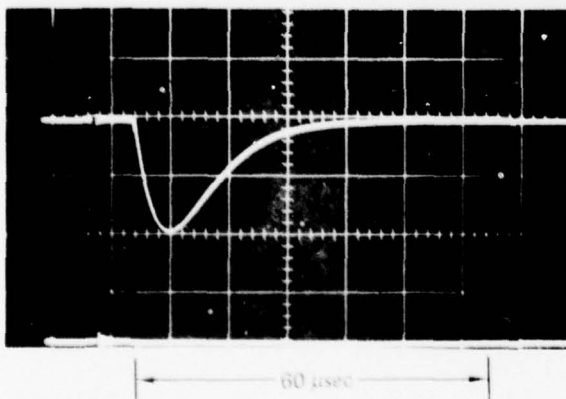
FIGURE 10  
EXAMPLES OF HPC WAVEFORMS FROM 600 kJ GENERATOR



Medium Unipolar  
125 kA Peak  
Reference 10



Wide Unipolar  
52 kA Peak  
(Approx 3 ft Long Arc)  
Reference 11



Narrow Unipolar  
7.6 kA Peak

GP78-8302-7

FIGURE 10 (Continued)  
EXAMPLES OF HPC WAVEFORMS FROM 600 kJ GENERATOR

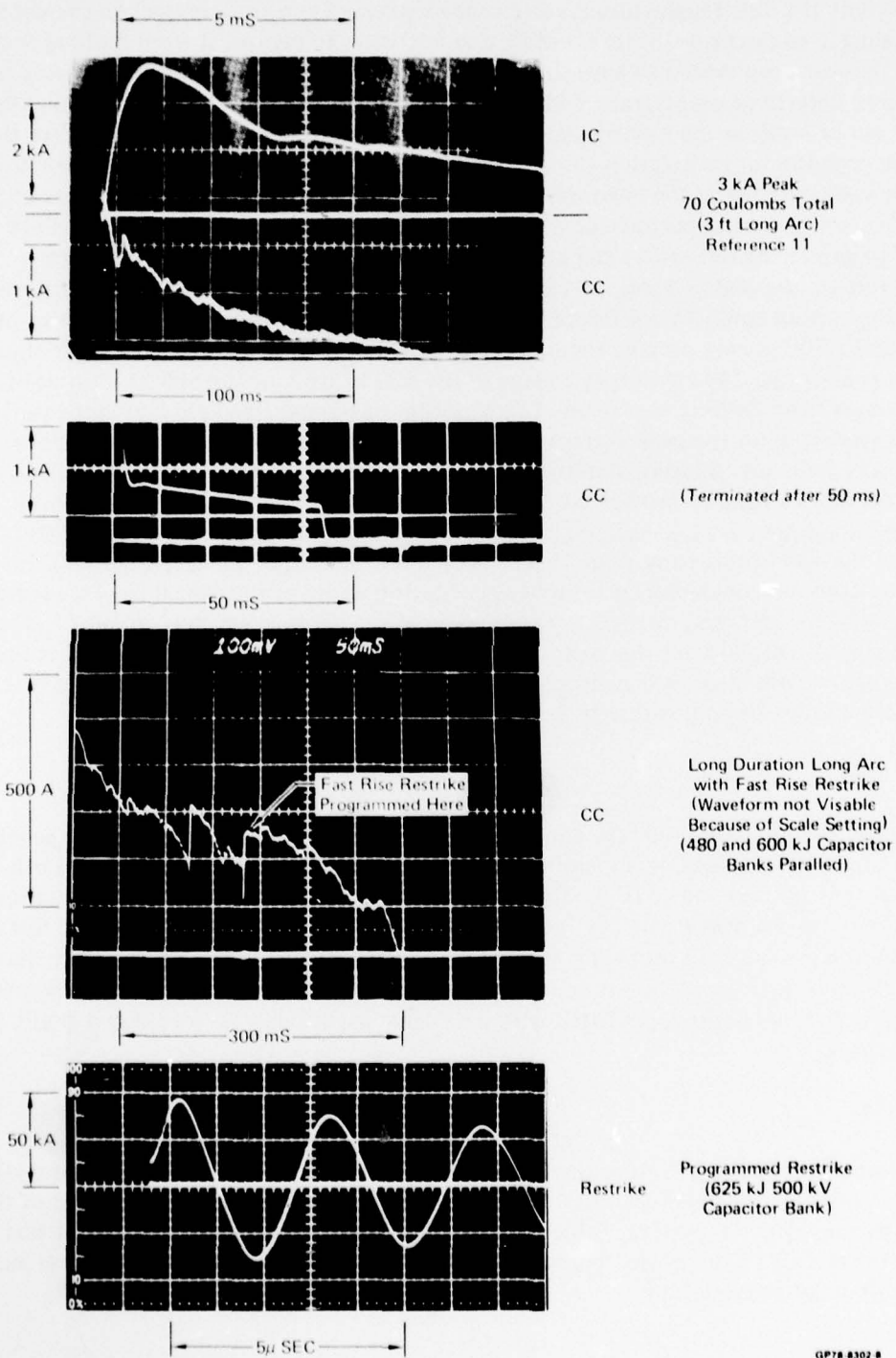


FIGURE 11  
EXAMPLES OF IC, CC, AND FAST RISE RESTRIKE WAVEFORMS  
FROM MCAIR LIGHTNING SIMULATORS



Circuit components such as high power inductors, resistors, capacitors and spark gaps are needed for isolation, thus posing some unique problems. For example, if a resistor and spark gap are used to isolate the initial high-current surge capacitor bank from an intermediate current supply, the resistor must have the high-voltage standoff characteristics to prevent it from flashing over. The resistor and the spark gap must also have the structural integrity to prevent magnetic forces from causing them to deform or disintegrate, and they must have sufficient heat capacity so that they do not burn out or erode as the intermediate and continuing current components pass thru them. The principle criterion for an isolation element or system is that it must develop a voltage drop such that the voltage rating of the most sensitive element in the system being protected is not exceeded. The voltage on the output side of the element must simultaneously remain high enough to close the air gap to the test article and generate the specified HPC or restrike waveform.

In this system, the 600 kJ bank and restrike generator are decoupled from the intermediate and continuing current banks by a series of inductive resistor elements (encased in 40-inch, oil-filled PVC tubes) and a 300  $\mu$ henry air core inductor. The oil bath provides the needed voltage standoff capability to prevent the 240 kV output voltage of the 600 kJ bank or the 500 kV output of the restrike generator from flashing over to the 12 kV output of the intermediate current bank. The resistors also serve to limit the peak current of the intermediate current bank in conjunction with the large air core inductor. Additional inductive resistor elements mounted in oil are utilized between portions of the 480 kJ bank to provide current limiting for the CC portion of the waveform. This filter network simplifies the high current switching difficulty somewhat by allowing the HPC generator and the 480 kJoule bank to be triggered by the same output gap (see Figure 7). However, this technique cannot be applied to the restrike generator because of the time difference between pulse initiation of the HPC and restrike. A time delay pulse generator, which is coupled to the HPC generator's firing circuit, initiates the high voltage trigger pulse to the restrike generator at the designated time. As with diagnostic instrumentation, isolated power sources are required to eliminate ground loops and premature triggering.

#### Instrumentation

In order to accurately monitor the combined waveform from the 600 kJoule pulse generator and the 480 kJoule capacitor bank, at least two different current sensors must be used. Both current transformers (CT's) and coaxial current shunts are used. CT's are preferred to monitor the HPC because they have a high frequency response and they are easier to isolate from the test circuit and thus minimize ground loop problems. Whenever coaxial current shunts or more than one CT are used, all readout instrumentation is operated from isolated power sources. The waveforms are commonly recorded by oscilloscopes fitted with data cameras, but may be recorded digitally for computer analysis.

#### Applications

The versatility which results from the many adjustable parameters of this combined system cannot be overemphasized. This versatility can probably be best illustrated by a sampling of the variety of tests run using this system. Table I shows a few of the tests performed and the test levels required for them. Table I in no way represents the total capability of the simulator. New innovations are still under investigation.

**TABLE 1**  
**REPRESENTATIVE LIGHTNING TESTS USING THE**  
**ONE MEGAJOULE LIGHTNING SIMULATION FACILITY**

Test Title	Peak Current (kAmps)	Waveform Type	Waveform Specification
F-15 External Fuel Tank Qualification	200	HPC	MIL-B-5087B
F-15 Wing Tip Light Qualification	100	HPC	MIL-B-5087B
Space Shuttle Aft Propulsion System (APS)	50	HPC-IC-CC	NASA
Space Shuttle External Fuel Tank	50	HPC-IC-CC	NASA
Space Shuttle Pyrotechnics	200	HPC-CC (100 kA/ $\mu$ sec)	NASA
Graphite/Epoxy Composite Panels	120	HPC-IC-CC	SAE
Electrical Properties of Boron/Epoxy Composites	1-13	HPC	R&D Scaled MIL-B-5087B
<i>Stressed Composite Beams</i>	94-208	HPC-CC	R&D Scaled MIL-B-5087B
Stressed F-111 Horizontal Stabilizer	64-204	HPC	MIL-B-5087B
Harrier Wing Internal Arcing Evaluation	25-204	HPC	SAE
Advanced Lightning Protection Systems	8-82	HPC-CC	R&D
F-18 Gr/Ep Composite Door Lightning Penetration Evaluation	100	HPC-CC	SAE
Slotted Metal Radome Direct Strike Evaluation	200	HPC	MIL-B-5087B

GP76-8302-10

#### Summary

The One Megajoule lightning simulator is a significant extension of the industry's lightning test capability. Not only can a much wider range of tests be performed but the test credibility is also enhanced. Some of the principal advantages of this system are:

1. The output probe can be located up to approximately 10 cm from the test sample so as to minimize probe effects.

2. The high output voltage (240 kV) is sufficient to produce puncture or flashover of dielectric materials.
3. After the arc channel has been initiated, it can be extended up to approximately one meter in length. Swept stroke tests require this condition.
4. Test specimen resistance and inductance normally has little effect on the discharge waveform.
5. Both single polarity and oscillatory discharge waveforms can be produced for testing.
6. The peak amplitude and pulse width of the discharge can be easily and reliably adjusted.
7. A full threat waveform (HPC, IC, CC and restrike) or any combination of the waveform components can be produced for synergistic testing.
8. A HPC restrike can be programmed to occur at any time during a CC. The restrike can come from the 600 kJoule pulse generator or from the high rate-of-rise restrike generator. The fast rate-of-rise of the restrike is up to 50 kAmp/ $\mu$ sec, so that threat level time-indicated voltage effects and inductive sparking can be produced by the composite waveform.



## REFERENCES

1. J.A. Plummer and J.D. Robb, "Aerospace Recommended Practice: Lightning Effects Tests on Aerospace Vehicles and Hardware," 1975 Lightning and Static Electricity Conference, Culham Laboratories, England, April 1975.
2. "Space Shuttle Program Lightning Protection Criteria Document," JSC-07636, Rev. A, 4 November 1975.
3. N. Cianos and E.T. Pierce, "A Ground-Lightning Environment for Engineering Usage," Stanford Research Institute Technical Report 1, SRI Project 1834, August 1972.
4. J.E. Nanevich, R.T. Bly and R.C. Adam, "Airborne Measurement of the Electromagnetic Environment Near Thunderstorm Cells," 1977 IEEE International Symposium on Electromagnetic Compatibility
5. M.A. Uman, "Lightning", McGraw Hill, New York, 1969
6. H.T. Clark, "Advanced Development on Vulnerability/Survivability of Advanced Composite Structures," Air Force Materials Laboratory, Technical Report AFML-TR-73-152, May 1973.
7. "A Look At Lightning," Product Support Digest Reprint, P.S. 1005, McDonnell Aircraft Co., 25 May 1977.
8. E.H. Schulte, "Effects of "Lightning Waveform Components on Graphite/Epoxy Material," Society for the Advancement of Material and Process Engineering 23rd National Symposium, Anaheim, California, May 1978.
9. R. Cohen and E.H. Schulte, "Lightning Tests of the Orbiter Pyrotechnic Escape System," 9th IES-AIAA-ASTM-NASA Space Simulation Conference, Los Angeles, California, April 1977.
10. E.H. Schulte, "High Current Lightning Simulation-Waveshape Evaluation," 11th National Conference on Environmental Effects on Aircraft and Propulsion Systems, Trenton, New Jersey, May 1974.
11. A. Anderson, E. Mumme, E.H. Schulte, "High Current Lightning Test of Space Shuttle External Tank Lightning Protection System," 9th IES-AIAA-ASTM-NASA Space Simulation Conference, Los Angeles, California, April 1977.



ABSTRACT

PROTECTION AGAINST LIGHTNING-INDUCED LINE SURGES AND TRANSIENTS

by

Rodney B. Bent  
Atlantic Scientific Corporation  
Indian Harbour Beach, Florida

Presented at

Federal Aviation Administration - Georgia Institute of Technology  
Workshop on Grounding and Lightning Protection

May 1978

PRECEDING PAGE BLANK

## ABSTRACT

In order to understand and protect against lightning surges and transients several basic facts must be understood. This presentation will introduce these problems to the attendees. The major source of lightning surges in conductors will be described, with descriptions of their magnitudes and accuracies. The effects of insulation, grounding and bonding and skin effect will be introduced. The characteristics of the basic protection devices will be presented and the types of circuits they are best suited to. Problem areas of each protector will be discussed in particular with respect to AC protection. The presentation will make people aware of the problems associated with electrical effects, as well as the different physical problems of the magnetic field effects from lightning. It is proposed that the presentation will not be biased toward any particular product, but will be a general overview of surge protection. Actual results of protected and unprotected systems will be illustrated.

PAPER NOT AVAILABLE AT TIME OF RELEASE  
FOR PRINTING

LIST OF ATTENDEES

Richard C. Abercrombie  
Dynalectron Corporation  
Transportation Test Center  
Pueblo, CO 81001

Blair R. Adams  
Federal Aviation Administration  
AAC-943E  
P. O. Box 25082  
Oklahoma City, OK 73125

Blanton R. Adams  
Federal Aviation Administration  
AAF-640  
Atlantic City, NJ 08405

M. P. Amason  
Douglas Aircraft Company  
3585 Lakewood Blvd.  
Long Beach, CA 90846

Herman D. Anderson  
Defense Electronics Supply Center  
ATTN: DESC-EMM  
1507 Wilmington Pike  
Kettering, OH 45444

C. J. Andrasco  
Federal Aviation Administration  
ARD-350  
Washington, DC 20590

Shigeo Ashida  
Tanegashima Space Center  
National Space Development  
Agency of Japan  
Minamitane-CHO KUMAGE-GUN  
Kagoshima, 891-37 Japan

Jack L. Atkinson  
Lockheed-Georgia Company  
D/72-75-280  
86 South Cobb Drive  
Marietta, GA 30063

Hugh Barber  
Federal Aviation Administration  
AAL-430  
632 Sixth Avenue  
Anchorage, AK 99501

Raymond R. Barkalow  
Federal Aviation Administration  
ARD-350  
2100 2nd Street, SW  
Washington, DC 20590

Tom Beaver  
Atlanta Gas Light Company  
P. O. Box 4596  
Atlanta, GA 30302

Jack Bell  
Federal Aviation Administration  
601 E. 12th  
ACE-430 Room 1625  
Kansas City, MO 64106

C. W. Bergman  
2340 Old Trail Drive  
Reston, VA 22091

Dumas Bernard  
Ministere de la Defense  
STTA  
129 Rue de la Convention  
Paris, France 75015

J. E. T. Black  
Rome Air Development Center  
RADC/DCLD  
Griffiss AFB, NY 13441

Warren Bogin  
Hazeltine Corporation  
Pulaski Road  
Greenlawn, NY 11740

Greg Von Bokern  
The Boeing Company  
P. O. Box 3707  
Seattle, WA 98124

Leonard Bosin  
Federal Aviation Administration  
ARD-223  
2100 2nd Street, SW  
Washington, DC 20590

T. L. Boulay  
Onera  
29 Division Leclerc  
92320 Chatillon, France

Warren Braun  
P. O. Box 1106  
Harrisonburg, VA 22801

George E. Briggs  
GTE Sylvania, Inc.  
189 "B" Street  
Needham Height, MA 02194



Art Brockschmidt  
Boeing Aerospace Company  
M/S 43/44  
P. O. Box 3999  
Seattle, WA 98124

Neal Browder  
GA ETV Network  
1540 Stewart Avenue, SW  
Atlanta, GA 30310

A. Gary Brown  
University of California  
P. O. Box 45  
Mercury, NV 89023

Jack Brown  
Atlanta Gas Light Company  
P. O. Box 4569  
Atlanta, GA 30302

Lou Brown  
Federal Aviation Administration  
P. O. Box 20636  
Atlanta, GA 30320

Frank Bugg  
GA ETV Network  
1540 Stewart Avenue, SW  
Atlanta, GA 30310

Donald H. Burchnell  
Dons Electric & Lightning Control  
7813 Napoleon Street  
Orlando, FL 32807

Bill Burgess  
University of South Alabama  
University Boulevard  
Mobile, AL 36688

William G. Butters  
McDonnell Aircraft Company  
Department 256, Bldg. 66  
P. O. Box 516  
St. Louis, MO 63166

Miguel Cabello  
Proyeccion Dinamica Industrial, S.A.  
Gomez Farias 56-102  
Mexico 4, D.F., Mexico

Carl B. Cahill  
c/o J. E. Sicre  
8906 Fairhaven Avenue  
Upper Marlboro, MD 20870

Reed W. Campbell  
U. S. Forest Service  
324 25th Street  
Ogden, UT 84401

Audrey R. Carlson  
Georgia Institute of Technology  
School of Electrical Engineering  
Atlanta, GA 30332

Don R. Carroll  
Federal Aviation Administration  
10455 E. 25th Avenue  
Aurora, CO 80010

George C. Carver  
Federal Aviation Administration  
ASO 213  
P. O. Box 20636  
Atlanta, GA 30349

J. Cecconi  
NOAA-NWS  
8060 13th Street  
Silver Springs, MD 20910

John T. Chasteen  
A. T. & T. Company  
Long Lines  
10 South Canal  
Chicago, IL 60606

James F. Clayton, Jr.  
Federal Aviation Administration  
ASO 213  
P. O. Box 20636  
Atlanta, GA 30349

J. D. Cline  
Dayton Granger Aviation, Inc.  
P. O. Box 14007  
Ft. Lauderdale, FL 33302

Gerald B. Cook  
Federal Aviation Administration  
Chinese CAA, Taiwan, ROC  
CAAG/FAA Box 18  
APO San Francisco, CA 96263

Roger B. Cook  
Mission Research Corporation  
1400 San Mateo, SE  
Albuquerque, NM 87108

H. R. Cooper  
Beech Aircraft Corporation  
9709 East Central  
Wichita, KS 67002

Paul Cork  
Gates Learjet Corporation  
P. O. Box 7707  
Wichita, KS 67277

Philip B. Corn  
Air Force Flight Dynamics Laboratory  
AAFDL/FEA  
Wright-Patterson AFB, OH 45433

Richard D. Cortright  
Extel Corporation  
310 Anthony Trail  
Northbrook, IL 60062

Richard M. Cosel  
Florida Institute of Technology  
Electrical Engineering Department  
P. O. Box 1150  
Melbourne, FL 32901

George Costache  
Bell-Northern Research  
P. O. Box 3511  
Ottawa, Canada

James Coyle  
Federal Aviation Administration  
NAFEC ANA-330  
Atlanta City, NJ 08405

Michael J. Coyle  
MCG Electronics, Inc.  
160 Brook Avenue  
Deer Park, NY 11729

Michael J. Coyle  
MCG Electronics Inc.  
160 Brook Avenue  
Deer Park, NY 11729

William T. Croker  
Georgia Power Company  
P. O. Box 4545  
Atlanta, GA 30302

David Culliford  
Transport Canada  
4900 Yonge Street, Suite 300  
Willowdale, Ontario, M2N, 6A5

Ed Dalman  
Powers Regulator Company  
2942 Mac Arthur Blvd.  
Northbrook, IL 60062

Larry Day  
Continental Telephone Service Corp.  
56 perimeter Center East  
Atlanta, GA 30346

George Deger  
TII Industries, Inc.  
100 North Strong Avenue  
Lindenhurst, NY 11757

Hugh W. Denny  
Georgia Institute of Technology  
EES/ETL/EMC  
Atlanta, GA 30332

Wilbur R. Dodge  
Singer Company Link Division  
Kirkwood Industrial Park  
Department 4917  
Binghamton, NY 13902

Joe. L. Downs  
Federal Aviation Administration  
AGL-436  
2300 East Devon Avenue  
Des Plaines, IL 60018

John C. Duane  
Jacksonville Port Authority  
14200 Pecan Park Road  
Jacksonville, FL 32229

Capt. Frank Eisenbarth  
Defense Nuclear Agency  
6801 Telegraph Road  
Alexandria, VA 22310

Martin C. Elliott  
Federal Aviation Administration  
AWE-430  
P. O. Box 92007, WWPC  
Los Angeles, CA 90009

Charles L. Elmore  
Federal Aviation Administration  
P. O. Box 20636  
Atlanta, GA 30320

Jim Eubanks  
Atlanta Gas Light Company  
P. O. Box 4569  
Atlanta, GA 30302

John R. Fields  
FM Associates, Ltd.  
P. O. Box 9901  
Atlanta, GA 30319

James Folkl  
U. S. Army  
Aviation Research & Deveopment Command  
P. O. Box 209  
St. Louis, MO 63166

Marlin H. Forstrom  
USAF  
3246 TESTW/TEERL  
Eglin AFB, FL 32542

A. C. Foss, Jr.  
General Electric Company  
MD 750  
P. O. Box 5000  
Binghamton, NY 13902

Anthony J. Froehlich, Jr.  
Federal Aviation Administration  
AAF-530  
Washington, DC 20591

Charle R. Fulton  
Naval Air Test Center  
(Lightning Facility)  
Naval Air Test Center SY82  
Patuxent River, MD 20670

Larsen L. Furr  
Federal Aviation Administration  
P. O. Box 20636  
Atlanta, GA 30349

Ben Gallo  
J. G. Biddle Company  
Township Line & Jolly Road  
Plymouth Meeting, PA 19462

Frank Galuppo  
Grumman Aerospace Corporation.  
South Oyster Bay Road  
Bethpage, NY 11714

A. Anthony Garka  
Federal Aviation Administration  
AAF-325  
800 Independence Avenue  
Washington, DC 20591

Jerry N. George  
Federal Aviation Administration  
Room 1611  
601 E. 12th Street  
Kansas City, MO 64106

Paul Gerard  
French Air Technic Service  
246 Rue Lecourbe  
Paris, France

H. Niles Gloer  
Transtector Systems  
Lake Tahoe, NV 89501

Richard A. Glover  
Federal Aviation Administration  
P. O. Box 1689  
Ft. Worth, TX 76101

James A. Goble, Jr.  
E-Systems, Inc.  
ECI Division  
P. O. Box 12248  
St. Petersburg, FL 33704

Dr. Donald J. Grace  
Director, EES  
Georgia Institute of Technology  
Atlanta, GA 30332

Emile Grenier  
L. P. Grenier & Fils, Inc  
Grounding & Lightning Protection  
4134, Boul. Hamel  
Quebec, Canada

Algirdas Grigaitis  
Federal Aviation Administration  
AGL-624  
2300 Devon Avenue  
Des Plaines, IL 60018

David H. Gunn  
Federal Aviation Administration  
FSDO-62  
9275 Genaire Drive  
Berkeley, MO 63134

Hal Hamann  
A. T. &T.  
Room 1039  
811 Main  
Kansas City, MO 64141

Robert L. Hammack  
A. T. &T.  
100 Edgewood Avenue NE  
Atlanta, GA 30303

Frederick A. Hansen  
Powers Regulator Company  
2942 Mac Arthur Blvd.  
Northbrook, IL 60062



William C. Hart  
Mission Research Corporation  
735 State Street  
Santa Barbara, CA 93102

Kenneth P. Heary  
Heary Brother Lightning Products  
Mfg. Company Inc.  
Moore Road  
Springville, NY 14141

James C. Henry, Jr.  
University of West Florida  
Physical Plant, Bldg. 19  
Pensacola, FL 32504

Robert N. Hokkanen  
Naval Training Equipment Center  
N411  
Orlando, FL 32813

Gene K. Huddleston  
Georgia Institute of Technology  
School of Electrical Engineering  
Atlanta, GA 30332

Curtis A. Jackson  
Federal Aviation Administration  
P. O. Box 20636  
Atlanta, GA 30320

Wilbur Jarmon  
Federal Aviation Administration  
ASO-400  
P. O. Box 20636  
Atlanta, GA 30349

William B. Johnson  
Department of Army  
CDR USAMIRADCOM  
ATTN: DRCPM-PE-EG  
Redstone Arsenal, AL 35809

Douglas E. Johnson  
Minn. Dept. of Transportation  
Aeronautic Division  
Room 417 Transportation Building  
St. Paul, MN 55155

Aaron U. Jones  
U. S. Department of Labor  
Mine Safety & Health Administration  
Building F  
P. O. Box 1166  
Beckley, WV 25801

Doanld T. Jones  
Copperweld Bimetallies Division  
P. O. Box 1000  
Glassport, PA 15045

Gary M. Jones  
U. S. Army Engineer District  
210 North 12th Street  
St. Louis, MO 63101

Dr. Richard D. Jones  
Sandia Laboratories  
P. O. Box 5800  
Albuquerque, NM 87185

C. W. Kaise  
Federal Aviation Administration  
ASO-213  
P. O. Box 20636  
Atlanta, GA 30349

Joseph Kaiser  
Federal Aviation Administration  
ACE-430, Room 1625  
601 E. 12th Street  
Kansas City, MO 64106

Chester J. Kawiecki  
Lightning Protection Corporation  
P. O. Box 6086  
Santa Barabara, CA 93111

Edwin L. Kesler  
Naval Electronic Systems Command  
Code 52021  
Washington, DC 20360

James R. Ketterer  
McDonnell Douglas Corporation  
Dept. 313, Bldg. 34  
P. O. Box 516  
St. Louis, MO 63166

Capt. Michael King  
Defense Nuclear Agency  
6801 Telegraph Road  
Alexandria, VA 22310

Wayne L. Kinney  
TCOM Corporation  
5775 Sterrett Place  
Columbia, MD 21044

J. L. Kirkman  
A. T. & T. Company  
100 Edgewood Avenue NE  
Atlanta, GA 30303



Richard Kline  
Elta Electronics  
P. O. Box 330  
Ashdod, Israel

Eugene D. Knowles  
Parsons-Brinckerhoff/Tudor  
401 W. Peachtree Street  
Atlanta, GA 30303

Lawrence V. Kriger  
Air Force System Command  
ESD/DCMV, S-51  
Hanscom AFB, MA 01731

Frank LaDieu  
Air Force Command Service  
1842 EEG/EETW  
Scott AFB, IL 62225

John J. Leahy  
Federal Aviation Administration  
ANE-436  
12 New England Executive Park  
Burlington, MA 01803

Lawrence Levey  
Bell Telephone Labs  
Whippany Road  
Whippany, NJ 07981

Donald F. Loomis  
Federal Aviation Administration  
AWE-434  
P. O. Box 92008, WWPC  
Los Angeles, CA 90009

Albert F. Lowas, Jr.  
USAF  
DEEE  
438 Civil Engineering Squadron  
McGuire AFB, NJ 08641

Melvin B. Luxenberg  
Federal Aviation Administration  
2300 East Devon Avenue  
Des Plaines, IL 60018

Wallace T. Lynch  
Georgia ETV Network  
WDCO-TV  
P. O. Box 269  
Cochran, GA 31014

Ian MacDonald  
Telecommunication & Electronics Branch  
Canadian Coast Guard Central Region  
1 Yonge Street, 20th Floor  
Toronto, Ontario, Canada

T. L. Mahoney  
Dayton T. Brown Company  
Church Street  
Bohemia, NY 11721

Ed Malone  
Reynolds Industries, Inc.  
89 Vereda Cordillera  
Goleta, CA 93017

M. E. Mann  
National Aeronautics & Space Admin.  
MSFC, Alabama  
Huntsville, AL 35812

John D. Marley  
Federal Aviation Administration  
P. O. Box 92007 WWPC  
Los Angeles, CA 90009

G. T. Martin  
Lockheed Georgia Company  
Department 72-39, Z316  
86 South Cobb Drive  
Marietta, GA 30063

Philip T. Martin  
ITT North Electric Company  
P. O. Box 20345, N.W. Station  
Columbus, OH 43220

George Matrigali  
U. S. Coast Guard Headquarters  
400 7th Street SW  
G-EOE-3/61  
Washington, DC 20590

William G. Michels  
Federal Aviation Administration  
ANW-456  
Boeing Field  
Seattle, WA 98003

Tom Miller  
Grumman American Aviation Corporation  
P. O. Box 2206  
Savannah, GA 31402

J. Gary Mitchell  
General Telephone of Southeast  
P. O. Box 1412  
Durham, NC 27702

Bruce E. Montgomery  
Lockheed Georgia Company  
Dept. T2-97, Zone 12  
Marietta, GA 30063

Fred Morris  
Federal Aviation Administration  
ASO-431.12  
P. O. Box 20636  
Atlanta, GA 30320

Roger Mull  
Federal Aviation Administration  
ASO-430  
P. O. Box 20636  
Atlanta, GA 30320

John W. Naglich  
Federal Aviation Administration  
P. O. Box 20636  
Atlanta, GA 30320

Sudin B. Naik  
MARTA  
2200 Peachtree Summit  
401 West Peachtree Street  
Atlanta, GA 30308

Harold E. Newcomb  
U. S. Department of Labor  
Mine Safety & Health Admin.  
P. O. Box 112  
Mt. Hope, WV 25880

Sunao Nomachi  
National Space Development  
Agency of Japan  
Z-4 Hamamatsucho Minatoko  
Tokyo, Japan

Richard D. Nussbaum  
Naval Air Development Center  
Mail Code 4053  
Warminster, PA 18974

Donald H. O'Bryhim  
Naval Electronics Systems Command  
Code 5103200  
Washington, DC 20360

Daniel T. O'Connell  
National Weather Service  
Room 616  
8060 13th Street  
Silver Springs, MD 20910

William L. Olsen  
Federal Aviation Administration  
AGA-100  
800 Independence Avenue, SW  
Washington, DC 20591

Wildon A. Ott  
U. S. Coast Guard Headquarters  
400 7th Street  
Washington, DC 20590

Charles Owen  
Heery & Heery  
880 W. Peachtree Street, NW  
Atlanta, GA 30309

Howell Pabian  
Continental Telephone Service Corp.  
P. O. Box 307  
Wentzville, MO 63385

G. W. Parkinson  
Sikorsky Aircraft  
N. Main Street  
Stratford, CT 06497

Albert D. Paul  
Federal Aviation Administration  
P. O. Box 92007, WWPC  
Los Angeles, CA 90009

W. M. Peacock  
Federal Aviation Administration  
ASO-213  
P. O. Box 20636  
Atlanta, GA 30349

William A. Phipps  
Federal Aviation Administration  
ASW-442  
P. O. Box 1689  
Ft. Worth, TX 76101

Louis D. Piszker  
Boeing Commercial Airplane Company  
MS 47-47  
P. O. Box 3707  
Seattle, WA 98124

Joseph J. Pizzicaroli  
General Semiconductor Industries, Inc.  
2001 W. 10th Place  
Tempe, AZ 85281

J. A. Plumer  
Lightning Technologies, Inc.  
560 Hubbard Avenue  
Pittsfield, MA 01201

George E. Pupera  
Climax Molybdenum Company  
Climax, CO 80429

Darryl Ray  
Williams Research Corporation  
2280 W. Maple  
Walled Lake, MI 48088

James Reed, Jr.  
Federal Aviation Administration  
Federal Building  
JFK International Airport  
Jamaica, NY 11430

John E. Reed  
Federal Aviation Administration  
ARD-530  
2100 2nd Street, SW  
Washington, DC 20591

Andrew W. Revay, Jr.  
Florida Institute of Technology  
P. O. Box 1150  
Melbourne, FL 32901

Bob Ridging  
Federal Aviation Administration  
P. O. Box 20636  
Atlanta, GA 30320

Douglas W. Robertson  
Georgia Tech/EES  
EES/ETL  
Atlanta, GA 30332

James P. Roby  
Brandy & Anglin Consulting Engineers  
Suite 970  
1800 Century Parkway, NE  
Atlanta, GA 30345

Norman G. Royer  
Federal Aviation Administration  
Airport Division  
601 E. 12th Street  
Kansas City, MO 64106

Carl J. Rubino  
Federal Aviation Administration  
P. O. Box 592057  
Miami, FL 33189

Farrest S. Rudd  
U. S. Forest Service  
324 25th Street  
Ogden, UT 84401

Bertrand F. Ruggles  
Federal Aviation Administration  
AAP-720  
Washington, DC 20591

F. S. Sakate  
Federal Aviation Administration  
ARD-350  
2100 2nd Street SW  
Washington, DC 20590

Leroy E. Savage  
Continental Telephone Company  
NE. Division  
85 Sheep Davis Road  
Concord, NH 03301

Donald E. Schmidt  
Elite Electronic Engineering Company  
1516 Centre Circle  
Downers Grove, IL 60515

Herman W. Schoob  
Naval Electronic System  
Engineering Center, Great Lakes  
Building 3209  
Great Lakes, IL 60088

R. W. Schult  
Aerospace Corporation  
2350 E. El Segundo Blvd.  
El Segundo, CA 90245

Len Sessler  
Bell Laboratories  
Room 2A261  
Whippany Road  
Whippany, NJ 07981

Billy E. Shipp  
Federal Aviation Administration  
4165 M.L. King, Jr. Drive, SW  
Atlanta, GA 30336



Jean-Pierre Simi  
Ingenieur-Cables de Lyon  
65 Rue Jean-Jaures-g58f7  
Bezons, France

Charles R. Smith  
U.S. Coast Guard Headquarters  
GECV-3  
400 7th Street, SW  
Washington, DC 20590

David L. Smith  
Parsons Brinckerhoff/Tudor  
P. O. Box 469  
Atlanta, GA 30301

Richard S. Smith  
Georgia Institute of Technology  
EES/ETL/EMC  
Atlanta, GA 30332

Sanford L. Smith  
Copperweld Bimetallics Division  
2496 Brookhurst Drive  
Atlanta, GA 30338

William S. Smith  
Federal Aviation Administration  
NAFEC ANA-710  
Atlanta City, NJ 08405

Felipe C. Solis  
General Services Administration  
Construction Management Division  
3PCS-Room 2319  
7th & G Street, SW  
Washington, DC 20407

Stephen J. Sorger  
W. N. Phillips, Inc.  
356 Bacon Street  
Lake City, MI 49651

John B. Sowell  
Federal Aviation Administration  
ASO-441  
P. O. Box 20636  
Atlanta, GA 30320

Richard J. Specht  
Federal Aviation Administration  
632 W. 6th Avenue  
Anchorage, AK 99502

Vernon P. Speiser  
Trans World Airlines  
1-448 MC1  
P. O. Box 20126  
Kansas City, MO 64195

Charles J. Spinks  
Atlanta Gas Light Company  
P. O. Box 4569  
Atlanta, GA 30302

Edward A. Spitzer  
Department of Transportation  
Transportation Systems Center  
Kendall SQ  
Cambridge, MA 02142

Bill Stager  
Aids & Ways Branch  
Canadian Coast Guard  
1 Yonge Street, 20th Floor  
Toronto, Ontario Canada, M5E 1E5

James R. Stahmann  
Planning Research Corporation  
PRC 1217  
P. O. Box 21266  
Kennedy Space Center, FL 32815

E. K. Stanek  
West Virginia University  
Dept. of Electrical Engineering  
Morgantown, WV 26506

Carroll L. Stang  
National Weather Service  
NOAA-NWS Engineering Division  
8060 13th Street  
Silver Spring, MD 20910

William Statter  
Federal Aviation Administration  
AAF-530  
800 Independence Avenue, SW  
Washington, DC 20591

Basil J. Steele  
Sandia Laboratories  
P. O. Box 5800  
Albuquerque, NM 87185

Walter W. Stevens  
Federal Aviation Administration  
King County International Airport  
Seattle, WA 98108



Howard P. Stickley  
NAVAL Facilities Engineering  
Command Headquarters  
Code 0442  
200 Stovall Street  
Alexandria, VA 22332

Roger L. Sullivan  
GTE Sylvania  
189 B. Street  
Needham, MA 02194

Phillip H. Swatek  
Federal Aviation Administration  
ASO-1  
P. O. Box 20636  
Atlanta, GA 30320

Keith Switzer  
ERICO Products, Inc.  
34600 Solon Road  
Cleveland, OH 44139

Dalton Szelle  
Sperry Gyroscope  
Marcus Avenue & Lakeville Road  
Great Neck, NY 11020

Allen Tate  
Federal Aviation Administration  
Federal Building  
J.F.K. International Airport  
Jamaica, NY 11430

Edward E. Taylor  
National Aeronautics & Space Admin.  
Kennedy Space Center, FL 32899

Herman R. Tharrington  
Federal Aviation Administration  
AAF-340  
800 Independence Avenue, SW  
Washington, DC 20591

Donald W. Thomas  
GA State Department of Education  
WJSP-TV  
P. O. Box 5  
Warm Spring, GA 31830

Richard W. Thompson  
Federal Aviation Administration  
P. O. Box 92007, WPC  
Los Angeles, CA 90009

Ed Threm  
Federal Aviation Administration  
AGL-437.2  
2300 Devon Avenue  
Des Plaines, IL 60018

W. H. Trammell  
Federal Aviation Administration  
ASO-213  
P. O. Box 20636  
Atlanta, GA 30349

Robert L. Truax  
The Truax Company  
604 Danley Drive  
Ft. Myers, FL 33901

Donald W. Turner  
HQ FORSCOM  
AFEN-FEU-E  
Ft. McPherson, GA 30330

C. B. Upchurch  
Atlanta Gas Light Company  
P. O. Box 4569  
Atlanta, GA 30302

Edward F. Vance  
SRI International  
333 Ravenswood Avenue  
Menlo Park, CA 94025

John F. Vaughan  
ITT Telecommunications  
2000 S. Wolf Road  
Des Plaines, IL 60018

Peter Versage  
Federal Aviation Administration  
NAFEC ANA 410  
Atlantic City, NJ 08405

Dr. Aleksandar Vorgucic  
Visiting Professor  
Georgia Institute of Technology  
School of Electrical Engineering  
Atlanta, GA 30332

Hung Chin Wang  
China Civil Aero Administration  
Air Nav Facilities Division  
Taipei, Taiwan, ROC

Ricahard C. Ward  
Atlanta Gas Light Company  
P. O. Box 4569  
Atlanta, GA 30302

Donald R. Wasson,  
Federal Aviation Administration  
AAC-54B5  
6500 S. MacArthur  
Oklahoma City, OK 73125

Gerald M. Waterfall  
Federal Aviation Administration  
AAP-550  
800 Independence Avenue, SW  
Washington, DC 20590

B. G. Weaver  
National Aeronautics & Space Admin.  
MSFC, Alabama  
Huntsville, AL 35812

Glenn Welch  
Atlanta Gas Light Company  
P. O. Box 4569  
Atlanta, GA 30302

Michael E. White  
Federal Aviation Administration  
2300 E. Devon Avenue  
Des Plaines, IL 60018

Curtis B. White  
Sundstrand Aviation  
Department 763SW  
4747 Harrison Avenue  
Rockford, IL 61101

Dr. Carrell D. Whitescarver  
Martin Marietta Aerospace  
Orlando Division  
P. O. Box 5837 MP 246  
Orlando, FL 32855

Lanny Keith Wiley  
GA Educational Television Network  
1540 Stewart Avenue, SW  
Atlanta, GA 30310

C. L. Wilkerson, Jr.  
Martin Marietta Aerospace  
MP-246  
P. O. Box 5837  
Orlando, FL 32855

Donald E. Williams  
Federal Aviation Administration  
10455 E. 25th Avenue  
Aurora, CO 80010

B. I. Wolff  
General Electric Company  
Building 7, Room 333  
Electronics Park Box 41  
Syracuse, NY 13201

Gordon L. Wood  
CESSNA Aircraft Company  
Department 80  
P. O. Box 1521  
Wichita, KS 67201

Jimmy A. Woody  
Georgia Institute of Technology  
EES/ETL/EMC  
Atlanta, GA 30332

C. R. Wright  
NAFEC AAF-640  
Atlantic City, NJ 08405

Y. C. Wu  
China Civil Aero Administration  
Air Nav Facilities Division  
Taipei, Taiwan, ROC

Donald E. Young  
Boeing Aerospace Company  
M/S 8C-52  
P. O. Box 3999  
Seattle, WA 98124

Klaus P. Zaepfse  
NASA Langley Research Center  
M.S. 477  
Hampton, VA 23665

William T. Zafaris  
Ace Lightning Protection Company  
4125 William Penn Highway  
Monroeville, PA 15146

Anthony G. Zimbalatti  
Grumman Aerospace Corporation  
Plant 35, Mail Stop B25-35  
Bethpage, NY 11748